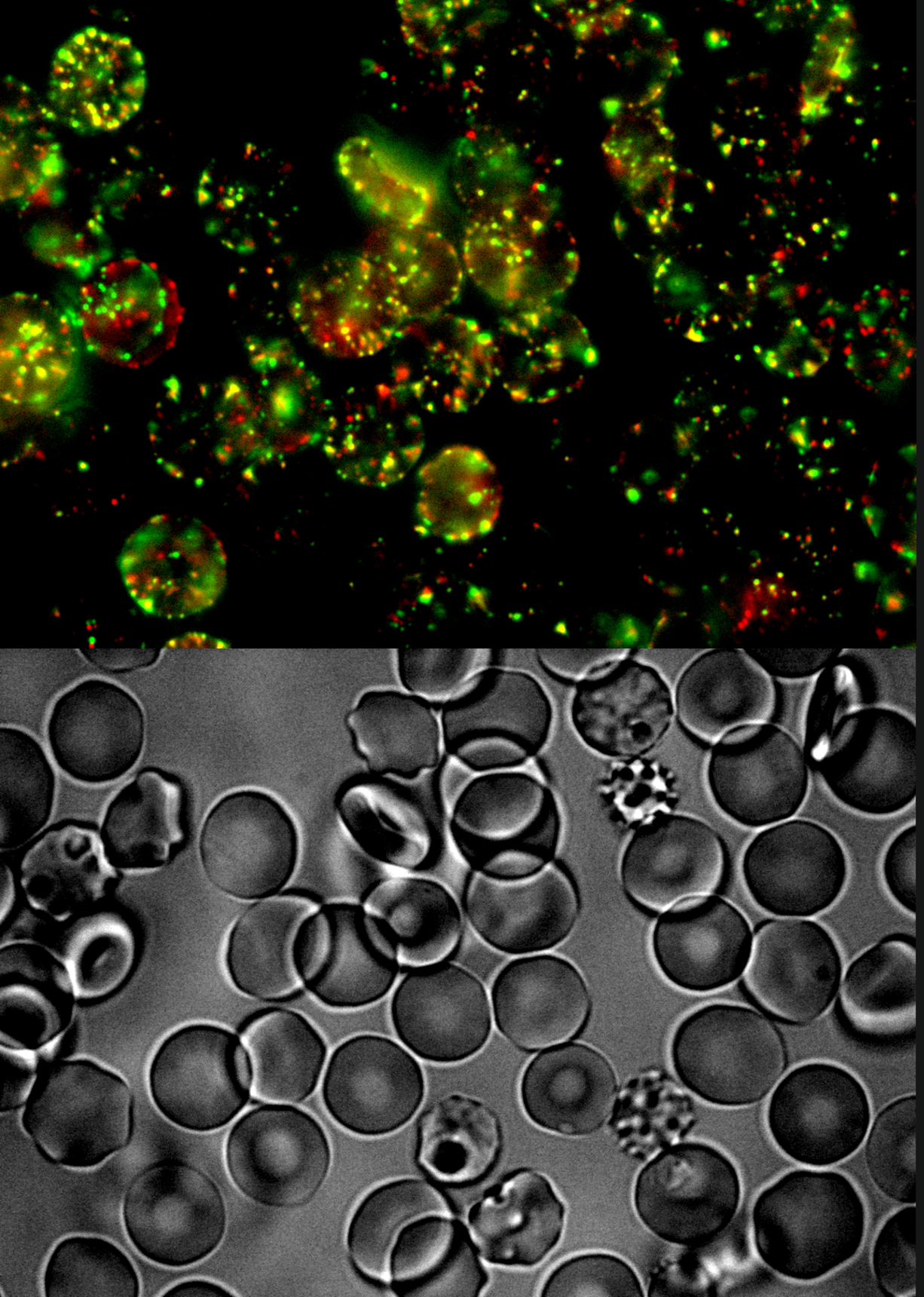

2015

PhD THESIS

Ernest Moles Meler

IBEC
Institute for Bioengineering of Catalonia

UNIVERSITAT DE BARCELONA

ISGlobal Barcelona Institute for Global Health

Development of polyvalent erythrocyte- and parasitized erythrocyte-targeted nanovectors as novel site-specific drug delivery approaches for *Plasmodium falciparum* malaria chemotherapy

ERNEST MOLES MELER

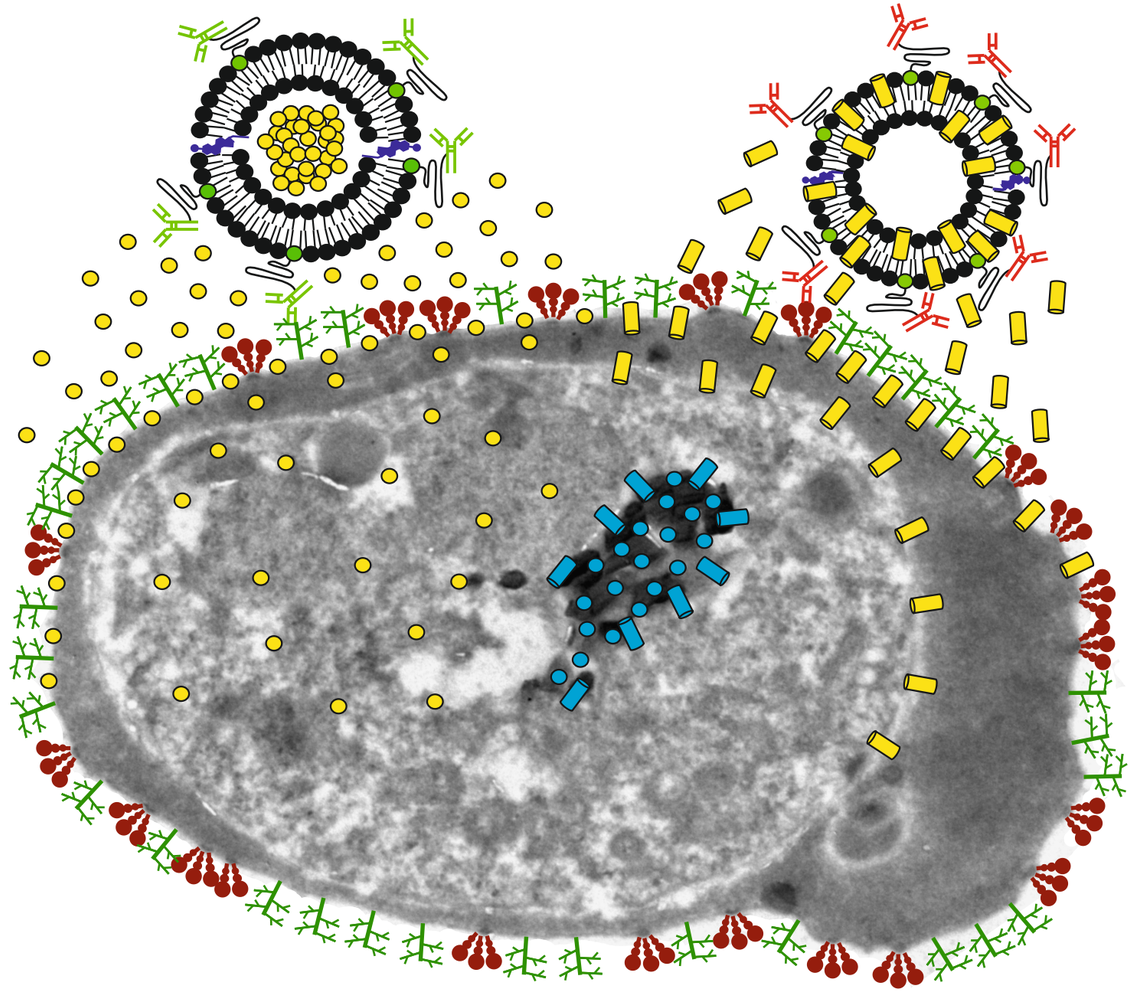

UNIVERSITAT DE BARCELONA

FACULTAT DE FARMÀCIA

PROGRAMA DE DOCTORADO EN BIOTECNOLOGÍA

INSTITUTE FOR BIOENGINEERING OF CATALONIA

BARCELONA INSTITUTE FOR GLOBAL HEALTH

DEVELOPMENT OF POLYVALENT ERYTHROCYTE- AND PARASITIZED ERYTHROCYTE-TARGETED NANOVECTORS AS NOVEL SITE-SPECIFIC DRUG DELIVERY APPROACHES FOR *PLASMODIUM FALCIPARUM* MALARIA CHEMOTHERAPY

Memoria presentada por el licenciado en Biotecnología

ERNEST MOLES MELER

para optar al título de Doctor por la Universidad de Barcelona.

Esta tesis ha sido inscrita en el programa de doctorado en Biotecnología de la Universidad de Barcelona. El trabajo experimental y la redacción de la presente tesis han sido realizados bajo la dirección del Dr. Xavier Fernàndez Busquets, Profesor Investigador Asociado y director del Grupo de Nanomalaria -unidad mixta participada por el Instituto de Bioingeniería de Cataluña y el Instituto de Salud Global de Barcelona-, y bajo tutela del Dr. Santiago Imperial Ródenas, Profesor titular del Departamento de Bioquímica y Biología Molecular de la Universidad de Barcelona.

Barcelona, 2015.

Director de la tesis	El doctorando	Tutor de la tesis
Dr. Xavier Fernàndez Busquets	Ernest Moles Meler	Dr. Santiago Imperial Ródenas

"The most exciting phrase to hear in science, the one that heralds the most discoveries, is not "Eureka!" (I found it!) but 'That's funny…'"

Isaac Asimov

ACKNOWLEDGEMENTS

Primer de tot m'agradaria agrair al meu cap i supervisor, el doctor Xavier Fernàndez Busquets, la confiança que ha dipositat en el meu treball -e idees esbojarrades algun cop...- al llarg d'aquests cinc anys (que es diuen ràpid) i haver-me donat l'oportunitat d'iniciar la tesi doctoral. Actualment la situació de la investigació catalana com la espanyola es troba en un punt molt delicat i es molt difícil iniciar-se en aquest apassionant món que és la recerca, sobretot la que es du a terme en un àmbit tan necessari com la sanitat. Per això sempre recordaré aquest suport dedicat i que la nostra amistat pugui perdurar, moltes gràcies! També voldria reconèixer l'ajuda i temps dedicat de la Patricia Urbán sobretot durant els primers dies en l'IBEC així com per tenir la possibilitat de poder continuar una línea d'investigació tan interessant com la seva.

Potser la part mes important, l'he de dedicar als meus companys sentimentals-investigadors-estudiants-familiars. Tot un grup d'intel·lectuals que són un exemple de com la societat civil hauria d'actuar en el món d'avui en dia. Tot va començar amb una carrera que a priori ningú creia que donaria unes relacions tan longeves. Biotecnologia va ser el punt de trobada on vaig poder gaudir de la companyia del Jordi Rosselló, Oriol Senan, Albert Escobedo, Dani Trujillano, Eduard Pèrez, Uxue Zorrilla (¡ya queda poco, un último esfuerzo!), Eduard Cruz, Octavi Domingo, Núria Estiarte, Judit Puigpinós. Tots vosaltres heu estat grans companys, la principal causa d'haver gaudit els anys universitaris de la millor manera possible i la millor raó per començar la tesi doctoral. Des de els viatges amb el Batmòbil, agrònom de ferro, festes als corresponents pisos, Cappond i medicina etc... Sobretot donar molts ànims a l'Albert en la cerca del *dorado* post-doct (algun dia trobaràs un lloc digne on reconeguin el teu inestimable treball no et preocupis!), al Jordi en la seva tesi en Cambridge (ostres tinc un company que treballa a Cambridge, que wapo!!) i a l'aventura americana de l'Eduard, molta sort company en aquest territori amic! I també, Oriol, que et vagi genial per Lausanne, ciutat fantàstica per viure-hi (i a veure si podem venir a fer un concertillo jaja).

A Lleida també he pogut gaudir de la companyia i suport dels *masters in law* Jordi Solé, Sergi Carvajal i Pol Ishanda, i el *boss enginyer teleco* Marc Vilà! També dels meus companys del grup més conegut mundialment, que com ja sabeu es FOO jaja, Pol, Oriol i Dani, tots molt peculiars i sempre grans persones vivint al límit! Espero que en el pròxim disc siguem tots doctors, músics professionals o juristes i ja definitivament ser un grup d'intel·lectuals jaja (bueno, i estil rock dels 60s clar...). Un record també al gran músic Jose Ramón Madrid i la seva gira marítima i al gran productor Marc Molas, grans artistes! Y un recuerdo de corazón también a mis antiguos compañeros de piso -¡los forestales!- en Lleida Adrián, Lorenzo y David, espero poder veros pronto, fuisteis imprescindibles durante mi estada en esta bonita ciudad.

I no m'oblido del principal recolzament, sosteniment per iniciar, tirar endavant i ara finalitzar la tesi. Tu Cristina has sigut la millor companyia que he pogut desitjar mai i m'has ajudat d'una manera que crec no podré agrair-te mai en la vida. Si mes no, des de que ens vam trobar per primer cop al Máster, hem tingut vides paral·leles i ens hem ajuntat en un moment de la vida similar on hem pogut iniciar-nos en el món de la recerca e iniciar la vida en parella. Disculpa si he sigut una pesat amb la tesi, ho visc massa potser xD!! Hem passat uns anys fantàstics aquí a Barcelona-Hospitalet i segur que els que vindran seran també molt bons. Estem en un camp

difícil però amb força i ganes ens en sortirem, ja sigui al Canadà o Australia qui sap :p. Molta sort en la cerca de post-doc y un petó enorme!!!!!

Tanmateix voldria recordar a tots aquells companys-investigadors que han compartit amb mi aquests anys de esperances, patiments e il·lusions. Desde mis primeros pasos en el IBEC-CRESIB, Joana, estuviste acompañándome y por supuesto ayudándome a organizar mi puesto de trabajo jaja nose que haríamos sin ti la verdad... De hecho, como ya te he dicho alguna vez, has sido lo más parecido a una hermana que he tenido, gracias por tus consejos, soporte moral diario, (¡los cafés de las 13:00h puntuales!) broncas instructivas :) y recordatorios, me has enseñado a ser mejor investigador y persona. Y siento mucho no haber podido estar más en el laboratorio, con nuestras estadas y ahora escribiendo la tesis ¡casi no nos hemos visto! Por cierto, espero que consigas un Super Cum Laude y la defensa te vaya genial (seguro que si, ya me gustaría hacer las presentaciones tan bien como tu…). Un recordatori especial també per als demés companys del fantàstic grup de Nanomalaria: Elisabet Martí i Míriam Ramírez, que seran unes grans mare-investigadores! (cosa molt difícil de dur a terme avui en dia... i que te molt de mèrit es clar), l'Arnau Biosca (viva imatge de la motivació 100%) i la Cinta Díez que espero estigui gaudint d'una tesi profitosa!

No m'oblido dels demés!! Vaig començar al CEK amb el selecte club d'Antonios/es liderat per la Maria Bernabeu (no es del Madrid encara que tingui aquest cognom...), la Lorena Martín, la Mireia Ferrer, la Diana Barrios i el Pep Astola. També teníem ja els fantàstics Alfons Jiménez, Ariel Magallón que mola mogollón i Pau Cisteró i el grup de l'Alfred que vindria una mica més endavant amb la genial Núria Rovira i la Cristina Bancells. La veritat es que m'ho vaig passar genial i teníem moooolt espai a les cabines de cultiu (de fet jo, la Maria i el Pau teníem cadascú una per cap!). M'agradaria sobretot agrair el suport moral de la Maria durant els primers dies de feina a cultius i les seves xerrades didàctiques, de fet ella i la Núria han sigut unes grans mentores i quasi bé tot el que se de cultius ho he après gràcies a elles. Gràcies Núria també per ser tan *accurate*, cal mes gent com tú! I per suposat, una gran abraçada al Pau i la Ruth. Crec sincerament que s'han unit les dues persones mes bones de l'univers (del de *2001*, no el d'aquella pel·lícula indescriptible d'*Interstellar*...) i que seran molt bons pares. I moltes moltes gràcies a tu Pau per ser com ets, tan amable i amb ganes d'ajudar a tothom a tot moment (i sobretot per poder comentar amb tu els concerts de Marilyn Manson, un músic fantàstic i gran incomprès). Sempre recordaré el dia que vas pujar a l'escenari a recollir el micro que se li havia caigut al nostre cantant jaja, merci! També recordar la sempre positiva actitud de l'Alfons i l'Ariel, grans persones i alegres companys. Els podeu trobar a algún karaoke, tenen un molt bon repertori de cançons per poder gaudir les estones perdudes en el lab! I'd like to give my thanks as well to Bogachan Tahirbegi!, the great turkish labmate I met during my early times in the IBEC and even greater friend. I hope your research goes fine and to hear from you soon!

Posteriorment, vindrien els fantàstics Aleix Elizalde, Sívia Sanz, Aida Valmaseda i Míriam Díaz (¡que grande es León!). Uns grans amics-doctorands amb els quals hem pogut compartir moltes estones alegres a cultius, realment gràcies a vosaltres la vida en el lab ha estat molt més lleugera i agradable. Se m'ha passat el temps volant! Espero que vagi molt bé la estada a Brasil Aleix, molta sort i que no contraguis *Vivax*! Voldria també remarcar el valor que ha tingut, sent

metge, en iniciar-se en el món de la investigació. Ho respectaré immensament doncs aquí en aquest país sembla una anomalia. I la Sílvia, doncs que hem de dir, una persona sense maldat i sempre positiva que pot trobar un somriure en un dia negre. Juntament amb el Borja López i la Marta Cova formen un dels millors grups tant com companys com treballadors, sempre ajudant-se i tots ells amb un gran sentiment d'humanitat. Moltes gràcies *Glycos* sou molt dolços! I m'estic deixant molta gent, disculpeu, realment hi ha moltes persones a qui recordar en el CEK: Martes, Sofia, Mario, Marc, Patricia, Gemma, Joe... gràcies a tots!

També m'agradaria agrair als caps de l'extint CRESIB i nou ISGlobal (- recerca) el seu suport directe e indirecte, ja sigui via col·laboracions, suport científic o mitjançant l'aportació de noves idees durant els importants i vitals Journal Clubs, a la recerca desenvolupada durant aquests cinc anys i plasmada en aquesta tesi. Moltes gràcies Alfred Cortès, Hernando del Portillo, Carmen Hernández, Luis Izquierdo, Carlota Dobaño i Alfredo Mayor. Tots grans persones i encara més, grans científics.

I'd like to thank as well Professor Mats Wahlgren and Kirsten Moll for giving me the opportunity to work in their exceptional group, particularly famous and worldwide acknowledged due to their findings about the rosetting processes caused by *Plasmodium* parasites. I spent such a great time with you and, importantly, this stage allowed us to characterize several features of our nanovectors and considerably move forward in our research. I'll always remember the awesome researchers I met and work with in MTC: Junhong, Xiaogang, Chim, Maria del Pilar, Daisy, Pablo, Mia, Martina… I hope Pilar, Xiaogang and Sherwin are still as industrious as they were during my stage! You were fantastic guys and a great example of how a researcher should work and behave with others! I'll always remember the day of the blackout jaja… really scary. Only the cell incubators were still running…

And, of course, I have a special remember for the people from KI, Norsborg. A village placed a few meters away of the end of the world but still pleasant and full of friendly researchers. Lauro, Mike and Albert (and Emeka of course!!), you guys were likely the main reason to come back to Norsborg with a smile on my face, even if the experiments had gone wrong! All the films and TV serials we saw, the days eating stevia, chickpeas and drinking vinegar, they were so great… (well even the day we destroyed the kitchen xD jajaj). I miss you so much! And thank you Albert for helping me with the bags in the road to the plane! The bass guitar was extremely weighty… I guess in the future we'll meet again I don't know if as group leaders jaja or at the post-doc.

Ya para terminar, me gustaría dar un abrazo inmenso a mis padres que siempre me han ayudado en la vida y han sido un soporte muy importante tanto durante mi época universitaria como ahora en el doctorado. Lo siento mucho por no haber podido estar más por casa pero gracias al trabajo hecho he podido sacar adelante esta magnífica tesis. Muchas gracias por vuestro apoyo, ¡os quiero un montón!

TABLE OF CONTENTS

TABLE OF CONTENTS I

LIST OF ABBREVIATIONS VII

LIST OF FIGURES AND TABLES XIII

PROLOGUE XIX

INTRODUCTION 1

1. MALARIA 3

1.1. Malaria global burden 3

1.2. *Plasmodium* life cycle 4

1.3. Malaria pathophysiology and *Plasmodium* species 5

1.4. Treatment of malaria and limitations of current antimalarial drug therapies 7

1.5. Anopheles vector control 12

1.6. *Plasmodium* antigenic variation and malaria vaccine design 13

2. *PLASMODIUM FALCIPARUM* 19

2.1. *P. falciparum* intraerythrocytic cycle 19

2.2. *P. falciparum* biochemistry and research of specific drug targets 28

2.3. The host red blood cell 37

3. NANOTECHNOLOGY 43

3.1. A brief history of nanotechnology 43

3.2. Medical application of nanotechnology 44

3.3. Liposomal nanocarriers for drug delivery applications 50

3.4. Immunoliposomal targeted drug delivery 61

3.5. Nanotechnology applied to the treatment of malaria 66

OBJECTIVES 75

RESULTS 79

SUMMARY OF PUBLICATIONS 81

CHAPTER 1 83

Immunoliposome-mediated drug delivery to *Plasmodium*-infected and non-infected red blood cells as a dual therapeutic/prophylactic antimalarial strategy 83

Loading antimalarial drugs into noninfected red blood cells: an undesirable roommate for *Plasmodium* 111

CHAPTER 2 **115**

Development of drug-loaded immunoliposomes for the selective targeting and elimination of rosetting *Plasmodium falciparum*-infected RBCs 115

CHAPTER 3 **149**

Proposal of 2-picolylamine derivatization and LC-ESI-MS/MS analysis for the ultra-sensitive detection of abscisic acid in apicomplexan blood-infecting parasites and first validation test in *Plasmodium falciparum* extracts 149

SUMMARY OF RESULTS **171**

DISCUSSION **177**

1. JOINT DISCUSSION OF CHAPTERS 1 AND 2: RBC- AND PRBC-TARGETED LPS AS DRUG DELIVERY SYSTEMS FOR *P. FALCIPARUM* MALARIA THERAPEUTICS **179**

1.1. LPs, a practical and versatile nanocarrier 179

1.2. Potential drawbacks of iLP-based therapies 182

1.3. Passive encapsulation of antimalarials into LPs 184

1.4. Active encapsulation of weakly basic antimalarials into LPs through pH gradients 185

1.5. Depletion of liposomal-pH gradient systems and sustained release of drugs: CQ-/PQ-loaded, GPA-iLP model 186

1.6. Applicability of liposomal-pH gradient systems in malaria 192

1.7. Depletion of small pH gradients and collision-based transference of hydrophobic drugs: LMF-loaded, PfEMP1-iLP model 193

1.8. Active encapsulation of weakly acid antimalarials into LPs through pH gradients 198

1.9. Clinical application of the GPA- and PfEMP1-iLP models 199

1.10. Attainable improvements in iLP-based drug delivery systems against malaria 205

2. DISCUSSION OF CHAPTER 3: ANALYSIS OF ABA BIOSYNTHESIS IN *P. FALCIPARUM* **211**

2.1. Research for new parasite-specific metabolic pathways as novel drug targets 211

2.2. Improvement in ABA detection 211

2.3. Application of the optimized ABA detection method to late form-pRBC extracts 212

2.4. Proposal of a mechanism regulating *P. falciparum* egress 213

2.5. Parasite-encoded, amyloid-forming proteins as potential targets against *Plasmodium* IEC and cerebral malaria 214

CONCLUSIONS **217**

ANNEX I: THEORETICAL CALCULATIONS 221

1. Analysis of CQ and PQ encapsulation into LPs and determination of a more precise model defining the membrane/solution partitioning mechanism followed by diprotic weak bases 223

1.1. Solubility-diffusion theory 223

1.2. Transient pore model 223

1.3. Influence of pH over the release kinetics of proton-ionizable weakly basic compounds from LPs 223

1.4. Determination of the new partitioning model for proton-ionizable drugs 226

2. Theoretical calculation of LP numbers as a function of lipid molarity and the size of the nanoparticle 230

3. Alternative determination of LP numbers by nanoparticle tracking analysis (NTA) 230

ANNEX II: EXPLORATION OF AMPHIPHILIC DENDRITIC NANOPARTICLES AS ALTERNATIVE ANTIMALARIAL DRUG DELIVERY SYSTEM TO LP-BASED APPROACHES 233

RESULTS 235

SUMMARY OF RESULTS 277

DISCUSSION 277

1. Amphiphilic dendritic nanoparticles as antimalarial agents 277

2. Physicochemical properties of dendrimers and encapsulation of active molecules 278

3. Targetability and antimalarial activity of dendritic nanoparticles 279

4. *In vivo* antimalarial activity and clinical applicability of dendritic nanoparticles 281

ANNEX III: POSSIBLE ROLES OF AMYLOIDS IN MALARIA PATHOPHYSIOLOGY 283

ANNEX IV: PHD STUDENT PARTICIPATION IN PUBLICATIONS AND THEIR IMPACT FACTOR 293

BIBLIOGRAPHY 295

LIST OF ABBREVIATIONS

Ab	antibody
ABA	abscisic acid
Ac-CoA	Acetyl-Coenzyme A
ACT	artemisinin-based combination therapy
APs	acidic phospholipids
Aβ	amyloid beta peptide
BM1234-iLP	LP targeted with the BM1234 Ab against *P. falciparum* Maurer's clefts
C_{40}-CBP	C_{40}-carotenoid biosynthetic pathway
CDD	controlled drug delivery
CDPK	calcium-dependent protein kinase
CIDR	cysteine-rich interdomain region
CPPs	cell penetrating peptides
CPs	choline phospholipids
CQ	chloroquine
CRT	chloroquine resistance transporter
CSP	circumsporozoite protein
DBL	Duffy-binding like domain
DC	tandem domain cassette
DHA	dihydroartemisinin
DMAPP	dimethylallyl pyrophosphate
DOPC	1,2-dioleoyl-*sn*-glycero-3-phosphocholine
DOPC-based LPs	DOPC:cholesterol (80:20 mol%) LPs
DOXP	1-deoxy-D-xylulose 5-phosphate
DPPC	1,2-dipalmitoyl-*sn*-glycero-3-phosphocholine
DSPC	1,2-distearoyl-*sn*-glycero-3-phosphocholine
DSPC-based LPs	DSPC:cholesterol (90:10 mol%) LPs
DSPE-PEG2000	1,2-distearoyl-*sn*-glycero-3-phosphoethanolamine-N-[methoxy(polyethylene glycol)-2000]
DXR	DOXP reductoisomerase
DXS	DOXP synthase
EC	endothelial cell
EDV	electron-dense vesicle
EE	encapsulation efficiency
EPR	enhanced permeation and retention effect
EV	extracellular vesicle
F(ab')$_2$	double antigen-binding fragment (2 × Fab')
Fab'	single antigen-binding fragment
FLU	fluridone
FP	ferriprotoporphyrin IX
G6PD	glucose-6-phoshate dehydrogenase

LIST OF ABBREVIATIONS

GAG	glycosaminoglycan
GPA	glycophorin A
GPA-iLP	LP targeted against GPA
GPB	glycophorin B
GSH	glutathione
HRP	histidine-rich protein
HS-GAGs	highly sulfated glycosaminoglycans
IC50	concentration at which growth is inhibited by 50%
IEC	intraerythrocytic cycle
iLP	immunoliposome particle
IPP	isopentenyl pyrophosphate
IspD	MEP cytidylyltransferase
KAHRP	knob-associated histidine-rich protein
late form-pRBC	parasitized-red blood cell at the trophozoite or schizont stage
LMF	lumefantrine
Lo	liquid-ordered phase
Log *P*	log10 [octanol/water] partition coefficient
LP	liposome particle
LUV	large-unilamellar vesicle
Lα	liquid-crystal phase
Lβ'	gel phase
M17.1-iLP	LP targeted against the SD3 loop of the PfEMP1-FCR3S1.2 ^{IT4var60} variant
MAb	monoclonal antibody
MAHRP1	membrane-associated histidine-rich protein 1
MCs	Maurer's clefts
MEP	2-*C*-methyl-D-erythritol 4-phosphate
MLV	multilamellar vesicle
mRBC	mature red blood cell
MSP2	merozoite surface protein 2
$MSP2_{NSP}$	N-terminal signal peptide of the MSP2 protein
MVA	mevalonic acid
NCED	neoxanthin cleavage enzyme
NDGA	nordihydroguaiaretic acid
NPPs	new permeability pathways
NTS	N-terminal segment
p	permeability coefficient
p.i.	post-invasion
PA	phosphatidic acid
parasitemia	percentage of infected erythrocytes
PBS	phosphate buffered saline

PC	phosphatidylcholine
PCR	polymerase chain reaction
PDPH	3-[2-Pyridyldithio]propionyl hydrazide
PDS	phytoene desaturase
PE	phosphatidylethanolamine
PEG	poly(ethylene glycol)
PEGylated	PEG-conjugated
PfEMP1	*P. falciparum* erythrocyte membrane protein-1
PfEMP1-iLP	LP targeted against PfEMP1
PfSBP1	*P. falciparum* skeleton binding protein 1
PKG	cGMP-dependent protein kinase
PLC/IP$_3$	phospholipase C/inositol 1,4,5-triphosphate system
PPM	parasite plasma membrane
PPP	pentose phosphate pathway
PQ	primaquine
pRBC	parasitized-RBC (by *Plasmodium falciparum* if otherwise indicated)
pRBCM	parasitized-RBC plasma membrane
PS	phosphatidylserine
PV	parasitophorous vacuole
PVM	parasitophorous vacuole membrane
Pβ'	ripple phase
R29-iLP	LP targeted against the R29^{IT4var9} variant of PfEMP1
RBC	red blood cell, mRBC if otherwise specified
RBCM	red blood cell plasma membrane
RDT	rapid diagnostic test
RES	reticuloendothelial system
ROS	reactive oxygen species
SATA	N-Succinimidyl S-Acetylthioacetate
SD	subdomain
SP	sulfadoxine-pyrimethamine drug combination
sp./spp.	species singular/plural
SUV	small-unilamellar vesicle
T	temperature
$t_{1/2}$	time it takes for a molecule to halve its concentration
TCA	tricarboxylic acid
T_m	melting temperature/main lipid phase transition temperature
T_p	lipid phase pre-transition temperature
TVN	tubulovesicular network
VLS	small uncoated vesicle-like structure
WHO	World Health Organization

LIST OF FIGURES AND TABLES

INTRODUCTION

Figure 1. Countries with ongoing malaria transmission in 2013. 3

Figure 2. *Plasmodium* life cycle. 5

Figure 3. Structures of the naturally-occurring antimalarial drugs quinine and artemisinin. 8

Table 1. Pharmacokinetic profiles of orally administered antimalarial drugs. 12

Figure 4. Description of *var* genes and PfEMP1 variants for the *P. falciparum* 3D7 reference clone. 15

Figure 5. *P. falciparum* IEC. 19

Figure 6. Relative transport rates of low-molecular weight solutes throughout the *P. falciparum*-induced NPPs. 21

Figure 7. Illustration of the pRBC ultrastructure obtained through electron microscope tomography and 3D reconstruction. 23

Figure 8. EDV-mediated trafficking of proteins forming the virulent cytoadherence complex at the pRBCM. 24

Figure 9. Theorized molecular transport routes in the pRBC and macromolecular uptake of 10 kDa dextrans. 25

Figure 10. *P. falciparum* essential metabolic pathways during the asexual IEC. 28

Figure 11. *P. falciparum* isoprenoid biosynthetic pathways. 30

Figure 12. Hypothesized PKG-induced egress of *P. falciparum* merozoites from infected erythrocytes. 33

Figure 13. *P. falciparum*-mediated hemoglobin uptake and digestion. 34

Figure 14. Architecture and phospholipid composition of the mRBC plasma membrane. 38

Figure 15. Alterations in the phospholipid distribution of the RBCM after *P. falciparum* infection. 40

Figure 16. Nanomaterials size in comparison with other particles and structures on the length scale. 43

Figure 17. Organ distribution analysis of PEGylated, lung-specific immunoliposomal nanoparticles (90-130 nm). 46

Figure 18. Ringsdorf's proposal of a targeted polymer-drug conjugate for the first time in history. 48

Figure 19. Basic nanomaterials currently available for the design of drug delivery approaches. 49

Figure 20. Illustration of all possible phospholipid acyl chain organization states. 51

Table 2. Differences in the time required for the release of one-half or nine-tenths of LP-encapsulated solutes in accordance with their permeability coefficient values. 54

Figure 21. Classification of drugs and their theorized incorporation into the LP according to their physicochemical properties. 56

Figure 22. Calculated ionization species as a function of solution pH for a weakly basic drug model containing proton-ionizable groups. 58

Figure 23. Lipophilic drug-membrane association examples. 60

Figure 24. Antibody conjugation strategies based on the generation of sulfhydryl groups and their subsequent reaction with maleimide-containing reagents. 63

Figure 25. iLP-target cell possible interaction mechanisms and the major types of lipidic structures. 64

Figure 26. Examples of *P. falciparum* and *P. yoelii* IEC-targeted chemotherapeutic approaches developed so far. 72

Figure 27. Analysis of antimalarial drugs timing of action over *P. falciparum in vitro* growth. 74

DISCUSSION

Figure 28. Size distribution analysis of the LPs developed in Chapter 1. 181

Figure 29. LP clearance kinetics from circulation in rats. 181

Table 3. Calculation of the cost of a complete treatment course for a single *P. falciparum*-infected humanized mouse model using CQ delivered through the BM1234- and GPA-iLPs. 183

Table 4. Relative abundances of drug ionization species as a function of solution pH. 185

Figure 30. Illustration of the theorized events taking place during depletion of liposomal-pH gradient systems and the subsequent release of encapsulated weakly basic drugs. 188

Figure 31. Molecular structures of the main antimalarial drug families and their classification according to their suitability for our liposomal-pH gradient system. 191

Figure 32. Exposure of GPA and PfEMP1 antigens at the pRBC surface and illustration of the principal epitopes recognized by Abs generated against rosette-forming PfEMP1 variants. 194

Figure 33. PfEMP1-iLPs retention into *P. falciparum* cultures. 195

Figure 34. Analysis of glycophorin A protein sequence similarity among animal orthologs. 203

Figure 35. CSP-conjugated LPs distribution in mouse organs and hepatocyte subcellular targeting. 207

ANNEX I

Table 5. Experimental encapsulation efficiencies for CQ and PQ drugs into LPs (DOPC:cholesterol, 80:20 mol%). 224

Table 6. Exemplification of the LP/solution theorized partitioning for CQ diprotic weak base according to the distribution coefficient *D* model. 225

Figure 36. Determination of CQ and PQ encapsulated amounts at non-membrane-saturating concentrations into LPs (DOPC:cholesterol, 80:20 mol%). 226

Figure 37. New partitioning model illustrating the main interaction events taking place between a diprotic weak base and a PC:cholesterol-based LP membrane. 227

Table 7. Exemplification of the LP/solution novel partitioning model for CQ diprotic weak base if passively encapsulated at physiological pH or actively encapsulated through a pH 4.0-7.4 gradient. 228

Figure 38. Determination of *D* and *D** distribution coefficients for CQ and PQ drugs as a function of solution pH. 229

PROLOGUE

This PhD thesis was initiated in October 2010 at the Institute for Bioengineering of Catalonia (IBEC) being part of a global research line headed by Dr. Xavier Fernàndez Busquets and focused on the obtainment of novel and effective targeted drug delivery systems based on liposomal and polymeric nanocarriers and employing antibodies as well as glycosaminoglycans as targeting agents against *P. falciparum*-infected erythrocytes for their vectorization. The experiments performed throughout this PhD thesis have been principally funded by grants BIO2011-25039, project entitled “Exploration of new efficient targeting molecules for nanovector-mediated antimalarial drug delivery”, and BIO2014-52872-R, project named “Engineering of nanovectors for antimalarial drug delivery to *Plasmodium* transmission stages”, both provided by the Ministerio de Economía y Competitividad, Spain.

In the light of the absence of an effective preventive vaccine against malaria and the nearly half a million deaths this disease causes every year, malaria chemotherapy along with its ultimate eradication demand for novel drug delivery approaches (i) more efficacious, (ii) completely biocompatible and innocuous to humans, as well as (iii) exhibiting a reduced likelihood of generating drug-resistant parasites. Such concerns have been addressed in this PhD thesis by means of (1) the development of RBC- and pRBC-targeted immunoliposomal nanocarriers loaded with antimalarial drugs and displaying multiple mechanisms of action, and (2) the research of new and vital *Plasmodium*-specific metabolic pathways.

"It is not the strongest of the species that survives, nor the most intelligent that survives. It is the one that is most adaptable to change"

Charles Darwin

INTRODUCTION

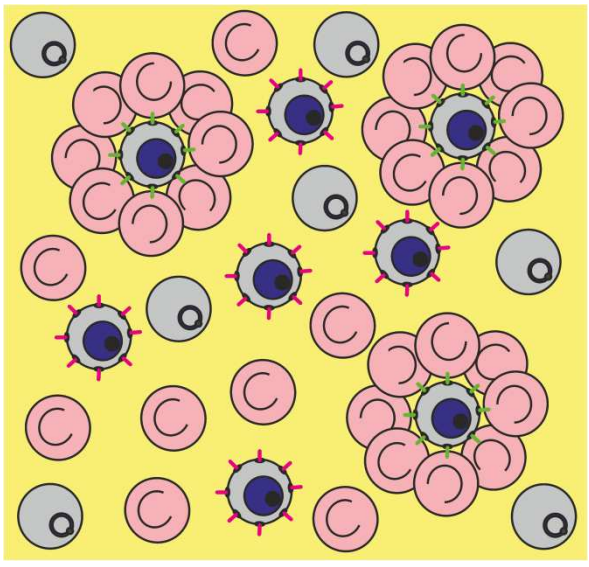

1. MALARIA

1.1. Malaria global burden

Malaria is a vector-borne infectious disease affecting humans and caused by protist parasites of the genus *Plasmodium* that remains nowadays as one of the major life-threatening concerns throughout the world. Interestingly, malaria-related features such as its characteristic periodic fevers and its close association with marshes and sources of settled water have been reported across all civilized societies since ancient China in 2700 BC (Cox 2002). Fevers first characterization was actually done by Hippocrates in 400 BC. Nevertheless, the parasite causing malaria would not be identified in human blood until 1880 by Dr. Alphonse Laveran (Laveran 1880).

Since the discovery of the human malaria causative agent, an enormous effort has been invested by several countries and health organizations in improving the knowledge and treatment of the disease. Malaria mortality rate has been eventually reduced in more than 40% over the last decade (Murray et al. 2012). However, in spite of this optimistic trend, malaria is still the most important parasitic disease at present due to its huge number of cases and deaths. In accordance with the last malaria epidemiological report from the World Health Organization (WHO) (World Health Organization 2014), 198 million cases occurred only in 2013 leading to 584,000 deaths and 3.2 billion people were at risk of contracting the disease (45% of the total world population).

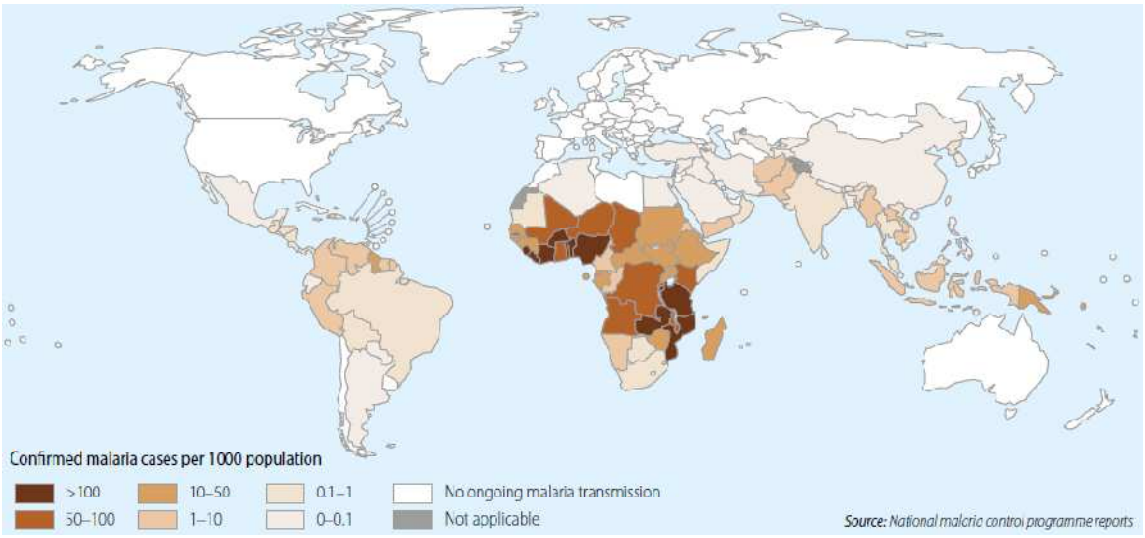

Figure 1. *Countries with ongoing malaria transmission in 2013*. Figure reproduced from (World Health Organization 2014).

Geographically, malaria incidence is distributed worldwide but irregular. Though it is mostly widespread across tropical and subtropical regions, tracing the distribution of the transmission vector, *Plasmodium* infection reported cases do concentrate within the sub-Saharan Africa region (Fig. 1) accounting for 90% of all malaria deaths. Importantly, 78% of all deaths occur before the

age of 5, being young children the most affected age group. The WHO in the African region does also concentrate at present 72% of the global funding for malaria control and elimination (US$ 2.7 billion in 2013). Remarkably, malaria is estimated to cost a total of US$ 12 billion annually considering the whole African continent (Tuteja 2007) and, consequently, represents such a daunting challenge for those least developed countries.

Remainder cases of malaria do concentrate within South and Central America, Oceania, Southeast Asia, India and Middle East. Finally, sporadic infections are also commonly reported in malaria-free countries affecting those travelers that return from areas in which malaria is endemic. In this regard, around 30,000 inhabitants from developed countries are estimated to be affected every year (Montero 2013).

1.2. Plasmodium life cycle

The discovery of the *Plasmodium* pathogen in humans in 1880 was followed by its identification within a mosquito of the genus *Anopheles* by Dr. Ronald Ross in 1897 (Ross 1897), defining this insect as transmission vector for malaria. The overall knowledge of the parasite life cycle would be provided for the first time in history only a few years later by the Italian malariologists Giovanni Battista Grassi, Amico Bignami, and Giuseppe Bastianelli (Grassi 1901). Parasite replication inside the liver during the first days of infection would be finally identified in 1947 by Henry Shortt and Cyril Garnham (Shortt 1948) giving the complete definition of *Plasmodium* life cycle. This encompasses two different stages in development and type of replication as a common feature shared by most of apicomplexan obligate endoparasites: (i) an asexual replication stage taking place in the animal host and (ii) a completely different sexual replication step occurring inside the mosquito vector (Fig. 2).

Plasmodium asexual cycle begins in humans when an *Anopheles* mosquito female inoculates the parasite in its infectious sporozoite form. Importantly, only ~20 parasites are usually injected during a mosquito blood meal (Barry & Arnott 2014). Sporozoites then migrate to the liver infecting hepatocytes (pre-erythrocytic stage), undergoing several rounds of replication and ultimately spilling thousands of merozoites into the bloodstream after one week of infection (variable incubation period determined by the *Plasmodium* species). Red blood cells (RBCs) will subsequently become infected starting the well-known intraerythrocytic cycle (IEC), asexual replication stage completed in 24 to 72 h depending on the *Plasmodium* species and finally leading to the reinfection of new erythrocytes by the second generation of merozoites. In comparison with the few sporozoites initially injected by the mosquito, more than 10 billion parasitized RBCs (pRBCs) can be found in a single human infection (Borrmann & Matuschewski 2011). Some of these blood stage parasites will eventually differentiate into gametocyte sexual forms (around 10 million parasites per host), which remain in circulation without invading new cells until being taken by a new mosquito blood meal.

Plasmodium sexual replication stage takes place inside the mosquito midgut (Fig. 2) in which male flagellated gametes fertilize the female counterpart forming a zygote that develops into an ookinete. This parasitic form crosses the wall of the gut where it encysts and maturates into an oocyst that eventually bursts releasing hundreds of sporozoites. Few of these nascent sporozoites will finally migrate towards the salivary glands of the insect ready for a new human host infection. Remarkably, similar mosquito vector-animal host *Plasmodium* life cycles to human-infecting species (spp.) have been further indentified in nature primarily affecting monkeys, higher primates, lizards, reptiles and birds.

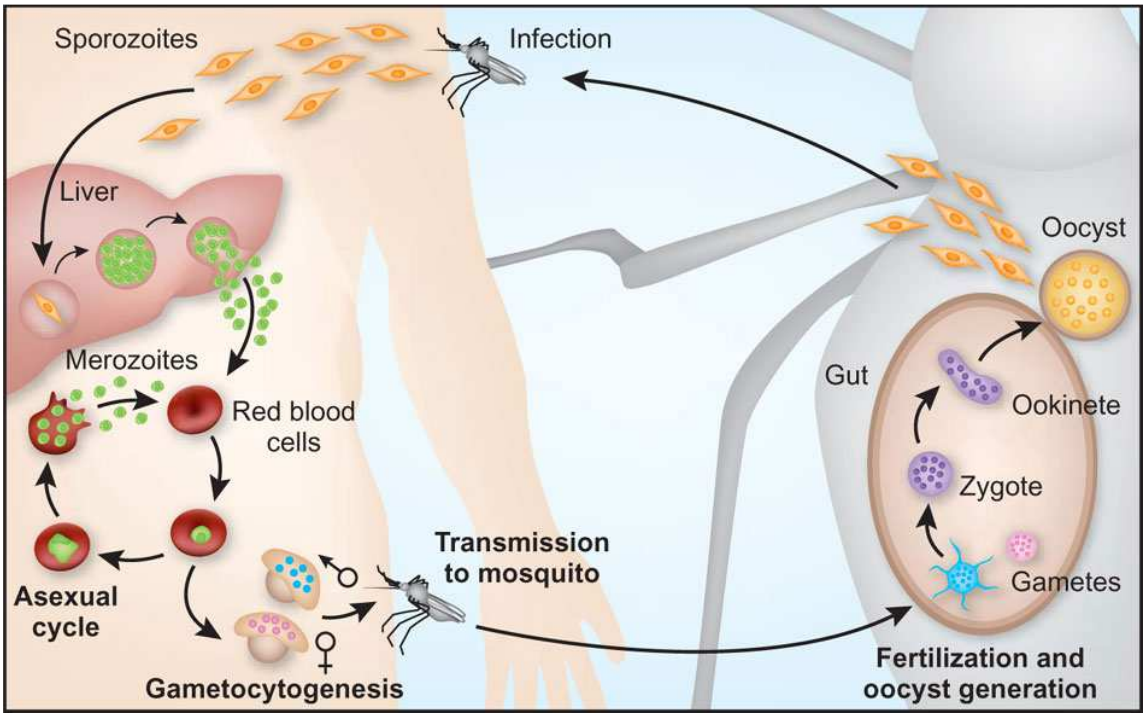

Figure 2. *Plasmodium life cycle*. Figure reproduced from (Pasvol 2010).

1.3. Malaria pathophysiology and Plasmodium species

Malaria parasites induce several pathogenic mechanisms. The most common among *Plasmodium* spp. are those associated with the invasion of RBCs such as anemia, particularly severe during infections with high parasitemia levels, changes in the pRBC discoid shape and alterations of the erythrocyte surface by insertion of parasite-derived proteins. These structural modifications of the RBC upon infection promote in turn an increased rigidity of its plasma membrane and the subsequent removal of parasites by splenic clearance, mechanism characterized by (i) a pRBC-filtering process that leaves the host RBC almost intact when crossing the interendothelial slits of sinus walls (Chotivanich et al. 2002) as well as (ii) the simultaneous phagocytosis of pRBCs and released parasites by spleen-resident macrophages (Tosta et al. 1984). Importantly, the parasite clearance rate in this organ is enhanced during antimalarial drug treatment courses (Chotivanich et al. 2002) and such splenic activity can

eventually result in splenomegaly in those individuals suffering from repeated malaria infections (Buffet et al. 2011).

The release of merozoites and parasite metabolism subproducts throughout the IEC, which is performed in a cyclic and synchronous fashion, produces the malaria associated periodicity in symptoms appearing every 2 (tertian fever) or 3 days (quartan fever, occurring only during *Plasmodium malariae* infection) as paroxysmal attacks. These include fever, shivering, headache, cough, joint pain, vomiting, convulsions, diarrhea and respiratory distress among other signs (Miller et al. 2002; Tuteja 2007). Other pathogenic processes may include lactic acidosis and hypoglycemia as a result of parasites anaerobic metabolism of glucose.

Moreover, severe complications in malaria strongly depend on the type of *Plasmodium* sp. To date, five species have been reported to cause malaria in humans: *Plasmodium falciparum*, *Plasmodium vivax*, *Plasmodium malariae*, *Plasmodium ovale* and *Plasmodium knowlesi*. *P. knowlesi* would be the last species to be incorporated in the list, being identified in humans for the first time in history in 1965 (Chin et al. 1965). Differences between *Plasmodium* spp. comprise mainly (i) the incubation time that encompasses between the mosquito bite and the establishment of the IEC, (ii) the degree of RBCs maturation required for invasion and (iii) the severity of the infection.

Pre-erythrocytic incubation time (period of time between the mosquito bite and Plasmodium IEC): Whereas *P. falciparum* begins erythrocytes infection within 2 weeks after sporozoites inoculation in non immune individuals, longer incubation periods of 35 days or 2-24 months are required for *P. malariae* or *P. vivax* and *P. ovale*, respectively.

RBC maturation stage: *P. vivax* and *P. ovale* infections are restricted to only immature cells (reticulocytes) as an hypothesized self-regulating process (Kerlin & Gatton 2013) that lowers the maximum percentage of infected erythrocytes (parasitemia) in less than 3% (Walker et al. 1990). These *Plasmodium* spp. do also present dormant stages, termed hypnozoites, that can remain undetectable in the liver before the beginning of a new replication round and the resultant relapse of malaria infection even a few years later. By contrast, *P. malariae* preferentially invades aged RBCs leading to low parasitemia levels able to sustain over several years in a mechanism similar to *P. vivax and P. ovale*. Infective RBC tropism for *P. knowlesi* still remains to be identified (Kerlin & Gatton 2013).

In this scenario, *P. falciparum* appears as the predominant, human-infecting species capable of invading erythrocytes regardless of the cell degree of maturation and, importantly, this lack of RBC tropism allows this species to reach extremely high parasitemias of more than 50%. *P. falciparum* presents an additional characteristic and severe pathogenic feature: exported parasite proteins cluster together beneath the plasma membrane of the pRBC in the form of knob-like excrescences that sustain transmembrane proteins with adhesive properties towards host cell receptors. Such sticky structures enabling *P. falciparum*-infected RBCs to avoid the

aforementioned splenic clearance mechanism by means of (i) remaining attached to the endothelium of blood vessels or (ii) forming cell aggregates with either uninfected RBCs (rosetting) or other pRBCs (platelet-induced clumping). All these cytoadhesive events result in turn in an obstruction of blood circulation and can eventually lead to severe malaria outcomes such as cerebral or placental malaria depending on the targeted organ. The binding of pRBCs to placental receptors during pregnancy is further associated with anemia in the mother and a major cause of low birthweight, impaired development and increased mortality in the newborn (De Beaudrap et al. 2013).

Importantly, the above-mentioned complications can be fatal if not treated rapidly and particularly severe in individuals with weakened immunity, making *P. falciparum* the deadliest species causing malaria in humans. Indeed, *P. falciparum* accounts for most of malaria deaths worldwide and still remains at present highly endemic in several sub-Saharan Africa countries (Gething et al. 2011). *P. vivax* infection, though much less virulent than *P. falciparum*, represents nearly the 40% of the malaria global burden (Wells et al. 2009) and is mainly distributed throughout Asia as well as Central and South America. Remaining *Plasmodium* spp. are only responsible for a small percentage of all malaria cases.

In addition to the already mentioned cell-binding properties of *P. falciparum*, specific sequestration of pRBCs into the barrier cells of the spleen after parasite-mediated organ restructuration has been described during *P. vivax* infection as a protective mechanism against host immunity (Del Portillo et al. 2004; Bernabeu et al. 2012; Fernández-Becerra, Yamamoto, et al. 2009). The spleen additionally provides an important source of reticulocytes for *P. vivax* replication. Cytoadhesive events of *P. vivax*-infected reticulocytes to human endothelial cells have been further identified in clinical isolates and claimed to be responsible for the newly appearing severe *P. vivax*-malaria cases (Carvalho et al. 2010).

1.4. Treatment of malaria and limitations of current antimalarial drug therapies

1.4.1. Malaria diagnosis

Malaria outcome will strongly depend on the type of *Plasmodium* sp. and the infection status at the time that the disease is diagnosed. *P. falciparum* untreated infections can easily progress to more severe symptoms with mortality rates of almost 100% and even higher than 15% under best chemotherapies (Montero 2013). Severe complications for *P. vivax* and *P. knowlesi* have also been reported but in a much lower extent (Bartoloni & Zammarchi 2012).

Moreover, malaria is asymptomatic within the first weeks of infection and shares similar clinical manifestations to other common diseases such as influenza, dengue, gastroenteritis or typhoid fever; usually leading to wrong diagnoses and, as a consequence, requiring the application of malaria-specific diagnostic tests. Those available at present comprise: (i) blood films, (ii) antigen

detection tests (also known as 'Rapid Diagnostic Tests', RDT) for the histidine-rich protein 2 (HRP2) and *Plasmodium* lactate dehydrogenase (pLDH) parasite proteins, (iii) *Plasmodium* DNA amplification by polymerase chain reaction (PCR) or (iv) the quantitative buffy-coat method (QBC). However, their use is restricted in less developed countries in which the access to public health centers is limited as well. In consequence, only the 62% of all patients with malaria-like symptoms living in the WHO African Region received a diagnostic test in 2013 (World Health Organization 2014).

1.4.2. Malaria chemotherapy

Bearing in mind that no preventive vaccine against *Plasmodium* infection is currently available, malaria treatment and control most importantly rely on the activity of drugs against the asexual blood stages, which are in turn responsible for malaria clinical manifestations. Antimalarial drugs can be classified into families or groups on the basis of similarities in their chemical structure and/or their mode of action. The aminoquinolines (including the 4- and 8-aminoquinolines) and artemisinin drug families (Fig. 3), which are obtained by derivatization of the naturally-occurring molecules quinine (from the *Cinchona calisaya* tree bark) and artemisinin (from the leaves of the sweet wormwood *Artemisia annua* (Miller & Su 2011)), have been probably the most commonly employed antimalarials. A third well-known family includes the inhibitors of folate biosynthesis.

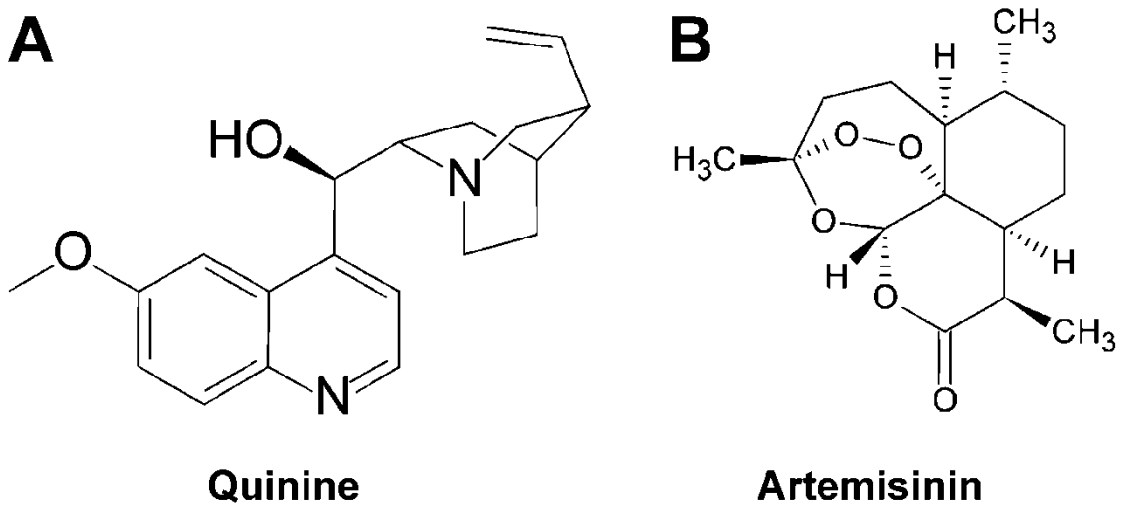

Figure 3. *Structures of the naturally-occurring antimalarial drugs (A) quinine and (B) artemisinin*.

Although the use of artemisinin dates back to ancient China by 168 BC, the first antimalarial to be used in the Western world would be Quinine in the 17th century. Chloroquine (CQ), member of the 4-aminoquinolines drug family discovered in 1934 by Hans Andersag (Bayer laboratories) will be later the drug of choice until 1990s. However, the quick emergence and nowadays widespread resistance of *P. falciparum* to CQ (particularly significant in malaria endemic areas) has restricted its use, and the application of other compounds of the 4-aminoquinolines family as well, to combination therapies with drugs of the artemisinin family (named 'Artemisinin-based

Combination Therapies', ACTs). These latter compounds are currently still highly active against *P. falciparum*.

Moreover, CQ administration remains as first-line treatment for *P. falciparum* and *P. vivax* in those regions where it is still effective (e.g. Central America and the Caribbean (World Health Organization 2014)). Sulfadoxine-pyrimethamine drug combination (SP) from the folate inhibitors family have promoted the generation of resistant *Plasmodium* strains even faster than CQ and its application has been limited to those areas where other antimalarials are no longer useful.

Considering the above-mentioned fast appearance of drug-resistant strains and following WHO recommendations, fixed-dose ACTs constitute the main therapeutic tool against malaria at present and have been approved as first-line treatment in more than 90% of *P. falciparum* endemic countries. Furthermore, orally administered artemether-lumefantrine ACT has been described as gold standard for treating uncomplicated malaria (World Health Organization 2014).

Special antimalarial drug therapies adapted to specific target profiles

The 8-aminoquinoline compound primaquine (PQ) is commonly used as drug supplement for the treatment of *P. vivax* and *P. ovale* malaria on the basis of its activity against the hypnozoite and gametocyte parasitic forms. Preventing in this way infection relapses and/or avoiding transmission of the parasite when following malaria eradication strategies. However, 14-day course therapies are required when fighting dormant stages, which demands for a high degree of compliance sometimes unreachable (Galappaththy et al. 2013).

Other special drug combinations comprise the parenteral administration of quinine or artesunate for the treatment of severe malaria (Dondorp et al. 2010), the use of SP for malaria chemoprevention in pregnant women (World Health Organization 2014) or the application of atovaquone-proguanil drug combination for disease prevention and alternative treatment to ACTs for uncomplicated malaria (Thybo et al. 2004).

1.4.3. Current limitations of antimalarial drug therapies: drug resistance

One of the major limitations in the use of antimalarial drugs, as explained above, is the fast and spontaneous emergence of drug resistance for which *Plasmodium* has demonstrated to be remarkably effective throughout history. In this regard, mutations in the parasite genome by means of (i) spontaneous single nucleotide variants due to DNA polymerase errors and (ii) gene copy amplification through telomeres recombination events (Hastings et al. 2009), both mechanisms triggered during *Plasmodium* asexual replication and particularly selected under drug pressure, are likely the main responsible factors following the Darwinian trend of natural selection.

Examples of mutations in parasite genes that generate drug resistance

Mutations in the genes encoding for the malaria parasite proteins cytochrome *b* and the ABC transporter multidrug resistant protein 1 have been demonstrated to occur *in vitro* after one year exposure of *P. falciparum* to atovaquone, eventually generating drug-resistant clones (Bopp et al. 2013). Alterations in the parasitic cytochrome bc_1 complex leading to atovaquone resistance have also been identified in *Plasmodium in vivo* isolates (Korsinczky et al. 2000; Siregar et al. 2008; Happi et al. 2006). Other important mutations accounting for drug resistance include (i) those in the chloroquine resistance transporter (CRT) protein (Summers et al. 2014; Fernández-Becerra, Pinazo, et al. 2009; Happi et al. 2006 (1)), which increase the CQ efflux from its site of action though displaying a limitation in the transport capacity (Summers et al. 2014), and (ii) alterations in the dihydrofolate reductase/dihydropteroate synthase protein pair as target molecules for SP anti-folate drugs (Sridaran et al. 2010). The utilization of drug combinations affecting different parasite cellular functions is in consequence a crucial requisite when designing antimalarial chemotherapeutic strategies in order to decrease the rate at which resistant strains emerge.

Parasite fitness cost of mutations

However, the aforementioned mutations taking place in *Plasmodium* genes and required to elude drugs action demand an important fitness cost since those cellular functions affected are in many cases vital for the parasite. As a result, drug-resistant yet metabolically impaired parasites would only outcompete those drug-sensitive yet fully active ones in hosts carrying intermediate/residual drug concentrations (Hastings et al. 2002; Peters et al. 2002). Highly effective drugs delivered in amounts (i) large enough to kill even drug-resistant parasites while at the same time (ii) being quickly removed from the organism would be therefore preferable. Artemisinin derivatives match pretty well with this condition. These compounds are rapidly absorbed into the body displaying peak plasma levels at 0.5 to 3 h post oral administration and are quickly eliminated with reported plasma half-lives of less than 2.5 h (Table 1). In comparison, the elimination rate of almost all other antimalarial drugs is significantly prolonged to 24 h (PQ, proguanil, quinine), a few days (SP, lumefantrine, atovaquone) or even more than a week (CQ and SP in some cases) (World Health Organization 2015a).

Drug resistance generation rate would furthermore decrease if following short treatment courses and designing properly controlled mass administration programs, considerably reducing in this manner the likelihood of undergoing impaired treatments. Unfortunately, there is no antimalarial drug at present capable of completely eliminating *Plasmodium* infection in a single dose. At least 3 days of continuous treatment and the administration of several doses (e.g. 6 doses for artemether-lumefantrine ACT) are commonly required for most of drugs (World Health Organization 2015a). Other important factors not directly related to parasite evolution under drug pressure must be considered when handling drug resistance. These take into account the mosquito vector as well as the human host and include, among other factors: (i) malaria

transmission rates and treatment policies, (ii) host body condition and immunity, and (iii) human migration routes.

1.4.4. Current limitations of antimalarial drug therapies: toxicity

Antimalarial drugs are in general well tolerated with the artemisinin derivatives, lumefantrine and atovaquone displaying the least number of adverse effects (World Health Organization 2015a). Nevertheless, numerous side effects may occur. The most frequent complications include: (i) Gastrointestinal disturbances such as abdominal pain, nausea, vomiting and diarrhea. (ii) Blood disorders comprising anemia and other types of cytopenia. (iii) Dizziness and headache. More severe side effects are commonly associated with hypersensitivity reactions. These have been described to occur more frequently during sulfadoxine and quinine treatment courses and with a less extent when administering artemisinin. Furthermore, the ingestion of drugs in amounts larger than those recommended can be particularly severe for CQ, pyrimethamine, proguanil and quinine antimalarials, which might cause death in some cases through serious blood disorders and cardiac complications.

The generation of hemolytic anemia is an additional well-known complication caused by PQ administration to patients deficient for glucose-6-phosphate dehydrogenase (G6PD). This enzyme takes part in the pentose phosphate pathway preserving the glutathione reduced pool inside the erythrocyte and, consequently, protecting it from oxidative stress. In this regard, the RBCs of G6PD deficient patients will be more prone to suffer from oxidative damage, which can be in turn triggered by drugs that generate free oxygen radicals such as PQ (Bolchoz et al. 2002; Augusto et al. 1986; Hong et al. 1992). Remarkably, this oxidizing process can finally result in anemia through the phagocytosis and spleen removal of those damaged erythrocytes.

1.4.5. Current limitations of antimalarial drug therapies: pharmacokinetics

Maybe it is in the pharmacokinetic profile of antimalarial drugs in which the greatest number of limitations can be found (Table 1). All compounds are absorbed quickly and almost completely a few hours after oral administration and become extensively distributed into body tissues and fluids (World Health Organization 2015a). In this regard, quinine, CQ and SP are by far the most widespread drugs capable of reaching the placenta, breast milk and even the cerebrospinal fluid. Moreover, nearly all drugs are metabolized in the body into diverse products with modified properties as well as antimalarial activities and circulate in the bloodstream mainly associated with plasma proteins (>60%).

In light of the above-mentioned limitations of antimalarials, only a minor fraction of the total amount of drug administered will remain available and functional in circulation and thereby capable of reaching the pRBC. Large drug payloads and several continued doses are

consequently required in order to reach an efficient antimalarial effect, being this issue directly related to drug resistance generation, host toxicity and an increased treatment cost.

Drug	Absorption	Distribution	Metabolization	% bound plasma	Half-life
CQ	Complete	Whole body tissues*	Yes (monodesethyl-CQ)	60%	7-12 days
Sulfadoxine	Complete	Whole body tissues*	No	90-95%	4-11 days
Pyrimethamine	Complete	Kidneys, lungs, liver and spleen**	Yes	80-90%	2-19 days
Artemisinin	Complete	n.d.	Yes (DHA)	n.d.	1-2.5 h
Artemether	Complete	n.d.	Yes (DHA)	95%	1-2.5 h
Artesunate	Complete	n.d.	Yes (DHA)	n.d.	1-2.5 h
DHA	Complete	n.d.	No	55%	1-2.5 h
LMF	Variable***	n.d.	Yes (desbutyl-LMF)	n.d.	6 days
PQ	Complete	Whole body tissues	Yes (carboxyprimaquine)	n.d.	16-17 h
Atovaquone	Variable***	n.d.	n.d.	99%	1-6 days
Proguanil	Complete	n.d.	Yes (cycloguanil)	75%	16-23 h
Quinine	Complete	Whole body tissues**	Yes (3-hydroxyquinine)	70-90%	3-26 h

Table 1. *Pharmacokinetic profiles of orally administered antimalarial drugs*. Parameters analyzed comprise: the degree of drug absorption from the gastrointestinal tract; drug distribution into organs and tissues; drug metabolization in the body and the resulting main metabolite; % of drug bound to plasma proteins; half-life of the drug major metabolization product in plasma. *drug distribution to placenta and breast milk, **drug distribution to placenta, breast milk and cerebrospinal fluid, ***combined administration with fatty acids considerable increases drug absorption. Chloroquine (CQ), dihydroartemisinin (DHA), primaquine (PQ) and lumefantrine (LMF) drugs. No data available (n.d.). Parameters information for all drugs has been retrieved from (World Health Organization 2010; World Health Organization 2015a).

1.5. Anopheles vector control

Another essential approach to avoid malaria transmission and reach the final goal of malaria eradication consists in taking care of the *Anopheles* mosquito vector. At least 400 *Anopheles* spp. have been identified throughout the world among which 60 are malaria vectors. The most relevant *P. falciparum*-carrying species in sub-Saharan Africa are *Anopheles gambiae s.s., Anopheles arabiensis* and *Anopheles funestus.*

Insecticide-treated nets (ITNs) and the newer long-lasting insecticidal nets (LLINs), both incorporating insecticides such as permethrin and deltamethrin, are one of the best malaria preventive measures in terms of cost-effectiveness protecting people at risk of being infected while simultaneously killing the vector. Furthermore, their use has considerable increased over the last decade being ITNs and LLINs nowadays distributed free of charge in most of countries with ongoing malaria transmission (World Health Organization 2014). Nevertheless, in 2013 only

approximately 44% people at risk were sleeping under an ITN and no more than 29% of houses had sufficient ITNs for all household members. Additional preventive strategies include indoor residual spraying (IRS), individual insect repellents and larval source management. The latter approach being principally based on the treatment of mosquito water habitats for the elimination of their larval developing stages (Tusting et al. 2013).

Importantly, the efficacy of all the aforementioned anti-mosquito measures has been clearly demonstrated in the field with an extraordinary indoor density reduction of >90% in female *P. falciparum*-carrying *Anopheles* spp. from 1997 to 2010. Unfortunately, such unprecedented result has been accompanied by an exchange of the mosquito vectors feeding indoors (e.g. endophilic *An. gambiae s.s.*) to those feeding outdoors (e.g. exophilic *An. arabiensis* and *An. funestus*), which are less dangerous but less sensitive to the ITNs and IRS indoor mosquito repellent methods (Futami et al. 2014; Lwetoijera et al. 2014).

1.6. Plasmodium antigenic variation and malaria vaccine design

1.6.1. *Plasmodium* antigenic variation

The design of a vaccine capable of simultaneously preventing malaria infection and transmission has been a topic of extensive research over several years. However, mainly because of the high antigenic variation associated with *Plasmodium* spp., no effective vaccine has been introduced into clinical practice to date. The surface exposition of polymorphic and multi-variant parasite-derived proteins throughout both liver and intraerythrocytic stages is probably the main responsible factor leading to such low antigen conservation and thereby allowing all *Plasmodium* stages in the human body (sporozoites, merozoites and pRBCs comprising even gametes) to easily elude host immunity by means of:

1. Parasite populations displaying multiple polymorphisms and protein variants at a time (Barry & Arnott 2014).
2. Alternating single-cell protein variant expression over time through transcriptional switching between genes of the same family (Paget-McNicol et al. 2002; Frank et al. 2007).
3. Complex post-transcriptional regulations such as those involved in switching the merozoite invasion pathway in accordance with the erythrocyte receptors available (Kuss et al. 2012; Stubbs et al. 2005).

Genes encoding multi-variant proteins are present in the parasite genome in multiple copies, each one leading to a unique protein variant composed of a specific arrangement of basic domains. In *P. falciparum*, the latter are finally classified into tandem domain cassettes (DC) that define pRBC adhesion tropism towards specific host cell receptors (Turner et al. 2013). Besides, 149, 59 and 28 gene copies for the *rif*, *var* and *stevor* families (encoding the RIFIN, PfEMP1 and STEVOR variant proteins), among others, have been identified in the *P. falciparum* 3D7 clone

genome (Gardner et al. 2002). Similar multigene families occur in other less-cytoadhesive *Plasmodium* spp. (e.g. VIR proteins in *P. vivax*) but their function is still unclear in most of cases (Singh et al. 2014; Fernández-Becerra, Yamamoto, et al. 2009; Tachibana et al. 2012).

Additional mechanisms increasing even more the *Plasmodium* antigen repertoire during the IEC as well as in other infection stages include meiotic and mitotic recombination events (Kyes et al. 2007; Bopp et al. 2013) and a high mutation rate (both already described in 1.4.3.).

Furthermore, an important factor rarely considered and significantly delaying the identification of efficacious vaccine candidates has been the design of vaccine antigens based on a few *Plasmodium* isolates (e.g. 3D7 and FVO for *P. falciparum* and Sal-1 for *P. vivax*) that have been in turn extensively cultured *in vitro* for several years, thereby scarcely representing the huge parasite genetic diversity circulating in the field (Barry et al. 2009).

1.6.2. Conserved protein regions and antigen candidates for vaccination

Fortunately, *Plasmodium* requires some degree of protein sequence conservation in order to preserve the functionality of those pathogenic mechanisms essential in maintaining parasite viability within the human host. In this regard, preserved regions have been identified as potential antigen candidates for vaccination in proteins involved in pRBC microvascular sequestration (i.e. in an attempt to confer protection against severe falciparum malaria) as well as taking part in invasive processes in which the parasite is completely exposed to the immune system (Barry & Arnott 2014; Schwartz et al. 2012). The latter set of antigens would be directed to the blockage of merozoite and sporozoite infection and, as a result, the interruption either the IEC and pre-erythrocytic *Plasmodium* stages.

PfEMP1: pRBC antigen candidate against severe malaria

The *P. falciparum* erythrocyte membrane protein-1 (PfEMP1, Fig. 4) is codified by the *var* multigene family (Fig. 4A). Variants of this protein family are clonally expressed (i.e. a single PfEMP1 variant per pRBC at a time) in a process defined as ‘mutually exclusive expression’ (Scherf et al. 1998) and subsequently presented on the pRBC surface.

Moreover, in an attempt to elude host immunity, the parasite is further capable of spontaneously changing the PfEMP1 variant exposed by means of the transcriptional switching between *var* genes to a different variant with distinct sequence and cytoadhesive properties as well (Paget-McNicol et al. 2002; Frank et al. 2007). PfEMP1 is also one of the most important virulent elements in *P. falciparum* being responsible for pRBCs sequestration into host microvasculature and, as a consequence, a key parasitic component in triggering the severe malaria clinical manifestations described in 1.3.

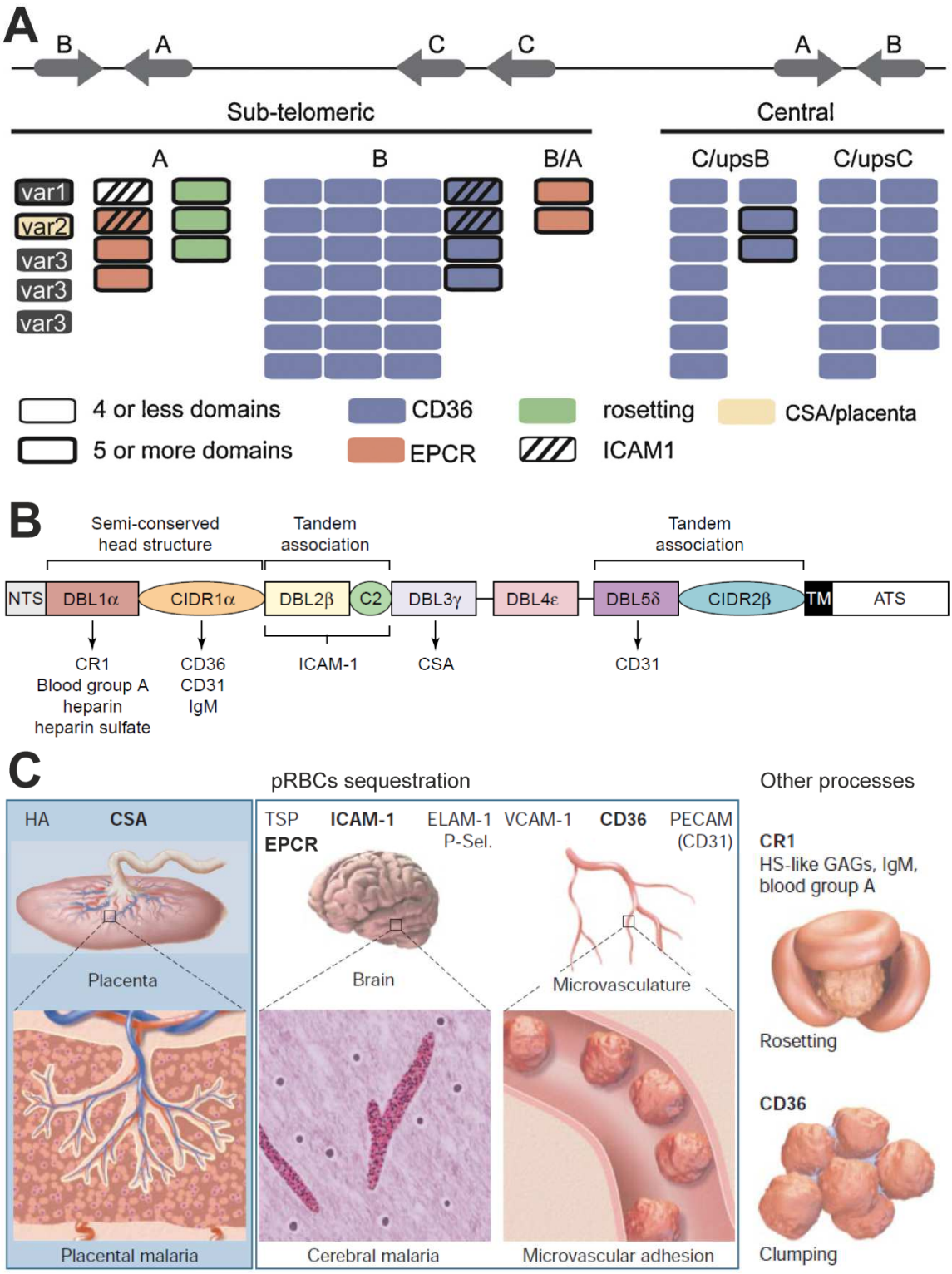

Figure 4. *Description of var genes and PfEMP1 variants for the P. falciparum 3D7 reference clone*. (A) *var* genes classification according to their chromosome location, transcription orientation and upstream sequence (ups) into: A (upsA), B (upsB), B/A chimeric sequence, C/upsC (upsC) and C/upsB (sharing features of B and C groups). (B) Example of a PfEMP1 protein variant architecture and binding domains along with their associated host receptors. (C) *P. falciparum* severe pathogenic processes and the related PfEMP1 receptors causing them. Figure adapted from (Smith 2014; Smith et al. 2001; Miller et al. 2002).

The PfEMP1 extracellular fragment is composed of four basic elements (Fig. 4B): (i) an N-terminal segment (NTS), (ii) Duffy-binding like domains (DBL), (iii) cysteine-rich inter-domain regions (CIDR) and (iv) C2 domains. Such specific domain architecture define PfEMP1 binding tropism to specific protein and glycosaminoglycan (GAG) host cell receptors (Smith et al. 1995). Furthermore, conserved protein sequences and particularly those specific **domains/DCs** and epitopes involved in pRBCs cytoadhesion have been identified together with their ***interacting counterparts***. The most remarkable include:

1. **DBL1X-DBL2X-DBL3X-DBL4ε-DBL5ε-DBL6ε** (VAR2CSA variant) specific head structure enabling pRBC binding to ***placenta*** (Salanti et al. 2004; Gill et al. 2009).
2. **NTS-DBL1α1-CIDRβ/γ/δ**, and particularly the SD3-loop subdomain of DBL1α1, interaction with ***RBC receptors*** and ***non-immune IgM*** during rosetting (Rowe et al. 2002; Albrecht et al. 2011; Rowe et al. 1997; Vigan-Womas et al. 2008; Angeletti et al. 2012; Angeletti et al. 2013; Vigan-Womas et al. 2010; Ghumra et al. 2012).
3. **NTS-DBL1α-CIDR1α2-6** adhesion to ***CD36*** endothelial cell (EC) receptor (Baruch et al. 1997; Turner et al. 2013; Robinson et al. 2003).
4. **NTS-DBL1α-CIDR1α1** (**DC8** and **DC13**) interaction with ***endothelial protein C receptor*** (EPCR) (Bertin et al. 2013; Lavstsen et al. 2012; Avril et al. 2012; Turner et al. 2013; Claessens et al. 2012).
5. Central **DBL2β** domain associated with the ***intercellular adhesion molecule 1*** (ICAM1) EC receptor as interacting partner (Ochola et al. 2011; Turner et al. 1994).

Even domain architectures capable of binding multiple receptors have been described: (i) a rosette-mediating PfEMP1 variant containing a central **DBL2γ** domain that further interacts with brain endothelial cells (***heparan sulfate*** receptor) (Adams et al. 2014) and (ii) the simultaneous interaction of a PfEMP1 molecule with ***CD36*** and ***ICAM1*** receptors through the **CIDR1α-DBL2β DC17** cassette (Avril et al. 2012; Cooke et al. 1994).

Finally, an association between the seroprevalence of PfEMP1-reactive antibodies and protection against severe disease has also been detected in *P. falciparum*-infected individuals, nominating this protein as the main pRBC-surface target of humoral immunity (Vigan-Womas et al. 2010; Chan et al. 2012). Unfortunately, even though animal immunization assays with some of the above-mentioned PfEMP1 preserved regions have proved their efficacy as preventive tools against severe malaria, their restricted *P. falciparum* strain cross-reactivity has significantly hampered their progression towards clinical assays (Baruch et al. 2002; Makobongo et al. 2006; Angeletti et al. 2012; Angeletti et al. 2013).

CS: sporozoite antigen candidate against Plasmodium pre-erythrocytic stage

Parasite-derived proteins from the sporozoite surface as well as those exposed on the infected hepatocyte surface have been extensively explored as potential vaccine candidates against the

Plasmodium pre-erythrocytic stage on the basis of their potential capacity to prevent both the initial liver infection and the beginning of the IEC (Barry & Arnott 2014). Among these candidates, the most remarkable and widely used has been the circumsporozoite protein (CSP). This highly abundant molecule on the sporozoite surface was originally identified as major antigenic determinant during irradiated whole-sporozoite vaccination studies (Nussenzweig & Nussenzweigt 1985) and anti-CS antibodies have additionally proved to effectively block sporozoite infection (John et al. 2008). Noteworthy, a recombinant subunit vaccine composed mainly of the central repeat region and T-cell epitopes of CSP fused with a viral envelope protein of Hepatitis B (RTS,S: developed by the non-profit PATH Malaria Vaccine Initiative and GlaxoSmithKline), is the unique malaria vaccine that has reached Phase III clinical trials evaluation (World Health Organization 2015b).

Latest results from vaccination assays in sub-Saharan Africa have demonstrated a significant decrease in malaria clinical cases in both children (aged 5-17 months at first vaccination) and infants (aged 6-12 weeks at first vaccination) by 36% and 26%, respectively, once completed the study (RTS,S Clinical Trials Partnership 2015). Unfortunately, the moderate preventive efficacy obtained together with the observation of a reduced activity over time demands for further research on new vaccine prototypes in order to meet the WHO strategic goals of 75% clinical malaria protection and efficient transmission blockage against *P. falciparum* and *P. vivax* by 2030 (Moorthy et al. 2013).

PfRh5, DBP and PfSEA-1: antigen candidates against the IEC

Nowadays, one of the best antigen candidates is probably the *P. falciparum* reticulocyte-binding protein homologue 5 (PfRh5). The interaction of this parasite ligand with the RBC receptor basigin has been identified as an essential event triggering *P. falciparum* invasion in several *in vitro* culture-adapted strains as well as field isolates (Baum et al. 2009; Crosnier et al. 2011). Antibodies generated against PfRh5 efficiently block RBC infection (Bustamante et al. 2013; Douglas et al. 2014) and even vaccine candidates have been proposed (Ord et al. 2014; Douglas et al. 2015). Remarkably, PfRh5-based viral vectored vaccines are being developed and assayed by Professor Simon J. Draper (The Jenner Institute, University of Oxford) and currently running Phase I/II clinical trials.

Alternative parasite potential targets include the cysteine-rich protective antigen (CyRPA) from the PfRh5/PfRipr/CyRPA multiprotein complex (Reddy et al. 2015) and other common merozoite ligands: *P. falciparum* Rh4, Rh2, AMA1, RON2, EBA175, EBL1, MSP1 and 38 (Tham et al. 2010; Williams et al. 2012; Srinivasan et al. 2011; Mayer et al. 2009). Antigens of this latter group are only essential for RBC infection in a few *P. falciparum* strains due to the existence of multiple redundant invasion pathways (Persson et al. 2008; Wright & Rayner 2014) and, as a consequence, vaccine prototypes composed of these parasite ligands have not progressed yet beyond Phase II clinical trials (Graves & Gelband 2006; World Health Organization 2015b).

Moreover, the Duffy binding protein (DBP) of the *P. vivax* merozoite surface is the main proposed antigen for vaccination against this *Plasmodium* sp. (Ntumngia et al. 2013) and a vaccine candidate is running Phase I clinical trials at present (World Health Organization 2015b).

Finally, additional potential antigens against *P. falciparum* blood stages have been identified in pRBCs during late schizogony, being the *P. falciparum* schizont egress antigen-1 (PfSEA-1) the most remarkable (Raj et al. 2014). Anti-PfSEA1 antibodies have proved their effectiveness by virtue of blocking merozoites egress, thereby interrupting the IEC while ultimately reducing parasitemia levels and avoiding severe malaria in Tanzanian children (Raj et al. 2014).

Pfs25: Antigen candidate against malaria transmission

Specific antigens of *Plasmodium* sexual forms have also been studied as potential preventive agents against malaria transmission by means of blocking gametes fertilization once inside the mosquito: Pfs25 (Kaslow et al. 1988; Barr et al. 1991; Sharma 2008; Miura et al. 2007) and Pfs48/45 (Rener et al. 1983), together with the *P. vivax* homologues Pvs25 and Pvs48/45, are a few examples. Among all these parasite-derived antigens, only a vaccine candidate based on the Pfs25 protein, which is present on the gametocyte surface up to the early oocyst stage, is currently running Phase I clinical trials (World Health Organization 2015b).

2. *PLASMODIUM FALCIPARUM*

2.1. P. falciparum intraerythrocytic cycle

As introduced in 1.3., *P. falciparum* accounts for the most severe malaria clinical manifestations in humans, which are in turn produced by the parasite blood stages (Fig. 5). *P. falciparum* IEC lasts 48 hours to complete and shares common features to other *Plasmodium* spp.

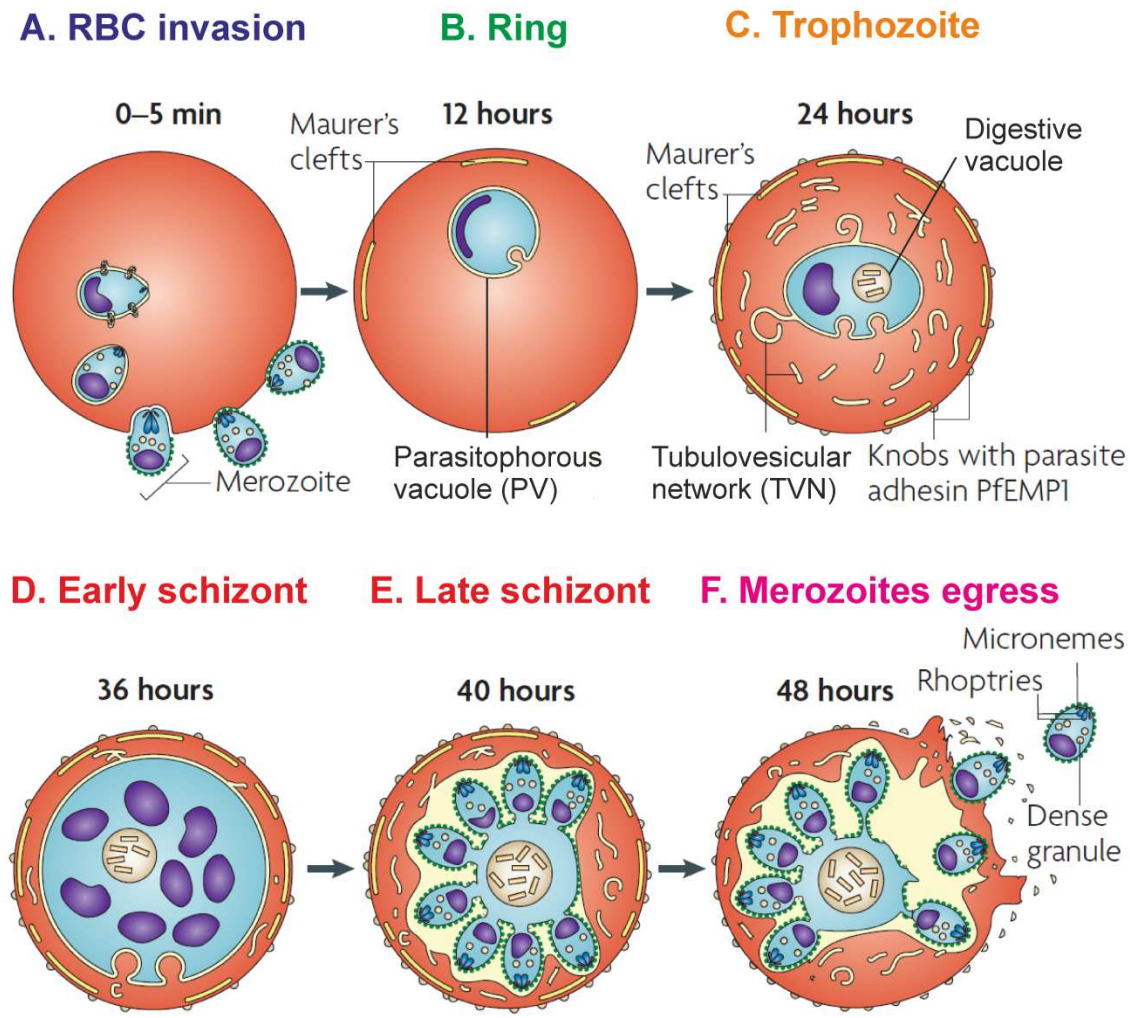

Figure 5. *P. falciparum IEC.* Figure adapted from (Maier et al. 2009).

2.1.1. RBC invasion (0-24h)

The *P. falciparum* IEC begins with the invasion of a healthy erythrocyte by the merozoite infective form of the parasite (0-5 min, Fig. 5A) in a process that encompasses the following sequence of events:

A) Interaction with the host RBC, parasite apical reorientation and irreversible formation of a tight junction. Remarkably and as already mentioned, this infective process involves the participation of multiple invasion pathways as a protective mechanism against host immunity and RBC

receptor polymorphisms (Stubbs et al. 2005). In this regard, several merozoite surface ligands and erythrocyte receptors take part in *P. falciparum* invasion. Some examples include the AMA1, EBA, MTRAP, MSP1 and PfRh proteins (Baum et al. 2009) as parasite ligands, and the CR1, basigin (Crosnier et al. 2011) and glycophorin proteins as well as GAGs (Y. Zhang et al. 2013; Boyle et al. 2010) as RBC receptors.

B) Merozoite signal transduction triggered by RBC binding and release of intracellular contents from the rhoptry and microneme organelles, which subsequently induce the formation of a vacuole by derivatization of the RBC plasma membrane (RBCM).

C) Merozoite invagination into the host cell and sealing of the RBC-derived compartment forming the parasitophorous vacuole (PV) (Dluzewski et al. 1992).

The parasite remains then almost inactive during the initial 12 h post-invasion (p.i.), period also known as the ring stage (Fig. 5B). Importantly, in a maturation process parallel to trophozoite progression, a few parasites in the early ring form will eventually give rise to gametocyte sexual stages (micro and macrogametocyte corresponding to the male and female parasite sexual forms). Gametocytogenesis is stimulated under stress conditions (Tilley & McConville 2013) and essential for the parasite transmission to the mosquito host.

2.1.2. Remodeling of the host RBC (24-36 h): parasite feeding

Parasite metabolic activities progressively increase while entering the trophozoite stage (24 h p.i., Fig. 5C) and are mainly based on (i) glucose lactic fermentation as major energy source and (ii) digestion of RBC hemoglobin. This latter process being essential in generating amino acid building blocks for protein and *de novo* pyrimidine biosynthesis and provides as well an important carbon skeleton supply for the mitochondrial tricarboxylic acid (TCA) cycle.

Hundreds of proteins are exported beyond the parasite's plasma membrane throughout the trophozoite stage remodeling the host RBC for feeding and mechanical cytoadhesive purposes (Goldberg & Cowman 2010; Maier et al. 2009). During this maturation process, hemoglobin and other essential nutrients are endocyted by the intracellular parasite from the host cell cytoplasm through the cytostome specialized organelle (Kirk 2001). The resulting cytostome-endocytosed vesicles will eventually fuse with an internal acidic digestive vacuole, parasite fundamental organelle responsible for hemoglobin digestion and storage of hemozoin waste product.

Furthermore, *P. falciparum* largely increases the permeability of the pRBC plasma membrane (pRBCM) to a wide range of low-molecular weight solutes between 10-20 h p.i. (Staines et al. 2001; Kirk 2001). Anions and electroneutral molecules are preferentially transported across the pRBCM and include essential substrates, electrolytes and metabolic waste products (Fig. 6). This restructuration process is defined as 'New Permeability Pathways' (NPPs) and primarily involves (i) the export and insertion of parasite-derived proteins into the pRBCM (Alkhalil et al. 2004) and (ii) the activity modulation of several endogenous RBC transporters. The latter regulating the

traffic of amino acids, purines and lactate, among other solutes, in the host erythrocyte (Quashie et al. 2010; Poole & Halestrap 1993; Huber et al. 2005).

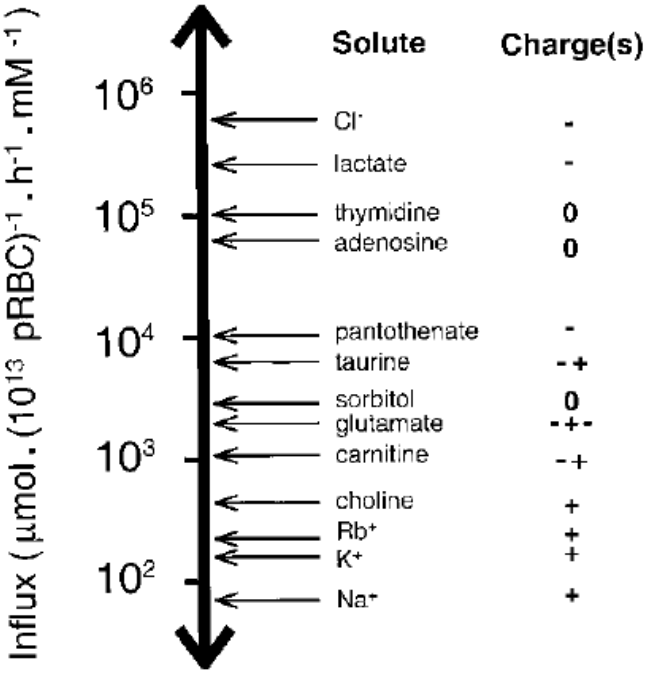

Figure 6. *Relative transport rates of low-molecular weight solutes throughout the P. falciparum-induced NPPs*. Influx rates were determined for pRBCs in the trophozoite maturation stage at 22 ºC and using an extracellular concentration of 1 mM solutes. Figure reproduced from (Kirk 2001).

Alterations in the RBCM mostly comprising variations in lipid composition and arrangement (e.g. lower unsaturation index, shorter fatty acid chains and changes in lipid asymmetry) have also been identified taking place throughout the *P. falciparum* IEC (Hsiao et al. 1991; Maguire et al. 1991; Moll et al. 1990).

2.1.3. Remodeling of the host RBC (24-36 h): cell ultrastructure alteration and vesicular transport of virulent proteins

Knobs, tubulovesicular network and Maurer's clefts

Dramatic changes in pRBC morphology occur during the trophozoite maturation stage (Fig. 7). The parasitized-cell shape becomes more irregular as a consequence of the host cytoskeleton restructuration and several small cup-like protrusions, defined as 'knobs', appear beneath the pRBCM (Fig. 7G). These knobby structures are composed mainly of the knob-associated histidine-rich protein (KAHRP) and serve as supporting platforms for the cell surface exposure of the PfEMP1 virulent adhesin (Maier et al. 2009). Additional parasite-induced structures and organelles participate in the intracellular transport of molecules (Fig. 7A,C,D). Small tubes and whorls emanate from the PV membrane (PVM) forming the 'tubulovesicular network' (TVN) while highly electron-dense and disc-shaped membrane-bound compartments of 500 nm diameter, termed 'Maurer's clefts' (MCs), emerge as single bodies distributed far and wide the host RBC cytoplasm (Hanssen et al. 2008; Hanssen, Carlton, et al. 2010; Hanssen, McMillan, et al. 2010).

MC organelles are built by the parasite 10-15 h p.i. (3D7 *P. falciparum* clone) and are characterized by (i) displaying an electron-lucent lumen of ~30 nm depth and (ii) containing specific resident proteins such as the membrane-associated histidine-rich protein 1 (MAHRP1), the ring exported protein 1, and *P. falciparum* skeleton binding protein 1 (PfSBP1). Furthermore, MCs play an essential role in the storage of proteins participating in pRBC cytoadherence and their controlled delivery to the pRBCM (Wickham et al. 2001; Bhattacharjee et al. 2008).

Tethers

A further deep analysis of the pRBC ultrastructure would be carried out by the group of Professor Leann Tilley through the application of electron microscope tomography techniques for the 3D reconstruction of MCs in 2008 and the whole infected cell in 2010 (Hanssen et al. 2008; Mcmillan et al. 2013; Pachlatko et al. 2010). Such awesome work led to the identification of membrane-bound, striated tether-like structures of 30 nm in diameter and 200-300 nm in length known as 'tethers' (Fig. 7A,C,D). These elongated structures contain an electron-dense lumen and were found to connect physically the MCs with: (i) the cytoplasmic side of the pRBCM in a process involving the restructuration of host cytoskeleton (Cyrklaff et al. 2011), (ii) the PV-TVN membranous system and (iii) other surrounding MCs. All these features ultimately resulting in a complex interconnected network that has been suggested to be involved in the intracellular traffic of parasite proteins.

Moreover, the cytoskeleton-binding PfSBP1 protein and particularly the membrane-associated histidine-rich protein 2 (MAHRP2) have been found to localize to tethers, highlighting the close association of these structures with MCs. MAHRP2 was identified as a major and specific component of tethers as well as indispensable for parasite survival (Pachlatko et al. 2010). Importantly, lipid bilayer continuum between tethers and the aforementioned connected pRBCM and MC organelles was found to be absent (Hanssen et al. 2008; Hanssen, Carlton, et al. 2010), fact that hinted at the participation of additional mechanisms for a functional molecular transport.

Vesicular transport of parasite-derived proteins: VLS, EDVs, J-dots and EVs

In light of the above, a *de novo* vesicular trafficking system induced by the intracellular parasite has been considered as responsible for the transport of proteins beyond the PVM. Small uncoated vesicle-like structures of ~25 nm in diameter (VLS, Fig. 7G) have been identified localizing in large numbers both to the MCs and beneath the pRBCM regardless of the *P. falciparum* IEC maturation stage (Hanssen et al. 2008; Hanssen, Carlton, et al. 2010).

Electron-dense vesicles (EDVs, Fig. 7A,E) constitute a second type of vesicles freely distributing throughout the host RBC compartment. In comparison with VLS, EDVs are (i) bigger in size (~80 nm in total but displaying an internal diameter of 25 nm), (ii) coated, (iii) less abundant and (iv) have only been identified in parasites at the trophozoite stage (Hanssen, Carlton, et al. 2010; Taraschi et al. 2001).

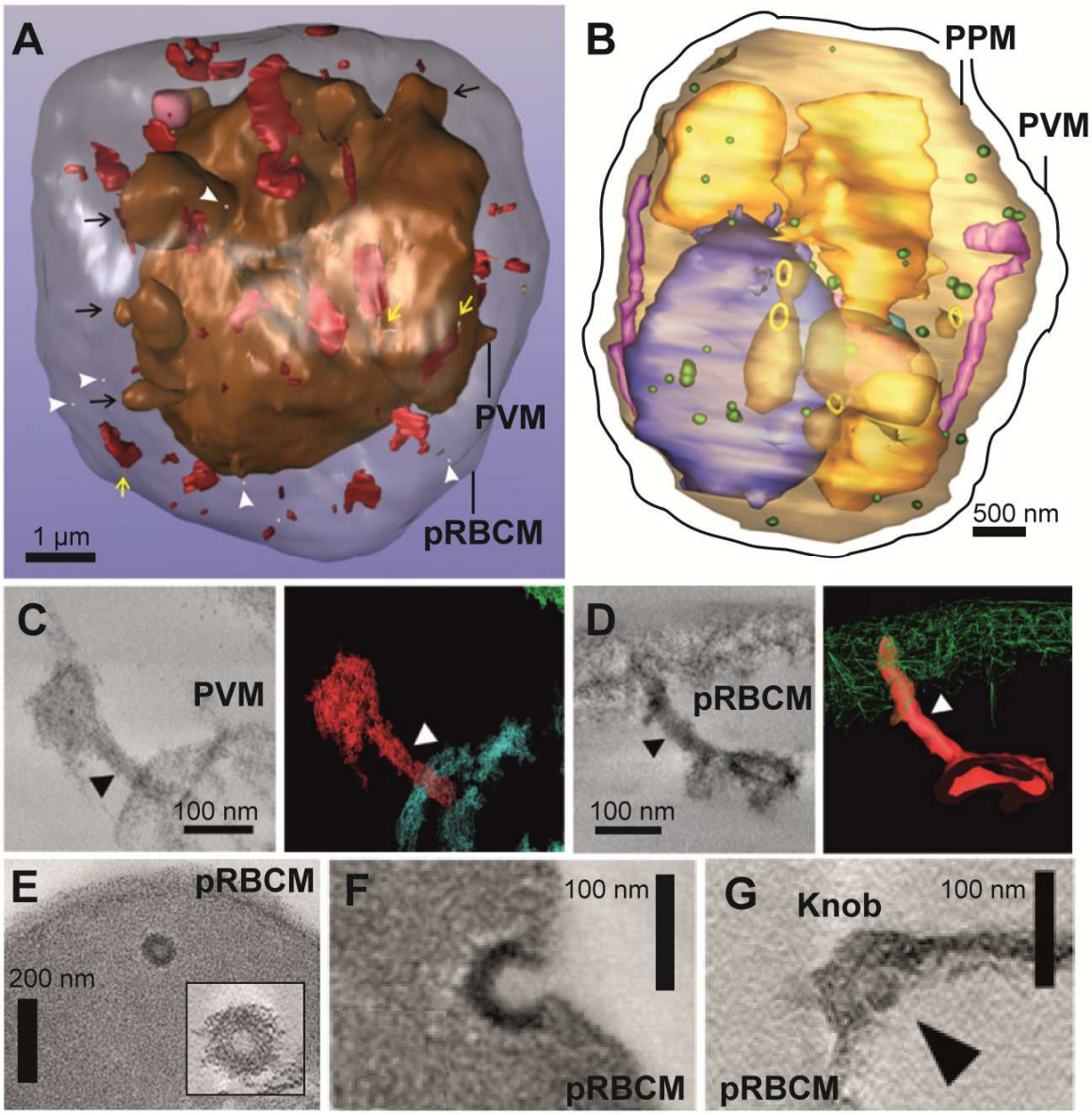

Figure 7. *Illustration of the pRBC ultrastructure obtained through electron microscope tomography and 3D reconstruction.* (A) Exomembrane system localized in the host RBC compartment. pRBCM and PVM are depicted in gray and brown, respectively. TVN structures are indicated by black arrows. MCs are shown in red and their tether-like connections with either the PVM or pRBCM are shown as beige cylinders (yellow arrows). EDVs are represented as white dots and marked with white arrowheads. A compartment for hemoglobin supply is depicted in magenta. (B) Parasite subcellular reconstruction: nuclei (gold), cytostome (yellow rings), cytostomal vesicles (yellow translucent intracellular invaginations), digestive vacuole (blue), mitochondrion (purple), acidocalcisomes (green vesicles), apicoplast (soft blue) and parasite plasma membrane (PPM). (C,D) Electron tomography of MCs (red) and their link with either (C) the PVM (blue), or (D) the pRBCM (green). (E-G) Transmission electron microscopy images of intracellular vesicles distributed throughout the host RBC cytoplasm: (E) 80 nm-EDV and its maximization, (F) EDV fusing with the pRBCM and (G) 25 nm-VLS localized beneath a knob structure. Figure adapted from (Hanssen et al. 2008; Hanssen, Carlton, et al. 2010; Hanssen, McMillan, et al. 2010; Hanssen, Goldie, et al. 2010).

Moreover, the detection of the parasite-derived PfEMP1 and *P. falciparum* erythrocyte membrane protein-3 (PfEMP3) proteins within EDVs and the further observation of some of these coated vesicles fusing with the pRBCM (Fig. 7F), has suggested a possible role of EDVs in transporting integral membrane proteins from MCs to the pRBCM (Taraschi et al. 2001; Mcmillan et al. 2013; Hanssen, Carlton, et al. 2010). Once in the membrane, these parasite proteins might in turn rearrange forming the aforementioned electron-dense knob structures (Fig. 8) (Taraschi et al. 2001; Mcmillan et al. 2013).

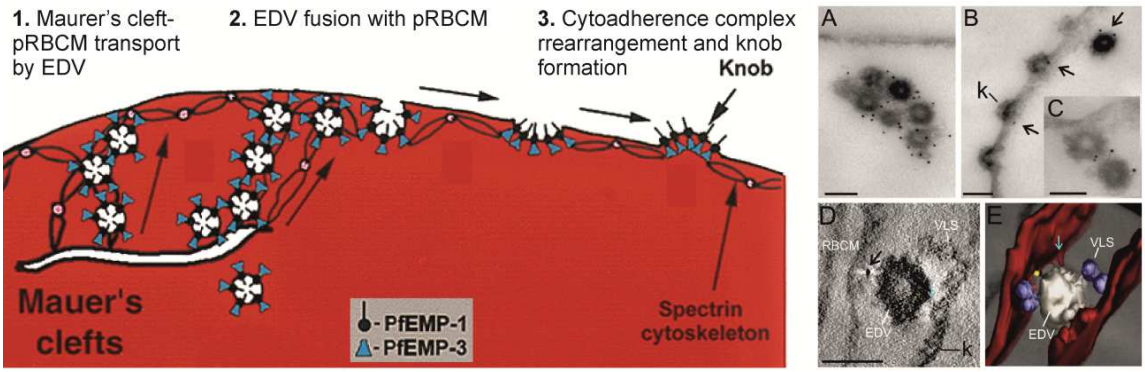

Figure 8. *EDV-mediated trafficking of proteins forming the virulent cytoadherence complex at the pRBCM*. (Left) Schema depicting the transport of virulent proteins from MCs to the pRBC surface and later knob formation. (Right) Electron microscopy (EM) of EDVs labeled through PfEMP1 gold immunostaining. Scale bar: 100 nm. (A-C) Immuno-EM examples of PfEMP1 (black dots)-loaded EDVs at the host RBC cytoplasm. Knobs (k, black arrows). (D-E) EM tomography and 3D reconstruction of EDVs carrying PfEMP1 (yellow dot) and VLS. Figure adapted from (Taraschi et al. 2001; Mcmillan et al. 2013).

A third type of vesicle-like structures, termed 'J-dots' (Külzer et al. 2012; Külzer et al. 2010), are characterized by lacking a visible membrane and carrying chaperone protein complexes (hsp40/hsp70). Remarkably, J-dots have been considered as responsible vesicles for the transport of PfEMP1 between the PV and MCs in a process dependent on the *P. falciparum* PfEMP1 trafficking protein 1 (PfPTP1) (Rug et al. 2014).

Finally, extracellular vesicles (EVs) have been recently identified throughout the *P. falciparum* IEC in the form of exosome-like structures of ~70 nm in diameter (Regev-Rudzki et al. 2013), and microvesicles of 0.1-1 µm in size (Mantel et al. 2013). The latter type of EV are produced through RBC membrane bleeding, contain several parasite and RBC proteins and are involved in inter-pRBC communication as well as immune regulation.

Besides, exosomes have been described as genetic information carriers (i) improving parasite survival during the IEC and particularly under stress pressure and (ii) having an additional role in stimulating gametocytes differentiation (Mantel et al. 2013; Regev-Rudzki et al. 2013). The protein PfPTP2 has been further identified as directly involved in generation, trafficking and reception of such exosome-like vesicles (Regev-Rudzki et al. 2013). It is important to highlight that both the mechanism by which exosomes are produced and secreted and if they are actually the same structures as the above-mentioned EDVs still remains unknown.

2.1.4. Remodeling of the host RBC (24-36 h): uptake of extracellular macromolecules

The study of the mechanisms by which the pRBC internalizes high-molecular weight solutes (macromolecules), process described to take place only during the trophozoite and schizont maturation stages (also termed 'late form-pRBCs'), has been an area of extensive research yet highly controversial. First of all it is important to highlight that the human mature erythrocyte (major RBC population in blood) lacks subcellular organelles and, as a consequence, cellular activities such as endocytosis and internal vesicular transport are absent in this cell (Mohandas & Chasis 1993). A similar fate has been attributed to the pRBC, being incapable of undergoing endocytic processes through the pRBCM (Haldar & Uyetake 1992; Pouvelle et al. 1994) and thereby requiring the *de novo* generation of an intracellular trafficking system based on vesicle-like structures for an efficient exchange of macromolecules (see 2.1.3.).

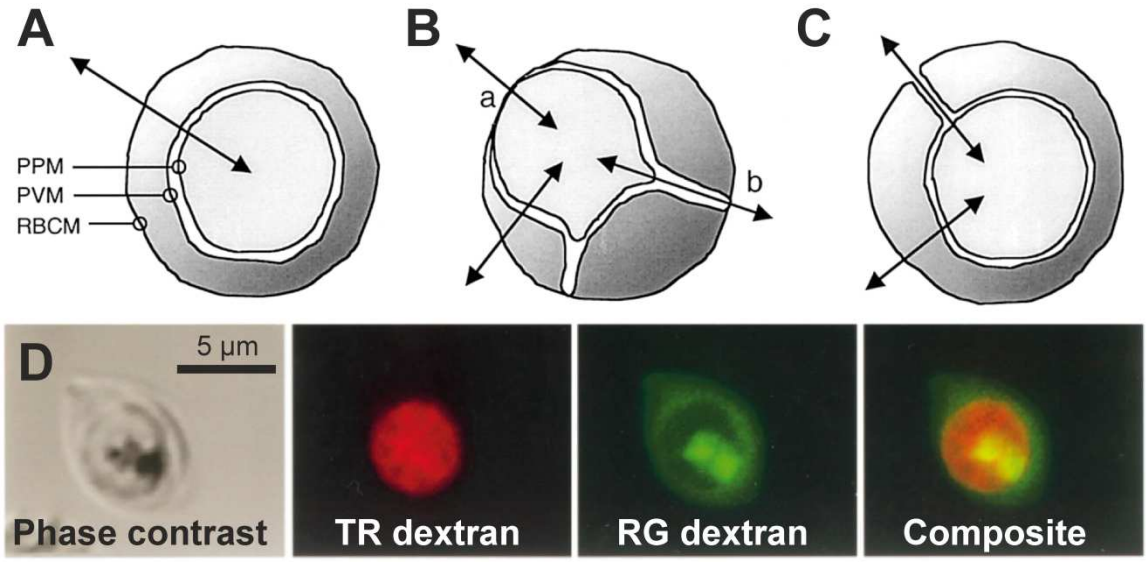

Figure 9. *Theorized molecular transport routes in the pRBC and macromolecular uptake of 10 kDa dextrans*. (B-C) Representation of the parallel uptake pathways as alternatives to the sequential route (A). Metabolic window (B,a) and parasitophorous duct with parasite-controlled (B,b) or direct (C) access to the extracellular medium. (D) Confocal microscopy assay of a 10 kDa dextran transport into the pRBC (early schizont form). Live images of a *P. falciparum* parasite infecting a RBC previously-loaded with Rhodamine green-labeled (RG) dextran and further incubated with medium containing a Texas red-labeled (TR) dextran. Figure adapted from (Goodyer et al. 1997; Kirk 2001).

Moreover, several independent experiments with live pRBCs hint at the existence of parallel routes that would mediate the incorporation of extracellular macromolecules following alternative pathways to the traditional sequential route (Fig. 9A): pRBCM→PVM→parasite plasma membrane (PPM). This conventional path would be extensively used by low-molecular weight solutes including hydrophobic, hydrophilic and amphiphilic molecules and mediated by either

passive or active diffusion mechanisms. In the latter condition, additional elements such as membrane channels and transporter proteins will be required.

By contrast, the hypothesized parallel routes (Fig. 9B-C) include: (i) specific regions of the PPM with direct access to the external medium, termed 'metabolic windows' (Bodammer & Bahr 1973) and (ii) membranous extensions of the PVM that reach the pRBCM, described later and named 'parasitophorous duct' (Pouvelle et al. 1991). Importantly, these parallel uptake pathways have been theorized to provide the intracellular parasite with a mechanism for the fast and straightforward uptake of a wide range of extracellular, high-molecular weight solutes with different sizes and physicochemical properties. Some reported examples are detailed below.

Oligonucleotides and peptides

Ribozimes (Flores et al. 1997) and 30 to 90-amino acid chains including dermaseptin polycationic peptides and gelonin (Nicolas et al. 1997; Ghosh et al. 1997). Remarkably, all these macromolecules inhibited parasite growth within a single IEC when added into the culture medium.

Proteins and polymers

Small proteins such as the 42 kDa-Protein A (Pouvelle et al. 1991) and antibodies either labeled with fluorescent markers or exhibiting antimalarial activity (Pouvelle et al. 1991; Kara et al. 1988; Raj et al. 2014) have been described to (i) cross the pRBCM, (ii) subsequently localize to the theorized parasitophorous duct-PV space and (iii) eventually becoming concentrated into the parasite cytoplasm through PPM-mediated endocytosis. A similar mechanism was hypothesized for the incorporation of fluorescent dextrans (10-70 kDa) and dextran-latex bead polymer conjugates of up to 100 nm in diameter (Pouvelle et al. 1991; Goodyer et al. 1997). Goodyer et al. would provide in 1997 the first visual evidence of multiple parasite uptake pathways taking place in parallel (Fig. 9D).

On one hand, a cytostomal macromolecular transport from the host RBC cytoplasm was indentified in parasites infecting erythrocytes that had been previously-loaded with rhodamine green-labeled dextrans. These polymers were then transported directly to the digestive vacuole in a process similar to the cytostome-mediated hemoglobin uptake and processing.

On the other hand, when the same pRBCs were incubated in the presence of a texas red-labeled dextran, a direct accumulation of this polymer into the parasite cytoplasm along with an absence of signal in the host RBC compartment was obtained. Such behavior suggested the existence of a trafficking route communicating the PV with the extracellular medium and particularly directed to the incorporation of extracellular macromolecules, though probably in a distinct way to the originally proposed parasitophorous duct route. Similar uptake processes have been reported latterly for the direct incorporation of charged polyamidoamine-based polymers (with sizes in the range of 3-7 nm) and heparin into pRBCs at the trophozoite-schizont maturation stage (Urbán et

al. 2014; Marques et al. 2014). Again, no signal was observed in the host RBC cytoplasm for both types of polymers.

Nevertheless, in spite of all invested efforts, the exact mechanism controlling such an important process for drug delivery and vaccination approaches remains still unknown. Moreover, the possibility that low-molecular weight fluorescent molecules get released from labeled polymer conjugates, process that could lead in turn to an indirect dye uptake by the parasite likely through the *P. falciparum*-induced NPPs or passive membrane diffusion, has been a focus of intensive debate. Such undesired process might occur during long incubation periods by either simple degradation or following a dilution-stimulated dissociation of the initial conjugated structure and would additionally result in the complete absence of the active polymer inside the pRBC. Importantly, this indirect labeling mechanism has been proposed against the previously described parallel routes, which in some cases have been claimed to be artifacts (Hibbs et al. 1997; Kirk 2001).

2.1.5. Nuclear division and merozoite egress (36-48 h)

The end of the *trophic* trophozoite stage is defined by multiple events of nuclear division (~36 h p.i.) and the resulting generation of about 20 merozoites. This period is known as the schizont stage (Fig. 5) and the pRBC is mainly characterized by an intracellular parasite containing multiple nuclei that occupies most of the host RBC volume. Both PVM and PPM closely approximate the host RBC plasma membrane and a peak release of extracellular microvesicles has been further described to occur at this maturation stage (Mantel et al. 2013).

Moreover, the pRBCM exhibits both the highest stiffness along the *P. falciparum* IEC as well as a major exposure of virulent proteins, which include the important PfEMP1 cytoadherence-mediating protein. Remarkably, such increase in microvascular sequestration capacity makes the schizont the deadliest parasite stage responsible for the most severe outcomes in malaria. As explained in 1.3. and 1.6.2., the formation of rosette RBC aggregates and pRBC cytoadherence to endothelial cells in the brain or placenta are just a few examples of PfEMP1-mediated virulent processes.

During the last hours of the IEC (~42 to 48 h p.i.), the pRBCM begins to fragment and daughter merozoites are subsequently released to the external medium ready for a new round of infection while leaving the cell remains of the parent pRBC. Importantly, this step produces at the same time the liberation of parasite-derived pro-inflammatory molecules, coinciding in this manner the discharge of merozoites taking place every 48 h with the malaria-associated frequency in fever peaks (Montero 2013).

2.2. P. falciparum biochemistry and research of specific drug targets

2.2.1. Glucose metabolism

Processing of glucose during the entire *P. falciparum* IEC is vital for the parasite. Indeed, its uptake in the pRBC increases by more than 75-fold during the trophozoite stage and is mediated by a parasite-encoded hexose transporter (Sherman 1979), which has been validated as novel drug target (Joet et al. 2003). Considering the sugar-rich environment that constitutes the human bloodstream, glycolysis and lactic acid fermentation are the main parasite metabolic activities for energy supply generating a total of 2 ATP net molecules per hydrolyzed glucose (Fig. 10).

Importantly, although fermentation is much less efficient than aerobic respiration (30-32 ATP net molecules per glucose) it provides an essential and fast ATP source vital to supply the high metabolic demand of parasite metabolism and its rapid growth. Actually, *P. falciparum* genome encodes all enzymes constituting the complete TCA cycle but only 7% of the total digested glucose is metabolized in the mitochondria during the asexual IEC (MacRae et al. 2013). Pyruvate decarboxylation in this organelle has been recently suggested to be developed by the *P. falciparum*-encoded 2-oxoglutarate dehydrogenase enzyme complex (Chan et al. 2013).

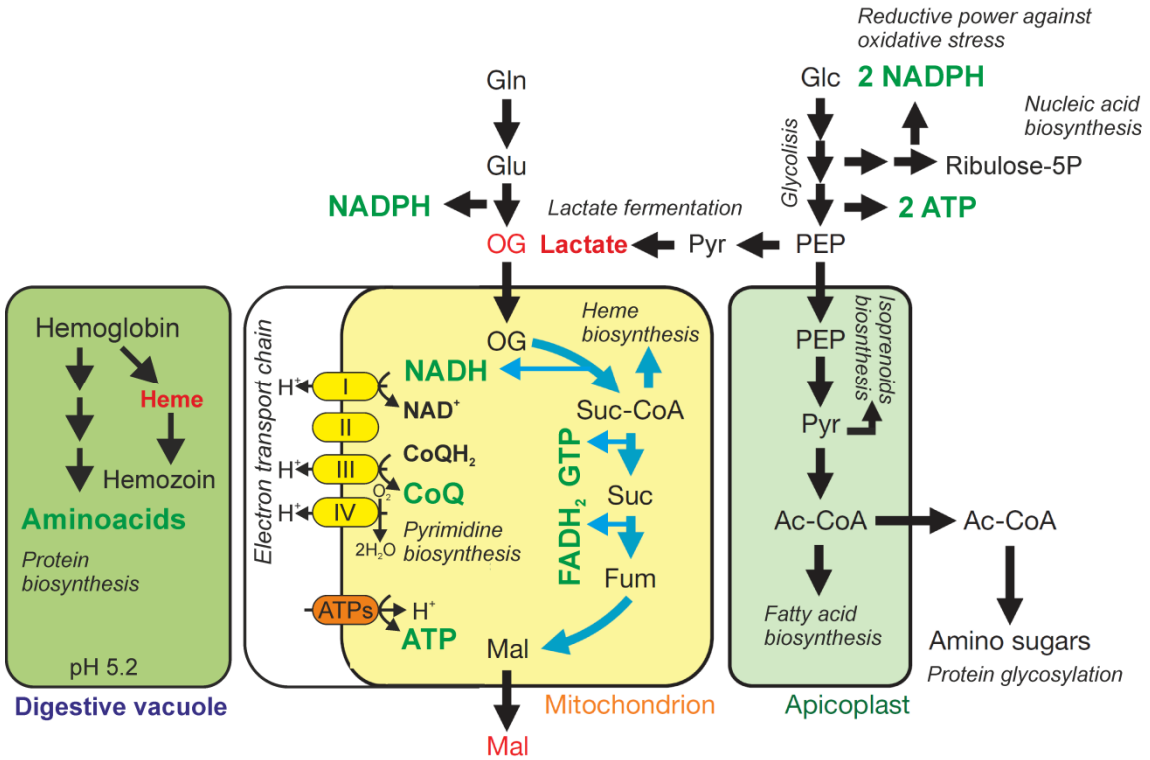

Figure 10. *P. falciparum essential metabolic pathways during the asexual IEC*. Key metabolites are highlighted in green color and their corresponding indispensable function is written in italics. Waste-toxic products are indicated in red color. Glucose (Glc), phosphoenolpyruvate (PEP), pyruvate (Pyr), acetyl-Coenzyme A (Ac-CoA), glutamine (Gln), glutamate (Glu), 2-oxoglutarate (OG), succinyl-Coenzyme A (Suc-CoA), succinate (Suc), fumarate (Fum), malate (Mal), ubiquinone (CoQ), ATP synthase (ATPs). Figure adapted from (Olszewski et al. 2010).

Moreover, the glycolytic intermediate glucose-6-phosphate is further metabolized through the Pentose Phosphate Pathway (PPP). This metabolic route is carried out by both erythrocyte and *P. falciparum* and provides (i) ribose sugars for nucleotide biosynthesis and (ii) a major source of reduced NADPH to be used in anabolic reactions as well as an essential reducing agent for the maintenance of thioredoxin and glutathione (GSH) redox systems in the pRBC (Barrett 1997).

The aforementioned redox pathways constitute an important defense against oxidative stress and participate in other vital cellular functions including cell growth and the preservation of protein functionality (Preuss et al. 2012). Remarkably, such important role of the PPP in parasite viability is supported by the reduced severity of malaria infection found in G6PD-deficient patients (Allison 1960).

2.2.2. Glucose metabolism in the apicoplast

Pyruvate obtained from glycolysis is alternatively metabolized in the apicoplast, a non-photosynthetic plastid-like organelle common in protist parasites of the Apicomplexa phylum, to Acetyl-Coenzyme A (Ac-CoA) and the isopentenyl pyrophosphate (IPP) / dimethylallyl pyrophosphate (DMAPP) building block pair for isoprenoids biosynthesis (Fig. 10 and 11).

Biosynthesis of amino sugars and fatty acids

Production of Ac-CoA through the *P. falciparum*-encoded pyruvate dehydrogenase complex, which has been found to uniquely localize to the parasite apicoplast (Foth et al. 2005), is necessary for the synthesis of amino sugars including N-acetylglucosamine and N-acetylgalactosamine, among others, as fundamental substrates for protein glycosylation (Gowda & Davidson 1999). Ac-CoA serves in parallel as building block for fatty acid synthesis through the type II pathway. Nevertheless, this biosynthetic route is only essential for parasite viability in the liver and mosquito stages (Yu et al. 2008; van Schaijk et al. 2014), being the human host the major lipid supplier during the asexual blood stage.

Isoprenoids biosynthesis

Isoprenoids are a large class of organic compounds obtained through the assembly of multiple five carbon-IPP molecules and involved in several *P. falciparum* downstream biosynthetic activities. Remarkably, whereas all organisms are able to synthesize IPP through the mevalonic acid pathway present in the cell cytoplasm, only those containing a plastid-like organelle (such as algae, plants, some bacteria and protists) display an alternative route that utilizes a distinct key intermediate metabolite: the 2-*C*-methyl-D-erythritol 4-phosphate (MEP) (Fig. 11).

In this regard, the synthesis of ubiquinone (Painter et al. 2010), carotenoids (Tonhosolo et al. 2009) and farnesyl/geranylgeranyl groups (Glenn et al. 2006; Nallan et al. 2005; Howe et al. 2013) through the MEP pathway has been identified in all *P. falciparum* asexual blood stages (Cassera et al. 2004). These metabolites participate in essential functions for parasite survival

such as the biosynthesis of hormones and pyrimidines as well as protein prenylation as a few examples, validating in this manner the research of antimalarial drugs against the synthesis of MEP and other downstream indispensable metabolites. Importantly, because most of the aforementioned processes are specific for plastid-containing organisms, drugs targeting intermediate metabolites of these pathways would theoretically be harmless to humans.

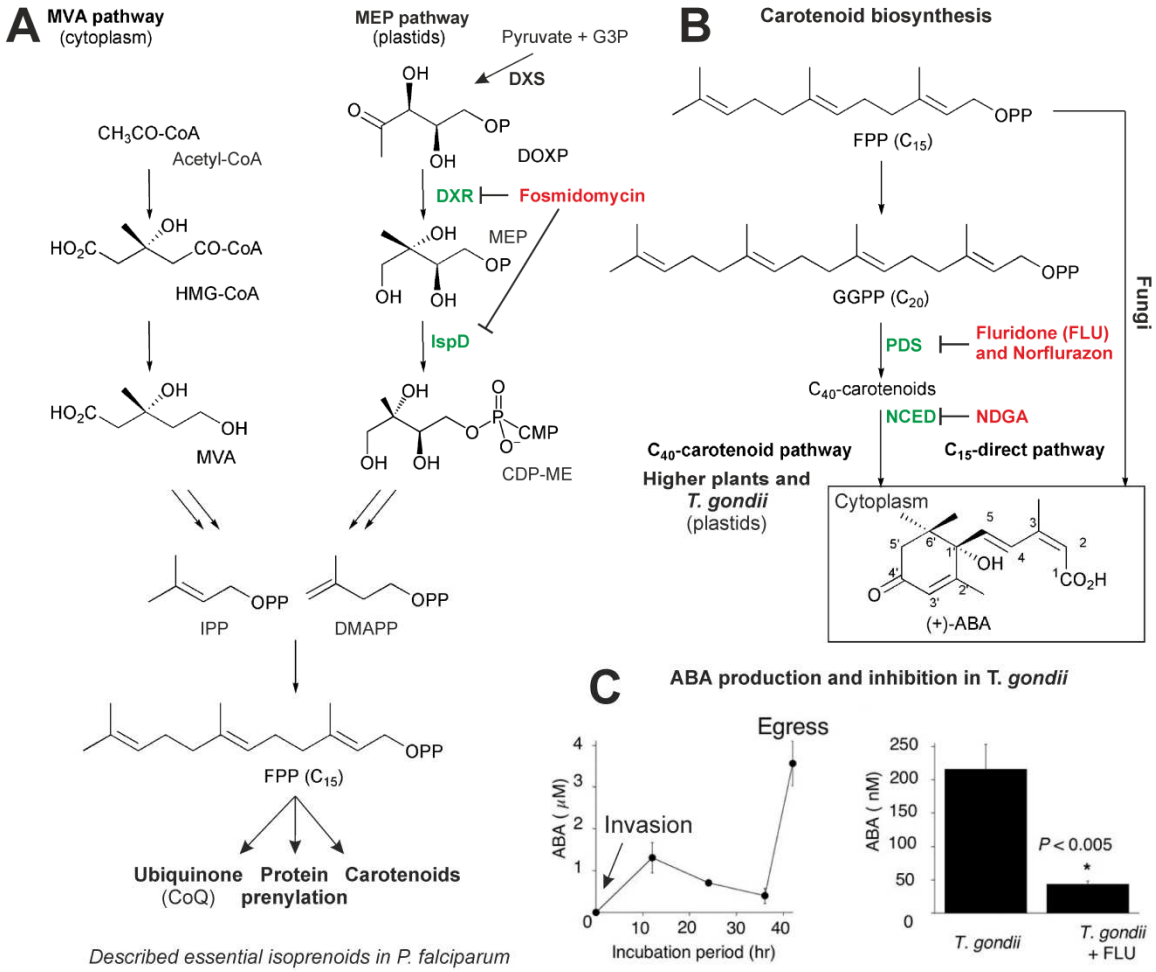

Figure 11. *P. falciparum isoprenoid biosynthetic pathways*. Drugs and their corresponding targeted enzymes are indicated in red and green colors. (A) MVA and MEP routes leading to IPP/DMAPP precursors and isoprenoid essential roles described in *P. falciparum*. (B) Naturally-occurring mechanisms for abscisic acid biosynthesis comprising the C_{15}-direct pathway in fungi and the C_{40}-carotenoid-indirect pathway in plants and *Toxoplasma gondii* (Hirai et al. 2000). (C) Abscisic acid (ABA) synthesis in *T. gondii* throughout a complete intracellular replication cycle and ABA levels after parasite treatment with fluridone (FLU). 1-deoxy-D-xylulose 5-phosphate (DOXP), DOXP synthase (DXS), 4-diphosphocytidyl-2-C-methylerythritol (CDP-ME), farnesyl pyrophosphate (FPP) and geranylgeranyl pyrophosphate (GGPP). Figure adapted from (Oritani & Kiyota 2003; Nagamune et al. 2008).

Fosmidomycin would be the first anti-MEP drug to be tested against *P. falciparum* (Jomaa et al. 1999) showing specific inhibition of the 1-deoxy-D-xylulose 5-phosphate reductoisomerase (DXR) enzyme activity and *in vitro* parasite growth impairment. Furthermore, the fact that parasite

development was completely blocked after fosmidomycin treatment indicated that MEP is the key metabolite/pathway leading to IPP production in *P. falciparum* together with a negligible action of the MVA cytoplasmic counterpart. An additional role of this drug against MEP-based isoprenoid synthesis by inhibiting the MEP cytidylyltransferase (IspD) enzyme would be identified later (Zhang et al. 2011) (Fig. 11). However, in spite of all this success, fosmidomycin is still undergoing Phase II clinical trials (Wells et al. 2015).

Carotenoid biosynthesis

Biosynthesis of carotenoids was first characterized in *P. falciparum* asexual blood stages (Tonhosolo et al. 2009), thereby considered as potential target for drugs design (Fig. 11). In the same work, the herbicide norflurazon, which inhibits the phytoene desaturase (PDS) enzyme in the early steps of the C_{40}-carotenoid biosynthetic pathway, efficiently prevented parasite multiplication (norflurazon *in vitro* 50% growth inhibitory concentration, IC50, of 25 µM) while simultaneously lowering the amounts of downstream metabolites. Additional promising inhibitors comprise: (i) fluridone, herbicide with analogous activity to norflurazon and an antiplasmodial effect already patented (Leef & Carlson 1997), and (ii) the nordihydroguaiaretic acid (NDGA). The latter compound is an inhibitor of lipoxygenase activity as well as a scavenger of reactive oxygen species and used in this way as antioxidant agent for a wide range of applications in mammals that include cardiovascular dysfunctions and cancer treatment (Lü et al. 2010).

NDGA has also been predicted as a potential antimalarial drug against *P. falciparum* liver stages (Mahmoudi et al. 2008) though never been tested against asexual blood forms. Importantly, this compound has been described to inhibit the plastid-resident lipoxygenase-like 9-cis-Epoxycarotenoid dioxygenase (alternatively termed 'neoxanthin cleavage enzyme', NCED) enzyme in plants (Creelman et al. 1992; Burbidge et al. 1997) by means of a dioxygenation step (i.e. incorporation of O_2) that eventually cleaves the 9-*cis*-neoxanthin and 9-*cis*-violaxanthin downstream carotenoids into the intermediate molecule xanthoxin. This compound is further metabolized in the cell cytoplasm obtaining the abscisic acid (ABA) hormone in a process stimulated by water shortage stress and subsequently triggering the stomatal closure of the plant as well as the blockage of its root growth (Zeevaart & Creelman 1988).

In agreement with NDGA behavior, additional compounds with analogous lipoxygenase inhibitory activity (e.g. 5,8,11-eicosatriynoic acid, 5,8,11,14-eicosatetraynoic acid, naproxen and abamine (Creelman et al. 1992; Han et al. 2004)) would therefore be interesting as inhibitory agents against carotenoid downstream functions.

Moreover, considering the absence of photosynthetic activity in apicoplasts, a role of carotenoid derivatives as antioxidant agents in apicomplexan parasites was suggested due to the observation in *P. falciparum* of increased carotenoid levels occurring during oxidative stress (Tonhosolo et al. 2009). Other hypothesized functions comprise: (i) simultaneous regulation of nuclear and plastid gene expression (Gray et al. 2003), (ii) changes in the fluidity of lipid bilayers

(Gruszecki & Strzałka 2005) and (iii) synthesis of plant-like hormones such as the aforementioned ABA.

Abscisic acid production in T. gondii

Endogenous ABA synthesis was identified in the apicomplexan parasite *Toxoplasma gondii* (*T. gondii*) being directly associated with its capacity to reinvade (Nagamune et al. 2008). In this work, *T. gondii* culture supplementation with exogenous ABA induced tachyzoites egress from infected cells through a mechanism controlled by intracellular calcium signaling and using cyclic ADP ribose as intermediate messenger molecule. By contrast, inhibition of ABA endogenous production after treatment with the carotenoid biosynthesis-inhibitor fluridone arrested *T. gondii* growth by delaying parasite release in a dose-dependent manner and inducing its differentiation into the dormant bradyzoite stage in the form of cysts. Furthermore, parasite egress was completely blocked at 50 µM fluridone.

T. gondii egress has been recently described to be further dependent on the activity of two proteins regulated by calcium (Lourido et al. 2012): the *T. gondii* calcium-dependent protein kinase 1 and 3 (*Tg*CDPK1 and *Tg*CDPK3); and an additional cGMP-dependent protein kinase (PKG). Importantly, CDPKs are the mandatory calcium-regulated kinases in plants and apicomplexan parasites (Harper & Harmon 2005; Nagamune & Sibley 2006).

Possible abscisic acid production in P. falciparum

The identification of ABA plant-like hormone in *T. gondii* opened the possibility of finding similar biosynthetic routes in other organisms of the phylum Apicomplexa such as *Plasmodium* or *Babesia* spp., thereby providing new potential therapeutic targets against these endoparasites. Similar calcium-dependent pathways to *T. gondii* regulating parasite escape from infected cells occur in *P. falciparum* (Fig. 12). In this regard, a function of the calcium-dependent *Pf*CDPK5 kinase in a process downstream of the cGMP/PKG intermediate signaling system has been identified in this parasite triggering merozoites egress through the disruption of the pRBCM (Dvorin et al. 2010; Collins et al. 2013). Moreover, an additional function of calcium in regulating *P. falciparum* growth during its asexual IEC has been suggested in virtue of the significant impairment of parasite development and maturation arrest at the late schizont stage caused by means of the inhibition of calcium release at the level of the phospholipase C (PLC)/inositol 1,4,5-triphosphate (IP_3) system (Enomoto et al. 2012).

Nevertheless, the presence of ABA or analogous hormones has never been reported in other protists than *T. gondii*. Considering the punctual ABA production pattern observed in this apicomplexan parasite (Fig. 11) and its amphiphilic nature (log_{10} [octanol/water] partition coefficient, log *P*, of 2.09 units and its uncharged form accounting for 0.55-0.22 % of total ABA molecules at the pH range 7.0-7.4, pKa 4.74, http://www.chemicalize.org), such hormone could become distributed throughout (i) all parasite subcellular compartments, (ii) non-infected host cells and even (iii) the extracellular medium. Derivatization of ABA as an activity regulatory

mechanism similar to those already found in plants (Oritani & Kiyota 2003) could take place in protists as well, considerably increasing in this manner the variability of ABA naturally-occurring derivatives. All these points would eventually result in scarce ABA overall amounts difficult to be detected, and therefore the research of new methodologies with ultra-low detection limits and capable of discerning between ABA-derivatization byproducts would be crucial in order to definitely ascertain if this plant-like hormone is produced by other apicomplexans than *T. gondii*.

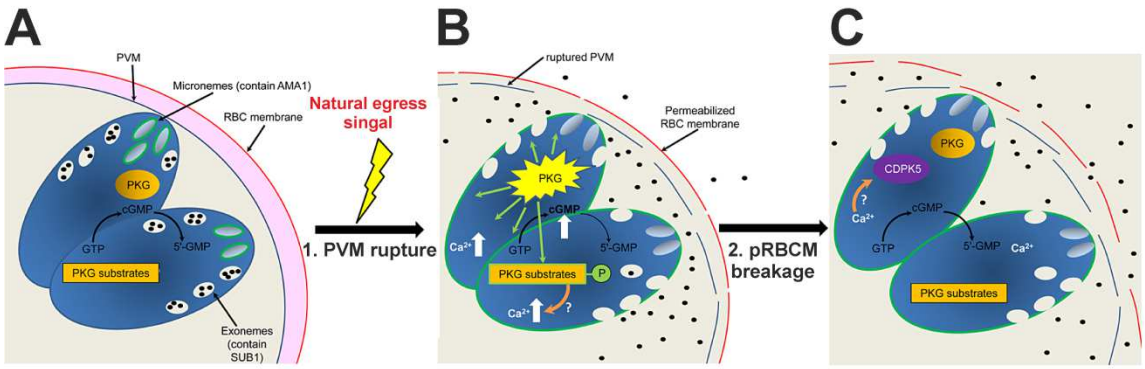

Figure 12. *Hypothesized PKG-induced egress of P. falciparum merozoites from infected erythrocytes*. (A) *P. falciparum* PKG basal state at low amounts of cGMP. (B) Activation of PKG at increased cGMP levels in response to a naturally-occurring egress signal and the subsequent release of parasite-derived proteins that disrupt the PVM. Process accompanied by an intracellular release of calcium. (C) Secreted calcium activates downstream kinases such as the *Pf*CDPK5 that ultimately trigger pRBCM breakage. cGMP returns to the initial basal concentration. Figure adapted from (Collins et al. 2013).

2.2.3. Hemoglobin digestion

In consideration of the restricted *de novo* biosynthesis of amino acids in *P. falciparum* (Payne & Loomis 2006), key components essential for protein biosynthesis and other metabolic pathways necessary for parasite survival, these are obtained during its IEC primarily through digestion of host RBC hemoglobin (Fig. 10) as well as by virtue of the *Plasmodium*-induced NPPs. The latter being indispensable for isoleucine uptake (Martin & Kirk 2007). Hemoglobin accounts for >90% of the total available protein in the RBC cytoplasm and it is almost completely incorporated into the parasite via cytostome-mediated endocytosis, process that generates double-membrane-bound endocytic vesicles filled with host RBC cytoplasm (Fig. 13). These vesicles will subsequently (i) fuse with the parasite's digestive vacuole, organelle that displays late endosome/lysosome-like properties, (ii) their inner membrane will become degraded releasing key lipids, and (iii) hemoglobin will be finally secreted (Lazarus et al. 2008). In total, about 60-80% of RBC hemoglobin is consumed throughout the *P. falciparum* IEC as a result of proteases activity and this digestive process is particularly important for parasite development during the trophozoite blood stage (Francis et al. 1997).

Moreover, reactive oxygen species (ROS, e.g. superoxide and hydroxyl radicals and hydrogen peroxide) are produced at the time hemoglobin is hydrolyzed by way of the release of heme.

Although this moiety is an essential cofactor for numerous enzymes, hemoglobin-derived heme (composed mostly of ferrous iron) is highly toxic for the parasite owing to the transference of electrons to molecular oxygen as a result of heme iron oxidation (ferrous Fe^{2+} to ferric Fe^{3+}). Such process ultimately generating the aforementioned ROS and described as one of the major causes of oxidative stress to the parasite (Francis et al. 1997).

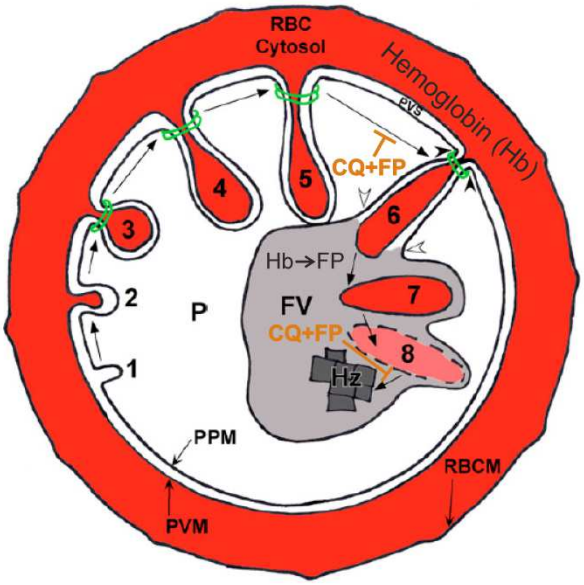

Figure 13. *P. falciparum-mediated hemoglobin uptake and digestion*. (1-3) Cytostome formation events comprising: (1) PPM and (2) PVM invagination, and (3) formation of a double-membrane collar around the neck of the host RBC-laden cytostome. (4-5) Elongation of the cytostome approaching the digestive vacuole (also called 'food vacuole', FV). (6) Cytostome fusing event with the FV membrane (white arrowheads) while being detached from the PPM-PVM (black arrowheads). (7) Release of a single-membrane-bound vesicle and (8) degradation of its membrane by lipases delivering hemoglobin and unsaturated lipids that will sequester free ferriprotoporphyrin IX (FP) and stimulate its polymerization into hemozoin crystals (Hz). CQ forms a complex with FP (CQ+FP) that blocks hemozoin synthesis and alters cytostome physiological processing into the FV. Intracellular parasite (P). Figure adapted from (Lazarus et al. 2008; Fitch 2004).

Other toxic effects of heme liberation include alterations in membranes that can eventually trigger cell lysis (Orjih et al. 1981) and inhibition of enzymes activity (Vander Jagt et al. 1986). Nevertheless, *P. falciparum* has evolved several protective mechanisms that comprise: (i) the action of superoxide dismutase and the thioredoxin/GSH redox systems against oxidative stress, and (ii) the polymerization of oxidized heme into an inert and insoluble crystalline substance termed 'hemozoin' (Fig. 13). Both parasite-derived, histidine-rich proteins (HRPs) and unsaturated lipids released after the incorporation of cytostome-endocytosed vesicles into the digestive vacuole, have been further suggested to be involved in hemozoin formation through the sequestration of free heme as well as triggering its polymerization (Sullivan et al. 1996; Tripathi et al. 2002; Fitch 2004; Huy et al. 2003). Remarkably, hemozoin contains more than 90% of the heme liberated during hemoglobin digestion (Egan et al. 2002), fact that evidences the major importance of heme sequestration and polymerization for parasite viability.

Antimalarial drugs targeting hemozoin formation: 4-aminoquinolines and artemisinin derivatives

In light of the above, hemozoin formation has been one of the most explored routes for antimalarial drugs research, being the 4-aminoquinoline drug CQ the most successful inhibitory agent (at least until resistance emergence). CQ binds the heme oxidation product, which is known as hematin or ferriprotoporphyrin IX (FP), forming a complex (FP+CQ) that inhibits further FP polymerization into hemozoin (Fig. 13) while simultaneously increasing the concentration of free FP and CQ+FP up to a level lethal for the parasite (Dorn et al. 1995; Egan et al. 1997). CQ does also primarily concentrate into the digestive vacuole (acidic organelle with an approximate pH of 5.18, (Wunderlich 2012)) on the basis of its weakly basic nature and the complex formation with FP (Madden et al. 1990; Warhurst et al. 2003; Fitch 2004).

An additional role of the FP+CQ complex has been described in impeding the physiological processing of the cytostome-endocytosed, hemoglobin-laden vesicles through the digestive vacuole route (Fig. 13) by means of an hypothesized binding to intracellular phospholipids (Shviro et al. 1982; Ginsburg & Demel 1984; Dutta & Fitch 1983). Such interaction causing the premature docking of the aforesaid cytostomal vesicles and triggering later the formation of an autophagic vacuole. These altered conditions finally giving rise to hemoglobin denaturation and an enhanced release of heme while avoiding its polymerization, thereby increasing even more the intracellular amounts of toxic free heme (Fitch, Cai, et al. 2003; Fitch, Chen, et al. 2003).

Moreover, those resistance strategies evolved by *P. falciparum* against CQ action all rely on (i) a decreased drug accumulation in the parasite digestive vacuole by virtue of mutations in the CQ-resistance transporter protein (CRT, see 1.4.3.) and (ii) a reduced amount of FP available for interaction with CQ. The latter process has been suggested to be mediated by a timely synchronized release of both FP and the aforementioned heme-binding, polymerization-inducing unsaturated lipids and parasite HRPs (Huy et al. 2003; Fitch 2004). A similar mechanism of action to CQ has been attributed to other antimalarial drugs of the 4-aminoquinoline family such as amodiaquine and hydroxychloroquine (Famin & Ginsburg 2002).

Finally, an analogous role to CQ with regard to the impairment of heme detoxification has been attributed to lumefantrine (Premji 2009; Kokwaro et al. 2007) and artemisinin derivatives. Antimalarial drugs of this latter group contain an endoperoxide bridge (-O-O-) cleavable by free heme and with which they form a heme-drug covalent adduct (O'Neill et al. 2010). This interaction generates free radical intermediates that ultimately result in the alkylation of integral parasite proteins and the disruption of membranes (Pandey et al. 1999; Wei & Hossein Sadrzadeh 1994). Other theorized antimalarial functions of the artemisinin derivatives include: (i) the inhibition of protein biosynthesis -through alterations in the structure of ribosomes and the endoplasmic reticulum of the parasite- in the case of dihydroartemisinin (DHA), and (ii) the inhibition of DNA replication as well as the blockage of the mitochondrial electron transport chain at the level of the cytochrome c oxidase with respect to artesunate (Vangapandu et al. 2007).

By contrast, a completely separate function has been described for those drugs of the quinoline-4-methanol subclass (e.g. the amino alcohols quinine and mefloquine among others) when compared to CQ. These antimalarials inhibit the cytostome-mediated uptake of hemoglobin, additionally interfere with the intracellular docking of endocytosed vesicles and impede the recovery of membrane components (Famin & Ginsburg 2002; Chou & Fitch 1993).

2.2.4. Mitochondrial electron transport chain, pyrimidine biosynthesis and TCA cycle

Mitochondrial electron transport chain and pyrimidine biosynthesis

The single mitochondria of *P. falciparum* is essential in sustaining a functional electron transport chain (Fig. 10) that is required for the parasite in order to maintain: (i) the organelle membrane potential established by proton gradient, (ii) an operative transport of proteins and metabolites into the mitochondria, and (iii) the recycling of fundamental metabolites such as the regeneration of ubiquinone by the cytochrome bc_1 complex. The latter role being indispensable for the *de novo* biosynthesis of pyrimidines (MacRae et al. 2013; Olszewski et al. 2010; Painter et al. 2007).

Drugs interfering with the parasite mitochondrial electron transport chain include atovaquone and proguanil (importantly not the case of the proguanil metabolization product: cycloguanil). Whereas the first antimalarial competes with ubiquinol (reduced from of ubiquinone) for binding to the cytochrome bc_1 complex, the second collapses the transmembrane proton gradient (Nixon et al. 2013; Painter et al. 2007). Furthermore, a reduction in atovaquone IC50 has been observed *in vitro* during combination treatments with proguanil highlighting their synergistic effect (Painter et al. 2007; Painter et al. 2010).

Additional antimalarials against pyrimidines biosynthesis include those agents impairing the synthesis of folic acid cofactor, which inhibit either the dihydropteroate synthase (sulfadoxine) or the dihydrofolate reductase (pyrimethamine and cycloguanil) enzymes of the parasite (Khalil et al. 2002; Peterson et al. 1990). Furthermore, the mechanism of action of the 8-aminoquinoline drug PQ has been hypothesized to be involved in blocking the mitochondrial activity of *P. falciparum* through an inhibition of ubiquinone function in electron transport as well as producing reactive oxygen species (Hill et al. 2006; Fernando et al. 2011).

Mitochondrial TCA cycle

It is important to highlight that the reducing equivalents utilized in the *P. falciparum* electron transport chain are provided mainly through a TCA cycle fuelled by: (i) glutamate as principal carbon source throughout the parasite asexual blood stages (segmented TCA cycle, Fig. 10), or (ii) glucose during sexual intraerythrocytic forms as a more efficient alternative to fermentation. The complete TCA cycle providing much more ATP molecules per hydrolyzed glucose during gametocyte stages (MacRae et al. 2013). In this regard, amino acid transaminases that regulate

the incorporation of glutamate into the TCA cycle through its conversion to 2-oxoglutarate, have been considered as potential targets for novel antimalarial drug therapies against the *P. falciparum* IEC (MacRae et al. 2013). Furthermore, the parasite's TCA cycle supplies the succinyl-Coenzyme A substrate required for the *de novo* biosynthesis of heme, process particularly important during *P. falciparum* mosquito stages (Mogi & Kita 2010; Ke et al. 2014).

2.3. The host red blood cell

The mature human erythrocyte (mRBC or RBC if otherwise specified) displays several distinctive features in comparison with other cells in the organism. Intracellular organelles comprising the nucleus, vesicular trafficking systems and membranous structures are absent in the RBC, being the cell plasma membrane the key element responsible for the transmembrane trafficking of molecules, the exposure of protein antigens and defining cell structure (Mohandas & Gallagher 2008). In this regard, the RBC is capable of deforming considerably its shape, characteristic that allows erythrocytes to cross the splenic interendothelial slits.

However, alterations in such deformable properties, which can be caused in turn by: (i) their own senescence (e.g. oxidative stress or after multiple passages through capillaries and splenic slits), (ii) genetic disorders (e.g. sickle cell disease) or (iii) owing to intracellular parasites (e.g. *P. falciparum*); drastically induce their sequestration and subsequent phagocytosis in the spleen.

Moreover, the mRBC dimensions are of about 6-8 µm in disk diameter along with 1-2.5 µm thickness. This mature cell does also display a surface of ~140 μm^2 (Schrier 2012), an average intracellular volume of 90 fL (McLaren et al. 1987) and constitute the major RBC population in circulation with those immature RBCs (reticulocytes) accounting for only ~1% of the total erythrocytes. Bearing in mind such excess mRBCs, this population will be the one primarily infected by intracellular parasites displaying an absence of RBC-maturation tropism such as in the case of *P. falciparum*.

Finally, RBCs exhibit such an incredibly long life span of 120 days in circulation together with a 24 h-recycling rate of 0.86% of the total 25 trillion erythrocytes found in the human body (i.e. 2.2×10^{11} RBCs are destroyed once a day, ~2.5 million cells every second).

2.3.1. Host RBC membrane

The erythrocyte membrane is composed basically of three distinct sections (Fig. 14):

A) An external glycocalyx (Fig. 14A) formed by carbohydrates located at the extracellular region of glycoproteins and glycolipids (e.g. the ABO and glycophorin blood group antigens). The presence of heparan sulfate proteoglycans at the human RBC surface has been further suggested playing a role as receptor for pRBC adhesion during rosetting processes (Vogt et al. 2004; Vogt et al. 2003; Angeletti et al. 2015) and might contribute as well to the glycocalyx negative charge.

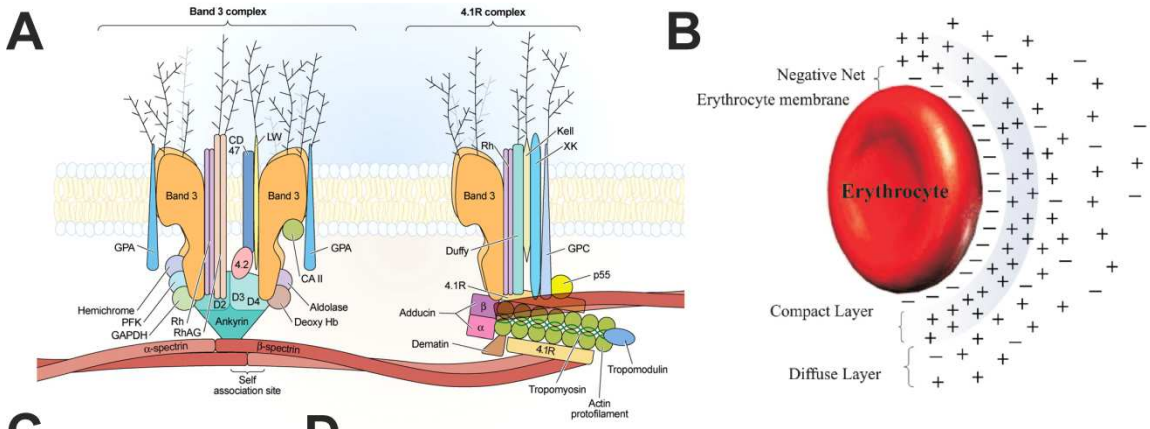

C

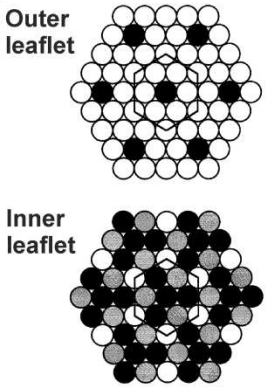

D

Phospholipid	% of whole membrane, ±SD	Outer leaflet, %	Inner leaflet, %
PC	29.3 ± 1.5	44.8	14.0
SM	25.5 ± 1.4	42.1	9.1
LPC	1.0 ± 0.8	2.0	—
CPs	**55.8** ± 2.2 (55.6)	**88.9** (88.9)	**23.1** (22.2)
PE	**27.6** ± 1.5 (27.8)	**11.1** (11.1)	**43.9** (44.4)
PS	14.9 ± 1.7	—	29.6
PI	0.6 ± 0.5	—	1.2
PA	1.1 ± 0.5	—	2.2
APs	**16.6** ± 1.8 (16.7)	**0.0** (0.0)	**32.9** (33.3)

Figure 14. *Architecture and phospholipid composition of the mRBC plasma membrane*. (A) Membrane multiprotein complexes composition. (B) Representation of the cell surface electrical properties. (C) Theorized lateral arrangement of membrane phospholipids through superlattice unit prediction and according to their headgroups: ethanolamine (black), acidic (gray) and choline (white). (D) Detailed phospholipid composition of the whole cell membrane and both outer and inner membrane leaflets. Phosphatidylcholine (PC), sphingomyelin (SM), lysophosphatidylcholine (LPC), phosphatidylinositol (PI) and phosphatidic acid (PA). Figure adapted from (Salomao et al. 2008; Virtanen et al. 1998; Fernandes et al. 2011).

B) An asymmetric lipid bilayer (Fig. 14C-D) with approximately half its mass constituted by more than 50 different transmembrane proteins and the other half by lipids. Phospholipids and cholesterol account for about 60% and 40%, respectively, of the total membrane lipid components. Remarkably, cholesterol is found inserted between phospholipid fatty acid tails and is a fundamental element in maintaining RBC membrane stability and impermeability to small hydrophilic molecules and ions (Chabanel et al. 1983; Arbustini 2007).

C) An intracellular protein skeleton linked to the inner layer of the RBC membrane and essential for maintaining the cell structure (Fig. 14A). Importantly, the stability of this protein network is critically dependent on (i) the formation of spectrin dimmers and their interaction with other key cytoskeletal components (e.g. ankyrin, actin and protein 4.1 R) and (ii) its association with aminophospholipids placed at the inner layer of the cell plasma membrane (Manno et al. 2002; R. Zhang et al. 2013; Mohandas & Gallagher 2008).

RBC membrane proteins

Band 3 (also known as anion exchanger 1 and responsible for the bicarbonate/chloride transmembrane exchange) and glycophorins are the major integral membrane proteins of the RBCM, in which they assemble in 2 main macromolecular clusters that are defined by their cytoskeleton-interacting partner (Fig. 14A): (i) the ankyrin-band 3 and (ii) protein 4.1R complexes (Salomao et al. 2008).

Moreover, glycophorin A (GPA), GPB, GPC and GPD, constitute a family of highly-sialoglycosylated transmembrane proteins that, owing to their large number of sialic acid incorporated residues, account for about 60% of the overall glycocalyx negative charge (Silva et al. 2012; Fernandes et al. 2011; Joel Anne Chasis 1992). Such cell surface charge (Fig. 14B) with approximately an average zeta potential of -14 mV is fundamental for the RBC in order to avoid: (i) the formation of cell aggregates by means of RBC-RBC electrostatic repulsion forces, and (ii) undesired interactions with other cells in the body.

GPA is the most abundant member of the glycophorin family with 0.5 to 1 million molecules per RBC and, along with GPB, specific for the erythroid lineage. Other functions than providing the aforementioned cell surface negative charge have not been clearly described, though possible suggested roles include their interaction with cytokines and/or used as receptors by RBC-infecting pathogens (especially in the case of *Plasmodium* infection). Besides, no complications have been described in individuals lacking one of these proteins, fact that indicates a non-essential role of GPA/GPB in RBC functionality (Dean 2005; Pang & Reithmeier 2009). The codominant allelic forms of the genes GYPA and GYPB, which encode the GPA and GPB proteins, determine the MNS antigenic blood group. Remarkably, the sequences of these glycophorins are highly conserved with only differences in 1 and 2 amino acids for the GPB-defined S-s and the GPA-defined M-N antigens, respectively (Dean 2005). Additional polymorphisms have been identified giving rise to the currently known 46 antigens of the MNS system, though most of them less frequent and minimally affecting the N-terminal region of GPA and GPB proteins (Reid 2009).

RBC-pRBC phospholipid composition and arrangement

RBCs display a particular phospholipid composition on each leaflet of the plasma membrane, characteristic defined as ‘lipid asymmetry’, and such membrane phospholipids have been predicted to be organized in superlattice-like structural units (Fig. 14C) according to the properties of their head groups (Virtanen et al. 1998; Maguire et al. 1991). Whereas choline phospholipids (CPs, neutrally-charged and their head group being composed of a choline moiety) are the major component of the outer membrane leaflet constituting about 88.9% of the total phospholipid molecules (Fig. 14D), the inner membrane leaflet is mainly integrated by phosphatidylethanolamine (PE, neutrally-charged and bearing a small headgroup) and negatively-charged phospholipids (acidic phospholipids group, APs, headed by

phosphatidylserine, PS) with relative abundances of 44 mol% and 33 mol%, respectively. Furthermore, only a minor fraction of the inner leaflet (~23 mol%) is occupied by choline phospholipids.

RBCM lipid asymmetry ultimately defines an overall net negative charge distributed throughout the cytoplasmic side of the membrane and controls the exposure of PS on the cell surface. Importantly, the presence of PS at the surface of RBCs is indicative of cell damage and/or aging and triggers their removal from circulation by spleen-resident macrophages (Mohandas & Gallagher 2008; Nguyen et al. 2011). The exposure of PS can lead as well to nonspecific interactions with other cells in the microvasculature (Yamaja Setty et al. 2002). Besides, phospholipids incorporating short (i.e. 16 carbons or 16C) and medium-length (18C) fatty acid chains predominate in the RBCM with relative abundances of 25 mol% and 42 mol%, respectively. Long-chain-lengths of >20C occur in nearly 30 mol%. Polyunsaturations are furthermore present in almost 40% of the total phospholipid acyl chains (Hsiao et al. 1991).

Moreover, several changes altering the RBCM lipid asymmetry as well as the length and degree of unsaturation of phospholipid fatty acid tails take place during *P. falciparum* infection. An increase in aminophospholipids (PS and PE) abundance on the outer leaflet of the pRBCM (Fig. 15) occurs during parasite growth in a process mediated by: (i) alterations in cytoskeletal components that regulate lipid asymmetry, (ii) PC influx to the inner pRBCM leaflet, and (iii) oxidative stress generation (Wallach et al. 1981). PE has been identified in this regard as the major lipid component of the pRBC surface at the trophozoite and schizont intraerythrocytic stages (Maguire et al. 1991).

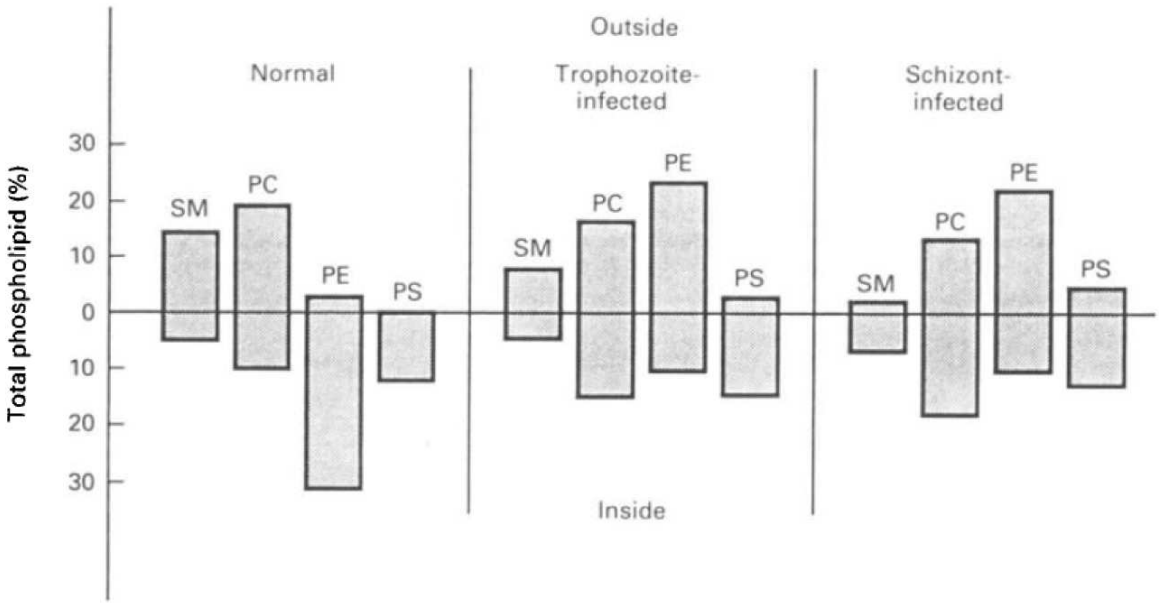

Figure 15. *Alterations in the phospholipid distribution of the RBCM after P. falciparum infection*. Figure reproduced from (Maguire et al. 1991).

The above-mentioned changes in cell exposed phospholipids as a result of *P. falciparum* infection have been described to stimulate pRBC phagocytosis in the spleen and mediate pRBC-cytoadherence to microvascular endothelial cells. Furthermore, due to the increased presence of PE and PS at the cell surface (both phospholipids inducing the inverted hexagonal lipid phase), an enhanced membrane fusibility has been suggested in the pRBC (Nakornchai et al. 1983; Maguire et al. 1991). Additional modifications include a reduction in phospholipid polyunsaturation index (40→24% of total fatty acid tails) and a shortening of their acyl chains. The latter phospholipid alteration is reflected by a significant decrease in 20-22C (30→17%) along with a considerable increase of 16C (25→34%) fatty acid chain-lengths and it is additionally in accordance with an increased pRBCM fusogenic capacity (Hsiao et al. 1991).

3. NANOTECHNOLOGY

3.1. A brief history of nanotechnology

The concept of nanotechnology comprises every manipulation of matter from the atomic level and up to the supramolecular scale, thereby building up structures, particles and complex materials in the 1-100 nm size range (the so-called 'nanomaterials', Fig. 16). Importantly, the behavior and physical properties of particles at the nanoscale will be influenced by those forces predominating at the same level such as the subatomic fundamental forces (area of knowledge explained by quantum mechanics) and intermolecular interactions (e.g. ionic and dipole interactions, hydrogen bonds and Van der Waals forces). Nanomaterials performance and physicochemical properties: optical, electrical, density, magnetic, solubility or fluidic properties, among others; will therefore be defined by the effect and combination of the aforementioned forces (Panneerselvam & Choi 2014; Kim et al. 2010).

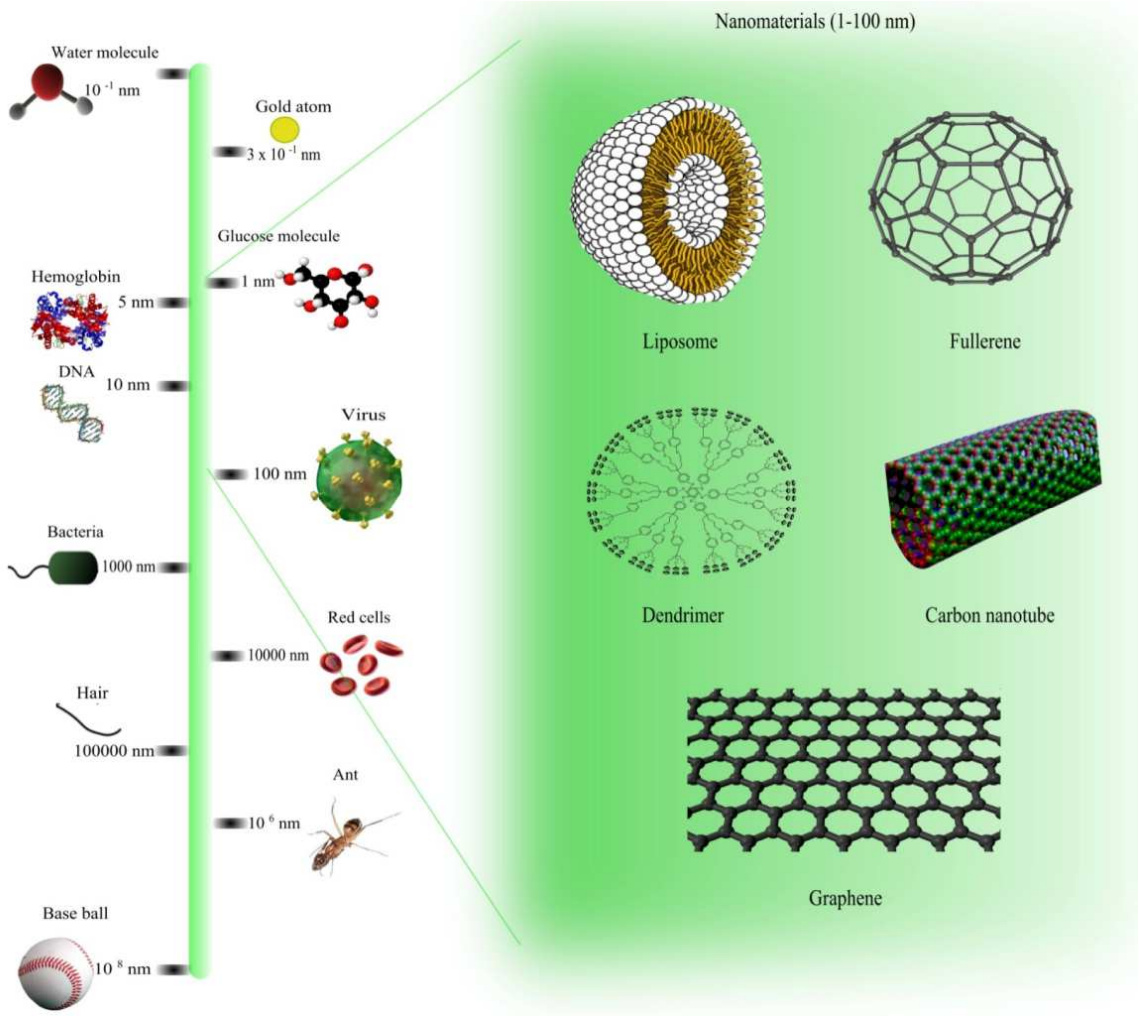

Figure 16. *Nanomaterials size in comparison with other particles and structures on the length scale*. Figure reproduced from (Panneerselvam & Choi 2014).

Nanotechnology is at present an area of extensive investigation, growing exponentially and receiving enormous investments of up to billions of dollars by governments and numerous private companies. Moreover, due to the versatility of nanomaterials in: (i) composition, (ii) physicochemical properties, (iii) complexity and (iv) structure; these can be designed for a wide range of applications in the industry, military and health research sectors as a few examples.

The origin of nanotechnology traces back to 1959 when Richard P. Feynman, one of the most important physicists of the 20th century and winner of the Physics Nobel Prize in 1965, introduced in his talk "*There's Plenty of Room at the Bottom"* the idea of building complex structures through the manipulation of more basic elements in a lower scale (e.g. the synthesis of a tissue of a few micrometers in size by means of the direct assembly of single carbon atoms). Feynman furthermore warned about the technical difficulties in understanding the new and different physical phenomena that would arise when operating below the molecular level.

However, nanotechnology would not appear as a single field until the 1980s when two major breakthroughs astonished the scientific community:

A) The invention of the scanning tunneling microscope in 1981 by the Physics Novel Prize-awarded Gerd Binnig and Heinrich Rohrer physicists (Binnig & Rohrer 1983). This innovative microscope allowed to visualize separate atoms for the first time in history and evolved later to diverse microscopy approaches that include (i) atomic force microscopy, (ii) photon scanning microscopy and (iii) scanning tunneling potentiometry among other techniques.

B) The discovery of the C_{60}:Buckminsterfullerene spherical molecule in 1985 by Harry Kroto, Richard Smalley and Robert Curl (Kroto et al. 1985), for which they received the Chemistry Novel Prize in 1996. Fullerenes comprise a family of carbon allotropes with many different shapes (e.g. spherical-C60, tubular-carbon nanotubes or ellipsoid), though all these distinct carbon atom rearrangements being primarily composed of a basic structural element, the 2D hexagonal lattice layer termed 'graphene' (Fig. 16). The unique properties of fullerenes along with their enormous capacity of derivatization have conferred to this nanomaterial a potential use in electronics, medical applications and the synthesis of new tissues (Bakry et al. 2007).

3.2. Medical application of nanotechnology

Nanomedicine involves the utilization of nanotechnology in the health sector. Some of the most important medical applications include the use of nanomaterials as: (i) imaging and biosensor tools, (ii) purification systems for complex matrices (e.g. using magnetic nanoparticles that have been coated with targeting agents specific for cells/proteins/toxins (Herrmann et al. 2013; Lee et al. 2014)), (iii) building block for tissue engineering, and (iv) carriers for the controlled delivery of drugs due to their prolonged half-lives in the body. Nevertheless, the major limitation in the medical use of nanomaterials probably encompasses a proper evaluation and understanding of their potential toxicity and environmental impact since in numerous cases, nanomaterials

incorporate elements of non-biological origin that have been seldom tested in biological conditions (van der Merwe & Pickrell 2012; Sharifi et al. 2012).

With regard to the use of nanomedicine for a better therapy visualization, it is important to highlight the application of quantum dots (i.e. cadmium selenide fluorescent nanoparticles whose emission wavelength is directly dependent on their size) as luminescent tags for the diagnosis and imaging of cancer, improving in this manner the magnetic resonance image acquisition (MRI) of tumoral tissues. Quantum dots can provide as well an excellent analysis of the distribution and metabolism in the body of targeted nanoparticles and other biologically active compounds (Walling et al. 2009; Schipper et al. 2009).

Moreover, biosensor devices based on lab-on-a-chip and microfluidic technologies as well as containing ligand-conjugated magnetic nanoparticles, have been developed as highly efficient diagnostic tools (Ying & Wang 2013). Finally, fullerenes and other nanoparticle-based structures serve as building blocks and/or biodegradable supports ameliorating the regeneration of damaged tissues and therefore being considered as a potential alternative to organ transplantation and synthetic implants in the future (Zhang & Webster 2009).

3.2.1. Controlled drug delivery

The first evidence of a controlled drug delivery (CDD) process was provided by the pioneer MD Judah Folkman in 1964 (Folkman & Long 1964). By means of the loading of small sealed silicone tubes with drugs (device named ‘Silastic capsule’) and their subsequent insertion in the left ventricular myocardium of dogs, he demonstrated that the cargo of such capsules could be released in a sustained manner once inside the body. Furthermore, such delivery mechanism was suggested to follow a zero order constant release rate.

First devices based on the CDD concept would be later designed in the 1970s-1980s as macroscopic inserts composed mainly of non-degradable silicone and poly(ethylene-vinyl acetate) (PEVA) polymers. Such inserts were successfully applied to the eye, the uterine cavity and the skin (Hoffman 2008). Importantly, Folkman and Bob Langer demonstrated in 1976 that sensitive compounds (e.g. proteins) could be administered still active using hydrophobic polymers such as PEVA (Langer & Folkman 1976).

The clinical practice of the CDD field evolved later in the second half of the 1980s to the synthesis of drug-loaded microscopic biodegradable polymers, mainly poly(glycolic acid) (PGA), poly(lactic acid) (PLA), and poly(lactic-*co*-glycolic acid) (PLGA). An additional remarkable polymeric particle composed of poly(hydroxypropyl methacrylamide) (PHPMA) and containing drugs covalently conjugated by a pendant-tetrapeptide and biodegradable linkage, would subsequently be synthesized and characterized by Jindra Kopecek, Karel Ulbrich and Ruth Duncan (Duncan et al. 1983; Ulbrich et al. 1980). Basically, all these vectors provided novel sustained drug delivery systems controlled by polymer degradation once administered. Efforts

were afterwards made in order to obtain much more uniform particles as well as improve drug loading efficiencies (Gombotz et al. 1991; Hoffman 2008).

In parallel to the obtention of the aforementioned CDD devices, three major successes would stimulate the development and engineering of nanoparticles as feasible drug delivery vehicles: (i) PEGylation, (ii) active targeting and (iii) the enhanced permeation and retention effect (EPR).

3.2.2. PEGylation

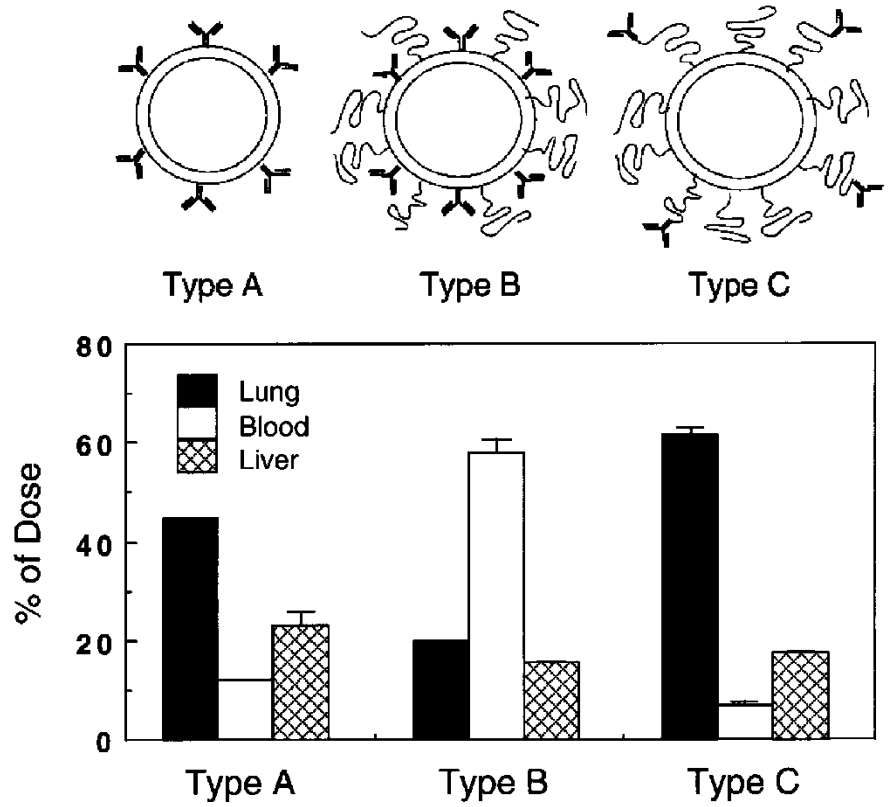

Figure 17. *Organ distribution analysis of PEGylated, lung-specific immunoliposomal (iLP) nanoparticles (90-130 nm)*. (Type A) Bulk iLP, (Type B) PEGylated iLP with antibodies conjugated at the lipid surface, (Type C) PEGylated iLP with antibodies attached at the distal end of PEG chains. Figure reproduced from (Maruyama 2002).

This derivatization process was defined for the first time by Frank Davis in the 1960s (Davis 2002) and refers to the attachment of poly(ethylene glycol) (PEG) chains to the surface of drug carrier particles (Fig. 17) (Maruyama 2002) or active macromolecules (e.g. proteins such as antibodies or even drugs). In both cases, the inclusion of PEG generates a steric barrier that protects the conjugated device once delivered inside the organism from: (i) immune system surveillance/reticuloendothelial system (RES)-mediated removal in the liver and spleen, (ii) nonspecific interaction and adsorption processes, (iii) self-aggregation by means of improving the solubility of hydrophobic elements, (iv) insertion of serum proteins and opsonization, (v) renal clearance of small nanoparticles by virtue of increasing their hydrodynamic diameter, and (vi)

enzymatic attack. All these features finally resulting in PEG-conjugated (PEGylated) constructs displaying longer retention times in circulation and, consequently, a prolonged therapeutic effect when loaded with active compounds (Longmire et al. 2008; Maruyama 2002).

Furthermore, PEG is well tolerated showing an absence of relevant toxic side effects at the concentration range and polymer size usually required for CDD strategies and very low immunogenic (Webster et al. 2009; Webster et al. 2007; Knop et al. 2010). Importantly, accelerated blood clearance rates have been observed for PEGylated vesicles when following repetitive injections (Ishida et al. 2002). Toxic cases have additionally been reported when administering PEG at too small (<0.4 kDa) or extremely large (>60 kDa) polymer sizes owing to either the formation of oxidation side-products or an inefficient removal from the body (PEG is not biodegradable), respectively. Considering the molecular weight threshold for a complete renal clearance of about 20-60 kDa, PEG in the 1-20 kDa size range has therefore been used in most of assays with PEGylated particles (Manjappa et al. 2011; Knop et al. 2010).

3.2.3. Enhanced permeation and retention (EPR) effect

The EPR effect by which nanoparticles and macromolecules do accumulate into solid tumors, mechanism referred as passive targeting as well, would be identified in 1984 by Ken Iwai, Hiroshi Maeda and coworkers using a dye-labeled, styrene-maleic anhydride (SMA) polymer (Iwai et al. 1984; Matsumura & Maeda 1986; Prabhakar et al. 2013). The presence of (i) fenestrated and leaky blood vessels in the tumor nearby area, feature that allows circulating bodies to extravasate into this damaged tissue, along with (ii) an impaired tumor draining capacity were suggested as capital elements responsible for the development of EPR.

3.2.4. Active targeting and its implications to CDD

The idea of a therapeutic agent selectively targeting a pathogen or a particular tissue/cell once inside the body was first time postulated by Paul Ehrlich in the early 1900s through the ‘magic bullet’ concept (Strebhardt & Ullrich 2008). Such site-specific strategy would be extraordinarily effective and extensively explored as drug delivery system for toxic and resistance-inducible compounds by virtue of concentrating the therapeutic agent into its site of action and, as a consequence, leading to local-high but overall-low drug amounts. Furthermore, reduced total drug payloads would be necessary in order to reach the desired therapeutic effect, significantly decreasing in this way both the likelihood of causing toxic side effects for the patient and the generation of drug-resistant pathogens.

However, the vast majority of therapeutic molecules do not concentrate at their site of action on their own -such behavior only displayed by a few macromolecules including antibodies (Allen 2002; Manjappa et al. 2011) and small peptides such as the RGD (Ruoslahti 1996)-, being largely distributed into body tissues once administered and therefore requiring their

encapsulation into ligand-functionalized, biodegradable carriers (Fig. 17). As an alternative approach, active compounds can also be directly conjugated with targeting ligands. The first proposal of a feasible site-specific CDD system would be provided by Professor Helmut Ringsdorf in 1975 with a germinal design of a targeted polymer-drug conjugate (Fig. 18). As an example, probably one of the first designs of a targeted nanocarrier prototype consisted of a drug-PHPMA polymer conjugate functionalized with galactose as hepatocyte-specific ligand, being employed as anti-cancer agent (Duncan et al. 1983 (1)).

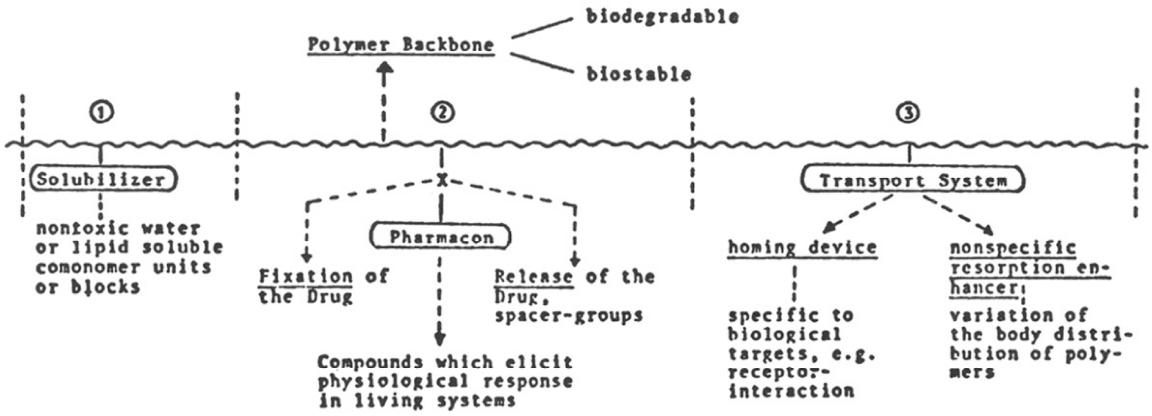

Figure 18. *Ringsdorf's proposal of a targeted polymer-drug conjugate for the first time in history*. Figure reproduced from (Ringsdorf 1975).

3.2.5. New nanomaterials for the design of novel drug delivery strategies

The repertoire of nanocarriers suitable for drug delivery strategies as well as capable of being conjugated with targeting ligands would considerably increase during the time period comprising the end of 1980s and the 1990s by means of the utilization of the following new nanomaterials: (i) polymeric micelles, (ii) nanocapsules, (iii) dendrimers, and (iv) liposomes (Fig. 19).

A) Polymeric micelles (Fig. 19C) are basically synthesized through the lipid micelle-like aggregation of amphiphilic copolymer tandem subunits (e.g. PEG-hydrophobic block as main combination). Such structure generates a water-repulsive core appropriate for the entrapment of lipophilic drugs (Kabanov et al. 1989). Besides, the generation of copolymers incorporating inner polycationic blocks have allowed their application as cell transfection agents (Harada 1999).

B) Dendrimers (Fig. 19D) comprise a vast family of polymers that are synthesized in a branched fashion, either following a convergent (i.e. the assembly of separated sections that are finally joined together) or divergent (i.e. the formation of extended branches from a single core) building strategy. Due to their precise and controlled synthesis, dendrimers can be conceivable in a wide range of shapes, sizes and physicochemical properties (Jain & Asthana 2007). Furthermore, targeting agents or other functionally active molecules can be appended to their surface allowing this branched polymers to be applied as site-specific drug carriers (Asthana et al. 2005; Nanjwade et al. 2009).

C) Polymeric and liposomal particles (Fig. 19A-B) comprising single or multiple peptide/lipid-based amphiphilic layers constitute the capsule-like group of nanocarriers. Remarkably, such biphasic feature enables the simultaneous encapsulation of hydrophilic, amphiphilic and lipophilic compounds within these vectors (Conniot et al. 2014). More recently, porous nanoparticle-supported lipid bilayers named 'protocells', which are composed of a single membrane adsorbed onto a spherical nanoporous silica particle, have been proposed as alternative nanocarriers for liver cancer therapeutics (Ashley et al. 2011). An unprecedented capacity for doxorubicin drug encapsulation together with an improved specificity towards the desired cancerous cells (after their conjugation with a targeting peptide in this case) was obtained for protocells when compared to liposomes and silica nanoparticles delivered on their own.

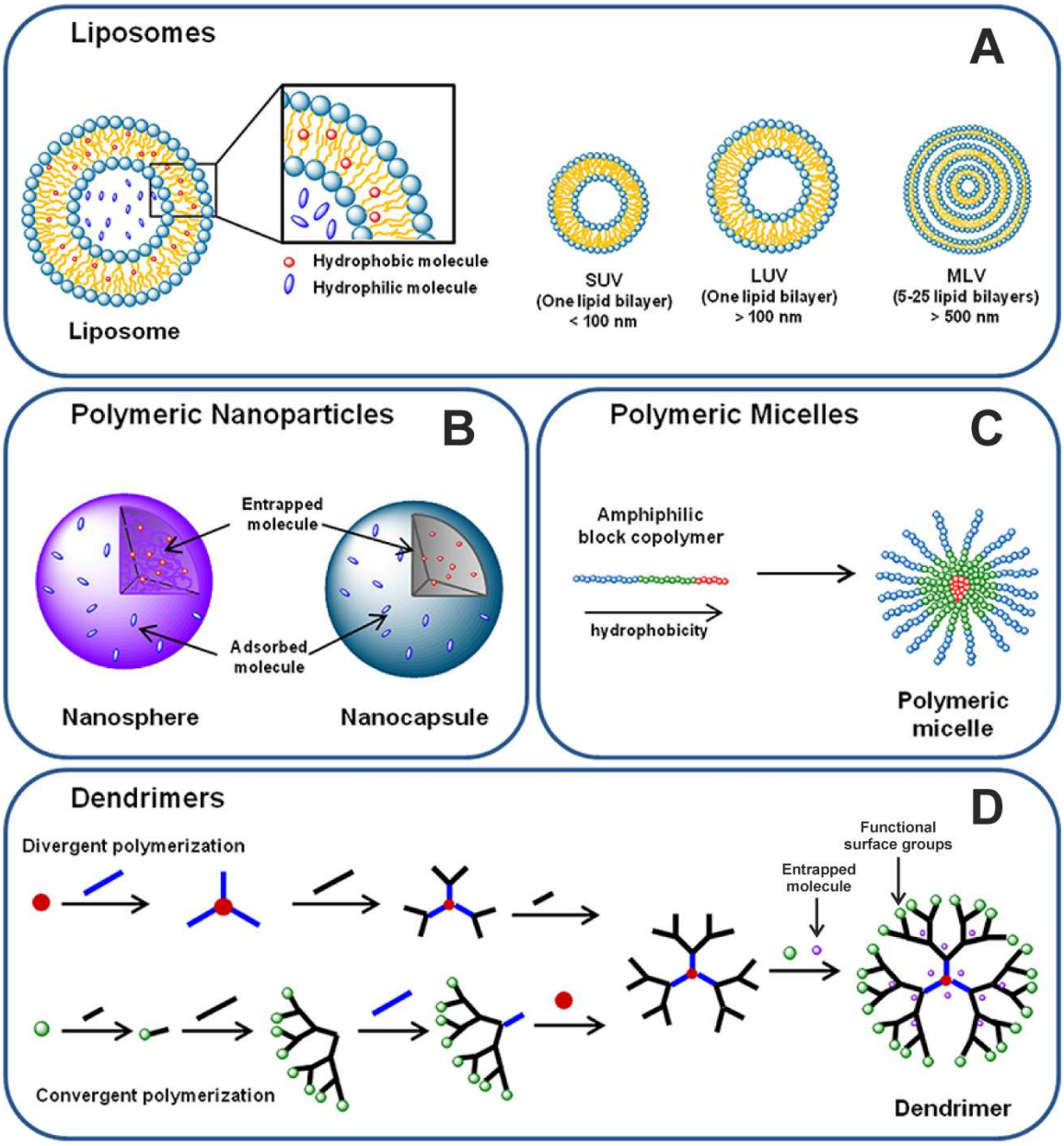

Figure 19. *Basic nanomaterials currently available for the design of drug delivery approaches*. Figure adapted from (Conniot et al. 2014).

3.3. Liposomal nanocarriers for drug delivery applications

3.3.1. Discovery and main properties of LPs

Liposome particles (LPs, Fig. 19A) were described for the first time in the early 1960s by Alec D. Bangham through the negative staining of phospholipids and their later observation under an electron microscope (Bangham & Horne 1964). Moreover, the complete characterization of this particles as (i) lipid-enclosed structures of up to a few micrometers in diameter as well as (ii) disruptable by treatment with detergents, would be thereafter provided in collaboration with Malcolm Standish and Gerald Weissmann (Bangham et al. 1965). It is important to point out that such important discovery gave rise to the current liposome industry. Finally, the word '*liposome'* (*lipo*/'fat' + *soma*/'body') would be later popularized by Weissmann.

Since their first identification, LPs have been the most widely used type of capsule-like nanoparticles owing to their:

- **Biocompatibility**; most of lipid components are biodegradable and non-toxic.
- **Prolonged blood circulation times** as a result of LP limited extravasation from blood vessels (LPs size >50 nm in diameter), which can be further improved through the attachment of PEG chains to the LP surface (see 3.2.2.). In this regard, plasma half-lives ranging from several hours to even a few days have been described for PEGylated LPs (Gabizon, Shmeeda, et al. 2003; Immordino et al. 2006), being these nanocarriers remarkably useful for the long-term maintenance of high drug levels in the bloodstream.
- **Easy particle surface chemical derivatizability** of either plain or crosslinker-derivatized phospholipids with functionally active molecules. Antibodies, carbohydrates, enzymes or fluorescent molecules are just a few examples of active elements for conjugation.
- **Lipid bilayer composition is easily adjustable** by just modifying the initial phospholipid mixture. Additional lipophilic compounds can be incorporated at this step, characteristic that makes LPs such an enormous versatile carrier.
- **Biphasic nature** comprising a lipophilic core (i.e. lipid hydrocarbon chains) along with a polar lipid bilayer surface and an aqueous lumen. All these compartments allowing LPs to simultaneously encapsulate hydrophobic, hydrophilic and amphiphilic molecules.
- **Improved stability of the encapsulated compounds**, which are protected inside the LP against external conditions that could trigger their degradation or inactivation. These undesired events are most likely to occur during *in vivo* applications.

Furthermore, LP size can be rapidly and uniformly adjusted by means of downsizing mechanisms (i.e. using filters with specific pore sizes). An extraordinarily uniform particle population can be thereby obtained displaying in turn the desired number of lipid bilayers. In this regard, LPs composed of a single membrane are classified according to their size into either small- or large-unilamellar vesicles (Fig. 19A): SUV (50-100 nm in diameter) or LUV (100-250 nm in diameter),

respectively. By contrast, those LPs containing multiple layers (multilamellar vesicles, MLV) are bigger in size and can reach diameters of up to 1-5 µm (Fig. 19).

3.3.2. Versatility of LPs: lipid bilayer acyl chains organization

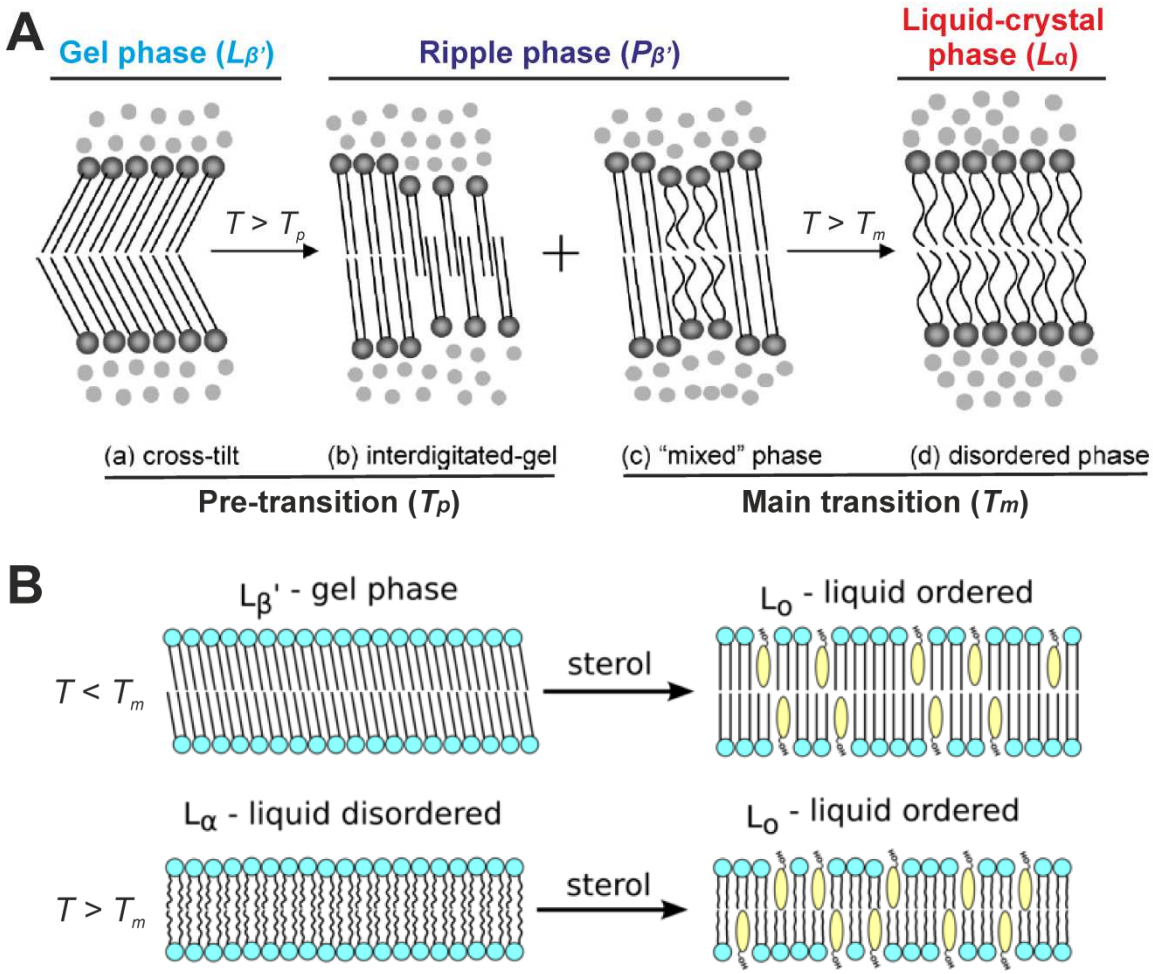

Figure 20. *Illustration of all possible phospholipid acyl chain organization states.* (A) Schema depicting the two principal lipid phase transitions (T_p and T_m) as a function of temperature (T). (B) Generation of a liquid but ordered and stabilized lipid bilayer through the inclusion of sterols. Figure adapted from (Qin et al. 2009) and http://physwiki.ucdavis.edu/Wikitexts/UCD_BPH241/Membrane_Phase_Transitions.

The phospholipid composition and their physicochemical properties have a major role in defining the characteristics of the LP in such a way that vesicle stability and solute permeation rate will be influenced by the hydrocarbon chain ordering of the membrane-constituting lipids (Maurer et al. 2001).

Lipid bilayer in the gel phase

Neutrally-charged, saturated phospholipids such as the 1,2-distearoyl-*sn*-glycero-3-phosphocholine (DSPC, C18:0, T_m 55 ºC) or the 1,2-dipalmitoyl-*sn*-glycero-3-phosphocholine (DPPC, C16:0, T_m 41 ºC) will form once dispersed in aqueous solution and at room temperature

(*T*), highly ordered, compact and low permeable membranes in which lipid acyl chains are organized in a cross-tilted manner (Qin et al. 2009; Riske et al. 2009). Such strong arrangement is defined as the 'gel phase' ($L\beta'$, $T < T_p$, Fig. 20) and protects the lipid bilayer against the insertion of external elements (e.g. plasma proteins), process that could otherwise destabilize the LP inducing in turn the leakage of internal contents or, alternatively, trigger its removal by phagocytic cells under *in vivo* conditions (Semple et al. 1998).

Lipid bilayer in the liquid ordered phase and PEGylation of LPs

Cholesterol is commonly included into this well-organized $L\beta'$ phospholipid structure in order to (i) improve its fluidity, (ii) avoid membrane packing defects, and (iii) eventually increase the LP plasma half-life in a few hours or even longer (Gabizon & Papahadjopoulos 1988). The resulting physical state of the lipid bilayer has been named as the 'liquid ordered phase' (L_o, Fig. 20B). LP circulation half-life can be further prolonged when PEGylated as aforesaid, obtaining the so-called 'sterically stabilized' or 'stealth liposome' (Immordino et al. 2006; Maurer et al. 2001; Allen & Hansen 1991). PEG-conjugated lipids such as the 1,2-distearoyl-*sn*-glycero-3-phosphoethanolamine-N-[methoxy(polyethylene glycol)-2000] (DSPE-PEG2000, C18:0) are commonly employed for this purpose.

Lipid bilayer in the liquid-crystal state and phase transition

The physical state of the lipid bilayer is influenced by the temperature of the system and is defined by a phase transition-melting temperature (T_m) specific for each type of phospholipid. Such parameter describes the temperature at which the tightly packed $L\beta'$ arrangement undergoes a drastic conformational change becoming more fluid, disorganized and less compacted. This new state has been named as the 'liquid-crystal disordered phase' ($L\alpha$, Fig. 20A) and is associated with a high solute permeability and an increased capacity for the insertion of plasma proteins (Gabizon & Papahadjopoulos 1992; Ishida et al. 2002). However, the stability of LP membranes in the $L\alpha$ phase can also be improved through the incorporation of cholesterol, obtaining again the ordered L_o phase (Fig. 20B), and PEG-conjugated lipids (Maurer et al. 2001).

Some examples of phospholipids forming lipid bilayers in the disordered $L\alpha$ state at room temperature include the 1,2-dioleoyl-*sn*-glycero-3-phosphocholine (DOPC, C18:1, T_m -17 ºC) and the 1,2-dioleoyl-*sn*-glycero-3-phospho-(1'-*rac*-glycerol) (DOPG, C18:1, T_m -18 ºC). The presence of unsaturations in these phospholipids, in the form of carbon-carbon *cis* double bonds, introduce bends in their fatty acid chains that consequently impair their ordered state and significantly decrease in turn the temperature required for the $L\beta'$ to $L\alpha$ lipid phase transition. Finally, both the T_m and the lipid bilayer packing degree are also influenced by phospholipid tails length, proportionally increasing for longer hydrocarbon chains (i.e. more stable bilayers): DSPC-C18 (T_m 55 ºC) > DPPC-C16 (T_m 41 ºC) (Xiang & Anderson 1997; Paula et al. 1996).

It is important to highlight that an intermediate sate ($L\beta' - L\alpha$) displaying partially-disordered acyl chain structures occurs in lipid bilayers at approximately 5-15 degrees below the T_m of their

constituting lipids. Such arrangement is known as the 'ripple phase' ($P\beta'$, Fig. 20A) and is only found in some groups of lipids such as the phosphatidylcholines (PCs). Membranes in the $P\beta'$ state are composed of phospholipid tails organized in: (i) interdigitated $L\beta'$ arrangements and (ii) mixtures of both $L\beta'$ and $L\alpha$ structures; such complex lipid organization giving rise to the formation of membrane ripples (de Vries et al. 2005; Riske et al. 2009; Yamazaki et al. 1992). Besides, a pre-transition temperature (T_p) has been identified defining the conformational change from the $L\beta'$ to the $P\beta'$ state. As an example, a T_p of 40 ºC has been described for the DSPC-cholesterol 80:20 molar mixture (Xiang & Anderson 1997) in comparison with the DSPC specific T_m of 55 ºC.

Optimized LP formulations for their application in vivo

In light of the above, LP formulations containing (i) saturated phospholipids, (ii) cholesterol and (iii) PEG-conjugated lipids, are one of the most preferred for *in vivo* applications. Actually, some of these LP compositions are running clinical trials at present and even a few of them have been approved for clinical use (Fan & Zhang 2013). Doxil® and Lipodox products, which have been authorized for the treatment of Kaposi's sarcoma and metastatic ovarian cancer, are just a few examples (Barenholz 2012; Andreopoulou et al. 2007; Chou et al. 2006).

Alternative LP formulations including charged and/or non-bilayer-forming lipids have been investigated in parallel as: (i) gene carriers for cell transfection purposes in the form of cationic liposome-DNA complexes, also named 'lipoplexes' (Masotti et al. 2009), and (ii) fusion-mediated delivery approaches (Bailey & Cullis 1997; Holovati et al. 2008). Unfortunately, undesired events including nonspecific interactions (e.g. stimulated macrophage uptake (Hsu & Juliano 1982)), an increase in plasma protein binding as well as an enhanced complement activation, have been reported for these LP compositions taking place during *in vivo* assays and, as a consequence, hampering their clinical application (Gabizon & Papahadjopoulos 1992; Ishida et al. 2002). Moreover, improved LP blood circulation times have been reported through the incorporation in restricted amounts (≤ 20% of the total lipids) of phosphatidylinositol and monosialogangliosides (Gabizon & Papahadjopoulos 1992). These glycolipids are composed of a polar carbohydrate-containing headgroup and a negatively-charged but sterically-hindered moiety.

3.3.3. Versatility of LPs: lipid bilayer permeability

Description of the permeability coefficient and examples

The time required for a particular permeant to cross an interface (e.g. a biological membrane) is defined by the permeability coefficient (p) as the distance of interface traversed per unit of time and usually expressed as centimeters per second (cm/s). With regard to LP membranes, their permeability to water and solutes, the latter mainly including uncharged polar molecules and small ions, has been extensively studied and their p values have been retrieved under a wide range of experimental conditions.

As a general overview, considerably high *p* values of 1E-02 to 1E-04 cm/sec have been obtained for water across LP membranes in a *Lα*-disordered state (Paula et al. 1996; Maurer et al. 2001; Cullis et al. 1996), which correspond to times ranging from 0.2 to 20 milliseconds for the release of half the encapsulated material ($t_{1/2}$, Table 2). Similar *p* values of about 1E-03 to 1E-06 cm/sec along with a related $t_{1/2}$ of less than 2 seconds have been observed for small polar organic molecules such as acetic acid, glycerol and urea (Xiang & Anderson 1997; Paula et al. 1996).

By contrast, lipid membranes are almost impenetrable to ionized molecules (Warhurst et al. 2003) and particularly impermeable to small ions such as calcium, sodium and potassium. Quite small *p* values of approximately 1E-11 to 1E-14 cm/sec have been reported for these ions (Paula et al. 1996; Maurer et al. 2001), thereby requiring more than 2 days and even several years to halve their encapsulated amounts when considering a LP system.

Finally, amphiphilic organic drugs (e.g. CQ, PQ and artemisinin derivatives) lye in between the aforementioned groups with *p* values ranging from 1E-05 to 1E-07 cm/sec (Fade 1998) and, consequently, these molecules are highly membrane permeable and will be theoretically completely released from LPs in less than a minute (Table 2).

p (cm/sec)	$t_{1/2}$ (ms)	$t_{9/10}$ (ms)	permeant examples
1.E-01	0.02	0.07	
1.E-02	0.20	0.65	water
1.E-03	1.96	6.52	
1.E-04	19.64	65.24	small polar organic molecules, H^+/OH^- under small pH gradients (<3 pH units)
1.E-05	196.35	652.40	
p (cm/sec)	$t_{1/2}$ (min)	$t_{9/10}$ (min)	
1.E-06	0.03	0.11	amphiphilic organic drugs
1.E-07	0.33	1.09	
1.E-08	3.27	10.87	H^+/OH^- under large pH gradients (≥3 pH units)
1.E-09	32.73	108.73	
p (cm/sec)	$t_{1/2}$ (h)	$t_{9/10}$ (h)	
1.E-10	5.45	18.12	small ions (K^+) across lipid bilayers containing short-chain phospholipids (<C18)
1.E-11	54.54	181.22	
p (cm/sec)	$t_{1/2}$ (days)	$t_{9/10}$ (days)	
1.E-12	22.73	75.51	small ions (Ca^{2+}, K^+) across lipid bilayers containing long-chain phospholipids (C18 or longer)
1.E-13	227.26	755.09	
p (cm/sec)	$t_{1/2}$ (years)	$t_{9/10}$ (years)	
1.E-14	6.23	20.69	small ions (Na^+)

Table 2. *Differences in the time required for the release of one-half ($t_{1/2}$) or nine-tenths ($t_{9/10}$) of LP-encapsulated solutes in accordance with their permeability coefficient values (p)*. Permeant examples are included from bibliography (references are appended throughout the text). Theoretical times calculated for a vesicle 85 nm in radius (R) and encapsulating an initial concentration Ci(0) of a solute according to the formula $Ci(t) = Ci(0) \times \exp(-3 \times p \times t/R)$, which is described in (Maurer et al. 2001; Cullis et al. 1996). A negligible external solute concentration is considered for its LP-release calculation.

Proton/hydroxide flux across the lipid bilayer

Large variations in membrane permeability to protons have been reported with regard to membrane fluidity, the size of the pH gradient and the incorporation of buffering agents. Whereas LPs containing unsaturated bilayers in the $L\alpha$ phase could theoretically release protons in a few milliseconds (Table 2, reported *p* of ~1E-04 cm/sec (Paula et al. 1996)), those saturated and in the $L\beta'$ phase would display prolonged release $t_{1/2}$ of a few seconds (observed *p* ranging from 1E-05 to 1E-06 cm/sec (Elamrani & Blume 1983).

Moreover, proton leaking can be further delayed in the presence of large pH gradients (≥ 3 pH units) resulting in theoretical $t_{1/2}$ from a few minutes to approximately half an hour (Table 2, described *p* from 1E-08 to 1E-09 cm/sec (Zeng et al. 1993; Deamer & Nichols 1983)). Such gradient has been suggested to generate a diffusion potential that limits in turn the proton/hydroxide net transmembrane flux. Besides, large pH gradients can be further stabilized for long-term purposes (proton $t_{1/2}$ from days up to even a month) by means of loading LPs with low membrane permeable buffering agents at high molarities (e.g. incorporation of 0.1-0.2 M citrate buffer, pH 3.0-4.0, into LPs suspended in 10 mM phosphate-buffered saline, pH 7.4 (Madden et al. 1990; Qiu et al. 2008; Stensrud et al. 2000)). LP-encapsulated buffering agents quickly neutralize in this regard the efflux/influx of proton/hydroxide ions through small changes in their proton-ionizable species.

3.3.4. Factors regulating the release kinetics of LP-encapsulated molecules

Observed parameters modulating the aforementioned coefficient *p* and, as a consequence, having a major influence on the LP membrane permeability to encapsulated substances include: (i) the temperature of the system with a positive correlation (Xiang & Anderson 1997) and (ii) phospholipid acyl chains packing degree (i.e. the free surface area available between lipid molecules) along with the permeant volume and its cross-sectional area with a negative correlation (Xiang & Anderson 1997; Xiang & Anderson 1998).

Moreover, the presence of membrane-stabilizing agents such as the already mentioned sterols (Fig. 20B), not only considerably lowers the fluidity and permeability of $L\alpha$-membranes in almost one order of magnitude through the formation of the L_o phase, but also competes with the permeant molecules for the above-mentioned inter-lipid free space (Dordas & Brown 2000; Xiang & Anderson 1997). By contrast, an opposite behavior is observed for $L\beta'$ lipid bilayers, in which sterols increase their fluidity and permeability (Fig. 20B). Such differences are reflected in their coefficient *p*, which becomes augmented in about one order of magnitude after the incorporation of sterols (Xiang & Anderson 1997; Stensrud et al. 2000).

Besides, the physicochemical properties of encapsulated molecules will also define their preferential route to cross the lipid bilayer and so to escape from LPs. Two main mechanisms have been theorized to account for the leakage of water-soluble compounds: the ‘solubility-

diffusion theory' (Finkelstein 1988) and the 'transient pore model' (Lawaczeck 1988). Moreover, a third kind of physical events regulate the LP encapsulation and release kinetics of poorly water-soluble compounds (Loew et al. 2011).

Solubility-diffusion theory and pH gradient-driven accumulation of proton-ionizable compounds

The 'solubility-diffusion theory' (Finkelstein 1988) has been broadly used to characterize the permeability of membranes to organic compounds and particularly applied to the knowledge of drugs distribution throughout the organism. This concept treats the LP as a biphasic system (Fig. 21) in which a thin layer of hydrophobic matter (LP membrane hydrocarbon core) is surrounded by an aqueous environment. Considering this system, amphiphilic encapsulated molecules initially distributed far and wide the LP inner aqueous space will (i) dissolve-partition first into the membrane hydrophobic core, (ii) diffuse across it, and finally (iii) solubilize again into a second, external aqueous phase. Besides, such migration mechanism has been found to be modestly dependent on membrane thickness, fact that indicates a fast movement of solutes once dissolved into the lipid bilayer inner core (Paula et al. 1996).

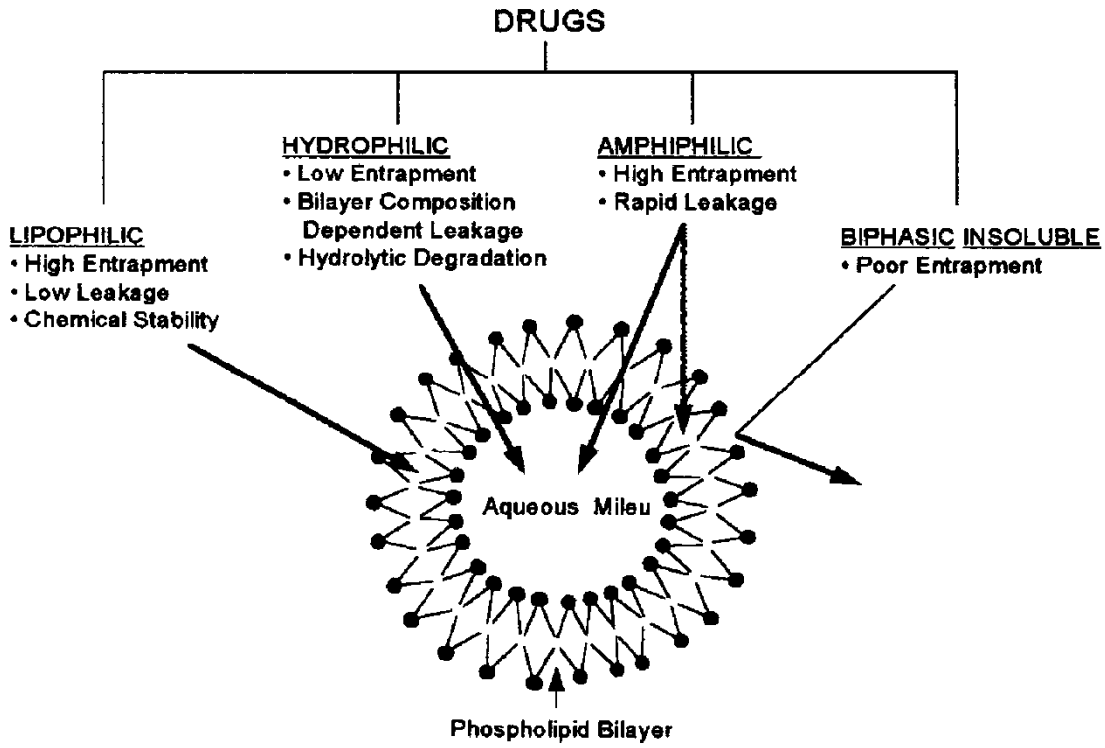

Figure 21. *Classification of drugs and their theorized incorporation into the LP according to their physicochemical properties*. Figure reproduced from (Gulati et al. 1998).

The movement of molecules following the aforementioned transmembrane diffusive pathway is driven by differences in their concentration among the distinct vesicular compartments and such flux will continue until an equilibrium concentration between phases is reached. In this regard, the organic/aqueous (org/aq) phase concentration ratio for unionized compounds at equilibrium is expressed as the partition coefficient (*P*). This coefficient is commonly measured in the

octanol/water biphasic system (Leo et al. 1971) and is described in detail in Eq. 1 (left) using a drug as permeant example.

(1) $$P = \frac{\frac{\text{mol Drug}_{org}}{\text{Vol}_{org}}}{\frac{\text{mol Drug}_{aq}}{\text{Vol}_{aq}}}, \quad D = \frac{\frac{\text{mol Drug}_{org}}{\text{Vol}_{org}}}{\frac{\text{mol Drug}_{aq} + \text{mol Drug}^{H+}{}_{aq} + \text{mol Drug}^{2H+}{}_{aq}}{\text{Vol}_{aq}}}$$

(2) $$\log D = \log\left[\frac{\text{mol Drug}_{org} \times \text{Vol}_{aq}}{\text{Vol}_{org} \times \text{mol Drug}_{aq}}\right] - \log\left[1 + \frac{\text{mol Drug}^{H+}{}_{aq}}{\text{mol Drug}_{aq}} + \frac{\text{mol Drug}^{2H+}{}_{aq}}{\text{mol Drug}_{aq}}\right]$$

(3) $$\text{pH} = \text{pK}_{a1} + \log\left(\frac{\text{mol Drug}}{\text{mol Drug}^{H+}}\right), \quad \text{pH} = \text{pK}_{a2} + \log\left(\frac{\text{mol Drug}^{H+}}{\text{mol Drug}^{2H+}}\right)$$

(4) $$\log D = \log[P] - \log\left[1 + 10^{(\text{pK}_{a1} - \text{pH})} + 10^{(\text{pK}_{a1} + \text{pK}_{a2} - 2\times\text{pH})}\right]$$

(5) $$\frac{[\text{All drug spp.}_{aq}]_{in}}{[\text{All drug spp.}_{aq}]_{out}} = \frac{1 + 10^{(\text{pK}_{a1} - \text{pH}_{in})} + 10^{(\text{pK}_{a1} + \text{pK}_{a2} - 2\times\text{pH}_{in})}}{1 + 10^{(\text{pK}_{a1} - \text{pH}_{out})} + 10^{(\text{pK}_{a1} + \text{pK}_{a2} - 2\times\text{pH}_{out})}}$$

Moreover, a distribution coefficient (*D*) has been reported (Scherrer & Howard 1977; Warhurst et al. 2003) defining the organic/aqueous partition of partially ionized substances at a particular pH and considering the unionized species as the only form able to solubilize into the membrane organic core. This coefficient *D* is described in detail in Eq. 1 (right) and Eq. 2 (log *D*) using a diprotic, weakly basic drug (e.g. quinine, chloroquine or primaquine antimalarials) as permeant example with the corresponding ionization species in solution: Drug (unionized-deprotonated) and the ionized-protonated Drug^{H+} and Drug^{2H+} forms.

Coefficient *D* can be calculated from a knowledge of *P*, pK_a and pH (Eq. 3-4) in cases where pKa-pH difference is more than one log unit (Scherrer & Howard 1977; Hansch et al. 1995). Besides, on account of the variations in the relative molar amounts of permeant ionized species occurring as a function of solution pH (Eq. 3, adapted from the Henderson-Hasselbalch equation, and Fig. 22), drug accumulation ratios in vesicular compartments and in response to transmembrane pH gradients can be calculated (Eq. 5) (Krogstad & Schlesinger 1986). In light of the weakly basic drug permeant example exposed here (e.g. containing proton-ionizable groups with pKas of >7.4), its almost full protonation inside an acidic vesicle (e.g. pH_{in} of 4.0) results in a complete ionization of the molecule and, consequently, hinders its capability to solubilize into the vesicle bilayer and the subsequent leakage. Such encapsulation mechanism is efficiently

stabilized by placing the former acidic vesicle into a basic aqueous environment (e.g. pH_{out} of 7.4).

Finally, it is important to note that the aforesaid pH gradient-dependent cumulative strategy has been successfully applied to the CDD field for the active encapsulation of weakly basic (Stensrud et al. 2000; Warhurst et al. 2003; Cullis et al. 1991; Madden et al. 1990) and acid (Clerc & Barenholz 1995; Hwang et al. 1999; Avnir et al. 2011) compounds into liposomal nanocarriers.

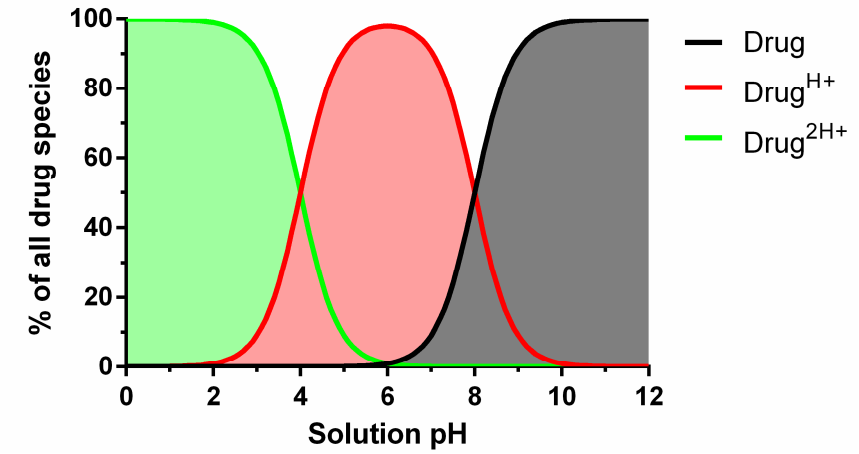

Figure 22. *Calculated ionization species as a function of solution pH for a weakly basic drug model containing proton-ionizable groups (pK_{a1} 8.0 and pK_{a2} 4.0).*

In light of the above, the leaking speed of proton-ionizable amphiphilic compounds from LPs (Fig. 21) will be particularly influenced by: (i) their lipophilicity, property reflected in coefficients *P* and *D*, and (ii) the percentage of their unionized species among all ionization forms at physiological pH. In this regard, (i) log *P* values ranging from 2 to 5 units along with (ii) relative molar amounts of >0.01% corresponding to the unionized species of compounds at pH 7.4, are commonly reported for highly effective drugs that freely diffuse across biological membranes. Some examples of antimalarials displaying such properties include, among others, CQ, PQ and the artemisinin derivatives (Warhurst et al. 2003; Shah et al. 2012; Nair et al. 2012).

By contrast, proton-ionizable, highly hydrophilic molecules would leak out of LPs following the solubility-diffusion theory as well but requiring much longer times than the aforementioned amphiphilic compounds. Drugs exhibiting these properties are characterized by a small uncharged population at physiological pH and negative log *P* values. Probably the best antimalarial example is fosmidomycin with a log *P* of -2.21 and 2.5 × 10^{-4}% of total drug molecules corresponding to the unionized species (http://www.chemicalize.org)

Liposomal encapsulation of fully ionized compounds and small ions

Completely ionized substances such as the acidic fluorescent dye pyranine (also named 8-hydroxypyrene-1,3,6-trisulfonic acid or HPTS), which simultaneously contains 3 to 4 negatively-charged moieties at the pH range 1.0-14.0 (http://www.chemicalize.org), will remain enclosed into the LP aqueous core with a negligible release over time and, as a consequence, this type of

molecules has been commonly classified as membrane-impermeable. In this regard, fully ionized compounds have been extensively used as fluorescent indicators for the LP inner aqueous cargo (Avnir & Barenholz 2005; Straubinger et al. 1990; Kono et al. 1997).

Moreover, particularly high release rates have been described for small ions from LPs composed of short-chain phospholipids (14-17 carbons) and a membrane in the *Lα* phase (Paula et al. 1996). As some examples, permeability coefficient (*p*) values have been reported of about (i) 1E-02 to 1E-04 cm/sec in the case of protons (LP-release $t_{1/2}$ of <20 ms, Table 2), and (ii) ~1E-10 cm/sec with regard to potassium (LP-release $t_{1/2}$ of a few hours, Table 2). Such ion leaking process has been found to be largely dependent on the packing degree of membrane phospholipids as well as the length of their fatty acid chains, and has been theoretically explained through the 'transient pore model' (Lawaczeck 1988). This approach considers the formation of hydrated transient pores throughout the LP membrane hydrocarbon core, which are in turn caused by structural defects or thermal fluctuations.

Finally, the transmembrane flux of small ions at longer phospholipid tail lengths (≥ 18 carbons) has been predicted by the 'solubility-diffusion model' and thus modestly dependent on further changes in the lipid bilayer thickness (Paula et al. 1996). Significantly decreased *p* values are obtained under these conditions with ~1E-05 and 1E-12 cm/sec in the case of protons and potassium, respectively (Table 2).

Liposomal encapsulation of hydrophobic compounds

Lipophilic compounds, which are characterized by large partition coefficient (*P*) values, will become almost completely internalized within the hydrocarbon region of the LP membrane (Fahr et al. 2005). Such entrapment has been proposed to occur with the long axis of cylinder-shaped substances placed in parallel to phospholipid acyl chains (Fig. 23A). Indeed, most of drugs display this cylinder-like structure with approximately 1 to 2 nm-length and 0.6 to 1.2 nm-width (http://www.chemicalize.org), feature that allows their stable internalization into the LP membrane once unionized. One of the best examples of hydrophobic antimalarials in this regard is lumefantrine displaying an observed log *P* of about 8 to 9 units (Wahajuddin et al. 2014; Amin et al. 2013), remarkably high if compared to other well-known lipophilic molecules such as cholesterol and DOPC (log *P* values of 7.11 and 9.17, respectively, http://www.chemicalize.org).

Besides, the aforesaid lipophilic drug-lipid bilayer association (Fig. 23A) would be the most thermodynamically favorable (Xiang & Anderson 1998; Fahr et al. 2005) by means of (i) minimizing the membrane structural perturbation effects caused after drug inclusion while at the same time (ii) allowing the surface exposure of polar and/or ionizable groups present at the hydrocarbon tail edge of the entrapped molecule (e.g. members of the 4- and 8-aminoquinoline antimalarial drug families). By contrast, other molecules with structures differing from the phospholipid-like cylinder model (e.g. the spherical-shaped artemisinin antimalarial) would induce

membrane structural defects resulting in unstable drug-membrane associations (Fig. 23B) and, finally, leading to lower amounts of LP-encapsulated drug.

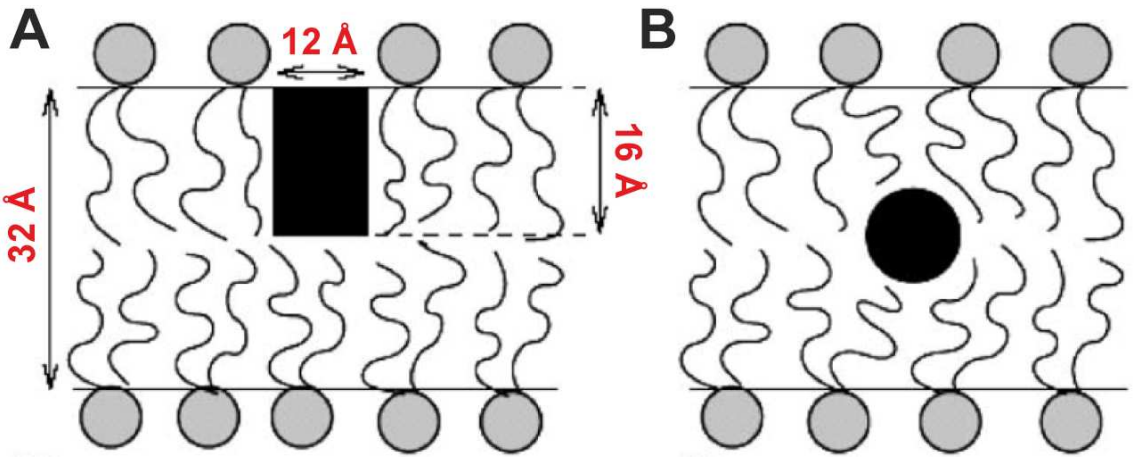

Figure 23. *Lipophilic drug-membrane association examples*. (A) Energetically-favorable interaction for cylinder-shaped molecules. (B) Unfavorable association for spherical-shaped molecules. Figure adapted from (Fahr et al. 2005).

Once incorporated into the lipid bilayer, poorly water-soluble compounds can be exchanged with other bilayers by either (i) random collision events taking place between LPs and cells or even between LPs themselves (Jones & Thompson 1989; Loew et al. 2011), or (ii) through their passive transference across the external aqueous environment in the case of separated membranes (Lange et al. 1983; McLean & Phillips 1981). The latter exchange mechanism has been proposed as predominant for compounds displaying energetically-unfavorable interactions with membranes as well as those less lipophilic, and particularly dependent on the dilution applied to the encapsulating vesicle (i.e. an increase in the volume of the external aqueous phase).

In light of the above, whereas times as short as a few minutes have been reported for the transference of low lipophilic elements (e.g. LP-release $t_{1/2}$ of 4.5 min for the spherical-shaped drug cyclosporin A, log *P* of 3.64), much longer times have been observed for more lipophilic and cylinder-shaped compounds such as cholesterol (log *P* of 7.11) and cholesteryloleoylether (log *P* of >9.0) with LP-release $t_{1/2}$ of 60 min and 256 days, respectively (Fahr et al. 2005; Fahr & Seelig 2001). All three mentioned log *P* values have been retrieved from http://www.chemicalize.org.

Finally, in this particular LP-lipophilic drug encapsulation model, the overall phospholipid concentration (i.e. the organic phase of the system) will define the amount of drug capable of being internalized. Drug to lipid molar ratios exceeding 1:20 have been described in this regard to form anomalous structures such as distorted bilayers and drug-lipid aggregates, not only impairing in this way the correct transference of the drug but also irreversibly increasing the size of the carrier vesicle (Fahr et al. 2005).

3.4. Immunoliposomal targeted drug delivery

3.4.1. LP surface chemical derivatizability

Liposomal nanocarriers can be designed for a wide range of applications such as (i) targeting agents for the specific labeling of cells or tissues, (ii) therapeutic agents for the site-specific delivery of biologically active compounds, and (iii) cell transfection purposes among others. Such functional LPs can be easily obtained through the attachment of active molecules to the vesicle membrane, either as individual elements with a lipophilic region embedded into the LP membrane or, alternatively, conjugated to surface-exposed and reactive phospholipid headgroups. Polymers (Zalipsky 1993), proteins (mostly antibodies), peptides (Xiong et al. 2005; Kondo et al. 2004), carbohydrates (Eliaz et al. 2004), vitamins (Gabizon, Horowitz, et al. 2003), fluorescent lipids (Baumgart et al. 2007), and nucleic acid aptamers (Sun et al. 2014), as a few examples, have been successfully incorporated into LPs and their effect favorably validated.

Among the aforementioned types of functionalized liposomal particles developed, those conjugated with antibodies (defined as 'immunoliposomes' or iLPs) have been one of the most used and are particularly suitable for the targeted delivery of anticancer therapeutic agents into tumoral cells. Besides, antibodies against the HER2, EGFR, MT1-MMP, GAH, VCAM-1 and CD19 receptors as well as specific for the GD2 ganglioside, among others, have been reported as successful targeting agents for LP-based approaches (Torchilin 2005; Manjappa et al. 2011; Baryshnikova & Baryshnikov 2013). Even some of these targeted nanocarriers are currently running clinical trials, though none approved yet (Manjappa et al. 2011; Baryshnikova & Baryshnikov 2013).

Furthermore, LP-based anticancer therapies have been remarkably improved by means of their conjugation with (i) antibodies recognizing cancer cell-exposed epitopes that trigger receptor-mediated endocytosis (Sapra & Allenz 2002), along with (ii) peptides that mediate the iLP escape from endosomal organelles (Mastrobattista et al. 2002; Nakase et al. 2010). Importantly, the latter step allows to the delivery of the iLP cargo into the targeted cell cytoplasm.

3.4.2. Antibody conjugation strategies

Several antibody coupling approaches for the functionalization of LPs are currently available (Manjappa et al. 2011; Hermanson 2008; Ansell et al. 2000), though four principal reactions are employed in most of these methodologies: (i) disulfide bond formation between pyridyldithiols and thiols (both molecules providing carbon-bonded sulfhydryl groups, R-SH, Fig. 24A-C), (ii) the reaction of hydrazides (R-NH-NH_2) with aldehyde groups, which yields hydrazone bonds (Fig. 24B), (iii) the formation of amide bonds between amino and either carboxyl or N-hydroxysuccinimide (NHS) ester groups (Fig. 24C), and (iv) the generation of thioether bonds between thiols and maleimide groups (Fig. 24D).

Importantly, those reactions involving the formation of amide and thioether linkages provide the most stable conjugations over a wide range of pH (Manjappa et al. 2011; Loughrey et al. 1990; Martin & Papahadjopoulos 1982). In comparison, hydrazone bonds are stable at physiological pH but become slowly hydrolyzed over time. Such degradation process is particularly noteworthy after one month storage and becomes further accelerated under acidic conditions (Ansell et al. 1996; Manjappa et al. 2011), thereby hydrazone conjugates commonly requiring the application of special stabilizing-reducing agents (e.g. sodium cyanoborohydride) or, alternatively, the generation of multiple hydrazone linkages between the antibody and the liposomal carrier (Hermanson 2008; Hage 2000; Abraham et al. 1991). Finally, because disulfide bonds are highly sensitive to reducing conditions and become as well easily disrupted in the presence of serum (Martin & Papahadjopoulos 1982), antibody conjugation approaches based on this linkage are no recommended for *in vivo* applications.

LP-antibody functionalization strategies have been optimized through the incorporation of heterobifunctional crosslinking agents, allowing in this way to: (i) the chemical accessibility of otherwise sterically hindered reactive groups, (ii) an increase in the mobility of the conjugated antibody for a better antigen recognition (Fleiner et al. 2001), and (iii) avoid the formation of antibody self-aggregates while, at the same time, preserve their functionality. In this regard, the 3-[2-Pyridyldithio]propionyl hydrazide (PDPH) (Ansell et al. 1996) and the N-Succinimidyl S-Acetylthioacetate (SATA) (Fleiner et al. 2001) have been some of the most widely employed and efficient crosslinking molecules (Fig. 24B-C).

Furthermore, polyethylene glycol (PEG)-derivatized phospholipids incorporating a reactive moiety at the end of the PEG-spacer chain, such as the DSPE-PEG-Hydrazide (Zalipsky 1993) and the commercially available DSPE-PEG-Maleimide (Kirpotin et al. 1997) (Avanti Polar Lipids, Inc.), have been synthesized and included into LP formulations (Fig. 17) providing a further improvement in antibody coupling efficiency and iLP targetability (Maruyama 2002; Manjappa et al. 2011). Remarkably, those LP-antibody conjugation strategies leading to high coupling yields while preserving at the same time antibody functionality and a minimal immunogenicity will always be prioritized. In addition to this, the antibody coupling reaction of choice should not interfere with either liposomal components or the drug-loading mechanism employed.

Latest advances in iLP preparation include a preliminary step based on the coupling of antibodies to micelles containing reactive PEG-lipid derivatives, which is then followed by the transference of these antibody-linked lipids into preformed PEGylated vesicles. This strategy has been named as the ‘post-insertion technique’ (Ishida et al. 1999; Moreira et al. 2002). Unfortunately, incubation times ranging from several minutes to even a few hours under high temperatures of >37 ºC are commonly required for a proper incorporation of the antibody-conjugated micelles into LPs. Such conditions might eventually trigger the leakage of LP-encapsulated compounds and, consequently, this strategy must be explored and characterized in detail when designing iLP-based drug delivery systems.

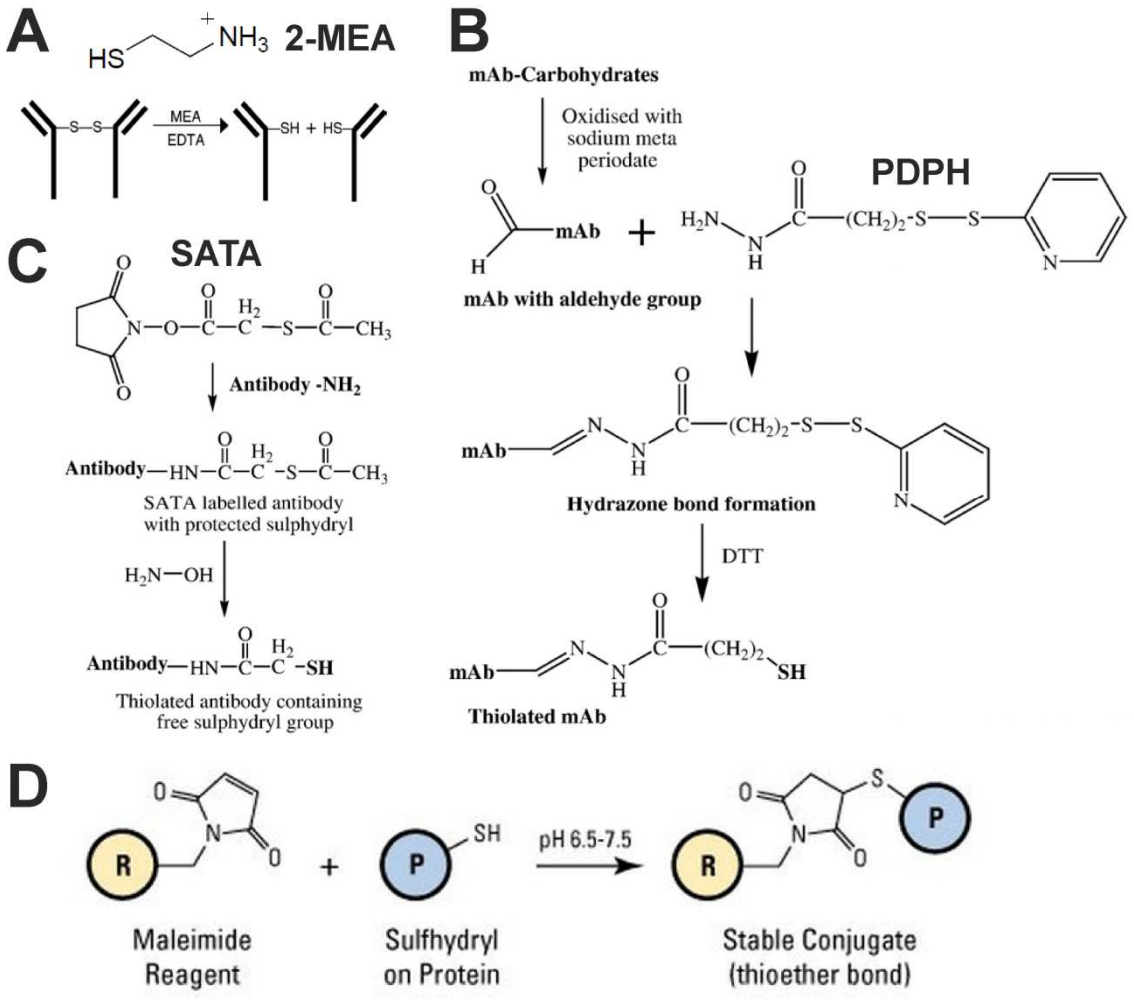

Figure 24. *Antibody conjugation strategies based on the generation of sulfhydryl groups (thiolation) and their subsequent reaction with maleimide-containing reagents*. (A) Antibody thiolation through the selective cleavage of internal disulfides from the IgG hinge region using a mild reducing agent (2-mercaptoethylamine, 2-MEA, or dithiothreitol alternatively) and finally obtaining half antibody thiolated fragments (Martin & Papahadjopoulos 1982; Urbán, Estelrich, Cortés, et al. 2011). (B) Derivatization of previously oxidized antibody carbohydrates with the PDPH crosslinker (hydrazone bond) and the subsequent DTT-mediated sulfhydryl group deprotection. (C) Antibody conjugation through its primary amines with the SATA crosslinker (amide bond) and the following hydroxylamine-mediated sulfhydryl group deprotection. (D) Thioether bond formation between a thiolated protein and a reagent containing maleimide groups. Figure adapted from (Manjappa et al. 2011) and Thermo Fisher Scientific Inc. reactive datasheets.

3.4.3. Immunoliposome interaction with cells

Immunoliposomes can interact with target cells in many different ways depending on their lipid composition and physicochemical properties (e.g. lipid geometry, degree of ionization and acyl chains organization). Additional factors playing a major role in the LP-cell interaction mechanism include the conditions of the system (pH, temperature) as well as the capacity of the target cell to

mediate endocytic processes. In this regard, targeted drug delivery strategies will be specifically designed according to each particular type of cell and its environmental conditions.

Stable adsorption on the target cell surface

Drug-loaded iLPs can be tightly adsorbed onto the surface of target cells without being internalized (Fig. 25A). Such process is commonly associated with iLPs comprising a highly stable and compact *Lβ'*-membrane composed mainly of neutrally-charged, cylinder-shaped phospholipids (Fig. 25B) (Papahadjopoulos et al. 1973) which in turn bind to non-internalizing receptors (e.g. the CD20 molecule exposed on human B-lymphoma cells) (Sapra & Allenz 2002) or cells lacking endocytic pathways (e.g. mature erythrocytes) (Holovati et al. 2008).

CDD-based strategies would be therefore required in the aforesaid situations in order to obtain a sustained release of iLP-encapsulated compounds into the extracellular medium once the nanovector has been docked to the target cell (Fig. 25A1-2). Liberated substances would subsequently cross the cell membrane by means of either passive diffusion (molecules with high coefficient *p* values, Table 2) or transporter-mediated pathways (e.g. the *P. falciparum*-induced NPPs, Fig. 6). Alternatively, lipophilic compounds can be directly exchanged between membranes in close contact (Fig. 25A3, see 3.3.4. for further information).

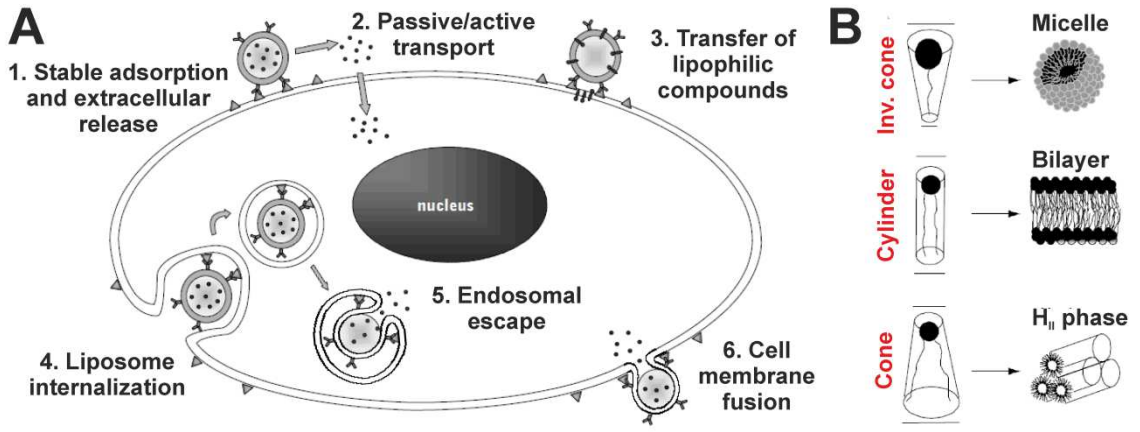

Figure 25. *iLP-target cell possible interaction mechanisms and the major types of lipidic structures*. (A) Illustration of the most common LP-cell association events and the subsequent delivery of the nanovector cargo. (B) Main lipid arrangements according to phospholipid geometry: cone (e.g. PE and neutrally-charged PS/DOTAP), cylinder (e.g. PC) and inverted cone (e.g. fatty acids). Figure adapted from (Janthur et al. 2012; Maurer et al. 2001).

Cell-mediated iLP internalization

Alternatively, ligand-conjugated nanocarriers can be internalized by the target cell by means of the clathrin- and the caveolae-dependent, receptor-mediated endocytic pathways (Soriano et al. 2010) (Fig. 25A4) as well as employing other distinct and non-specific mechanisms such as the macropinocytosis and phagocytosis processes. Besides, phagocytosis has been efficiently promoted through the inclusion of the negatively-charged lipids PS and phosphatidylglycerol into

LP formulations (Kelly et al. 2011; Makino et al. 2003). It is important to note that a final step involving the endosomal escape of the endocytosed nanocarrier (Fig. 25A5) is mandatory when following these internalization pathways for an efficient delivery of the nanovector cargo into the target cell cytoplasm. This decisive step can be achieved through the incorporation of pH-sensitive lipids (e.g. PS) and/or specific peptides (Mastrobattista et al. 2002; Nakase et al. 2010), as a few examples, into LPs.

Liposome-cell membrane fusion

A third mechanism based on the merge of lipid bilayers has been explored for the direct intracellular delivery of iLP contents (Fig. 25A6). Membrane fusion events are triggered in this regard when incorporating phospholipids with an inducible conical geometry, special molecular shape that eventually leads to the H_{II} phase lipidic structure (also named 'inverted micelle', Fig. 25B) and promotes in turn the formation of interlamellar micelles and stalk intermediate structures (Bailey & Cullis 1997). Such complex lipid rearrangement process ultimately results in the generation of membrane fusion pores and the subsequent mixture of intravesicular contents. Unfortunately, the H_{II} phase is only induced under specific conditions and the membrane fusion process is completely independent of the cell type as well as the presence of cell surface receptors in most of cases, fact that considerably hampers the applicability of this drug delivery strategy in complex cell cultures and, especially, if considering *in vivo* practices.

Some of the conditions promoting the H_{II} phase and thus stimulating membrane fusion include:

- Incorporation of unsaturated phospholipids with small headgroups (e.g. dioleoyl-PE) in either PC- or PS-based bilayers (Bailey & Cullis 1997).
- Negative charge neutralization of phosphatidic acid (PA)- and PS-based membranes through the addition of multivalent cations (e.g. Ca^{2+}) (Papahadjopoulos et al. 1990), (Mondal Roy & Sarkar 2011) and/or under acidic environments (pH below 3.0) (Bailey & Cullis 1997).
- Low pH-induced charge neutralization of bilayers containing mixtures of fatty acids and PE (Düzgüneş et al. 1985).
- Positive charge neutralization of membranes composed solely of cationic lipids (e.g. DODAC, DOTMA and DOTAP) or in combination with PE, in the presence of anionic lipids such as cells exposing PS (Stebelska et al. 2006) and within endosomes containing acidic phospholipids. Alternatively, the H_{II} phase can be found in the cationic LP-DNA mixtures (named 'lipoplexes') commonly employed for cell transfection purposes (Zuhorn et al. 2007; Cao et al. 2006).

In light of the above, the use of LPs composed of PS:PC:cholesterol has been successfully validated for the trehalose delivery into RBCs *in vitro* and in the presence of Ca^{2+} (Holovati et al. 2008). Besides, such an extreme reduction in the amount of delivered trehalose was observed in

this work when employing PC:cholesterol vesicles under the same conditions. A total of about 35-fold less intracellular trehalose was detected in this regard if compared to PS-containing LPs.

Novel cellular delivery mechanisms: cell penetrating peptides

Recent advances in the targeted drug delivery field include the use of cell penetrating peptides (CPPs) as membrane-permeabilizing agents for the translocation of functional molecules and drug-loaded carriers into cells (Bechara & Sagan 2013; Gupta et al. 2005). Such peptides, which mainly originate from viral proteins (e.g. TATp and $S4_{13}$-PV peptides from HIV-1 and SV40 virus, respectively) (Trabulo et al. 2010), are capable of being internalized into cells by means of either their direct translocation into the cell cytoplasm (He et al. 2014) or using cell-mediated endocytic processes (Montrose et al. 2013). The pathway of choice is further influenced by the size of the CPP-bound cargo, thereby the entry of large carrier sizes being dramatically limited when following direct translocation approaches (Trabulo et al. 2010). Unfortunately, most CPPs display a considerable lack of cell type specificity, requiring in this manner their incorporation in drug delivery systems in the form of masked but cleavable groups that are released once the nanovector has been docked to the desired cell or tissue (Zhu et al. 2012).

3.5. Nanotechnology applied to the treatment of malaria

The application of nanotechnology to malaria therapeutics has been proposed as a promising approach for the amelioration of those drawbacks commonly associated with the freely administration of antimalarial compounds such as: (i) the emergence of drug resistance (see. 1.4.3.), (ii) causing toxicity to the patient (see 1.4.4.) and (iii) drug pharmacokinetics (see 1.4.5.). The latter limitation including large biodistribution volumes and either a fast elimination-metabolization or the maintenance of residual drug levels for long periods of time.

In light of the above, CDD strategies (see 3.2.1.) using LP- and polymer-based nanocarriers have been explored by a few groups for the encapsulation and sustained release of antimalarial drugs, improving in this manner their pharmacokinetic profiles in the organism with longer plasma half-lives and reduced biodistribution volumes due to the limited extravasation of the aforesaid carriers from blood vessels. Furthermore, the conjugation of these nano-sized vectors with targeting molecules has provided a further step beyond more efficient malaria chemotherapies by means of novel pRBC-specific approaches. The most important advances in antimalarial CDD systems are described below.

3.5.1. Drug delivery systems against *Plasmodium* pre-erythrocytic stages

Probably the first assay utilizing a nanovector-based drug delivery strategy for malaria chemotherapy would be reported by (Pirson et al. 1979). In this pioneer work, PQ-encapsulating multilamellar liposomes (PC:PS:cholesterol) completely eliminated *Plasmodium berghei* liver-stage infection in mice with a described minimal single dose of 40 mg PQ/kg. Besides, PQ

toxicity was significantly diminished when encapsulated in comparison with freely-administered drug, being their respective 50% lethal doses (LD_{50}) of 139 and 39 mg PQ/kg.

More recently, a second LP prototype targeted against highly sulfated glycosaminoglycans (HS-GAGs) would be developed by (Longmuir et al. 2006). This GAG-specific nanovector was successfully accumulated into mouse liver with more than 100-fold retained LPs in comparison with other organs (though only 10-fold when compared to the spleen) and consequently proposed as a potential drug delivery system for the treatment of *Plasmodium* pre-erythrocytic stages (Robertson et al. 2008; Tsai et al. 2011).

Such meaningful tropism towards the liver was achieved through the conjugation of LPs with a 19-amino-acid sequence of the *P. berghei* CSP that had been previously identified to bind heparin and heparan sulfate HS-GAGs with high affinity (Tewari et al. 2002; Ancsin & Kisilevsky 2004). In this regard, proteoglycans containing heparan sulfate are primarily located on the surface of hepatocytes and across the perisinusoidal space of the liver, though present in other organs and tissues such as the spleen and the basement membrane of brain microvasculature among others (Miller et al. 2008; Steiner et al. 2014; Lau et al. 2013), and have been importantly identified as receptors during *Plasmodium* sporozoites liver infection (John et al. 2008; Frevert et al. 1993; Ancsin & Kisilevsky 2004).

3.5.2. Pioneering targeted drug delivery strategies against *P. berghei* intraerythrocytic stages

RBC-specific iLPs

The first site-specific antimalarial drug delivery system was developed by the group headed by Dr. Chhitar M. Gupta in the late 1980s with the novel design of a liposomal nanocarrier capable of specifically targeting rat erythrocytes *in vivo* (Singhal et al. 1986; Singhal & Gupta 1986). Such targetability was provided by coupling anti-rat RBC polyclonal $F(ab')_2$ through their amino groups to carbohydrate-containing LPs (PC:cholesterol:gangliosides in a 1:1:0.2 molar ratio), resulting in a total amount of conjugated antigen-binding fragments of about 65 µg protein/µmol lipid along with a coupling efficiency of <20%. Approximately 20% of the total intravenously administered iLPs were retained onto RBCs and among these cell-bound nanocarriers, only nearly 20-30% delivered their encapsulated cargo (i.e. isotope-labeled sucrose and inulin) into the RBC cytoplasm. Besides, an insignificant reduction in the number of RBC-bound iLPs was observed up to 3 h post-administration, result that suggested an absence of iLP-induced harmful effects over RBCs, and a minimal iLP-organ association was reported over the same period of time.

The efficacy of this RBC-targeted iLP prototype as chemotherapeutic agent would be later assayed in *P. berghei*-infected mice (Agrawal et al. 1987; Chandra et al. 1991). A single intravenous injection of CQ-loaded iLPs (either 2.5 or 5 mg CQ/kg) at the 4^{th} day post-infection notably reduced parasitemia levels when compared to freely administered drug and, furthermore,

parasitemia elimination rates of more than 50% were reached from 24 h to even one week post-treatment with iLPs. Importantly, a significant improvement in drug efficacy as well as in the number of surviving mice was also observed when CQ-loaded iLPs were assayed in mice infected with a CQ-resistant *P. berghei* strain.

Moreover, a similar iLP model to that designed by Gupta, Singhal and coworkers was developed in parallel (Peeters et al. 1988), though using anti-mouse RBC Fab' thiolated antigen-binding fragments coupled to maleimide-containing LPs instead. In this work, iLP binding to mouse RBCs (moRBCs) triggered their uptake by host organs (mostly spleen and the liver) and subsequent elimination when administered to mouse blood-grafted rats. A considerable removal of >50% of the total circulating moRBCs was obtained only a few minutes after iLPs intravenous injection. Nevertheless, such rapid elimination would be undoubtedly influenced by the presence of RBCs from a different organism, which could in turn substantially aggravate their recognition by the immune system after iLPs binding and, as a consequence, lead to results that seriously differ from a physiological state.

pRBC-specific iLPs

Later on, the antimalarial activity of the aforementioned iLP prototype developed by Gupta's group would be further improved thanks to its functionalization with a monoclonal $F(ab')_2$ specific for *P. berghei*-infected RBCs (the so-called MAb F_{10}) (Owais et al. 1995). Remarkably, this targeting agent was generated by mice immunization with cell membranes obtained from mouse pRBCs mainly in the trophozoite stage. The intravenous administration of MAb F_{10}-iLPs loaded with CQ (5 mg drug/kg) on days 4 and 6 post-infection completely eliminated CQ-resistant *P. berghei* parasites in most of mice leading to survival rates of >75% at day 30 post-treatment. By contrast, only half the infected mice survived when delivering CQ through RBC-targeted LPs (either using polyclonal or monoclonal antibodies) and, furthermore, all animals died when the same amount of drug was administered in free form.

Limitations in the treatment of P. berghei infection using iLPs

Unfortunately and spite all the aforesaid success, no other works employing either RBC- or pRBC-targeted iLPs as therapeutic agents against murine malaria have been reported. Problems in finding an appropriate antibody leading to 100% iLP retention into parasitized cells (see 1.4.3. and 1.6.1. for a detailed explanation of *Plasmodium* antigenic variation) as well as troubles in controlling CQ encapsulation into liposomes (see 3.3.4.) are probably the most likely reasons. Moreover, additional limitations found in the iLP prototypes described in this section and thus requiring further optimization include:

- All *in vivo* assays have been performed using mice infected with *P. berghei*, *Plasmodium* sp. that displays a meaningful tropism for reticulocyte infection (Cromer et al. 2006) though capable of invading mature erythrocytes as well (Harris et al. 2012). Reticulocytes are still endocytically active (Harding et al. 1983; Griffiths, S. Kupzig, et al. 2012), thereby

allowing to a much more efficient internalization of cell surface-bound iLPs in comparison with mRBCs. Moreover, bearing in mind the requirement of finding novel and effective chemotherapeutic strategies against the lethal and human-infecting *P. falciparum* sp., which primarily infects the non-endocytic mRBCs and displays a particular set of cell surface-exposed proteins completely different to the other *Plasmodium* spp., iLP-based drug delivery strategies against *P. falciparum* should be mostly assayed in those parasite species exhibiting a similar host cell tropism. In this regard, *Plasmodium yoelii* XL (lethal strain) and the human RBC-grafted, immunosuppressed mouse model infected with *P. falciparum* (Vaughan et al. 2012) are a few examples.

- RBC-specific iLPs have been prepared using polyclonal antibodies generated against total erythrocytes (i.e. regardless of the cell maturation stage), fact that could impair their binding to *P. berghei*-infected reticulocytes.
- The delivery of iLP contents into the target cell cytoplasm has been analyzed by isotopes quantification and not determined visually under fluorescence or confocal microscope using fluorescent markers instead (i.e. more reliable intracellular localization of the delivered material).
- No information is given about LPs long-term stability and drugs leakage over time.
- Only a minor fraction of about 10-20% of the administered iLPs was retained into target cells in all studies performed (either RBC- or pRBC-targeted iLPs).
- The antigen recognized by the pRBC-specific MAb F_{10} is unknown and could be also a RBC endogenous molecule exposed only during *P. berghei* infection.
- A moderate reduction in parasitemia levels has been obtained after two-dose treatment with CQ-loaded, MAb F_{10}-iLPs. Complete parasite elimination has only been reported at day 30 post-treatment.

Alternative LP-based approaches

Additional drug delivery systems to the aforementioned cell-targeted strategies have been designed for the treatment of *Plasmodium* IEC. A liposomal model for the sustained release of recombinant human tumor necrosis factor-α (rhTNF-α) was developed by (Postma et al. 1999) and proposed in this work as a successful approach in preventing the development of experimental cerebral malaria (ECM) in *P. berghei*-infected mice. Remarkably, rhTNF-α-conjugated LPs through thioether linkage (SATA-maleimide) proved to notably decrease the number of mice suffering from ECM when compared to the administration of free rhTNF-α. This cytokine plays an important a role in regulating immune cells as well as triggering inflammatory reactions and has been described to mediate protection against malaria infection when dispensed in low amounts (Jacobs et al. 1996; Kremsner et al. 1995).

Moreover, artemether-loaded multilamellar LPs efficiently diminished *Plasmodium chabaudi* parasitemia in mice (Chimanuka et al. 2002). A single dose administration of liposomized 4.8 mg drug/kg completely cured *P. chabaudi*-infected mice. By contrast, no surviving animal was reported when the same dose of artemether was delivered in combination with Mygliol® triglycerides oil. Artemether was mostly incorporated within LP multiple bilayers due to its hydrophobic properties (i.e. completely unionized molecule with a log *P* of 3.48, http://www.chemicalize.org) and minimal drug leakage was observed during storage. Nevertheless, artemether was easily released in a dilution-dependent manner and entirely exchanged between LPs.

3.5.3. Pioneering targeted, LP-based drug delivery strategies against *P. falciparum* intraerythrocytic stages

The enormous antigenic variation displayed by *Plasmodium* spp. (see 1.6.1.) as well as the pRBC-exposure of almost completely distinct endogenous elements on each species (e.g. the cytoadhesive protein families PfEMP1 and RIFINs (Goel et al. 2015) in *P. falciparum*, VIR in *P. vivax* (Bernabeu et al. 2012) and other ligands still unknown in *P. berghei* (Pasini et al. 2013; El-Assaad et al. 2013)), led to both a considerable reduction in the use of murine *Plasmodium* spp. and the emergence of novel targeted drug delivery approaches specific and directly tested on the human-infecting *P. falciparum* sp. The simultaneous development of *in vivo* mouse models capable of sustaining human RBCs in circulation and their subsequent infection with *P. falciparum* (Vaughan et al. 2012) would importantly encourage this trend change.

BM1234-conjugated LP

The first nanovector model specifically designed against *P. falciparum* would be developed by conjugating quantum dot-loaded LPs (DOPC:cholesterol:MPB-PE, 77.5:20:2.5) with the BM1234 commercial monoclonal antibody as targeting ligand against the late form-pRBC Maurer's clefts (Urbán, Estelrich, Cortés, et al. 2011). Besides, the thiol (half antibody)-maleimide coupling strategy was employed for LP functionalization (Fig. 24D). Remarkably, the BM1234-iLP model specifically recognized pRBCs in the trophozoite/schizont stages and delivered its cargo into these cells in less than 1.5 h (Fig. 26A). The same iLP prototype but loaded with CQ and fosmidomycin antimalarials instead of quantum dots, provided parasite elimination rates by 10-fold higher in the best case when compared to freely delivered drugs (Urbán, Estelrich, Adeva, et al. 2011). Furthermore, a complete absence of cytotoxic and hemolytic activity was observed on either fibroblasts or endothelial cells even at the high LP concentration of 1 mM lipid.

Heparin-conjugated LP

An additional liposomal model targeting *P. falciparum*-infected RBCs would be later developed by (Marques et al. 2014). Importantly, this work would be the first in exploring the dual activity of heparin as both targeting molecule and antimalarial agent:

- **Targeting agent**: the affinity of heparin to pRBCs had been previously demonstrated by means of atomic force microscopy assays displaying an interaction strength that positively correlated with the parasite maturation stage (Valle-Delgado et al. 2013). Furthermore, the PfEMP1 protein, which is chiefly exposed on the surface of late form-pRBCs, has been identified as ligand for heparan sulfate and heparin during parasite rosetting and cytoadhesive processes (Barragan et al. 2000; Angeletti et al. 2015).

- **Antimalarial agent**: heparin has been identified as a RBC receptor-like molecule involved in merozoite invasion (likely analogous to heparan sulfate), thereby inhibiting *P. falciparum* replication when extracellularly added to parasite cultures. In this regard, an averaged *in vitro* IC50 of about 1 to 10 µg heparin/ml has been reported (Boyle et al. 2010; Kobayashi et al. 2013). The specific attachment of heparin to merozoites has also been observed when assayed in *P. yoelii*-infected mice (Fig. 26B) (Marques et al. 2014).

Marques et al. further demonstrated that fluorescently-labeled heparin can be specifically incorporated into *P. falciparum*- and *P. yoelii*-infected RBCs only after 30 to 90 min incubation (Fig. 26B). Anticoagulation activity was found in mouse for heparin concentrations above 1 µg/ml. Moreover, cationic liposomes (DOPC:cholesterol:DOTAP, 76:20:4) loaded with PQ and conjugated with heparin through electrostatic interaction, significantly reduced parasitemia levels when added at 1 µg heparin/ml to *P. falciparum in vitro* cultures by nearly (i) 4-fold compared with PQ-loaded untargeted vesicles (equimolar drug amount) and (ii) 3.5-fold when compared to heparin-conjugated LPs lacking of drug (equimolar lipid and heparin amount). Such improvement in drug efficacy was attributed to the synergistic effect of heparin as antimalarial agent as well as targeting molecule for the specific delivery of PQ into pRBCs.

Limitations in the treatment of P. falciparum using pRBC-targeted LPs

In spite of the promising short incubation time required by BM1234 and heparin molecules for a complete pRBC recognition and their remarkable contribution in improving drug efficacy, the mechanism by which LPs conjugated with these targeting agents deliver their cargo into the target pRBC remain unclear. There is a substantial lack in data concerning live cell assays for the analysis of nanovector targeting and intracellular delivery. In this regard, all fluorescence microscopy assays reported so far rely on the analysis of cells fixed before their observation.

Moreover, no information is given about (i) the antibody coupling yield as well as (ii) drug encapsulation efficiencies and (iii) LP-release kinetics in the aforesaid models. Furthermore, a binding tropism has been reported for BM1234 and heparin to late form-pRBCs, leading in this manner to a scarce recognition of those parasites in the early ring maturation stage (Valle-Delgado et al. 2013; Urbán, Estelrich, Cortés, et al. 2011; Marques et al. 2014). The *in vivo* application of these pRBC-targeted LP approaches would be therefore limited to the presence of *P. falciparum* intraerythrocytic late stages in circulation.

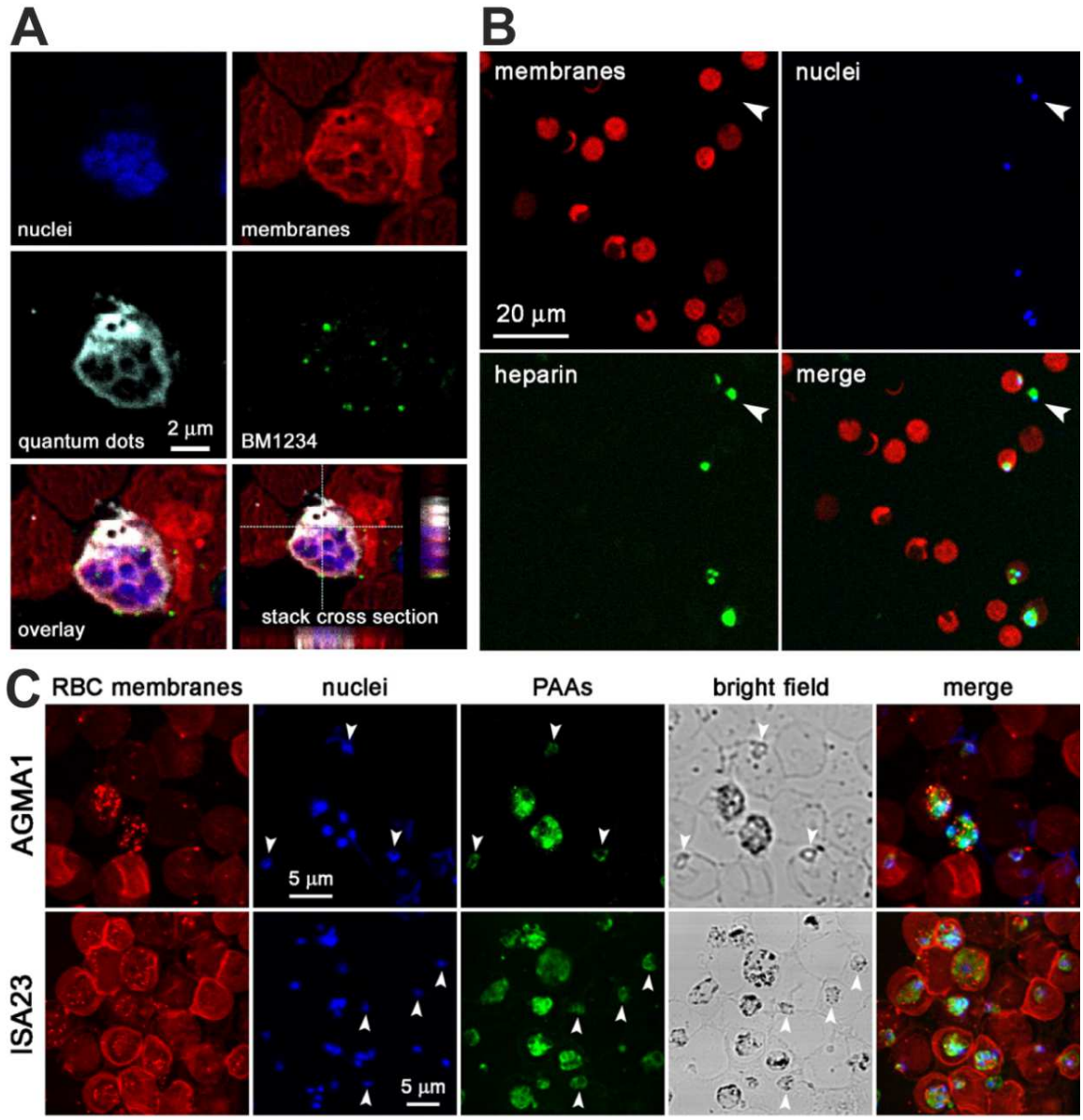

Figure 26. *Examples of P. falciparum and P. yoelii IEC-targeted chemotherapeutic approaches developed so far*. (A) BM1234-conjugated, quantum dot-loaded LPs against *P. falciparum*-infected RBCs. (B-C) Specific accumulation into *P. yoelii*-infected RBCs of FITC-labeled (B) heparin and (C) PAA-derived polymers (ISA23 and AGMA1). RBC membranes have been stained with rhodamine-labeled wheat germ agglutinin. White arrow heads indicate (B) a heparin-bound merozoite and (C) pRBCs at young stages. Figure adapted from (Urbán, Estelrich, Cortés, et al. 2011; Marques et al. 2014; Urbán et al. 2014).

3.5.4. Pioneering targeted, polymer-based drug delivery strategies against *P. falciparum* intraerythrocytic stages

In parallel to the research of LPs as antimalarial drug vehicles, polyamidoamine (PAA)-derived polymers displaying an hydrodynamic radius of approximately 2 to 7 nm in size (Fig. 19B, 'nanosphere' structure) have been simultaneously explored as alternative drug carrier nanoparticles (Urbán et al. 2014). Remarkably, an endogenous pRBC-targeting capacity was

identified in these PAA carriers allowing to their specific internalization into *P. falciparum*- and *P. yoelii*-infected RBCs only after 1.5 h incubation (Fig. 26C).

AGMA1 and ISA23 PAAs were capable of inhibiting *P. falciparum* growth *in vitro* and, furthermore, a particular effect of AGMA1 in impairing the RBC invasion by the parasite was proposed. Finally, the triple combinatorial activity of PAA nanoparticles as (i) targeting elements, (ii) chemotherapeutic agents, and (iii) antimalarial drug carriers, was analyzed by loading them with CQ and the resulting constructs were assayed in *P. yoelii*-infected mice. Whereas no animal treated with free drug at 0.8-1.9 mg CQ/kg survived at day 30 post-infection, all those receiving PAA-vectorized CQ were completely cured. Besides, parasitemias were almost cleared at day 4 post-administration.

3.5.5. RBCs as drug carriers

In addition to the above-mentioned liposomal and polymeric types of carriers, erythrocytes have also been considered as potential vehicles for CDD systems on the basis of their:

- Prolonged plasma half-lives commonly described of as long as 4 months in humans, being considerably higher in comparison with most of reported carriers.
- Restricted extravasation from blood vessels (Muzykantov 2010).
- Almost complete biocompatibility (if immunologically compatible) and biodegradability.
- Physicochemical properties (e.g. negatively-charged glycocalyx), dimensions and huge intracellular loading capacity (see 2.3. to know more details about RBC characteristics).

Some examples of approaches using RBCs as carriers include the encapsulation into these cells and subsequent sustained delivery of anti-cancer agents (Skorokhod et al. 2007), anti-retroviral compounds (Benatti et al. 1996) and anti-inflammatory molecules (Magnani et al. 2002). Importantly, their efficacy has been validated *in vivo* in several cases (Magnani et al. 2002; Skorokhod et al. 2007; Muzykantov 2010), thereby demonstrating their potential capacity as drug delivery vectors.

However, probably the main limitation associated with this particular CDD system is the strategy followed for the intracellular loading of biologically active compounds. In this regard, protocols based on: (i) an initial ex-vivo isolation of RBCs, (ii) the consequent internalization of the active compound through simple diffusion or, alternatively, employing harsh techniques in which membrane pores are formed, and (iii) a final transfusion into an immunologically compatible recipient; are frequently employed (Muzykantov 2010). Alternative and clinically feasible approaches avoiding the aforesaid complicated steps rely mainly on the direct administration of RBC-targeted active agents for either cell labeling or functionalization purposes (Zaitsev et al. 2006). Nevertheless, such promising strategy has never been considered as a tool for the *in vivo* loading of drugs into the RBC.

Finally, the potential role of erythrocytes as drug carriers for malaria chemotherapy has been additionally demonstrated due to the observation of several antimalarial compounds freely diffusing into the RBC, becoming stably internalized after cells washing and eventually preventing *P. falciparum* growth (Fig. 27) (Wilson et al. 2013). However, such applicability has never been explored as a clinical strategy against malaria.

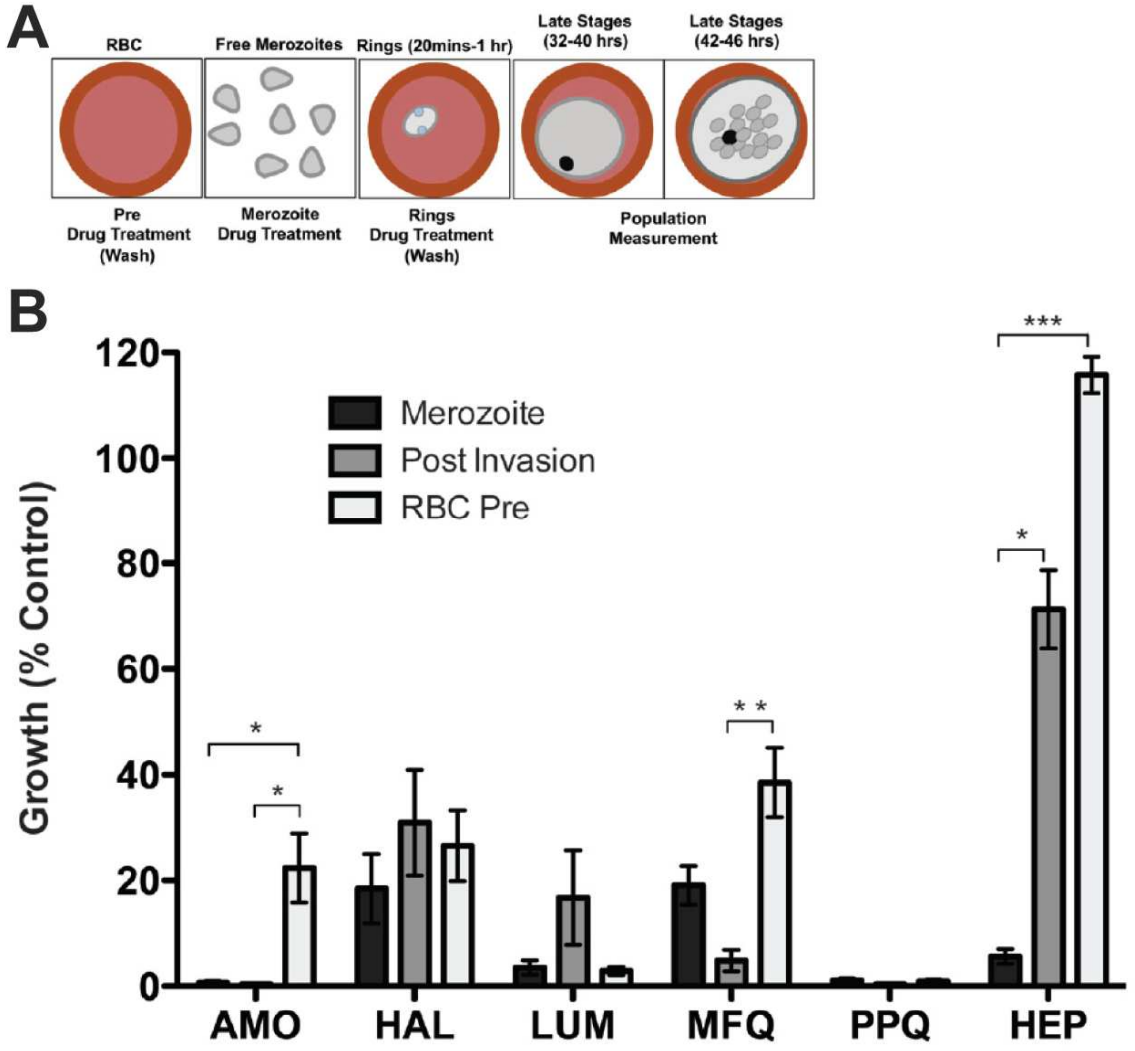

Figure 27. *Analysis of antimalarial drugs timing of action over P. falciparum in vitro growth*. (A) Schema depicting the different parasite intraerythrocytic stages at which drug activity was assayed: healthy RBCs prior to *Plasmodium* infection (RBC Pre, 1 h drug incubation) and *P. falciparum* cultures either in the merozoite (10 min drug incubation) or ring (parasites 20 min post RBC-invasion, 1 h drug incubation) parasite forms. (B) Overall results of the growth inhibition assays. Antimalarial compounds tested included: amodiaquine (AMO, 2 µM), halofantrine (HAL, 86 nM), lumefantrine (LUM, 612 nM), mefloquine (MFQ, 8 µM), piperaquine (PPQ, 1.6 µM) and heparin (HEP, concentration not reported). Figure reproduced from (Wilson et al. 2013).

"Everything should be made as simple as possible... but not simpler"

Albert Einstein

OBJECTIVES

Malaria in its clinical severe manifestations is one of the most life-threatening diseases worldwide and a major limitation to progress in undeveloped countries having limited economic and health resources. ***Plasmodium falciparum*** **appears as the most virulent species causing malaria in humans due to its capacity to invade erythrocytes (RBCs) regardless of their maturation stage and its particular ability to export cytoadhesive proteins to the parasitized-RBC (pRBC) surface**. Importantly, the latter feature ultimately enables the pRBC to bind to host cells distributed throughout the blood vessels of various organs and tissues in a sequestering mechanism employed by the parasite to avoid splenic clearance.

Moreover, because **malaria associated symptoms do principally originate from RBCs infection, this intraerythrocytic and asexual stage of the parasite's life cycle is the most common target of currently marketed chemotherapeutic agents**. Nevertheless, several obstacles are commonly associated with the utilization of antimalarial compounds, which are in turn directly delivered to the patient. (i) **Large biodistribution volumes**, (ii) a **fast absorption from blood circulation**, (iii) their **metabolization into inactive byproducts**, and (iv) their **association with plasma proteins**, are just a **few examples of pharmacokinetic handicaps** that basically lead to the **obligatory administration of large drug doses in order to completely clear *Plasmodium* infection**. Such high drug payloads consequently increase the likelihood of causing toxic side effects to the patient and, furthermore, promote the emergence of resistant parasites in malaria endemic areas.

Additionally, the above-mentioned **disadvantages of antimalarial drug therapies could even aggravate during severe malaria clinical cases in which parasites remain sequestered in the form of RBC-pRBC clumps (rosettes) and/or adhered to the microvasculature of diverse essential organs**. The formation of rosettes causes an important obstruction to blood flow and has been identified as one of the most important pathogenic processes in triggering severe malaria. Besides, the NTS-DBL1α N-terminal domain of the parasite-derived PfEMP1 protein has been reported as a key fragment directly involved in rosetting and antibodies generated against this domain from different PfEMP1 rosetting variants have efficiently prevented the formation of such cellular aggregates.

Nanotechnology in the form of targeted, drug-embedded liposome- and polymer-based nanocarriers has been successfully validated as a feasible and huge potential alternative to ongoing antimalarial therapies. Preliminary assays using immunoliposomes (iLPs) specifically recognizing murine RBCs and *Plasmodium berghei*-infected RBCs, performed by Dr. C. M. Gupta and co-workers in the late 1980s, significantly improved the activity of chloroquine (CQ) antimalarial drug with a considerably larger number of surviving animals at the end of the assay in comparison with the freely delivered compound. Similarly, an iLP model targeted against a Maurer's clefts-resident protein specific for the human-infecting *Plasmodium falciparum* sp. and loaded with CQ/fosmidomycin antimalarials would be later reported by Dr. Urbán et al. in 2011 markedly increasing the activity of drugs against parasite growth when encapsulated.

However, the **aforementioned liposomal nanovector prototypes have been poorly characterized** with a minimal knowledge regarding (i) their **mechanism of interaction and internalization into the target cell**, (ii) **release kinetics of LP-encapsulated material** and (iii) **antibodies coupling yield**. In addition to this, the **RBC- and pRBC-specific antigens recognized by these iLPs have either not been reported or are still unknown**. A more detailed analysis of these issues as well as their optimization is therefore required for the design of more potent nanovectors with even greater antimalarial activities.

Moreover, **a further step beyond in the development of more effective site-specific drug delivery approaches against *P. falciparum* malaria** has been provided by Dr. P. Urbán, J. Marques and co-workers in 2014 by means of **novel antimalarial combination therapies based on the application of targeted, drug-loaded nanocarriers displaying multiple and completely separated activities**. **Heparin** has been employed as pRBC-targeting agent with intrinsic antimalarial properties for the functionalization of positively-charged LPs containing primaquine. Besides, three different capabilities have been described for **polyamidoamine (PAA)-based nanoparticles**: (**1**) Targeting agents owing to their specific accumulation into pRBCs, (**2**) antiparasitic agents likely interfering with the invasion of RBCs by *Plasmodium*, and (**3**) nanocarriers for the selective delivery of antimalarial drugs into the pRBC. Nevertheless, the improvement in drugs activity after their encapsulation into heparin- and PAA-derived nanovectors has been rather modest when assayed against *P. falciparum*.

In light of the above, the main scope of this PhD thesis has been the **characterization and development of new and more effective targeted drug delivery systems against the human-infecting *P. falciparum* sp.** with special attention to the **obtainment and assessment of polyvalent therapeutic approaches** displaying multiple mechanisms of action. The latter aim being remarkably important in order to fight the infection at multiple sites simultaneously (e.g. distinct *P. falciparum* pathogenic processes, developmental stages and metabolic routes) while at the same time diminishing the capacity of the parasite to escape from treatment (e.g. through single point mutations or genetic recombination events affecting essential proteins).

In order to meet the proposed challenge, the following objectives have been considered:

- *Objective 1.* **Development of upgraded immunoliposomal prototypes** through the research of **better targeting agents** as well as **more efficient drug loading and antibody coupling strategies**.
- *Objective 2*. **Application of the liposomal prototype developed in *Objective 1.* for the selective targeting and elimination of rosette-forming pRBCs** as well as **the disruption of already formed rosettes** using antibodies specific for the rosetting-linked NTS-DBL1α domain of distinct PfEMP1 variants as targeting agents.
- *Objective 3*. **Exploration of novel biosynthetic routes necessary for parasite viability but absent in humans as new targets for antimalarial drug research** with a particular focus on those metabolic pathways taking place in the apicoplast organelle.

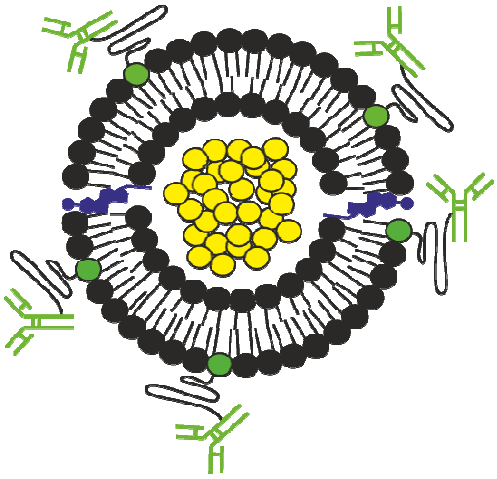

RESULTS

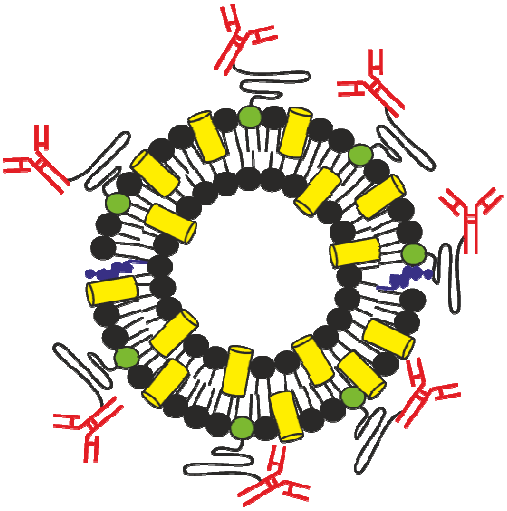

SUMMARY OF PUBLICATIONS

This PhD thesis is composed of two accepted manuscripts, which are included in Chapter 1, as well as two more Chapters containing data that have not yet been published. All results presented here have been obtained throughout the PhD. Two additional manuscripts that have been accepted for publication during the PhD are included in Annexes II and III.

Chapter 1

Immunoliposome-mediated drug delivery to *Plasmodium*-infected and non-infected red blood cells as a dual therapeutic/prophylactic antimalarial strategy.

Moles E, Urbán P, Jiménez-Díaz MB, Viera-Morilla S, Angulo-Barturen I, Busquets MA, Fernàndez-Busquets X. *J Control Release. 2015 Jul 28;210:217-29. doi: 10.1016/j.jconrel.2015.05.284. Epub 2015 May 23.*

Loading antimalarial drugs into noninfected red blood cells: an undesirable roommate for *Plasmodium*.

Moles E, Fernàndez-Busquets X. *Future Med Chem. 2015;7(7):837-40. doi: 10.4155/fmc.15.35.*

Chapter 2

Development of drug-loaded immunoliposomes for the selective targeting and elimination of rosetting *Plasmodium falciparum*-infected RBCs.

Moles E, Moll K, Ch'ng J, Parini P, Wahlgren M, Fernàndez-Busquets X. *In preparation.*

Chapter 3

Proposal of 2-picolylamine derivatization and LC-ESI-MS/MS analysis for the ultra-sensitive detection of abscisic acid in apicomplexan blood-infecting parasites and first validation test in *Plasmodium falciparum* extracts.

Moles E, Marcos J, Imperial S, Pozo OJ, Fernàndez-Busquets X. *In preparation.*

Annex II

Amphiphilic dendritic derivatives as nanocarriers for the targeted delivery of antimalarial drugs.

Movellan J, Urbán P, Moles E, de la Fuente JM, Sierra T, Serrano JL, Fernàndez-Busquets X. *Biomaterials. 2014 Sep;35(27):7940-50. doi: 10.1016/j.biomaterials.2014.05.061. Epub 2014 Jun 13.*

Annex III

Possible roles of amyloids in malaria pathophysiology.

Moles E, Valle-Delgado JJ, Urbán P, Azcárate IG, Bautista JM, Selva J, Egea G, Ventura S, Fernàndez-Busquets X. *Future Science OA. 2015;1(2), FSO43. doi:10.4155/fso.15.43.*

CHAPTER 1

Journal of Controlled Release 210 (2015) 217–229

Contents lists available at ScienceDirect

Journal of Controlled Release

journal homepage: www.elsevier.com/locate/jconrel

Immunoliposome-mediated drug delivery to *Plasmodium*-infected and non-infected red blood cells as a dual therapeutic/prophylactic antimalarial strategy

Ernest Moles [a,b,c], Patricia Urbán [a,b,c], María Belén Jiménez-Díaz [d], Sara Viera-Morilla [d], Iñigo Angulo-Barturen [d], Maria Antònia Busquets [c,e], Xavier Fernàndez-Busquets [a,b,c,*]

[a] Nanomalaria Group, Institute for Bioengineering of Catalonia (IBEC), Baldiri Reixac 10-12, ES-08028 Barcelona, Spain
[b] Barcelona Institute for Global Health (ISGlobal, Hospital Clínic-Universitat de Barcelona), Rosselló 149-153, ES-08036 Barcelona, Spain
[c] Nanoscience and Nanotechnology Institute (IN2UB), University of Barcelona, Martí i Franquès 1, ES-08028 Barcelona, Spain
[d] Tres Cantos Medicines Development Campus, GlaxoSmithKline, Severo Ochoa 2, ES-28760 Tres Cantos, Spain
[e] Departament de Fisicoquímica, Facultat de Farmàcia, University of Barcelona, Av. Joan XXIII, s/n, ES-08028 Barcelona, Spain

ARTICLE INFO

Article history:
Received 26 February 2015
Received in revised form 20 May 2015
Accepted 21 May 2015
Available online 23 May 2015

Chemical compounds studied in this article:
Chloroquine (PubChem CID: 2719)
Primaquine (PubChem CID: 4908)
DSPC (PubChem CID: 94190)
DOPC (PubChem CID: 6437081)
Cholesterol (PubChem CID: 5997)
Maleimide (PubChem CID: 10935)
SATA (PubChem CID: 127532)
Pyranine (PubChem CID: 61389)
Hoechst 33342 (PubChem CID: 1464)

Keywords:
Immunoliposomes
Malaria
Nanomedicine
Plasmodium
Targeted drug delivery

ABSTRACT

One of the most important factors behind resistance evolution in malaria is the failure to deliver sufficiently high amounts of drugs to early stages of *Plasmodium*-infected red blood cells (pRBCs). Despite having been considered for decades as a promising approach, the delivery of antimalarials encapsulated in immunoliposomes targeted to pRBCs has not progressed towards clinical applications, whereas in vitro assays rarely reach drug efficacy improvements above 10-fold. Here we show that encapsulation efficiencies reaching >96% are achieved for the weak basic drugs chloroquine (CQ) and primaquine using the pH gradient loading method in liposomes containing neutral saturated phospholipids. Targeting antibodies are best conjugated through their primary amino groups, adjusting chemical crosslinker concentration to retain significant antigen recognition. Antigens from non-parasitized RBCs have also been considered as targets for the delivery to the cell of drugs not affecting the erythrocytic metabolism. Using this strategy, we have achieved unprecedented complete nanocarrier targeting to early intraerythrocytic stages of the malaria parasite for which there is a lack of specific extracellular molecular tags. Immunoliposomes studded with monoclonal antibodies raised against the erythrocyte surface protein glycophorin A were capable of targeting 100% RBCs and pRBCs at the low concentration of 0.5 μM total lipid in the culture, with >95% of added liposomes retained on cell surfaces. When exposed for only 15 min to *Plasmodium falciparum* in vitro cultures of early stages, free CQ had no significant effect on the viability of the parasite up to 200 nM, whereas immunoliposomal 50 nM CQ completely arrested its growth. In vivo assays in mice showed that immunoliposomes cleared the pathogen below detectable levels at a CQ dose of 0.5 mg/kg, whereas free CQ administered at 1.75 mg/kg was, at most, 40-fold less efficient. Our data suggest that this significant improvement is in part due to a prophylactic effect of CQ found by the pathogen in its host cell right at the very moment of invasion.

1. Introduction

The majority of chemotherapeutic approaches against malaria are targeted at the *Plasmodium* stages infecting red blood cells (RBCs), which are responsible for all symptoms and pathologies of the disease [1]. Because of the amphiphilicity of most current antimalarial drugs, they are extensively distributed into body tissues after administration and can be rapidly metabolized in the liver [2]. In the blood vessels, antimalarial drugs circulate mainly associated to plasma proteins [3] and are usually quickly removed from circulation, presenting relatively short half-lives from less than 1 h to few hours [2]. These shortcomings are usually compensated through administration of increased doses, in a delicate narrow edge between high overall amounts causing toxic side effects [4] and low local concentrations inducing resistance evolution in most malaria-endemic countries [5].

Drugs specifically targeted to parasitized RBCs (pRBCs) would benefit from a reduction in the body distribution volume, lasting longer in the bloodstream while avoiding degradation, and increasing exposure of the pathogen to lethal doses. Liposomal nanovectors bearing cell-specific antibodies on their surfaces (immunoliposomes, iLPs) have

* Corresponding author at: Nanomalaria Group, Institute for Bioengineering of Catalonia (IBEC), Baldiri Reixac 10-12, ES-08028 Barcelona, Spain.
E-mail address: xfernandez_busquets@ub.edu (X. Fernàndez-Busquets).

http://dx.doi.org/10.1016/j.jconrel.2015.05.284
0168-3659/

been widely considered as chemotherapeutic drug carriers due to their non-toxic and biodegradable character [6], but they have not progressed yet towards a working strategy for malaria therapeutics. Pioneering assays to treat *Plasmodium berghei* infections in mice focused on the encapsulation of the antimalarial drug chloroquine into liposomes (LPs) and iLPs functionalized with antibodies against RBCs and pRBCs [7–9]. Drug efficacy was significantly improved upon encapsulation, especially when targeted towards pRBCs, and after treatment with iLPs, mice exhibited lower parasitemias and longer survival times even with drug-resistant strains. These improvements were attributed to the specific interaction of targeting antibodies with RBCs/pRBCs and to the efficient incorporation of LP contents into the cells, although liposomal models were poorly characterized with no direct evidence for LP internalization and absence of encapsulated drug stability and release kinetics analyses. Moreover, because all these studies were done in murine malarias, there was a lack of data for human-infecting parasites, particularly for the deadliest species, *Plasmodium falciparum*.

Recently, in vitro assays in *P. falciparum* have shown that LPs functionalized with pRBC-specific antibodies can specifically recognize target cells vs. non-infected erythrocytes in less than 90 min [10]. The short time required to achieve complete specificity was an encouraging result that opened good perspectives regarding the development of a rapid delivery nanovector capable of competing with LP clearance from blood by macrophages and the liver [11]. Nevertheless, this good targeting has not been able to provide improvements in drug efficacy above 10-fold [12], and parasitemia could not be completely eliminated from the cultures. In vivo assays in mice grafted with human erythrocytes and subsequently infected with *P. falciparum* [13] showed that some iLP-encapsulated antimalarials had a clearly improved efficacy (Fig. 1A). However, as in in vitro assays, *Plasmodium* parasites could not be completely cleared despite the continuous presence of iLPs in the blood of mice during the entire length of four-day tests (Fig. 1B).

Often, the particularities of malaria pathophysiology have not been sufficiently considered when designing iLPs for targeted antimalarial drug delivery. Most drugs used in the treatment of malaria are amphiphilic compounds whose capacity to solubilize in both aqueous and organic phases allows them to easily cross lipid bilayers, which complicates their liposomal encapsulation. Therefore, special liposome formulations including saturated long-chain phospholipids with elevated phase transition temperatures (>37 °C) together with low amounts of cholesterol are crucial components required to avoid the otherwise quick leakage of small molecules [14]. In addition, since lipid bilayers are highly impermeable to ionized species, working at the adequate pH is paramount to sustain a proton gradient and attain higher liposomal drug loads. Other factors to be taken into account are the nature, location, and abundance of markers on pRBC surfaces: although *Plasmodium* proteins are found in the plasma membrane of pRBCs [15], those currently known are highly variable or have a low abundance [16]. Given this scarcity of adequate antigens exposed on pRBCs, essential parameters that will be determinant in the capacity of iLPs to recognize and bind target cells are a careful selection of sufficiently specific antibodies, the way they are crosslinked to lipids, and their numbers on the liposome surface. Since RBCs have very poor endocytic processes [17], once iLPs are docked to them delivery of cargo into the cell has been proposed to occur through a membrane fusion process [7,10,18,19]. Nevertheless, considering the lack of strong evidence and the poor characterization of this fusion process using RBCs and pRBCs as targeted cells, alternative mechanisms of interaction should be considered. These include, but are not limited to, the stable adsorption on the target cell surface or the entry through the tubulovesicular network (TVN) [17] and other modifications suffered by erythrocyte membranes when the cell has been parasitized by *Plasmodium*.

Here we have dissected the different iLP parts to propose a rational design strategy for the administration of lethal amounts of drugs to the intraerythrocytic pathogen. The results presented can significantly contribute to developing new and optimized targeted drug delivery approaches against malaria based on a dual and simultaneous (i) therapeutic activity on pRBCs and (ii) prophylactic effect against erythrocyte infection by *Plasmodium*.

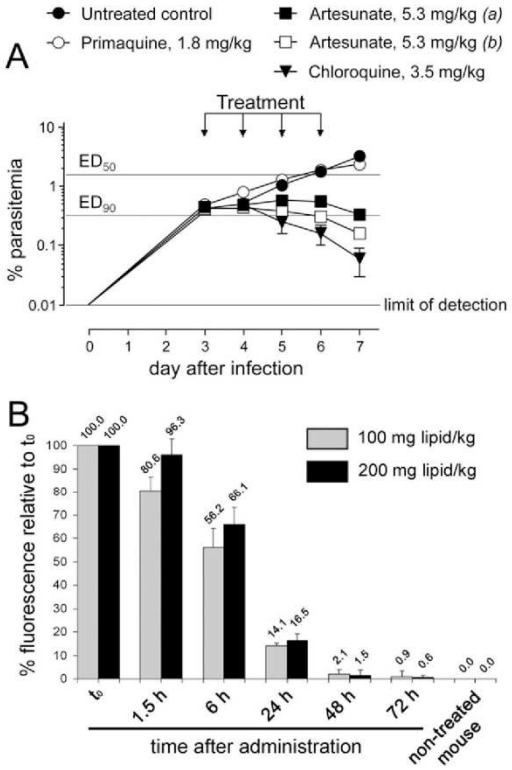

Fig. 1. (A) 4-day test in female immunodeficient mice engrafted with human erythrocytes and infected i.v. with *P. falciparum*. The different curves correspond to drug-containing iLPs functionalized with the pRBC-specific antibody *BM1234* as previously described [10]. *(a)* and *(b)* correspond to artesunate-containing iLPs where the drug was added, respectively, to the lipid mixture before evaporation of the solvent, or to the aqueous buffer added to the dry lipids to form LPs. (B) Residence time in the bloodstream of mice of rhodamine-labeled LPs with the same lipid composition as in (A).

2. Materials and methods

2.1. Materials

Except where otherwise indicated, reactions were performed at room temperature (20 °C), and reagents were purchased from Sigma-Aldrich Corporation (St. Louis, MO, USA). The lipids (all ≥99% purity according to thin layer chromatography analysis) 1,2-dioleoyl-*sn*-glycero-3-phosphocholine (DOPC), 1,2-distearoyl-*sn*-glycero-3-phosphocholine (DSPC), 1,2-dioleoyl-*sn*-glycero-3-phosphoethanolamine-N-[4-(p-maleimidophenyl)butyramide] (MPB-PE), 1,2-distearoyl-*sn*-glycero-3-phosphoethanolamine-N-[maleimide(polyethylene glycol)-2000] (DSPE-PEG2000-Mal), 1,2-dioleoyl-*sn*-glycero-3-phosphoethanolamine-N-[lissamine rhodamine B sulfonyl] (DOPE-Rho), and 1,2-dioleoyl-*sn*-glycero-3-phosphoethanolamine-N-[methoxy(polyethylene glycol)-2000] (PE-PEG2000) were purchased from Avanti Polar Lipids Inc. (Alabaster, AL, USA). Mouse monoclonal IgG anti-human GPA SM3141P, rabbit polyclonal IgG anti-human GPA AP05437PU-N, mouse monoclonal anti-HRP2 AM01200PU-N, and mouse monoclonal IgM BM1234 were purchased from Acris Antibodies, Herford, Germany.

2.2. Preparation of LPs and encapsulation of drugs

LPs with a basic formulation of neutrally charged unsaturated (DOPC:cholesterol, 80:20) or saturated (DSPC:cholesterol, 90:10) phospholipids were prepared by the lipid film hydration method [20]. Briefly, stock lipids in chloroform were mixed and dissolved in chloroform:methanol (2:1, v/v) in a round-bottomed flask. Organic solvents were removed by rotary evaporation under reduced pressure at 37 °C, in a progressive vacuum range from −20 to −70 mm Hg, to yield a thin lipid film on the flask bottom and walls. For passive drug encapsulation, the dried lipids were then hydrated to 10 mM total lipid in 10 mM phosphate buffer, pH 6.5, containing the desired drug/molecule to encapsulate and osmotically adjusted to 320 mOsm/kg (isotonic with *P. falciparum* growth medium) by addition of 5 M NaCl. Multilamellar LPs were formed by 3 cycles of constant vortexing followed by bath sonication for 3 min each, and downsized to unilamellar vesicles by extrusion through 200 nm polycarbonate membranes (Poretics, Livermore, CA, USA) in an extruder device (LiposoFast, Avestin, Ottawa, Canada). Throughout the lipid film hydration and downsizing process samples were maintained above lipid transition temperature. LP size was determined by dynamic light scattering using a Zetasizer NanoZS90 (Malvern Ltd, Malvern, UK). Unencapsulated material was removed by buffer exchange in 7-kDa Zeba™ spin desalting columns (Thermo Fisher Scientific, Inc.) using isotonic phosphate buffered saline (PBS) at the desired pH (7.5 unless otherwise indicated). Finally, liposomal suspensions to be used in assays with live cells were sterile filtered through 0.22 μm pore size polyvinylidene difluoride (PVDF) filters (Millex-GV Syringe Filter Units, 4 mm, Millipore). Active encapsulation by the pH gradient method was done following an adaptation of established protocols [21], substituting saturated DSPC for unsaturated DOPC to obtain a lipid bilayer capable of sustaining a proton gradient. LPs were prepared in 200 mM citrate buffer at pH 4.0 and buffer exchanged with isotonic PBS containing 10 mM ethylenediaminetetraacetic acid (EDTA) in order to establish a pH gradient across the LP membrane. One volume of drug was then mixed with ten volumes of LPs to reach final concentrations of 500 μM chloroquine (CQ) and 1 mM primaquine (PQ) and the mixture was stirred for 30 min at room temperature before immediately proceeding, when required, to antibody coupling.

2.3. Generation of polyclonal antibodies against $MAHRP1_{21-40}$ peptide

$MAHRP1_{21-40}$ (ADVPTEGMDVPFGFFDKNTL) was synthesized (Peptide Synthesis Service, Scientific and Technological Centers, University of Barcelona) with an additional cysteine at the carboxy terminal end. Immunization of rabbits was done at the facilities of the Animal Experimentation Services (University of Barcelona) following standard protocols. Serum antibodies were purified by affinity chromatography using the corresponding peptides immobilized on agarose beads (SulfoLink Kit, Pierce Biotechnology, Rockford, IL, USA), assayed by Enzyme-Linked ImmunoSorbent Assay (ELISA), and finally stored at −20 °C.

2.4. Generation of iLPs

Freshly prepared maleimide-containing LPs were conjugated with thiolated antibodies following established protocols [22]. The generation of sulfhydryl groups in antibodies was performed through three alternative approaches: (i) Half-antibodies bearing free thiols generated by reduction with 2-mercaptoethylamine-HCl (MEA, Thermo Fisher Scientific, Inc.) were obtained as described previously [10]. (ii) Reactive aldehyde groups (CHO) were generated in the carbohydrate moieties of antibody (Ab) Fc regions by oxidation in PBS containing 5 mM sodium periodate (1 h, protected from light) [23]. Oxidized antibodies were then recovered by buffer exchange in PBS, pH 7.2, and conjugated by hydrazone linkage through a 2-h incubation with a 150-fold molar excess of freshly dissolved 3-(2-pyridyldithio)propionyl hydrazide crosslinker (PDPH, Thermo Fisher Scientific, Inc.). The number of reactive aldehyde groups available (ca. 2/Ab) was quantified before PDPH conjugation by incubation of oxidized antibodies with Lucifer Yellow CH fluorescent dye, as described previously [24]. Excess of crosslinker was removed by buffer exchange in SAS buffer (100 mM sodium acetate, 50 mM NaCl, pH 4.4) and thiol groups were finally exposed through pyridyldithiol group cleavage by addition of 25 mM dithiothreitol (DTT) and incubation for 20 min. (iii) For the non-oriented binding through primary amino groups, antibodies in PBS were reacted for 30 min with a 10× to 100× molar excess relative to antibody molecules of the crosslinker N-succinimidyl S-acetylthioacetate (SATA, Thermo Fisher Scientific, Inc.) freshly dissolved in dimethyl sulfoxide. Unreacted SATA was removed by buffer exchange in PBS and protected thiols in SATA-conjugated antibodies were exposed by addition of 50 mM hydroxylamine and 2.5 mM EDTA. After thiolation, antibodies were recovered by buffer exchange in PBS supplemented with 10 mM EDTA and the number of available sulfhydryl groups was determined by reaction with 5,5′-dithio-bis-(2-nitrobenzoic acid) (DTNB, Thermo Fisher Scientific, Inc.). 400 μg DTNB/ml was added to the thiolated antibody solution, and after 20 min the formation of 2-nitro-5-thiobenzoic acid was quantified by measuring its absorbance at 412 nm. Finally, coupling of freshly thiolated antibodies to freshly prepared maleimide-containing LPs was done overnight (12 to 15 h) in PBS supplemented with 10 mM EDTA. Unbound antibodies were removed by ultracentrifugation (150,000 *g*, 1 h, 4 °C), maintaining the same tonicity and LP concentration (10 mM lipid) during the whole process. For the intercalation of a polyethylene glycol (PEG) linker between LP and antibody, DSPE-PEG2000-Mal was substituted for MPB-PE in the LP formulation. Pelleted iLPs were taken up in PBS and stored at 4 °C for up to one month before being used. Antibody coupling was quantitatively assessed by protein determination with the DC™ Protein Assay (Bio-Rad). Coupling efficiency (%) was determined as the fraction of LP-bound antibody relative to total antibody added; the number of bound antibodies per LP was determined considering an IgG molecular mass of 150 kDa and the theoretical lipid content of a LP 170 nm in diameter composed solely of phosphatidylcholine [25]. For qualitative SDS-polyacrylamide gel electrophoresis (PAGE) coupling analysis, supernatant and pelleted iLP samples were heated at 90 °C for 3 min in 1× Laemmli sample buffer, supplemented with 355 mM 2-mercaptoethanol, and electrophoresed in 7.5% SDS-polyacrylamide gels using the Mini Protean II System (Bio-Rad). For silver staining of gels [26], they were fixed (40% ethanol, 10% acetic acid) during 30 min and activated (30% ethanol, 41 mg/ml sodium acetate, 1.27 mg/ml sodium thiosulfate) for 30 min. After washing with deionized water (Milli-Q system, Millipore), gels were stained (1 mg/ml silver nitrate, 0.02% formaldehyde) for 40 min and protein bands were developed (25 mg/ml sodium carbonate, freshly prepared 0.01% formaldehyde). Finally, the reaction was terminated by addition of 1% acetic acid and gels were stored in 10% glycerol solution.

2.5. Quantification of drugs and fluorescent dyes in LP samples

Encapsulated CQ and PQ were quantified by measuring their respective absorbances at 342 and 352 nm after LP (0.5 mM lipid) disruption by treatment with 2% v/v Triton X-100 in PBS, subtracting the lecture of drug-free LPs. Encapsulated fluorescent dye quantification was performed by fluorescence analysis (Synergy HT Multi-Mode Microplate Reader, BioTEK) of pyranine ($\lambda_{ex/em}$ = 488/520 nm), and of rhodamine-conjugated lipid (DOPE-Rho; $\lambda_{ex/em}$ = 530/590 nm). Encapsulation efficiency (EE, %) represents the encapsulated fraction relative to total compound added to the LP-containing solution. High performance liquid chromatography–tandem mass spectrometry (HPLC–MS/MS) was used to quantify CQ concentrations below the detection limit of UV–Vis spectroscopy (20 nM and 2 μM CQ detection limits for HPLC–MS/MS and UV–Vis spectroscopy, respectively), according to established protocols [12]. The release rate from LPs of encapsulated CQ and PQ was determined at selected timepoints by drug quantification in the supernatants

and corresponding pelleted LPs obtained after ultracentrifugation (100,000 *g*, 45 min, 4 °C). Release rates were expressed as the percentage of drug in the supernatant relative to the total drug present in the sample. All experimental values are represented as mean ± SD for 3 replicates.

2.6. *P. falciparum* in vitro culture and growth inhibition assays

P. falciparum strain 3D7 was grown in vitro in group B human erythrocytes using previously described conditions [27]. Parasites (thawed from glycerol stocks) were cultured at 37 °C in Petri dishes with RBCs at 3% hematocrit in Roswell Park Memorial Institute (RPMI) complete medium containing Albumax II (RPMI-A, Invitrogen), supplemented with 2 mM L-Glutamine, under a gas mixture of 92% N_2, 5% CO_2, and 3% O_2. Synchronized cultures in early ring stages (0–24 h post-invasion) were obtained by 5% sorbitol lysis [28]. Late-form trophozoite and schizont stages (24–36 h and 36–48 h post-invasion, respectively) were purified in 70% Percoll (GE Healthcare) [28,29]. Parasitemia was determined by microscopic counting of blood smears fixed briefly with methanol and stained with Giemsa (Merck Chemicals) diluted 1:10 in Sorenson's buffer, pH 7.2, for 10 min. For culture maintenance, parasitemia was kept below 5% late forms and 10% early forms by dilution with freshly washed RBCs and the medium was changed every 1–2 days. For *P. falciparum* in vitro growth inhibition assays, cultures synchronized (>95%) in early ring or late form stages were brought to 4% hematocrit and 1% parasitemia by dilution with fresh RBCs. After adding one culture volume of 2× concentrated drug solution in RPMI-A, cultures were incubated for 15 min in 2-ml Petri dishes under orbital stirring, transferred to microcentrifuge tubes, and cells were spun down, finally replacing the medium with fresh RPMI-A. Unless otherwise specified, the data presented throughout the manuscript refer to samples containing 2% hematocrit. The resulting cell suspension was then seeded on 96-well plates (Merck Chemicals) and further incubated for a complete 48-h growth cycle under the conditions described above. For growth inhibition determination, samples were diluted 1:100 in PBS, and the nuclei of pRBCs (the only nucleated cells present in the culture) were stained by addition of 0.1 μM Syto11 (Thermo Fisher Scientific, Inc.) in the final mixture before proceeding to flow cytometry analysis.

2.7. Protein expression analysis throughout the 48-h intraerythrocytic cycle

For the analysis of MAHRP-1 (*BM1234* antigen) and HRP2 protein expression throughout the whole intraerythrocytic cycle of *P. falciparum*, tightly synchronized cultures (0–5 h range, 8% parasitemia) were obtained using a combination of 70% Percoll and 5% sorbitol (5 h after release of merozoites) stage-selection methods as described above. Culture samples corresponding to 3 μl pRBCs were obtained at the following post-infection timepoints: 12 h and 20 h (rings); 26 h, 35 h and 38 h (trophozoites); 42 h, 44 h and 46 h (schizonts). Protein expression was analyzed by subcellular detergent fractionation (see below) and SDS-PAGE/Western blot, as previously described [10], using the primary monoclonal antibodies *BM1234* (2 μg/ml) and anti-HRP2 (0.5 μg/ml), and as secondary antibody goat anti-mouse IgG horseradish peroxidase-conjugated (1 μg/ml, Thermo Fisher Scientific, Inc.).

2.8. Fluorescence microscopy

Antigen localization in fixed cells by fluorescence confocal microscopy was done according to established protocols [10]. Briefly, air-dried blood smears were fixed in 1% formaldehyde and cell membranes were labeled with 3.3 μg/ml wheat germ agglutinin-tetramethylrhodamine (WGA-Rho) conjugate (Molecular Probes, Eugene, OR, USA). Slides were then incubated in the presence of 20 μg/ml of the mouse monoclonal antibodies *BM1234* or anti-HRP2, and the rabbit polyclonal antibodies anti-PfEMP1 (raised against the conserved C-terminal domain, gently provided by Dr. Alfred Cortés) and MAHRP1$_{21–40}$, followed by incubation in the presence of 6.7 μg/ml of the corresponding Alexa Fluor® secondary antibodies goat anti-mouse AF488 or AF660, or goat anti-rabbit AF488 (all from Molecular Probes), and of 1 μg/ml 4′ 6-diamino-2-phenylindole (DAPI, Invitrogen) for nuclei staining. All antibody treatments were done for 1 h in the presence of 0.75% w/v bovine serum albumin as blocking agent. Finally, slides were washed with PBS, mounted with ProLong® Gold antifade reagent (Molecular Probes), and examined with a Leica TCS SP5 laser scanning confocal microscope as described [10].

For immunofluorescence assays with live cells of the targeting efficiency of free antibodies and iLPs, *P. falciparum* cultures at 5% parasitemia were washed 3× with RPMI-A (700 *g*, 2 min) and nuclei were stained for 30 min with 2 μg/ml Hoechst 33342 (Molecular Probes). Excess dye was removed by washing cells 3× with RPMI-A and hematocrit was lowered to 2.5% trough RPMI-A addition. Four volumes of this culture were then added to 1 vol of antibody- or iLP-containing samples to reach, respectively, 70 μg antibody/ml or 1 mM lipid, and 2% hematocrit, and samples were incubated for 1.5 h at 37 °C under orbital mixing. When using the free monoclonal antibody anti-GPA, its concentration was lowered to 1 μg/ml because of excessive RBC agglutination found at higher concentrations, with no significant difference in targeting. iLPs loaded with the fluorescent dye pyranine were observed directly, whereas antibodies were detected with the corresponding fluorescent secondary antibodies as described above, but diluted in RPMI-A. Finally, cells were washed 3× with RPMI-A and placed at 0.2% hematocrit into MatTek culture plates for further analysis with an Olympus IX51 inverted system microscope, equipped with an IX2-SFR X–Y stage, a U-TVIX-2 camera, and a fluorescence mirror unit cassette for UV/blue/green excitation and detection of their respective blue/green/red emission ranges. Phase contrast images were acquired simultaneously.

2.9. Flow cytometry

For growth inhibition determination and quantitative live cell targeting examination of antibodies and iLPs, samples were analyzed at 0.02% hematocrit in PBS with a BD LSRFortessa flow cytometer (Becton, Dickinson and Company, New Jersey, USA). Forward- and side-scatter in a logarithmic scale were used to gate the RBC population. Green fluorescent dyes (Syto11, pyranine, and AF488) and Hoechst 33342 were detected, respectively, by excitation through a 488 or 355 nm laser at 50 mW power and emission collection with a 530/30 or 450/50 nm bandpass filter. Acquisition was configured to stop after recording 20,000 events within the RBC population. Parasitized erythrocytes in late forms were distinguished from those in young forms, when required, by means of their increased DNA and RNA content giving higher Syto11 signal intensity values.

2.10. Transmission electron microscopy (TEM)

P. falciparum cultures sorbitol-synchronized at ring, trophozoite, and schizont stages were washed 3× with PBS (470 *g*, 5 min), and 6-μl volumes of pelleted cells were fixed in 500 μl of 4% v/v formaldehyde in PBS for 1 h at 4 °C under orbital stirring. The fixing solution was changed to 2% v/v formaldehyde in PBS and cells were left in the same solution at 4 °C for 24 h until gelatine embedding. Prior to fixation, ring samples were at 10% parasitemia, whereas trophozoite and schizont stages were enriched to >90% parasitemia in 70% Percoll. After fixation, sample processing for the preparation of ultrathin cryosections was done as previously described [30]. Cryosections were incubated for 30 min in PBS containing 5% fetal bovine serum with the corresponding primary antibodies (mouse *BM1234*, anti-HRP2 and anti-GPA at 40 μg/ml, and rabbit anti-MAHRP1$_{21–40}$ at 21 μg/ml), followed by secondary antibodies (50 μg/ml goat anti-mouse or goat anti-rabbit IgG H + L) coupled to 12-nm colloidal gold particles (Jackson ImmunoResearch Laboratories Inc., West Grove, PA, USA). As control for non-specific secondary antibody binding the primary antibody was omitted; non-infected red blood cells were also processed as a control for non-specific interactions

of the primary antibodies. Sample observations were done in an electron microscope Jeol J1010 (Jeol, Japan) with a CCD SIS Megaview III camera.

For immunocryo-TEM analysis of anti-GPA targeted iLPs, a thin aqueous film was formed by dipping a glow discharged holey carbon grid in the iLP suspension and then blotting the grid against filter paper. The resulting thin sample films spanning the grid holes were then incubated with a 1:20 v/v dilution of goat anti-mouse IgG (H + L) antibody coupled to 6-nm colloidal gold particles (Jackson ImmunoResearch Laboratories Inc.) for 30 min and washed twice in PBS. Sample vitrification and microscope analysis were done as described previously [10].

2.11. Subcellular protein fractionation

Differential detergent fractionation of pRBC proteins was essentially performed as previously described [31]. PBS supplemented with 1× complete protease inhibitor cocktail (Roche) was used for the washing of cells and as buffer for all detergent-containing samples; all fractions were obtained using the same detergent extraction volume, calculated as 6× pRBC pellet starting volume. Cells were extensively washed and extracted with 0.15% saponin for 10 min at 4 °C, pelleted by centrifugation (10,000 *g*, 15 min, 4 °C), and the resulting supernatant was rescued as the saponin-soluble fraction. The saponin-insoluble pellet was washed again before being extracted with 1% Triton X-100 (30 min, 4 °C). Samples were centrifuged (20,000 *g*, 30 min, 4 °C) and the resulting supernatant was rescued as the Triton-soluble fraction. Finally, the Triton-insoluble pellet was washed again before the final extraction with 2× SDS-containing reducing Laemmli sample buffer (supplemented with 355 mM 2-mercaptoethanol) for 30 min at 60 °C while vigorously mixing by vortex every 10 min. The final SDS-soluble fraction was then collected after spinning down cell debris (16,000 *g*, 15 min). For two-dimensional-PAGE, the Triton-insoluble pellet was extracted with O'Farrell lysis buffer (5% v/v 2-mercaptoethanol, 2% w/v NP-40, 9.5 M urea) [32] for 30 min at 30 °C under sonication (30-second pulses, 100% amplitude) until pellet disaggregation. Saponin, Triton, and SDS fractions mainly contained, respectively, cytosolic proteins, membrane and organelle proteins, and nuclear and detergent-resistant cytoskeletal/matrix proteins. Because erythrocytes lack a cell nucleus and have few organelles, most of the proteins from the last two fractions will belong to *P. falciparum*.

2.12. Two-dimensional (2D)-SDS-PAGE

To two 140-μl protein samples (containing 80 μg of total protein each) were added a trace amount of Bromophenol blue and an aliquot of immobilized pH gradient (IPG) buffer to reach a final concentration of 0.5% v/v. For the first dimension isoelectric focusing, samples were loaded onto two 7-cm immobilized pH gradient strips, pH 3–10 (Immobiline® DryStrip, GE Healthcare, Life Sciences), subjected to overnight passive rehydration (13 h, 20 °C) and then run on a IPGphor device (first step-and-hold, 1 h, 50 V; second step-and-hold, 0.5 h, 300 V; third gradient step 0.5 h to reach 1000 V; fourth gradient step, 1.5 h to reach 5000 V; and finally a fifth step-and-hold, 2.5 h, 5000 V; the accumulated voltage was 5632 KV·h). Prior to the second dimension, the IPG strips were equilibrated in two steps for 15 min each with gentle shaking in 3 ml of equilibration buffer (first equilibration solution: 50 mM Tris–HCl, pH 8.8, 6 M urea, 30% w/v glycerol, 2% SDS, 65 mM DTT and a trace amount of Bromophenol blue; for the second equilibration solution, DTT was replaced by 135 mM iodoacetamide). The second dimension SDS-PAGE was performed in a vertical Mini Protean Hoefer system (Hoefer, Inc.). After equilibration, strips were transferred to the second dimension in two 12.5% polyacrylamide gels (0.375 M Tris–HCl, pH 8.8, 0.1% SDS) run for 1 h at 100 V and 20 mA/gel (running buffer: 25 mM Tris-base, 192 mM glycine, 0.1% SDS, pH 8.6). The BenchMark™ Protein Ladder 10747-012 (Invitrogen) was run in parallel as molecular mass marker. One of the gels was silver-stained as described above, scanned (GS 800 Calibrated Densitometer M, Bio-Rad), and the image obtained was processed (Quantity One software image analysis, Bio-Rad). The other gel was transferred to a PVDF membrane (Hybond-P, Amersham Biosciences) and processed for Western blot analysis of proteins as previously described [10]. After incubation with the mouse monoclonal antibody *BM1234* (2 μg/ml) followed by goat anti-mouse IgG horseradish peroxidase-conjugated (1 μg/ml, Thermo Fisher Scientific, Inc.), chemiluminescence was recorded (ImageQuant LAS 4000, GE Healthcare Life Sciences) and the membrane was finally stained with Ponceau S (0.1% w/v in 5% v/v acetic acid) for 10 min. The region containing the two spots detected by *BM1234* was identified by triangulation using protein spots common to Ponceau and silver stains, excised from the silver-stained gel, and subjected to LC–MS/MS for protein identification.

2.13. Liquid chromatography with tandem mass spectrometry (LC–MS/MS)

Trypsin digestion of proteins in silver-stained gel slabs was performed in a ProGest™ automatic digestor (Genomic Solutions). Each sample was washed with 50 mM NH_4HCO_3 and acetonitrile (ACN), reduced in 10 mM DTT (30 min, 56 °C), alkylated in 55 mM iodoacetamide (30 min, 30 °C, protected from light), and digested with 80 ng of porcine trypsin (Trypsin Gold, Promega) for 16 h at 37 °C. The resulting peptides were extracted from the gel matrix with 5% formic acid (FA) and ACN, and dried in a SpeedVac concentrator. LC–MS/MS identification was performed in a Cap-LC-nano-ESI-Q-TOF system (Micromass-Waters). Dried peptides were taken up in 100 μl of 1% FA and 4–10 μl of the resulting solution was injected into the liquid chromatography system equipped with a reverse phase C18 column (75 μm internal diameter, 3 μm particle, 15 cm length; NanoEase Atlantis, Waters), with a mobile phase gradient 5–60% B in 35 min (A: 2% ACN, 0.1% FA; B: 90% ACN, 0.1% FA). Eluted peptides were ionized trough electrospray (NanoES PicoTip™ emitter, New Objective) with an applied voltage of 2 KV to capillary/needle and 60 V to cone. A 400–1800 m/z range of peptide masses was analyzed in full scan MS mode (1 s scan time, 10,000 full width at half maximum resolution). Within this range, the 10 most abundant peptides were selected (minimum intensity of 28 counts/s) for their fragmentation by collision-induced dissociation (20 eV collision energy, Ar gas) in the MS/MS analysis (1 s scan time, 100–1700 m/z range). Peptide fragmentation generated a pkl file (MassLynx MS software) and sequences were matched with the NCBInr on-line database using the MASCOT search engine.

2.14. Determination of LP half-life time in blood plasma

LPs fluorescently labeled and PEG-grafted (DOPC:cholesterol:DOPE-Rho:PE-PEG2000, 64:20:1:15), were injected intravenously at 200 mg/kg doses to ICR-CD1 mice females of ca. 23 g (Harlan Laboratories). Blood samples of ca. 30–40 μl were then collected in Microvette heparinized tubes (Sarstedt) from the terminal portion of the tail at the post-administration times: t_0 (2 min), 1.5 h, 6 h, 24 h, 48 h and 72 h. Samples were separated into supernatant (plasma, stored at −80 °C until analysis) and cells by centrifugation at 4000 *g* for 3 min. For fluorescence quantification of LPs containing the rhodamine-conjugated lipid DOPE-Rho, plasma samples were thawed on ice, diluted with one volume of 2% Triton X-100 in PBS and 5 replicas of 2-μl drops were placed on a methanol-activated PVDF membrane. Fluorescence signal from spotted samples was imaged and analyzed with an ImageQuant LAS 4000 biomolecular imager with green RGB light source and 1/100- to 30-s exposure time. Plasma autofluorescence signal was subtracted from samples using plasma collected from an untreated mouse. LP concentration was calculated by linear regression using serial-fold dilutions of stock LPs in PBS spotted on the same membrane at known concentrations. Finally, concentration values were normalized to t_0 (100%) and LP half-life time ($t_{1/2}$, time after which 50% of the administered LPs are removed from plasma), was determined.

2.15. In vivo 4-day test in P. falciparum-infected mice

Female immunodeficient NOD.Cg-*Prkdc*^{scid} *Il2rg*^{tm1Wjl}/SzJ (NOD scid gamma, NSG) mice were engrafted with human erythrocytes and infected i.v. with the *P. falciparum* 3D7$^{0087/N9}$ strain generated in GlaxoSmithKline (Tres Cantos, Spain), using established methods [33]. These mice sustain in circulation high amounts of human RBCs (ca. 1 to 1.75 × 10^{10} in 2.5 ml blood). The inoculum was 2 × 10^{7} *P. falciparum*-infected erythrocytes, and free or encapsulated drugs were administered i.v. in PBS for four consecutive days starting at day 3 after infection, using 2 mice/compound. Parasitemia was measured by flow cytometry as described [34], with 0.01% sensitivity of detection. Sampling was every 24 h after the start of treatment until the end of assays. Effective dose 50% (ED_{50}) and ED_{90} are defined as the dose in mg/kg that reduces parasitemia at day 7 after infection by 50% and 90%, respectively, relative to vehicle-treated mice. The human biological samples were sourced ethically and their research use was in accord with the terms of the informed consents. All animal studies were ethically reviewed and carried out in accordance with European Directive 86/609/EEC and the GSK Policy on the Care, Welfare and Treatment of Animals.

3. Results

3.1. Passive vs. active encapsulation methods for the entrapment of antimalarial drugs into LPs

Because of their amphiphilic nature, depending on pH the weak basic antimalarial drugs chloroquine (CQ) and primaquine (PQ) are found in their uncharged, monoprotonated and diprotonated forms (Fig. 2), which have different organic/aqueous partitioning degrees. The encapsulation efficiencies (EEs) of CQ and PQ passively loaded through the lipid film hydration method [20] into LPs composed mainly of neutrally charged unsaturated phospholipids (DOPC:cholesterol, 80:20) were determined at different lipid film hydration solution pHs and initial drug concentrations (Table 1). Passive EE was several-fold higher for PQ vs. CQ, which can be explained because of their different protonation degree. Whereas for the wide pH range 4.0–7.4 CQ becomes fully protonated (≥99% CQ^{2H+}), PQ is found mainly in its monoprotonated species (≥86% PQ^{H+}), which confers PQ a lower ionization state and therefore higher hydrophobicity and interaction with the LP lipid bilayer. The significant EE increase for lower drug amounts at a fixed pH (Supplementary Table 1) indicates saturation of passive LP encapsulation capacity. On the other hand, in agreement with previous reports [21,35,36], active encapsulation of CQ and PQ by establishing a pH gradient 4.0–7.5 inside-outside of LPs composed mainly of neutrally charged saturated phospholipids (DSPC:cholesterol, 90:10) resulted in EE values close to 100% (Table 1). Drug amounts during active encapsulation into LPs were selected according to the aforementioned works as those highest possible while avoiding a significant consumption of the internal liposomal proton pool.

Table 1
Passive (DOPC LPs) and active (DSPC LPs) encapsulation efficiencies (EE) for CQ and PQ into LPs at 10 mM total lipid.

Liposomal samples	Added drug (μM)	Encapsulated drug (μM)	EE (%)
DOPC CQ pH 7.4	10,000	999.0 ± 5.2	10.0 ± 0.1
DOPC CQ pH 6.5	10,000	499.0 ± 12.1	5.0 ± 0.1
DOPC CQ pH 6.5	25	3.5 ± 0.6	14.1 ± 2.5
DSPC CQ pH 4.0–7.5	500	491.7 ± 1.6	98.3 ± 0.3
DOPC PQ pH 7.4	10,000	3392.6 ± 70.9	33.9 ± 0.7
DOPC PQ pH 6.5	10,000	3215.0 ± 61.9	32.2 ± 0.6
DOPC PQ pH 6.5	4000	1945.9 ± 78.0	48.7 ± 2.0
DSPC PQ pH 4.0–7.5	1000	966.7 ± 2.1	96.7 ± 0.2

After 2 weeks in storage conditions (PBS, pH 7.4, 4 °C) insignificant release (<5%) was obtained for actively encapsulated drugs (Fig. 3A). By contrast, drugs were quickly released when passively encapsulated, with ca. 60% and 30% of originally encapsulated CQ and PQ, respectively, being found outside LPs after only 5 min storage. In accordance with passive encapsulation data for DOPC LPs (Table 1), PQ was significantly more retained than CQ (Supplementary Table 2), with respective encapsulated amounts at equilibrium of ca. 60% and 20%. Similar drug release results were obtained in *P. falciparum* culture conditions (PBS, pH 7.4, 37 °C, diluted samples; Fig. 3B). Whereas passively encapsulated CQ was almost completely released after 48 h under culture conditions, 30% of PQ was still retained in LPs, reflecting the higher hydrophobicity of PQ and its stronger lipid bilayer interaction. On the other hand, no significant release of actively encapsulated drug was observed under the same experimental conditions during the first 3 h of incubation, illustrating the capacity of the pH gradient method for amphiphilic drug containment into LPs.

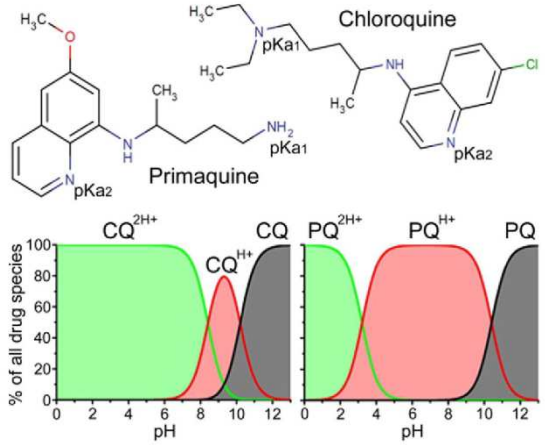

Fig. 2. Ionization species in solution as a function of pH for the weak basic drugs chloroquine (CQ, pKas 10.2 and 8.4 [37]) and primaquine (PQ, pKas 10.4 and 3.2 [38]). Chemical formulae were obtained from http://www.chemicalize.org/.

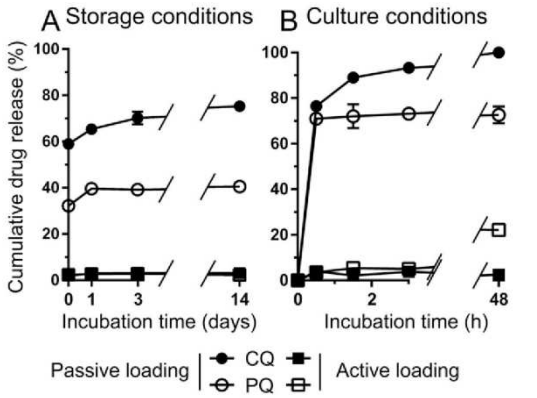

Fig. 3. Cumulative drug release of encapsulated CQ and PQ passively loaded (DOPC liposome pH 7.4, 10 mM drug during encapsulation) and actively loaded (DSPC liposome, drug concentrations in Table 1) under (A) storage conditions (4 °C, 10 mM total lipid) and (B) culture conditions (liposomal samples in storage conditions further diluted 1:10 and 1:40 in PBS for CQ and PQ, respectively, and incubated at 37 °C).

3.2. Targeting antibodies against different pRBC antigens

A previous iLP prototype developed in our group was able to improve ca. 10-fold the efficacy of CQ in vitro [10], although most of this effect was due to liposomization of the drug, and only a relatively minor effect could be attributed to antibody (Ab) targeting [12]. Since the antigen of the pRBC-binding *BM1234* commercial monoclonal antibody used was not known, we set out to identify it. The *BM1234*-positive, Triton X-100-insoluble fraction of a pRBC extract (Fig. S1) was analyzed in a 2D-SDS-PAGE/Western blot and the area containing the two spots detected by *BM1234* (Fig. S2A) was excised from an identical 2D-SDS-PAGE run in parallel (Fig. S2C) and subjected to LC-MS/MS analysis (data not shown). The resulting peptides indicated that the *BM1234* antigen was the membrane-associated histidine-rich protein 1 (MAHRP1), found in two major isoforms as previously described [39]. Subcellular fractionation analysis along the intraerythrocytic *P. falciparum* cycle (Fig. S3) confirmed the presence of the antigen mostly within insoluble membrane fractions of the late stages trophozoites and schizonts, in agreement with the expected preferential localization of the protein in Maurer's clefts [40], organelles involved in trafficking of several proteins towards the pRBC membrane [16,41]. Despite the intracellular location of MAHRP1, the improved pRBC targeting of *BM1234* iLPs over LPs [10] suggested that at some time the recognized antigen should be exposed on the pRBC membrane. Indeed, MAHRP1 had been described as being essential for the translocation to the pRBC surface of PfEMP1, a mediator of pRBC cytoadherence to cell membrane receptors [42]. The association between these two proteins in pRBC plasma membrane regions has been confirmed by confocal fluorescence microscopy (Fig. S4). Consistent with these observations, TEM data showed the expected preferential intracellular localization of the *BM1234* antigen, but with some occasional host cell plasma membrane-associated signal (Fig. S5). Since MAHRP1 was suggested to bind erythrocytes through a 20-mer-long amino acid region [43], we decided to generate polyclonal antibodies against this peptide (ADVPTEGMDVPFGFFDKNTL). As expected, the antigen detected by the resulting antibodies, MAHRP1$_{21–40}$, showed a subcellular localization similar to that of the *BM1234* antigen (Figs. S6 and S7).

Knowing the preferential intracellular localization of MAHRP1, we explored other protein targets present on pRBC surfaces for which commercial antibodies were available: Histidine-rich protein 2 (HRP2) [44] and glycophorin A (GPA) [45]. HRP2 is expressed during most of the *P. falciparum* life cycle (Fig. S3) and secreted by pRBCs, being therefore at some point present on the extracellular side of the plasma membrane (Figs. S8 and S9). GPA is a conserved and highly abundant membrane protein present in all RBCs and pRBCs (Fig. 4A). To test the targeting capacity of the selected antibodies, these were incubated with live pRBC cultures and analyzed directly without fixation by flow cytometry (Fig. 4B) and by fluorescence microscopy (Figs. 4C and S10). In these conditions, anti-GPA proved to be the only antibody capable of completely recognizing the entire RBC and pRBC populations, whereas *BM1234*, anti-HRP2, and anti-MAHRP1$_{21–40}$ bound just a small fraction of pRBCs (<1%), in agreement with the different extracellular exposures of the respective antigens.

3.3. Binding of targeting antibodies to LPs

The capacity of the antibodies raised against MAHRP1 (*BM1234* and anti-MAHRP1$_{21–40}$), HRP2, and GPA as targeting agents for the functionalization of iLPs (DOPC:cholesterol:MPB-PE, 65:20:15) was tested in vitro with live cells by fluorescence microscopy. iLPs containing in their formulation 0.5% of the rhodamine-labeled lipid DOPE-Rho, and loaded with 30 mM pyranine for tracking purposes, were subsequently functionalized with free thiol-bearing half-antibodies by crosslinking these to lipids containing thiol-reacting maleimide (Mal) groups as previously described [10] (Fig. S11). Consistently with the results obtained using free antibodies, of the four LP-Mal-antibody (LP-Mal-Ab), only

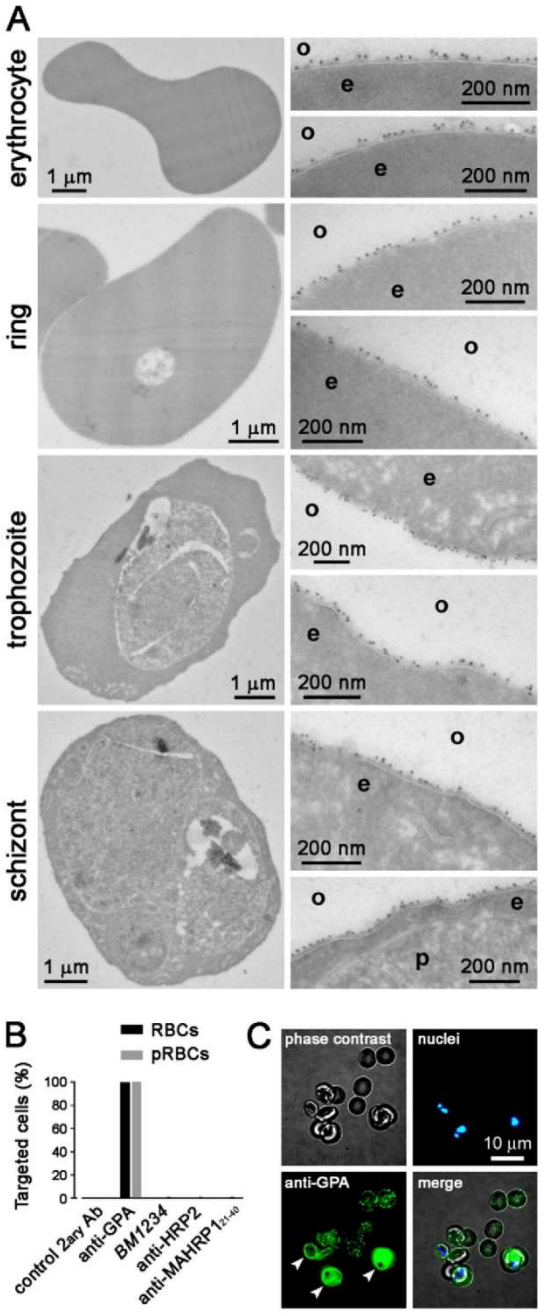

Fig. 4. Cell targeting analysis of monoclonal anti-GPA antibody. (A) Immuno-TEM subcellular localization analysis in RBCs and in pRBCs at the ring, trophozoite, and schizont stages of erythrocytic glycophorin A. o: outside of the cell; e: erythrocyte cytoplasm; p: *P. falciparum*. (B) Flow cytometry analysis of the binding of targeting antibodies to non-fixed RBCs and pRBCs. (C) Epifluorescence microscopic analysis of the binding of anti-GPA to live RBCs and pRBCs. Arrowheads indicate the three pRBCs present in the image.

anti-GPA iLPs were capable of completely recognizing target cells in live pRBC cultures (Fig. S12), though only at the high LP concentration of 1 mM total lipid. In an attempt to improve anti-GPA-iLP targeting, three alternative iLP models were designed (Fig. 5). A lipid bearing a 2-kDa polyethylene glycol (PEG) linker terminated with a Mal group (DSPE-PEG-Mal) was included in the LP formulation (5% of total lipid; LP-PEG-Mal) with the double objective of (i) providing better antigen access to targeting Abs and (ii) improving the coupling reaction otherwise sterically hindered in the original iLP model by the polar heads of surrounding lipids [46,47]. This strategy was used for the oriented binding of half-antibodies through their free thiols (LP-PEG-Mal-Ab) or of whole antibodies through the carbohydrate moieties in antibody Fc regions (LP-PEG-Mal-CHO-Ab), and for the non-oriented binding through primary amino groups on Ab amino acid residues (LP-PEG-Mal-NH_2-Ab). To support a pH gradient required for the active encapsulation of amphiphilic drugs, the LP formulation was adapted by including the saturated lipid DSPC and lowering the cholesterol content. The relative amounts of Mal-conjugated lipid and antibody were adjusted to a lipid:Ab 75-fold molar excess during coupling to maximize binding yield, with a final lipid composition DSPC:cholesterol:DSPE-PEG-Mal 85:10:5. Analysis of anti-GPA iLPs showed that all four methods resulted in good coupling efficiencies above 30% of total antibody added (≥55 Ab molecules/LP), with LP-PEG-Mal-NH_2-Ab showing the best results (Fig. 6 and Table 2). Protein smears observed in the gel lanes corresponding to samples coupled through primary amines indicate an efficient incorporation of maleimide-containing lipids and SATA crosslinker molecules, which decreased the electrophoretic mobility of antibody chains.

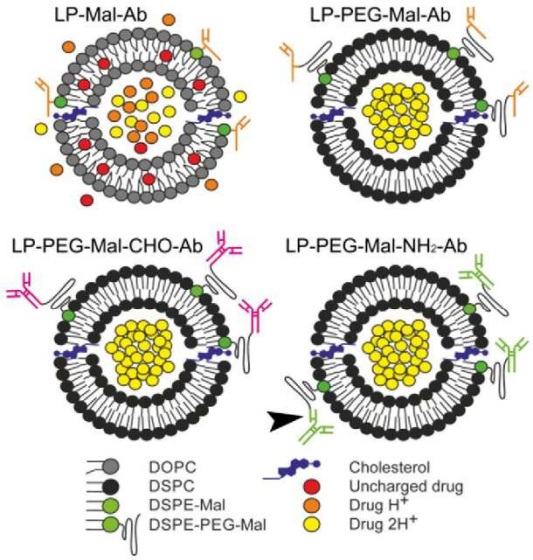

Fig. 5. Representation of iLP models encapsulating an amphiphilic weak basic drug and functionalized with antibodies linked through four different conjugation strategies, all based on the formation of a thioether bond between a thiolated antibody and a maleimide-conjugated lipid. For cell targeting assays, drugs were substituted by the fluorescent dye pyranine as a tracker for the LP aqueous core and a rhodamine-conjugated lipid (DOPE-Rho) was included in the LP formulation. LP-Mal-Ab and LP-PEG-Mal-Ab: half-antibody is conjugated in oriented position, in the second model at the distal end of a 2-kDa PEG linker. LP-PEG-Mal-CHO-Ab: whole antibodies are conjugated in oriented position through the carbohydrate chains in the Fc region. LP-PEG-Mal-NH_2-Ab: whole antibodies are conjugated in non-oriented position through primary amino groups, which in some cases can be placed within the antigen binding site, interfering with antigen recognition (arrowhead). In the first model the drug is represented as being passively loaded, whereas the other three models represent drug actively loaded with the pH gradient method.

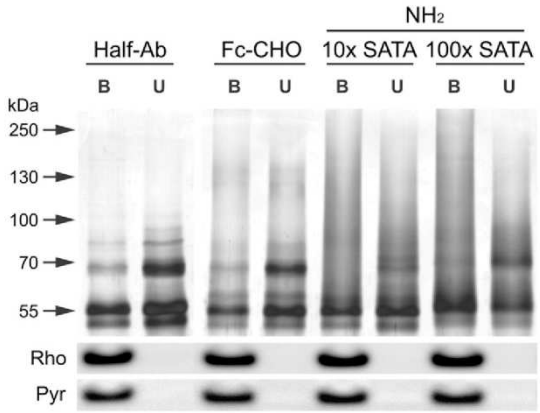

Fig. 6. Silver-stained, reducing SDS-PAGE analysis of different strategies for the coupling of anti-GPA polyclonal antibodies to LPs. Coupling was via a PEG-Mal linker through: (Half-Ab) the free thiol of half-antibodies, LP-PEG-Mal-Ab model; (Fc-CHO) the carbohydrate moiety in Fc regions, LP-PEG-Mal-CHO-Ab model; (NH_2) primary amino groups with different amounts of the crosslinking agent SATA (10× and 100× molar excess relative to antibody molecules), LP-PEG-Mal-NH_2-Ab model. Prior to electrophoresis, samples containing 2 μg protein were centrifuged for the analysis of LP-bound antibodies in the pellet (B) and of unbound antibodies in the supernatant (U). The ca. 70-kDa band with a relatively minor incorporation into LPs when compared to the ca. 55-kDa band of IgG heavy chains, corresponds to rabbit albumin, which is highly abundant in animal serum and interacts with Protein G during IgG purification [48]. When using monoclonal antibodies, albumin is absent (Fig. S13). The fluorescence emission of rhodamine (Rho) conjugated to lipids included in the formulation of LPs, and of pyranine dye (Pyr) with which they were passively loaded, are used as controls of the LP-containing fractions.

3.4. Cell targeting of iLPs

Flow cytometry studies on non-fixed RBCs using the different iLP models indicated a cell targeting efficiency LP-PEG-Mal-NH_2-Ab ≫ LP-PEG-Mal-CHO-Ab ≫ LP-Mal-Ab/LP-PEG-Mal-Ab (Fig. 7A). After a 30-min incubation, only ca. 10% of cells were bound by LP-Mal-Ab anti-GPA iLPs at 250 μM lipid in culture, whereas LP-PEG-Mal-NH_2-Ab generated using the relatively low crosslinker:Ab 10× molar excess resulted in ~100% cell targeting at a concentration of 100 μM lipid. This complete targeting could be maintained when using a monoclonal anti-GPA (LP-PEG-Mal-NH_2-MAb-10×) even at a LP concentration of 50 μM lipid, and down to 0.5 μM lipid according to fluorescence microscopy analysis (Fig. S14). Cryo-TEM images showed that >90% of LPs in this last model carried antibodies (Fig. S15), result consistent with the observation that >80% of LPs are retained on target cells at ≤50 μM lipid, whereas retention values were below 15% for all other iLP models (Fig. 7B). It is important to note that using a 10-fold increase of the chemical crosslinker SATA (100× molar excess) inhibited cell targeting (Fig. 7), likely due to massive crosslinking of NH_2 groups near the antigen recognition site of antibodies. When LP-PEG-Mal-NH_2-MAb-10× iLPs

Table 2
Characterization of the different methods used to conjugate the polyclonal anti-GPA antibody to maleimide-PEG-grafted LPs (LP-PEG-Mal model).

Parameter	Half-Ab	Fc-CHO	NH_2 10× SATA	NH_2 100× SATA
Sulfhydryl groups/Ab	0.7 ± 0.4	1.9 ± 0.5	2.9 ± 0.4	10.2 ± 0.1
Coupling efficiency (%)	32.5 ± 5.0	39.6 ± 2.2	44.1 ± 1.5	54.4 ± 0.0
μg Ab/μmol lipid	34.6 ± 5.3	32.1 ± 1.8	53.3 ± 1.8	67.1 ± 0.0
Ab number per LP	55.6 ± 8.5	51.6 ± 2.8	85.6 ± 2.8	107.6 ± 0.0
Size increment (nm)	4.9 ± 3.4	0.0 ± 4.4	8.7 ± 3.3	17.1 ± 1.3

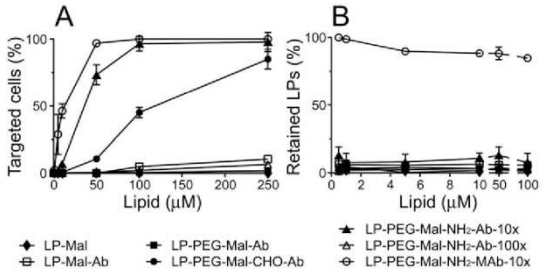

Fig. 7. RBC targeting analysis after a 30-min incubation with anti-GPA iLPs loaded with 30 mM pyranine and prepared through different antibody conjugation methods. (A) Flow cytometry results showing the fraction of RBCs positive for pyranine signal. (B) Determination by pyranine fluorescence quantification in the culture supernatant of the iLP fraction bound to cells. All samples were prepared with polyclonal antibodies except LP-PEG-Mal-NH_2-MAb-10×, where a monoclonal antibody was used.

were incubated with live pRBC cultures for 90 min, confocal fluorescence microscopy analysis showed colocalization of rhodamine and pyranine signals on RBCs and pRBCs as a punctate pattern (Fig. 8A–C). This suggested that erythrocyte-bound iLPs did not immediately fuse with the plasma membrane, but rather remained adsorbed onto the cell. The observation of the presence of diffuse fluorescence areas in some RBCs (Fig. 8B), but especially on pRBCs (Fig. 8C), suggests that eventually iLPs could fuse with the cell, despite the lipid formulation used here (dominated by saturated lipids) significantly inhibits such fusion events. Free pyranine controls showed passive entry of this highly hydrophilic dye only into pRBCs (Fig. 8D).

3.5. P. falciparum growth inhibition activity of anti-GPA iLPs encapsulating antimalarial drugs

The iLP prototype having both best targeting efficiency and retention into pRBC cultures (LP-PEG-Mal-NH_2-MAb-10× functionalized with monoclonal antibodies against human GPA) was selected for in vitro growth inhibition assays of *P. falciparum*. Drug concentrations during active encapsulation of 500 μM CQ and 1 mM PQ (for 10 mM total lipid) were selected to avoid an excessive consumption of the LP internal proton pool and subsequent disruption of the liposomal pH gradient [21,35], yielding EEs of 98.3 and 96.7% for CQ and PQ, respectively (Table 1). After only 15 min of incubation in the presence of iLPs, pRBC cultures were washed and incubated for a further 48 h (one replication cycle). CQ activity significantly improved when actively encapsulated into iLPs, with an IC50 of ca. 35 nM when administered to *P. falciparum* cultures synchronized in either ring or late blood stages (trophozoites + schizonts), whereas at a concentration of 50 nM encapsulated CQ, parasite growth was completely inhibited (Fig. 9A, B). In contrast, free CQ was only capable of completely inhibiting *Plasmodium* growth when added to late forms at a concentration in culture of 200 nM, although this dose was ineffective when added to ring stages. Neither agglutination nor morphological alterations of RBCs were observed upon microscopic examination of Giemsa-stained slides from growth inhibition assays (Fig. S16). Fluorescence microscopy and flow cytometry analysis (Fig. S17), as well as hemolysis assays (Fig. S18), further confirmed an absence of adverse effects on non-infected RBCs within the liposome molar range leading to complete *P. falciparum* growth inhibition (1–4 μM lipid, corresponding respectively to ca. 19–75 iLPs/RBC; Fig. S19), indicating that erythrocyte viability was not compromised by iLP binding. When ≥50 nM CQ encapsulated in iLPs was added at ring stage, the parasites were killed before completing their intraerythrocytic cycle, as evidenced by a lack of increase in pRBC numbers after 48 h and the microscopic observation of picnotic *Plasmodium* nuclei indicative of cell death (Fig. S16A). On the other hand, when added to late stages, treated parasites egressed from pRBCs but had a low invasion rate and those which could invade RBCs failed to mature into late forms, dying at ring stage. Again, this growth inhibitory effect was evidenced by pRBC counts and microscopic examination (Fig. S16B). Fluorescence microscopy detection at the end of growth inhibition assays of DOPE-Rho lipid that had been incorporated into the LP formulation confirmed the expected iLP binding to all RBCs and pRBCs (Fig. S20). In late forms, lipid fluorescence was often observed to be homogeneously distributed throughout the cell, hinting at LP fusion with the pRBC membrane during the length of 48-h growth inhibition assays. Dramatic activity increases were also obtained for actively encapsulated PQ, which at 10 μM eliminated parasitemia almost completely in both ring and late form cultures, whereas the same concentration of free drug did not have any significant effect on the parasite (Fig. 9C). However, PQ-containing iLPs had in vitro an RBC agglutinating effect (Fig. 9D–F), likely due to the need to add a large amount of drug-encapsulating LPs (50–100 μM lipid, corresponding respectively to 940–1880 iLPs/RBC; Fig. S19) because of the high in vitro IC50 of PQ, which is in the μM range. This agglutinating effect was especially significant under static incubation conditions for high iLP amounts >10 μM lipid (Figs. S17 and S19). The absence of hemolysis was observed even for the highest agglutinating iLP amount of 100 μM lipid (Fig. S18).

Preliminary in vivo 4-day tests in mice grafted with human erythrocytes and subsequently infected with *P. falciparum* showed that anti-GPA iLPs (LP-PEG-Mal-NH_2-MAb-10×) encapsulating CQ cleared the pathogen below detectable levels (<0.01% parasitemia in peripheral blood) at a CQ dose of 0.5 mg/kg, whereas free CQ administered at 1.75 mg/kg was, at most, 40-fold less efficient (ca. 0.4% parasitemia; Fig. 10). 0.5 mg CQ/kg administered in non-targeted liposomes had a much diminished effect, which highlights the crucial role of GPA targeting. The survival of iLP-treated mice suggests that the function of non-infected RBCs was not significantly affected in vivo by CQ-loaded iLPs at the concentration required to eliminate parasitemia from infected animals.

4. Discussion

Plasmodium early stages are ideal therapeutic targets because drugs delivered to them would have a longer time to kill the parasite before it completes its development, although the permeability of the infected erythrocyte to ions and small nonelectrolytes, including some drugs, does not increase until ca. six hours after invasion [17]. During its maturation the parasite hydrolyzes hemoglobin in a digestive vacuole, which is the target of many amphiphilic drugs that freely cross the RBC membrane and accumulate intracellularly. As a result, most antimalarials start affecting the infected cell relatively late in the intraerythrocytic parasite life cycle, when their effect is probably often too short to be lethal for *Plasmodium*.

A strategy to improve the activity of antimalarial drugs contemplates their encapsulation in nanocarriers specifically targeted to pRBCs [49], which requires the existence of specific pRBC markers. 200-nm LPs studded with heparin or specific antibodies raised against pRBCs have been shown to bind late stages with high specificity [10,50], increasing up to tenfold the efficacy of encapsulated antimalarial drugs in vitro [12,50]. However, the therapeutic administration of such liposomal models against late stages has to be timed to the precise moment when trophozoites and schizonts are present in blood, between 24 and 48 h into the *P. falciparum* intraerythrocytic cycle. The relatively short blood half-life of, in the best case, <10 h for polyethylene glycol-coated stealth LPs [51], guarantees that if injected when early stage pRBCs are present, by the time late forms mature most LPs will have been removed from the blood circulation. Polymeric nanovectors were observed to penetrate trophozoites and schizonts [30], most likely through the TVN, although entry of nanoparticles into early ring stages has not been observed so far for *P. falciparum* or any other human malaria species. As an additional obstacle to antimalarial targeted delivery strategies, most externally recognizable pRBC proteins are present in the parasite

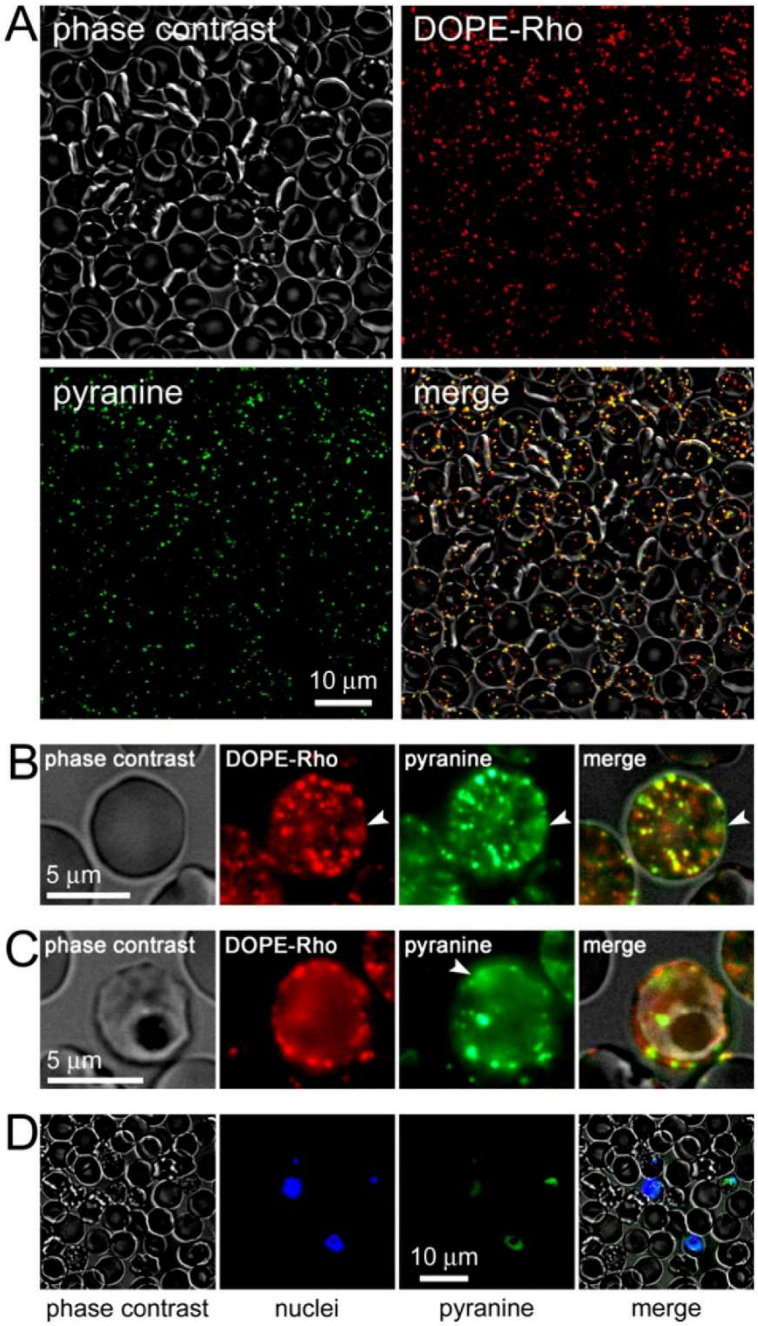

Fig. 8. Fluorescence microscopy analysis of the interaction of anti-GPA iLPs with target cells. Rhodamine-labeled anti-GPA LP-PEG-Mal-NH_2-MAb iLPs loaded with pyranine (concentrations in the culture of 500 μM lipid and 26 μM pyranine) were added to live pRBC cultures, incubated for 90 min and visualized without fixation by (A) confocal fluorescence microscopy and (B, RBC; C, pRBC) epifluorescence microscopy. The arrowheads indicate diffuse fluorescence areas. (D) Control sample where 26 μM free pyranine was added to the culture.

genome as multiple variants that can be clonally expressed [15]. In vitro, the targeting of pRBCs using laboratory strains of *Plasmodium* that present known, homogeneously expressed antigens is a valid approach allowing for the use of the corresponding antibody specific for each particular target molecule, but in a clinical setting this strategy is invalidated by the large clonal variability inherent to a typical malaria infection.

Malaria is a systemic infection of erythrocytes, where targeted drug delivery approaches are complicated by the fluidics conditions found in

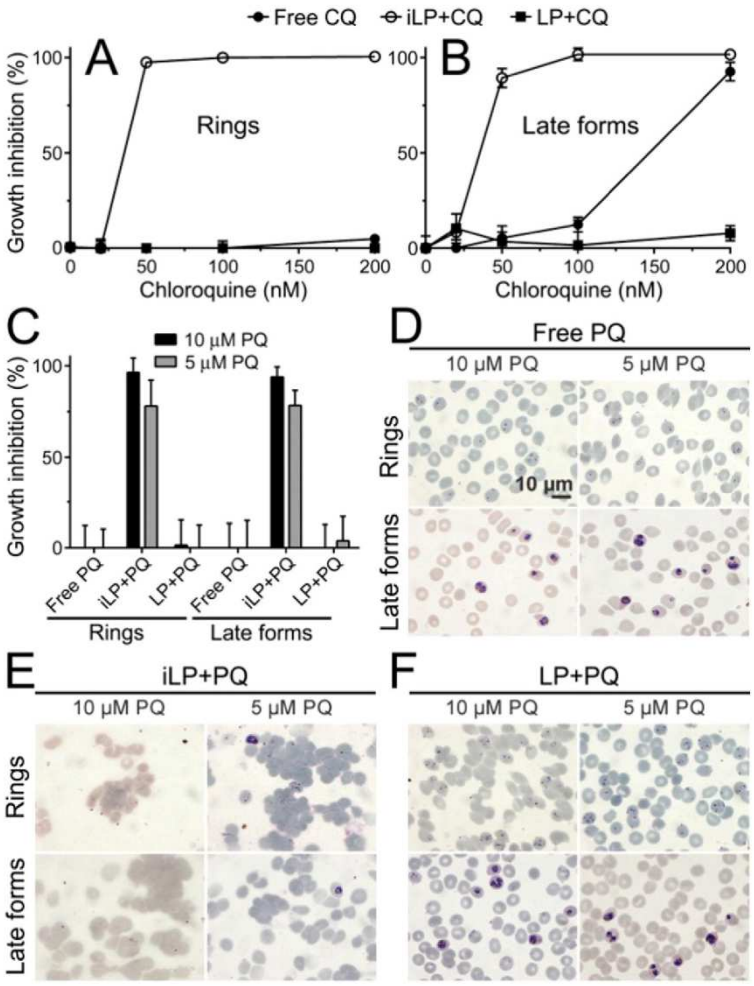

Fig. 9. *P. falciparum* growth inhibition assays of the effect of CQ and PQ as free drugs and encapsulated in LPs and iLPs. CQ (A, B) and PQ (C) encapsulated in LP-PEG-Mal-NH_2-Mab anti-GPA iLPs, in LP-PEG-Mal LPs, or in non-encapsulated form were added at the same final concentrations to either ring or late blood stages (trophozoites and schizonts) and let to act for 15 min before removing them by changing the incubation medium. After a further 48 h incubation the samples were analyzed by flow cytometry to determine *P. falciparum* growth. For PQ samples are presented images of cultures treated with free PQ (D), iLP+PQ (E), and LP+PQ (F), to show agglutination in the iLP-treated samples. Highest LP concentrations in *P. falciparum* cultures were 100 μM and 4 μM lipid for 10 μM PQ and 200 nM CQ, respectively.

the blood circulation, whose strong flow drag and shear forces necessarily affect the interaction of molecular components with target cells. In this adverse physical environment, the design of iLPs engineered to encapsulate antimalarial drugs for their specific entry into pRBCs has to be especially careful regarding the liposomal nanocapsule composition, which will define drug encapsulation and partition within the vesicle, and the selection of targeting antibody/antigen pairs. Although the oriented binding of half-antibodies through their free thiols or of whole antibodies through their carbohydrate moieties in the Fc region is a priori a guarantee to increase antigen binding site exposure and thus target binding efficiency, our results indicate that non-oriented binding through primary amino groups significantly increases the number of antibodies bound per LP, whereas carefully choosing the amount of chemical crosslinker used preserves a high antigen binding capacity, at least for the monoclonal anti-GPA antibody used here. Considering the limitations exposed above for an efficient pRBC targeting, efforts have to be invested in encapsulating the highest drug cargo possible. Using the pH gradient active loading method [36] and LP formulations high in saturated lipids capable of sustaining a proton gradient, we have obtained for the weak basic drugs CQ and PQ encapsulation efficiencies close to 100% and high intraliposomal retention levels >95% for several hours in both storage and culture conditions. However, the varied physicochemical properties of present and future antimalarial drugs will determine their location within the liposomal structure [52,53], calling for encapsulation strategies adapted to each particular compound.

Antimalarial drug carriers should provide optimal drug half-lives in circulation, adequate clearance mechanisms, restriction of unintended drug effects in non-target cells, specific delivery to the correct tissue, and a timely initiation and termination of the therapeutic action. Considering the interest in targeting intraerythrocytic *Plasmodium* as early in its life cycle as possible and the lack of strategies to shuttle drugs into it, alternative approaches must be explored without preconceptions. A way to overcome the aforementioned exposed obstacles to

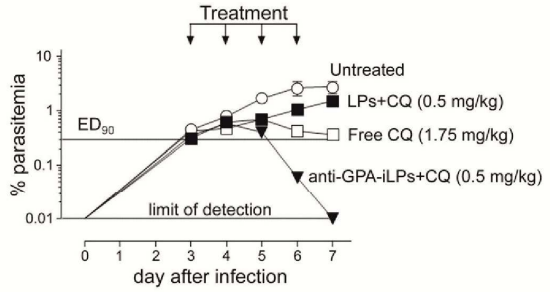

Fig. 10. 4-day test in female immunodeficient mice engrafted with human RBCs and infected i.v. with *P. falciparum*. The animals were treated with the indicated drug preparations at days 3 to 6 after infection. The anti-GPA-iLP + CQ sample contained 48 mmol CQ/mol lipid, whose administered dose corresponded to ca. 100 iLP/erythrocyte, assuming 1×10^{10} human RBCs in the mouse blood circulation.

the design of pRBC-targeted nanocarriers can perhaps be provided by one of the most adequate vascular carriers ever proposed; namely, red blood cells themselves [54]. Human erythrocytes have a life span in the blood of up to 120 days, which makes them attractive carriers for intravascular delivery because they prolong drug circulation. In addition, their large size (ca. 7 μm across and around 2 μm thick) significantly restricts unintended extravasation and in principle allows for a much larger encapsulation capacity than LPs. Other interesting features of RBCs as drug carriers are their biocompatibility and the existence of natural mechanisms for their safe elimination from the body. Actually, delivery of antimalarials to non-infected red blood cells to study the effects on later invading parasites has been an approach used for chemotherapeutic investigations, where pretreatment of erythrocytes with the drugs halofantrine, lumefantrine, piperaquine, amodiaquine, and mefloquine showed that these diffuse into and remain within the cell, inhibiting downstream growth of *Plasmodium* [55]. Nevertheless, the loading of drugs into non-infected RBCs has not yet been explored in detail as a clinically feasible therapeutic strategy against malaria, since most currently available protocols use a harsh ex vivo erythrocyte isolation followed by drug loading through diffusion [54].

RBC-targeted iLPs could be used to shuttle into the cell antimalarial drugs, although the incapacity of mature erythrocytes to endocyte [56] calls for the development of specific targeted delivery strategies independent from the receptor-mediated endocytic pathway. Delivery of iLP cargo into RBCs had been proposed to occur through membrane fusion [7], a highly controlled process that requires the incorporation of specific fusogenic agents into the lipid bilayer [57,58]. Nevertheless, because of little evidence for liposomal fusion observed with RBCs, alternative routes for the incorporation of LP contents into targeted erythrocytes should be examined [53]. The TVN induced by *Plasmodium* during its intraerythrocytic growth [17] extends from the parasitophorous vacuole membrane and connects the intracellular parasite with the host RBC surface. However, this confers to the pRBC the capacity of internalizing a wide range of particles up to diameters of only 70 nm [17,59], well below the mean size of the LPs used here. Other potential mechanisms to consider include LP adsorption on the cell surface followed by either the exchange of hydrophobic molecules (e.g., the antimalarial drugs lumefantrine and halofantrine) between apposed lipid bilayers [60,61], or a sustained release of the entrapped material [53]. This process would be mediated by a depletion of the liposomal proton gradient by means of temperature, LP-cell interaction events [62] and lipid sequestration by plasma components [63], and might be highly effective for the delivery of weak basic drugs such as those from the aminoquinoline family. These compounds, positively charged at acidic/neutral pH, will theoretically accumulate inside the cell by virtue of the electrochemical gradient created by the phospholipid asymmetry in RBC membranes [64], which maintains a negatively charged intracellular membrane lining. Although the slow drug release observed for pH gradient-loaded LPs is a requirement for storage periods and to avoid drug leaking before reaching their target, once docked to RBCs and pRBCs liposomal contents must enter the cell. Here, we have observed for CQ a similar in vitro IC50 when present either for 48 h as free drug or for only 15 min encapsulated in iLPs, suggesting an adequate drug transfer from iLP to cell.

Other foreseeable limitations to targeting RBCs as an antimalarial strategy will have to be considered. First, to avoid erythrocyte agglutination, an upper iLP concentration threshold must be established in vivo, which will complicate the application of this model to drugs with a high IC50. In this regard, according to the data reported here for drugs having a low IC50 like CQ, a ratio of ca. 100 iLP/RBC (lacking agglutination and hemolysis activity in vitro) led in mice grafted with human erythrocytes to complete elimination of parasitemia. A second requirement for the use of RBCs as antimalarial carriers is that when present at therapeutically active concentration, the drug has to be innocuous for the cell physiology, which might not be an unsurmountable obstacle given the reduced metabolic activity of erythrocytes. However, loading of some antimalarial drugs like clotrimazole had been observed to predispose RBCs to oxidative damage [65], an undesirable scenario since oxidized RBCs are rapidly taken up by hepatic reticuloendothelial system macrophages. Finally, because LPs adsorbed on RBC surfaces would probably sufficiently modify cell shape to target it for removal through spleen filtration, a compromise between stable drug containment and lipid bilayer fusion might have to be reached through the adequate LP formulation, with the objective of achieving LP-RBC merging before spleen removal while avoiding rapid drug leaking from LPs.

5. Conclusion

Antigens found in all RBCs can be a target to consider for antimalarial drug delivery, trading pRBC specificity for a far larger abundance of anchoring points on the cell surface. Because the selected RBC markers are also found on pRBCs, targeted iLPs would have a double activity as therapeutic and prophylactic agents when simultaneously delivering drug to, respectively, infected and non-infected cells. It is reasonable to predict that the nanovector design limitations exposed above can be satisfactorily dealt with, and that some of the future antimalarials yet to be discovered will be harmless for erythrocytes, thus allowing for the loading into them of drug amounts being lethal for *Plasmodium*. If so, the pathogen might encounter its enemy at home, right at the very moment of entering the host cell, which would have devastating effects for the parasite and significantly compromise its survival capacity.

Acknowledgment

This work was supported by grants BIO2011-25039 and BIO2014-52872-R from the Ministerio de Economía y Competitividad, Spain, which included FEDER funds, and by grant 2014-SGR-938 from the Generalitat de Catalunya, Spain. A fellowship of the Instituto de Salud Carlos III (Spain) is acknowledged by P.U. We thank L. D. Shultz and The Jackson Laboratory for providing access to nonobese diabetic scid IL2Rγc null mice through their collaboration with GSK Tres Cantos Medicines Development Campus.

Appendix A. Supplementary data

Supplementary data to this article can be found online at http://dx.doi.org/10.1016/j.jconrel.2015.05.284.

References

[1] K.S. Griffith, L.S. Lewis, S. Mali, M.E. Parise, Treatment of malaria in the United States: a systematic review, JAMA 297 (2007) 2264–2277.
[2] World Health Organization, Guidelines for the Treatment of Malaria, World Health Organization, Geneva, Switzerland, 2010.

[3] P. Newton, Y. Suputtamongkol, P. Teja-Isavadharm, S. Pukrittayakamee, V. Navaratnam, I. Bates, et al., Antimalarial bioavailability and disposition of artesunate in acute falciparum malaria, Antimicrob. Agents Chemother. 44 (2000) 972–977.
[4] T.K. Chan, D. Todd, S.C. Tso, Drug-induced haemolysis in glucose-6-phosphate dehydrogenase deficiency, BMJ 2 (1976) 1227–1229.
[5] M. Chinappi, A. Via, P. Marcatili, A. Tramontano, On the mechanism of chloroquine resistance in *Plasmodium falciparum*, PLoS One 5 (2010) e14064.
[6] G. Gregoriadis, Liposomes as a drug delivery system: optimization studies, Adv. Exp. Med. Biol. 238 (1988) 151–159.
[7] A. Singhal, C.M. Gupta, Antibody-mediated targeting of liposomes to red cells in vivo, FEBS Lett. 201 (1986) 321–326.
[8] A.K. Agrawal, A. Singhal, C.M. Gupta, Functional drug targeting to erythrocytes in vivo using antibody bearing liposomes as drug vehicles, Biochem. Biophys. Res. Commun. 148 (1987) 357–361.
[9] M. Owais, G.C. Varshney, A. Choudhury, S. Chandra, C.M. Gupta, Chloroquine encapsulated in malaria-infected erythrocyte-specific antibody-bearing liposomes effectively controls chloroquine-resistant *Plasmodium berghei* infections in mice, Antimicrob. Agents Chemother. 39 (1995) 180–184.
[10] P. Urbán, J. Estelrich, A. Cortés, X. Fernàndez-Busquets, A nanovector with complete discrimination for targeted delivery to *Plasmodium falciparum*-infected versus non-infected red blood cells *in vitro*, J. Control. Release 151 (2011) 202–211.
[11] D.D. Lasic, F. Martin, Stealth Liposomes, CRC Press, Boca Raton, FL, USA, 1995.
[12] P. Urbán, J. Estelrich, A. Adeva, A. Cortés, X. Fernàndez-Busquets, Study of the efficacy of antimalarial drugs delivered inside targeted immunoliposomal nanovectors, Nanoscale Res. Lett. 6 (2011) 620.
[13] A.M. Vaughan, S.H. Kappe, A. Ploss, S.A. Mikolajczak, Development of humanized mouse models to study human malaria parasite infection, Future Microbiol. 7 (2012) 657–665.
[14] S. Paula, A.G. Volkov, A.N. Van Hoek, T.H. Haines, D.W. Deamer, Permeation of protons, potassium ions, and small polar molecules through phospholipid bilayers as a function of membrane thickness, Biophys. J. 70 (1996) 339–348.
[15] S. Kyes, P. Horrocks, C. Newbold, Antigenic variation at the infected red cell surface in malaria, Annu. Rev. Microbiol. 55 (2001) 673–707.
[16] B.M. Cooke, K. Lingelbach, L.H. Bannister, L. Tilley, Protein trafficking in *Plasmodium falciparum*-infected red blood cells, Trends Parasitol. 20 (2004) 581–589.
[17] K. Kirk, Membrane transport in the malaria-infected erythrocyte, Physiol. Rev. 81 (2001) 495–537.
[18] J.C. Shillcock, R. Lipowsky, Tension-induced fusion of bilayer membranes and vesicles, Nat. Mater. 4 (2005) 225–228.
[19] J.J. Wheeler, L. Palmer, M. Ossanlou, I. MacLachlan, R.W. Graham, Y.P. Zhang, et al., Stabilized plasmid-lipid particles: construction and characterization, Gene Ther. 6 (1999) 271–281.
[20] R.C. MacDonald, R.I. MacDonald, B.P. Menco, K. Takeshita, N.K. Subbarao, L.R. Hu, Small-volume extrusion apparatus for preparation of large, unilamellar vesicles, Biochim. Biophys. Acta 1061 (1991) 297–303.
[21] G. Stensrud, S. Sande, S. Kristensen, G. Smistad, Formulation and characterisation of primaquine loaded liposomes prepared by a pH gradient using experimental design, Int. J. Pharm. 198 (2000) 213–228.
[22] H.C. Loughrey, L.S. Choi, P.R. Cullis, M.B. Bally, Optimized procedures for the coupling of proteins to liposomes, J. Immunol. Methods 132 (1990) 25–35.
[23] S.M. Ansell, P.G. Tardi, S.S. Buchkowsky, 3-(2-Pyridyldithio)propionic acid hydrazide as a cross-linker in the formation of liposome–antibody conjugates, Bioconjug. Chem. 7 (1996) 490–496.
[24] D.S. Hage, Periodate oxidation of antibodies for site-selective immobilization in immunoaffinity chromatography, Methods Mol. Biol. 147 (2000) 69–82.
[25] N. Maurer, D.B. Fenske, P.R. Cullis, Developments in liposomal drug delivery systems, Expert Opin. Biol. Ther. 1 (2001) 923–947.
[26] R.C. Switzer III, C.R. Merril, S. Shifrin, A highly sensitive silver stain for detecting proteins and peptides in polyacrylamide gels, Anal. Biochem. 98 (1979) 231–237.
[27] S.L. Cranmer, C. Magowan, J. Liang, R.L. Coppel, B.M. Cooke, An alternative to serum for cultivation of *Plasmodium falciparum in vitro*, Trans. R Soc. Trop. Med. Hyg. 91 (1997) 363–365.
[28] C. Lambros, J.P. Vanderberg, Synchronization of *Plasmodium falciparum* erythrocytic stages in culture, J. Parasitol. 65 (1979) 418–420.
[29] A. Radfar, D. Méndez, C. Moneriz, M. Linares, P. Marín-García, A. Puyet, et al., Synchronous culture of *Plasmodium falciparum* at high parasitemia levels, Nat. Protoc. 4 (2009) 1899–1915.
[30] P. Urbán, J.J. Valle-Delgado, N. Mauro, J. Marques, A. Manfredi, M. Rottmann, et al., Use of poly(amidoamine) drug conjugates for the delivery of antimalarials to *Plasmodium*, J. Control. Release 177 (2014) 84–95.
[31] M. Ramsby, G. Makowski, Differential detergent fractionation of eukaryotic cells, Cold Spring Harbor Protocols 2011. http://dx.doi.org/10.1101/pdb.prot5592.
[32] P.H. O'Farrell, High resolution two-dimensional electrophoresis of proteins, J. Biol. Chem. 250 (1975) 4007–4021.
[33] I. Angulo-Barturen, M.B. Jiménez-Díaz, T. Mulet, J. Rullas, E. Herreros, S. Ferrer, et al., A murine model of *falciparum*-malaria by *in vivo* selection of competent strains in non-myelodepleted mice engrafted with human erythrocytes, PLoS One 3 (2008) e2252.
[34] M.B. Jiménez-Díaz, T. Mulet, V. Gómez, S. Viera, A. Alvarez, H. Garuti, Y. Vázquez, A. Fernández, J. Ibáñez, M. Jiménez, D. Gargallo-Viola, I. Angulo-Barturen, Quantitative measurement of *Plasmodium*-infected erythrocytes in murine models of malaria by flow cytometry using bidimensional assessment of SYTO-16 fluorescence, Cytometry 75A (2009) 225–235.
[35] L. Qiu, N. Jing, Y. Jin, Preparation and in vitro evaluation of liposomal chloroquine diphosphate loaded by a transmembrane pH-gradient method, Int. J. Pharm. 361 (2008) 56–63.
[36] T.D. Madden, P.R. Harrigan, L.C.L. Tai, M.B. Bally, L.D. Mayer, T.E. Redelmeier, et al., The accumulation of drugs within large unilamellar vesicles exhibiting a proton gradient: a survey, Chem. Phys. Lipids 53 (1990) 37–46.
[37] F. Omodeo-Salè, L. Cortelezzi, N. Basilico, M. Casagrande, A. Sparatore, D. Taramelli, Novel antimalarial aminoquinolines: heme binding and effects on normal or *Plasmodium falciparum*-parasitized human erythrocytes, Antimicrob. Agents Chemother. 53 (2009) 4339–4344.
[38] A. Nair, B. Abrahamsson, D.M. Barends, D.W. Groot, S. Kopp, J.E. Polli, et al., Biowaiver monographs for immediate-release solid oral dosage forms: primaquine phosphate, J. Pharm. Sci. 101 (2012) 936–945.
[39] E. Pachlatko, S. Rusch, A. Müller, A. Hemphill, L. Tilley, E. Hanssen, et al., MAHRP2, an exported protein of *Plasmodium falciparum*, is an essential component of Maurer's cleft tethers, Mol. Microbiol. 77 (2010) 1136–1152.
[40] C. Spycher, N. Klonis, T. Spielmann, E. Kump, S. Steiger, L. Tilley, et al., MAHRP-1, a novel *Plasmodium falciparum* histidine-rich protein, binds ferriprotoporphyrin IX and localizes to the Maurer's clefts, J. Biol. Chem. 278 (2003) 35373–35383.
[41] L. Tilley, G. McFadden, A. Cowman, N. Klonis, Illuminating *Plasmodium falciparum*-infected red blood cells, Trends Parasitol. 23 (2007) 268–277.
[42] C. Spycher, M. Rug, E. Pachlatko, E. Hanssen, D. Ferguson, A.F. Cowman, et al., The Maurer's cleft protein MAHRP1 is essential for trafficking of PfEMP1 to the surface of *Plasmodium falciparum*-infected erythrocytes, Mol. Microbiol. 68 (2008) 1300–1314.
[43] J. García, H. Curtidor, O.L. Gil, M. Vanegas, M.E. Patarroyo, A Maurer's cleft-associated *Plasmodium falciparum* membrane-associated histidine-rich protein peptide specifically interacts with the erythrocyte membrane, Biochem. Biophys. Res. Commun. 380 (2009) 122–126.
[44] R.J. Howard, S. Uni, M. Aikawa, S.B. Aley, J.H. Leech, A.M. Lew, et al., Secretion of a malarial histidine-rich protein (Pf HRP II) from *Plasmodium falciparum*-infected erythrocytes, J. Cell. Biol. 103 (1986) 1269–1277.
[45] P.D. Siebert, M. Fukuda, Isolation and characterization of human glycophorin A cDNA clones by a synthetic oligonucleotide approach: nucleotide sequence and mRNA structure, Proc. Natl. Acad. Sci. U. S. A. 83 (1986) 1665–1669.
[46] M. Fleiner, P. Benzinger, T. Fichert, U. Massing, Studies on protein–liposome coupling using novel thiol-reactive coupling lipids: influence of spacer length and polarity, Bioconjug. Chem. 12 (2001) 470–475.
[47] K. Maruyama, T. Takizawa, N. Takahashi, T. Tagawa, K. Nagaike, M. Iwatsuru, Targeting efficiency of PEG-immunoliposome-conjugated antibodies at PEG terminals, Adv. Drug Deliv. Rev. 24 (1997) 235–242.
[48] P.A. Nygren, M. Eliasson, L. Abrahmsén, M. Uhlén, E. Palmcrantz, Analysis and use of the serum albumin binding domains of streptococcal protein G, J. Mol. Recognit. 1 (1988) 69–74.
[49] P. Urbán, X. Fernàndez-Busquets, Nanomedicine against malaria, Curr. Med. Chem. 21 (2014) 605–629.
[50] J. Marques, E. Moles, P. Urbán, R. Prohens, M.A. Busquets, C. Sevrin, et al., Application of heparin as a dual agent with antimalarial and liposome targeting activities towards *Plasmodium*-infected red blood cells, Nanomedicine 10 (2014) 1719–1728.
[51] D. Papahadjopoulos, T.M. Allen, A. Gabizon, E. Mayhew, K. Matthay, S.K. Huang, et al., Sterically stabilized liposomes: improvements in pharmacokinetics and antitumor therapeutic efficacy, Proc. Natl. Acad. Sci. U. S. A. 88 (1991) 11460–11464.
[52] M. Gulati, M. Grover, S. Singh, M. Singh, Lipophilic drug derivatives in liposomes, Int. J. Pharm. 165 (1998) 129–168.
[53] V.P. Torchilin, Recent advances with liposomes as pharmaceutical carriers, Nat. Rev. Drug Discov. 4 (2005) 145–160.
[54] V.R. Muzykantov, Drug delivery by red blood cells: vascular carriers designed by Mother Nature, Expert Opin. Drug Deliv. 7 (2010) 403–427.
[55] D.W. Wilson, C. Langer, C.D. Goodman, G.I. McFadden, J.G. Beeson, Defining the timing of action of antimalarial drugs against *Plasmodium falciparum*, Antimicrob. Agents Chemother. 57 (2013) 1455–1467.
[56] D.M. Harmening, The red blood cell: structure and function, Clinical Hematology and Fundamentals of Hemostasis, F. A. Davis Company, Philadelphia, PA, 1996. 54–70.
[57] A.L. Bailey, P.R. Cullis, Membrane fusion with cationic liposomes: effects of target membrane lipid composition, Biochemistry 36 (1997) 1628–1634.
[58] S. Mondal Roy, M. Sarkar, Membrane fusion induced by small molecules and ions, J. Lipids 2011 (2011) 528784.
[59] I.D. Goodyer, B. Pouvelle, T.G. Schneider, D.P. Trelka, T.F. Taraschi, Characterization of macromolecular transport pathways in malaria-infected erythrocytes, Mol. Biochem. Parasitol. 87 (1997) 13–28.
[60] S. Loew, A. Fahr, S. May, Modeling the release kinetics of poorly water-soluble drug molecules from liposomal nanocarriers, J. Drug Deliv. 2011 (2011) 376548.
[61] A. Fahr, P.V. Hoogevest, S. May, N. Bergstrand, S. Leigh, Transfer of lipophilic drugs between liposomal membranes and biological interfaces: consequences for drug delivery, Eur. J. Pharm. Sci. 26 (2005) 251–265.
[62] H. Kercret, J. Chiovetti, M.W. Fountain, J.P. Segrest, Plasma membrane-mediated leakage of liposomes induced by interaction with murine thymocytic leukemia cells, Biochim. Biophys. Acta Biomembr. 733 (1983) 65–74.
[63] G. Scherphof, F. Roerdink, M. Waite, J. Parks, Disintegration of phosphatidylcholine liposomes in plasma as a result of interaction with high-density lipoproteins, Biochim. Biophys. Acta Gen. Subj. 542 (1978) 296–307.
[64] J.A. Virtanen, K.H. Cheng, P. Somerharju, Phospholipid composition of the mammalian red cell membrane can be rationalized by a superlattice model, Proc. Natl. Acad. Sci. U. S. A. 95 (1998) 4964–4969.
[65] I.L. Lisovskaya, I.M. Shcherbachenko, R.I. Volkova, F.I. Ataullakhanov, Clotrimazole enhances lysis of human erythrocytes induced by t-BHP, Chem. Biol. Interact. 180 (2009) 433–439.

SUPPLEMENTARY DATA

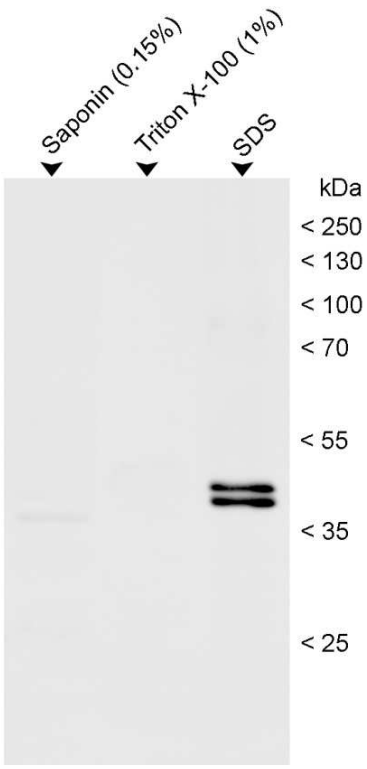

Fig.S1. pRBC subcellular fractionation analysis by Western blot using the monoclonal antibody *BM1234*.

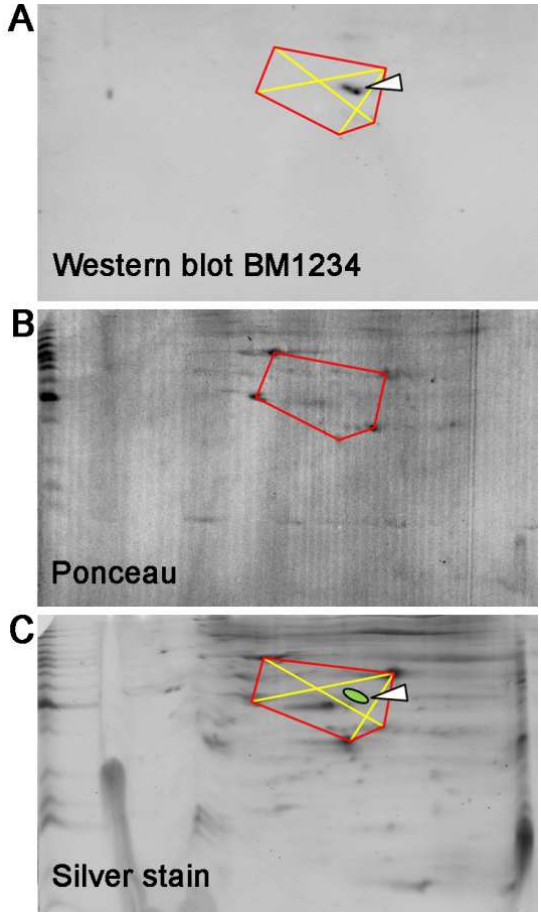

Fig.S2. 2D PAGE analysis of the cytoskeletal-matrix protein fraction obtained during pRBC subcellular fractionation. A first gel was blotted onto a PVDF membrane and subjected to Western blot hybridization with the monoclonal antibody *BM1234* (A), followed by Ponceau staining (B). A second identical gel was silver-stained (C) and the region containing the spots detected by *BM1234* (arrowhead in A and C) was identified by triangulation using common protein spots detected by Ponceau and silver stains in membrane and gel, respectively, excised (green oval area in C), digested with trypsin, and subjected to LC-MS/MS analysis.

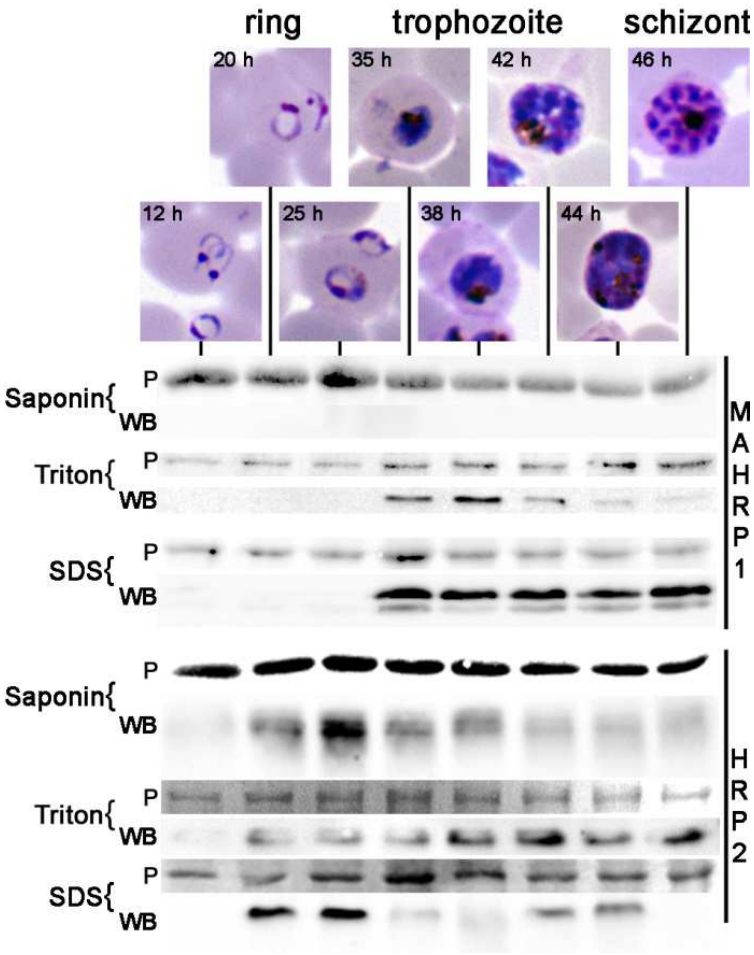

Fig.S3. Subcellular fractionation analysis along the intraerythrocytic *P. falciparum* cycle of MAHRP1 and HRP2 expression. P: Ponceau stain of endogenous RBC proteins as control for homogeneous sample loading; WB: Western blot for the detection of MAHRP1 (using the monoclonal antibody *BM1234*) and HRP2. The upper images show representative Giemsa-stained pRBCs from the different time points.

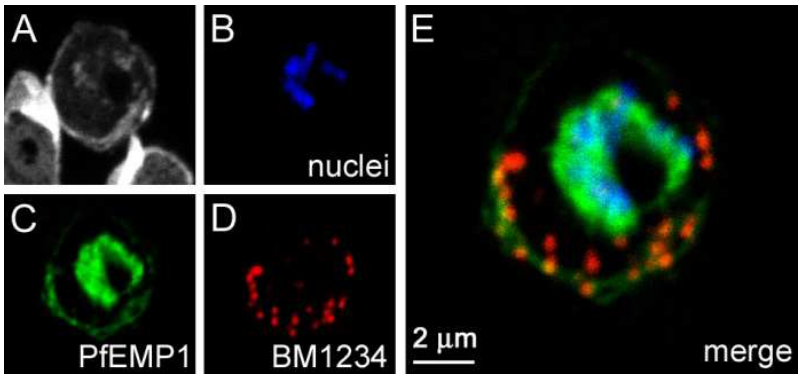

Fig.S4. Fluorescence confocal microscopy analysis of the subcellular localizations of PfEMP1 and MAHRP1 (using the *BM1234* antibody) in fixed pRBCs.

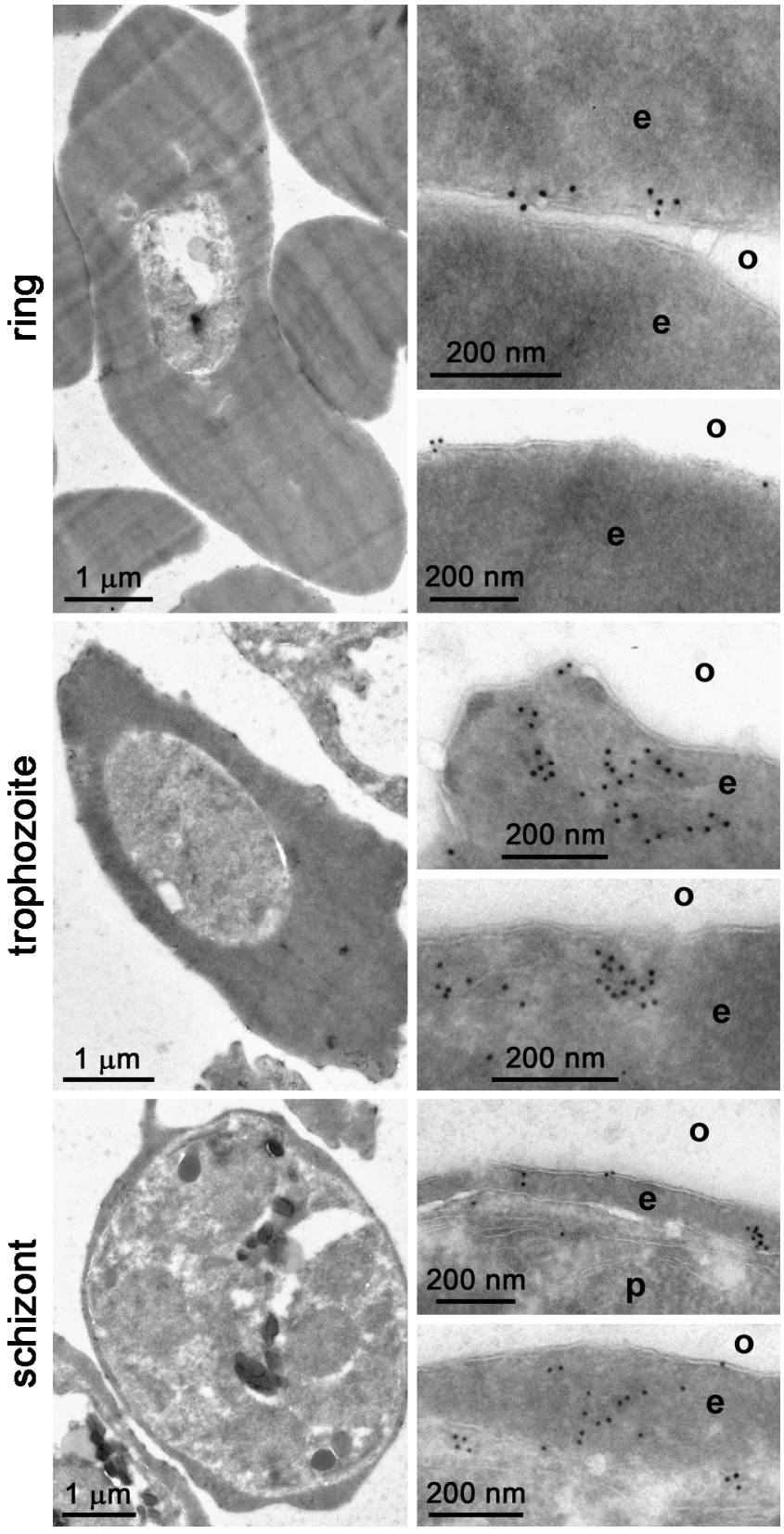

Fig.S5. Immuno-TEM subcellular localization analysis in pRBCs at the ring, trophozoite, and schizont stages of *P. falciparum* MAHRP1, using the monoclonal antibody *BM1234*. o: outside of the cell; e: erythrocyte cytoplasm; p: *P. falciparum*.

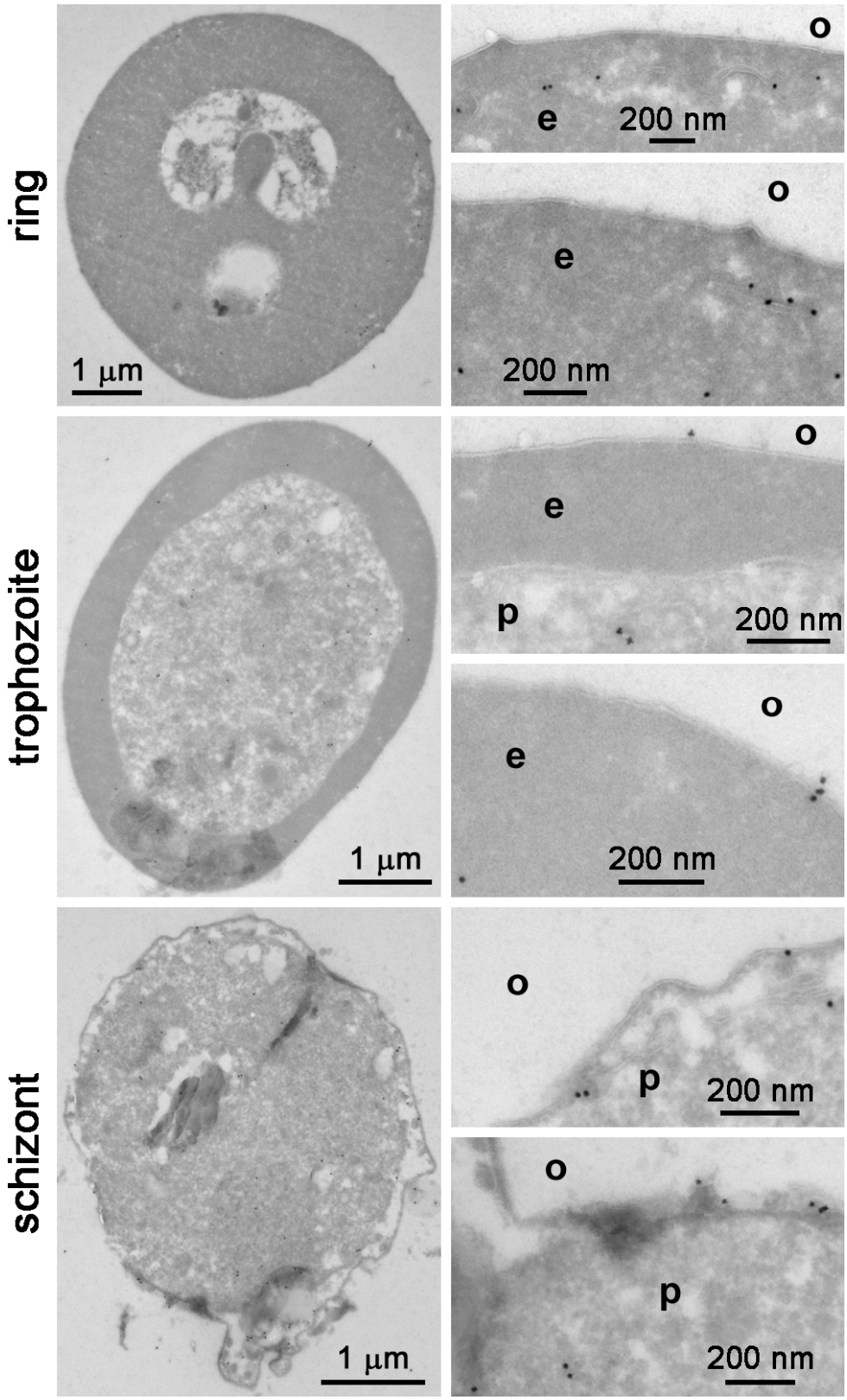

Fig.S6. Immuno-TEM subcellular localization analysis in pRBCs at the ring, trophozoite, and schizont stages of *P. falciparum* MAHRP1, using the polyclonal antibody raised against MAHRP1$_{21\text{-}40}$. o: outside of the cell; e: erythrocyte cytoplasm; p: *P. falciparum*.

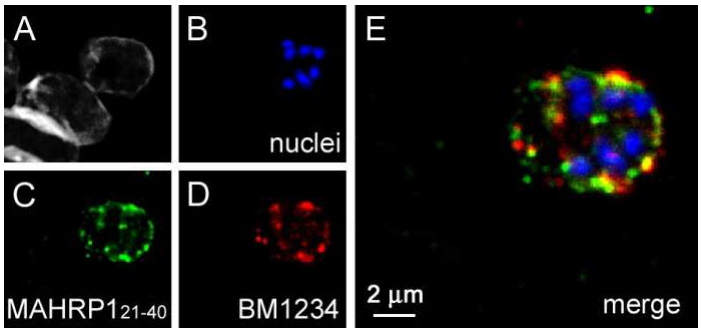

Fig.S7. Fluorescence confocal microscopy analysis of the subcellular localization of MAHRP1 (using anti-MAHRP1$_{21-40}$ and *BM1234* antibodies) in fixed pRBCs.

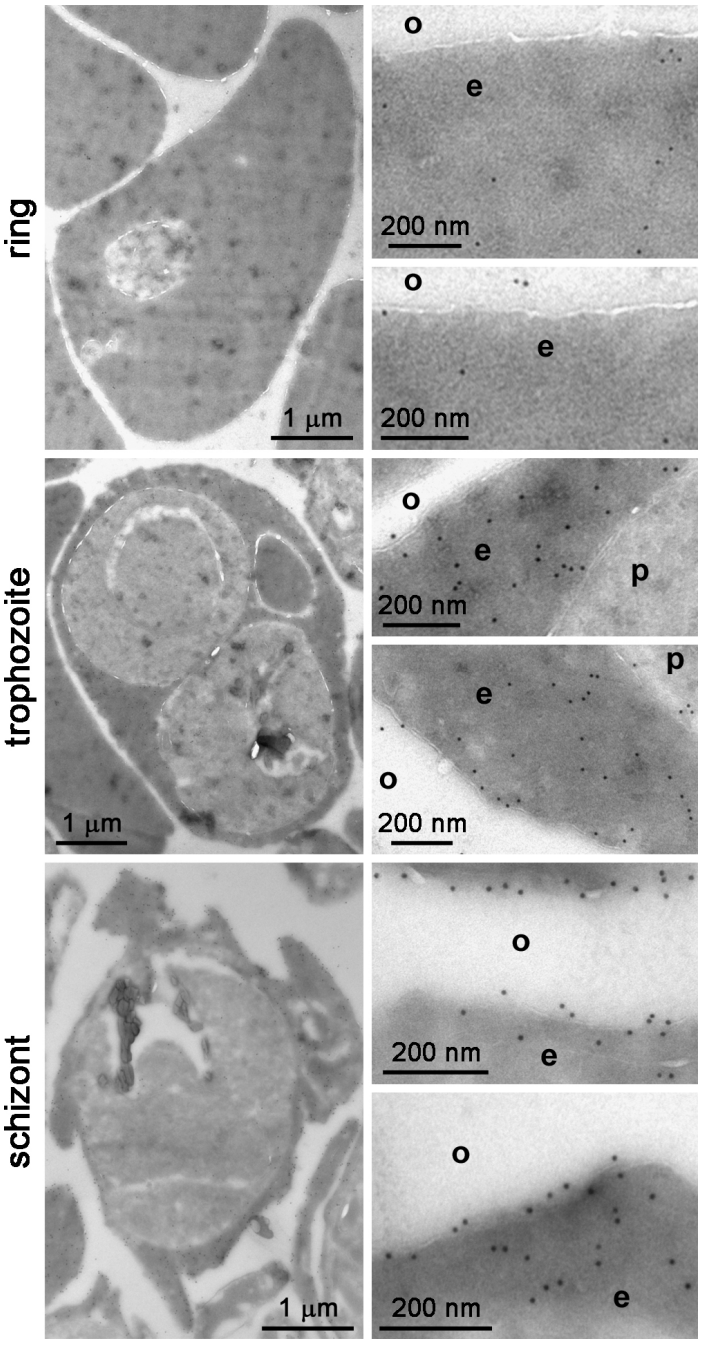

Fig.S8. Immuno-TEM subcellular localization analysis in pRBCs at the ring, trophozoite, and schizont stages of *P. falciparum* HRP2, using the monoclonal antibody specified in the manuscript. o: outside of the cell; e: erythrocyte cytoplasm; p: *P. falciparum*.

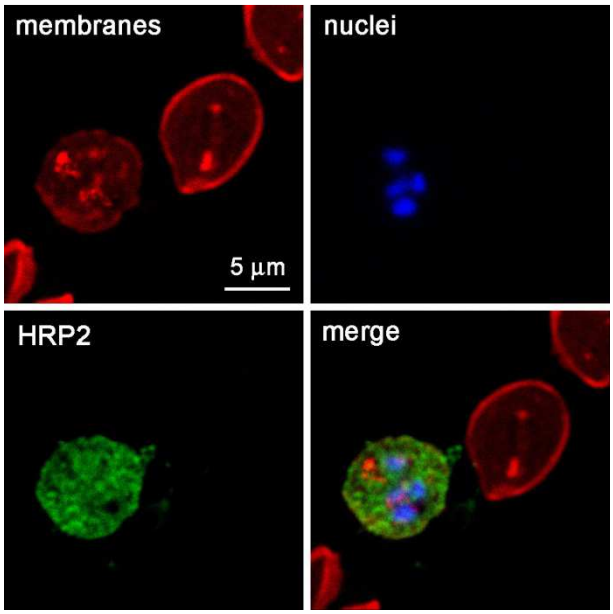

Fig.S9. Fluorescence confocal microscopy analysis in fixed cells of the presence of HRP2 on pRBCs.

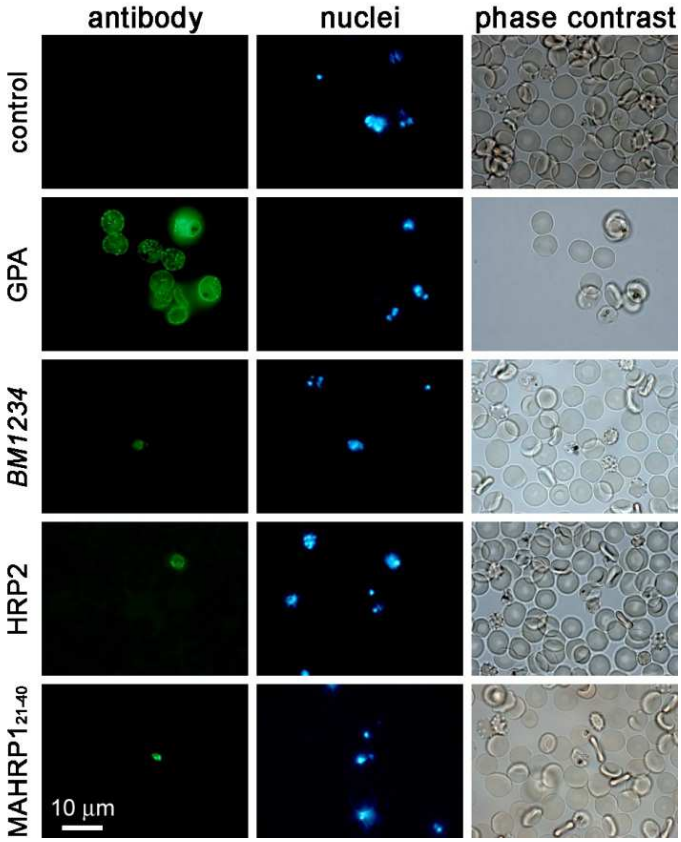

Fig.S10. Fluorescence microscopy analysis of the binding of targeting antibodies to live pRBC cultures after 30 min incubation at 37 °C. Monoclonal anti-GPA was used at 1 µg/ml because at higher concentrations it was found to induce excessive agglutination; all other antibodies were used at 70 µg/ml. Control: cells incubated only with the secondary fluorescent antibody.

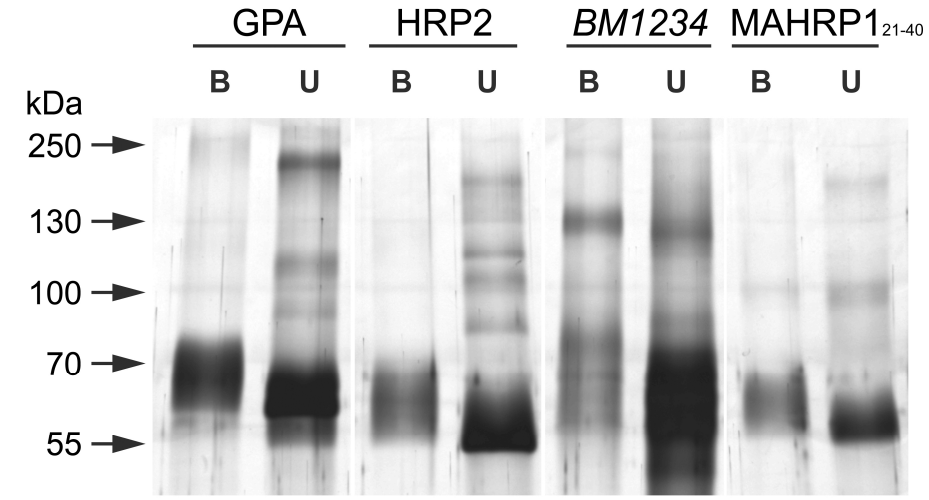

Fig.S11. Silver-stained gel of the electrophoretic analysis under reducing conditions of the coupling of half-antibodies against GPA, HRP2, and MAHRP1 (monoclonal *BM1234* and polyclonal anti-MAHRP1$_{21-40}$) to liposomes containing in their formulation 15% of the maleimide-conjugated lipid MPB-PE (LP-Mal-Ab model). Prior to electrophoresis, samples containing 2 µg protein were centrifuged for the analysis of liposome-bound antibodies in the pellet (B) and of unbound antibodies in the supernatant (U).

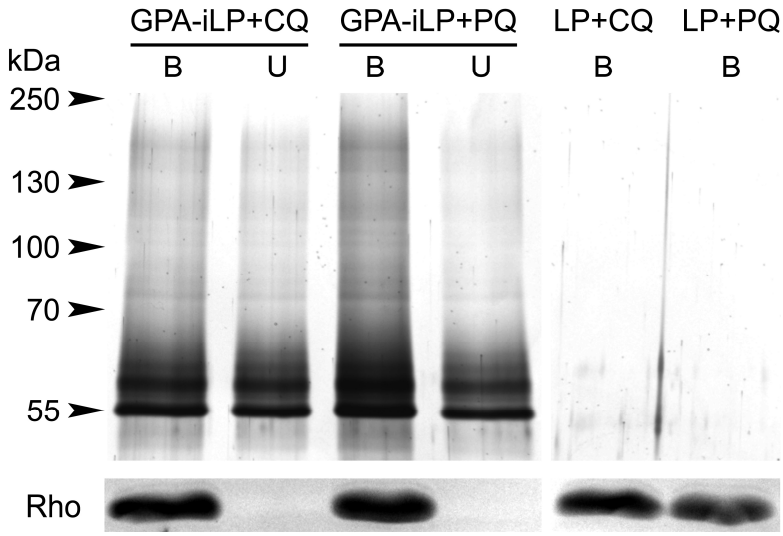

Fig.S13. Silver-stained, reducing SDS-PAGE analysis of monoclonal anti-GPA coupling to LPs encapsulating CQ and PQ (GPA-iLP). Coupling was performed via a PEG-Mal linker through antibody primary amino groups using a 10× molar excess relative to antibody molecules of SATA crosslinking agent. Prior to electrophoresis, samples containing 2 µg protein were centrifuged for the analysis of LP-bound antibodies in the pellet (B) and of unbound antibodies in the supernatant (U). Identically prepared liposome samples where the antibody was omitted (LP) were included as a control. The fluorescence emission of rhodamine conjugated to lipids included in the formulation of LPs is used as control of the LP-containing fractions (Rho).

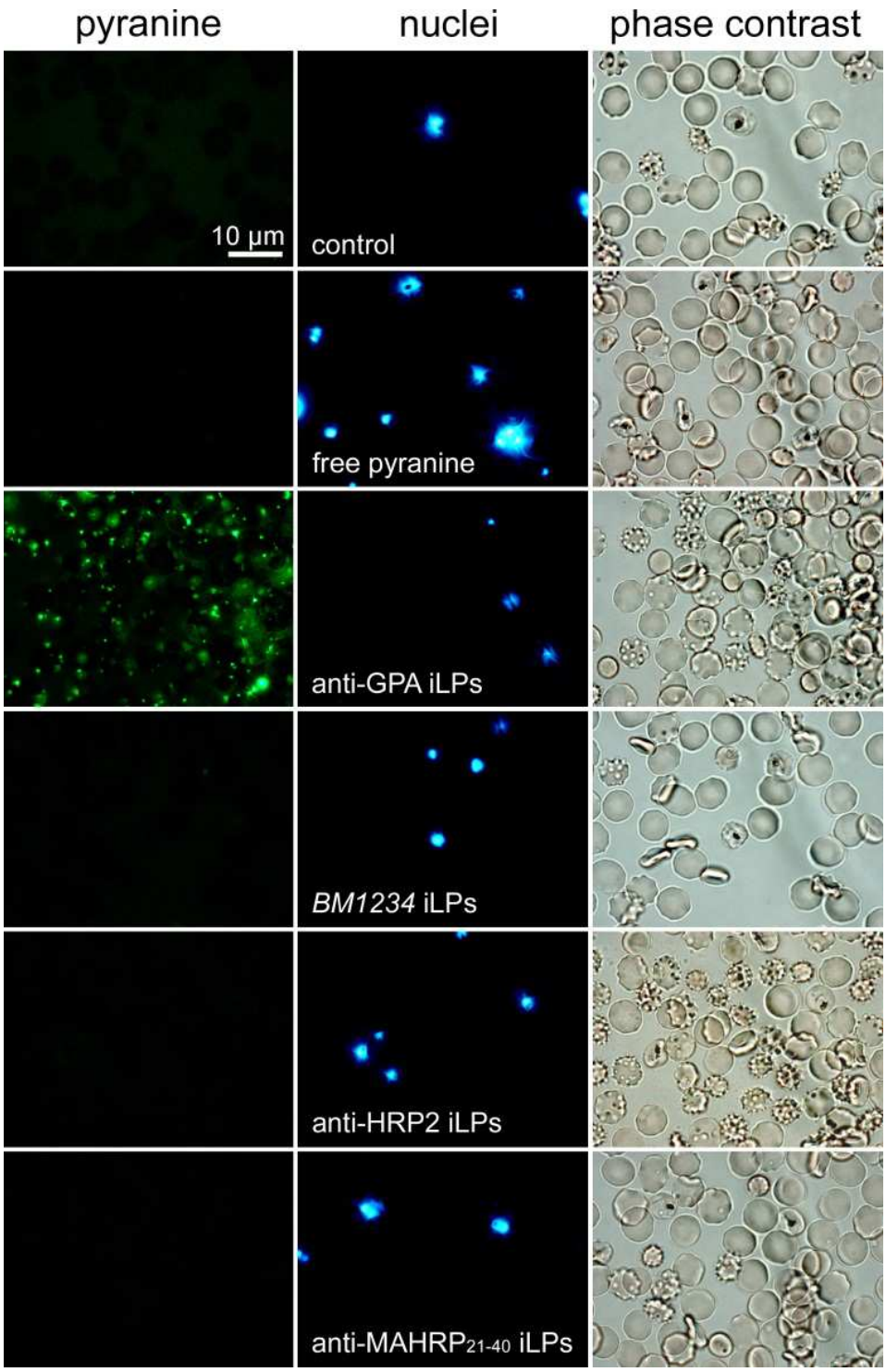

Fig.S12. Fluorescence microscopy targeting analysis in live *P. falciparum* cultures of pyranine-loaded iLPs functionalized with the different antibodies studied according to the LP-Mal-Ab model. Lipid concentration in the culture was 1 mM and samples were incubated for 90 min at 37 °C before microscopic observation. A sample not treated with iLPs was included as autofluorescence control.

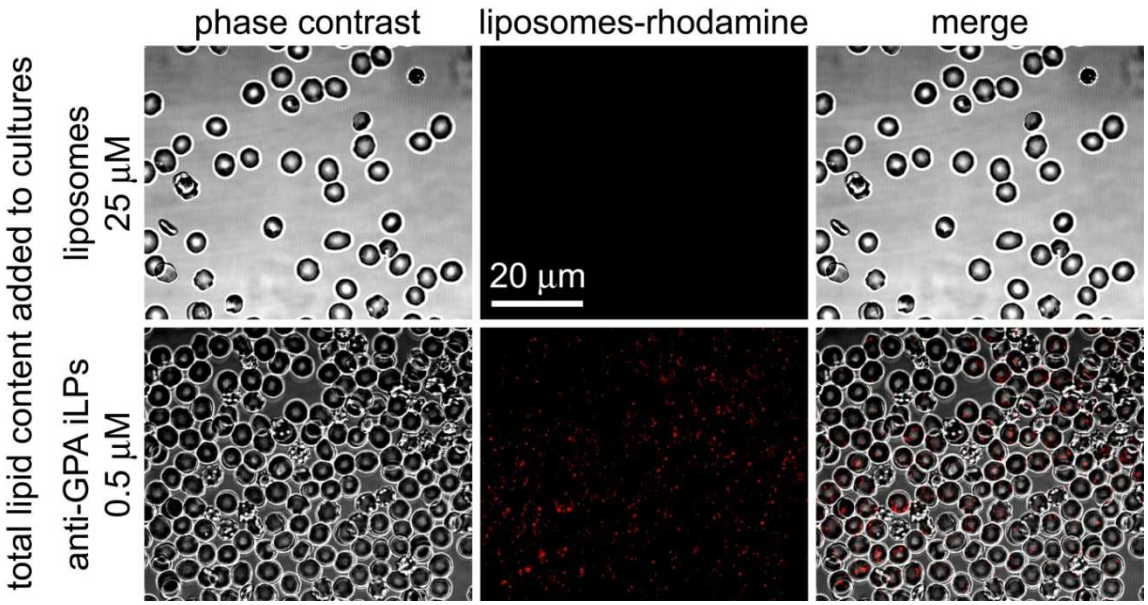

Fig.S14. Confocal fluorescence microscopy assay of live *P. falciparum* cultures showing the fraction of cells targeted by small amounts of monoclonal anti-GPA iLPs (LP-PEG-Mal-NH_2-MAb model). Liposomes contained 0.5% of the rhodamine-labeled lipid DOPE-Rho in their formulation, and the samples were incubated for 30 min under orbital stirring before microscopic examination.

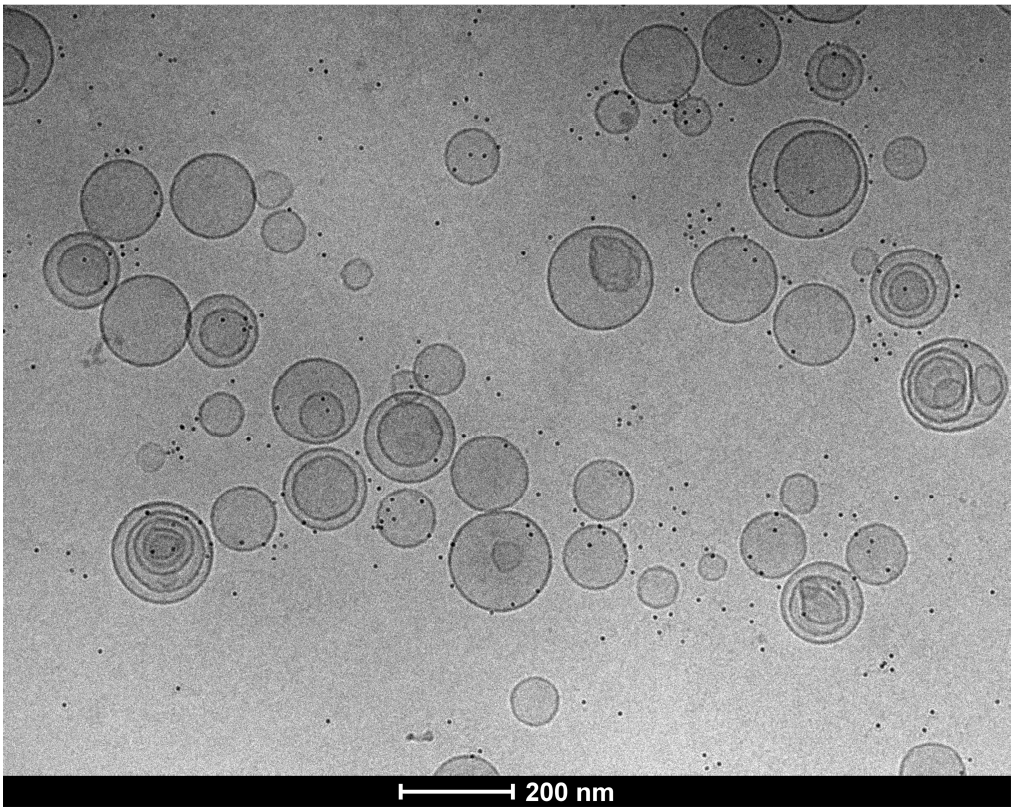

Fig.S15. Cryo-TEM image of iLPs conjugated with monoclonal anti-GPA at the distal end of maleimide-PEG-grafted lipids (LP-PEG-Mal-NH_2-MAb model). Anti-GPA antibodies were detected with anti-mouse IgG conjugated to 6-nm colloidal gold particles.

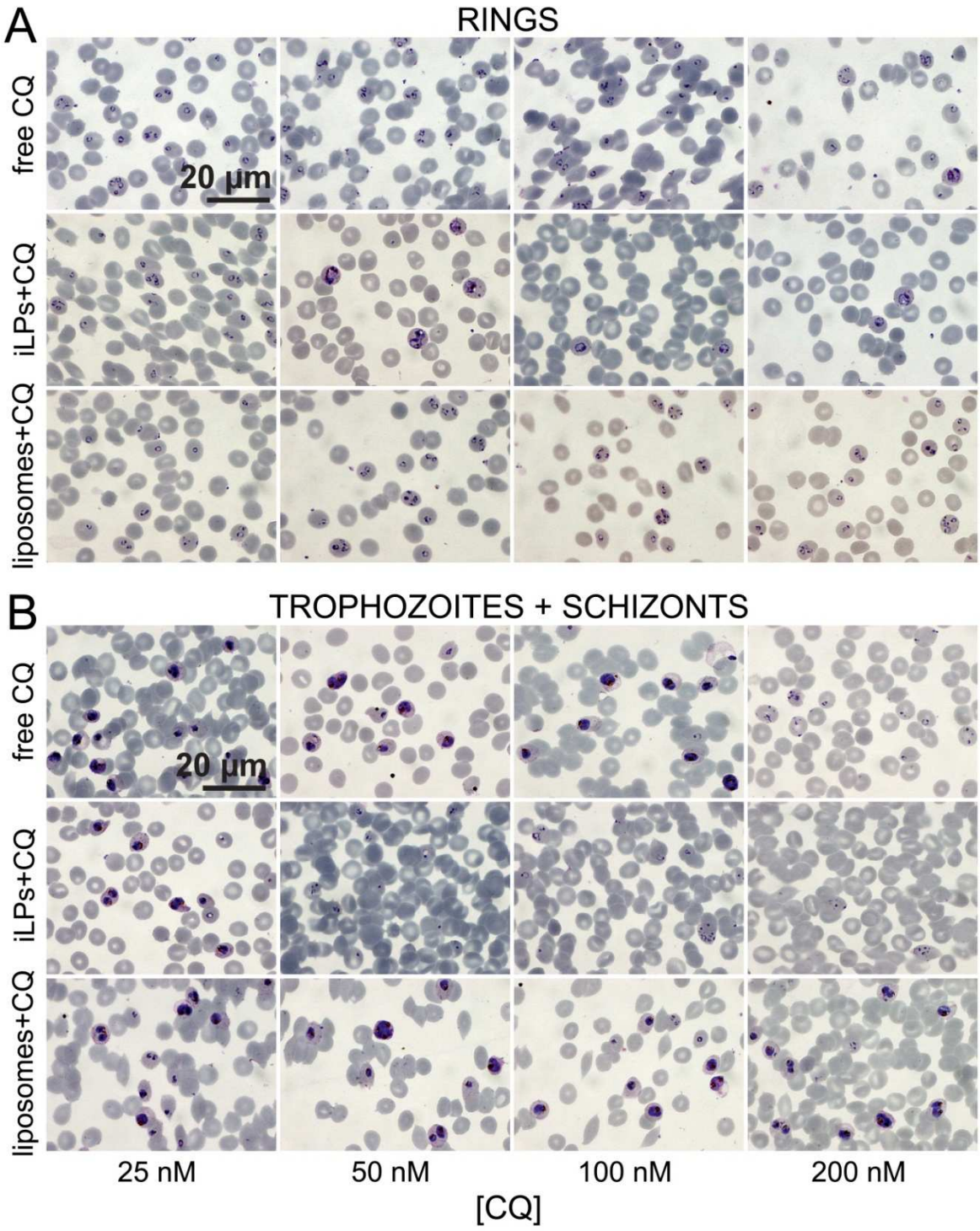

Fig.S16. Microscopy images of *P. falciparum* growth inhibition assays. Giemsa-stained cultures had been treated for 15 min with different amounts of CQ as a free drug or encapsulated into rhodamine-labeled LPs or anti-GPA iLPs (LP-PEG-Mal-NH_2-MAb) added to either (A) ring or (B) trophozoite+schizont stages, and incubated for 48 h before microscopic examination.

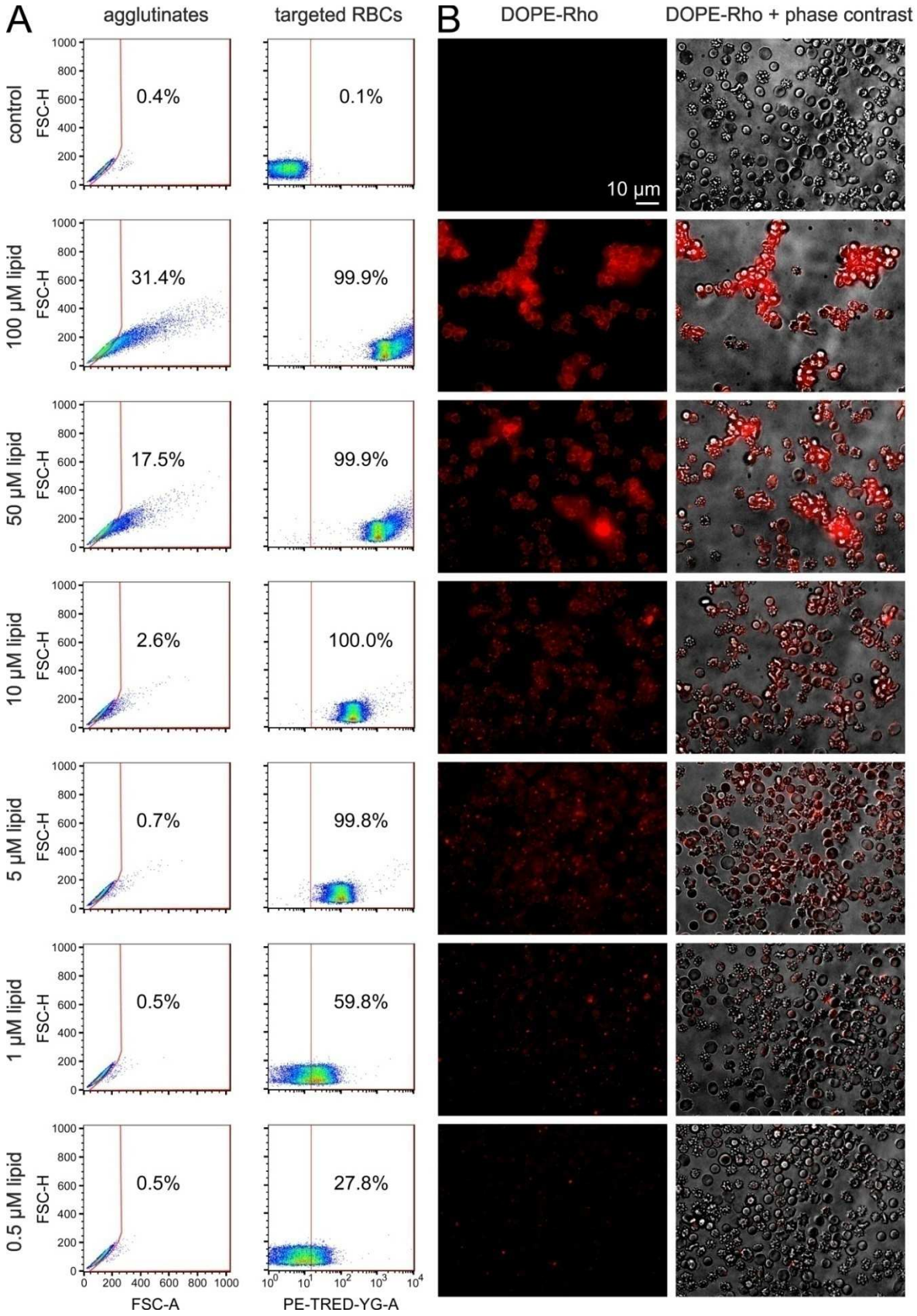
A
agglutinates
targeted RBCs
B
DOPE-Rho
DOPE-Rho + phase contrast
control
100 µM lipid
50 µM lipid
10 µM lipid
5 µM lipid
1 µM lipid
0.5 µM lipid
FSC-H
0.4%
0.1%
31.4%
99.9%
17.5%
99.9%
2.6%
100.0%
0.7%
99.8%
0.5%
59.8%
0.5%
27.8%
10 µm
FSC-A
PE-TRED-YG-A

Fig.S17. *In vitro* analysis of the agglutinating effect and targeting against RBCs of liposomes functionalized with the monoclonal antibody anti-GPA (GPA-iLPs) and containing the red fluorescent lipid DOPE-Rho. RBCs at 2% hematocrit samples were incubated in RPMI-A for 30 min with different liposome amounts. Agglutinates were detected during flow cytometry analysis (A) as those cells having a disproportion between forward light scatter area (FSC-A) and height (FSC-H) values in a linear scale. Cell targeting was determined by measuring rhodamine fluorescence signal by excitation through a yellow-green 561 nm laser at 50 mW power and emission collection with a 610/20 nm bandpass filter and a 600 nm long pass dichroic mirror (PE-TRED-YG channel). The agglutinating effect and targeting under static conditions from the same GPA-iLP samples was analyzed in parallel by fluorescence microscopy (B) using an Olympus IX51 inverted system microscope equipped with a green 532 nm laser and red fluorescence emission collection.

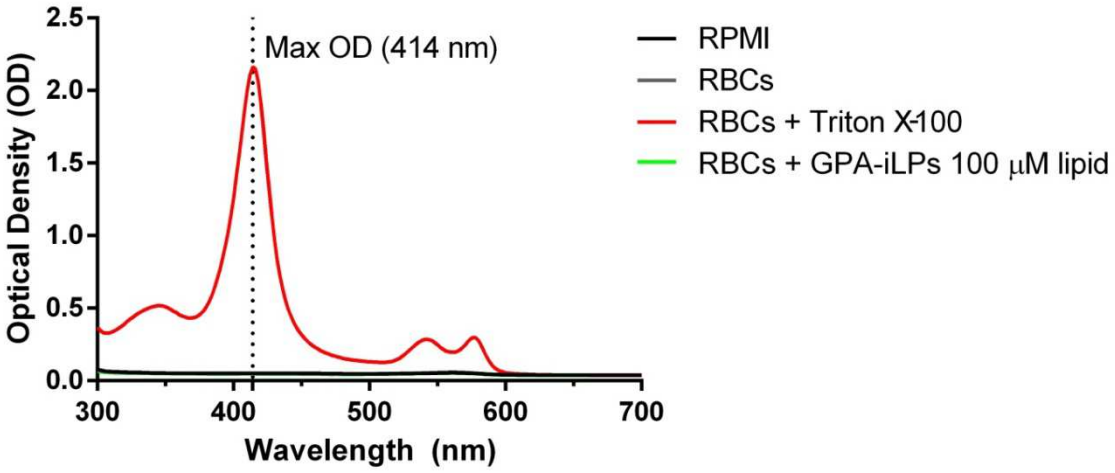

Fig.S18. Absorption spectral analysis of the *in vitro* hemolytic effect of liposomes functionalized with the monoclonal antibody anti-GPA (GPA-iLPs). After 30 min incubation with 2% hematocrit RBCs in RPMI-A, cells were spun down and supernatants analyzed in a Synergy HT spectrophotometer. RPMI-A and the supernatants from RBCs alone or treated for 30 min with 2% Triton X-100 are included as negative and positive controls. Maximum optical density indicative of hemolysis was obtained at 414 nm.

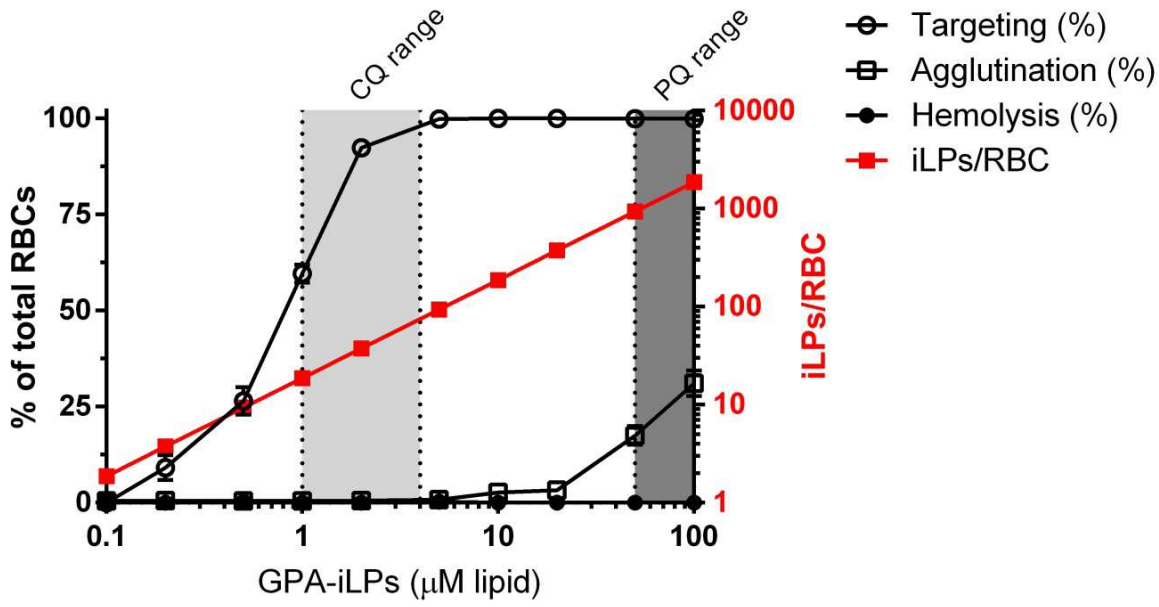

Fig.S19. Analysis of the overall *in vitro* effects on red blood cells at 2% hematocrit of liposomes functionalized with the monoclonal antibody anti-GPA (GPA-iLPs). (Left Y axis) Targeting and agglutination were determined by flow cytometry after 30 min incubation with GPA-iLPs (Fig. S17A). Hemolysis was determined by light absorption at 414 nm relative to the positive control consisting of RBCs treated with 2% Triton X-100 (Fig. S18). (Right Y axis) iLP/RBC ratio, calculated as described in the Methods section 2.4. The ranges of GPA-iLP amounts assayed in this work where the corresponding encapsulated CQ and PQ amounts led to a complete *P. falciparum* growth inhibition are highlighted in grey.

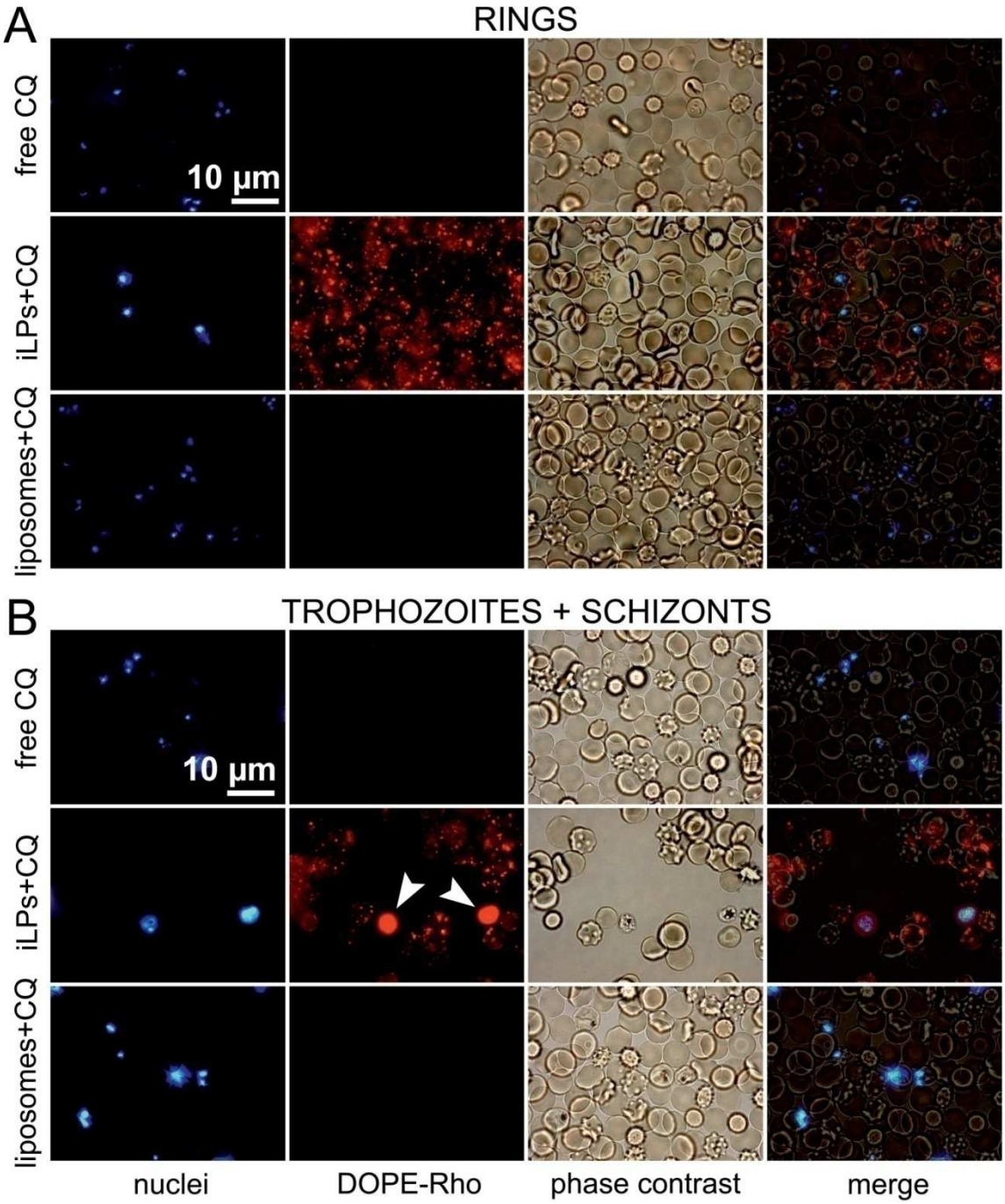

Fig.S20. Fluorescence microscopy images of live *P. falciparum* cultures corresponding to the 100 nM CQ sample from Figure S16 to show retention on the cells of anti-GPA iLPs added to either (A) ring or (B) trophozoite+schizont stages. Free drug-treated samples are shown as autofluorescence control. The arrowheads in (B) indicate schizonts.

Supplementary Table 1. Statistical significance of the differences between empirical encapsulation efficiencies from Table 1.

Parameters to compare (EE %)		Fold change	p-value	t-test
CQ pH 7.4	CQ pH 6.5	2	0.003	unpaired
PQ pH 7.4	PQ pH 6.5	1.1	0.12	unpaired
25 µM CQ pH 6.5	10 mM CQ pH 6.5	2.8	0.005	unpaired
4 mM PQ pH 6.5	10 mM PQ pH 6.5	1.5	2.4^{-6}	unpaired

Fold change represents the ratio of left vs. right compared parameters.

Supplementary Table 2. Statistical significance of the differences between average drug releases from unsaturated DOPC liposomes in Figure 3.

Average release from DOPC LPs (%)		Fold change	p-value	t-test
Storage CQ	Storage PQ	1.8	7.3^{-4}	paired
Culture CQ 1:10	Culture PQ 1:40	1.3	1.1^{-3}	paired

Fold change represents the ratio of left vs. right compared parameters.

Editorial

For reprint orders, please contact reprints@future-science.com

Future Medicinal Chemistry

Loading antimalarial drugs into noninfected red blood cells: an undesirable roommate for *Plasmodium*

"...most antimalarials start affecting the infected cell relatively late in the intraerythrocytic parasite life cycle, when their effect is probably often too short to be lethal to *Plasmodium*."

Keywords: malaria • nanomedicine • *Plasmodium* • red blood cell • targeted drug delivery

Ernest Moles
Nanomalaria Unit, Institute for Bioengineering of Catalonia (IBEC), Baldiri Reixac 10–12, Barcelona ES-08028, Spain
and
Barcelona Institute for Global Health (ISGlobal, Barcelona Ctr. Int. Health Res. [CRESIB], Hospital Clínic-Universitat de Barcelona), Rosselló 149–153, Barcelona ES-08036, Spain
and
Nanoscience & Nanotechnology Institute (IN²UB), University of Barcelona, Martí i Franquès 1, Barcelona ES-08028, Spain

Xavier Fernàndez-Busquets
Author for correspondence:
Nanomalaria Unit, Institute for Bioengineering of Catalonia (IBEC), Baldiri Reixac 10–12, Barcelona ES-8028, Spain
and
Barcelona Institute for Global Health (ISGlobal, Barcelona Ctr. Int. Health Res. [CRESIB], Hospital Clínic-Universitat de Barcelona), Rosselló 149–153, Barcelona ES-08036, Spain
and
Nanoscience & Nanotechnology Institute (IN²UB), University of Barcelona, Martí i Franquès 1, Barcelona ES-08028, Spain
xfernandez_busquets@ub.edu

The malaria parasite, *Plasmodium* spp., is a delicate unicellular organism unable to survive in free form for more than a couple of minutes in the bloodstream. Upon injection in a human by its *Anopheles* mosquito vector, *Plasmodium* sporozoites pass through the liver with the aim of invading hepatocytes. Those which succeed spend inside their host cell a recovery time before replicating and entering the blood circulation as fragile merozoites, although their exposure to host defenses is extraordinarily short. Quick invasion of red blood cells (RBCs) in a process lasting just a few minutes allows the parasite to escape immune system surveillance. For most of its erythrocytic cycle the pathogen feeds mainly on hemoglobin as it progresses from the early blood stages, termed rings, to the late forms trophozoites and schizonts. Early stages are ideal targets for antimalarial therapies because drugs delivered to them would have a longer time to kill the parasite before it completes its development. However, only 6 h after invasion does the permeability of the infected erythrocyte to anions and small nonelectrolytes, including some drugs, start to increase as the parasite matures [1]. During this maturation process the parasite hydrolyzes hemoglobin in a digestive vacuole, which is the target of many amphiphilic drugs that freely cross the RBC membrane and accumulate intracellularly. As a result, most antimalarials start affecting the infected cell relatively late in the intraerythrocytic parasite life cycle, when their effect is probably often too short to be lethal to *Plasmodium*.

Malaria-infected erythrocytes: an elusive target

Several strategies to improve the activity of antimalarial drugs concern their encapsulation in nanocarriers targeted to parasitized RBCs (pRBCs), an approach that requires the existence of specific pRBC markers. 200-nm liposomes studded with heparin or antibodies raised against pRBCs have been shown to bind late forms with high selectivity [2,3], improving the activity of encapsulated antimalarial drugs up to tenfold [2,4]. In addition to the inconvenient late-stage targeting, such liposomal delivery models will also have to overcome the obstacle of timing nanocarrier administration to the precise moment of the parasite's life cycle when trophozoites and schizonts are present. The relatively short blood half-life of liposomes (in the best cases, <10 h for polyethylene glycol-coated stealth liposomes) guarantees that if injected at the wrong moment (too soon or too late), they will not last the 48 h needed to ensure that they are present for the pathogen's next cycle. In another display of cunningness, *Plasmodium* leaves virtually no external signal on the parasitized cell, and only after spending half its life inside the erythrocyte does the parasite export a significant number of receptors and transporters to the host cell plasma membrane. Most of these externally recognizable clues are present in the parasite genome as multiple variants that can be clonally expressed [5], which further complicates delivery approaches designed to specifically target pRBCs. A receptor-independent alternative for the nanovector-mediated delivery of antimalarial drugs to *Plasmodium* blood

10.4155/FMC.15.35 © 2015 Future Science Ltd **Future Med. Chem.** (2015) 7(7), 837–840 ISSN 1756-8919

stages can be provided by the tubulovesicular network induced in the host cell by the pathogen during its intraerythrocytic growth, which confers pRBC accessibility to a wide range of particles up to diameters of 70 nm [6]. Indeed, polymeric nanovectors were observed to penetrate trophozoites and schizonts [7,8], possibly in a significant fraction through the tubulovesicular network, although entry of nanoparticles into early ring stages has not been unambiguously observed so far.

Is there an ideal carrier for blood-circulating drugs?

Antimalarial drug carriers should provide optimal compound half-lives in circulation, adequate clearance mechanisms, restriction of unintended drug effects in non-target cells, specific delivery to the correct tissue, and a timely initiation and termination of the therapeutic action. Considering the need to target intraerythrocytic *Plasmodium* as early in its life cycle as possible and the lack of strategies currently out there for shuttling drugs into pRBCs, it is imperative that these issues are addressed and that alternative approaches are explored. A solution to the aforementioned problems in the design of pRBC-targeted nanocarriers can perhaps be provided by one of the most adequate vascular carriers, RBCs themselves [9]. Human erythrocytes have a life span in the blood of up to 120 days, which makes them attractive carriers for intravascular delivery because they prolong drug circulation. In addition, their large size (approximately 7 μm across and around 2 μm thick) significantly restricts unintended extravasation and in principle allows for a much larger encapsulation capacity than liposomes. Other interesting features of RBCs as drug carriers are their biocompatibility and the existence of natural mechanisms for their safe elimination from the body. Actually, delivery of antimalarials to noninfected RBCs has been previously carried out in chemotherapeutic investigations, in order to examine the effects on later invading parasites. In one such study, RBCs were pretreated with the drugs halofantrine, lumefantrine, piperaquine, amodiaquine and mefloquine, which were observed to diffuse into and remain within the erythrocyte, inhibiting downstream growth of *Plasmodium* [10]. However, it should be noted that the loading of drugs into noninfected RBCs has not yet been explored in detail as a clinically feasible therapeutic strategy against malaria, in part because of a number of restrictions that must be taken into consideration.

Which are the limitations of erythrocytes as drug carriers?

A significant limiting factor for the use of RBCs as antimalarial carriers is that when present at therapeutically active concentration, the drug has to be innocuous for the cell physiology, which might not be an unsurmountable obstacle given the reduced metabolic activity of eryrthrocytes. However, loading of some antimalarial drugs like clotrimazole had been observed to predispose RBCs to oxidative damage [11], an undesirable scenario because oxidized RBCs are rapidly taken up by hepatic reticuloendothelial system macrophages. Another obstacle for the incorporation of antimalarial drugs into RBCs is drug loading itself, since most currently available protocols use a harsh *ex vivo* isolation of erythrocytes followed by drug loading through diffusion [9]. In a clinical setting, perhaps RBC-targeted immunoliposomes can come to rescue, although the incapacity of mature erythrocytes to endocyte [12] calls for the development of specific targeted drug delivery strategies independent from the receptor-mediated endocytic pathway. Moreover, the physicochemical properties of each particular antimalarial drug will constrain the nanovector composition and the corresponding drug delivery mechanism. As an example, the optimal approach for delivery of membrane-impermeable hydrophilic drugs such as fosmidomycin would be immunoliposomal fusion with the RBC membrane, which requires the incorporation of special fusogenic agents into highly fluid vesicles. Including negatively charged phospholipids in the liposome formulation has been found to be crucial for the delivery of trehalose into RBCs *in vitro* [13], but nanovector fusion can be inhibited by components found in plasma [14], and charged vesicles are quickly complexed by serum proteins that target them for clearance from circulation [15]. A possible solution consists of incorporating stealth agents onto the nanovector surface like polyethylene glycol chains or gangliosides, which neutralize vesicle charge and significantly reduce unspecific interaction events, although they can also interfere with fusion if excessive amounts are used.

> "...the loading of drugs into noninfected red blood cells has not yet been explored in detail as a clinically feasible therapeutic strategy against malaria..."

The capacity of amphiphilic antimalarial drugs (which comprise the extensive aminoquinoline and artemisinin drug derivative families) to easily cross lipid bilayers demands a careful design of their targeting liposomes. Active loading techniques based on pH gradients across liposome membranes [16] are required to efficiently encapsulate the fully ionized species of amphiphilic drugs, in combination with a saturated lipid-enriched bilayer capable of maintaining a proton gradient. As a consequence of the reduced fluidity of the resulting membrane, fusion events with targeted

cells are significantly inhibited; sustained drug delivery while the liposome is docked onto the RBC is the most likely mechanism through which such nanovectors operate. This process would be mediated by a depletion of the liposomal proton gradient by means of temperature, liposome–cell interaction events [17] and lipid transference to plasma components [18], and might be highly effective for the delivery of weak basic drugs such as those from the aminoquinoline family. These compounds, positively charged at neutral pH, will theoretically accumulate inside the cell and become entrapped by virtue of the electrochemical gradient created by the phospholipid asymmetry in RBC membranes [19], which maintains a negatively charged intracellular membrane lining. Liposomal nanovectors are also efficient carriers for hydrophobic drugs like lumefantrine and halofantrine, which can be delivered to RBCs following a sustained release process by an exchange mechanism of hydrophobic material between the apposed membranes of liposome and erythrocyte [20]. Since the liposomes adsorbed on RBC surfaces would probably sufficiently modify cell shape to target it for removal through spleen filtration, a compromise between stable drug containment and lipid bilayer fusion will have to be reached through the adequate liposome formulation, with the objective of achieving liposome–RBC merging before spleen removal while avoiding rapid drug leaking from liposomes.

It is reasonable to predict that the nanovector design limitations exposed above can be satisfactorily dealt with, and that some of the future antimalarials yet to be discovered will be harmless for erythrocytes, thus allowing for the loading in these cells of drug amounts that are lethal for *Plasmodium*. If so, the pathogen might encounter its enemy at home, right at the very moment of entering the host cell, which would have devastating effects for the parasite and significantly compromise its survival capacity. Such a strategy could be likely developed into a prophylactic treatment against erythrocyte infection.

Financial & competing interests disclosure

This work was supported by grants BIO2011–25039 and BIO2014-52872-R from the Ministerio de Economía y Competitividad, Spain, which included FEDER funds, 2014-SGR-938 from the Generalitat de Catalunya, Spain, and 2013–0584 from the FondSazione Cariplo, Italy. The authors have no other relevant affiliations or financial involvement with any organization or entity with a financial interest in or financial conflict with the subject matter or materials discussed in the manuscript apart from those disclosed.

No writing assistance was utilized in the production of this manuscript.

References

1 Kirk K. Membrane transport in the malaria-infected erythrocyte. *Physiol. Rev.* 81(2), 495–537 (2001).

2 Marques J, Moles E, Urbán P *et al.* Application of heparin as a dual agent with antimalarial and liposome targeting activities towards *Plasmodium*-infected red blood cells. *Nanomedicine* 10, 1719–1728 (2014).

3 Urbán P, Estelrich J, Cortés A, Fernàndez-Busquets X. A nanovector with complete discrimination for targeted delivery to *Plasmodium falciparum*-infected versus non-infected red blood cells *in vitro*. *J. Control. Release* 151(2), 202–211 (2011).

4 Urbán P, Estelrich J, Adeva A, Cortés A, Fernàndez-Busquets X. Study of the efficacy of antimalarial drugs delivered inside targeted immunoliposomal nanovectors. *Nanoscale Res. Lett.* 6, 620 (2011).

5 Kyes S, Horrocks P, Newbold C. Antigenic variation at the infected red cell surface in malaria. *Ann. Rev. Microbiol.* 55, 673–707 (2001).

6 Goodyer ID, Pouvelle B, Schneider TG, Trelka DP, Taraschi TF. Characterization of macromolecular transport pathways in malaria-infected erythrocytes. *Mol. Biochem. Parasitol.* 87(1), 13–28 (1997).

7 Movellan J, Urbán P, Moles E *et al.* Amphiphilic dendritic derivatives as nanocarriers for the targeted delivery of antimalarial drugs. *Biomaterials* 35(27), 7940–7950 (2014).

8 Urbán P, Valle-Delgado JJ, Mauro N *et al.* Use of poly(amidoamine) drug conjugates for the delivery of antimalarials to *Plasmodium*. *J. Control. Release* 177, 84–95 (2014).

9 Muzykantov VR. Drug delivery by red blood cells: vascular carriers designed by Mother Nature. *Expert Opin. Drug Deliv.* 7(4), 403–427 (2010).

10 Wilson DW, Langer C, Goodman CD, McFadden GI, Beeson JG. Defining the timing of action of antimalarial drugs against *Plasmodium falciparum*. *Antimicrob. Agents Chemother.* 57(3), 1455–1467 (2013).

11 Lisovskaya IL, Shcherbachenko IM, Volkova RI, Ataullakhanov FI. Clotrimazole enhances lysis of human erythrocytes induced by t-BHP. *Chem. Biol. Interact.* 180(3), 433–439 (2009).

12 Harmening DM. The red blood cell. Structure and function. In: *Clinical Hematology and Fundamentals of Hemostasis. 3rd Edition*. F. A. Davis Company, Philadelphia, PA, USA, 54–70 (1996).

13 Holovati JL, Gyongyossy-Issa MIC, Acker JP. Effect of liposome charge and composition on the delivery of trehalose into red blood cells. *Cell Preserv. Tech.* 6(3), 207–218 (2008).

14 Pires P, Simões S, Nir S, Gaspar R, Düzgünes N, Pedroso de Lima MC. Interaction of cationic liposomes and their DNA complexes with monocytic leukemia cells. *Biochim. Biophys. Acta* 1418(1), 71–84 (1999).

15 Maurer N, Fenske DB, Cullis PR. Developments in liposomal drug delivery systems. *Expert Opin. Biol. Ther.* 1(6), 923–947 (2001).

▶16 Madden TD, Harrigan PR, Tai LCL *et al.* The accumulation of drugs within large unilamellar vesicles exhibiting a proton gradient: a survey. *Chem. Phys. Lipids* 53(1), 37–46 (1990).

▶17 Kercret H, Chiovetti J, Fountain MW, Segrest JP. Plasma membrane-mediated leakage of liposomes induced by interaction with murine thymocytic leukemia cells. *Biochim. Biophys. Acta* 733(1), 65–74 (1983).

▶18 Scherphof G, Roerdink F, Waite M, Parks J. Disintegration of phosphatidylcholine liposomes in plasma as a result of interaction with high-density lipoproteins. *Biochim. Biophys. Acta* 542(2), 296–307 (1978).

▶19 Virtanen JA, Cheng KH, Somerharju P. Phospholipid composition of the mammalian red cell membrane can be rationalized by a superlattice model. *Proc. Natl. Acad. Sci. USA* 95(9), 4964–4969 (1998).

▶20 Fahr A, Hoogevest Pv, May S, Bergstrand N, Leigh S. Transfer of lipophilic drugs between liposomal membranes and biological interfaces: Consequences for drug delivery. *Eur. J. Pharm. Sci.* 26(3–4), 251–265 (2005).

CHAPTER 2

Development of drug-loaded immunoliposomes for the selective targeting and elimination of rosetting *Plasmodium falciparum*-infected RBCs

Ernest Moles[a,b,c,*], Kirsten Moll[d], Jun-Hong Ch'ng[d,e], Paolo Parini[f], Mats Wahlgren[d], Xavier Fernàndez-Busquets[a,b,c,*].

[a] Nanomalaria Group, Institute for Bioengineering of Catalonia (IBEC), Baldiri Reixac 10-12, ES-08028 Barcelona, Spain

[b] Barcelona Institute for Global Health (ISGlobal, Hospital Clínic-Universitat de Barcelona), Rosselló 149-153, ES-08036 Barcelona, Spain

[c] Nanoscience and Nanotechnology Institute (IN2UB), University of Barcelona, Martí i Franquès 1, ES-08028 Barcelona, Spain

[d] Department of Microbiology, Tumor and Cell Biology (MTC), Karolinska Institutet, Stockholm, Sweden

[e] Department of Microbiology, National University of Singapore, Singapore

[f] Department of Laboratory Medicine (LABMED), H5, Division of clinical chemistry, Karolinska Institutet, Huddinge, Sweden

* Corresponding author at: Nanomalaria Group, Institute for Bioengineering of Catalonia (IBEC), Baldiri Reixac 10-12, ES-08028 Barcelona, Spain.

E-mail address: ernest.moles@isglobal.org; xfernandez_busquets@ub.edu

ABSTRACT

Parasite proteins exported to the surface of *Plasmodium falciparum*-parasitized red blood cells (pRBCs) have a major role in severe malaria clinical manifestation. Importantly, pRBC cytoadhesion and rosetting processes have been strongly linked with high microvascular sequestration while avoiding both spleen filtration and immune surveillance. The parasite-derived and pRBC surface-exposed PfEMP1 protein has been identified as one of the responsible elements for rosetting and, therefore, considered as a potential vaccine candidate for the generation of rosette-disrupting antibodies and a desirable protection against severe malaria. However, the potential role of anti-rosetting antibodies as targeting molecules for the functionalization of nanovectors has never been studied. In this proof-of-concept study, we assay *in vitro* the activity of an immunoliposomal vehicle with a dual activity capable of: i) specifically recognizing and disrupting rosettes while ii) simultaneously eliminating those pRBCs forming them. Using a polyclonal antibody against the NTS-DBL1α N-terminal domain of a rosetting PfEMP1 variant as targeting molecule and lumefantrine as the antimalarial payload, a 70% growth inhibition was achieved for all parasitic forms in culture only after 30 min incubation with 2 μM encapsulated drug ($IC50_{growth}$: 613 nM). Moreover, this result was accompanied by a reduction in ca. 60% of those pRBCs with a rosetting phenotype ($IC50_{rosettes}$: 747 nM). This immunoliposomal approach represents an innovative combination therapy for the improvement of severe malaria therapeutics having a broader spectrum of activity than either anti-rosetting antibodies or free drugs on their own.

1. Introduction

Malaria infection by the blood-borne parasites of the genus *Plasmodium* remains one of the most life-threatening diseases around the world with more than 198 million cases and 584,000 deaths reported only in 2013. Remarkably, children under 5 years account for 78% of all malaria deaths [1]. Red blood cells (RBCs) infected with mature stages (trophozoites and schizonts) of the malaria parasite bind to the endothelial cells in the capillaries of tissues through cytoadhesion events, which allows *Plasmodium* to replicate while evading splenic clearance [2]. Parasitized RBCs (pRBCs) can also adhere to non-infected erythrocytes giving rise to rosettes [3], and they can form clumps through platelet-mediated binding to other pRBCs. These events, which may lead to occlusion of the microvasculature, are thought to play a major role in the fatal outcome of severe malaria. Because the blood-stage infection is responsible for all symptoms and pathologies of malaria, pRBCs have traditionally been a main chemotherapeutic target [4].

Rosetting has been extensively studied and described [5]–[9] in order to develop therapeutic strategies for the treatment of severe malaria. Noticeably, this association between rosetting processes and clinical severe manifestation has been highlighted by the association found between host erythrocyte polymorphisms interfering with rosetting and an increased protection against severe malaria [10], [11]. The *var* gene-encoded, pRBC surface-exposed *Plasmodium falciparum* erythrocyte membrane protein 1 (PfEMP1) contains a tandem repetition of Duffy Binding Like domains (DBL) and Cysteine-rich InterDomain Regions (CIDR). PfEMP1 has been identified as one of the key molecules responsible for cytoadhesion and rosetting [12], [13] and one of the most important proteins promoting antigenic variation at the pRBC surface being encoded by around 60 *var* genes widely distributed throughout the parasite genome [14].

Several antibodies have been raised against rosetting variants of the NTS-DBL1α N-terminal domain of PfEMP1, which are chiefly encoded by group A *var* genes. Some examples of rosette-inducing transcripts include the IT4*var*60 [13], IT4*var*9 [15] and PA*var*O [16] from the FCR3S1.2, R29 and PAvarO *P. falciparum* strains, respectively. These antibodies have been shown to prevent the rosetting phenotype [13], [17], [18] and promote the opsonization of antibody-targeted pRBCs [19]. The SD3-loop of DBL1α subdomain has been identified as a target in anti-rosetting activity [17] and consistently predicted as a B-cell-recognized epitope [18]. However, despite the potential role of antibodies as rosette disrupting tools, no direct effect against pathogen viability has been observed, thus requiring immune system stimulation [19] or antimalarial drug supplementation therapies in order to successfully remove malaria parasites.

An underestimated application of rosetting-associated PfEMP1 variants is their potential role as targets for drug-loaded nanovectors [20], [21]. The capability of these vehicles to carry a diverse range of molecules, including fluorescent tracers, antimalarial drugs and proteins such as antigenic determinants or phagocytic markers [22], could make them interesting polyvalent

tools for the targeting, disruption and elimination of both rosettes and those parasites causing them, as part of future new clinical strategies against severe malaria.

Lipid-based nanovectors (liposomes, LPs) bearing cell-specific ligands have been widely considered as efficient drug carriers in targeted drug delivery therapies because of their organic-aqueous biphasic character and their *in vivo* biodegradability and low toxicity [23]–[25]. Antibody-conjugated liposomes (immunoliposomes, iLPs) against pRBCs were first assayed for the treatment of *Plasmodium berghei* infections in mice [26], [27] and more recently in targeting assays against the pRBC antigens MAHRP1 and glycophorin A [28]–[30] from *Plasmodium* and human origin, respectively. Other studies include the use of glycosaminoglycans such as heparin [31], [32] as anti-pRBC targeting molecules of drug-loaded liposomes, or polymeric nanoparticles as drug carriers with self-targeting capacity against pRBCs [33], [34]. In these works the efficacy of antimalarial drugs was significantly improved when specifically targeted against pRBCs. On the other hand, the use of RBC antigens opened the possibility of loading drugs within erythrocytes as a strategy to eliminate *P. falciparum* during its early development stages, or as a prophylactic approach inhibiting parasite growth right after erythrocyte invasion.

However, no specific drug delivery system towards sequestered parasites has been designed yet. pRBCs adhered to microvasculature capillaries or hidden within erythrocyte clumps would remain undetected by the aforementioned nanovectors during severe malaria complications. This study reports the application as targeting agents for the functionalization of liposomal nanovectors of polyclonal antibodies raised against the rosetting-linked NTS-DBL1α domains of FCR3S1.2^{IT4var60}, R29^{IT4var9} and PAvarO PfEMP1 protein variants [18] and the monoclonal antibody mAbV2-17.1 (M17.1) specific for a conformational epitope identified within the SD3-loop subdomain of NTSDBL1α-FCR3S1.2^{IT4var60} [17]. We have explored the capacity of this model for the detection, disruption and elimination of rosetting pRBCs using lumefantrine as antimalarial drug.

2. Materials and methods

2.1. Materials

Except where otherwise indicated, reagents were purchased from Sigma-Aldrich Corporation (St. Louis, MO, USA), and reactions were performed at room temperature (22 to 24 °C). The lipids (all≥99% purity according to thin layer chromatography analysis) 1,2-distearoyl-*sn*-glycero-3-phosphocholine (DSPC), 1,2-distearoyl-*sn*-glycero-3-phosphoethanolamine-N-[maleimide(polyethylene glycol)-2000] (DSPE-PEG2000-Mal), and 1,2-dioleoyl-*sn*-glycero-3-phosphoethanolamine-N-[lissamine rhodamine B sulfonyl] (DOPE-Rho) were purchased from Avanti Polar Lipids Inc. (Alabaster, AL, USA). Polyclonal FCR3S1.2, R29 and PAvarO and monoclonal M17.1 antibodies raised against the NTS-DBL1α domain of PfEMP1 variants were obtained in [17], [18].

2.2. Preparation of liposomes and encapsulation of lumefantrine.

Liposomes (LPs) with the lipid composition DSPC:cholesterol:DSPE-PEG2000-Mal:DOPE-Rho, 84.5:10:5:0.5, were prepared by the lipid film hydration method [35]. Briefly, stock lipids in chloroform were mixed and dissolved in chloroform:methanol (2:1 v/v) in a round-bottomed glass tube. Organic solvents were removed by evaporation (P-12 Multivapor, BÜCHI Labortechnik AG) under progressive reduced pressure and orbital agitation at 41 °C to yield a thin lipid film on the tube bottom. The dried lipids were then hydrated to 10 mM total lipid in 10 mM phosphate buffer (PB), pH 6.5, supplemented with 10 mM EDTA and osmotically adjusted to 280 mOsm/Kg (isotonic with *P. falciparum* growth medium) by addition of 5 M NaCl. Multilamellar liposomes were formed by 3 cycles of constant vortexing followed by bath sonication (3 min each). For the generation of unilamellar vesicles, multilamellar liposomes were downsized by serial extrusion through 400 and 200 nm polycarbonate membranes in a Mini-extruder device equipped with a heating block (Avanti Polar Lipids, Inc.). Throughout the lipid film hydration and downsizing processes samples were maintained at 65 °C, above lipids transition temperature. Liposome size and concentration (LP number/ml) was determined by nanoparticle tracking analysis (NanoSight NS500, Malvern Instruments Ltd) using samples at 1 µM lipid after dilution in phosphate-buffered saline (PBS) sterile-filtered through 0.22 µm pore size polyvinylidene difluoride (PVDF) filters (Millex-GV Syringe Filter Units, 4 mm, Millipore). For the preparation of LPs encapsulating lumefantrine (LMF), the drug diluted in chloroform was incorporated in the initial lipid mixture at 1:40 lipid/drug molar ratio (250 µM drug in the final 10 mM lipid suspension). Alternatively, for tracking purposes, the green fluorescent dye pyranine was included in the lipid film hydration solution at a concentration of 30 mM and in a fluorescence quenched state at pH 6.5 for 450-480 nm excitation range. Pyranine experiences a shift in maximum excitation wavelength from 400 nm at pH ≤ 6.5 to 460 nm at pH ≥ 7.4 (Fig. S1) [36], leading to a significant increase in fluorescence emission at 488 nm excitation once released from liposomes in a neutral pH environment. Finally, unencapsulated material was removed by ultracentrifugation (150,000 *g*, 1 h, 4 °C) and pelleted LPs were resuspended in isotonic PB. Liposomal suspensions to be used in assays with live cells were sterile-filtered.

2.3. Generation of immunoliposomes (iLPs)

Following established protocols, freshly prepared maleimide-containing LPs were conjugated with previously thiolated antibodies [30], [37] using the N-succinimidyl S-acetylthioacetate crosslinker (SATA, Thermo Fisher Scientific, Inc.), which contains a protected yet exposable sulfhydryl group [38]. This strategy, as described in [30], enables the covalent, efficient and stable conjugation onto liposome surfaces of antibodies through their primary amino groups. Briefly, antibodies in PBS were reacted for 30 min with 1× to 10× molar excess relative to antibody molecules of the SATA crosslinker (freshly dissolved in dimethyl sulfoxide) and unreacted SATA was removed by buffer exchange in PBS. Protected thiols in SATA-conjugated antibodies were then exposed by addition of 50 mM hydroxylamine containing 2.5 mM EDTA and thiolated antibodies were finally recovered by buffer exchange in PBS

supplemented with 10 mM EDTA. The presence of available sulfhydryl groups was determined by reaction with 5,5'-dithio-bis-(2-nitrobenzoic acid) (DTNB, Thermo Fisher Scientific, Inc.) following established protocols [30]. Finally, coupling of thiolated antibodies to freshly prepared maleimide-containing LPs was left overnight (12 to 24 h) in PBS supplemented with 10 mM EDTA. Unbound antibodies were removed together with unencapsulated material by ultracentrifugation as described above.

2.4. Antibody coupling analysis

Antibody coupling was quantitatively assessed by QuickStart™ Bradford Protein Assay (Bio-Rad), and coupling efficiency (%) was determined as the fraction of LP-bound antibody relative to the total antibody added. The number of bound antibodies per vesicle was determined considering an IgG molecular mass of 150 kDa and the LP concentration determined by nanoparticle tracking analysis as described above. For qualitative SDS-polyacrylamide gel electrophoresis (PAGE) coupling analysis, supernatant and pelleted iLP samples containing 2.5 µg total protein were heated at 70 °C for 10 min in 1× NuPAGE® LDS Sample Buffer (Thermo Fisher Scientific) supplemented with 355 mM 2-mercaptoethanol and electrophoresed in 10% acrylamide Tris-Glycine gels using the Mini Protean II System (Bio-Rad). Protein bands were resolved by the SilverQuest™ Silver Staining Kit (Thermo Fisher Scientific, Inc.) and gels were finally stored in 10% glycerol solution and scanned through a Gel Doc™ XR+ System (BIO-RAD) equipped with a CCD high-resolution camera and software-controlled motorized lens.

2.5. Absorption spectra analysis of liposomal samples

For the determination of LMF encapsulation into LPs, absorption spectra of 2-µl liposomal samples were obtained with a NanoDrop 2000c UV-Vis spectrophotometer (Thermo Fisher Scientific, Inc.). Plain liposomes (10 mM lipid in PBS) lacking LMF and the lipid film hydration solution were included as blank samples for the pellet and supernatant fractions obtained after ultracentrifugation of LPs during LMF encapsulation. LMF absorption was analyzed in the range of 200-400 nm as previously described [39], [40], and areas under curves (AUC) were calculated by the trapezoidal approximation for pellet and supernatant LP fractions, obtained after blank absorbance subtraction. Encapsulating efficiency was determined as the AUC retrieved for LP pellet relative to the total area corresponding to the drug (pellet and supernatant fractions). Absorption spectra (300-500 nm) were also used for the analysis of pH-dependent pyranine excitation in the blue visible light spectral range. All samples were adjusted to 300 µM dye.

2.6. P. falciparum cultures

P. falciparum strains FCR3S1.2, R29 and PAvarO were cultivated in blood group O RBCs and malaria culture medium (MCM) supplemented with 10% human AB+ serum (complete medium or MCM+), according to standard protocols [41]. For the maintenance of the rosetting

phenotype, cultures were enriched in rosette-forming parasites by Ficoll-Isopaque [41] and/or monoclonal antibody pull-down [16].

2.7. Rosette disruption and reformation assays

The capacity of anti-PfEMP1 antibodies and their corresponding iLPs to disrupt *P. falciparum* rosettes or prevent their formation was performed through an adaptation of standardized protocols [41]. For disruption assays, rosetting *P. falciparum* strains in late forms at 2% hematocrit were incubated with one culture volume of 2× concentrated iLPs or free antibodies for 1 h under orbital stirring and cell nuclei where stained with Hoechst 33342 (10 µg/ml) for 30 min immediately before flow cytometry analysis. In formation assays, rosetting pRBCs were stained with Hoechst 33342 as described above, washed three times in PBS supplemented with 0.75% w/v bovine serum albumin (PBS-BSA) and rosettes were mechanically disrupted by passing cells 6 times through a 0.6 mm-gauge needle. pRBCs were thereafter incubated with iLPs or free antibodies for 1 h under orbital stirring. Cells were spun down (2 min, 470 *g*), washed twice with PBS-BSA and finally taken up in MCM+ for at least 1 h before flow cytometry analysis. Samples were finally diluted to 0.02% hematocrit in PBS-BSA right before analysis and the efficacy of iLPs and free antibodies in either disruption and reformation assays was finally expressed as the percentage of rosettes in treated samples relative to the total number of rosettes found within untreated control samples. Free antibodies were assayed in parallel to iLPs using equal protein amounts as a control in order to check for possible antibody inactivation effects induced by liposome-Ab conjugation.

2.8. Growth inhibition assays

Rosetting *P. falciparum* R29 cultures brought to 2% hematocrit and 1% parasitemia by addition of fresh RBCs were washed three times with MCM+. After adding one sample volume containing 2× concentrated drug in the same medium, cultures were incubated for 30 min under orbital mixing before spinning cells down and replacing the supernatant with fresh medium. The resulting cell suspension was then seeded into 96-well plates (Becton, Dickinson and Company) and further incubated for a complete 48 h growth cycle under the conditions described above before proceeding to flow cytometry analysis. Growth inhibition in drug-treated samples was defined as the percentage decrease in parasitemia within the second generation of parasites relative to untreated control samples.

2.9. Flow cytometry

For rosette disruption and reformation assays, *P. falciparum* samples stained with Hoechst 33342 and diluted to 0.02% hematocrit in PBS-BSA were analyzed in a BD™ LSR II flow cytometer (Becton, Dickinson and Company). Forward- and side-scatter in a linear scale were used to gate the RBC population and Hoechst-stained pRBCs (the sole population of nucleated cells present in culture) were detected by excitation through a 405 nm laser and emission collection with a 450/50 nm bandpass filter in a logarithmic scale (Pacific Blue-A).

Parasites in late forms were discerned from those in early stages by their increased Hoechst signal resulting from the presence of segmented parasites with multiple nuclei while presenting high rosetting percentages for the untreated control sample. pRBCs targeted by immunoliposomes including the rhodamine-conjugated lipid DOPE-Rho in their composition were detected by excitation through a 532 nm laser and emission collection with a 555 nm LP dichroic mirror and a 575/25 nm bandpass filter in a logarithmic scale (PE-A).

For growth inhibition determination, samples were first stained with a mixture of 10 µg/ml Hoechst 33342 and 5 µg/ml dihydroethidium (DHE, redox indicator of metabolic activity) in PBS. After 30 min incubation, cells were resuspended and diluted 16-fold in PBS (0.06% hematocrit) for analysis in a BD FACSVerse™ flow cytometer (Becton, Dickinson and Company) equipped with a BD™ high throughput sampler. Forward- and side-scatter in a linear scale were used to gate the RBC population and Hoechst-stained cells (pRBCs) were detected by excitation through a 405 nm laser and emission collection with a 448/45 nm LP dichroic mirror and a 448/25 nm bandpass filter in a logarithmic scale (V450-A). pRBCs in late forms (DHE positive cells) were detected by excitation through a 488 nm laser and emission collection with a 560 nm LP dichroic mirror and a 586/42 nm bandpass filter in a logarithmic scale (PE-A).

Acquisition was configured to stop after recording 30,000 events for the RBC population and rosettes were determined within the parasitized erythrocyte population in late forms by means of their disproportion in Forward Scatter (FSC) height-area (H-A) or width-area (W-A) confronted parameters, which indicated the presence of cell doublets as previously described in [42]. FSCH-A values were used when working with FACSVerse™ (used in growth inhibition assays) and FSCW-A values with BD™ LSR II (used during rosette reformation and disruption assays).

2.10. Fluorescence microscopy

For immunofluorescence assays with live cells of the targeting efficiency of iLPs, *P. falciparum* cultures were brought to 2% hematocrit and washed three times before nuclei staining with 2 µg/ml Hoechst 3334. After 30 min incubation, excess dye was removed by washing samples three times and pRBCs cultures were thereafter incubated with one volume of 2× concentrated iLP samples under orbital stirring. Unless otherwise indicated, iLP incubations lasted 90 min and cells remained in MCM+ throughout the whole experiment. Unretained material was removed by washing cells three times and pRBC cultures at 0.1% hematocrit were placed onto Lab-Tek™ chambered coverglass slides (Thermo Fisher Scientific, Inc) for analysis by a Zeiss Axio Observer (Carl Zeiss) inverted confocal microscope system. Hoechst 33342, pyranine and iLP-rhodamine signals were recorded by excitation through, respectively, 405, 458 nm Argon and 561 nm solid state lasers together with their corresponding emission filters. Phase contrast images were acquired simultaneously. For routine analysis of iLP targeting, live pRBC cultures were analyzed onto glass slides with a Nikon Eclipse80i fluorescence

microscope suitable for analysis of the absorption ranges 340-380 nm (DAPI), 465-496 nm (FITC), and 540-580 nm (Texas Red).

3. Results

3.1. Characterization of the anti-rosetting immunoliposomal model

Liposomal nanovectors (10 mM total lipid) with an average size distribution of 169 ± 5 nm and a vesicle concentration of 1.2×10^{13} particles/ml (Fig. S2 and Table S1) were functionalized with the polyclonal antibodies (Abs) raised against rosetting-linked NTS-DBL1α domains of the PfEMP1 variants FCR3S1.2^{IT4var60} (FCR-iLPs), R29^{IT4var9} (R29-iLPs) and PAvarO (PAvarO-iLPs) and the monoclonal antibody mAbV2-17.1 (M17.1-iLPs), specific for the SD3-loop subdomain of NTSDBL1α-FCR3S1.2^{IT4var60}. For the first preparation of iLPs, a 10-fold molar excess of SATA crosslinker agent relative to total antibody (SATA/Ab ratio) was used (iLPs 10×) and the reaction was left to proceed for 24 h with a molar ratio total lipid:Ab of 187.5:1 or 750:1 for either polyclonal or monoclonal antibodies, respectively. Coupling efficiencies higher than 69 % were obtained resulting in around 2,400 polyclonal or 460 monoclonal antibodies per vesicle (Table 1). Antibody conjugation was also qualitatively analyzed by SDS-PAGE under reducing conditions (Fig. 1). Protein bands indicative of IgG heavy and light chains were observed for all antibody-bound fractions, indicating an efficient incorporation of antibodies into liposomes.

Parameter	FCR-iLPs	R29-iLPs	PAvarO-iLPs	M17.1-iLPs
Coupling efficiency %	90.7 ± 7.1	85.7 ± 3.7	97.3 ± 2.3	69.1 ± 2.8
µg Ab / µmol lipid	725.4 ± 56.6	685.4 ± 29.9	778.2 ± 18.2	138.2 ± 5.7
Ab number per LP	2,426.7 ± 189.2	2,292.9 ± 100.1	2,603.4 ± 60.8	462.2 ± 19.0

Table 1. Quantitative determination of the coupling to liposomes of anti-rosetting antibodies. Data are represented as the mean ± standard deviation of at least three independent measurements.

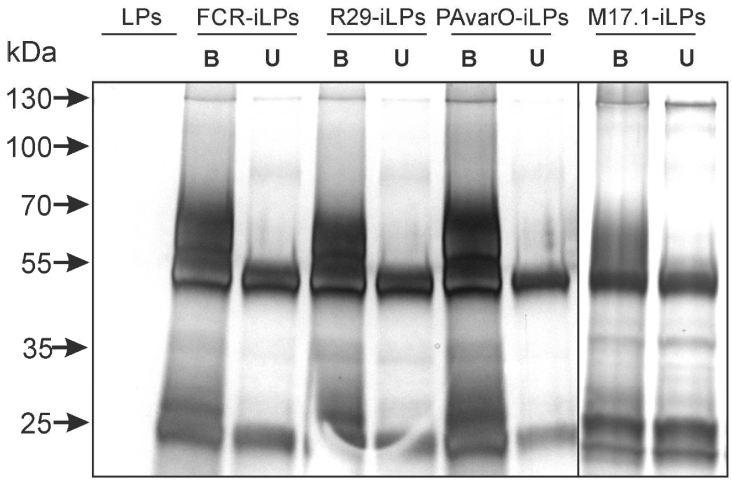

Fig. 1. SDS-PAGE qualitative analysis of the coupling to liposomes of anti-rosetting antibodies. For each Ab are shown liposome-bound (B) and unbound (U) fractions.

3.2. Determination of iLP targeting efficiency with homologous P. falciparum strains

The targeting of anti-rosetting iLPs against their homologous *P. falciparum* strains was examined by confocal fluorescence microscopy using liposomes incorporating the rhodamine-conjugated lipid DOPE-Rho. Rosette-specific iLPs recognized pRBCs exposing their homologous PfEMP1 variants at the concentration of 100 µM lipid (about 14-72 µg Ab/ml), showing a distinctive punctate pattern on pRBCs, together with an absence of unspecific signal observed on RBCs (Fig. 2). Despite the large excess of iLPs relative to the number of pRBCs in culture (ca. 1.8×10^5 iLPs/pRBC for 100 µM lipid in culture, Fig. S3), a significant dose-dependent decrease in signal was observed, with targeting limits for FCR-, PAvarO-, M17.1- and R29-iLPs being detected at 10, 5, 1 and 0.5 µM lipid, respectively (Fig. S4).

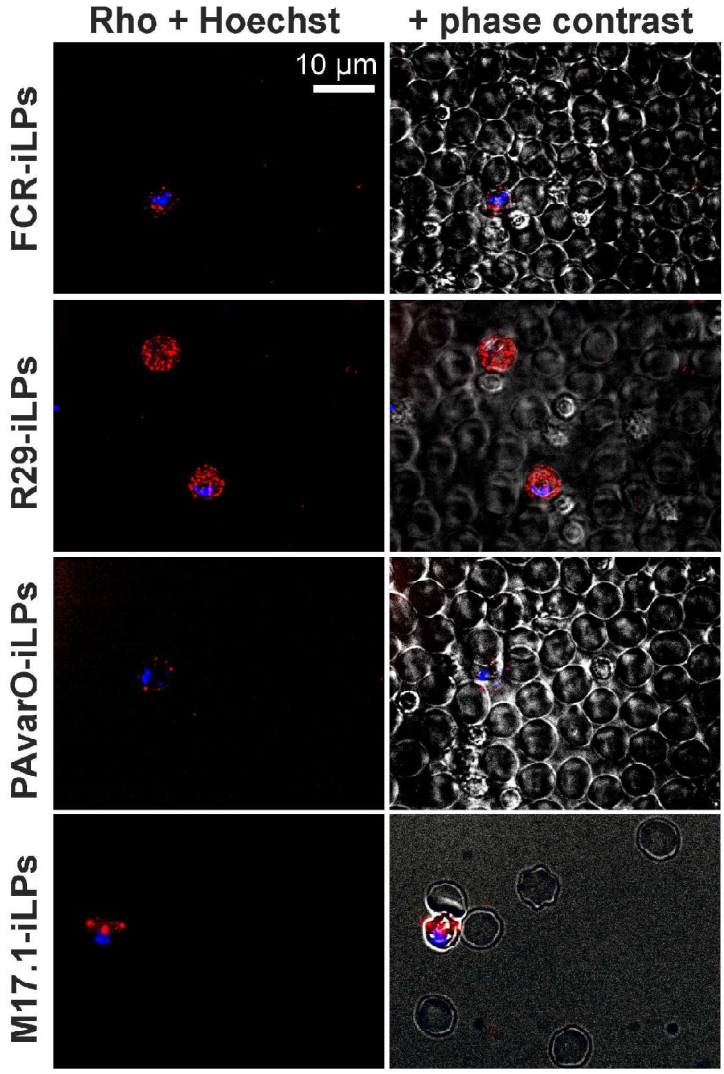

Fig. 2. Confocal fluorescence microscopy targeting analysis of different amounts of anti-rosetting iLPs against their homologous strains at 100 µM lipid. Images correspond to the stack of individual z axis sections spanning the whole cell.

Fluorescence microscopy revealed the formation of aggregates after antibody coupling to liposomes (10× SATA/R29 Ab molecular ratio, Fig. S5), result in accordance with the high incorporation yield of Abs into liposomes (Table 1). To minimize aggregation, we reduced both the chemical crosslinking agent to 5× and 1× SATA/Ab ratios and the coupling incubation time from 24 to 12 h. For R29- and M17.1-iLPs prepared under these new conditions, a significant reduction in aggregates formed was observed (Fig. S5). SDS-PAGE analysis indicated the maintenance of ca. 50% coupling efficiency (Fig. 3A). A significant improvement of iLP targeting efficiency was observed by confocal fluorescence microscopy, with final detection thresholds of ca. 100 nM lipid in culture (Fig. 3B), corresponding to the non surface-saturating amount of 200 iLPs/pRBC (Fig. S3).

3.3. Characterization of iLP/pRBC interaction

To better understand the mechanism of interaction between PfEMP1-specific iLPs and their homologous *P. falciparum* strains, R29-iLP (5× SATA/Ab molecular ratio) containing the rhodamine-conjugated lipid DOPE-Rho were loaded with the highly hydrophilic green fluorescent dye pyranine in a fluorescence quenched state for 450-480 nm excitation at pH 6.5 (Fig. S1) as tracer for the liposome aqueous phase. After 3 h of incubation with R29 rosetting pRBCs, a punctate pattern was observed on host cell surfaces as a result of iLP adsorption (Fig. 4A). The pyranine-rhodamine colocalization on the pRBC surface indicated an absence of transference of the liposomal cargo into the target cell (pyranine otherwise unquenched at the intracellular pRBC pH of 7.3 [43] while being diluted throughout the cell cytoplasm), and of lipid exchange events between liposome and cell lipid bilayers. As a control, free pyranine administered to pRBC cultures in the same incubation conditions was capable of entering the host cell and accumulate inside the parasite (Fig. 4B), likely through the *Plasmodium*-induced tubulovesicular network or the new permeation pathways [44], [45]. Similar results were obtained for M17.1-iLPs and the corresponding homologous FCR3S1.2 strain (data not shown).

3.4. Analysis of iLP-mediated rosette disruption

The capacity of iLPs functionalized with anti-rosetting antibodies to specifically recognize those pRBCs displaying homologous PfEMP1 variants was explored as a dual tool for the disruption of rosettes while simultaneously targeting drugs into rosette-forming pRBCs. In this regard, the capability of R29- and M17.1-iLPs in either avoiding the reformation of rosettes or directly disrupt them was analyzed by flow cytometry (Figs. 5 and S6). Both iLPs against R29 and FCR3S1.2 strains showed high rosette reforming inhibition and disrupting efficacy similar to the corresponding free antibodies (Fig. 5), indicating that Ab affinity against PfEMP1 was not affected by coupling to LPs. Moreover, despite higher amounts of R29-iLPs were retained on the surface of pRBCs (Fig. S7), a lower rosette reforming inhibition and disrupting capacity was observed when compared to M17.1-iLPs. Such distinctive behavior was probably caused by differences in the respective PfEMP1 epitopes recognized and their role in rosetting. Besides, an absence of *P. falciparum* strain cross-reactivity was observed with no detectable amounts of

pRBC-bound R29-/M17.1-iLPs when tested on the heterologous FCR3S1.2/R29 parasite cultures, respectively (Fig. S7).

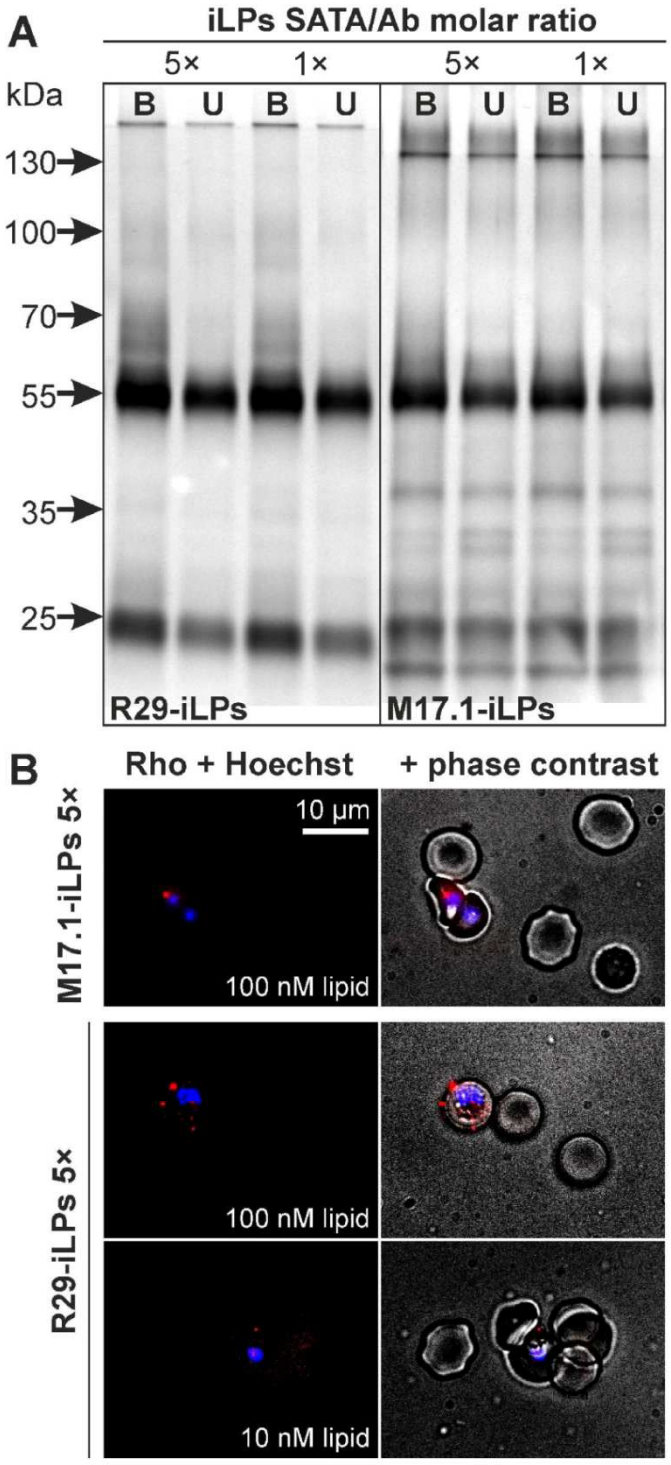

Fig. 3. iLP functionalization using reduced SATA/Ab ratios and shorter reaction times. (A) Qualitative SDS-PAGE analysis of Ab incorporation into iLPs. (B) Confocal fluorescence microscopy analysis of iLP targeting thresholds.

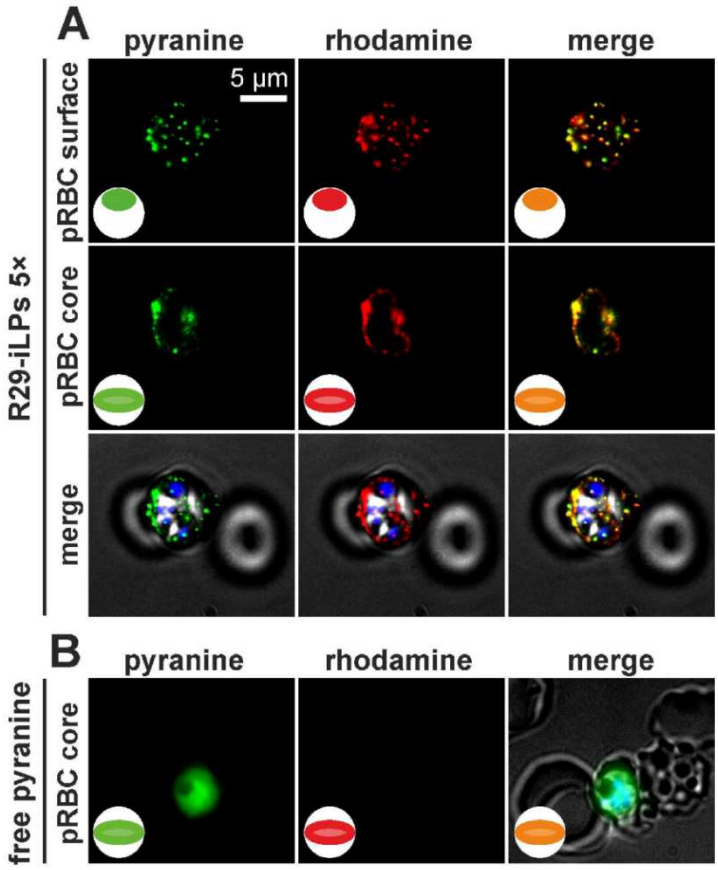

Fig. 4. Confocal fluorescence microscopy analysis of the subcellular distribution of anti-rosetting iLPs. R29-iLPs 5× SATA/Ab ratio (10 µM lipid) were incubated for 3 h with the *P. falciparum* R29 homologous strain. (A) Images from the surface and the core of a selected pRBC. (B) Free pyranine control for unquenched fluorescence signal. Merge panels include Hoechst and phase contrast images.

Some of the rosettes detected by flow cytometry for the highest iLP concentrations in culture of 2-40 µg conjugated Ab/ml (corresponding to ca.10-100 µM lipid) were actually autoagglutinated pRBCs identified by a strong rhodamine fluorescence coming from surface-bound iLPs, feature which was especially significant for the R29 strain (Figs. S7 and S8). R29-iLPs could be unambiguously identified throughout the pRBC surface down to the relatively low antibody concentration of 0.04 µg/ml and even within already formed rosettes (Fig. S8). These observations suggest that although rosettes were not completely disrupted, iLPs were capable of reaching the pRBC in detectable amounts (Fig.S7 and S8). In addition, R29-iLPs were more efficient in avoiding the reformation of rosettes than in disrupting them (Fig. 5). The best performance in rosette number reduction was obtained for R29- and M17.1-iLPs conjugated through 1× and 5× SATA/Ab molar ratios (Fig. 5), in accordance with the improved targeting efficiency observed for iLPs prepared through this optimized Ab coupling strategy, which led to lower detection thresholds by confocal microscopy and a reduction in iLP aggregate formation (Fig. 3 and Fig. S5). These results likely indicate a higher number of functional antigen binding sites in those iLP samples with a reduced presence of vesicle aggregates.

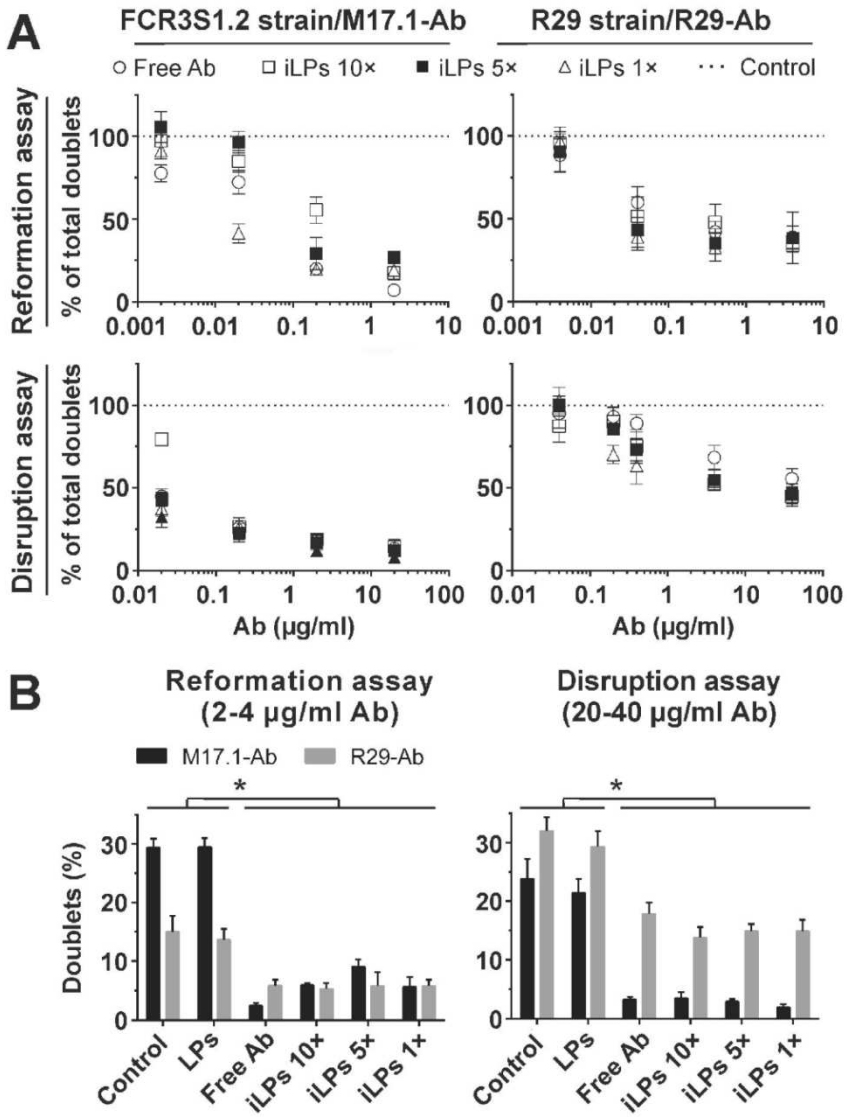

Fig. 5. Flow cytometry analysis of rosettes disruption activity by anti-rosetting iLPs and free antibodies against the homologous FCR3S1.2 and R29 strains. (A) The fraction of total rosettes/cell doublets within pRBCs in late-forms after treatment compared to untreated control (100% rosettes) was determined for both reformation and disruption assays. (B) Absolute rosetting rate values within late-form pRBCs for the highest iLP and free antibody amounts used in the assay (* $p < 0.05$).

Rosette disruption was also assessed by fluorescence microscopy and manual counting for the highest Ab amounts of 20 to 40 µg/ml (Fig. S9). Although according to microscopy analysis absolute rosetting pRBCs numbers were significantly higher than those reported in Fig. 5B derived from flow cytometry data (70-80% vs. 25-35% of total late-form pRBCs respectively), the ratios obtained when comparing control vs. Ab or iLPs-treated samples in both methodologies were comparable. Such difference has been previously discussed by [42], work in which the use of flow cytometry was successfully validated as a high throughput alternative approach to fluorescence microscopy for rosette analysis.

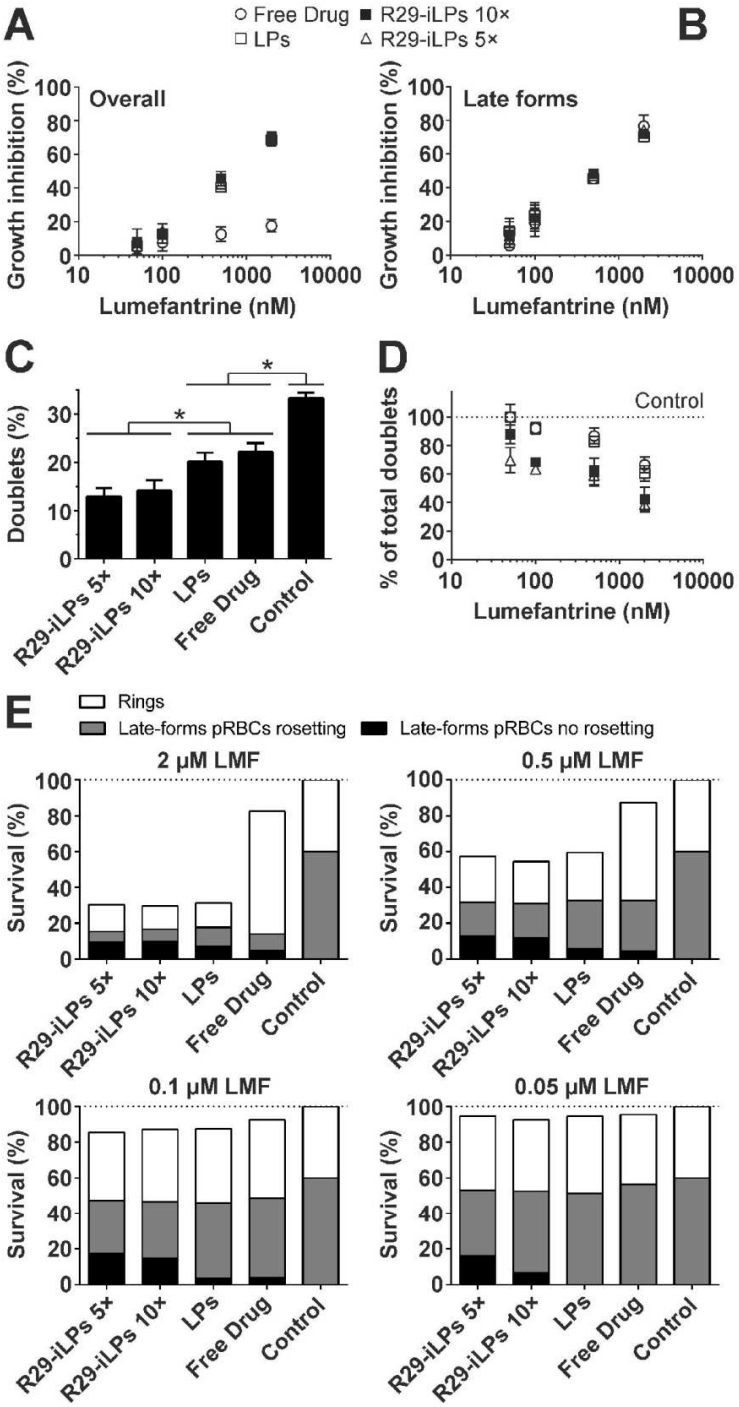

Fig. 6. Flow cytometry analysis of R29 strain growth inhibition assay by anti-rosetting iLPs encapsulating lumefantrine after 30 min incubation at 37 °C. (A) Overall growth inhibition considering all parasitic forms in culture; (B) late forms (trophozoites and schizonts) growth inhibition; (C) absolute rosetting/cell doublets percentages within late form pRBCs for the highest drug concentration (2 µM) used in the assay (* $p < 0.05$); and (D) determination of % of total rosettes/cell doublets after treatment compared to untreated control (100% rosettes). (E) Stacked clustered chart representation of the surviving *P. falciparum* forms. Relative survival % for each parasite maturation stage was calculated by normalization with the untreated control culture (100% survival), composed by 40% rings plus 60% rosetting late-forms.

3.5. Analysis of the growth inhibition activity of lumefantrine loaded into R29-iLPs

R29 polyclonal antibody was selected as the best targeting agent for liposomal drug delivery because it provided the highest number of retained iLPs for the homologous rosetting *Plasmodium* R29 strain together with a significant anti-rosetting disruption activity. SATA crosslinker/antibody ratios of 10× and 5× were chosen for iLP preparation to study the effect of liposome aggregation on their growth inhibition activity. Given the absence of detectable anti-PfEMP1 iLP fusion with targeted pRBCs (Fig. 4), the highly hydrophobic drug lumefantrine (LMF) was selected for growth inhibition assays due to its capacity of being transferred between lipid bilayers. Such process not requiring nanovector internalization [46]. LMF was incorporated into the liposome suspension at the non-saturating concentration of 250 µM, corresponding to a 1:40 drug/lipid ratio for 10 mM total lipid. The spectrophotometric properties of LMF [39] allowed quantifying its encapsulation by UV-visible (200-600 nm) absorption spectra analysis, indicating a high encapsulation efficiency of 89 % of total added drug (Fig. S10, Table S2). This efficient encapsulation was possible due to LMF high organic/water partition coefficient log *P* value of 9.19 [47].

Growth inhibition efficiency of R29-iLPs loaded with LMF was determined *in vitro* in *P. falciparum* non-synchronized cultures of the homologous R29 rosetting strain (approximately 40% rings and 60% late forms, Fig. S11A) and the same amounts of drug in free form were administered in parallel for comparison. After 30 min exposure of parasites with either drug-loaded R29-iLPs or free drugs (1st generation of parasites), cells were washed in order to remove unbound material and further cultured for one replication cycle of 48 h (2nd generation of parasites), time point at which growth inhibition was determined (Fig. 6).

LMF growth inhibition activity considering parasites in all growth stages (Fig. 6A) was significantly improved when encapsulated into liposomes, with ca. 70% reduction in parasitemia for 2 µM liposomized LMF (mean IC50 of 613 nM liposomized drug, Fig. S12) compared to only 20% elimination for the same amount of drug in the free form (IC50 not determinable). However, LMF either liposomized or in free form showed similar performance if considering only pRBCs in late forms (Fig. 6B). Nevertheless, significant differences were found in the number of surviving ring stage parasites (Fig. 6E): whereas a >60% reduction was obtained for encapsulated 2 µM LMF when compared to the untreated control, a >70% increase was observed when delivered in free form, indicating in the latter case a significant growth arrest after parasite replication but still presenting high overall pRBC amounts.

To determine the selective elimination of rosetting pRBCs (presenting the R29^{IT4var9} PfEMP1 variant), the presence of rosettes within the second generation of parasites was determined. A preferential activity of LMF, either freely administered or delivered through plain liposomes, in eliminating rosette-forming parasites was observed with a significant reduction in total rosettes at 2 µM drug when compared to the untreated control sample (Fig. 6C). Rosette prevalence further significantly decreased when delivered by R29-iLPs leading to a maximum

60% reduction in cell doublets (Fig. 6C and Table S3), although no complete removal of rosettes was obtained at this drug concentration. The improved selective removal of rosetting parasites by R29-iLPs remained constant for lower drug amounts with still 30% doublets reduction at 50 nM LMF for R29-iLPs 5× (Figs. 6D-E). The lowest rosette disruptive IC50 was obtained at 0.75 µM LMF for R29-iLPs 5× (Fig. S12 and Table S4), being slightly lower than that of R29-iLPs 10× (1.1 µM), in accordance with the improved targeting against R29 pRBCs for the lowest 1× and 5× SATA/Ab molar ratios. By contrast, significantly higher estimated IC50 values of 3.4 µM and 4.8 µM LMF were obtained for LPs and free drug, respectively.

4. Discussion

The NTS-DBL1α domain of PfEMP1 has been identified as one of the key mediators for rosetting and antibodies raised against this region can successfully prevent rosette formation [12], [18]. However, the potential role of these anti-rosetting antibodies as targeting agents for the functionalization of nanovectors encapsulating antimalarial drugs has never been considered. The conjugation of antibodies to liposomes formulated with lipids containing maleimide groups can be achieved through the incorporation of sulfhydryls at different sites in the antibody molecule [48], [49]. Ab thiolation at primary amines through the incorporation of crosslinkers bearing SH-protected groups such as SATA, has been described as one of the most efficient approaches in terms of coupling efficiency and Ab-LP bond stability while preserving antibody bivalency [30], [38], [48]. However, since primary amines are distributed throughout Ab sequence, there is a high risk of obscuring antigen binding sites if excess crosslinker is used. In accordance with other works [30], [50], [51], the antibodies used in this work have shown to maintain acceptable antigen recognition when using crosslinker/Ab ratios of up to 10-fold, which result in ≤ 5 SH groups per antibody molecule. Another risk when using iLPs for targeted drug delivery is that large crosslinker amounts do proportionally increase the number of lipid molecules bound to antibodies, which in turn presumably induces the formation of iLP self-aggregates. Such process would ultimately result in nanovectors with increased size as well as a reduction in the total number of free vesicles available in suspension. This aggregating effect was found to be more common when working with polyclonal antibodies, although it was also minimized by reducing the crosslinker/antibody ratio and conjugation time.

In comparison to PfEMP1-specific monoclonal Abs (mAbs) such as M17.1, which are selected against single cell surface-exposed epitopes involved in pRBC interactions with RBCs [19], polyclonal Abs recognize multiple epitopes distributed throughout the DBL1α domain of PfEMP1, including those in conserved and non-exposed regions [18]. This limitation in the use of polyclonal antibodies is even more significant considering the presence of contaminating PfEMP1-unspecific immunoglobulins collected during Protein G purification from animal antiserum. These different properties between monoclonal and polyclonal antibodies would explain the improved anti-rosetting activity of M17.1 iLPs over iLPs conjugated to polyclonal R29-Ab despite its reduced presence over the pRBC surface. Because the PfEMP1 epitope

recognized by the M17.1 mAb is directly involved in rosetting [17], presumably only one antibody molecule would be enough to break the PfEMP1-RBC interaction. Moreover, the capability of polyclonal antibodies to recognize multiple epitopes at distinct sites of the antigen make them such a more efficient tool for targeting purposes than mAbs, providing iLPs with much more anchoring points at the target cell surface. Accordingly, the largest amounts of pRBC-bound iLPs were identified when using the R29 polyclonal antibody as targeting agent. Furthermore, considering that a significant region of PfEMP1 molecule would remain obscured by interacting with RBC receptors, antibodies specific for exposed regions not involved in rosetting would improve pRBCs detection and, as a consequence, lead to more efficient chemotherapeutic strategies when conjugated to drug-loaded nanovectors.

One of the major limitations in the application of targeted chemotherapeutic approaches against RBCs and pRBCs is the absence of endocytosis [44], [52], [53]. Accordingly, iLP targeting analysis against rosetting pRBCs indicated a stable adsorption over the target cell surface as the most likely mechanism of interaction, in agreement with other assays using immunoliposomal vehicles with a similar composition [30], [54]. This saturating effect, limiting in turn the number of iLPs capable of interacting with the pRBC surface, indicates that mechanisms other than the receptor-mediated endocytosis pathway [55], [56] must be invoked in order to design efficient drug delivery strategies capable of reaching the intracellular parasite. These include, but are not limited to, the fusion of lipid bilayers between liposome and cell plasma membrane, and the sustained drug delivery from stably adsorbed nanovectors on the target cell surface [25], [30].

Membrane merging requires the inclusion of special fusogenic agents in the liposome formulation, such as charged or small-headgroup lipids, promoting the formation of stalk intermediates and the subsequent fusion of lipid bilayers releasing the nanovector contents directly into the cell cytoplasm [57]. However, the resulting increased membrane fluidity and the incorporation of charged elements also leads to unspecific interaction events with non-target cells and plasma components upon *in vivo* administration, significantly limiting their clinical use. Sterically stabilized nanovectors incorporating neutral-charged and fully saturated lipids, such as those used in this work, emerge as an alternative to overcome the stability disadvantages discussed above [58], [59]. Due to the inhibited fusogenicity of this model, once the nanovector is docked on the cell surface, liposome cargo delivery likely proceeds through sustained release of amphiphilic drugs [60] and/or the transference of hydrophobic material between the liposome and cell membranes [46]. In this scenario, a saturating amount of nanovectors, factor dependent on the abundance of the receptor on the target cell surface, would limit their use to drugs with relatively low IC50 values in the nanomolar range.

The combination of R29 polyclonal antibody and PfEMP1 as ligand/receptor pair proved to be an efficient tool for the targeting of homologous rosetting pRBCs using sterically stabilized liposomal nanocarriers. The iLP design presented here further improved the growth inhibitory efficacy of LMF once encapsulated within nanovector bilayer leaflets (Fig. 7A), significantly

reducing the overall amounts of infected erythrocytes within the second generation of parasites (Fig. 7C,F) when compared to the positive growth control parasite population (Fig. 7D). Importantly, a selective removal of those pRBCs with a rosetting phenotype was observed within surviving parasites (Fig. 7F). By contrast, free LMF was only capable of delaying parasite growth but resulted inefficient in avoiding erythrocyte reinfection. Such behavior was reflected by an increase in the number of *P. falciparum* intraerythrocytic ring forms (Fig. 7B,E) in comparison to the untreated culture (Fig. 7D). Moreover, a considerable number of rosettes were still present at the end of free LMF treatment (Fig. 7E). This improvement in simultaneously eliminating parasite replication in ring as well as late form, *P. falciparum*-infected RBCs with liposomized LMF could be attributed to a much more efficient drug distribution into the culture. Bearing in mind the high hydrophobic properties of LMF, this drug could form self-aggregates when freely delivered but will readily dissolve into the liposome membrane. In this regard, the organic/water partition coefficient described for LMF (log *P* of 9.19, [47]) is very similar to common phospholipids (e.g. log *P* of 9.17 for dioleoylphosphatidylcholine, obtained from http://www.chemicalize.org/).

Future improvements in the nanovector model would include strategies to limit LMF leaking in order to avoid unspecific drug release before reaching rosetting pRBCs. As a feasible strategy, the pH gradient active loading method [61] allows for a highly efficient encapsulation of amphiphilic drugs within liposomal vehicles. Drug release in these systems can be triggered by temperature increase, dilution of the vector, or lipid bilayer destabilization following the interaction of liposomes with cells [62] or plasma components [63]. This active encapsulation method would maintain LMF facing the inward side of the liposome lipid bilayer long enough to minimize unspecific drug transference events by random encounters with uninfected cells during the first minutes of incubation. Furthermore, due to the limited *P. falciparum* strain cross-reactivity commonly displayed by Abs generated against single rosetting PfEMP1 variants [18], [64], a remarkable improvement in the recognition of heterologous strains by our liposomal model might be provided through its conjugation with multiple strain-specific ligands. The applicability of anti-rosetting Ab pools (at least composed of six different PfEMP1 variant-specific Abs) has been remarkably demonstrated in this regard due to their pRBC surface reactivity and rosette disruption efficacy when assayed against *P. falciparum* clinical isolates [64].

The concept that antimalarial treatment combinations could delay the evolution of resistance in the parasite and prolong in this manner the useful life of existing drugs is not new [65], [66]. If resistance results from spontaneous genetic mutations, the chance of a parasite to become resistant simultaneously to two drugs with unrelated modes of action becomes exponentially decreased. As a result, drug combinations will considerably postpone the selection of multiple drug resistance and interrupt the spread and further increase of established resistance.

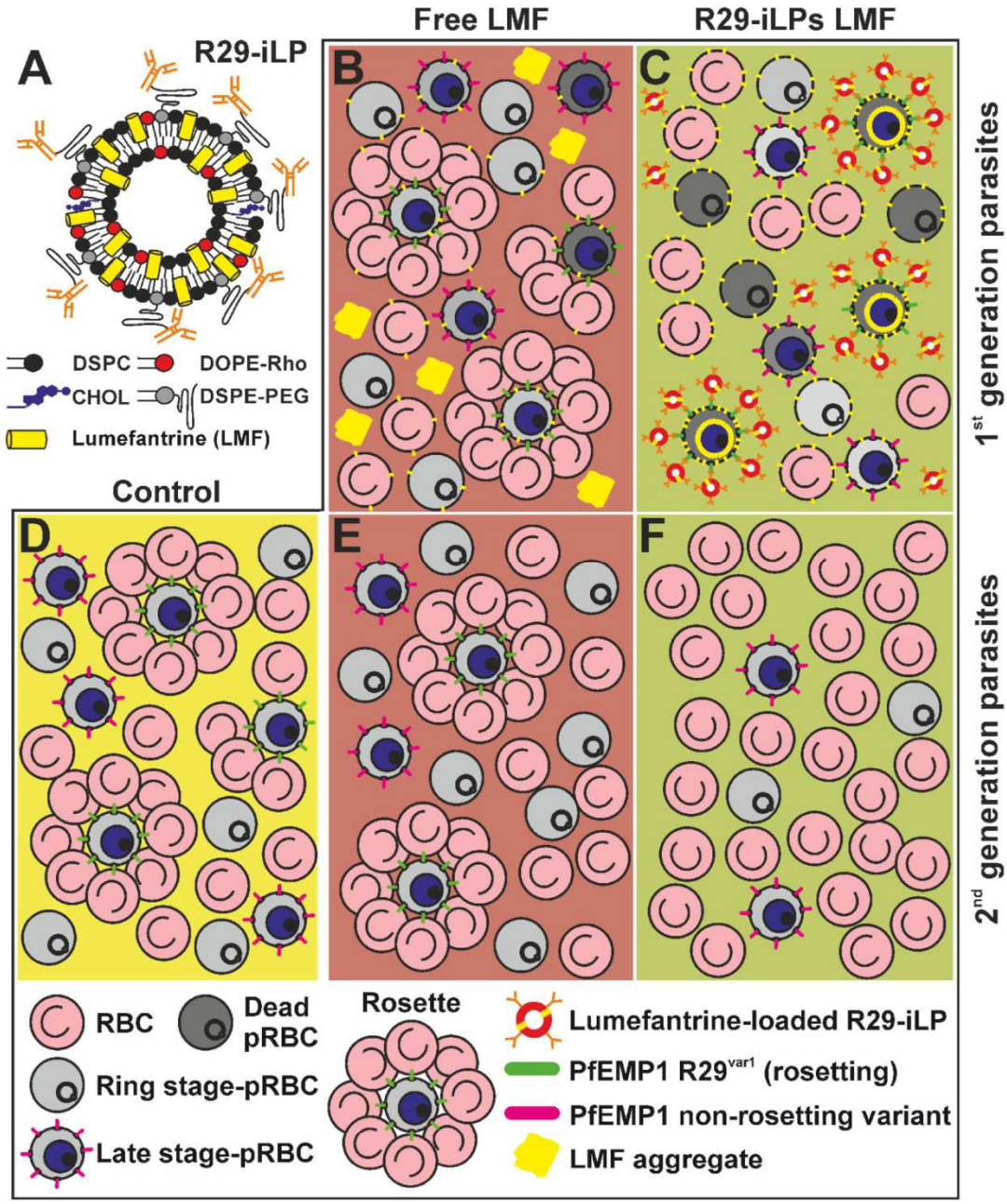

Fig. 7. (A) Cartoon showing the components of the immunoliposomal nanovector designed in this work targeted against the rosette-forming $R29^{IT4var9}$ PfEMP1 variant. (B-C) Hypothesized main interaction events occurring during growth inhibition assays (GIAs) and corresponding to the 1st generation of parasites incubated with (B) LMF delivered in free form (free LMF) or (C) encapsulated within R29-iLPs. (D-F) Observed parasite surviving forms at the end of the GIAs (2nd generation of parasites) for (D) untreated control culture, (E) free LMF or (F) encapsulated within R29-iLPs.

However, we suggest an expanded concept of combination therapy based on the simultaneous use of different therapeutic approaches. pRBC-targeted poly(amidoamine) (PAA)-based nanocarriers have been shown to have a role as carriers of drugs towards *Plasmodium*-infected cells, but also a second antiparasitic activity in themselves [33]. The antimalarial

mechanism of PAAs is most likely based on the inhibition of RBC invasion due to the polymer binding to merozoite surfaces or, alternatively, coating host erythrocytes and consequently blocking parasite adhesion. Moreover, the failure of egressed merozoites to quickly invade a new host cell will expose the pathogen to the immune system for a longer time thus reducing its chances of survival and possibly improving protection to subsequent *Plasmodium* infections. In a second targeting/therapeutic combination approach we applied the known capacities of heparin as antimalarial drug and as a specific marker of pRBCs vs. RBCs [31] to develop liposomal nanocarriers where heparin was used first as a targeting molecule and secondly as an antimalarial in itself [32]. Recently, we have shown that drug-loaded iLPs targeted against the RBC surface protein glycophorin A exhibit a dual activity as therapeutic antimalarial carriers towards pRBCs and as prophylactic agents when delivering their contents to non-infected erythrocytes, effectively protecting these cells against *P. falciparum* infection [30]. Here, we demonstrate a combinational therapy which juxtaposes improved drug efficacy and reduction in rosetting capacity of the parasite. These new combination therapies targeting unrelated pathologically-relevant modalities can provide useful alternatives to drive malaria eradication.

Acknowledgments

This work was supported by grants BIO2011-25039 and BIO2014-52872-R from the Ministerio de Economía y Competitividad (MINECO), Spain, which included FEDER funds, and by grant 2014-SGR-938 from the Generalitat de Catalunya, Spain. A fellowship from the Subprograma de Formación de Personal Investigador, MINECO, Spain, is acknowledged by E.M. We would like to thank to Helena Sork and Cristina Rocha from the Department of Laboratory Medicine (LABMED), H5, Karolinska Institutet, Huddinge, Sweden, for providing support with the liposome size and concentration measurement.

References

[1] World Health Organization, “World malaria report 2014,” Switzerland, 2014.

[2] L. H. Miller, D. I. Baruch, K. Marsh, and O. K. Doumbo, “The pathogenic basis of malaria.,” *Nature*, vol. 415, no. 6872, pp. 673–679, 2002.

[3] A. Juillerat, S. Igonet, I. Vigan-Womas, M. Guillotte, S. Gangnard, G. Faure, B. Baron, B. Raynal, O. Mercereau-Puijalon, and G. A. Bentley, “Biochemical and biophysical characterisation of DBL1α1-varO, the rosetting domain of PfEMP1 from the VarO line of Plasmodium falciparum,” *Mol. Biochem. Parasitol.*, vol. 170, no. 2, pp. 84–92, 2010.

[4] K. S. Griffith, L. S. Lewis, S. Mali, and M. E. Parise, “Treatment of malaria in the United States: a systematic review.,” *JAMA*, vol. 297, pp. 2264–2277, 2007.

[5] J. Carlson, H. Helmby, A. V Hill, D. Brewster, B. M. Greenwood, and M. Wahlgren, “Human cerebral malaria: association with erythrocyte rosetting and lack of anti-rosetting antibodies.,” *Lancet*, vol. 336, pp. 1457–1460, 1990.

[6] A. Rowe, J. Obeiro, C. I. Newbold, and K. Marsh, “Plasmodium falciparum rosetting is associated with malaria severity in Kenya,” *Infect. Immun.*, vol. 63, no. 6, pp. 2323–2326, 1995.

[7] J. Normark, D. Nilsson, U. Ribacke, G. Winter, K. Moll, C. E. Wheelock, J. Bayarugaba, F. Kironde, T. G. Egwang, Q. Chen, B. Andersson, and M. Wahlgren, “PfEMP1-

DBL1alpha amino acid motifs in severe disease states of Plasmodium falciparum malaria.," *Proc. Natl. Acad. Sci. U. S. A.*, vol. 104, pp. 15835–15840, 2007.

[8] M. Wahlgren, J. Carlson, H. Helmby, I. Hedlund, and C. J. Treutiger, "Molecular mechanisms and biological importance of Plasmodium falciparum erythrocyte rosetting.," *Mem. Inst. Oswaldo Cruz*, vol. 87 Suppl 3, pp. 323–9, 1992.

[9] U. Ribacke, K. Moll, L. Albrecht, H. Ahmed Ismail, J. Normark, E. Flaberg, L. Szekely, K. Hultenby, K. E. M. Persson, T. G. Egwang, and M. Wahlgren, "Improved In Vitro Culture of Plasmodium falciparum Permits Establishment of Clinical Isolates with Preserved Multiplication, Invasion and Rosetting Phenotypes," *PLoS One*, vol. 8, 2013.

[10] R. M. Fairhurst, D. I. Baruch, N. J. Brittain, G. R. Ostera, J. S. Wallach, H. L. Hoang, K. Hayton, A. Guindo, M. O. Makobongo, O. M. Schwartz, A. Tounkara, O. K. Doumbo, D. A. Diallo, H. Fujioka, M. Ho, and T. E. Wellems, "Abnormal display of PfEMP-1 on erythrocytes carrying haemoglobin C may protect against malaria.," *Nature*, vol. 435, pp. 1117–1121, 2005.

[11] J. Carlson, G. B. Nash, V. Gabutti, F. al-Yaman, and M. Wahlgren, "Natural protection against severe Plasmodium falciparum malaria due to impaired rosette formation.," *Blood*, vol. 84, pp. 3909–3914, 1994.

[12] Q. Chen, F. Pettersson, A. M. Vogt, B. Schmidt, S. Ahuja, P. Liljeström, and M. Wahlgren, "Immunization with PfEMP1-DBL1α generates antibodies that disrupt rosettes and protect against the sequestration of Plasmodium falciparum-infected erythrocytes," *Vaccine*, vol. 22, pp. 2701–2712, 2004.

[13] L. Albrecht, K. Moll, K. Blomqvist, J. Normark, Q. Chen, and M. Wahlgren, "var gene transcription and PfEMP1 expression in the rosetting and cytoadhesive Plasmodium falciparum clone FCR3S1.2.," *Malar. J.*, vol. 10, p. 17, 2011.

[14] S. M. Kraemer and J. D. Smith, "A family affair: var genes, PfEMP1 binding, and malaria disease.," *Curr. Opin. Microbiol.*, vol. 9, no. 4, pp. 374–380, 2006.

[15] J. A. Rowe, J. M. Moulds, C. I. Newbold, and L. H. Miller, "P. falciparum rosetting mediated by a parasite-variant erythrocyte membrane protein and complement-receptor 1.," *Nature*, vol. 388, no. 6639, pp. 292–295, 1997.

[16] I. Vigan-Womas, M. Guillotte, C. Le Scanf, S. Igonet, S. Petres, A. Juillerat, C. Badaut, F. Nato, A. Schneider, A. Lavergne, H. Contamin, A. Tall, L. Baril, G. A. Bentley, and O. Mercereau-Puijalon, "An in vivo and in vitro model of Plasmodium falciparum rosetting and autoagglutination mediated by varO, a group A var gene encoding a frequent serotype," *Infect. Immun.*, vol. 76, no. 12, pp. 5565–5580, 2008.

[17] D. Angeletti, L. Albrecht, K. Blomqvist, M. P. de Quintana, T. Akhter, S. M. Bächle, A. Sawyer, T. Sandalova, A. Achour, M. Wahlgren, and K. Moll, "Plasmodium falciparum Rosetting Epitopes Converge in the SD3-Loop of PfEMP1-DBL1α," *PLoS One*, vol. 7, no. 12, 2012.

[18] D. Angeletti, L. Albrecht, M. Wahlgren, and K. Moll, "Analysis of antibody induction upon immunization with distinct NTS-DBL1α-domains of PfEMP1 from rosetting Plasmodium falciparum parasites.," *Malar. J.*, vol. 12, p. 32, 2013.

[19] I. Vigan-Womas, A. Lokossou, M. Guillotte, A. Juillerat, G. Bentley, A. Garcia, O. Mercereau-Puijalon, and F. Migot-Nabias, "The humoral response to Plasmodium falciparum VarO rosetting variant and its association with protection against malaria in Beninese children.," *Malar. J.*, vol. 9, p. 267, 2010.

[20] A. Z. Wilczewska, K. Niemirowicz, K. H. Markiewicz, and H. Car, "Nanoparticles as drug delivery systems," *Pharmacological Reports*, vol. 64, no. 5. pp. 1020–1037, 2012.

[21] G. Tiwari, R. Tiwari, B. Sriwastawa, L. Bhati, S. Pandey, P. Pandey, and S. K. Bannerjee, "Drug delivery systems: An updated review.," *Int. J. Pharm. Investig.*, vol. 2, no. 1, pp. 2–11, 2012.

[22] S. Rajesh Kumar, S. M. Syed Khader, T. K. Kiener, M. Szyporta, and J. Kwang, "Intranasal Immunization of Baculovirus Displayed Hemagglutinin Confers Complete Protection against Mouse Adapted Highly Pathogenic H7N7 Reassortant Influenza Virus," *PLoS One*, vol. 8, no. 6, 2013.

[23] G. Gregoriadis and A. T. Florence, “Liposomes in Drug Delivery,” *Drugs*, vol. 45. pp. 15–28, 1993.

[24] M. Langner and T. E. Kral, “Liposome-based drug delivery systems,” *Pol. J. Pharmacol.*, vol. 51, no. 3, pp. 211–222, 1999.

[25] V. P. Torchilin, “Recent advances with liposomes as pharmaceutical carriers.,” *Nat. Rev. Drug Discov.*, vol. 4, no. 2, pp. 145–160, 2005.

[26] A. K. Agrawal, A. Singhal, and C. M. Gupta, “Functional drug targeting to erythrocytes in vivo using antibody bearing liposomes as drug vehicles.,” *Biochem. Biophys. Res. Commun.*, vol. 148, no. 1, pp. 357–361, 1987.

[27] M. Owais, G. C. Varshney, A. Choudhury, S. Chandra, and C. M. Gupta, “Chloroquine encapsulated in malaria-infected erythrocyte-specific antibody-bearing liposomes effectively controls chloroquine-resistant Plasmodium berghei infections in mice.,” *Antimicrob. Agents Chemother.*, vol. 39, no. 1, pp. 180–184, 1995.

[28] P. Urbán, J. Estelrich, A. Adeva, A. Cortés, and X. Fernàndez-Busquets, “Study of the efficacy of antimalarial drugs delivered inside targeted immunoliposomal nanovectors.,” *Nanoscale Res. Lett.*, vol. 6, no. 1, p. 620, Jan. 2011.

[29] P. Urbán, J. Estelrich, A. Cortés, and X. Fernàndez-Busquets, “A nanovector with complete discrimination for targeted delivery to Plasmodium falciparum-infected versus non-infected red blood cells in vitro.,” *J. Control. Release*, vol. 151, no. 2, pp. 202–11, Apr. 2011.

[30] E. Moles, P. Urbán, M. B. Jiménez-Díaz, S. Viera-Morilla, I. Angulo-Barturen, M. A. Busquets, and X. Fernàndez-Busquets, “Immunoliposome-mediated drug delivery to Plasmodium-infected and non-infected red blood cells as a dual therapeutic/prophylactic antimalarial strategy,” *J. Control. Release*, vol. 210, pp. 217–229, 2015.

[31] J. J. Valle-Delgado, P. Urbán, and X. Fernàndez-Busquets, “Demonstration of specific binding of heparin to Plasmodium falciparum-infected vs. non-infected red blood cells by single-molecule force spectroscopy.,” *Nanoscale*, vol. 5, no. 9, pp. 3673–80, 2013.

[32] J. Marques, E. Moles, P. Urbán, R. Prohens, M. A. Busquets, C. Sevrin, C. Grandfils, and X. Fernàndez-Busquets, “Application of heparin as a dual agent with antimalarial and liposome targeting activities toward Plasmodium-infected red blood cells,” *Nanomedicine*, vol. 10, no. 8, pp. 1719–1728, 2014.

[33] P. Urbán, J. J. Valle-Delgado, N. Mauro, J. Marques, A. Manfredi, M. Rottmann, E. Ranucci, P. Ferruti, and X. Fernàndez-Busquets, “Use of poly(amidoamine) drug conjugates for the delivery of antimalarials to Plasmodium,” *J. Control. Release*, vol. 177, pp. 84–95, 2014.

[34] J. Movellan, P. Urbán, E. Moles, J. M. de la Fuente, T. Sierra, J. L. Serrano, and X. Fernàndez-Busquets, “Amphiphilic dendritic derivatives as nanocarriers for the targeted delivery of antimalarial drugs,” *Biomaterials*, vol. 35, pp. 7940–7950, 2014.

[35] R. C. MacDonald, R. I. MacDonald, B. P. Menco, K. Takeshita, N. K. Subbarao, and L. R. Hu, “Small-volume extrusion apparatus for preparation of large, unilamellar vesicles.,” *Biochim. Biophys. Acta*, vol. 1061, pp. 297–303, 1991.

[36] B. S. Gan, E. Krump, L. D. Shrode, and S. Grinstein, “Loading pyranine via purinergic receptors or hypotonic stress for measurement of cytosolic pH by imaging.,” *Am. J. Physiol.*, vol. 275, no. 4 Pt 1, pp. C1158–66, Oct. 1998.

[37] F. J. Martin and D. Papahadjopoulos, “Irreversible coupling of immunoglobulin fragments to preformed vesicles. An improved method for liposome targeting.,” *J. Biol. Chem.*, vol. 257, no. 1, pp. 286–288, 1982.

[38] M. Fleiner, P. Benzinger, T. Fichert, and U. Massing, “Studies on protein-liposome coupling using novel thiol-reactive coupling lipids: Influence of spacer length and polarity,” *Bioconjug. Chem.*, vol. 12, pp. 470–475, 2001.

[39] M. Phale, S. Pawar, P. Patil, M. Gandhi, and P. Hamrapurkar, “A simple and precise method for quantitative analysis of lumefantrine by planar chromatography,” *Pharmaceutical Methods*, vol. 2. p. 44, 2010.

[40] S. Suleman, K. Vandercruyssen, E. Wynendaele, M. D'Hondt, N. Bracke, L. Duchateau, C. Burvenich, K. Peremans, and B. De Spiegeleer, "A rapid stability-indicating, fused-core HPLC method for simultaneous determination of β-artemether and lumefantrine in anti-malarial fixed dose combination products.," *Malar. J.*, vol. 12, p. 145, 2013.

[41] K. Moll, I. Ljungström, H. Perlmann, A. Scherf, and M. Wahlgren, *METHODS IN MALARIA RESEARCH*. 2008.

[42] J.-H. Ch'ng, K. Moll, M. del P. Quintana, S. Chan, E. Moles, J. Liu, A. B. Eriksson, and M. Wahlgren, "Cell-based Screening Identifies a Rosette-Disrupting Antimalarial for the Treatment of Plasmodium falciparum Malaria Complications," 2015. **Manuscript currently in preparation for submission to Blood journal*.

[43] D. A. van Schalkwyk, K. J. Saliba, G. A. Biagini, P. G. Bray, and K. Kirk, "Loss of pH Control in Plasmodium falciparum Parasites Subjected to Oxidative Stress," *PLoS One*, vol. 8, no. 3, 2013.

[44] K. Kirk, "Membrane transport in the malaria-infected erythrocyte.," *Physiol. Rev.*, vol. 81, pp. 495–537, 2001.

[45] I. D. Goodyer, B. Pouvelle, T. G. Schneider, D. P. Trelka, and T. F. Taraschi, "Characterization of macromolecular transport pathways in malaria-infected erythrocytes.," *Mol. Biochem. Parasitol.*, vol. 87, no. 1, pp. 13–28, 1997.

[46] A. Fahr, P. Van Hoogevest, S. May, N. Bergstrand, and M. L. S. Leigh, "Transfer of lipophilic drugs between liposomal membranes and biological interfaces: Consequences for drug delivery," *European Journal of Pharmaceutical Sciences*, vol. 26. pp. 251–265, 2005.

[47] N. C. Amin, H. Fabre, M.-D. Blanchin, J. Montels, and M. Aké, "Determination of artemether and lumefantrine in anti-malarial fixed-dose combination tablets by microemulsion electrokinetic chromatography with short-end injection procedure," *Malar. J.*, vol. 12, p. 202, 2013.

[48] A. S. Manjappa, K. R. Chaudhari, M. P. Venkataraju, P. Dantuluri, B. Nanda, C. Sidda, K. K. Sawant, and R. S. R. Murthy, "Antibody derivatization and conjugation strategies: application in preparation of stealth immunoliposome to target chemotherapeutics to tumor.," *J. Control. Release*, vol. 150, no. 1, pp. 2–22, 2011.

[49] S. M. Ansell, T. O. Harasym, P. G. Tardi, S. S. Buchkowsky, M. B. Bally, and P. R. Cullis, "Antibody conjugation methods for active targeting of liposomes.," *Methods Mol. Med.*, vol. 25, pp. 51–68, 2000.

[50] M. A. Lindorfer, A. Nardin, P. L. Foley, M. D. Solga, A. J. Bankovich, E. N. Martin, A. L. Henderson, C. W. Price, E. Gyimesi, C. P. Wozencraft, J. B. Goldberg, W. M. Sutherland, and R. P. Taylor, "Targeting of Pseudomonas aeruginosa in the bloodstream with bispecific monoclonal antibodies.," *J. Immunol.*, vol. 167, no. 4, pp. 2240–2249, 2001.

[51] R. A. Schwendener, T. Trüb, H. Schott, H. Langhals, R. F. Barth, P. Groscurth, and H. Hengartner, "Comparative studies of the preparation of immunoliposomes with the use of two bifunctional coupling agents and investigation of in vitro immunoliposome-target cell binding by cytofluorometry and electron microscopy.," *Biochim. Biophys. Acta*, vol. 1026, no. 1, pp. 69–79, 1990.

[52] K. Haldar and N. Mohandas, "Erythrocyte remodeling by malaria parasites.," *Curr. Opin. Hematol.*, vol. 14, no. 3, pp. 203–209, 2007.

[53] L. Shang, K. Nienhaus, and G. U. Nienhaus, "Engineered nanoparticles interacting with cells: size matters.," *J. Nanobiotechnology*, vol. 12, no. 1, p. 5, 2014.

[54] J. L. Holovati, M. I. C. Gyongyossy-Issa, and J. P. Acker, "Effect of Liposome Charge and Composition on the Delivery of Trehalose into Red Blood Cells," *Cell Preservation Technology*, vol. 6. pp. 207–218, 2008.

[55] Z. M. Qian, H. Li, H. Sun, and K. Ho, "Targeted drug delivery via the transferrin receptor-mediated endocytosis pathway.," *Pharmacol. Rev.*, vol. 54, pp. 561–587, 2002.

[56] L. M. Bareford and P. W. Swaan, “Endocytic mechanisms for targeted drug delivery,” *Advanced Drug Delivery Reviews*, vol. 59. pp. 748–758, 2007.

[57] J. Zimmerberg and K. Gawrisch, “The physical chemistry of biological membranes.,” *Nat. Chem. Biol.*, vol. 2, pp. 564–567, 2006.

[58] D. D. Lasic and D. Needham, “The ‘Stealth’ Liposome: A Prototypical Biomaterial,” *Chem. Rev.*, vol. 95, pp. 2601–2628, 1995.

[59] M. L. Immordino, F. Dosio, and L. Cattel, “Stealth liposomes: Review of the basic science, rationale, and clinical applications, existing and potential,” *International Journal of Nanomedicine*, vol. 1. pp. 297–315, 2006.

[60] P. R. Cullis, M. B. Bally, T. D. Madden, L. D. Mayer, and M. J. Hope, “pH gradients and membrane transport in liposomal systems.,” *Trends Biotechnol.*, vol. 9, no. 8, pp. 268–72, Aug. 1991.

[61] T. D. Madden, P. R. Harrigan, L. C. Tai, M. B. Bally, L. D. Mayer, T. E. Redelmeier, H. C. Loughrey, C. P. Tilcock, L. W. Reinish, and P. R. Cullis, “The accumulation of drugs within large unilamellar vesicles exhibiting a proton gradient: a survey.,” *Chem. Phys. Lipids*, vol. 53, pp. 37–46, 1990.

[62] H. Kercret, R. Chiovetti, M. W. Fountain, and J. P. Segrest, “Plasma membrane-mediated leakage of liposomes induced by interaction with murine thymocytic leukemia cells,” *Biochim. Biophys. Acta - Biomembr.*, vol. 733, pp. 65–74, 1983.

[63] G. Scherphof, F. Roerdink, M. Waite, and J. Parks, “Disintegration of phosphatidylcholine liposomes in plasma as a result of interaction with high-density lipoproteins.,” *Biochim. Biophys. Acta*, vol. 542, pp. 296–307, 1978.

[64] A. Ghumra, J. P. Semblat, R. Ataide, C. Kifude, Y. Adams, A. Claessens, D. N. Anong, P. C. Bull, C. Fennell, M. Arman, A. Amambua-Ngwa, M. Walther, D. J. Conway, L. Kassambara, O. K. Doumbo, A. Raza, and J. A. Rowe, “Induction of strain-transcending antibodies against group A PfEMP1 surface antigens from virulent malaria parasites,” *PLoS Pathog.*, vol. 8, no. 4, 2012.

[65] W. Peters, “The prevention of antimalarial drug resistance.,” *Pharmacol. Ther.*, vol. 47, no. 3, pp. 499–508, 1990.

[66] N. White, “Antimalarial drug resistance and combination chemotherapy.,” *Philos. Trans. R. Soc. Lond. B. Biol. Sci.*, vol. 354, no. 1384, pp. 739–749, 1999.

SUPPLEMENTARY DATA

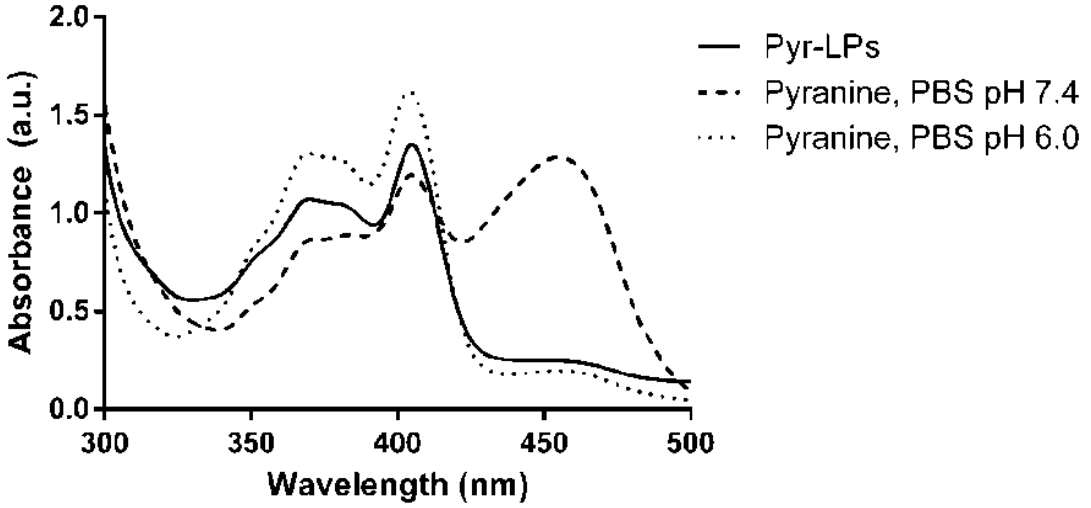

Fig.S1. Pyranine absorption spectra as a function of solution pH, either encapsulated inside liposomes (10 mM lipid) in PBS pH 6.5 as inner aqueous core and PBS pH 7.4 as outer aqueous phase (Pyr-LPs), or freely dissolved in PBS, pH 7.4 or 6.0.

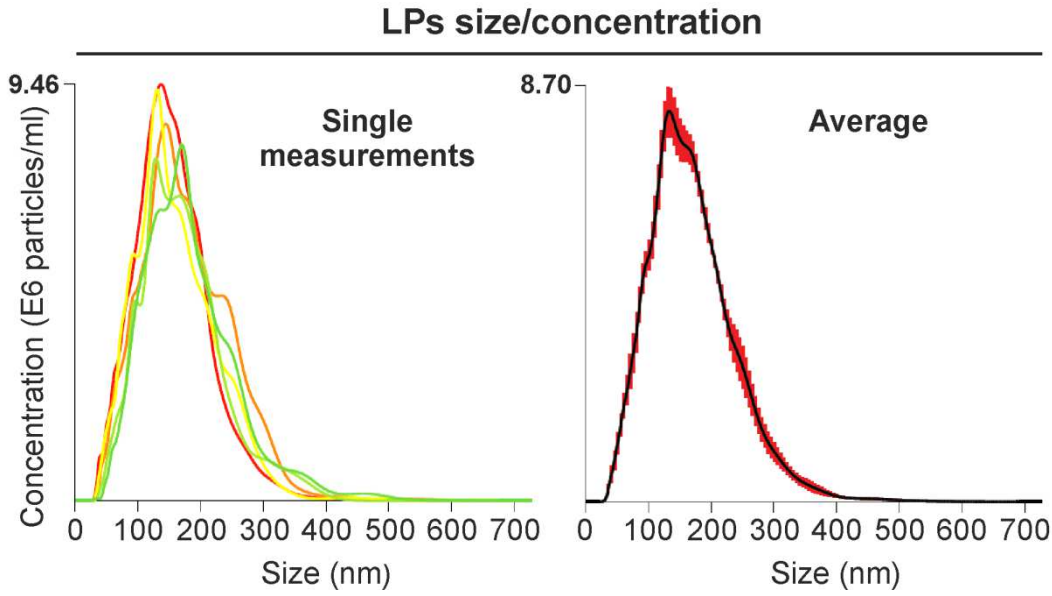

Fig.S2. Determination of liposome size and concentration by nanoparticle tracking analysis, which utilizes properties of both light scattering and Brownian motion. (A) Individual measurements and (B) averaged values for *n=5* individual replicates of liposome samples corresponding to 1 µM total lipid. Red error bars indicate ± standard error of the mean.

Table S1. Batch average results from liposome size and concentration determination by nanoparticle tracking analysis, corresponding to 1 µM total lipid. Results are presented as mean ± standard deviation from *n=5* individual replicates.

Size Distribution	
Mean (nm)	169 ± 5
Mode (nm)	142 ± 8
Total Concentration	
Particles/frame	55.6 ± 1.2
Particles/ml	$1.2 \times 10^9 \pm 0.3 \times 10^9$

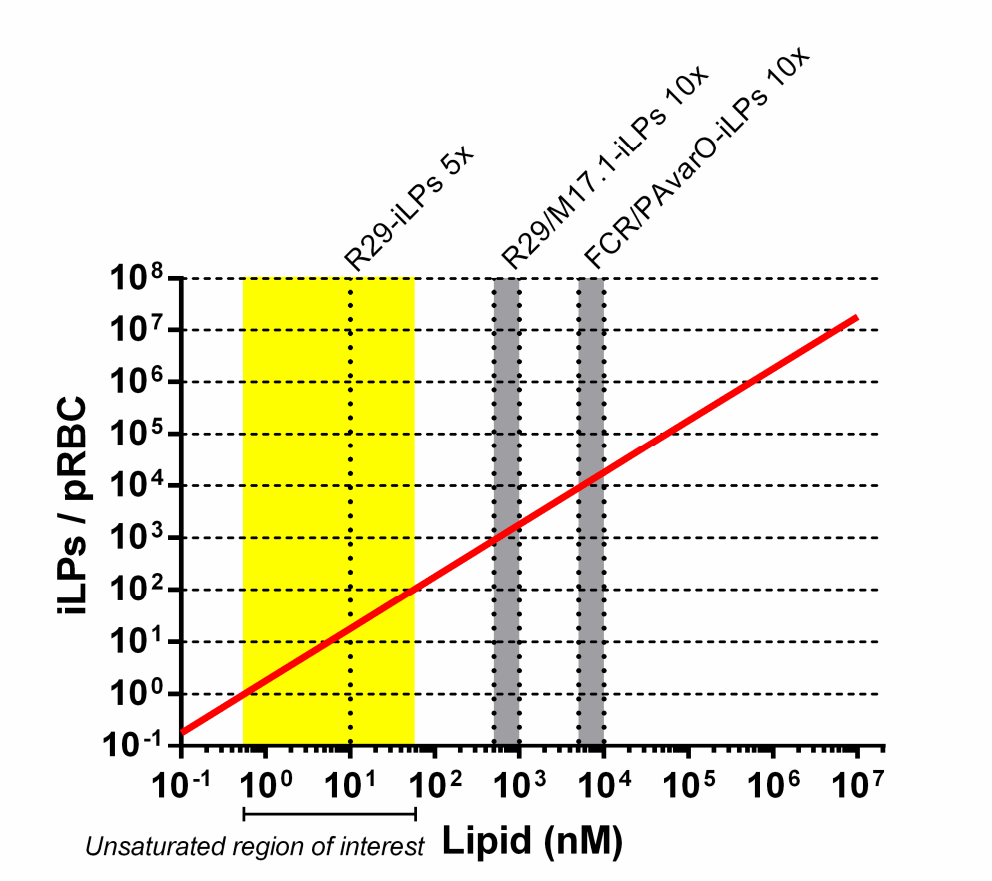

Fig.S3. Determination of the iLPs/pRBC ratio as a function of lipid concentration for a 1% hematocrit culture (6.7×10^7 RBCs/ml) with 1% *P. falciparum*-infected RBCs, parameters used during *in vitro* rosette disruption and growth inhibition assays. LP amount in pRBC cultures is expressed as total phospholipid concentration (Lipid, nM). Besides, LP particle concentration according to total lipid amount was determined by nanoparticle tracking analysis (Fig. S2 and Table S1). Confocal fluorescence microscopy detection limits for the different iLP models are indicated by dotted lines. The unsaturated region of interest, corresponding to ca. 1-100 iLPs/pRBC is highlighted in yellow.

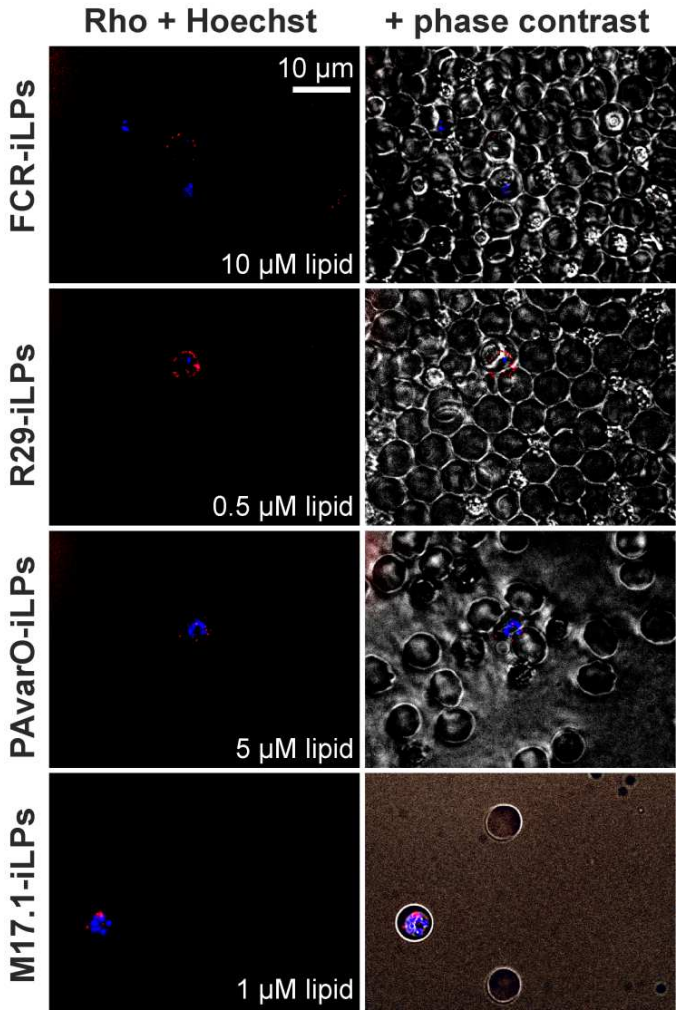

Fig.S4. Confocal fluorescence microscopy analysis of the iLPs targeting limit against their homologous strains. Images correspond to the stack of individual z axis sections spanning the whole cell.

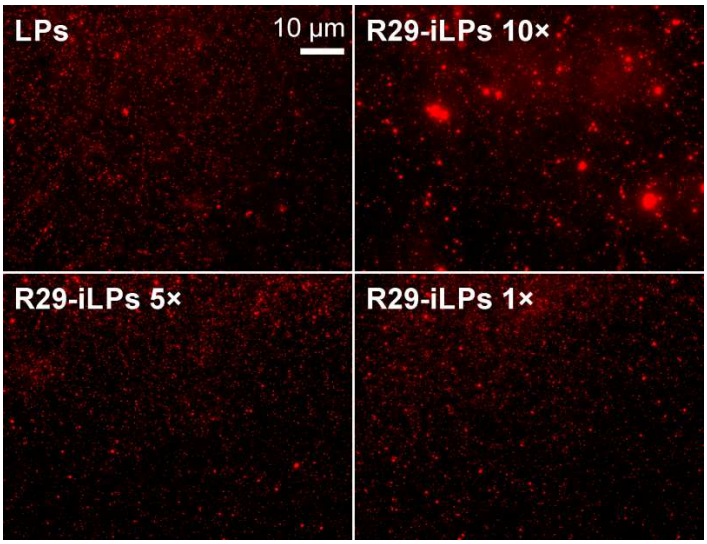

Fig.S5. Fluorescence microscopy analysis of liposome aggregates after R29 antibody coupling using 1×, 5× or 10× SATA/Ab molecular ratios. Plain LPs are included as control for absence of aggregates.

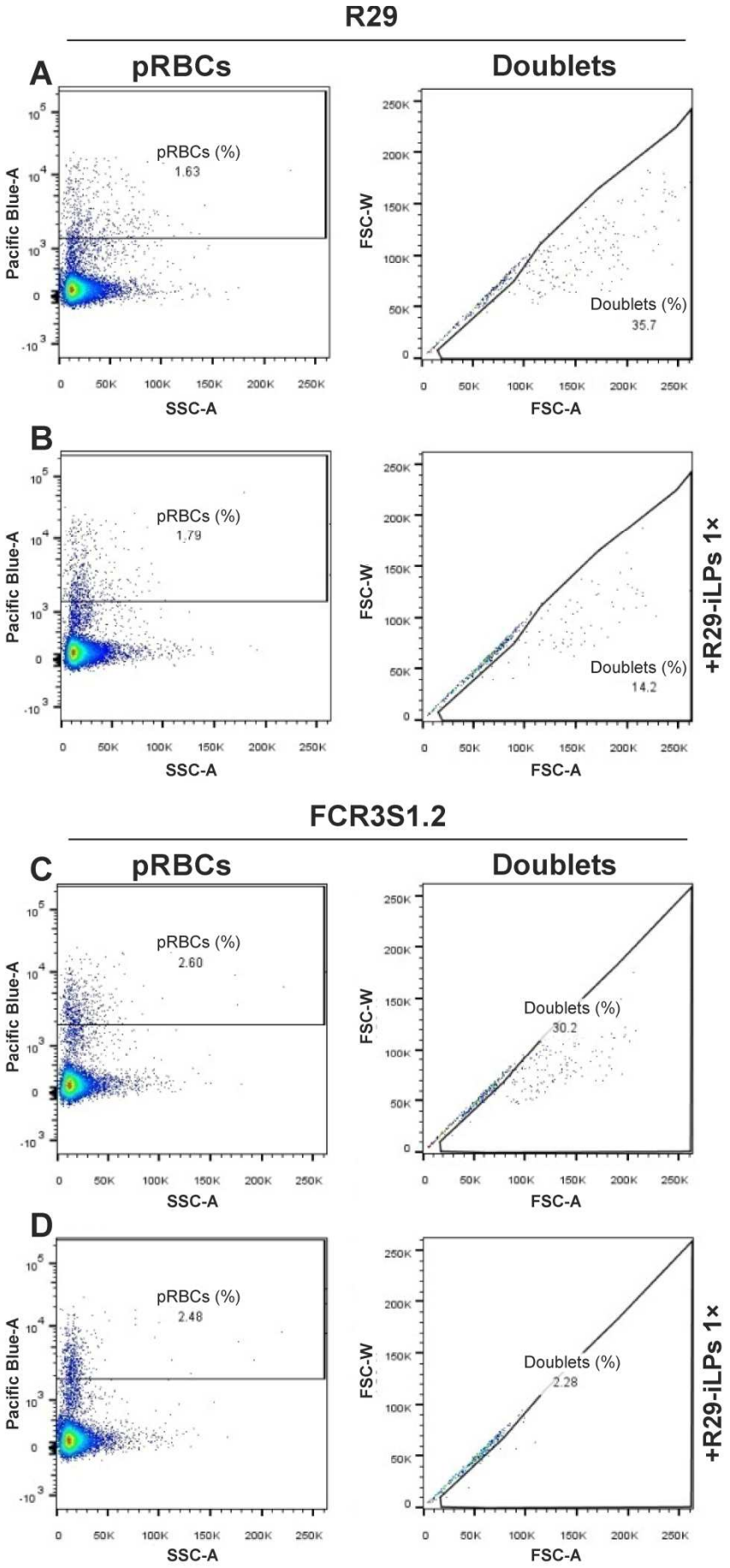
R29
A
pRBCs
Doublets
pRBCs (%)
1.63
Doublets (%)
35.7
Pacific Blue-A
SSC-A
FSC-W
FSC-A
B
pRBCs (%)
1.79
Doublets (%)
14.2
+R29-iLPs 1×
FCR3S1.2
C
pRBCs
Doublets
pRBCs (%)
2.60
Doublets (%)
30.2
D
pRBCs (%)
2.48
Doublets (%)
2.28
+R29-iLPs 1×

Fig.S6. Flow cytometry analysis of rosetting disruption before (A, C) and after iLP 1× treatment (B,D) against the homologous R29 (40 µg Ab/ml) and FCR3S1.2 (20 µg Ab/ml) pRBC strains in late forms (positive Hoechst signal, Pacific Blue-A channel).% of rosettes/cell doublets was calculated among pRBCs in late forms.

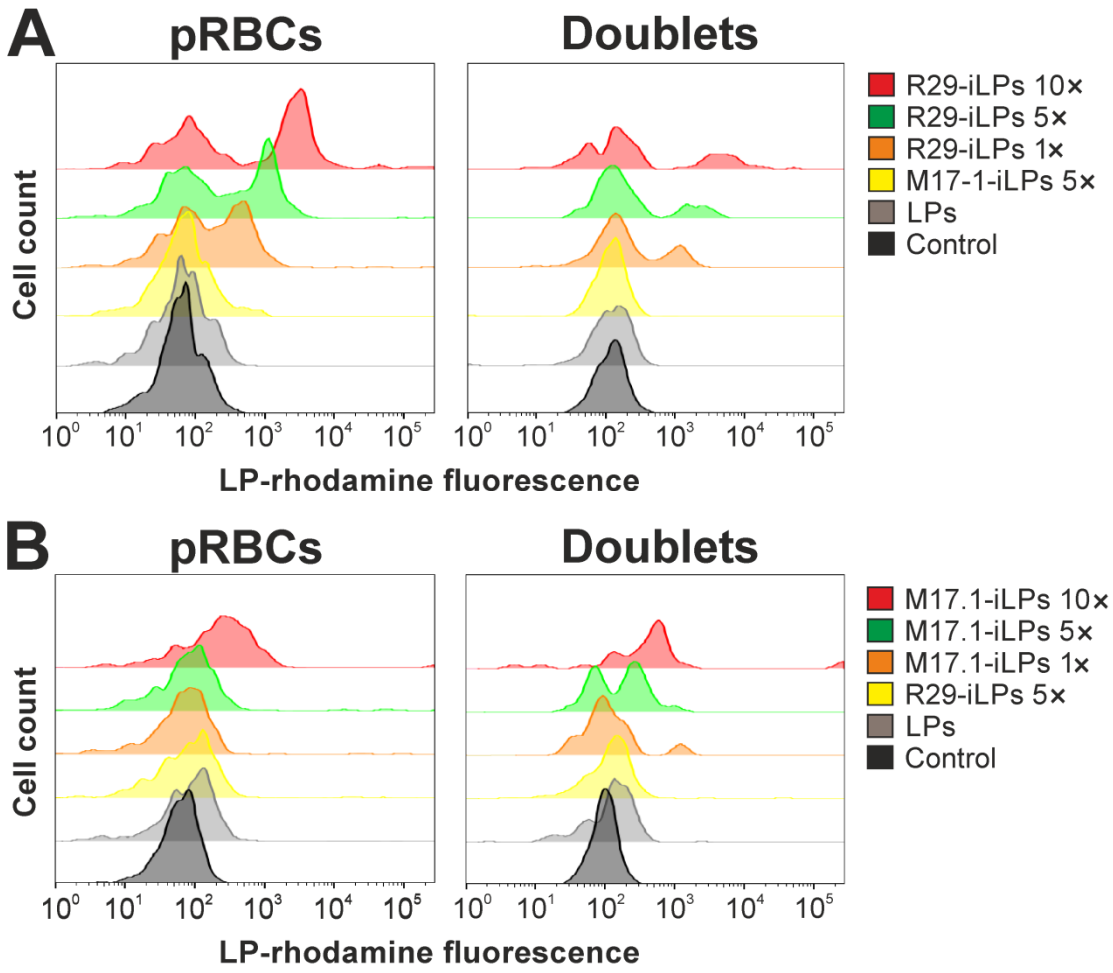

Fig.S7. Flow cytometry targeting analysis of rosetting disruption mediated by R29- and M17.1-iLPs against their homologous R29 (A) and FCR3S1.2 (B) pRBC strains in late forms. Cell count histograms represent the LP-rhodamine fluorescence signal acquired through the PE-A cytometer channel.

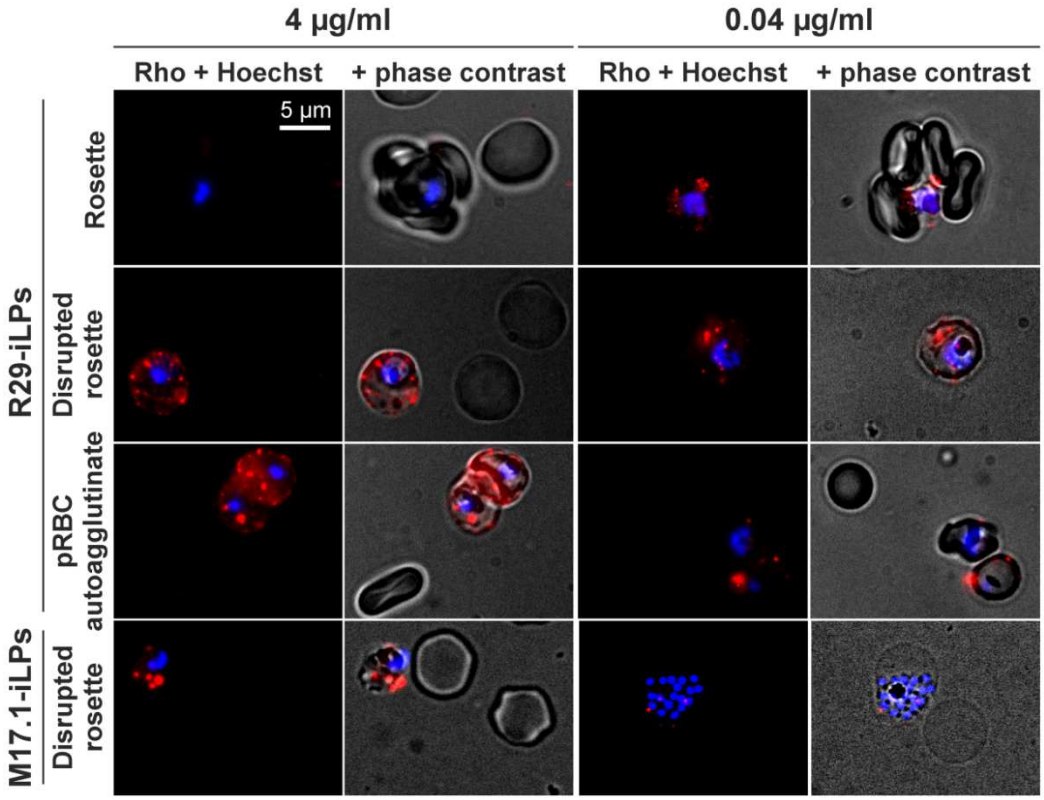

Fig.S8. Qualitative analysis of R29-iLP interacting events after incubation with the homologous R29 *P. falciparum* strain at the indicated amounts of conjugated antibody in culture. Targeting results for M17.1-iLPs with the same amounts of conjugated antibody, incubated with the homologous FCR3S1.2 *P. falciparum* strain, are included for comparison.

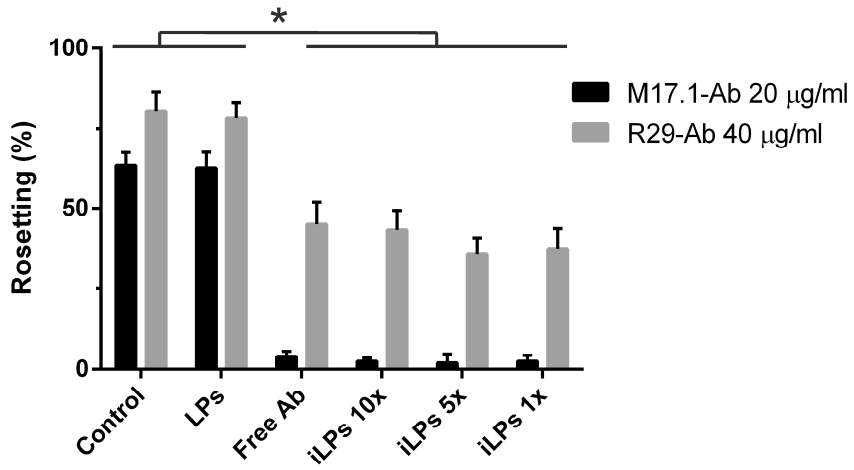

Fig.S9. Analysis of the rosette disrupting activity by fluorescence microscopy and manual counting (considering rosette as a late-form pRBC interacting with 2 or more RBCs) of anti-rosetting iLPs and the corresponding free antibodies against their homologous *P. falciparum* strains (M17.1 and R29 antibodies against FCR3S1.2 and R29 strains, respectively). Percentages represent the fraction of rosetting pRBCs relative to the total number of late-form pRBCs in the cultures (* $p < 0.05$).

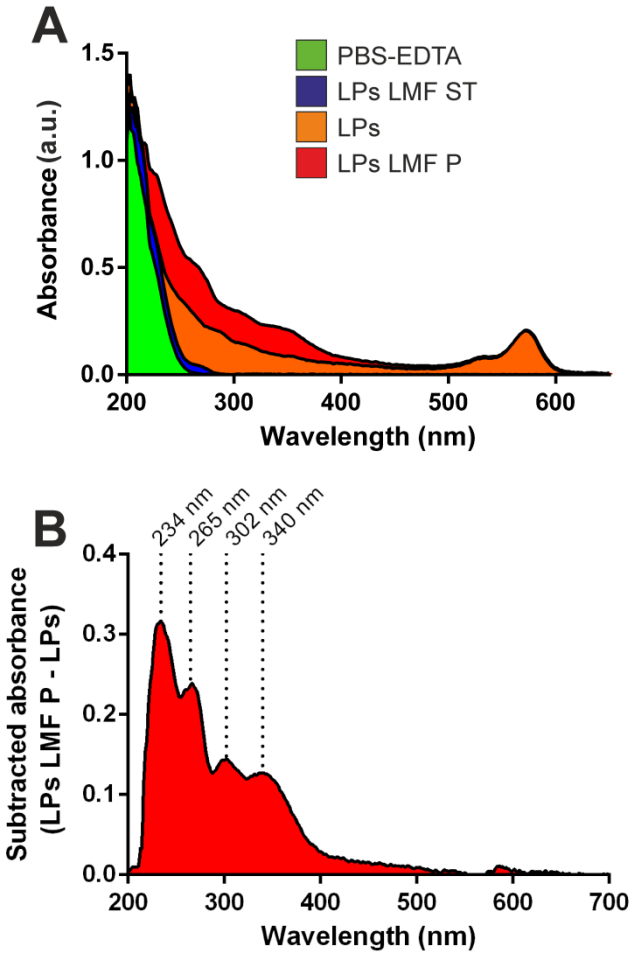

Fig.S10. (A) UV-visible absorption spectra analysis (arbitrary units, a.u.) of liposomes encapsulating lumefantrine (LPs LMF) used in *P. falciparum* growth inhibition assays. PBS-EDTA and plain LPs are included as controls for liposome supernatant (LPs LMF ST), and pellet (LPs LMF P) fractions obtained after separation of unencapsulated drug by ultracentrifugation. (B) LPs LMF pellet area under curve obtained after absorbance subtraction showing lumefantrine maximum absorption peaks.

Table S2. Areas under curves (AUC) results for lumefantrine encapsulation quantification into LPs by UV-visible absorption spectra analysis.

Samples	AUC Mean ± SD (a.u.)	Subtracted AUC (a.u.)	Lumefantrine (% of total drug)
PBS-EDTA	18.8 ± 0.2	-	-
LPs LMF ST	22.8 ± 0.5	3.9	**11.0**
LPs	61.0 ± 1.8	-	-
LPs LMF P	92.4 ± 0.7	31.4	**89.0**

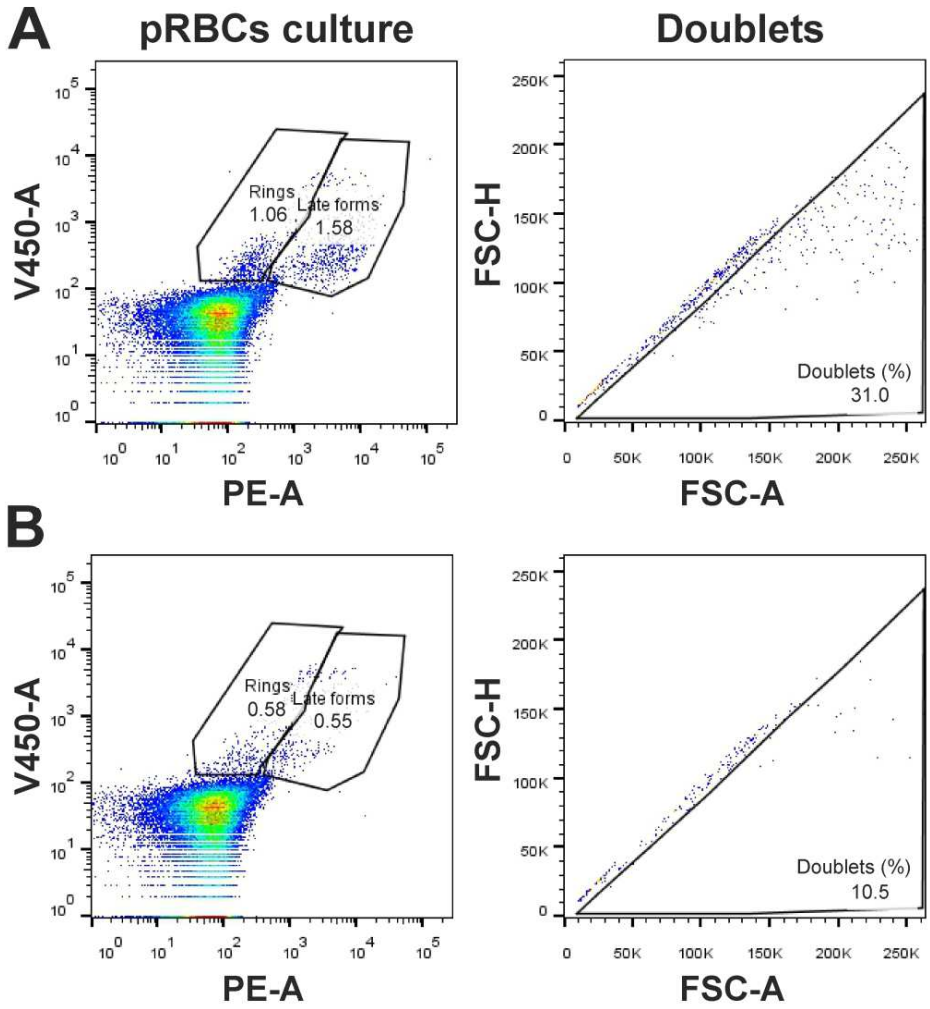

Fig.S11. Growth inhibition assay analysis by flow cytometry using R29-iLPs encapsulating lumefantrine. (A) Untreated R29 control. (B) Culture treated with 2 µM lumefantrine encapsulated within R29-iLPs 5×. % of rosettes/cell doublets was calculated among pRBCs in late forms within the 2nd generation of parasites.

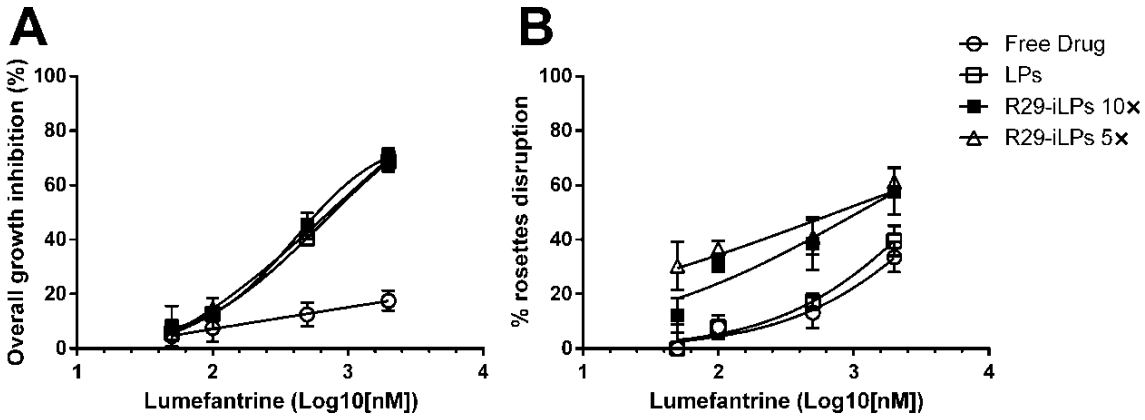

Fig.S12. Nonlinear regression analysis for (A) growth inhibition and (B) rosette disruption IC50 determination from *P. falciparum* R29 growth inhibition assays with lumefantrine. Data retrieved from the 2nd generation of parasites.

Table S3. Grid showing the inter-sample *p* values obtained in Fig. 6C experiment and corresponding to the comparison of absolute rosetting/doublets percentages analyzed within the second generation of *P. falciparum* R29 parasites after treatment with different lumefantrine (2 µM) sources.

	R29-iLPs 5x	R29-iLPs 10x	LPs	Free Drug	Control
R29-iLPs 5x	1	0.50	**7.61E-04**	**3.68E-04**	**1.41E-05**
R29-iLPs 10x	-	1	**8.68E-03**	**4.49E-03**	**1.03E-04**
LPs	-	-	1	0.41	**3.60E-04**
Free Drug	-	-	-	1	**6.78E-04**
Control	-	-	-	-	1

Table S4. IC50 values for growth inhibition and rosette disruption obtained by nonlinear regression analysis after *P. falciparum* R29 culture treatment with R29-iLPs encapsulating lumefantrine. N.A.: Not applicable. Data retrieved from the 2nd generation of parasites.

Lumefantrine IC50	R29-iLPs 5x	R29-iLPs 10x	LPs	Free Drug
Overall growth inhibition (nM)	765.8	413.7	661.5	N.A.
Rosettes disruption (nM)	747.3	1,085	3,361	4,833

CHAPTER 3

Proposal of 2-picolylamine derivatization and LC-ESI-MS/MS analysis for the ultra-sensitive detection of abscisic acid in apicomplexan blood-infecting parasites and first validation test in *Plasmodium falciparum* extracts

Ernest Moles[a,b,c,*], Josep Marcos[d,e], Santiago Imperial[f], Oscar J. Pozo[d], Xavier Fernàndez-Busquets[a,b,c,*]

[a] *Nanomalaria Group, Institute for Bioengineering of Catalonia (IBEC), Baldiri Reixac 10-12, ES-08028 Barcelona, Spain*

[b] *Barcelona Institute for Global Health (ISGlobal, Hospital Clínic-Universitat de Barcelona), Rosselló 149-153, ES-08036 Barcelona, Spain*

[c] *Nanoscience and Nanotechnology Institute (IN2UB), University of Barcelona, Martí i Franquès 1, ES-08028 Barcelona, Spain*

[d] *Bioanalysis Research Group, IMIM, Hospital del Mar, Doctor Aiguader 88, 08003 Barcelona, Spain*

[e] *Department of Experimental and Health Sciences, Universitat Pompeu Fabra, Doctor Aiguader 88, 08003 Barcelona, Spain*

[f] *Departament de Bioquímica i Biología Molecular, Universitat de Barcelona (UB), Avda Diagonal 645, E-08028 Barcelona, Spain*

* Corresponding author at: Nanomalaria Group, Institute for Bioengineering of Catalonia (IBEC), Baldiri Reixac 10-12, ES-08028 Barcelona, Spain.

E-mail address: ernest.moles@isglobal.org; xfernandez_busquets@ub.edu

ABSTRACT

Parasitic protists of the apicomplexan phylum represent a major life-threatening concern accounting annually for thousands of deaths and primarily affecting developing countries. Because the high replication rate of these pathogens is closely associated with the appearance of drug resistant clones, the discovery of novel parasite-specific pathways is of crucial importance for the development of new therapeutic agents. Of particular importance has been the identification of abscisic acid (ABA) biosynthesis in *Toxoplasma gondii* and its specific role in regulating parasite egress. Although ABA is produced as a by-product of the C_{40}-carotenoid metabolism in plastid-containing organisms, it has not been identified in other apicomplexa besides *Toxoplasma*. Nordihydroguaiaretic acid, an antioxidant compound blocking ABA synthesis, efficiently inhibited *Plasmodium falciparum* growth, suggesting the presence of an ABA biosynthetic route in this organism. We have developed a new liquid chromatography-electrospray ionization tandem mass spectrometry (LC-ESI-MS/MS) methodology based on 2-picolylamine derivatization and positive ion mode detection for ABA identification in red blood cell-infecting protists, obtaining excellent limits of detection (LOD) and quantification (LOQ) values of 0.03 and 0.15 ng/mL, respectively. ABA could not be detected in *P. falciparum*-infected red blood cell (pRBC) extracts suggesting that, if present, it will be found either in trace amounts or as brief bursts at defined time points within the intraerythrocytic cycle and/or in the form of a chemical derivative.

1. Introduction

Human infections by protist obligate endoparasites of the phylum Apicomplexa are responsible for millions of clinical cases resulting in thousands of deaths every year, thereby representing a major development constraint for low-income countries. Those Apicomplexa pathogens with higher clinical impact can be classified into three principal genera/diseases: *Plasmodium*/malaria, *Babesia*/babesiosis and *Toxoplasma*/toxoplasmosis. Malaria is a mosquito-borne disease where red blood cells (RBCs) are the main host cell in an infected human; such RBCs infection being responsible for all the malaria-associated clinical manifestations, from flu-like symptoms to life-threatening complications like severe anemia. Even more severe outcomes occur during *Plasmodium falciparum* infection due to parasitized-RBC cytoadherence to brain and placenta, leading to 584,000 deceases only in 2013 [1]. Babesiosis is a zoonotic tick-borne disease infecting RBCs and considered as an emerging disease in humans due to the increase in clinical cases since 1969 [2], being *Babesia microti* classified as the most frequently transfusion-transmitted intraerythrocytic pathogen [3]. Parasites of the *Toxoplasma* genus are propagated through raw food and/or untreated water in their cyst/oocyst dormant form, which invade intestinal cells at first. Latent cysts ultimately form in diverse tissues of the human host with a particular tropism towards brain, eyes and striated muscles [4]. Remarkably, about a third of the world's human population is estimated to be infected by *Toxoplasma gondii*, though clinically silent in most of cases and only lethal in immunocompromised patients [5].

All the aforementioned intracellular parasites share characteristic organelles and infective processes common in Apicomplexa. Among these specific features, the apicoplast, a non-photosynthetic plastid incorporated through endosymbiosis from algae during protozoan evolution, has several metabolic pathways absent in humans and therefore has been considered an exceptional target for antiparasitic drug research [6]. Isoprenoid biosynthesis, which operates in plastid-containing parasites mostly through the 2-*C*-methyl-D-erythritol 4-phosphate (MEP) pathway, has driven special attention being essential for the synthesis of numerous downstream metabolites that include ubiquinone, carotenoids and prenylation-groups [7]–[10]. The MEP pathway inhibitor fosmidomycin has been the first line drug against MEP-derived isoprenoids in *P. falciparum* [11] and its efficacy against *B. microti* and *T. gondii* has been proved. However, because of membrane impermeability to fosmidomycin, specific protein transporters are required for its uptake into the parasitized cell [12]. This transport mechanism is easily disruptable by single point mutations [13] and consequently the research of additional drugs and essential routes for the development of apicomplexan parasites is mandatory.

Carotenoid biosynthesis in the apicoplast has been recently described in *P. falciparum* [8] and in *T. gondii* [9]. Considering the absence of photosynthetic activity in apicomplexan plastids, diverse alternative roles have been theorized for carotenoid derivatives in these parasites as (i) antioxidant agents against oxidative stress [8], [14], (ii) messengers coordinating nuclear-plastid

gene expression [15], (iii) triggering changes in membrane fluidity [16] and (iv) substrates for the synthesis of plant-like hormones that regulate essential cellular processes [9], [17]–[19]. In this regard, abscisic acid (ABA, Fig. 1A) has been proved to be endogenously produced by *T. gondii* through the plant-like C_{40}-carotenoid biosynthetic pathway (C_{40}-CBP) [9]. ABA is necessary for *Toxoplasma* reinvasion regulating its maturation and the egress of daughter parasites from the host infected cell in a complex signaling process dependent on calcium delivery. Accordingly, the herbicide fluridone, which targets the phytoene desaturase enzyme (PDS) in the early steps of the C_{40}-carotenoid route, efficiently delayed the parasite growth and prevented its multiplication while significantly reducing ABA levels in the intracellular parasite. Other compounds with greater and more straight effect over ABA synthesis, such as the nordihydroguaiaretic acid (NDGA) lipoxygenase inhibitor, have been identified in plants [20], [21] but never assayed against apicomplexan parasites. Remarkably, due to NDGA antioxidant effects, it has been further proposed as an anticancer agent [22], [23].

Two calcium-dependent, plant-like protein kinases (*Tg*CDPK1 and 3), along with an additional cGMP-dependent protein kinase (PKG), have been further identified to be essential in *T. gondii* egress [24]. Similar calcium-regulated processes affecting parasite maturation and egress do also occur in other apicomplexan parasites, including *Plasmodium* and *Babesia* genera [25]–[29], although the initial endogenous event triggering such mechanisms remains still unknown. The identification in *P. falciparum* of an analogous host cell egress route to *T. gondii* involving PKG and *Pf*CDPK5 [30], as well as its growth dependence on intracellular oscillating calcium levels during most of the intraerythrocytic stage [26], supports the possible existence of ABA or an ABA-like hormone not yet identified as starting triggering element of diverse and vital calcium-dependent pathways and, therefore, a highly interesting forthcoming target for malaria and babesiosis chemotherapy.

Nowadays, liquid chromatography-electrospray ionization tandem mass spectrometry (LC-ESI-MS/MS) is considered the technique of choice for the determination of ABA and other phytohormones [31]–[35]. This technique provides an excellent sensitivity, specificity and throughput, allowing as well to the analysis of non-volatile and thermally-unstable compounds. Although the sensitivity of this approach (in the range of a few ng/mL) favored the detection of endogenous levels of ABA in vegetal material, smaller concentrations of this hormone would be expected to be produced by apicomplexan parasites due to the absence of most of plant-like, ABA-regulated processes in these pathogens (e.g. leaf senescence, stomatal closure and seed germination [36], [37]); which ultimately calls for the development of high-sensitivity ABA detection protocols. Several chemical derivatization procedures have been developed in order to enhance the detection responses of carboxylic acids, such as ABA, in LC-ESI-MS/MS [38]. Picolylamine (PA), a derivatizing agent displaying a highly ESI-active pyridyl group that reacts with carboxylic acids in the presence of a condensation agent to form an amide derivative, has

been employed in this regard for the analysis of fatty acids and other carboxyl-containing compounds [39].

In the present work we propose the use of PA for the derivatization of ABA as an ultra-high sensitive approach for the research and detection of this plant-like hormone in (i) those apicomplexan parasites in which it has never been identified yet and (ii) as a more efficient protocol for ABA study in *T. gondii* than the currently employed GC-MS assay, which requires the methylation of ABA [9]. In addition to the optimized detection parameters, the results obtained after the application of a full validation protocol for ABA detection in *P. falciparum* are presented.

2. Materials and methods

2.1. Chemicals and reagents

ABA and deuterated ABA ($[^2H_6]$ABA or ABA-d6), the latter used as internal standard (ISTD), PA, 2,2'-Dipyridyl disulfide (DPDS), triphenylphosphine (TPP) and saponin were purchased from Sigma-Aldrich Corporation (St. Louis, MO, EUA). Ethyl acetate, methanol (LC gradient grade), formic acid, and ammonium formate (LC/MS grade) were obtained from Merck (Darmstadt, Germany). Ultrapure water was obtained from a Milli-Q purification system (Millipore Ibérica, Barcelona, Spain). The Sep-Pak® Vac RC (500 mg) C18 cartridges were purchased from Waters (Milford, Massachusetts, USA).

2.2. P. falciparum in vitro culture and growth inhibition assays

P. falciparum strain 3D7 was grown *in vitro* in group B human erythrocytes using previously described conditions [40]. Parasites (thawed from glycerol stocks) were cultured at 37 °C in Petri dishes with RBCs at 3% hematocrit in Roswell Park Memorial Institute (RPMI) complete medium containing Albumax II (RPMI-A, Invitrogen), supplemented with 2 mM L-Glutamine and under a gas mixture of 92% N_2, 5% CO_2, and 3% O_2. Synchronized cultures in early ring stages (0-24 h post-invasion) were obtained by 5% sorbitol lysis [41]. Late-form trophozoite and schizont stages (24-36 h and 36-48 h post-invasion, respectively) were purified in 70% Percoll (GE Healthcare) [41], [42]. Parasitemia was determined by microscopic counting of blood smears fixed briefly with methanol and stained with Giemsa (Merck Chemicals) diluted 1:10 in Sorenson's buffer, pH 7.2, for 10 min. For culture maintenance, parasitemia was kept below 5% late forms and 10% early forms by dilution with freshly washed RBCs and the medium was changed every 1-2 days.

For *P. falciparum* in vitro growth inhibition assays, cultures synchronized (>95%) in the early ring maturation stage were brought to 6% hematocrit and 1% parasitemia by dilution with fresh RBCs. After adding one culture volume of 2× concentrated drug solution in RPMI-A, making 3% hematocrit, cultures were seeded on 96-well plates (Merck Chemicals) and

incubated for a complete 48 h growth cycle under the conditions described above. For growth inhibition determination, samples were processed and analyzed by flow cytometry as described in [43]. Briefly, cultures were diluted 1:100 in 1× phosphate buffered saline (PBS) and the nuclei of *P. falciparum*-infected RBCs (pRBCs, the only nucleated cells present in the culture) were stained by addition of 0.1 µM Syto11 (Thermo Fisher Scientific, Inc.) in the final mixture before proceeding to their analysis by a BD LSRFortessa flow cytometer (Becton, Dickinson and Company, New Jersey, USA).

2.3. ABA analysis from P. falciparum culture after treatment with C_{40}-CBP inhibitors

P. falciparum cultures at 6% parasitemia and 3% hematocrit synchronized in the ring maturation stage were washed several times with RPMI-A and cultured in the presence of C_{40}-carotenoid biosynthetic pathway (C_{40}-CBP) inhibitors for 24 h until the appearance of pRBCs at the trophozoite-schizont late forms. Fluridone herbicide and the nordihydroguaiaretic acid (NDGA) antioxidant compound were assayed at their previously-determined *in vitro* IC50 (112.2 µM and 46.8 µM for fluridone and NDGA, respectively, Fig. 2) separately and in combination. The same volume of methanol, used as solvent for inhibitors, was tested in parallel as control (0.1% v/v methanol/culture). An additional control corresponding to only uninfected RBCs at 3% hematocrit was also included.

After the aforementioned 24 h incubation period in the presence of C_{40}-CBP inhibitors, *P. falciparum* cultures were spun down and cells were subsequently extracted through the lyophilization-acetone method (described in 2.4.) as an adaptation of already established protocols for ABA purification [9], [44], [45]. Finally and in parallel to cells extraction, small aliquots of the cultures in the trophozoite stage were diluted 7.5-fold in RPMI, supplemented with new RBCs (making 3% hematocrit) and further incubated for additional 24 h (total of 48 h) in order to determine the parasite reinvasion capacity after treatment.

2.4. Lyophilization-acetone cell extraction method

Briefly, pelleted cells (1.2×10^{10} total cells) were frozen directly into a dry-ice ethanol bath and lyophilized overnight. Resulting pellets were thereafter weighted and solubilized in 8-volumes of ice-cold extraction solution (80:19:1 acetone:water:acetic acid). Samples were homogenized by vortex for few minutes, incubated for 15 min and spun down 10,000 g for 10 min at 4 ºC. The supernatants obtained were stored at 4 ºC and the remaining pellets were solubilized again in 8-volumes of ice-cold extraction solution. After homogenization and 5 min incubation, samples were spun down 8,000 g for 5 min at 4 ºC. The two previous steps were repeated for the 3rd final extraction and the latter supernatant was stored. All three obtained supernatants were subsequently pooled and dried first under nitrogen flow and, thereafter, left overnight in the lyophilizer for a complete removal of water remains.

2.5. ABA purification from cell extracts and derivatization

Liquid-liquid extraction (LLE)

The lyophilized cell extract (obtained as described in 2.4.) was re-dissolved in 1 mL of acetonitrile:water (8:2 v/v). An aliquot of 150 µL of the re-dissolved extract was supplemented with 25 µL of the ISTD solution (ABA-d6) and the mixture was evaporated under a nitrogen stream at 40 ºC. Afterwards, 1 mL of a saturated NaCl, and 1 mL of acetic acid 1 M solutions were added. The mixture was extracted with 6 mL of ethylacetate by shaking in a rocking mixer at 40 oscillations per minute during 20 min. After centrifugation (3000 g, 5 min), the organic layers rich in protonated ABA were separated and evaporated to dryness under a stream of nitrogen coupled to a water bath at 40 ºC. Due to the highest ABA extraction recovery obtained through the LLE approach (Table 2), it was selected as strategy of choice for the validation of the ABA optimized detection-quantification method and its later application in *P. falciparum* cultures.

Solid-phase extraction (SPE)

Alternatively to LLE, the lyophilized cell extracts obtained in 2.4. and re-dissolved in 1 mL of acetonitrile:water (8:2 v/v) were processed by solid-phase extraction using the Sep-Pak® Vac RC C18 (500 mg) cartridges. The mixture comprising 150 µL of re-dissolved extract and 25 µL of ISTD (ABA-d6) was vortex-mixed and passed through a C18 cartridge previously conditioned with MeOH and water (using 2 mL of each solution). The column was then washed with water (2 mL) and ABA was eluted with MeOH (2 mL). The methanolic extract was evaporated to dryness under a stream of nitrogen coupled to a water bath at 40 ºC.

ABA derivatization with 2-picolylamine (PA)

The resulting dry pellet from either LLE or SPE was derivatized based on the procedure described by Higashi *et al.* [32]. Briefly, a freshly prepared solution of TPP (10 mM) in acetonitrile (10 µl), DPDS (10 mM) in acetonitrile (10 µl) and PA (10 µg) in acetonitrile (10 µl) were successively added to the pellet. The mixture was incubated at 60 ºC for 10 min. After removal of the solvent, the product was reconstituted with 150 µL of a mixture of deionized water:acetonitrile (9:1, v/v) and 10 µL were injected into the LC-MS/MS system.

2.6. Liquid chromatography-electrospray ionization tandem mass spectrometry (LC-ESI-MS/MS)

PA-derivatized ABA (ABA-PA) was quantified by LC-ESI-MS/MS with a selected reaction monitoring (SRM) method using a triple quadrupole (Quattro Premier XE) mass spectrometer equipped with an orthogonal Z-spray-electrospray ionization source (ESI) (Waters Associates, Milford, MA, USA) interfaced to an Acquity UPLC system (Waters Associates) for the chromatographic separation. Nitrogen was employed as both drying and nebulising gas. The desolvation gas flow was set to approximately 1200 L/h and the cone gas flow to 50 L/h. A cone

voltage of 25 V and a capillary voltage of 3.0 kV were used in positive ionization mode. The nitrogen desolvation temperature was set at 450 ºC and the source temperature at 120 ºC.

The LC separation was performed using an Acquity UPLC BEH C18 column (100 x 2.1 mm i.d., 1.8 µm from Waters Associates, Milford, MA, USA) at a flow rate of 300 µL/min. Water and methanol, both containing formic acid (0.01%) and ammonium formate (1 mM), were selected as mobile phase solvents. A gradient program was used; the percentage of organic solvent was linearly changed as follows: at 0 min., 30%; at 0.5 min., 30%; at 5 min., 70%; at 5.5 min., 90%; at 6 min., 30%; at 7.5 min., 30%. ABA-PA and ABA-d6-PA (PA-derivatized ISTD) were determined by SRM considering three transitions for each compound. The optimized detection parameters are summarized in Table 1.

2.7. Method validation for ABA detection and quantification

Prior to the application of the optimized PA-based, LC-ESI-MS/MS method for ABA detection in *P. falciparum* cultures, a complete intra- and inter-assay validation was carried out. The samples selected for validation were processed through LLE plus PA-derivatization (as explained in 2.5.) and finally analyzed by means of the LC-ESI-MS/MS system described in 2.6. The protocol consisted in three validation assays. In each of them, seven calibration standards were prepared by spiking lyophilized RBC extracts with a known amount of ABA. Calibration standards were analyzed and calibration curves were calculated by least-squares linear regression. Precision and accuracy of the method were checked by analyzing quality control (QC) samples. QC samples were prepared by spiking lyophilized RBC extracts at two different concentrations of ABA (0.15 and 1.5 ng/mL).

In a first assay, repeatability and intra-assay accuracy were evaluated by analyzing six replicates for each level. For the rest of the assays, three replicates were included and their concentration was estimated against the calibration curve. Intra-assay precision of the method is expressed as the relative standard deviation (%) of the estimated concentrations obtained for the six QCs analyzed in one assay. Intra-assay accuracy is expressed as the recovery value (%) estimated for the QCs. Analogously, inter-assay precision is given as the relative standard deviation (%) of the estimated concentrations obtained for all replicates analyzed along the three validation assays as well as by two different operators (n = 12). Inter-assay accuracy is obtained as described for intra-assay accuracy but considering the replicates analyzed in all three analytical batches (n = 12). The limit of detection (LOD) was defined as the lowest concentration displaying a signal/noise ratio (S/N) value from the chromatogram of 3. Similarly, the limit of quantification (LOQ) was estimated as the concentration which gives a S/N value of 10. ABA concentration for the determination of LOD and LOQ was calculated considering the lyophilized RBC extract resuspended in 1 mL acetonitrile:water (8:2 v/v), as described in 2.5., which results in approximately 1.2×10^{10} total cells extract/mL.

Besides, RBC matrix effect was evaluated for both ABA and ABA-d6 (ISTD). For this purpose, six blank samples corresponding to 150 µl-replicates of a re-dissolved RBCs extract were processed through LLE (as described in 2.5.) and the resulting dry pellet was subsequently supplemented with 150 µL of ABA at 5 ng/mL and 25 µL of ISTD at 1 ng/mL. The same amounts of ABA and ISTD were added in parallel to three clean tubes. The derivatization reaction with PA (explained in 2.5.) was thereafter performed in all nine tubes. Matrix effect in both ABA and ISTD was calculated by means of the comparison between the responses of the RBCs extract blank samples spiked after LLE and the solvent standards prepared in clean tubes.

3. Results

3.1. P. falciparum growth inhibition by inhibitors of the C_{40}-carotenoid biosynthetic pathway

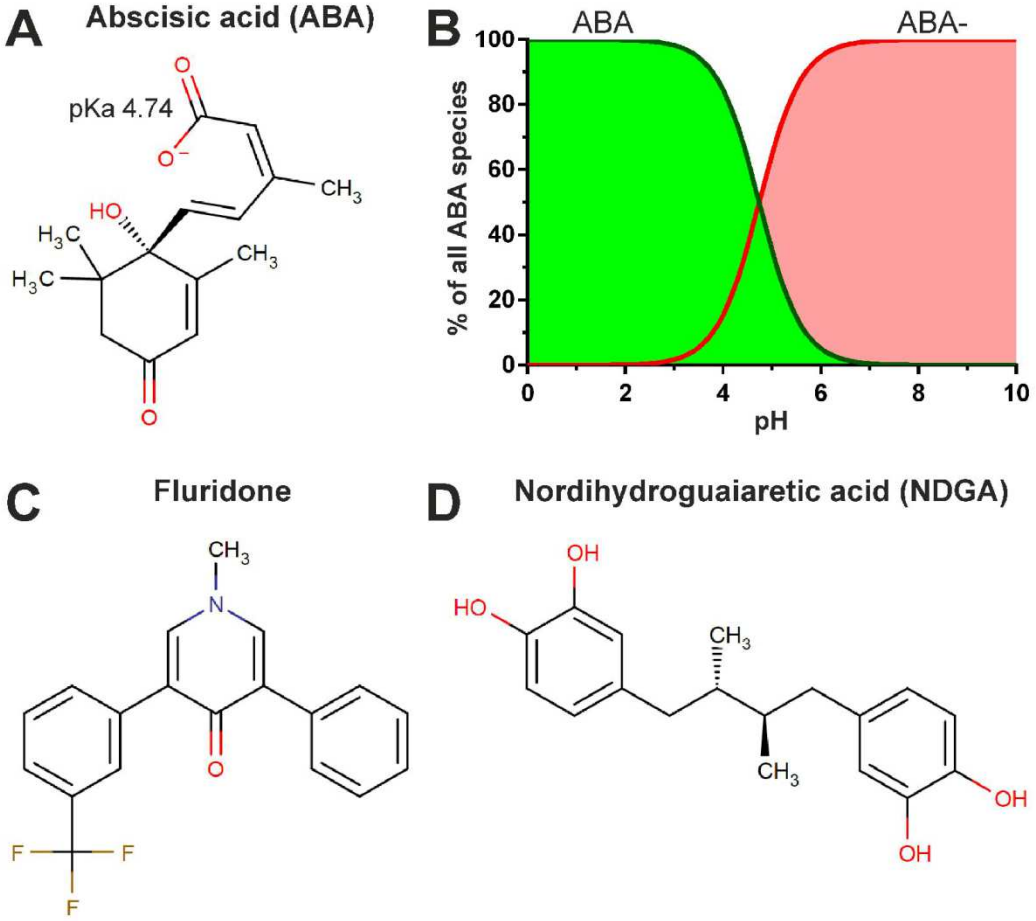

Fig. 1. Molecular structure and major ionization forms at physiological pH of ABA and fluridone/NDGA C_{40}-CBP inhibitors. (A) ABA structure and (B) relative abundances of its ionization species as a function of solution pH. (C) Fluridone structure. (D) NDGA structure. ABA pKa value and molecular structures were retrieved from http://www.chemicalize.org/.

The effect over parasite growth of two well known compounds interfering with the C_{40}-carotenoid biosynthetic pathway (C_{40}-CBP), and therefore directly affecting the production of downstream carotenoids as possible precursor molecules for a hypothesized ABA synthesis, was analyzed in *P. falciparum in vitro* cultures. The herbicide fluridone (Fig. 1C) inhibits the phytoene desaturase enzyme (PDS) at the beginning of the C_{40}-CBP, whereas the nordihydroguaiaretic acid (NDGA, Fig. 1D) antioxidant compound targets the lipoxygenase-like 9-cis-epoxycarotenoid dioxygenase (or neoxanthin cleavage enzyme, NCED) at the end of the route [46], [47]. Importantly, NCED is responsible for the dioxygenation step that cleaves 9-*cis*-neoxanthin and 9-*cis*-violaxanthin downstream of C_{40}-carotenoids. Such process generates the intermediate molecule xanthoxin, which in turn becomes subsequently processed in the cell cytoplasm to ABA-aldehyde and finally ABA. Therefore, a growth inhibitory effect of NDGA against *P. falciparum* would be indicative of cellular damage caused by the action of this antioxidant compound over essential parasite-derived metabolites likely involved in ABA biosynthesis.

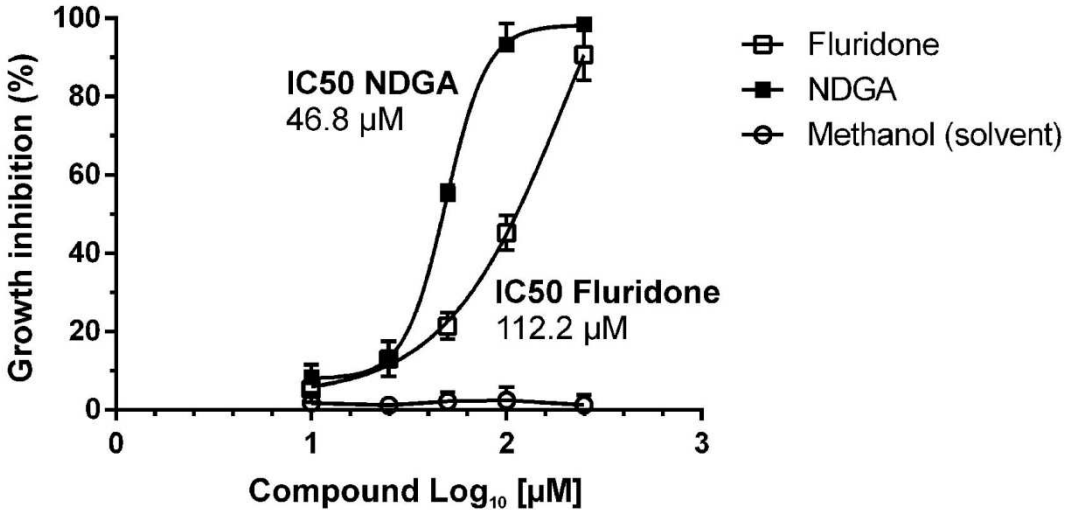

Fig. 2. *P. falciparum* growth inhibition assays of the effect of fluridone and NDGA added to ring blood stage cultures and analyzed after one replication cycle (48 h incubation).

Both fluridone and NDGA displayed activity against *P. falciparum* intraerythrocytic growth, with the respective 50%-growth inhibitory concentrations (IC50) of 112.2 and 46.8 µM (Fig. 2), in accordance with similar C_{40}-CBP inhibitors tested in *P. falciparum* and *T. gondii* [8], [9]. Parasite phenotypes similar to those described in the aforementioned works were observed during growth inhibition assays. Treated *P. falciparum* cultures displayed a significant delay in growth when compared to the untreated control (Fig. 3), feature illustrated by an increase in the number of parasites exhibiting a picnotic nucleus (phenotype indicative of cell death) after 24 h incubation in the presence of inhibitors and being particularly remarkable when parasites were treated simultaneously with both inhibitors. At the end of growth inhibition assays (48 h after the

addition of inhibitors to cultures), it was further observed a reduction in the number of parasites in the ring early maturation form together with the existence of few parasites in late forms preparing to egress (Fig. 2 and Fig. 3). All these results ultimately suggested a significant effect of fluridone and NDGA in impairing parasite development and replication. Because the observed *P. falciparum* growth-delayed phenotype was analogous to the ABA-producing *T. gondii* parasite, and considering the already known activity of NDGA as inhibitor of ABA biosynthesis, we proceeded to the optimization of ABA detection and the design of a validation method to be later applied to *P. falciparum* culture cell extracts.

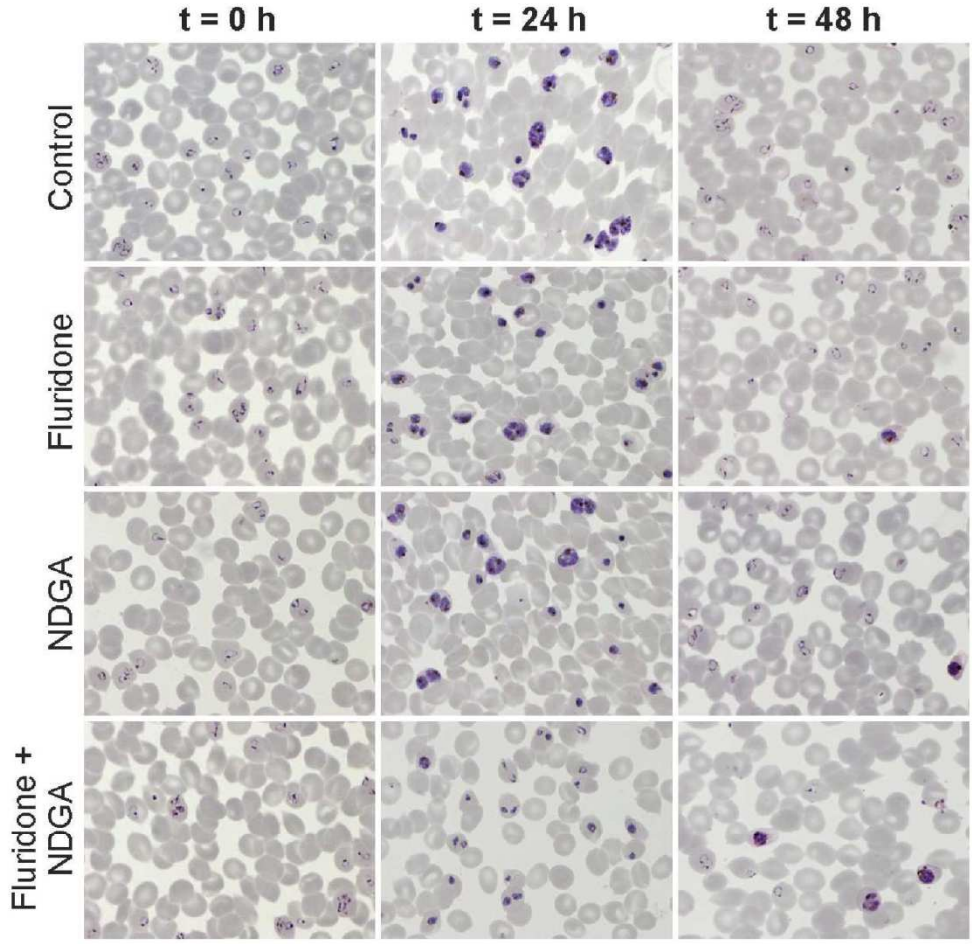

Fig. 3. Giemsa-stained, *P. falciparum* culture images corresponding to growth inhibition assays with fluridone and NDGA C_{40}-CBP inhibitors tested at their respective IC50. Samples were obtained at t = 0 h (parasites at ring stage), 24 h (trophozoite-schizont stages) and 48 h after (ring stage again in untreated cultures). Those parasites collected at 24 h were employed for ABA determination in 3.4.

3.2. Optimization of the method for ABA detection: PA derivatization and major ion transitions

The mass spectrometric parameters for PA-derivatized ABA (ABA-PA and ABA-d6-PA ISTD) were optimized in order to achieve the maximum signal. Optimized conditions are summarized in Table 1. ABA derivatization proved to notably increase the MS/MS response towards this metabolite when compared to the underivatized ABA, such effect being illustrated

by the chromatograms corresponding to the analysis of the same amounts of ABA (Fig. 4B) and ABA-PA (Fig. 4C). Remarkably, the intensity of the most abundant transition increased from 120 to 92,461 counts after ABA conjugation with PA.

Table 1. SRM method for the detection of ABA after PA derivatization (* transition used for quantification).

Analyte	Precursor ion (m/z)	Cone (V)	Collision E (eV)	Product ion (m/z)	Ion ratio
ABA-PA	355	30	22	109	0.7
			30	135	0.6
			22	**229***	1
ABA-d6-PA	361	30	22	109	0.8
			30	139	0.6
			22	**235***	1

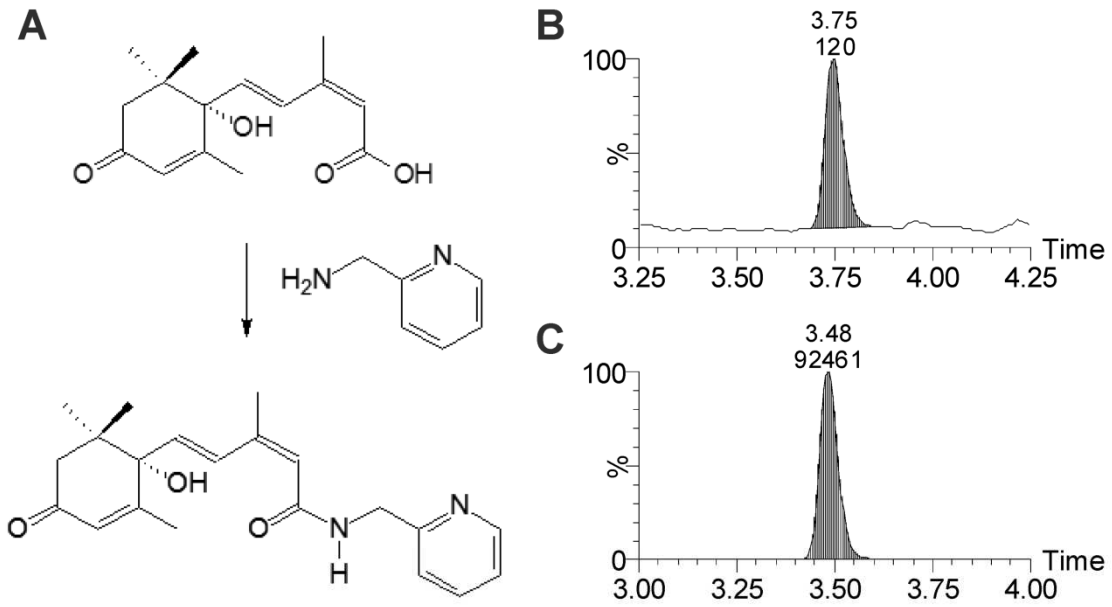

Fig. 4. ABA derivatization with PA and detection of ABA-PA vs. underivatized ABA by LC-ESI-MS/MS operating in SRM mode. (A) Derivatization reaction, (B) ABA detection in a solvent standard at 10 ng/mL using the ion transition 263 → 153 m/z as optimized in [31] and (C) ABA-PA detection in a solvent standard at 10 ng/mL using the 355 → 229 m/z major ion transition.

During the development of the method, the presence of ABA was identified in the plant-derived hemolytic agent saponin, which was used at first for the preparation of *P. falciparum*-infected RBC (pRBC) extracts. The unequivocal presence of ABA in a saponin solution, likely due to its plant origin, was proved by monitoring three different ion transitions of ABA-PA (Fig. 5). As a result, an alternative protocol based only on acetone as organic solvent was established and used in this work for the extraction of pRBCs.

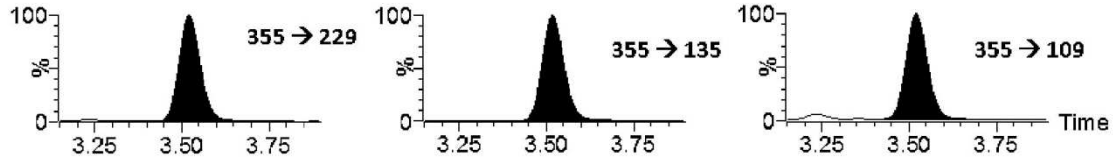

Fig. 5. Detection of ABA in 0.15% v/v saponin solution (PBS). LC-ESI-MS/MS chromatograms showing the three major ion transitions (m/z) of ABA-PA are included.

3.3. Method validation: ABA extraction recovery and RBC-matrix effects

A satisfactory liquid-liquid extraction (LLE) recovery and an adequate correlation coefficient (r = 0.998) for the studied range 0.05-10 ng/mL (Table 2) were obtained for ABA. Due to the fact that electrospray ionization is particularly prone to matrix effects, a specific study concerning this parameter was conducted. The results proved that the multiple compounds present in a complex sample such as RBC extracts in this case do not produce significant ionization enhancement or suppression, neither for ABA nor for its ISTD (Table 2). The chromatograms corresponding to the analysis of a blank RBC sample (1.2×10^{10} cells extract/mL) either alone or spiked with 0.15 ng/mL of ABA are included in Fig. 6.

Table 2. Results of the analytical parameters used for the validation of derivatized ABA quality controls. Solid Phase Extraction (SPE). Liquid-liquid extraction (LLE). Relative standard deviation (RSD). Recovery value (Rec). Limit of detection (LOD). Limit of quantification (LOQ). * % Average (% RSD).

Extraction recovery*		**Linearity**		**LOD**	**LOQ**	**Matrix effect***	
SPE	**LLE**	**Range (ng/mL)**	**r**	**(ng/mL)**	**(ng/mL)**	**ABA-PA**	**ABA-d6-PA**
36 (18)	86 (13)	0.05-10	0.998	0.03	0.15	89 (11)	95 (12)
Intra-day (n = 6)				**Inter-day (n = 12)**			
Low level (0.15 ng/mL)		**High level (1.5 ng/mL)**		**Low level (0.15 ng/mL)**		**High level (1.5 ng/mL)**	
Rec (%)	**RSD (%)**	**Rec (%)**	**RSD (%)**	**Rec (%)**	**RSD (%)**	**Rec (%)**	**RSD (%)**
93	10	113	8	96	10	116	9

Regarding sensitivity, due to the ionization improvement provided by the PA-derivative formed, the limits of detection (LOD) and quantification (LOQ) where 0.03 and 0.15 ng/mL ABA, respectively, over a RBC-based matrix of 1.2×10^{10} cells extract/mL. These results validate, up to date, this method as the most sensitive for ABA detection-quantification and, additionally, using a huge amount of RBCs extract as matrix. Furthermore, intra-day and inter-day accuracy at both tested concentrations (0.15 and 1.5 ng/mL ABA) gave excellent results with recovery values higher than 90%. Moreover, the validation results also showed the goodness of the method in terms of precision, with relative standard deviation (RSD) values equal to or below 10% in all cases.

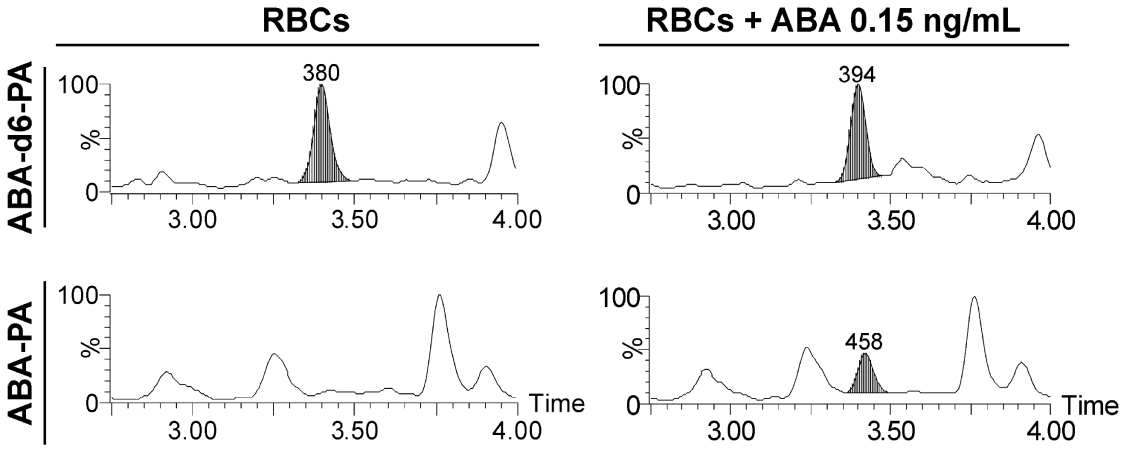

Fig. 6. LC-ESI-MS/MS chromatograms corresponding to ABA-PA and ABA-d6-PA (ISTD) for RBC blank samples (1.2×10^{10} cells extract/mL) either alone or spiked at 0.15 ng/mL ABA. Peaks obtained at the characteristic ABA-PA 355 → 229 m/z and ISTD 361 → 235 m/z major ion transitions and detected at the ISTD specific retention time are highlighted.

3.4. Application of the validated ABA detection method in P. falciparum cultures and analysis of a possible effect of C_{40}-CBP inhibitors over ABA synthesis

The already validated PA-based, LC-ESI-MS/MS method for ABA detection and quantification was applied in *P. falciparum* cultures in the trophozoite-schizont maturation stages (Fig. 3, t = 24 h) either untreated (control) or cultured in the presence of the C_{40}-CBP inhibitors fluridone and NDGA at their previously determined IC50 (Fig. 2). Total cells in culture were extracted through the lyophilization-acetone method, subsequently purified by liquid-liquid extraction plus PA derivatization and finally analyzed by LC-ESI-MS/MS: ISTD retention time of about 3.3-3.5 min and 355 → 229 m/z as major ABA-PA ion transition. Unfortunately, no peak was detected matching the aforementioned conditions (Fig. 7) indicating either the absence of ABA in pRBC extracts or its presence in amounts below the LOD of 0.03 ng/mL. Similarly, ABA could not be detected in *P. falciparum* samples treated with C_{40}-CBP inhibitors.

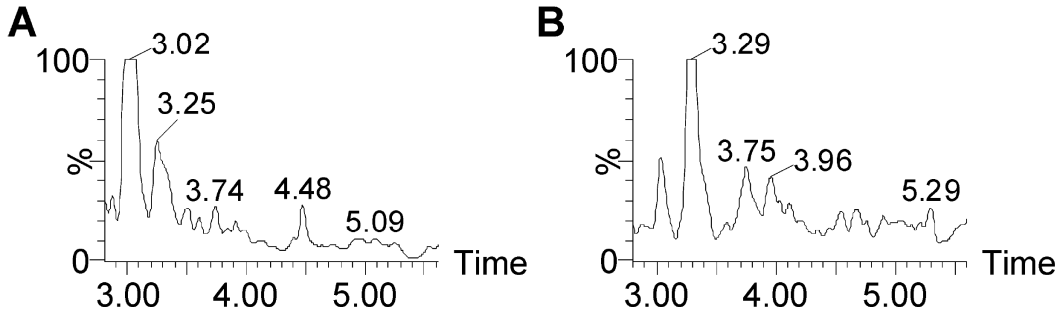

Fig. 7. ABA analysis in total cell extracts obtained from *P. falciparum* untreated cultures at the trophozoite-schizont intraerythrocytic late stages. LC-ESI-MS/MS chromatograms corresponding to (A) RBC and (B) pRBC extracts with no peak detected at the ABA-PA specific parameter conditions: ISTD retention time of 3.3 min, 355 → 229 m/z major ion transition.

4. Discussion

Several analytical approaches previously used for the quantification of ABA include ultraviolet or MS detection, either combined with high performance liquid chromatography [48] or capillary electrophoresis [49], with MS being the most powerful analytical tool because of its high sensitivity and specificity. Initial MS methods were based on gas chromatography coupled to mass spectrometry (GC–MS) [9], [50]–[52], with the highest reported sensitivity obtained by forming the pentafluorobenzyl ester of ABA and subsequently detecting this derivative in an electron capture negative ionization source (ion trap mass spectrometer [51], or a quadrupolar instrument [52]). However, this technique is not well suited for the analysis of non-volatile substances or temperature-sensitive compounds and is less sensitive than newer methodologies currently used for the detection of plant-derived ABA such as LC-ESI-MS/MS. By means of the latter approach and working in negative ion mode, excellent detection and quantification limits have been reported ranging from 0.3 to 4 ng/g dry weight [44], [53], [54].

A further improvement in the detection of compounds bearing carboxylic acids has been achieved by means of their conjugation with PA, allowing in this manner for a more sensitive detection through positive-ion mode. Nevertheless, this strategy has never been explored in the analysis of ABA. In this respect, we have successfully combined in this work an efficient LC-ESI-MS/MS system with ABA-PA derivatization, a conjugation step enabling this plant-like hormone to be quantified through selected reaction monitoring in positive ionization mode and ultimately resulting in a highly sensitive method with extraordinarily low LOD and LOQ values of 0.03 and 0.15 ng/mL ABA, respectively, besides employing a 1.2×10^{10} RBCs/mL extract as matrix. In the most sensitive determination to date using an acetone-based cell extraction and in which ABA was quantified through the negative ionization mode [54], the respective LOD and LOQ were 0.2 and 0.6 ng/g dry mass, ca. 7- and 4-fold higher, respectively, than those reported here. This improvement in ABA detection sensibility might be crucial for the analysis of this hormone in those organisms in which its presence has been suggested, such as parasitic protists of the phylum Apicomplexa including *Plasmodium* and *Babesia*, but never detected.

ABA is commonly quantified in plant extracts where sample availability is not a limitation. However, its determination in minute amounts in complex biological samples such as within intraerythrocytic apicomplexan pathogens, protist parasites that remarkably lack most of the ABA-controlled functions found in plants, requires a detailed optimization of the ABA chromatographic and mass spectrometric parameters. After choosing the right conditions for ABA purification and detection, we applied a full validation protocol using human blood as matrix in order to better characterize the newly developed method. The results presented here show that our optimized methodology is adequate for its intended purpose in terms of accuracy, precision and linearity. Importantly, as far as we know, this is the first developed and validated procedure capable of determining ABA synthesis in red blood cell-infecting parasites.

In spite of the high sensitivity of the method, ABA has not been detected in *P. falciparum* cultures. It still remains unresolved, however, by which mechanism the C_{40}-CBP inhibitors fluridone and NDGA exert their negative effect on *P. falciparum* growth. The observed NDGA antiplasmodial effect is in this regard of exceptional importance since it inhibits the neoxanthin cleavage enzyme (NCED), which is directly involved and essential for ABA synthesis in plants [19], [46], [47]. This compound has been extensively used as antioxidant agent [55]–[57] and, therefore, it should not cause any harmful effect to an organism like the malaria parasite in which reactive oxygen species are probably one of its major life-threatening concerns [58]. It is likely that an effect of NDGA on *P. falciparum* viability would consequently imply an impairment in ABA production by the intracellular parasite and would further suggest the existence of this hormone in other protist endoparasites besides *T. gondii* [9]. Remarkably, analogous signaling pathways controlling parasite egress and involving calcium-dependent protein kinases (CDPKs) to *T. gondii* have been described among apicomplexan parasites [25], [28], suggesting a possible role of ABA in these organisms as an essential element controlling diverse vital processes.

Some of the reasons that might account for the incapability of detecting ABA in *P. falciparum* cultures include: (i) its presence in a concentration below the limit of detection; (ii) the synthesis of this hormone only at a precise time of parasite maturation, such as the moment prior to escape from the host cell [9], and thereby remaining below detectable amounts during most of the parasite's intraerythrocytic cycle; and (iii) the simultaneous existence of ABA derivatives having distinct molecular masses or showing different chromatography retention times, the overall amount of unmodified-fully active ABA being regulated and diminished in this manner by the parasite. Besides, the amphiphilic properties of ABA, which are reflected in its high octanol/water partition coefficient of 123.03 units (http://www.chemicalize.org) together with the relative abundance of about 0.5-0.2 % for the ABA unionized-protonated sp. at physiological pH (Fig. 1B), would lead to a widespread distribution of this hormone throughout (i) the parasitized cell, (ii) the extracellular solution and (iii) probably reaching other cells present in the pRBC nearby such as healthy erythrocytes. All these points might eventually result in too low overall amounts of unmodified ABA in *P. falciparum* cultures below the LC-ESI-MS/MS detection level reported here of 0.03 ng/mL.

An unknown compound was detected in pRBC extracts having the same molecular mass as ABA-PA and eluting from the liquid chromatography column at the ABA-d6-PA (ISTD) characteristic retention time (3.3 to 3.5 min) but, however, displaying only the 355 → 109 m/z ion transition (Fig. 8) instead of the ABA-PA specific 355 → 229/135/109 m/z major ion transitions (Table 1). Moreover, this molecule exhibited the predicted ABA behavior after treatment with C_{40}-CBP inhibitors, being at its maximum level in untreated *P. falciparum* cultures but significantly reduced in the presence of fluridone and NDGA at their IC50. Further research is required in order to ascertain if this detected compound is actually a modified derivate of ABA

or an interfering and thus completely unrelated compound generating the ABA-PA-like 355 m/z precursor ion. Multiple derivates of ABA exhibiting diverse physicochemical properties (e.g. highly hydrophobic or comprising a modified carboxyl group) could be simultaneously present in pRBCs, a possible scenario in which the application of open metabolomic approaches would be of great interest in order to unveil the identity of such potentially existing derivates of ABA and, besides, properly understand the *P. falciparum* biological processes affected by C_{40}-CBP inhibitors.

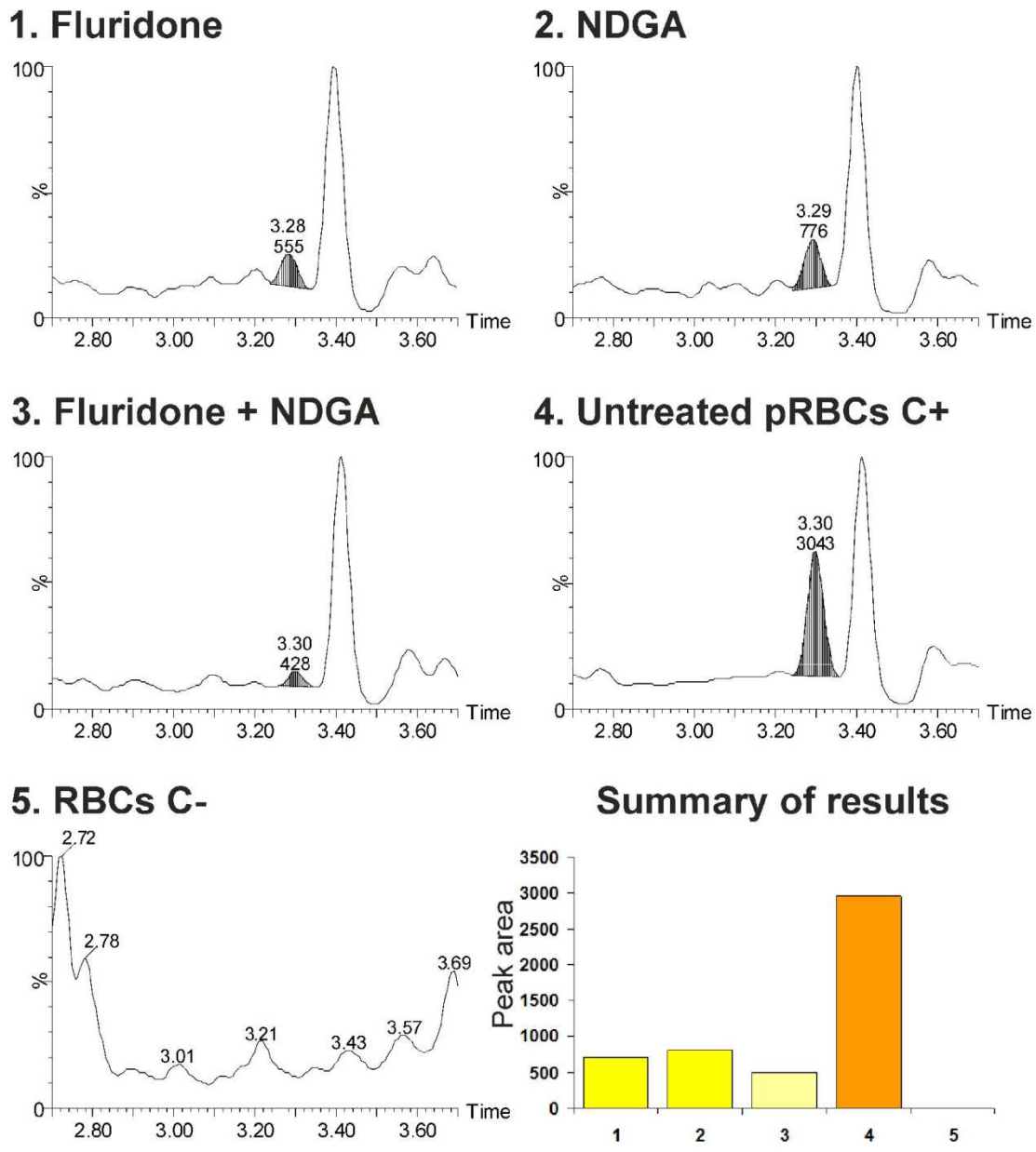

Fig. 8. Unknown compound detected in *P. falciparum* samples treated with C_{40}-CBP inhibitors and exhibiting the hypothesized behavior of ABA. (1-4) LC-ESI-MS/MS chromatograms corresponding to the total cell extracts obtained from fluridone, NDGA or untreated pRBCs. (5) RBCs as negative control. Peak detected at the ISTD retention time of 3.3. min and following the 355 →109 m/z ion transition.

5. Conclusion

The presence of a biosynthetic route for abscisic acid production in the *P. falciparum* apicomplexan parasite remains still unresolved despite the development of a highly sensitive LC-ESI-MS/MS approach for its detection, with respective LOD/LOQ values of 0.03/0.15 ng/mL and being furthermore validated in RBC matrices and finally applied to late form-pRBC extracts. Nevertheless, inhibitors affecting enzymes directly involved in ABA synthesis, such as the nordihydroguaiaretic acid acting on the NCED enzyme, arrest parasite intraerythrocytic growth prior to reaching late stages and thereby impede the subsequent infection of healthy erythrocytes. Some likely explanations for such dichotomy comprise the synthesis of ABA by the parasite in undetectable amounts, its production only at specific time points of the parasite's life-cycle or the presence of ABA derivatives with differences in their molecular mass and physicochemical properties. In this regard, further research is mandatory in order to finally resolve if *P. falciparum* and other protists of the phylum Apicomplexa besides *T. gondii* are capable of synthesizing ABA. Such discovery would provide novel parasite-specific pathways for the design of new drugs and, importantly, improved therapies against *Plasmodium* and *Babesia* RBC-infecting pathogens. Finally, the optimized method for ABA detection presented here could be applied as well to the study of this hormone in *T. gondii*.

Acknowledgements

This work was supported by grants BIO2014-52872-R from the Ministerio de Economía y Competitividad (MINECO), Spain, which included FEDER funds, and 2014-SGR-938 from the Generalitat de Catalunya, Spain. A fellowship from the Subprograma de Formación de Personal Investigador, MINECO, Spain, is acknowledged by E.M. The Spanish Health National System is acknowledged for O. J. Pozo contract (MS10/00576).

References

[1] World Health Organization, "World malaria report 2014," Switzerland, 2014.

[2] A. M. Kjemtrup and P. A. Conrad, "Human babesiosis: An emerging tick-borne disease," *International Journal for Parasitology*, vol. 30, no. 12–13. pp. 1323–1337, 2000.

[3] C. a. Lobo, J. R. Cursino-Santos, A. Alhassan, and M. Rodrigues, "Babesia: An Emerging Infectious Threat in Transfusion Medicine," *PLoS Pathog.*, vol. 9, no. 7, pp. 9–11, 2013.

[4] K. Kim and L. M. Weiss, "Toxoplasma gondii: The model apicomplexan," *International Journal for Parasitology*, vol. 34, no. 3. pp. 423–432, 2004.

[5] E. Scallan, R. M. Hoekstra, F. J. Angulo, R. V. Tauxe, M. A. Widdowson, S. L. Roy, J. L. Jones, and P. M. Griffin, "Foodborne illness acquired in the United States-Major pathogens," *Emerg. Infect. Dis.*, vol. 17, no. 1, pp. 7–15, 2011.

[6] J. Wiesner, a Reichenberg, S. Heinrich, M. Schlitzer, and H. Jomaa, "The plastid-like organelle of apicomplexan parasites as drug target.," *Curr. Pharm. Des.*, vol. 14, no. 9, pp. 855–871, 2008.

[7] I. Coppens, "Targeting lipid biosynthesis and salvage in apicomplexan parasites for improved chemotherapies.," *Nat. Rev. Microbiol.*, vol. 11, no. 12, pp. 823–35, 2013.

[8] R. Tonhosolo, F. L. D'Alexandri, V. V de Rosso, M. L. Gazarini, M. Y. Matsumura, V. J. Peres, E. F. Merino, J. M. Carlton, G. Wunderlich, A. Z. Mercadante, E. A. Kimura, and A. M. Katzin, "Carotenoid biosynthesis in intraerythrocytic stages of Plasmodium falciparum.," *J. Biol. Chem.*, vol. 284, no. 15, pp. 9974–9985, 2009.

[9] K. Nagamune, L. M. Hicks, B. Fux, F. Brossier, E. N. Chini, and L. D. Sibley, "Abscisic acid controls calcium-dependent egress and development in Toxoplasma gondii.," *Nature*, vol. 451, no. 7175, pp. 207–210, 2008.

[10] R. Howe, M. Kelly, J. Jimah, D. Hodge, and A. R. Odoma, "Isoprenoid biosynthesis inhibition disrupts Rab5 localization and food vacuolar integrity in Plasmodium falciparum," *Eukaryot. Cell*, vol. 12, no. 2, pp. 215–223, 2013.

[11] T. Umeda, N. Tanaka, Y. Kusakabe, M. Nakanishi, Y. Kitade, and K. T. Nakamura, "Molecular basis of fosmidomycin's action on the human malaria parasite Plasmodium falciparum," *Sci. Rep.*, vol. 1, no. Article 9, 2011.

[12] S. Baumeister, J. Wiesner, A. Reichenberg, M. Hintz, S. Bietz, O. S. Harb, D. S. Roos, M. Kordes, J. Friesen, K. Matuschewski, K. Lingelbach, H. Jomaa, and F. Seeber, "Fosmidomycin uptake into Plasmodium and Babesia-infected erythrocytes is facilitated by parasite-induced new permeability pathways," *PLoS One*, vol. 6, no. 5, 2011.

[13] S. C. Nair, C. F. Brooks, C. D. Goodman, A. Strurm, G. I. McFadden, S. Sundriyal, J. L. Anglin, Y. Song, S. N. J. Moreno, and B. Striepen, "Apicoplast isoprenoid precursor synthesis and the molecular basis of fosmidomycin resistance in Toxoplasma gondii.," *J. Exp. Med.*, vol. 208, no. 7, pp. 1547–1559, 2011.

[14] S. A. Paiva and R. M. Russell, "Beta-carotene and other carotenoids as antioxidants.," *J. Am. Coll. Nutr.*, vol. 18, no. 5, pp. 426–433, 1999.

[15] J. C. Gray, J. A. Sullivan, J.-H. Wang, C. A. Jerome, and D. MacLean, "Coordination of plastid and nuclear gene expression.," *Philos. Trans. R. Soc. Lond. B. Biol. Sci.*, vol. 358, no. 1429, pp. 135–145, 2003.

[16] W. I. Gruszecki and K. Strzałka, "Carotenoids as modulators of lipid membrane physical properties," *Biochim. Biophys. Acta - Mol. Basis Dis.*, vol. 1740, no. 2, pp. 108–115, 2005.

[17] A. Alder, M. Jamil, M. Marzorati, M. Bruno, M. Vermathen, P. Bigler, S. Ghisla, H. Bouwmeester, P. Beyer, and S. Al-Babili, "The Path from -Carotene to Carlactone, a Strigolactone-Like Plant Hormone," *Science*, vol. 335, no. 6074. pp. 1348–1351, 2012.

[18] E. Nambara and A. Marion-Poll, "Abscisic acid biosynthesis and catabolism.," *Annu. Rev. Plant Biol.*, vol. 56, pp. 165–185, 2005.

[19] T. Oritani and H. Kiyota, "Biosynthesis and metabolism of abscisic acid and related compounds.," *Nat. Prod. Rep.*, vol. 20, no. 4, pp. 414–425, 2003.

[20] S.-Y. Han, N. Kitahata, K. Sekimata, T. Saito, M. Kobayashi, K. Nakashima, K. Yamaguchi-Shinozaki, K. Shinozaki, S. Yoshida, and T. Asami, "A novel inhibitor of 9-cis-epoxycarotenoid dioxygenase in abscisic acid biosynthesis in higher plants.," *Plant Physiol.*, vol. 135, no. 3, pp. 1574–1582, 2004.

[21] S. Y. Han, N. Kitahata, T. Saito, M. Kobayashi, K. Shinozaki, S. Yoshida, and T. Asami, "A new lead compound for abscisic acid biosynthesis inhibitors targeting 9-cis-epoxycarotenoid dioxygenase," *Bioorganic Med. Chem. Lett.*, vol. 14, no. 12, pp. 3033–3036, 2004.

[22] N. Fujimoto, R. Kohta, S. Kitamura, and H. Honda, "Estrogenic activity of an antioxidant, nordihydroguaiaretic acid (NDGA)," *Life Sci.*, vol. 74, no. 11, pp. 1417–1425, 2004.

[23] S. Raisuddin, S. Rahman, R. A. Ansari, H. Rehman, and S. Parvez, "Nordihydroguaiaretic acid from creosote bush (Larrea tridentata) mitigates 12- O -tetradecanoylphorbol-13-Acetate-Induced inflammatory and oxidative stress responses of tumor promotion cascade in mouse skin," *Evidence-based Complement. Altern. Med.*, vol. 2011, 2011.

[24] S. Lourido, K. Tang, and L. D. Sibley, "Distinct signalling pathways control Toxoplasma egress and host-cell invasion.," *EMBO J.*, vol. 31, no. 24, pp. 4524–34, 2012.

[25] J. D. Dvorin, D. C. Martyn, S. D. Patel, J. S. Grimley, C. R. Collins, C. S. Hopp, A. T. Bright, S. Westenberger, E. Winzeler, M. J. Blackman, D. A. Baker, T. J. Wandless, and M. T. Duraisingh, "A plant-like kinase in Plasmodium falciparum regulates parasite egress from erythrocytes.," *Science*, vol. 328, no. 5980, pp. 910–912, 2010.

[26] M. Enomoto, S. ichiro Kawazu, S. Kawai, W. Furuyama, T. Ikegami, J. ichi Watanabe, and K. Mikoshiba, "Blockage of spontaneous ca2+ oscillation causes cell death in intraerythrocitic plasmodium falciparum," *PLoS One*, vol. 7, no. 7, 2012.

[27] E. Mossaad, M. Asada, D. Nakatani, N. Inoue, N. Yokoyama, O. Kaneko, and S. Kawazu, "Calcium ions are involved in egress of Babesia bovis merozoites from bovine erythrocytes," *J. Vet. Med. Sci.*, vol. 77, no. 1, pp. 53–58, 2015.

[28] R. Hui, M. El Bakkouri, and L. D. Sibley, "Designing selective inhibitors for calcium-dependent protein kinases in apicomplexans," *Trends Pharmacol. Sci.*, vol. 36, no. 7, pp. 452–460, 2015.

[29] C. R. Collins, F. Hackett, M. Strath, M. Penzo, C. Withers-Martinez, D. A. Baker, and M. J. Blackman, "Malaria Parasite cGMP-dependent Protein Kinase Regulates Blood Stage Merozoite Secretory Organelle Discharge and Egress," *PLoS Pathog.*, vol. 9, no. 5, 2013.

[30] J. D. Dvorin, J. D. Dvorin, D. C. Martyn, S. D. Patel, J. S. Grimley, C. R. Collins, C. S. Hopp, A. T. Bright, S. Westenberger, E. Winzeler, M. J. Blackman, D. A. Baker, T. J. Wandless, and M. T. Duraisingh, "A Plant-Like Kinase in Plasmodium Egress from Erythrocytes," vol. 910, no. 2010, pp. 10–13, 2014.

[31] A. Gómez-Cadenas, O. J. Pozo, P. García-Augustín, and J. V Sancho, "Direct analysis of abscisic acid in crude plant extracts by liquid chromatography--electrospray/tandem mass spectrometry.," *Phytochem. Anal.*, vol. 13, no. 4, pp. 228–234, 2002.

[32] A. Durgbanshi, V. Arbona, O. Pozo, O. Miersch, J. V. Sancho, and A. Gómez-Cadenas, "Simultaneous determination of multiple phytohormones in plant extracts by liquid chromatography-electrospray tandem mass spectrometry," *J. Agric. Food Chem.*, vol. 53, no. 22, pp. 8437–8442, 2005.

[33] Z. Ma, L. Ge, A. S. Y. Lee, J. W. H. Yong, S. N. Tan, and E. S. Ong, "Simultaneous analysis of different classes of phytohormones in coconut (Cocos nucifera L.) water using high-performance liquid chromatography and liquid chromatography-tandem mass spectrometry after solid-phase extraction," *Anal. Chim. Acta*, vol. 610, no. 2, pp. 274–281, 2008.

[34] S. Hou, J. Zhu, M. Ding, and G. Lv, "Simultaneous determination of gibberellic acid, indole-3-acetic acid and abscisic acid in wheat extracts by solid-phase extraction and liquid chromatography-electrospray tandem mass spectrometry," *Talanta*, vol. 76, no. 4, pp. 798–802, 2008.

[35] M. Almeida Trapp, G. D. De Souza, E. Rodrigues-Filho, W. Boland, and A. Mithöfer, "Validated method for phytohormone quantification in plants," *Front. Plant Sci.*, vol. 5, no. August, pp. 1–11, 2014.

[36] L. Xiong and J.-K. Zhu, "Regulation of abscisic acid biosynthesis.," *Plant Physiol.*, vol. 133, no. 1, pp. 29–36, 2003.

[37] C. Liang, Y. Wang, Y. Zhu, J. Tang, B. Hu, L. Liu, S. Ou, H. Wu, X. Sun, J. Chu, and C. Chu, "OsNAP connects abscisic acid and leaf senescence by fine-tuning abscisic acid biosynthesis and directly targeting senescence-associated genes in rice.," *Proc. Natl. Acad. Sci. U. S. A.*, vol. 111, no. 27, pp. 10013–8, 2014.

[38] T. Higashi, T. Ichikawa, S. Inagaki, J. Z. Min, T. Fukushima, and T. Toyo'oka, "Simple and practical derivatization procedure for enhanced detection of carboxylic acids in liquid chromatography-electrospray ionization-tandem mass spectrometry.," *J. Pharm. Biomed. Anal.*, vol. 52, no. 5, pp. 809–818, 2010.

[39] X. Li and A. A. Franke, "Improved LC-MS method for the determination of fatty acids in red blood cells by LC-orbitrap MS," *Anal. Chem.*, vol. 83, no. 8, pp. 3192–3198, 2011.

[40] S. Cranmer, C. Magowan, J. Liang, R. Coppel, and B. Cooke, "An alternative to serum for cultivation of Plasmodium falciparum in vitro.," *Trans R Soc Trop Med Hyg.*, vol. 91, no. 3, pp. 363–5, 1997.

[41] C. Lambros and J. P. Vanderberg, "Synchronization of Plasmodium falciparum erythrocytic stages in culture.," *J. Parasitol.*, vol. 65, pp. 418–420, 1979.

[42] A. Radfar, D. Méndez, C. Moneriz, M. Linares, P. Marín-García, A. Puyet, A. Diez, and J. M. Bautista, "Synchronous culture of Plasmodium falciparum at high parasitemia levels.," *Nat. Protoc.*, vol. 4, pp. 1899–1915, 2009.

[43] E. Moles, P. Urbán, M. B. Jiménez-Díaz, S. Viera-Morilla, I. Angulo-Barturen, M. A. Busquets, and X. Fernàndez-Busquets, "Immunoliposome-mediated drug delivery to Plasmodium-infected and non-infected red blood cells as a dual therapeutic/prophylactic antimalarial strategy," *J. Control. Release*, vol. 210, pp. 217–229, 2015.

[44] M. López-Carbonell and O. Jáuregui, "A rapid method for analysis of abscisic acid (ABA) in crude extracts of water stressed Arabidopsis thaliana plants by liquid chromatography - Mass spectrometry in tandem mode," *Plant Physiol. Biochem.*, vol. 43, no. 4, pp. 407–411, 2005.

[45] L. Tian, D. DellaPenna, and J. A. D. Zeevaart, "Effect of hydroxylated carotenoid deficiency on ABA accumulation in Arabidopsis," *Physiol. Plant.*, vol. 122, no. 3, pp. 314–320, 2004.

[46] R. A. Creelman, E. Bell, and J. E. Mullet, "Involvement of a lipoxygenase-like enzyme in abscisic Acid biosynthesis.," *Plant Physiol.*, vol. 99, no. 3, pp. 1258–1260, 1992.

[47] A. Burbidge, A. Burbidge, T. Grieve, T. Grieve, A. Jackson, A. Jackson, A. Thompson, A. Thompson, I. Taylor, and I. Taylor, "Structure and expression of a cDNA encoding a putative neoxanthin cleavage enzyme (NCE), isolated from a wilt-related tomato (Lycopersicon esculentum Mill.) library," *J. Exp. Bot.*, vol. 48, no. 12, pp. 2111–2112, 1997.

[48] P. I. I. Dobrev, L. Havlicek, M. Vagner, J. Malbeck, M. Kaminek, L. Havlíček, M. Vágner, and M. Kamínek, "Purification and determination of plant hormones auxin and abscisic acid using solid phase extraction and two-dimensional high performance liquid chromatography," *J Chromatogr A*, vol. 1075, no. 1–2, pp. 159–166, 2005.

[49] B. F. Liu, X. H. Zhong, and Y. T. Lu, "Analysis of plant hormones in tobacco flowers by micellar electrokinetic capillary chromatography coupled with on-line large volume sample stacking," *J. Chromatogr. A*, vol. 945, no. 1–2, pp. 257–265, 2002.

[50] E. A. Schmelz, J. Engelberth, H. T. Alborn, P. O'Donnell, M. Sammons, H. Toshima, and J. H. Tumlinson, "Simultaneous analysis of phytohormones, phytotoxins, and volatile organic compounds in plants.," *Proc. Natl. Acad. Sci. U. S. A.*, vol. 100, no. 18, pp. 10552–10557, 2003.

[51] A. G. Netting and B. V Milborrow, "Methane chemical ionization mass spectrometry of the pentafluorobenzyl derivatives of abscisic acid, its metabolites and other plant growth regulators," *Biol. Mass Spectrom.*, vol. 17, no. 4, pp. 281–286, 1988.

[52] P. H. Duffield and A. G. Netting, "Methods for the quantitation of abscisic acid and its precursors from plant tissues.," *Anal. Biochem.*, vol. 289, no. 2, pp. 251–259, 2001.

[53] C. M. Santiago, G. Habermann, M. R. R. Marchi, and G. J. Zocolo, "The role of matrix effects on the quantification of abscisic acid and its metabolites in the leaves of Bauhinia variegata L . using liquid chromatography combined with tandem mass spectrometry," *Brazilian J. Plant Physiol.*, vol. 24, no. 3, pp. 223–232, 2012.

[54] R. Zhou, T. M. Squires, S. J. Ambrose, S. R. Abrams, A. R. S. Ross, and A. J. Cutler, "Rapid extraction of abscisic acid and its metabolites for liquid chromatography-tandem mass spectrometry," *J. Chromatogr. A*, vol. 1010, no. 1, pp. 75–85, 2003.

[55] O. Gisvold, F. Bope, and C. H. Rogers, "A preliminary investigation of the antioxidant effect of nordihydroguaiaretic acid in cod-liver oil.," *J. Am. Pharm. Assoc. Am. Pharm. Assoc. (Baltim).*, vol. 37, no. 6, pp. 232–234, 1948.

[56] S. Guzmán-Beltrán, S. Espada, M. Orozco-Ibarra, J. Pedraza-Chaverri, and A. Cuadrado, "Nordihydroguaiaretic acid activates the antioxidant pathway Nrf2/HO-1 and protects cerebellar granule neurons against oxidative stress," *Neurosci. Lett.*, vol. 447, no. 2–3, pp. 167–171, 2008.

[57] P. Yam-Canul, Y. I. Chirino, D. J. Sánchez-González, C. M. Martínez-Martínez, C. Cruz, C. Villanueva, and J. Pedraza-Chaverri, "Nordihydroguaiaretic acid attenuates potassium dichromate-induced oxidative stress and nephrotoxicity," *Food Chem. Toxicol.*, vol. 46, no. 3, pp. 1089–1096, 2008.

[58] S. Müller, "Redox and antioxidant systems of the malaria parasite Plasmodium falciparum," *Molecular Microbiology*, vol. 53, no. 5. pp. 1291–1305, 2004.

SUMMARY OF RESULTS

Chapter 1

We have first characterized and optimized in **Chapter 1** the liposomal nanocarrier model provided by Dr. Urbán et al. (Urbán, Estelrich, Cortés, et al. 2011): DOPC-based, anti-*P. falciparum* Maurer's clefts-immunoliposome (BM1234-iLP); which importantly shares common features with the preliminary LP-based prototypes studied by Dr. Gupta and coworkers (Owais et al. 1995) including: (i) lipid compositions based on neutrally-charged, unsaturated phospholipids, (ii) the absence of PEGylation, (iii) the utilization of analogous passive drug encapsulation techniques, and (iv) the employment of low-efficiency, unstable and/or harsh antibody (Ab) coupling methods. The **BM1234-iLP model** studied here displayed in this regard a **rapid release of chloroquine (CQ) and primaquine (PQ) passively-loaded drugs** together with **low Ab coupling yields** and a **scarce targeting efficiency against live *P. falciparum*-infected red blood cells (pRBCs)**.

In the light of the above, the inclusion of **fully saturated phospholipids (DSPC lipid)** together with the employment of the **pH gradient method** as alternative and active drug encapsulation strategy has allowed to (i) the **almost complete encapsulation (>95%) of CQ and PQ** weakly basic antimalarials into LPs as well as (ii) their **stable entrapment with minimal release over time** during either storage (14 days at 4 ºC) or culture (2 days at 37 ºC) conditions. The latter drug liberation assays were performed in phosphate buffered saline (PBS) at physiological pH. Moreover, the **conjugation of N-succinimidyl S-acetylthioacetate (SATA)-derivatized Abs to maleimide-containing, PEG-grafted LPs**, which results in the highly stable and efficient thioether linkage, has provided **coupling efficiencies higher than 40%**. Furthermore, a **meaningful retention of Ab affinity** has been obtained when using a **10× SATA/Ab molar ratio** during LPs functionalization.

Additionally, thanks to the selection of a **monoclonal Ab specific for the RBC antigen glycophorin A (GPA) as targeting agent** for the vectorization of the previously optimized liposome nanocarrier, **a complete retention into RBCs/pRBCs (>95%) and targetability (~100%) were obtained for this anti-GPA immunoliposomal (GPA-iLP) model** when assayed in *P. falciparum* cultures. Remarkably, such excellent targeting results were still maintained up to the lowest iLPs amount of 0.5 µM lipid in culture. The attachment of a RBC-specific Ab enabled as well to the **recognition of erythrocytes infected by parasites at the early ring stage**.

The antiplasmodial growth inhibitory efficacy of this GPA-iLP prototype was validated both *in vitro* and *in vivo* **extraordinarily enhancing CQ activity in *P. falciparum* cultures and *P. falciparum*-infected humanized mice** (Angulo-Barturen et al. 2008). In this respect, a dosage regimen comprising four intravenous administrations of **0.5 mg CQ/kg encapsulated into GPA-iLPs cleared the parasite from mice circulation below detectable levels** (<0.01% parasitemia). Drug-loaded plain LPs had in comparison no effect over the pathogen and freely

administered CQ at 1.75 mg/kg was at least 40-fold less efficient in clearing the infection resulting in final parasitemias of ~0.4%.

Moreover, ***in vitro*** **incubation times of as short as 15 minutes were required to entirely inhibit *P. falciparum* growth** for a dose of **immunoliposomal 50-100 nM CQ** and, remarkably, **regardless of the parasite intraerythrocytic stage**. By contrast, the **same amount of CQ** delivered to *P. falciparum* cultures either in **free form or encapsulated in plain LPs**, and under the same culture conditions, **caused a negligible effect over parasites viability**. Furthermore, when the aforesaid dose of CQ-loaded, GPA-iLPs was assayed in *P. falciparum* synchronized cultures at the trophozoite-schizont late stages, daughter merozoites were capable to egress from pRBCs and invade new host RBCs but failed in maturating beyond the ring stage and even some of them displayed picnotic nuclei (feature indicative of cell death) (Kroemer et al. 2009).

Finally, it is important to mention that a **RBC-agglutinating effect was observed *in vitro* at GPA-iLP amounts of >10 µM lipid**, though lacking of hemolysis. Such adverse outcome was **remarkably important in the case of iLPs loaded with PQ due to its higher *in vitro* IC50 compared to CQ** (i.e. micromolar vs. nanomolar ranges). The amounts of iLPs employed during growth inhibition assays were in this regard 1-4 µM and 50-100 µM lipid for CQ and PQ, respectively. In spite of the aforesaid agglutination and regardless of the *P. falciparum* intraerythrocytic stage, whereas parasite growth was completely inhibited at 10 µM PQ when delivered by GPA-iLPs (30 minutes iLPs incubation with cells), no effect was detected if using free PQ or, alternatively, encapsulated into plain LPs.

Chapter 2

The optimized liposomal nanocarrier obtained in **Chapter 1** would be particularly modified in order to address a distinct target cell population, those pRBCs generating the severe malaria-associated rosettes through their binding to host RBCs (Carlson et al. 1990; Rowe et al. 1995). Such nanovector specific for rosette-forming pRBCs is described in **Chapter 2** and proposed as an innovative approach against RBC microvascular sequestration. For this purpose, **the anti-GPA Ab was replaced by anti-rosetting Abs** as alternative targeting agents that had been previously generated against the NTS-DBL1α N-terminal domain of the multivariant and parasite-encoded *Plasmodium falciparum* erythrocyte membrane protein 1 (PfEMP1) (Angeletti et al. 2013; Angeletti et al. 2012).

A **complete specificity for these novel anti-PfEMP1 immunoliposomal (PfEMP1-iLP) models was obtained towards pRBCs displaying homologous PfEMP1 variants** and **Abs rosette-disrupting activity was fully maintained after their conjugation to the liposomal carrier**. Moreover, because of the identification of **PfEMP1-iLPs stable adsorption on the**

pRBC surface as **major iLP-cell interaction mechanism** and, as a consequence, an absence of membranes fusion as well as nanovector cargo delivery, the highly hydrophobic and membrane exchangeable drug lumefantrine (LMF) was selected for *P. falciparum in vitro* growth inhibition assays.

In view of the above, LPs targeted against the $R29^{IT4var9}$ variant of PfEMP1 (R29-iLP, variant for which homologous PfEMP1-iLPs exhibited best targeting results) and encapsulating LMF significantly improved drug efficacy only after 30 minutes incubation by means of (i) an **increased parasite overall growth inhibition**, e.g. about 4-fold drug activity improvement (20% vs. 80% inhibitory efficacy considering free drug vs. iLP-encapsulated LMF) at 2 µM LMF and considering all the *P. falciparum* asexual intraerythrocytic stages present in culture, and (ii) a **selective elimination of those pRBCs displaying a rosetting phenotype** (4.5- to 6.5-fold smaller rosette disruptive IC50 within the 2^{nd} generation of parasites) when compared to freely delivered LMF.

Chapter 3

Finally, in **Chapter 3** we have investigated the possible existence of a biosynthetic pathway for abscisic acid (ABA) production in *P. falciparum* as a potential parasite-specific target route for the design of novel antimalarial compounds. The plant-like ABA synthesis through the C_{40}-carotenoid biosynthetic pathway (C_{40}-CBP), which takes place within plastid-type organelles, has already been described in the apicomplexan parasite *T. gondii* (Nagamune et al. 2008) controlling the egress of daughter parasites from the infected host cell in a process regulated by intracellular calcium release as intermediate signaling system. Moreover, the previously reported identification of an analogous calcium-dependent mechanism controlling *P. falciparum* maturation and egress (Enomoto et al. 2012; Dvorin et al. 2010; Hui et al. 2015), the latter biological process being vital for the parasite subsequent invasion of RBCs, led us to consider a possible ABA biosynthetic route in this parasite operating as starting key event regulating diverse signal transduction pathways essential for *P. falciparum* viability.

The requirement of the C_{40}-CBP for parasite growth and replication was firstly assessed by incubating *P. falciparum* cultures in the presence of inhibitors affecting key enzymes placed at distinct levels: (i) the herbicide fluridone (FLU) acting at the top of the route against the phytoene desaturase enzyme and (ii) the antioxidant agent nordihydroguaiaretic acid (NDGA). The latter compound works at the bottom of the C_{40}-CBP pathway inhibiting the neoxanthin cleavage enzyme and, therefore, would have a major role in impairing a likely production of xanthoxin by the parasite to be used as direct precursor of ABA. Remarkably, ***P. falciparum*** **intraerythrocytic growth was inhibited and arrested prior to merozoites egress after treatment with FLU and NDGA** (IC50 values of 112.2 and 46.8 µM, respectively).

Secondly, considering that ABA could be found in *P. falciparum* cultures in rather low levels, its detection was improved through derivatization with 2-picolylamine and the subsequent analysis by liquid chromatography-electrospray ionization tandem mass spectrometry (LC-ESI-MS/MS) operating in the positive ion mode. **Optimized limits of detection and quantification of 0.03 and 0.15 ng/ml ABA**, respectively, **were obtained using RBCs as matrix (1.2×10^{10} total cells extract/ml), and this ultrasensitive detection approach was applied to the analysis of pRBC extracts** obtained from *P. falciparum* cultures at the trophozoite-schizont late stages. **Unfortunately, ABA could not be detected within these parasites.**

"Nanotechnology in medicine is going to have a major impact on the survival of the human race"

Bernard Marcus

DISCUSSION

1. Joint discussion of Chapters 1 and 2: RBC- and pRBC-targeted LPs as drug delivery systems for *P. falciparum* malaria therapeutics

1.1. LPs, a practical and versatile nanocarrier

Liposome particles (LPs) have been one of the most employed nanocarriers for site-specific drug delivery strategies due to their: (i) high potential for particle surface derivatization with active molecules including targeting ligands and fluorescent markers, (ii) membrane-like structure allowing to the simultaneous entrapment of compounds displaying completely distinct physicochemical properties and (iii) biocompatibility, with very few reported cases of toxic lipids (e.g. LPs containing cationic phospholipids such as DOTAP or DSTAP) (Filion & Phillips 1997).

In this respect, throughout this PhD thesis we have (i) successfully conjugated LPs with polyclonal and monoclonal antibodies (Abs) employing distinct coupling approaches as well (Chapter 1), (ii) fluorescent phospholipids such as the rhodamine-conjugated lipid DOPE-Rho have been included in the LP formulation for labeling purposes, (iii) we have encapsulated a wide range of active agents displaying diverse physicochemical properties that comprise fully ionized fluorescent molecules (pyranine), amphiphilic drugs (e.g. the weakly basic chloroquine, CQ, and primaquine, PQ, antimalarials) and the highly hydrophobic drug lumefantrine (LMF). Furthermore, (iv) we have not observed hemolytic effects *in vitro* either for the DSPC:cholesterol:DSPE-PEG2000-Mal (85:10:5 mol%) basic LP composition used in this PhD thesis or after its conjugation with glycophorin A-specific Abs (GPA-iLP model).

Similar LP formulations composed of neutrally-charged phosphatidylcholines (PC) and cholesterol, both commonly purified from natural sources such as soybeans or egg yolk (van Hoogevest & Wendel 2014), have been previously shown an absence of detectable cytotoxic and hemolytic activity *in vitro* (Urbán, Estelrich, Cortés, et al. 2011). Moreover, although polyethylene glycol (PEG) is considered low or non biodegradable and even a few toxic cases have been reported, the polymer molar mass that we have employed of 2 kDa (PEG2000) lies within the 0.4-20 kDa safe range allowing to a complete renal clearance from the body (Knop et al. 2010).

Additional benefits not frequently noted of using LPs as nanovector of choice together with a PC:cholesterol-based lipid composition include:

- ✓ The **obtainment of highly uniform nanoparticle populations** (Fig. 28) exhibiting polydispersity indexes lower than 0.1 units by employing the lipid film hydration method, which additionally comprises multiple sonication cycles and a final extrusion step through 200 nm porous polycarbonate membranes (Moles et al. 2015). Besides, a minimal LPs size increment has been observed after their vectorization with Abs.
- ✓ **Complete solubility** and **low aggregation over time** (at least a few months at 4 ºC).

- ✓ **Easy preparation of sterically-stabilized LPs** (also known as 'stealth LPs') by incorporating PEG-grafted lipids (e.g. DSPE-PEG2000-Mal) into the nanocarrier formulation. PEGylation generates a protective steric barrier throughout the nanocarrier surface that eventually results in prolonged blood circulation times (see 3.2.2. and 3.3.1. from Introduction for a more complete explanation). More in detail, the 2kDa PEG that we have included in our LP models has been described to provide a 5 nm coating thickness (Woodle et al. 1994). Furthermore, plasma half-lives of about 12-13 h together with 20-30% retention rates into circulation 24 h after administration (both parameters being not significantly influenced by the amount of injected dose) have been reported in the literature for analogous liposomal nanocarriers in composition and PEGylation to the PC:cholesterol-based LPs developed in Chapters 1 and 2 (Fig. 29) (Papahadjopoulos et al. 1991; Allen & Hansen 1991). By contrast, similar LPs but lacking of PEG exhibited much shorter plasma half-lives of nearly 3-4 h in these works and their clearance rate from circulation was found to be dependent on the initially injected dose. It still remains to be determined in this regard the blood clearance kinetics of the GPA-iLP model, which could display considerably longer circulation times bearing in mind its efficient and stable binding to human RBCs.
- ✓ **Inclusion of derivatized, PEG-grafted lipids** containing a reactive group at the end of their PEG chain (e.g. the **DSPE-PEG2000-Mal lipid** containing a thiol-reactive maleimide moiety) into LPs additionally provides a spacer arm for a more efficient conjugation with targeting ligands (Fleiner et al. 2001). In agreement with this rationale, we have obtained increased Ab coupling efficiencies when substituting the DSPE-PEG2000-Mal lipid for DOPE-Mal (the latter lipid alternatively designated MPB-PE and, importantly, lacking of a spacer fragment). Such remarkable improvement can be observed by comparing the amounts of LP-conjugated half-Ab fragments between the LP-Mal-Ab and the LP-PEG-Mal-Ab iLP models (Fig. S11 and Fig. 6, respectively, from Chapter 1).
- ✓ **LPs having sizes >150 nm**, such as those prepared in this PhD thesis (Fig. 28), can be fully precipitated after 1 h ultracentrifugation (150,000 × g, 4 ºC) as well as entirely disrupted by means of detergent action (e.g. 2% Triton X-100 v/v in buffered solution). Both features allowing to the determination of LP-encapsulated material release kinetics.
- ✓ **Lipids do not interfere with the analysis of LP-coupled Abs** by either visible spectroscopic (e.g. Bradford or Bio-Rad protein assays) or SDS-PAGE plus protein staining methods (e.g. silver staining), fact that enables their easy quantification.
- ✓ **LP-encapsulated compounds can be easily extracted through HPLC-compatible methods** such as the biphasic chloroform/methanol-water system, which has been employed in Chapter 1 and is commonly described in the literature as well (Urbán, Estelrich, Adeva, et al. 2011), facilitating in this manner their determination at trace amounts by HPLC coupled to mass spectrometry techniques.

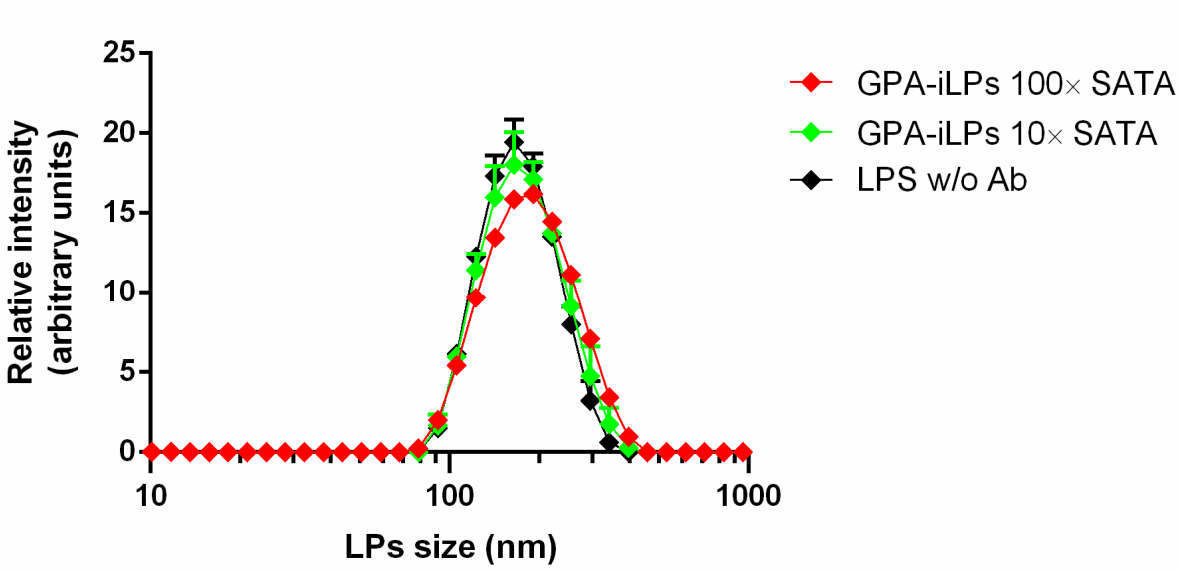

Figure 28. *Size distribution analysis of the LPs developed in Chapter 1.* LPs size-diameter (nm) was determined through Dynamic light scattering (Zetasizer series from Malvern Ltd.). (Black) Plain LPs without (w/o) Ab. (Green) and (Red) iLPs conjugated with anti-GPA Ab through their primary amines and the SATA crosslinking agent using the 10× and 100× SATA/Ab molar ratios, respectively.

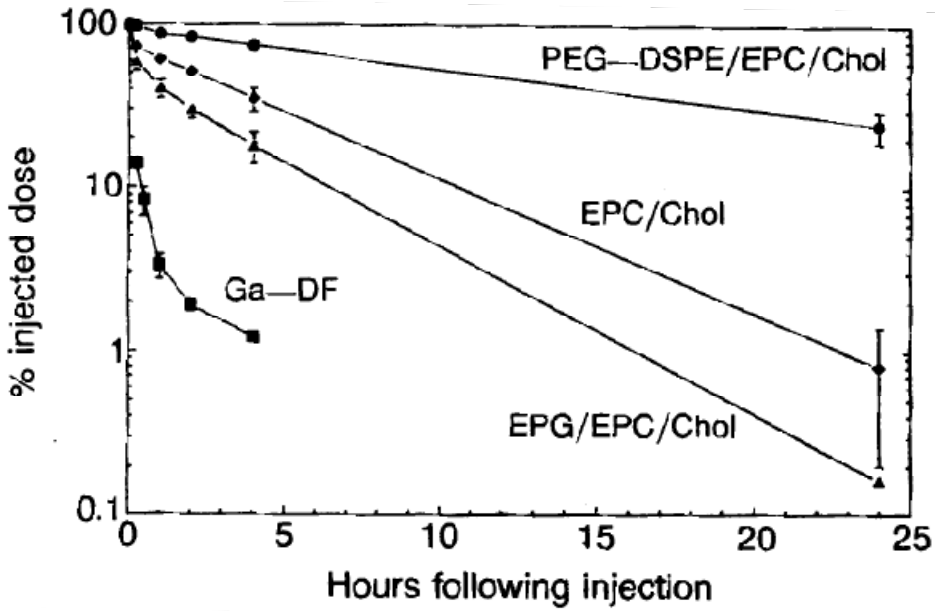

Figure 29. *LP clearance kinetics from circulation in rats.* LPs tracking was performed through their loading with ^{67}gallium-desferoxamine mesylate (^{67}Ga-DF). Conditions assayed comprise the administration of Ga-DF on its own or encapsulated into LPs composed of EPC/Chol, EPG/EPC/Chol or the PEGylated lipid mixture PEG-DSPE/EPC/Chol. Figure reproduced from (Papahadjopoulos et al. 1991). EPC (egg phosphatidylcholine), EPG (phosphatidylglycerol derived from EPC), Chol (cholesterol) and PEG-DSPE (2 kDa PEG-derivatized distearoyl phosphatidylethanolamine).

1.2. Potential drawbacks of iLP-based therapies

Nevertheless, some disadvantages are also associated with the utilization of immunoliposomal nanocarriers. The most important include:

- **Phospholipid non-enzymatic oxidation once hydrated** (Reis & Spickett 2012), degradative process that substantially limits the storage periods of LP suspensions to a maximum of a couple of months at 4 ºC. Among the currently available strategies to improve LP long-term stability, their lyophilization by incorporating lyoprotectant agents has been the most employed one (Chen et al. 2010). Nevertheless, this technique should be carefully tested for each particular LP model, considering in this regard several important factors such as the type of encapsulated drug and its concentration, LP formulation, solution pH and the surface attachment of functional agents, among others.
- **High cost of LP components**. Lipids derivatized with PEG, reactive groups or fluorescent dyes (e.g. DSPE-PEG2000-Mal, MPB-PE and DOPE-Rho) together with Abs are among the most expensive elements required for iLPs preparation, fact that is ultimately reflected in their prices (Table 3). Actually, Abs account for >95% of the BM1234- and GPA-iLPs total cost with prices per mg exceeding those of the aforementioned derivatized lipids in more than 100-fold.
- **LPs preparation further requires the availability of expensive equipment:**
  (i) **Extrusion systems** for LPs downsizing at temperatures (*T*) above lipids phase transition (T_m). In this regard, *T* higher than 65 ºC are commonly employed when handling saturated phospholipids, thereby requiring suitable extruders such as the LiposoFast LF-50 (~4,500 €, supplied by Avestin Inc.).
  (ii) **A rotary evaporator** (2-3,000 €; e.g. the Büchi® Rotavapor® distributed by Sigma-Aldrich Co., Z563994EU-1EA, with an associated cost of 2,595 €) for the removal of organic solvents from lipid components.
  (iii) **A water bath sonicator** necessary for the hydration of dried lipids obtained after rotary evaporation and the subsequent generation of unilamellar vesicles (500-2,000 €).
  (iv) Additional machinery usually required for LP characterization include a **dynamic light scattering system** for the analysis of nanoparticles size distribution (e.g. Zetasizer series from Malvern Ltd.) and an **ultracentrifuge** for LPs precipitation. Prices for these apparatus will largely depend on the supplier and the required specifications though might account for more than 50,000 €.
- **Intravenous is the only available route for iLPs administration** when following targeted drug delivery strategies, fact that restricts their application to trained health personnel. Bearing in mind their membrane-like composition and size (typically >100 nm in diameter), iLPs would get degraded and/or entrapped within body tissues if following either oral or intramuscular administration routes and finally result in minor amounts of nanocarriers reaching the bloodstream (Allen et al. 1993).

A. BM1234-iLP

Component	Reference	Supplier	µmol	MW	mg	€/mg	Date prize	Prize €
DOPC	850375C-1g	Avanti	11.38	786.11	8.95	0.14	Jun-14	1.24
Cholesterol	C8667-25G	Sigma	3.50	386.66	1.35	1.09E-02	Jul-15	1.47E-02
MPB-PE	870013C-100mg	Avanti	2.63	955.18	2.51	13.12	Mar-13	32.91
BM1234 MAb	BM1234	Acris	1.95E-03	900,000	1.75	360	Jul-15	630.26
CQ	C6628-250G	Sigma	0.88	319.87	0.28	9.18E-04	Jul-15	2.57E-04
Total prize for 1 x 20 g weight mouse treatment (4 doses, 3.5 mg CQ/kg)								**664.42**

B. GPA-iLP

Component	Reference	Supplier	µmol	MW	mg	€/mg	Date prize	Prize €
DSPC	850365C-1g	Avanti	2.19	790.15	1.73	0.13	Jun-14	0.23
Cholesterol	C8667-25G	Sigma	0.26	386.66	0.10	1.09E-02	Jul-15	1.09E-03
DSPE-PEG2000-Mal	880126P-100mg	Avanti	0.13	2941.61	0.38	6.91	Jun-14	2.63
DOPE-Rho	810150C-10mg	Avanti	1.30E-02	1301.73	0.02	33	Jun-14	0.56
Anti-GPA MAb	SM3141P	Acris	1.73E-03	150,000	0.26	2300	Jul-15	596.16
CQ	C6628-250G	Sigma	0.13	319.87	0.04	9.18E-04	Jul-15	3.67E-05
Total prize for 1 x 20 g weight mouse treatment (4 doses, 0.5 mg CQ/kg)								**599.58**

Table 3. *Calculation of the cost of a complete treatment course for a single P. falciparum-infected humanized mouse model (approximately 20 g weight) using CQ delivered through the (A) BM1234- and (B) GPA-iLPs at the doses used in Fig. 1A and Fig. 10 from Chapter 1*. Drug encapsulated amounts of 16 mg CQ/mmol lipid and 15.4 mg CQ/mmol lipid were considered for the BM1234- and GPA-iLP models, respectively. Monoclonal antibodies (MAbs) conjugation was performed at 100 mg MAb/mmol lipid.

The aforementioned high cost of LP preparation, particularly expensive in the case of iLPs, its high-priced related equipment and their mandatory intravenous administration are important disadvantages when considering the application of LP-based approaches in the fight against diseases affecting countries with insufficient and/or inadequate health centers as well as limited economic resources. Such situation is frequently found in malaria, disease that is mainly concentrated within the sub-Saharan Africa region and, as a consequence, the research of antimalarial agents having a low cost-associated production is fundamental.

In this scenario, probably the first issue that should be addressed when designing iLP-based targeted drug delivery strategies against diseases affecting low-income countries would be a considerable reduction in the Ab production cost. Prizes ranging from 200 € to >2,000 € per mg protein are commonly found when looking at the monoclonal Abs (MAbs) currently marketed (e.g. MAbs supplied by Acris Antibodies, Inc. or Sigma-Aldrich Co., Table 3). The generation of hybridoma cell lines for the production of our own MAbs would be therefore of major importance and greatly reduce the overall iLP preparation cost for more affordable antimalarial therapies.

Moreover, if we consider the improvement in drug efficacy that targeted delivery approaches provide, iLP-based therapies would be remarkably useful in those situations in which drugs delivered on their own exhibit limited or null activity and/or have a high potential risk of causing toxic side effects to the patient. Infections caused by drug-resistant parasites, patients sensitive to medication and severe clinical manifestations would be some examples. In these particular cases, the cost of immunoliposomal therapies might not be a constraint and such specific patients could be conveniently treated in the clinical centers available.

1.3. Passive encapsulation of antimalarials into LPs

Liposomal encapsulation strategies based on the entrapment of drugs at the time of LPs formation (i.e. by adding the drug directly into the lipid film hydration solution) have been the unique methodology followed for the preparation of the previously reported LP and iLP models in (Urbán, Estelrich, Adeva, et al. 2011; Marques et al. 2014; Owais et al. 1995; Pirson et al. 1979), which include the BM1234-iLP prototype further characterized in Chapter 1 and whose efficacy has been proved against *Plasmodium* infections using mainly CQ and PQ as antimalarial agents.

It is important to highlight that during these passive encapsulation approaches, unencapsulated drugs are removed by gel filtration chromatography. This step generates a drug concentration gradient inside vs. outside of the LP vesicle that in turn triggers the passive diffusion of the entrapped compound to the external solution until its concentration between all compartments-phases present in the system reaches the equilibrium (process described by the 'solubility-diffusion theory' in 3.3.4. from Introduction and Annex I). Considering that LPs only represent a minor fraction of the total solution volume (e.g. a LP concentration of 10 mM total lipid occupies only ~3.3% v/v) (Maurer et al. 2001), drugs can be thereby quickly released in times shorter than 30 min as we have described for aminoquinoline drugs passively encapsulated into unsaturated DOPC:cholesterol (80:20 mol%, DOPC-based) LPs (Chapter 1).

Such rapid leaking process would extremely decrease LP efficacy and might have as well a major impact when following targeted drug delivery strategies. Unfortunately, encapsulated CQ and PQ stability over time and their release kinetics during either storage or culture conditions has not been reported in none of the antimalarial LP prototypes mentioned above. In spite of this, if we consider their similarity in lipid composition (i.e. essentially PC:cholesterol) and the passive encapsulation strategy followed to our DOPC-based LP model, antimalarial drugs might be passively released as well from these LPs during their storage and, importantly, quickly lost upon sample dilution such as in the case of their *in vivo* administration. LPs would lose in this way most of their initially encapsulated drug payloads before reaching the target cell.

Furthermore, antimalarials at large LP bilayer-saturating amounts were employed at the time of their encapsulation in the aforesaid works (e.g. 6 mM PQ and 80 mM CQ for LPs at 10 mM total lipid in (Marques et al. 2014; Owais et al. 1995)), thereby leading to remarkably small encapsulation efficiencies (EEs) of less than 7% (Owais et al. 1995; Chandra et al. 1991) and the

resulting loss of >93% of drug payloads. These results are in accordance with the EE reported in Chapter 1 of about 5-10% and 32-34% for CQ and PQ aminoquinolines, respectively, both assayed at 10 mM drug for 10 mM total lipid.

Moreover, the incorporation of the negatively-charged lipids phosphatidylserine (PS) and gangliosides into the LP models described in (Owais et al. 1995; Pirson et al. 1979), accounting for the 10% of the total lipid molecules in both cases, might partially compensate for the rapid leakage of drugs by improving CQ and PQ stability (positively-charged drugs) once dissolved into the LP bilayer. Unfortunately, no information about this matter is given in these manuscripts.

1.4. Active encapsulation of weakly basic antimalarials into LPs through pH gradients

In an attempt to improve aminoquinoline drugs long-term encapsulation stability using LPs as nanocarriers and prevent their release after dilution of the samples, the pH gradient active loading method was explored (Cullis et al. 1991). Considering a liposomal system having a difference in pH of 4.0-7.4 inside-outside of the vesicles, if a weakly basic drug containing proton-ionizable groups is added to the sample (e.g. aminoquinoline antimalarials), this will become firstly distributed throughout all LP compartments as well as the external aqueous solution (pH 7.4). Nevertheless, its protonation-ionization degree will considerably increase once inside the LP due to its acidic aqueous core (pH 4.0, Table 4), reducing in this manner drug lipophilicity (decreased abundance of drug uncharged species) and eventually impairing its capacity to leak out from the LP once encapsulated. A more detailed explanation about CQ and PQ partitioning into a liposomal system comprising a pH gradient is included in Annex I.

Drug species (%)	**pH 4.0**	**pH 6.5**	**pH 7.4**
CQ	2.45E-09	2.42E-04	1.41E-02
CQ H^+	3.89E-03	1.22	8.90
CQ $2H^+$	100.00	98.78	91.08
PQ	3.44E-05	1.26E-02	9.99E-02
PQ H^+	86.32	99.94	99.89
PQ $2H^+$	13.68	5.01E-02	6.30E-03
LMF	1.86E-03	0.59	4.47
LMF H^+	100.00	99.41	95.53

Table 4. *Relative abundances of drug ionization species as a function of solution pH*. Data calculated by knowledge of pKa values at 25 ºC for the following weakly basic antimalarials: CQ (pKas 10.2 and 8.4 (Omodeo-Salè et al. 2009)), PQ (pKas 10.4 and 3.2 (Nair et al. 2012)) and LMF (pKa 8.73 (Amin et al. 2013)).

This pH-based active encapsulation strategy had been previously employed for the efficient entrapment of CQ and PQ (EEs of >90%) into LPs composed mainly of PC:cholesterol (e.g.

DSPC or soy-PC together with 10-16 mol% of cholesterol) and loaded with citric acid (0.1-0.2 M) as buffering agent at pH 3.0-4.0 (Qiu et al. 2008; Stensrud et al. 2000). The highest drug:lipid molar ratios displaying no harmful effect over the LP internal proton concentration (0.5:10 and 1.5:10 for CQ and PQ, respectively) were also reported in these works. Besides, the addition of DSPE-PEG2000 to the LP formulation (5 mol%) further improved the stability of encapsulated CQ (Qiu et al. 2008). Finally, it is important to mention that in spite of the improved drug encapsulation into these LP models, none of them was assayed against malaria.

In light of the above, we have used and validated in Chapter 1 the pH gradient methodology for the almost complete entrapment of CQ and PQ (EEs of >96%) into saturated DSPC:cholesterol (90:10 mol%, DSPC-based) LPs containing 0.2 M citrate buffer at pH 4.0 and suspended in a buffered-isotonic solution at pH 7.4. Remarkably, the lipid composition we have employed generates LP bilayers in the low-permeable gel phase ($L\beta'$) at temperatures below ~40 ºC (pre-transition and main transition temperatures of DSPC:cholesterol mixtures of about 40 ºC and 55 ºC, respectively) (Xiang & Anderson 1997) improving in this way the maintenance of the LP internal proton pool and the preservation of buffering agents during storage (4 ºC) and at room temperature (see 3.3.2. and 3.3.3. from Introduction for a more detailed explanation). DSPE-PEG2000-Mal was further incorporated into LPs (5 mol%) for Ab conjugation purposes and, as described in (Qiu et al. 2008), in order to improve their stability as well. In accordance with the above-mentioned works, we observed a negligible release of drugs under either storage (LPs undiluted for 2 weeks at 4 ºC) or culture conditions (LPs diluted for 2 days at 37 ºC). Interestingly, only a moderate release of PQ (~20%) was detected at the end of the latter assay likely due to its reduced ionization state at pH 4.0 in comparison with CQ (relative abundances of 13.7% and ~100% corresponding to the PQ $2H^+$ and CQ $2H^+$ ionization species, respectively, Table 4).

The next step in LP optimization will probably be the improvement in its long-lasting stability. In this regard, lyophilization-based approaches have been successfully employed for the long-term storage of citrate-loaded LPs by means of their supplementation with cryoprotectant agents such as 5% trehalose or 9.2% sucrose (Qiu et al. 2008; Stensrud et al. 2000). Remarkably, lyophilized LPs were still capable of actively-encapsulating CQ and PQ after their reconstitution displaying EEs of >90% and, therefore, indicating a minimal effect of the lyophilization process over the LP internal proton pool and the encapsulated buffering agent.

1.5. Depletion of liposomal-pH gradient systems and sustained release of drugs: CQ-/PQ-loaded, GPA-iLP model

One of the major concerns we have faced in this PhD thesis has been (i) the preservation of LP-encapsulated drug amounts after several-week storage and dilution of the samples while at the same time (ii) achieve an adequate release of the LP cargo at the desired site of action. In this regard, we decided to employ in Chapter 1 the already mentioned highly stable LP formulation DSPC:cholesterol:DSPE-PEG2000 (85:10:5 mol%) together with the citrate buffered-pH gradient

method (pH 4.0-7.5 inside-outside of the LP vesicle) as drug-encapsulating strategy of choice for the performance of both *in vitro* and *in vivo* assays against *P. falciparum*.

Nevertheless, in the light of the insignificant leakage of pH gradient-loaded CQ and PQ antimalarials observed after DSPC-based LPs dilution and a further 48 h incubation period at 37ºC, such performance could be a potential disadvantage for the correct delivery of liposomal contents into the target cell considering the limited or null fusogenic capacity of our neutrally-charged DSPC-based LP model. When conjugated with erythroid lineage-specific anti-glycophorin A Abs (GPA-iLP), these iLPs remained mostly stably adsorbed onto the surface of RBCs and pRBCs. Such scarce nanovector internalization was thereafter followed by an absence of detectable release of the iLP-encapsulated fully ionized dye pyranine into the target cell cytoplasm after 1.5 h incubation at 37 ºC.

Fortunately, as we have explained in 3.3.4. from Introduction and in Annex I as well, amphiphilic drugs do easily diffuse across lipid bilayers in the absence of pH gradients and this migratory mechanism is driven by differences in their concentration among the existing organic/aqueous phases in the system. In this regard, a depletion of the liposomal-pH gradient through the leakage of protons or, alternatively, the iLP-encapsulated buffering agent would result in the automatic release of the entrapped drug and its subsequent distribution throughout the target cell following a sustained drug delivery process.

In order to understand the mechanism underlining such important modulation of the iLP internal pH, it is important to keep in mind that citrate buffer is the principal regulatory element in our DSPC-based liposomal-pH gradient system (pH_{in}-pH_{out} 4.0-7.4). This buffering agent is encapsulated at a concentration 2,000-fold higher compared to protons (0.2 M considering all citrate buffer species vs. 1E-04 M H_3O^+) and consequently an eventual loss of H_3O^+ molecules would be simultaneously accompanied by the deprotonation of $C_6H_7O_7^-$ (citrate buffer main form at pH 4.0, Fig. 30A), ultimately leading to an insignificant iLP-internal [H_3O^+] reduction and the efficient maintenance of the pH gradient.

Furthermore, a particularly low permeability of lipid bilayers to H_3O^+/OH^- has been described under the following conditions:

- **Large transmembrane pH gradients** (≥ 3 pH units). Proton permeability coefficients (*p*) have been reported in such cases 100,000-fold smaller than in the absence of gradients, about 1E-09 vs. 1E-04 cm/sec, respectively (Deamer & Nichols 1983).

- **Incorporation of lipids with high melting temperatures and long fatty acid chains**, both having a remarkable effect in further lowering membrane permeability to protons (Elamrani & Blume 1983; Paula et al. 1996). The DSPC lipid is on this point an excellent example comprising two fully saturated 18-carbon acyl chains and a T_m at 55 ºC.

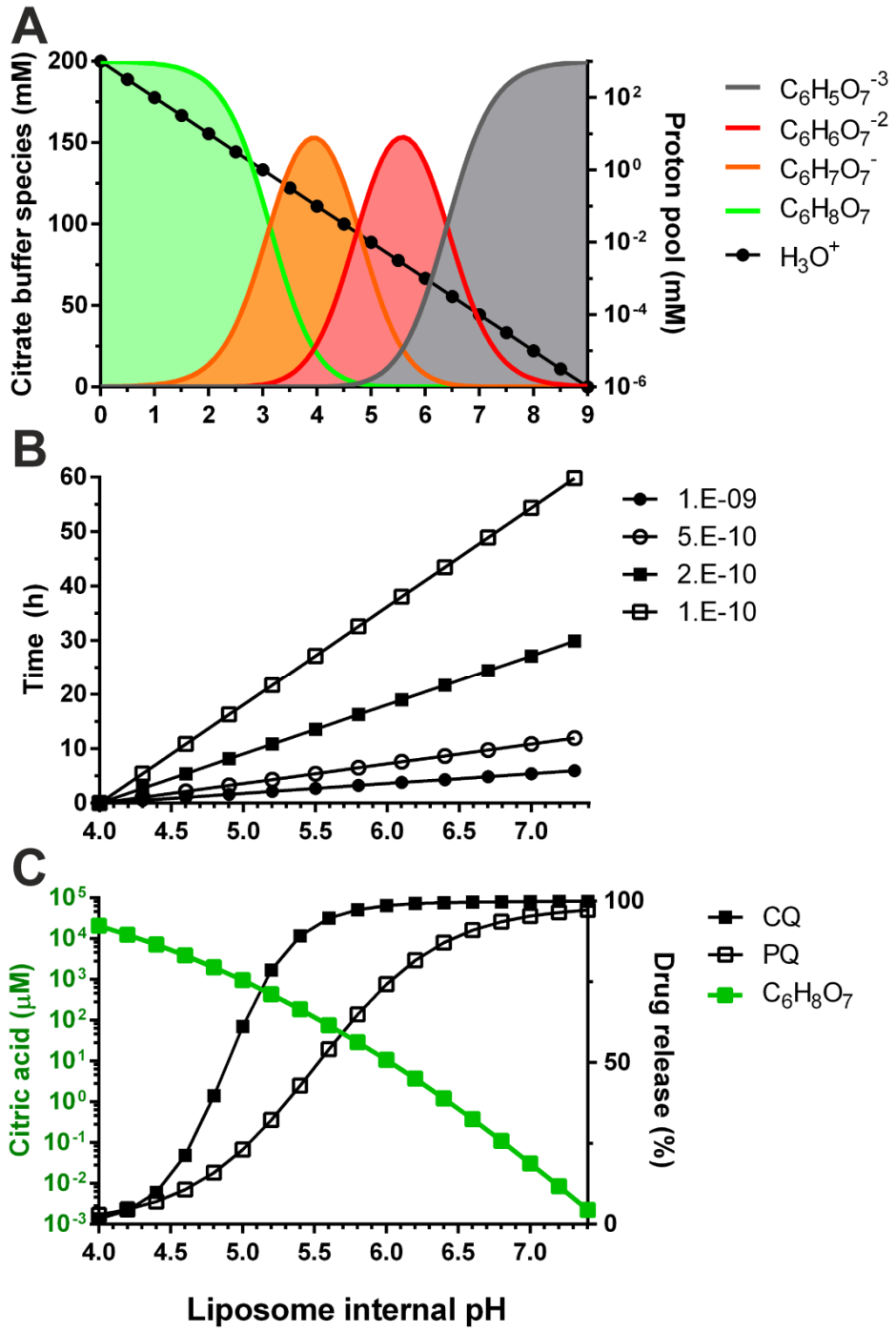

Figure 30. *Illustration of the theorized events taking place during depletion of liposomal-pH gradient systems and the subsequent release of encapsulated weakly basic drugs*. (A) Representation of the intraliposomal concentration of all citrate buffer species (pKas 3.13, 4.76 and 6.40, retrieved from Sigma-Aldrich Co.) as a function of pH. (B) Theorized times required for the increase in LP (170 nm in diameter) internal pH according to the leakage of protons through distinct permeability coefficients (1E-09 to 1E-10 cm/sec). Times calculated as described in Table 2 from Introduction. (C) Predicted liposomal release of pH gradient-loaded drugs at the highest concentrations assayed *in vitro* during *P. falciparum* growth inhibition assays (4 µM and 100 µM total lipid corresponding to 200 nM CQ and 10 µM PQ, respectively) and as a function of the LP internal proton pool. The pH-related amounts of LP internal citric acid are included for comparison. The liposomal system and the theoretical calculation of drugs release is described in Annex I.

In the light of the above considerations, proton *p* coefficients even lower than 1E-09 cm/sec might be expected in our DSPC-based liposomal-pH gradient system. Theoretical times longer than 30 min would be therefore required for this LP model in order to expel half of the internal proton pool (calculated as described in Table 2 from Introduction, $p \leq$ 1E-09 cm/sec). Remarkably, this leaking process would account for a pH increase in just 0.3 units and, consequently, a major shift in the LP internal pH from 4.0 to 7.4 units would only take place in more than 6 h (Fig. 30B). Considering the same pH difference, approximately two and a half days would be required if proton p = 1E-10 cm/sec. Furthermore, if we bear in mind the already mentioned presence of 0.2 M citrate buffering agent as principal regulatory proton source, our LP model might likely sustain the pH gradient over several weeks (as we have observed in Chapter 1 under storage conditions) or even months.

Nevertheless, such excellent system in maintaining LP internal pH has a major weakness that would allow in turn to the sustained release of encapsulated drugs. The unionized form of citrate buffer (citric acid or $C_6H_8O_7$, Fig. 30A,C) is present at a considerable amount of 20.6 mM inside of the LP (10.3% of all buffer species, pH 4.0). Similarly to other polar organic molecules, citric acid moderately diffuses across lipid bilayers and, remarkably, at a higher theoretical rate compared to protons, which makes this molecule the key membrane permeable element of our liposomal system. If we look at the physicochemical properties of citric acid, a permeability coefficient of 1E-07 cm/sec (≥ 2 orders of magnitude higher than protons) as well as an octanol/water partition coefficient (log *P*) of -1.72 have been reported (Collander et al. 1951; Gallmetzer et al. 1998). Following with this reasoning, the leakage of citric acid would be simultaneously accompanied by the protonation of $C_6H_7O_7^-$ (Fig. 30A), thereby consuming the LP internal proton pool and consequently gradually increasing the intraliposomal pH. This process would continue until citric acid is completely released and the consequent depletion of the pH gradient. In this regard, approximately 2.24 nM of citric acid would be found inside LPs at pH 7.4 upon reaching equilibrium compared to the initial 20.6 mM at pH 4.0 (Fig. 30C).

Finally, considering the encapsulation of a weakly basic drug containing proton-ionizable groups in our liposomal-pH gradient system, its release would be mostly dependent on the LP internal pH and, therefore, the amount of citric acid lost. We have represented in Fig. 30C the amounts of CQ and PQ drugs that would theoretically have been released during the *in vitro P. falciparum* growth inhibition assays performed in Chapter 1. As we can see in the figure, only an increase in 1-2 intraliposomal pH units would lead to the release of >50% of the initially encapsulated drug payload. Importantly, this sequence of events might be easily accomplished in view of:

1. The **large dilutions applied to drug-loaded, GPA-iLPs** from their 10 mM lipid stock (2,500 to 10,000-fold for CQ and 100 to 200-fold for PQ, Fig. S19 from Chapter 1).

2. The **incubation conditions used during *P. falciparum* culture** including **temperature** of 37 ºC and the **presence of membrane-destabilizing elements** such as: (i)

hydrophobic amino acids; (ii) albumin, which actually has a preference for DSPC-like ordered bilayers (Thakur et al. 2014); and (iii) lipids. These two latter ingredients originating from the AlbuMAX® II culture supplement (Thermo Fisher Scientific Inc.).

3. **iLP interaction events with the target cell** comprising (i) the transference of hydrophobic material (Fahr et al. 2005; Hefesha et al. 2011), mainly cholesterol and lipids (the latter in a much less extent), and (ii) the induction of structural malformations in iLPs through their collision with the target cell plasma membrane (Torchilin 2005).

4. **Partial consumption of the iLP internal proton pool** by the encapsulated weakly basic drugs, which become markedly protonated at pH 4.0 (Table 4). In Chapter 1, LPs at 10 mM total lipid (~2.4% v/v occupied by the vesicles internal aqueous compartment considering all LPs in solution) (Maurer et al. 2001) were supplemented with either 0.5 mM CQ or 1 mM PQ. Drug concentrations as high as 20.8 mM CQ and 41.7 mM PQ would be thereby reached inside LPs (in the light of their high EE of >95%), for which 2× and 1.14× protons are consumed per molecule (Table 4, total of 41.6/47.5 H_3O^+ molecules consumed by CQ/PQ), and ultimately resulting in the deprotonation of $C_6H_8O_7$ and $C_6H_7O_7^-$ citrate species for the maintenance of pH (Fig. 30A). All these events would lead to an overall pH increment in approximately 0.5 to 0.6 units (i.e. pH 4.5 to 4.6).

The aforesaid conditions would trigger the release of citric acid from LPs once in culture, the subsequent depletion of the liposomal-pH gradient and the final liberation of drugs. Such sustained release process has been demonstrated in Chapter 1 to occur *in vitro* late enough to allow GPA-iLPs to completely recognize RBCs/pRBCs (i.e. > 15 min) but early enough to provide an adequate delivery of antimalarials into pRBCs at early stages for their effective growth inhibition. Similarly, when the GPA-iLP model was assayed *in vivo* in *P. falciparum*-infected humanized mice, CQ was effectively delivered into RBCs and pRBCs during the extent of the assay leading to final mouse parasitemias below detectable levels. It is important to highlight that this drug release process was only observed when iLPs were incubated with *P. falciparum* cultures *in vitro* or when administered to a *P. falciparum*-infected mouse but, as already mentioned, no significant leakage of either CQ or PQ was detected during LPs storage at 4 ºC or after their dilution and 2-day incubation at 37 ºC indicating that citric acid remained still mostly encapsulated under these mild conditions.

Moreover, the observation of dead ring stage-parasites after RBCs invasion in *P. falciparum* cultures treated with CQ-loaded, GPA-iLPs might be explained by: (i) an adequate delivery of CQ into non-infected erythrocytes, (ii) its stable retention into these cells, and (iii) the subsequent inhibition of parasite growth right after RBC infection. Remarkably, this prophylactic effect had been previously reported in (Wilson et al. 2013) taking place after a first 1 h incubation of RBCs with the following antimalarials: amodiaquine (AMO), halofantrine (HAL), LMF, mefloquine (MFQ) and piperaquine (PPQ); and the later impairment of parasite development post-RBC invasion.

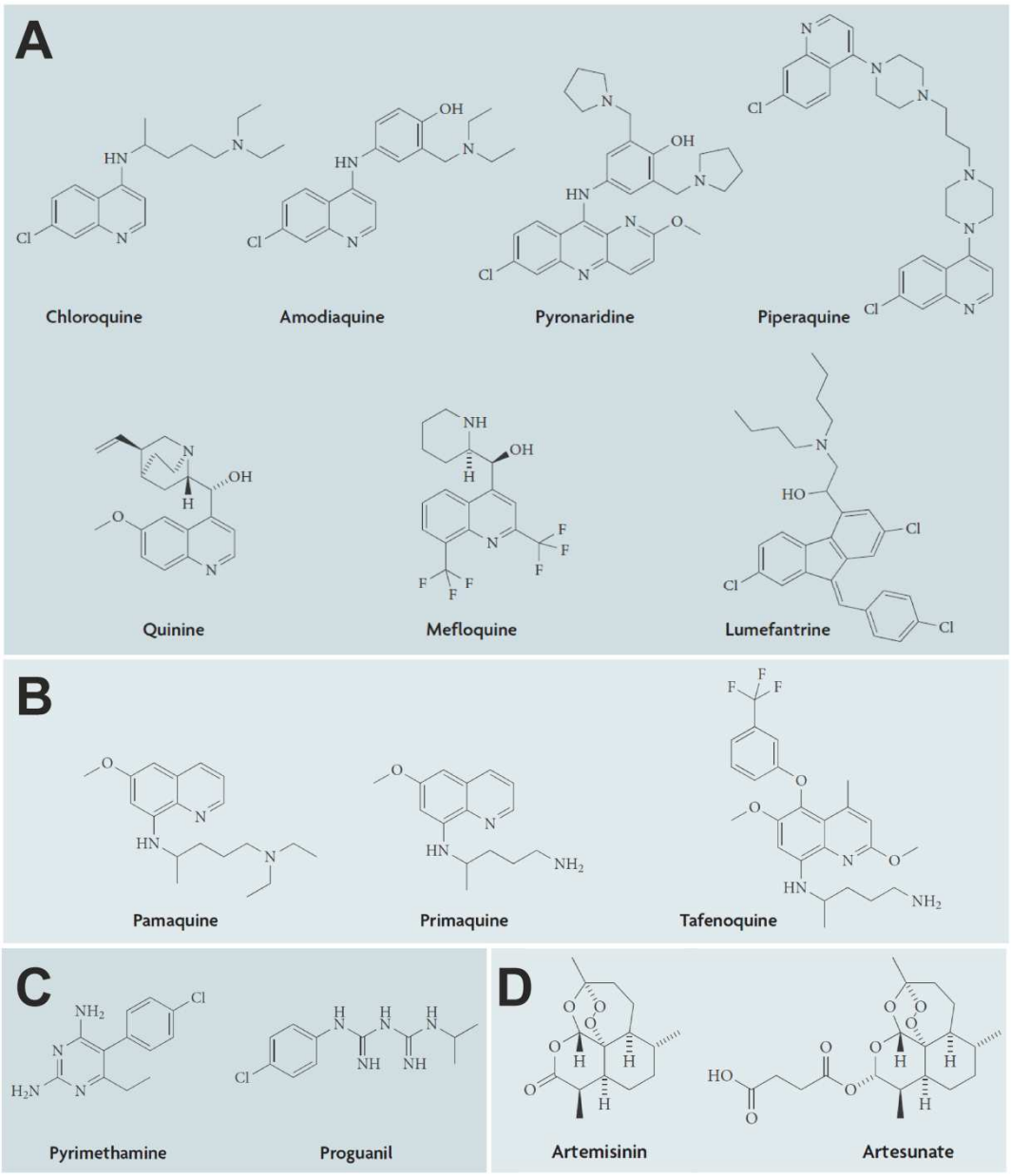

Figure 31. *Molecular structures of the main antimalarial drug families and their classification according to their suitability for our liposomal-pH gradient system.* Applicable (A) 4-aminoquinolines and amino alcohols, (B) 8-aminoquinolines and (C) protozoal dihydrofolate reductase inhibitors. (D) Not applicable drugs belonging to the artemisinin derivatives family. The physicochemical properties for all the drugs included in the figure such as: pKas and relative abundance of their ionization species as a function of solution pH, log *P*, distribution coefficient *D*, overall charge and structure; can be quickly viewed at the website http://www.chemicalize.org. Figure reproduced from (Wells et al. 2009).

If we look at the physicochemical properties of all the aforementioned antimalarials (including CQ and PQ as well), we can see that they share several major attributes (Fig. 31). Most importantly, all these compounds belong to the 4-aminoquinoline (CQ, AMO and PPQ) and amino alcohol (HAL, LMF, MFQ) antimalarial drug families. Besides, PQ is included in the 8-aminoquinolines family. Drugs from these closely related groups are (i) similar in shape and size (cylindrical and

~10 Å in length), (ii) display remarkable hydrophobic properties when uncharged (log *P* > 3.5 units, http://www.chemicalize.org), and (iii) all compounds are positively-ionized at physiological pH. Furthermore, having a look at their weakly basic moieties, we can see that in all drugs the first group to be ionized (pKas between 8.7 and 10.4 units, http://www.chemicalize.org) is located at the opposite end to the aromatic rings (Fig. 31), thereby leaving the rest of these monoprotonated molecules still lipophilic and capable of solubilizing into the lipid bilayer following an analogous mechanism to that theorized for CQ and PQ drugs in Annex I (Fig. 37).

In view of the above explanation, the particular properties of the RBC membrane (RBCM) comprising (i) a negatively-charged, sialic acid-rich glycocalyx and (ii) its asymmetric disposition of lipids, would have a major role in the intracellular accumulation of weakly basic drugs by attracting their positively-charged groups to the cell surface and, besides, stabilizing these antimalarials once dissolved into the plasma membrane (Fig. 37 from Annex I). Furthermore, the exclusion of anionic lipids into the inner leaflet of the RBCM, in which they constitute nearly the 33% of the total lipid components (Fig. 14 from Introduction) (Virtanen et al. 1998), would in turn generate an electrochemical gradient allowing to the intracellular retention and effective lipid bilayer-stabilization of drug monoprotonated species. In summary, such singular properties of the RBCM make erythrocytes:

- **Highly promising drug carriers** bearing in mind their biocompatibility and prolonged blood circulation times of about 4 months in humans (see 3.5.5. from Introduction).

- **Target of choice** for the **development of novel and clinically applicable site-specific drug delivery approaches**, such as our GPA-iLP model encapsulating either CQ or PQ antimalarials, based on a **prophylactic effect preventing *Plasmodium* intraerythrocytic growth right after infection**.

1.6. Applicability of liposomal-pH gradient systems in malaria

We have demonstrated in Chapter 1 that DSPC-based liposomal-pH gradient systems (pH_{in}-pH_{out} 4.0-7.4) can be successfully employed for the efficient encapsulation and sustained liberation of weakly basic antimalarials. Nevertheless, if we take into account the limited fusogenicity of this LP model, the sustained release of entrapped drugs is crucial so that these agents can diffuse across the target pRBC/RBC and satisfactorily reach the intraerythrocytic *P. falciparum* parasite or, alternatively, become accumulated into non-infected RBCs. Unfortunately, this condition considerably restricts the number of antimalarials that would fit into our nanovector model. In this regard and in the light of all points discussed in previous sections, the most suitable drugs should:

1. **Display unionized species at physiological pH with moderate hydrophobic properties** (e.g. log *P* values of > 0, which corresponds to ratios higher than 1:1 considering all unionized molecules distributed in organic:aqueous isovolumic phases) in

order to enable drugs to diffuse across both the LP bilayer and the plasma membrane of the target cell. Importantly, even low relative abundances of drugs unionized species at pH 7.4 would be enough for an effective delivery considering those occurring in CQ and PQ antimalarials (0.014% and 0.1% of all drug molecules, respectively, Table 4).

2. **Contain exclusively weakly basic groups** in order to become released from LPs after the depletion of their internal proton pool (i.e. through the generation of the unionized-membrane permeable species). Weakly acid groups would behave in an opposite manner exhibiting an increased ionization state (and thus reduced bilayer solubility) at lower proton concentrations.

3. **Have a shape and size similar to phospholipids** with a cross-sectional area of ~60 $Å^2$ (Maurer et al. 2001) and a maximum length of about 13.5 Å (Fig. 37 from Annex I). Such dimensions would improve drugs partition into the LP bilayer leaflets while at the same time minimize the risk of causing structural perturbations in the well-ordered arrangement of membrane-constituting lipids.

Some examples of antimalarials that fulfill the aforementioned requisites are shown in Fig. 31A-C and comprise mainly the following drug families: (i) 4- and 8-aminoquinolines, (ii) amino alcohols and (iii) antifolate compounds. Remarkably, many other antimalarials with similar properties (e.g. quinidine, lidocaine, dopamine, vincristine and codeine among others) have been successfully encapsulated into LPs through $acidic_{inside}$-$basic_{outside}$ pH gradient systems (Madden et al. 1990; Cullis et al. 1991) and applied to diseases other than malaria pointing out the large suitability of liposomal-pH gradient approaches. By contrast, atovaquone, sulfadoxine and those compounds obtained by derivatization of artemisinin (Fig. 31D) would be among the antimalarials not applicable to our LP model due to either the complete absence of ionizable moieties (null movement of molecules as a function of pH) or the presence of R-COOH/R-OH deprotonable groups at the pH range 4.0-7.5 (e.g. artesunate and atovaquone with pKas 3.77 and 5.73, respectively, http://www.chemicalize.org).

1.7. Depletion of small pH gradients and collision-based transference of hydrophobic drugs: LMF-loaded, PfEMP1-iLP model

1.7.1. Availability of PfEMP1 vs. GPA

PfEMP1 and pRBCs provide much less anchoring points in comparison with GPA and RBCs. On one hand, whereas GPA is exposed all over the RBC and pRBC surfaces, PfEMP1 is mainly located in the parasite-derived, electron-dense knobby protrusions termed ‘knobs’ (Fig. 32A-B). Moreover, cultures containing larger amounts of RBCs compared to *P. falciparum*-infected RBCs will always be required in order to preserve parasites infectivity and viability. Initial parasitemias of about 0.5 to 1%, which corresponds to 200- and 100-fold less pRBCs than RBCs, are commonly employed in this regard during *in vitro* growth inhibition assays.

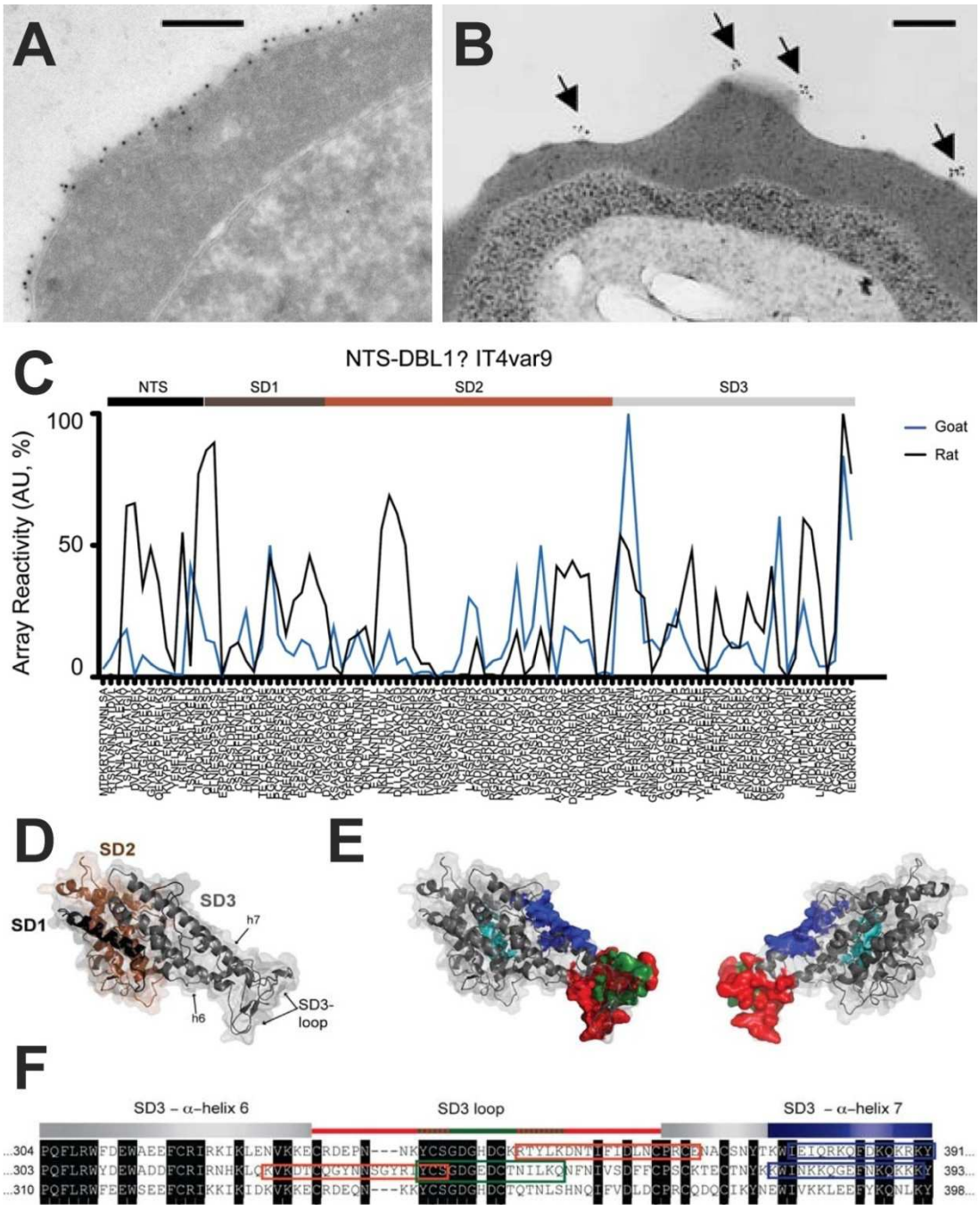

Figure 32. *Exposure of GPA and PfEMP1 antigens at the pRBC surface and illustration of the principal epitopes recognized by Abs generated against rosette-forming PfEMP1 variants*. Immuno-TEM images corresponding to pRBCs labeled with (A) anti-GPA MAb used in Chapter 1, (B) anti-PfEMP1 mAbBC6 MAb, A4 clone, reproduced from (Horrocks et al. 2005). Bars, 200 nm. PfEMP1 clusters are indicated by arrows. (C) Epitope average recognition pattern for the polyclonal Abs raised in goats (the ones used in Chapter 2) and rats against the NTS-DBL1α domain of PfEMP1-R29^{IT4var9}, reproduced from (Angeletti et al. 2013). (D) Representation of the NTS-DBL1α domain of PfEMP1-FCR3S1.2^{IT4var60} and subdomains (SDs) as well as (E) its orthogonal view displaying surface-exposed epitopes in red (M17.1 MAb used in Chapter 2) and other non-exposed in blue and green. (F) Sequence alignment of SD3 regions from R29^{IT4var9}-, FCR3S1.2^{IT4var60}- and PAvarO-PfEMP1 variants showing conserved residues in black and comprising the colored regions depicted in (E). (D-F) Figures adapted from (Angeletti et al. 2012).

Such differences in the abundance of both target cells and antigens were furthermore reflected in the number of cell-attached iLPs. Whereas GPA-iLPs were completely retained into RBCs/pRBCs for the total lipid range of 0.5-100 µM (about 10-2,000 GPA-iLPs/cell, Fig. S19 from Chapter 1) and only after 30 min incubation, less than 5% of all delivered PfEMP1-iLPs remained bound to pRBCs at 0.5 µM lipid (out of a total of nearly 900 PfEMP1-iLPs/pRBC during their incubation with *P. falciparum* cultures, Fig. S3 from Chapter 2) for the same period of time (Fig. 33). Look at Annex I for a detailed explanation about the calculation of iLPs/cell numbers.

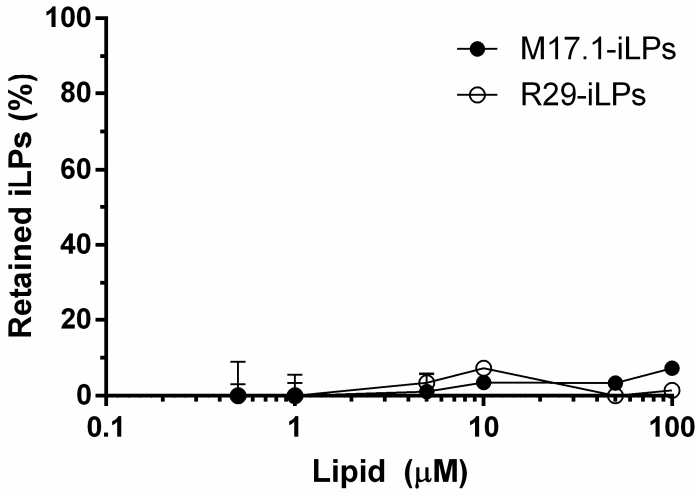

Figure 33. *PfEMP1-iLPs retention into P. falciparum cultures*. M17.1- and R29-iLPs were incubated with their homologous FCR3S1.2 and R29 *P. falciparum* rosetting strains (1% parasitemia, 1% hematocrit) in PBS-BSA for 30 min and iLP amounts in culture supernatants were determined by rhodamine fluorescence (0.5% DOPE-Rho lipid included into iLPs formulation) using several-fold dilutions of iLPs in PBS-BSA as calibration standards.

The reduced cell-binding capacity of PfEMP1-iLPs might probably be attributed to the already mentioned limited fusogenicity of the neutrally-charged DSPC-based LP formulation employed, which was indeed the same as in the GPA-iLP model. No cytoplasmic delivery of the iLP-encapsulated fluorescent dye pyranine was observed in this regard even after 3 h incubation with pRBCs. Such stable adsorption process occurring at the pRBC surface likely generates a saturation point with a maximum number of iLPs capable of binding to the cell being mostly dependent on (i) the amount of PfEMP1 molecules available for interaction as well as (ii) the number and accessibility of anchoring points-epitopes within the PfEMP1 protein that are recognized by the targeting ligand. With regard to this point, best targeting efficiencies along with a low rosette-disrupting capacity were obtained in Chapter 2 for LPs conjugated with the R29 polyclonal antibody (R29-iLP). More in detail, R29-Ab recognizes several epitopes distributed throughout the NTS region and SD1-3 subdomains (SDs) of the NTS-DBL1α fragment of the $R29^{IT4var9}$ variant of PfEMP1 (Fig. 32C-F) (Angeletti et al. 2013). Remarkably, some of these epitopes will be exposed at the pRBC surface providing R29-iLPs with multiple anchoring points but only a few of those comprised within the SD3 region would be involved in rosetting. As

described in (Angeletti et al. 2012), whereas all three SDs of PfEMP1-DBL1α can generate surface-specific Abs, only those targeting SD3 efficiently avoid the formation of rosettes.

Moreover, when the M17.1 MAb was employed as targeting agent (M17.1-iLP) less iLPs were found binding to pRBCs but, surprisingly, an increased rosette-disrupting activity was obtained for this iLP model. M17.1 MAb specifically recognizes a conformational and rosette-forming epitope from the DBL1α-SD3 loop of the FCR3S1.2^{IT4var60} variant of PfEMP1 (Fig. 32E-F). In this regard, only one MAb molecule or M17.1-iLP would be capable of either impeding or disrupting the PfEMP1-RBC interaction. However, just a single iLP would remain attached per PfEMP1 molecule in this case. Such behavior likely accounting for the reduced targeting efficiency observed for M17.1-iLPs in comparison with R29-iLPs.

A similar saturation process to PfEMP1-iLPs would be expected as well for the GPA-iLP model. Nevertheless, if we keep in mind the vast exposure of GPA (Fig. 32A) and the reported one million copies of this protein at the RBCM (Daniels & Bromilow 2013), much larger amounts of iLPs would be required in this respect in order to saturate the RBC/pRBC surfaces. Let us consider a typical erythrocyte with an approximate diameter of about 7 µm, which provides a total cell surface area of $4\times\pi\times r^2 = 1.54\times10^8$ nm^2, incubated with iLPs of nearly 170 nm in diameter. The latter corresponding to a maximum surface-occupied area of $\pi\times r^2$ = 22,700 nm^2. In this system, **a single RBC/pRBC would allow to a maximum attachment of ~6,785 GPA-iLPs** considering that the antigen is distributed throughout the whole cell surface. Remarkably, such large quantity of iLPs is well above the highest amounts that we have assayed either *in vitro* or *in vivo* (Chapter 1) with about 2,000 iLPs/erythrocyte (100 µM lipid in 2% hematocrit culture, 10 µM PQ) and nearly 100 iLPs/erythrocyte (~260 µM lipid in the bloodstream of a *P. falciparum*-infected humanized mouse, 1×10^{10} human RBCs in circulation and 0.5 mg CQ/kg), respectively. By contrast, if we take into account that PfEMP1 is primarily concentrated into knobs, its availability might be limited to only a 10-20% of the whole pRBC surface (Fig. 32B) resulting in **maximum iLP-retainable amounts of about 680 to 1,360 PfEMP1-iLPs/pRBC**.

1.7.2. Design of an alternative drug delivery approach for the pRBC membrane-saturable PfEMP1-iLP

Considering the above-mentioned limitation in the number of PfEMP1-iLPs that can remain anchored to the pRBC surface, we decided to use in this liposomal model (i) the highly hydrophobic and thereby membrane-exchangeable antimalarial drug LMF (log *P* of 9.19 units) (Amin et al. 2013) together with (ii) a small and easily breakable 10 mM phosphate-buffered pH gradient of 6.5-7.4 units inside-outside of vesicles. Remarkably, the steps comprising LPs preparation and loading of LMF as well as their later conjugation with the R29 polyclonal Ab were performed at pH 6.5. Thereafter, pH 6.5-stored iLPs were diluted into isotonic phosphate buffer at pH 7.4 just a few minutes prior to their addition to *P. falciparum* cultures. Such difference in pH of 0.9 units constitutes a small pH gradient that would theoretically reduce the amount of LMF

molecules exposed at the iLP surface. According to its weakly basic group, LMF should mostly become encapsulated within the inner leaflet of the iLP bilayer (slightly acidic pH 6.5, Table 4) following an analogous pH driven-mechanism to the already described in 1.4. and Annex I.

Later on, once in the presence of pRBCs and under culture conditions, LMF would gradually become exposed at the iLP surface and subsequently transferred to its pRBC interacting partner. This immunoliposomal system would remarkably not require the accumulation of iLPs in large numbers onto the cell surface for an effective drug delivery, such as in the case of CQ-/PQ-loaded GPA-iLPs in which drug release is performed in a long-lasting sustained manner, but the execution of a mixture of iLP-pRBC short-lived interactions and random collisions instead (Loew et al. 2011). As we observed during growth inhibition assays with the R29 iLP-parasite strain homologous pair in Chapter 2, such drug delivery mechanism based on LP-cell collisions did also effectively transferred LMF to ring stage-pRBCs (parasite form lacking of PfEMP1) improving in this manner *P. falciparum* overall growth inhibition when compared to freely supplemented LMF. Furthermore, a fraction of the total LP-encapsulated LMF might be transferred as well as intracellularly accumulated into non-infected RBCs, protecting these cells from an ulterior parasite infection as already described in 1.5. for CQ and PQ antimalarials and further reported in (Wilson et al. 2013).

In comparison with LMF-loaded LPs, a similar reduction in the percentage of late form-pRBCs was obtained when R29 *P. falciparum* cultures were treated with free LMF. Nevertheless, the observation of such a large proportion of pRBCs at the ring stage 48 h post-treatment suggested both (i) a negligible effect of free LMF over early *P. falciparum* intraerythrocytic stages as well as (ii) its incapability to avoid the egress of merozoites from pRBCs at late stages. In the latter case, freely delivered LMF might concentrate into parasites at trophozoite-schizont stages due to their acidic digestive vacuole as well as the presence of multiple membrane-bound intracellular compartments (i.e. an increased organic phase) in amounts enough to delay but not block parasite growth. The formation of drug self-aggregates due to LMF lipophilic nature might be theorized as responsible for this particular behavior, thereby reducing its capacity to become accumulated into parasitized cells and those non-infected as well compared to LP-delivered LMF.

Moreover, when looking at rosettes prevalence within those surviving late form-pRBCs at the end of growth inhibition assays (2^{nd} generation of parasites), an increased and significant removal of rosette-forming parasites was obtained when LMF was delivered through R29-iLPs in comparison with plain LPs and free LMF. Such differences could be attributed to LMF-loaded R29-iLPs improved recognition and drug transference to $R29^{IT4var9}$-expressing pRBCs. Interestingly, much moderate but still significant reduction in the percentage of rosetting parasites was found when 2 µM LMF was delivered either in free form or encapsulated into non-targeted LPs. If we bear in mind the already mentioned hydrophobic properties of LMF, this antimalarial drug could preferentially accumulate into rosettes because of their larger amounts of

membranous-lipophilic material (i.e. cellular aggregates comprising a single or a few pRBCs bound to multiple RBCs).

In summary, it is important to highlight that the proposed LP-cell collision-mediated mechanism for LMF delivery would explain both the improved parasite growth inhibitory efficacy obtained when encapsulated and the particular reduction in rosettes prevalence in the case of R29-iLPs given the large excess of both LPs and iLPs compared to pRBCs in culture. If we take into account all parasitized cells from a 1% hematocrit culture with 1% parasitemia (about 670,000 pRBCs/ml), theoretical amounts of 3.58×10^{3} and 1.43×10^{5} iLPs/pRBC can be calculated for the *in vitro* assayed LMF quantities of 0.05 and 2 µM, which corresponds in turn to 2 and 80 µM lipid (Fig. S3 from Chapter 2 and Annex I). Such large amounts considerably exceeding the aforesaid theoretical pRBC surface saturation point of nearly a thousand iLPs/pRBC. Nevertheless, if we consider a dynamic scenario in which Ab-antigen bounds are constantly broken and reformed, situation highly likely to happen bearing in mind the bulky features of our LP model (170 nm in diameter, PEGylated and containing saturated lipids), not only those iLPs interacting first with the pRBC but also others present in the cell nearby area could transfer their LMF cargo to the parasitized cell during subsequent iLP-pRBC interaction rounds.

1.8. Active encapsulation of weakly acid antimalarials into LPs through pH gradients

The LP-encapsulation and sustained release of amphipathic, proton-deionizable weakly acid antimalarials might be alternatively achieved by designing a completely opposite approach to the one described in 1.4. and 1.5. for weakly basic drugs. A weakly basic buffering agent containing proton-ionizable groups and displaying similar membrane permeability properties to citric acid (*p* = 1E-07 cm/sec and log *P* of -1.72) (Collander et al. 1951; Gallmetzer et al. 1998) would be required in this case. Considering the encapsulation of Tris buffer into LPs as a possible example (log *P* of -2.71, no data about permeability coefficient), the liberation of its unionized species (Tris base, $C_4H_{11}NO_3$) during culture conditions (e.g. stimulated by temperature or in a dilution-dependent manner) would trigger the deprotonation of its conjugate acid $C_4H_{12}NO_3^{+}$ in order to replace the molecules of Tris base lost. This process would continue until reaching equilibrium again and lowering in this way the intraliposomal pH.

Let us consider that a weakly acid drug has been actively encapsulated through a Tris-buffered pH gradient 10.0-7.4 inside-outside of the LP system. In such model, the aforementioned increase in intraliposomal proton concentration due to the leakage of Tris base would be accompanied by a protonation-charge neutralization of the simultaneously entrapped drug and its subsequent sustained release. Nevertheless, the lower buffering capacity of Tris in comparison with citrate buffer (i.e. 1 vs. 3 proton-ionizable/deionizable groups having pKas from 1.0 to 10.0 units, respectively) might result in a faster depletion of the pH gradient and, as a consequence, more unstable and less efficient drug encapsulations.

Finally, an additional mechanism for the LP-encapsulation of weakly acid compounds through the generation of transmembrane calcium acetate concentration gradients has been described in (Clerc & Barenholz 1995). Basically, this strategy relies on (i) the incorporation of calcium acetate at a high concentration into the LP (e.g. 120 mM calcium acetate at pH 6.0), which is followed by (ii) a rapid leakage of acetic acid ($C_2H_4O_2$, p > 1E-04 cm/sec) (Clerc & Barenholz 1995), and (iii) the subsequent consumption of protons by its conjugate base (acetate or $C_2H_3O_2^-$, pKa 4.75). All these steps ultimately lead to the increase of the LP internal pH and enable the simultaneous accumulation of a supplemented weakly acid drug that becomes stably precipitated in the presence of the intraliposomal calcium divalent cation (p < 1E-12 cm/sec, Table 2 from Introduction). Nalidixic acid, 5(6)-Carboxyfluorescein, diclofenac and the methylprednisolone hemisuccinate glucocorticoid are just a few examples of weak acids that have been successfully encapsulated using this methodology (Clerc & Barenholz 1995; Hwang et al. 1999; Avnir et al. 2008). However, a considerable proportion of the initially entrapped acetate buffering agent would leak out of the LP at the time of drug encapsulation, leading in turn to an easy depletion of the pH gradient and consequently a quick release of the drug if not properly precipitated once inside the LP. Furthermore and in the light of a permanent precipitation of the encapsulated drug, this strategy would not be convenient when using low fusogenic LP formulations (such as ours) in which antimalarials might not be effectively released in the presence of cells.

1.9. Clinical application of the GPA- and PfEMP1-iLP models

1.9.1. GPA-iLP

In summary, we have described in Chapter 1 an iLP model vectorized against the glycophorin A protein specific for the erythroid lineage and actively loaded with CQ and PQ antimalarials by the pH gradient method. The most important features of this GPA-iLP model that make it exceptionally interesting and potentially clinically applicable comprise:

1. **Complete retention of iLPs onto RBCs and pRBCs** *in vitro* in **<30 min** followed by the **sustained release of CQ/PQ weakly basic drugs** through a theorized **citric acid leakage** and **subsequent depletion of the intraliposomal proton pool under culture conditions**, process discussed in 1.4. and 1.5.
2. **Prophylactic activity against the intraerythrocytic cycle (IEC) of *P. falciparum*** by means of the **iLP-mediated delivery** and **stable entrapment of weakly basic antimalarials into non-infected RBCs**, mechanism discussed in 1.5.
3. The **pH gradient loading method** employed here (pH 4.0-7.4 inside-outside of vesicles) **could in principle be applied for the LP-encapsulation of all antimalarials** from the **4- and 8-aminoquinoline and amino alcohol families**, as explained in 1.6.
4. The **highly abundance of GPA** at the RBC/pRBC surfaces provides a theoretical **maximum retainable limit of ~6,785 iLPs/cell** as calculated in 1.7.1, well above the

largest amount of iLPs that we have employed *in vivo*: total of about **400 iLPs/human-RBC** considering the administration of **4 × 0.5 mg CQ/kg doses** into a single *P. falciparum*-infected humanized mouse; and allowing in this manner to a theoretical **complete retention *in vivo* of all delivered iLPs onto circulating RBCs/pRBCs**.

5. Such **efficient iLPs targeting to RBCs** together with the **capacity of these cells to accumulate weakly basic drugs inside**, would explain the **improved efficacy of CQ when delivered through GPA-iLPs to humanized mice** in which *P. falciparum* infection was cleared below detectable levels. In comparison with the iLP-vectorized drug, mice treated with free CQ at a dose 3.5-fold higher still presented infected erythrocytes at the end of the assay. Furthermore, **iLP-delivered CQ would preferentially localize into erythrocytes**, thereby **reducing its overall distribution into the body** and, as a consequence, **minimizing both the likelihood of causing toxic side effects and the generation of drug-resistant parasites**. In this regard, additional assays should be performed in the future in order to know the effectiveness and potential clinical applicability of the CQ-loaded, GPA-iLP model against *P. falciparum* resistant strains.

6. **Glycophorin A is a highly conserved and specific receptor of the erythroid lineage** with two major codominant alleles encoding for the M-N antigens, which differ only in two amino acids located at the N-terminal end of the molecule. Additional and less frequent polymorphisms are mainly positioned close to the transmembrane region leading to several antigenic forms of GPA (Reid 2009). In this regard, **antibodies generated against the N-terminal conserved region of GPA**, such as the MAb SM3141P (Acris Antibodies, Inc.) that we have employed as LP-targeting agent for both *in vitro* and *in vivo P. falciparum* growth inhibition assays, **can successfully recognize human RBCs regardless of the MNS antigens expressed**. Moreover, **given the variability of GPA in its central regions**, **the use of polyclonal Abs obtained against the full protein as targeting molecules should be avoided**. On this point, the capacity of LPs to recognize human RBCs considerably diminished when conjugated with the polyclonal Ab AP05437PU-N (Acris Antibodies, Inc.). Albumin contamination was further identified in this Ab due to antiserum-IgG affinity purification through Protein G.

7. The ability of our GPA-iLP model to bind RBCs regardless of the *P. falciparum* IEC stage allows to the effective delivery of antimalarials into the asexual ring, trophozoite and schizont forms as well as the sexual gametocyte stages. The **encapsulation of anti-gametocyte agents into our immunoliposomal system** could be therefore explored as a **clinically applicable approach blocking the transmission of parasites**. Antimalarials from the **8-aminoquinolines** family are **remarkably active against gametocytes** and currently recommended by the WHO for the reduction of *P. falciparum* transmission (Graves et al. 2014). **We have efficiently loaded GPA-iLPs with PQ** but the efficacy of this model against *P. falciparum* sexual stages has never been tested.

Nevertheless, we shall discuss the main disadvantages and those obstacles likely to be faced if considering a future clinical application of the GPA-iLP model:

1. As we have examined in 1.2., iLPs preparation must be more affordable if we want to bring this therapeutic tool to low-income countries. Probably the most important points to address would be (i) the **generation of our own MAbs** against the N-terminal region of GPA, (ii) **reduce the amount of Abs conjugated per vesicle** (about 100 Ab molecules are currently attached per LP for a total of 100 µg Ab/µmol lipid utilized during conjugation) while preserving the complete iLPs retention onto RBCs/pRBCs, and (iii) **improve iLPs storage through lyophilization-based approaches**. Alternatively, **erythrocyte-specific Abs** might be used for the **functionalization of polymer-based nanocarriers cheaper to produce than LPs** (e.g. dendritic nanoaggregates, Annex II) as a more economic approach for the targeted delivery of drugs into RBCs and pRBCs.

2. **Intravenous is the only practicable route for iLPs administration**, hampering their application to people with limited access to health centers. In this scenario and bearing in mind the considerable improvement in CQ efficacy provided by our GPA-iLP model, **iLPs utilization could be particularly directed to special cases of malaria** including (i) **patients infected with CQ-resistant strains**, (ii) **severe clinical manifestations** and (iii) **patients** sensitive to drugs or vomiting and so **unable to take oral antimalarials**.

3. We have identified **RBC-agglutination events** *in vitro* **caused by the attachment of GPA-iLPs at amounts greater than 100 iLPs/erythrocyte** and **particularly significant when binding >1,000 iLPs per cell**. The latter numbers were required when encapsulating PQ and considerably restrict in turn the employment of our immunoliposomal model to drugs displaying activities against the *P. falciparum* IEC below the micromolar range (e.g. CQ vs. PQ, *in vitro* IC50 of about 20 nM and 4 µM, respectively). This agglutinating undesired outcome might be further diminished if lowering the above-mentioned amount of nearly 100 Abs attached per LP. Finally, **humanized mice survived to 4 × ~100 iLPs/human-RBC administrations while completely clearing *P. falciparum* infection**. Nevertheless, a complete toxicity study must be performed in order to establish a maximum tolerable dose of GPA-iLPs and provide a more detailed knowledge of their potential toxic side effects.

4. **Antimalarial drugs must be selected** according to **causing an absence of harmful effects over RBC viability**. In this regard, probably the most well known contraindication would be the administration of PQ to G6PD-deficient patients, which leads to RBC oxidative damage and eventually results in hemolytic anemia. However, such undesired **toxicity of PQ could be lowered if encapsulated into LPs**, **preventing** in this manner **its metabolism in the liver and the subsequent generation of** either (i) **highly oxidizing by-products** such as the remarkably toxic 5-hydroxyprimaquine (Liu et al.

2013) or (ii) **metabolites with reduced antimalarial activity**, being carboxyprimaquine the principal metabolic product in circulation with a reported *in vitro* IC50 against liver-exoerythrocytic *P. berghei* stages of 14-fold higher than PQ (Bates et al. 1990).

5. **Glycophorin A expression** begins at the **nucleated proerythroblast**, continues throughout the distinct **erythroblast stages** to the **enucleated reticulocyte** and, finally, this protein is further present in the **mature erythrocyte** (Steinberg et al. 2009). All these cells of the erythroid lineage would potentially be recognized by GPA-iLPs and, therefore, **a possible effect of either iLPs interaction or their encapsulated antimalarial drugs over erythropoiesis should be carefully studied**. Nevertheless, if we bear in mind the huge amounts of circulating mature RBCs (~99% of all erythroid cells) and the exclusive localization of the erythrocyte precursor cells in the bone marrow, only a relatively minor fraction of the total iLPs administered would bind to these pre-RBC stages.

6. The **immunosuppressed NOD-scid gamma mouse engrafted with human RBCs** is the **unique animal capable of being infected with *P. falciparum* human-specific strains** and consequently the **only available model for this parasite at present** (Vaughan et al. 2012; Angulo-Barturen et al. 2008). Infections with *P. falciparum*-related species have been observed in gorilla, bonobos, chimpanzees and African monkeys but such parasites being genetically distinct to those pathogens affecting humans (Liu et al. 2010; Prugnolle et al. 2011; Otto et al. 2014). However, even though the aforesaid **humanized mouse model** provides a much better approximation to *P. falciparum in vivo* infections than murine-related *Plasmodium* spp., it **does also present an important disadvantage**. **These animals have no functional immune system** and, therefore, the **immunogenicity of our GPA-iLP model** as a possible **interference of such immune response against iLPs activity could not be tested**. Moreover, with regard to GPA as target molecule of choice, only **limited homology is shared between human GPA and its mouse ortholog to their four C-terminal exons** (Terajima et al. 1994), claiming to the research and utilization of other RBC-specific receptors and targeting molecules (e.g. the TER-119 Ab) (Kina et al. 2000) if considering the employment of murine *Plasmodium* spp. Besides, **full homology in the N-terminal region of human GPA** is observed when compared to **chimpanzee** (Pan troglodytes) and slightly lower but still considerable in comparison with **rhesus monkey** (Macaca mulatta) and **gorilla** (Fig. 34), being our **GPA-iLP model** probably **applicable to *P. knowlesi* infection in rhesus monkey**.

7. Finally, **in the event of triggering strong immune responses**, the GPA-iLP model could be optimized either (i) through the **preparation of Ab fragments** (e.g. Fab or $F(ab')_2$) lacking of the highly immunogenic Fc region or (ii) **conjugating the whole Ab** by means of the already employed **carbohydrate-based crosslinking approach** (LP-PEG-Mal-CHO-Ab model) in Chapter 1. Such strategy provided less amounts of LP-coupled Ab and resulted in a lower RBC-binding efficiency when compared to the primary

amines-based conjugation approach (LP-PEG-Mal-NH_2-Ab model). However, **the oriented binding of Abs through their carbohydrate-rich Fc fragment might hinder this region from the immune system surveillance**. Alternatively, **humanized Abs could also be generated**.

A

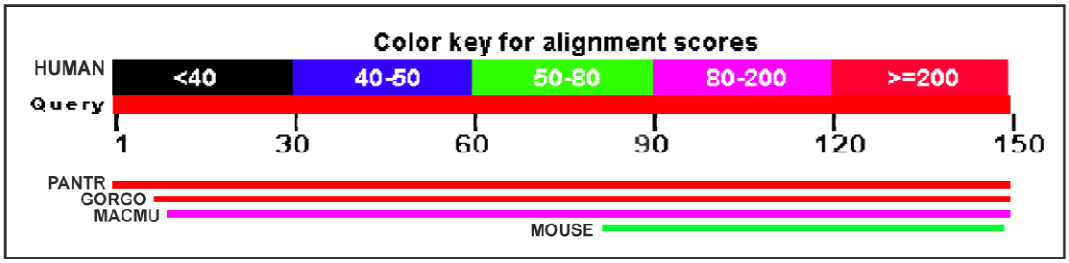

Description	Max score	Total score	Query cover	E value	Ident
sp|Q28913|GLPA_PANTR Glycophorin-A OS=Pan troglodytes GN=GYPA PE=2 SV=1	239	239	100%	9e-86	89%
tr|G3RHP3|G3RHP3_GORGO Uncharacterized protein (Fragment) OS=Gorilla gorilla gorilla GN=GYPA PE=4 SV=1	206	206	95%	7e-73	81%
gi|2564692|gb|AAB81840.1| glycophorin A, partial [Macaca mulatta]	191	191	94%	2e-67	73%
sp|P14220|GLPA_MOUSE Glycophorin-A OS=Mus musculus GN=Gypa PE=1 SV=2	62.4	62.4	44%	2e-17	51%

B

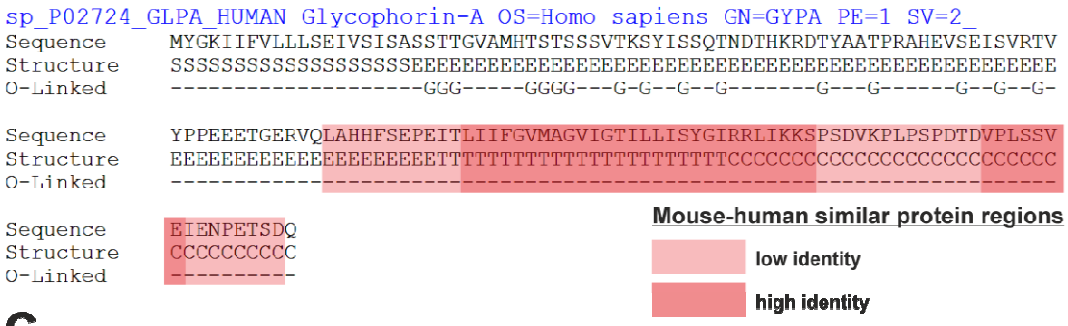

C

Score	Expect	Method	Identities	Positives	Gaps	Frame
62.4 bits(150)	2e-17()	Compositional matrix adjust.	35/68(51%)	44/68(64%)	1/68(1%)	

Features:

```
Query  83   LAHHFSEPEITLIIFGVMAGVIGTILLISYGIRRLIKKSPSDVKPLPSPDTDVPLSSVE-  141
            + H F    + LII GVMAG+IGTILLISY I R+ KKS  D++     D  VPLSS+E
Sbjct  100  IQHDFPALVMILIILGVMAGIIGTILLISYCISRMTKKSSVDIQSPEGGDNSVPLSSIEQ  159

Query  142  IENPETSD  149
             N E+S+
Sbjct  160  TPNEESSN  167
```

Query: GLPA_HUMAN
Sbjct: GLPA_MOUSE

Figure 34. *Analysis of glycophorin A protein sequence similarity among animal orthologs*. (A) Protein BLAST® (NCBI) sequence alignment using the human GPA sequence (GLPA_HUMAN UniProtKB entry) against its orthologs from pan troglodytes (GLPA_PANTR), gorilla gorilla (G3RHP3_GORGO), macaca mulatta (AAB81840.1) and mus musculus (GLPA_MOUSE). (B) Human GPA predicted structure (S, signal peptide; E, extracellular; T, transmembrane; and C, cytoplasmic regions) and glycosylation (O-Linked) sites, obtained through the OGlyco-RBF software (http://GlycoRBF.bioinfo.tw). Sequence similarity of GLPA_HUMAN compared to GLPA_MOUSE is highlighted in red. (C) Detailed human vs. mouse GPA sequence alignment by BLAST®.

1.9.2. Anti-rosetting, PfEMP1-iLP

In a nutshell, we have reported in Chapter 2 a distinct immunoliposomal approach based on the conjugation of LPs with Abs generated against rosette-forming variants of PfEMP1 for the targeted delivery of LMF into *P. falciparum* rosetting parasites. The most remarkable features to take into account when considering a possible clinical application of this rosette-specific, PfEMP1-iLP model comprise:

1. **Anti-rosetting approaches developed to date** are based on the **delivery of free agents** including **Abs against PfEMP1/RIFINs** or **highly sulfated glycosaminoglycans** as a few examples (Angeletti et al. 2013; Goel et al. 2015; Leitgeb et al. 2011; Barragan et al. 1999). Remarkably, only a **mechanical effect based on the disruption/prevention of rosettes is produced** when following most of these strategies with **no direct harmful action over parasite viability**. In this regard, the **LMF-loaded, PfEMP1-iLP model** might be a clinically applicable alternative due to its **dual activity** in (i) **disrupting rosettes at the time of administration** together with (ii) a **simultaneous growth inhibition of those parasites forming them**. PEGylated LPs would additionally display **prolonged blood circulation times** in comparison with the aforementioned freely assayed molecules.
2. Taking into account the large variability of PfEMP1 and its expression by the parasite only during intraerythrocytic late stages, the **application of our PfEMP1-iLP model would be particularly recommended to severe malaria clinical cases** in which rosette-forming, late form-pRBCs are more likely to be found and, besides, **administered in combination with antimalarial agents effective against all stages of the *P. falciparum* IEC** (e.g. freely delivered drugs or the CQ-/PQ-loaded, GPA-iLP model reported in Chapter 1) **for an efficient reduction of the overall parasite infection**. Moreover, due to the **limited cross-reactivity** displayed by the **anti-rosetting Abs employed in Chapter 2** against distinct *P. falciparum* clones and field isolates (Angeletti et al. 2013), the **research on the generation of Abs capable of recognizing multiple rosetting-linked PfEMP1 variants would be imperative**. In this regard, the rosette-forming and pRBC surface-exposed epitopes previously identified within the SD3 loop of PfEMP1-DBL1α domain might be further explored (Angeletti et al. 2012).
3. Given the **scarce docking points provided by PfEMP1 at the pRBC surface** (theoretical saturation limit of about a thousand iLPs/pRBC, as discussed in 1.7.1.), our **iLP model would additionally benefit from the incorporation of Abs specific for multiple surface-exposed regions distributed throughout the entire PfEMP1 molecule**. Following this reasoning and considering the absence of iLP-cell fusion events observed, the **loading of iLPs with membrane exchangeable drugs** (such as LMF) would be preferable. Finally, the strategy for Abs coupling should be optimized in order to avoid the formation of iLP-aggregates, which would in turn reduce the overall

number of freely available iLPs as well as ultimately result in a significant loss of material due to precipitation events or after the filter-sterilization of samples.

4. **No animal model is currently available for the study of *P. falciparum* severe malaria**, fact that might considerably delay its clinical validation. Nevertheless, the already mentioned **human RBC-engrafted, immunosuppressed mouse model could be adapted to sustain *P. falciparum* strains with rosetting phenotypes**.
5. In comparison with the GPA-iLP model, the **cost of a therapy based on PfEMP1-iLPs** is more complex to analyze. However, it **might be less expensive given the availability of** (i) **recombinant NTS-DBL1α domains from several *P. falciparum* rosetting strains**, which might be employed for the production of new Abs, and (ii) **already obtained MAbs**, both by the group headed by Prof. Mats Wahlgren (Angeletti et al. 2013; Angeletti et al. 2012). Future collaborations could be made in this regard in order to generate Abs displaying improved *P. falciparum* strain cross-reactivity and propose a final iLP prototype clinically affordable.

1.10. Attainable improvements in iLP-based drug delivery systems against malaria

In the light of RBCs and pRBCs incapability of performing endocytic processes, we have provided in Chapters 1 and 2 novel strategies for the targeted delivery of weakly basic antimalarials into these cells based on either (i) the fully attachment of iLPs onto RBCs/pRBCs for the subsequent sustained release of CQ and PQ drugs (GPA-iLP model) or (ii) the transference of the highly hydrophobic drug LMF through random collisions between iLPs and all cells in culture but displaying a particular tropism towards rosette-forming pRBCs (PfEMP1-iLP model). Importantly, both strategies being largely dependent on the number of both antigen molecules and epitopes available at the target cell surface if we bear in mind the stable membrane adsorption obtained for these immunoliposomal models. The latter process ultimately results in the deficient direct internalization of iLP contents and the generation of a cell surface saturation point; both disadvantages being particularly significant when targeting pRBCs. Alternative mechanisms might be explored in this regard for the development of improved drug delivery systems against malaria based on (i) receptor-mediated endocytosis for other *P. falciparum* host cells than the mature RBC and (ii) iLP-cell lipid bilayers fusion.

Moreover, bearing in mind the large sequence variability in those parasite-derived, pRBC-exposed proteins, it would be imperative to explore *Plasmodium* host cells and their specific and highly conserved receptors as targets. Remarkably, this drug delivery strategy would follow an analogous prophylactic/therapeutic effect to the CQ-loaded, GPA-iLP approach described in Chapter 1.

1.10.1. Receptor-mediated endocytosis in *Plasmodium* host cells

Cell-mediated internalization processes have probably been the most employed route for the delivery of LP-encapsulated drugs. However, as already mentioned several times throughout this PhD thesis, this strategy is not valid when fighting *P. falciparum* intraerythrocytic stages due to their lack of endocytic activity. If we look at the complete life cycle of *Plasmodium* spp. in humans, fortunately, we can find a few host cells displaying a fully operative intracellular vesicular transport and thereby being potential targets for the design of improved iLP-based chemotherapies: (i) reticulocytes invasion by *P. vivax* and *P. ovale* and (ii) hepatocytes, which are infected during the liver stage of all *Plasmodium* spp.

Reticulocytes as target cell

Blood circulating immature RBCs (reticulocytes) do still display an active autophagic activity mainly employed in the removal of plasma membrane proteins, which occurs through a two step process. A first maturation step takes place in the bone marrow and involves the selective removal of the transferrin receptor (CD71), CD98 and β1 integrin, among other proteins, along with intracellular organelles by means of an endosome-exosome pathway. These events differentiate the R1 early reticulocyte to the R2 mature and less endocytic reticulocyte stage. Secondly, an additional removal of membrane-bound elements together with their later exocytosis takes place once in circulation and results in the fully mature erythrocyte (Griffiths, S. Kupzig, et al. 2012; Griffiths, S. Kupzig, et al. 2012 (1)). Finally, reticulocytes exhibiting a high CD71 expression ($CD71^{hi}$) are located in mouse spleen and their overall amounts have been observed to considerably increase at the same time they reach peripheral circulation during infections with the *P. yoelii* 17X strain (Martín-Jaular et al. 2013).

In light of the above explanation and taking into account the predominant infection of $CD71^{hi}$ reticulocytes by the mouse-infecting *P. yoelii* 17X strain (murine parasite comparable to the human-infecting *P. vivax* sp.), analogous drug-loaded nanovectors to the GPA-iLP model but conjugated with Abs specifically recognizing CD71 instead could be designed against this immature host cell as a clinically feasible therapeutic approach against *P. vivax* malaria. Furthermore, the already mentioned endocytic activity of reticulocytes might improve the intracellular delivery of iLP contents.

Hepatocytes as target cell

The specific delivery of antimalarials into hepatocytes during *Plasmodium* liver stages has been considered as the chemotherapeutic approach of choice for the (i) blockage of parasite replication before the initiation of the IEC as well as (ii) impeding infection relapses through the elimination of *P. vivax* and *P. ovale* hypnozoite dormant stages. Besides, the receptor-mediated endocytosis of a wide range of macromolecules including exosomes, cell penetrating peptides and viruses, among others, has been reported to take place in hepatocytes by means of their

interaction with heparan sulfate proteoglycans exposed at the cell surface (Christianson & Belting 2014). This type of highly sulfated glycosaminoglycans is highly abundant in hepatocytes and the surrounding sinusoidal blood vessels, though it can also be found into other organs and tissues. A preferential localization into mouse liver and the subsequent internalization of LPs into hepatocytes has been achieved in this regard in (Longmuir et al. 2006) by means of their conjugation with a peptide from the *P. berghei* circumsporozoite protein (CSP-LP, Fig. 35), sporozoite ligand that binds to heparan sulfate with high affinity (Ancsin & Kisilevsky 2004).

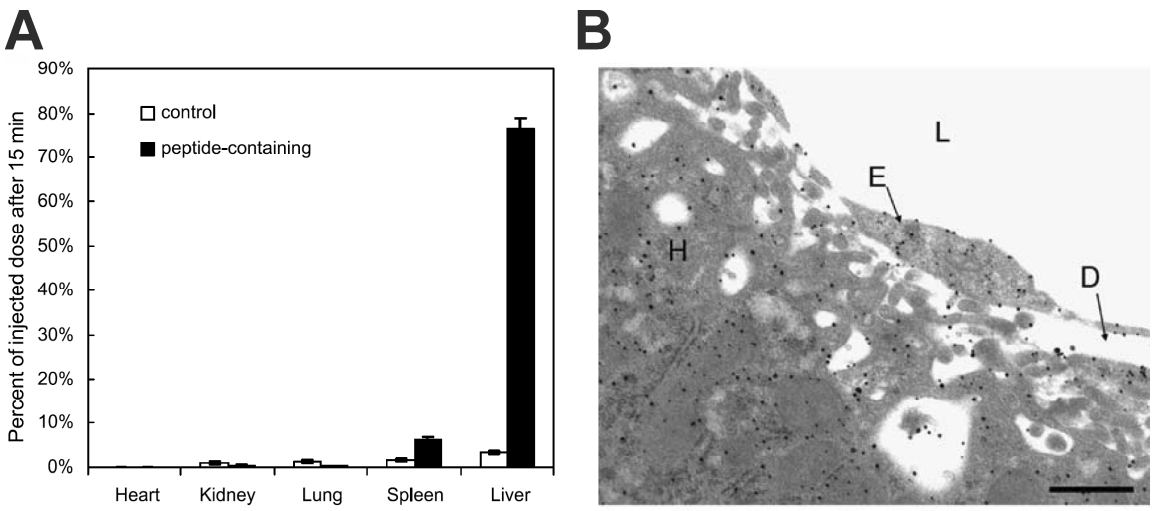

Figure 35. *CSP-conjugated LPs distribution in mouse organs and hepatocyte subcellular targeting*. (A) Overall CSP-LPs accumulation into organs. (B) Electron microscopy image showing gold labeled-LPs reaching the hepatocyte cytoplasm (H) as well as being endocytosed by an endothelial cell (E) from liver sinusoidal capillaries. Lumen of the capillary (L) and the space of Disse (D) are further indicated. Figure reproduced from (Longmuir et al. 2006).

LP-based therapies clinically applicable to all human-infecting *Plasmodium* spp. could be consequently designed through their functionalization with: (i) CSP-derived peptides from *Plasmodium* spp. affecting humans, (ii) other sporozoite ligands having a role in hepatocyte invasion, or (iii) Abs generated against hepatocyte-specific receptors as targeting agents; along with their encapsulation with antimalarials effective against *Plasmodium* liver stages (e.g. PQ) (Galappaththy et al. 2013).

Furthermore, more efficient liver-specific approaches might lead as well to (i) shorter treatment courses than those currently recommended by the WHO (e.g. the continuous administration of 15 mg/day doses and lasting 14 days in the case of PQ) as well as (ii) a reduction in the total amount of drug delivered. This latter improvement would be of extraordinarily importance bearing in mind the generation of hemolytic anemia when PQ is administered to glucose-6-phosphate dehydrogenase (G6PD)-deficient patients (Bolchoz et al. 2002; Alving et al. 1956).

1.10.2. iLP-cell lipid bilayers fusion

The intracellular delivery of liposomal contents comprising the merge of LP-cell membranes, process named as 'lipid bilayers fusion', has been extensively explored *in vitro* and successfully validated for cell transfection purposes. Basically, membrane fusion is mediated by lipids exhibiting a phase transition from the lamellar to the hexagonal H_{II} phase (already termed 'inverted micellar structure'). Such transition is commonly stimulated by the neutralization of LPs containing H_{II} phase-preferring, charged phospholipids in which their ionization state under physiological conditions and in aqueous solution allows them to maintain a stable lamellar arrangement (Hafez et al. 2001; Bailey & Cullis 1997; Stebelska et al. 2006). Some examples of lipids displaying the aforesaid properties include: (i) the cationic DOTAP and DOTMA or (ii) the anionic PA and PS (the latter contain a phosphate group with pKas 6.34 and 2.18, respectively, http://www.chemicalize.org). Both groups of H_{II} phase-preferring lipids are included in LP formulations in combination with PE and their charge neutralization can occur in the presence of, respectively, (i) anionic molecules (e.g. negatively-charged lipids and DNA) or (ii) divalent cations (e.g. Ca^{2+} or Mg^{2+}) and low pH environments.

However, several limitations must be taken into account if considering the clinical application of fusogenic liposomal formulations:

1. Even though LPs can be specifically targeted towards a particular cell type, the above-mentioned **events that trigger membrane fusion are completely nonspecific**. As an example, such minimal selectivity would enable cationic LPs to interact and deliver their contents into almost any type of cell in the organism exposing PS or other anionic lipids on its surface, which would be the case of macrophages and damaged cells that have lost their lipid asymmetry (Callahan et al. 2000). Moreover, anionic LPs could fuse nonspecifically between themselves as well as with any circulating cell in the presence of Ca^{2+} (there is actually about 2.1 to 2.6 mM calcium in the bloodstream) and following an equivalent mechanism to that described in (Holovati et al. 2008) for the *in vitro* delivery of trehalose into RBCs using PS-containing LPs and a buffer supplemented with 5 mM Ca^{2+}.

2. **Charged LPs** display both an **elevated protein binding level** and an **increased complement activation** (Ishida et al. 2002). Besides, **low amounts of serum** of nearly 3% v/v have been reported to **fully inhibit the fusion of cationic vesicles with cells** (Pires et al. 1999).

3. **Nonspecific LP interaction events with cells** could be **reduced by means of their PEGylation**. However, such **steric protection** has been proved in (Pires et al. 1999) to neutralize the LP overall charge and **significantly impair fusion** as well **when included in cationic vesicles** (5 mol% of total lipids).

4. **Lipid bilayers in a liquid crystalline state are required for an effective lamellar-to-H_{II} phase transition** (Bailey & Cullis 1997). Such condition would be easier to accomplish by incorporating unsaturated lipids into LPs but would likely result in turn in a considerably increased membrane permeability to encapsulated molecules.

Moreover, if we look at those changes in lipid asymmetry taking place during the *P. falciparum* IEC (see 2.3.1. from Introduction), PE appears as the major pRBC surface element along with a remarkable exposure of PS. Such increased presence in aminophospholipids has been reported to enhance pRBCs susceptibility to virus-induced fusion (Maguire et al. 1991) and might be employed as cell anchoring point for the interaction and internalization of cationic LPs. The DOPC-based, heparin-targeted LP model developed in (Marques et al. 2014) and containing a 4 mol% of DOTAP, provided in this regard a moderate improvement in PQ drug efficacy when assayed *in vitro* in *P. falciparum* cultures. Nevertheless, the mechanism by which LPs interacted with pRBCs and delivered their cargo was not characterized.

Membrane fusion had also been suggested as principal drug delivery mechanism for the DOPC:cholesterol (80:20 mol%)-composed, BM1234-iLP model firstly developed in (Urbán, Estelrich, Cortés, et al. 2011; Urbán, Estelrich, Adeva, et al. 2011) and further characterized in Chapter 1, which importantly comprises neutrally charged phospholipids and lacks of H_{II} phase-preferring lipids (i.e. nonfusogenic LP formulation). Even though internalization events of iLP contents into late form-pRBCs had been previously observed using PBS as buffer and after cells fixation (Urbán, Estelrich, Cortés, et al. 2011), evidences of such delivery process were scarcely detected in Chapter 1 when BM1234-iLPs were assayed and analyzed in live *P. falciparum* cultures in the presence of the serum-like AlbuMAX® II supplement (RPMI-A complete medium, Invitrogen).

In light of the above, cationic LPs composed mainly of DOTAP:PE along with a small amount of DSPE-PEG2000 for a minimal steric stabilization (i.e. overall charge neutralization and reduced protein binding) could be developed and explored as a potential clinically applicable strategy for the delivery of highly hydrophilic drugs (e.g. fosmidomycin, fully ionized at pH 7.4 due to its acidic groups with pKas 1.81, 8.09 and 8.72, together with a log *P* of -2.21, http://www.chemicalize.org), macromolecules or DNA into pRBCs. Even though PEGylation has been reported to inhibit LP fusion, different concentrations and sizes of PEG might be tested in order to obtain a particular liposomal formulation by which intracellular delivery is maintained but barely affected by serum components. Furthermore, if this LP prototype was conjugated with a pRBC-specific ligand, such as the anti-PfEMP1 Ab employed in Chapter 2, its binding to pRBCs would provide retention times onto these cells long enough to allow membrane fusion to take place.

Let us consider an iLP-pRBC interaction lasting 3 h and a lipid lateral diffusion coefficient of 5 μm^2/sec, value that has been described in (Lindblom et al. 2006) for a DOPC:DPPC:cholesterol (35:35:30 mol%) bilayer at 37 ºC. During this period of time, DOTAP lipids from stably adsorbed

iLPs on the pRBC membrane (pRBCM) might theoretically gather those surface-exposed PS molecules in a few minutes (i.e. one PS would cover the whole pRBC surface of about 154 μm^2 in only 30.8 seconds) and their charges would become thereafter neutralized, thereby promoting the lamellar-to-H_{II} lipid phase transition simultaneously at both apposed lipid bilayers. Such process would be followed by the formation of intermediate lipid mixtures and the final generation of a membrane fusion pore (Bailey & Cullis 1997). Besides, this strategy would be harmless to RBCs due to their absence of surface-exposed PS and, furthermore, the PEGylation of iLPs could perhaps avoid nonspecific interactions with other PS-displaying cells in circulation. Finally, additional fusion-based approaches, such as the PS-Ca^{2+} methodology already tested and validated *in vitro* in RBCs (Holovati et al. 2008), coupled to vesicles PEGylation might be alternatively explored.

2. Discussion of Chapter 3: Analysis of ABA biosynthesis in *P. falciparum*

2.1. Research for new parasite-specific metabolic pathways as novel drug targets

Bearing in mind the current scenario of malaria chemotherapy in which parasite resistance to the highly effective and widely employed chloroquine and artemisinin drugs, as well as their derivatives, is increasingly hampering their application, the research of novel antimalarial compounds is mandatory in order to continue with an active malaria control and eradication program. Besides, metabolic pathways essential for parasite viability but absent in humans, such as the CQ-inhibited hematin detoxification into the hemozoin polymer, are of special interest as drug targets due to a reduced likelihood of causing toxic side effects to the patient.

In the light of the above, those metabolic routes taking place in the apicoplast, a non-photosynthetic and essential organelle present in most of the apicomplexan pathogens, have emerged as potential antiparasitic targets (see 2.2.2. from Introduction for more detailed information). Fosmidomycin drug inhibiting the synthesis of IPP-DMAPP isoprenoid building blocks through the MEP pathway in the apicoplast (Umeda et al. 2011) would be the first compound of this class to be studied against malaria and is running Phase II clinical trials at present (Wells et al. 2015). Nevertheless, owing to the requirement of membrane transporters for its accumulation into pRBCs (Baumeister et al. 2011) and because fosmidomycin activity is based on the blockage of individual gene products, both processes being easily disruptible through single point mutations, its administration in combination with additional antiplasmodial agents directed against: (i) distinct levels of the isoprenoids biosynthetic pathway, (ii) essential isoprenoid-derived downstream products (e.g. carotenoids and ubiquinone), or (iii) targeting completely separate functions; would be crucial in order to prevent a quick generation of drug-resistant parasites.

In this PhD thesis we have focused on the utilization of inhibitors affecting key enzymes of the C_{40}-carotenoid biosynthetic pathway (C_{40}-CBP) against *P. falciparum* and, importantly, we have explored a possible production of abscisic acid (ABA) by this parasite as an essential final product of the C_{40}-CBP and therefore a potential chemotherapeutic target. Remarkably, the interest of finding this plant-like hormone in *Plasmodium* has been revived after its detection in *Toxoplasma gondii* controlling parasite egress through a mechanism regulated by calcium release (Lourido et al. 2012; Nagamune et al. 2008).

2.2. Improvement in ABA detection

Taking into account the ABA production pattern in *T. gondii*, apicomplexan parasite in which the maximum levels of this hormone are reached prior to egress (Nagamune et al. 2008), the first point we addressed was to improve both ABA limits of detection (LOD) and quantification (LOQ)

in order to be able to detect it throughout the IEC of *P. falciparum*, parasite in which low levels were expected due to the lack in this organism of most of the ABA-regulated processes taking place in higher plants (e.g. closure of the stomatal pores and embryogenesis in response to reduced water availability) (Li et al. 2000).

By means of ABA derivatization with 2-picolylamine (PA), which generates ABA-PA, and including RBCs as matrix for validation (lyophilized cell extract obtained from 1.2×10^{10} RBCs and finally re-dissolved in 1 ml solution containing known amounts of ABA and ABA-d6 as internal standard, ISTD), LOD and LOQ values of 0.03 and 0.15 ng/ml were obtained through LC-ESI-MS/MS working in ESI positive ion mode. This PA-based derivatization strategy has been proposed in this PhD thesis as a much more powerful analytical approach than the preliminary methods employed for ABA detection in *T. gondii* (Nagamune et al. 2008) and plants (Santiago et al. 2012; Zhou et al. 2003), which were remarkably based on:

- **Gas chromatography coupled to mass spectrometry** (Duffield & Netting 2001; Nagamune et al. 2008), methodology **not well suited for the analysis of low-volatile compounds** (e.g. ABA and carotenoids boiling point of >450 ºC) or those **unstable to high temperatures**.

- **LC-ESI-MS/MS** but detecting **unmodified ABA in the ESI negative ion mode** (Zhou et al. 2003). This newer strategy provided the most sensitive **LOD and LOQ** reported values to date of **0.2 and 0.6 ng ABA/g dry mass**, respectively, being **nearly 7- and 4-fold higher in comparison with our optimized ABA-PA analytical limits**.

Such improvement in ABA detection sensitivity was further observed when analyzing ABA-PA vs. unmodified ABA through the same LC-ESI-MS/MS system and conditions but running samples through either ESI positive or negative ion mode depending on the presence or not of PA. A total of 92,461 vs. 120 counts were obtained in this regard for ABA-PA vs. PA from the MS/MS chromatograms, both molecules initially spiked at 10 ng/mL. Besides, the RBC matrix did not produce any significant effect over ABA-PA or ABA-d6-PA detection and an exceptional calibration linearity ($r = 0.998$) together with an extraordinary intra-/inter-day accuracy and precision were obtained. All the aforementioned results ultimately validating the ABA-detection method described in Chapter 3 for its application to RBC-infecting apicomplexan parasites.

2.3. Application of the optimized ABA detection method to late form-pRBC extracts

ABA could not be detected in late form-pRBC extracts at the previously determined ABA-PA specific LC-MS/MS parameters of about 3.3 min retention time into the LC column and 355 → 229 m/z as major ion transition. Nevertheless, the *in vitro* observed growth inhibitory efficacy of the NDGA antioxidant compound against *P. falciparum* IEC claims for further investigation in order to finally ascertain if this parasite is capable of producing ABA. Indeed, NDGA has been

described to inhibit the neoxanthin cleavage enzyme (Creelman et al. 1992; Burbidge et al. 1997), which is directly responsible for the generation of the xanthoxin precursor essential in turn for ABA biosynthesis in the cytoplasm of plant cells.

The antiparasitic activity of fluridone, herbicide targeting the enzyme phytoene desaturase in an analogous way and IC50 to norflurazon (Tonhosolo et al. 2009), further highlighted the essential role of carotenoids in *P. falciparum* viability. So far, a major function in protecting the intracellular parasite against the oxidative stress produced by hemoglobin digestion has been attributed to carotenoids (Tonhosolo et al. 2009). Additionally proposed vital tasks carried out by these compounds, though not yet reported in *Plasmodium*, include gene expression and pRBCM stabilization (Gray et al. 2003; Gruszecki & Strzałka 2005). Finally, a synergistic effect was observed when treating pRBCs with NDGA and fluridone at the same time, which importantly increased the number of parasites displaying a cell-death phenotype with picnotic nuclei.

2.4. Proposal of a mechanism regulating P. falciparum egress

Bearing in mind: (i) the aforementioned antiplasmodial activity of NDGA (IC50 of about 47 µM) and (ii) the increased number of parasites in the presence of C_{40}-CBP inhibitors whose growth has been slowed and further stopped prior to merozoites release, phenotype similar to *T. gondii* after being treated with fluridone (Nagamune et al. 2008) and *P. falciparum* cultures in which intracellular calcium oscillations are blocked (Enomoto et al. 2012); ABA could still be present in pRBCs having a role in controlling parasite growth and the egress of merozoites from the host segmented schizont by means of a complex signaling system that, based on bibliography, might comprise the following steps:

1. **ABA-mediated activation** of the parasite **cyclic GMP-dependent protein kinase** (*Pf*PKG) and the subsequent **micronemal protein discharge** including merozoite surface ligands such as AMA1 (Collins et al. 2013) or EBA175. It still remains to be determined the dependence of this latter process on intracellular calcium levels.
2. **Intracellular secretion of calcium** triggered by (i) **cyclic ADP ribose/ryanodine receptor** and/or (ii) through the **PLC/IP_3 system**. Both mechanisms have been detected in *T. gondii* and *P. falciparum* having a fundamental function in the egress of parasites as well as the later host cell invasion and might participate in parallel (Nagamune et al. 2008; Lovett et al. 2002; Jones et al. 2009; Thomas et al. 2012). Additionally, the **PLC/IP_3 pathway** has been found to be **functional throughout the *P. falciparum* IEC** (Enomoto et al. 2012) and remarkably **essential during schizogony** in which high intracellular calcium levels are reached prior to merozoite egress (Agarwal et al. 2013).
3. **Calcium-induced** (i) **protein secretion from parasite exonemes**, being particularly important the **subtilisin-like serine protease *Pf*SUB1** that mediates PVM rupture and activates several merozoite surface proteins including MSP1 (Agarwal et al. 2013), and (ii) **activation of the parasite calcium-dependent protein kinase *Pf*CDPK5** for the final

disruption of the pRBCM and the consequent liberation of daughter merozoites (Dvorin et al. 2010). **Additional calcium-dependent kinases** have been reported to be involved in the **processing of parasite proteins required for invasion**, such as the *Pf*CDPK1 and the *P. falciparum* protein kinase B (Thomas et al. 2012). The latter being required by the parasite for the regulation of the glideosome associated protein 45.

A similar ABA-regulated mechanism could take place in *T. gondii* (Lourido et al. 2012; Lovett et al. 2002) and might be present in *Babesia microti* as well. Moreover, some of the reasons that might explain why ABA still remains undetected in *P. falciparum* include (i) its presence in amounts below the 0.03 ng/ml LOD during most of the parasite's IEC and probably only detectable prior to egress and/or (ii) the simultaneous existence of multiple ABA derivatives having distinct molecular masses as well as differing in their functional groups, likely following a mechanism for ABA activity regulation. Importantly, the latter suggestion has already been described to occur in plants (Oritani & Kiyota 2003) and even a compound was detected in our late form-pRBC extracts analyzed displaying the same LC retention time and molecular mass as ABA-PA. Furthermore, the MS/MS detected amounts of this unknown molecule were found to follow the ABA-expected behavior after parasites treatment with the C_{40}-CBP inhibitors.

Unfortunately, among the 355 → 229/135/109 m/z major ion transitions characteristic of ABA-PA, the aforementioned compound appeared only at the 355 → 109 m/z ion transition. Further research will be therefore required to finally verify if this molecule is actually a derivative of ABA or a completely unrelated compound. In addition to this, the application of new methodologies based on open metabolomic studies will be imperative in order to: (i) analyze several likely modifications of ABA at the same time, (ii) obtain a better knowledge about which parasite metabolic pathways are affected by C_{40}-CBP inhibitors and, (iii) in case that ABA is not the initial element leading to *Pf*PKG activation and merozoites egress, find out which is actually the starting event and what type of parasite functions are impaired by NDGA action.

2.5. Parasite-encoded, amyloid-forming proteins as potential targets against Plasmodium IEC and cerebral malaria

Alternative chemotherapeutic approaches against *Plasmodium* endogenous metabolic processes are being currently considered for the treatment of malaria most severe clinical manifestations, which chiefly comprise the cytoadhesion of pRBCs to the endothelium of brain capillaries in a pathogenic mechanism eventually leading to cerebral malaria. Importantly, such severe complication affects half million children in African areas every year and can be fatal even under best chemotherapies (e.g. intravenous administration of artesunate) with reported mortality rates of about 15 to 20% of all treated cases (Montero 2013; Idro et al. 2010).

Moreover, several intrinsically unstructured proteins (IUPs) have been identified within the *P. falciparum* genome as a common feature shared by apicomplexan parasites (Feng et al. 2006). Among these, the merozoite surface protein 2 (MSP2) has been observed to form *in vitro*

amyloid-like fibrils containing β-sheet structural arrangements (Adda et al. 2009; Yang et al. 2010). Key residues placed at the N-terminal conserved region of MSP2: amino acid positions 20-44 or 1-25 considering either the full-length translated protein (Fig. 3 from Annex III) or its mature-processed form; have been found in this regard responsible for such aggregative properties (Yang et al. 2010). MSP2 has been further identified at the merozoite surface in the form of fibrils and, as a consequence, these ligaments might in turn have an essential role for parasite viability during erythrocyte invasion as (i) stabilizing components of the merozoite surface coat and/or (ii) by means of their interaction with host cell receptors (Adda et al. 2009; Boyle et al. 2014). Drugs blocking the cell surface exposure of MSP2 or its aggregation would be in such case potential agents against parasite replication.

An alternative role of MSP2-derived oligomers and fibrils as neurotoxic elements triggering cerebral malaria has been additionally proposed (see Annex III for more detailed information). Amyloid-forming regions have also been identified within the naturally cleaved N-terminal signal peptide of MSP2 ($MSP2_{NSP}$), being actually predicted as the most amyloidogenic fragment of the whole parasite protein and, importantly, displaying an average score similar to the amyloid beta (Aβ) peptide causing Alzheimer's disease. However, an unknown function has been attributed to this excised fragment during MSP2 maturation. This amyloid-forming peptide could be released into circulation along with merozoites when the former schizont bursts or, furthermore, secreted by late form-pRBCs through the complex parasite-derived vesicular trafficking system described in 2.1.3. from Introduction (Mantel et al. 2013; Regev-Rudzki et al. 2013).

The liberated peptide might eventually aggregate once in the bloodstream leading to the formation of oligomers and fibrils in a mechanism stimulated by the presence of sulfated glycosaminoglycans, process that has already been described for the Aβ peptide (Valle-Delgado et al. 2010). In this regard, a considerable fibrillogenesis might take place in those organs rich in heparan sulfate-proteoglycans such as the liver and, importantly, the brain (Lau et al. 2013). In the latter case, similar pathogenic mechanisms to Alzheimer's disease might be triggered by the parasite-secreted $MSP2_{NSP}$ during cerebral malaria causing neuronal degeneration and cytotoxicity. Therefore, compounds interfering with either a hypothetical $MSP2_{NSP}$ aggregation *in vivo* or the subsequent heparan sulfate-stimulated formation of fibrils could theoretically be potential agents against severe malaria.

"Remember, you can always stoop and pick up nothing"

Charles Chaplin

"El triunfo del verdadero hombre surge de las cenizas de su error"

Pablo Neruda

CONCLUSIONS

1. Ab coupling yields of >40% have been obtained by means of (i) the incorporation of maleimide-containing, PEGylated phospholipids into LPs and (ii) the derivatization of Abs with the SATA crosslinker. Both steps performed in parallel and resulting in the highly stable thioether linkage. Besides, SATA/Ab molar ratios of up to 10× provided adequate antigen recognition and minimal iLP aggregation.

2. The pH-driven active encapsulation of CQ and PQ antimalarials into DSPC-based LPs together with their conjugation with a MAb specific for the GPA antigen of RBCs (GPA-iLP) provides (i) a complete recognition and retention of iLPs into both RBCs/*P. falciparum*-infected RBCs as well as (ii) a total and stable drug encapsulation along with its effective intracellular release over time under parasite culture conditions.

3. The improved antimalarial efficacy of CQ-loaded, GPA-iLPs has been proven *in vivo* in *P. falciparum*-infected, humanized mice through the reduction of their parasite densities to undetectable levels (<0.01% parasitemia) and following a 4 × 0.5 mg CQ/kg dosage schedule. Free CQ at a dosage 3.5 times higher was at least 40-fold less effective.

4. Considering the enormous antigenic variation intrinsic in *Plasmodium* spp. and their parasitic-intracellular nature, those conserved and cell surface-exposed proteins found in erythrocytes constitute potential targets for the development of novel site-specific nanovectors capable of delivering drugs into (i) all intraerythrocytic stages of *P. falciparum* and (ii) uninfected RBCs for a simultaneous therapeutic-prophylactic effect.

5. LMF-laden iLPs targeted against rosette-forming variants of PfEMP1 (PfEMP1-iLP) represent a further step beyond more effective severe malaria therapeutics by means of (i) mechanically disrupting already formed rosettes while at the same time (ii) eliminating those parasites forming them. In this regard, an increased activity of LMF in reducing the number of rosette-forming pRBCs (R29 clone) was obtained when delivered through homologous PfEMP1-iLPs with a 4.5- to 6.5-fold decreased IC50 compared to either free drug or non-targeted LPs. Besides, the rosette-disrupting activity of Abs has been preserved after their conjugation to LPs.

6. ABA has not been detected in late form-pRBC extracts even though the sensitivity for its detection has been extraordinarily improved (LOD of 0.03 ng/ml) through the generation of the ABA-picolylamine derivative and its subsequent analysis by LC-ESI-MS/MS operating in the positive ion mode. It still remains to be identified the essential function of *P. falciparum* affected by the NDGA antioxidant compound.

ANNEX I

Theoretical calculations

1. Analysis of CQ and PQ encapsulation into LPs and determination of a more precise model defining the membrane/solution partitioning mechanism followed by diprotic weak bases

1.1. Solubility-diffusion theory

Water and amphiphilic unionized molecules (including most of drugs) do easily cross lipid bilayers (e.g. <1 min for the release of one-half of the initially encapsulated drug cargo from LPs 170 nm in diameter, Table 2 from Introduction) in a process described by the 'solubility-diffusion theory' (Finkelstein 1988; Paula et al. 1996). This mechanism is defined by the solubility of molecules into the membrane hydrocarbon core and, therefore, the migratory speed of these substances will be largely dependent on their organic/aqueous partition coefficient *P* (Leo et al. 1971), which is commonly reported as log *P* and mostly determined by means of the octanol-water biphasic system.

1.2. Transient pore model

The 'transient pore model' has been theorized to describe the migration of small ions (e.g. hydronium, hydroxide, potassium and calcium) across lipid bilayers (Lawaczeck 1988), though being largely restricted to membranes containing short-chain phospholipids (acyl chains of <18 carbon in length, Table 2 from Introduction). By contrast, the movement of ions across membranes composed of C18 and longer hydrocarbon chains, such as our DOPC/DSPC-based LP models, has been alternatively predicted to occur through the solubility-diffusion model (Paula et al. 1996) and, consequently, times longer than a month can be calculated for the release of 50% LP-encapsulated amounts of ions. Bearing in mind the almost insignificant solubility of small ions into organic phases, membranes have been considered impermeable to ions bigger in size, such as the protonated forms of the weakly basic CQ and PQ antimalarials (Warhurst et al. 2003). Theoretical time periods of as long as several months or even a few years might be required for these ionized compounds to significantly leak out from a LP.

1.3. Influence of pH over the release kinetics of proton-ionizable weakly basic compounds from LPs

Considering the transmembrane migration models explained above, the leaking speed of LP-encapsulated proton-ionizable/deionizable compounds (i.e. molecules containing either weakly basic or weakly acid groups partially ionized at physiological pH) will be strongly influenced by the pH of the system, which defines the relative abundance of their ionization species. Importantly, among all these species occurring in solution, the unionized one will be the unique form of compounds capable of completely solubilizing into the membrane and, therefore, able to cross it. In this regard, we obtained in Chapter 1 times of as short as 30 min for the release of ~70% of the initially passively-encapsulated CQ and PQ drug amounts from DOPC:cholesterol

(80:20 mol%) LPs after >10-fold dilution of the 10 mM lipid stock (PBS, physiological pH). These results are in accordance with the already reported permeability coefficients of amphiphilic drugs (Fade 1998), which can range between 1E-05 to 1E-07 cm/sec and lead in turn to theoretical LP-release times of a few minutes for the complete loss of the entrapped compound (Table 2 from Introduction). Moreover, the unionized form of CQ and PQ consists of only 0.014% and 0.099% of all drug molecules in solution at pH 7.4 (Table 4 from Discussion), which importantly indicates that this neutral form is capable of mediating a fast transport of drugs across membranes even if present in very low amounts. Actually, the unionized species of CQ and PQ display highly hydrophobic properties with remarkably large log *P* values of 4.72 and 3.2, respectively (Omodeo-Salè et al. 2009; Nair et al. 2012). Such exceptional lipophilicity likely compensates for their small relative abundances occurring at neutral pH.

In addition to the fast release of drugs observed when following the passive LP-encapsulation approach, we did also obtain in Chapter 1 larger experimental encapsulation efficiencies (Exp EE%) than those theoretically expected (Theo EE%, Table 5) if following the currently accepted distribution coefficient *D* partitioning model (Eq. 1-2 from Introduction). The latter basically considers that only the unionized species of amphipathic molecules can become internalized into the lipid bilayer (Scherrer & Howard 1977; Warhurst et al. 2003). An illustration of this theorized partitioning model is included in Table 6 using CQ as example.

Liposomal samples	Added drug (μM)	Encapsulated drug (μM)	Exp EE%	Theo EE%	Theo* EE%
CQ pH 7.4	10,000	999.0 ± 5.2	10.0 ± 0.1	8.49	65.4
CQ pH 6.5	10,000	499.0 ± 12.1	5.0 ± 0.1	2.53	21.4
CQ pH 6.5	25	3.5 ± 0.6	14.1 ± 2.5	2.53	21.4
PQ pH 7.4	10,000	3392.6 ± 70.9	33.9 ± 0.7	3.79	74.6
PQ pH 6.5	10,000	3215.0 ± 61.9	32.2 ± 0.6	2.59	74.6
PQ pH 6.5	4,000	1945.9 ± 78.0	48.7 ± 2.0	2.59	74.6

Table 5. *Experimental encapsulation efficiencies (Exp EE%) for CQ and PQ drugs into LPs (DOPC:cholesterol, 80:20 mol%)*. LP samples (10 mM total lipid) were prepared in Chapter 1. Calculated theoretical (Theo) and modified theoretical (Theo*) EE% are described in Tables 6 and 7.

Remarkably, such differences between experimental and theoretical EE% suggested that additional drug ionization species to the unionized form might be interacting as well with the LP membrane. Besides, a substantial increase in Exp EE% was obtained for lower drug amounts indicating LP-encapsulation saturability at 10 mM drug vs. 10 mM lipid (Table 5). More accurate Exp EE% were observed at lower non-saturating drug concentrations with the highest entrapped payloads of 65.4% and 74.6% of the total CQ and PQ amounts in samples (LPs were maintained always at 10 mM lipid, Fig. 36). Such results highlighted the tremendous capacity of these antimalarial agents to interact with the LP membrane.

CQ pH 7.4	LP aqueous cargo	Inner LB	Outer LB	External solution
	Vol %	**Vol %**	**Vol %**	**Vol %**
	2.40	0.41	0.48	96.71
	pH	-	-	**pH**
	7.40	-	-	7.40
	Drug	**Drug**	**Drug**	**Drug**
Mol	2.48E-02	221.89	260.47	1
% total Drug	3.20E-04	2.86	3.36	1.29E-02
	Drug H^+	-	-	**Drug H^+**
Mol	15.66	-	-	630.96
% total Drug	2.02E-01	-	-	8.14
	Drug $2H^+$	-	-	**Drug $2H^+$**
Mol	160.23	-	-	6.46E+03
% total Drug	2.07	-	-	83.34
			Mol	% total Drug
		Total Drug	7.75E+03	100.00
		Encapsulated	6.58E+02	8.50
		Released	7.09E+03	91.50

Table 6. *Exemplification of the LP/solution theorized partitioning for CQ diprotic weak base according to the distribution coefficient D model.* Calculated considering: (i) pH 7.4, (ii) 10 mM total lipid concentration, (iii) LPs 100 nm in diameter, (iv) LP internal aqueous volume of 2.4 µl/µmol total lipid, (v) LP internal aqueous volume/membrane volume ratio of 2.7, (vi) LP-membrane external/internal leaflets lipid ratio of 54/46 mol%. Parameters described in (i-vi) have been retrieved from (Maurer et al. 2001). LP internal and external aqueous compartments (LP aqueous cargo, external solution) and membrane leaflets (Inner LB, Outer LB).

Moreover, whereas CQ encapsulation was largely dependent on pH, the Exp EE % obtained for PQ did not change at all when lowering the pH from 7.4 to 6.5 units (Table 5). These results pointed out that drugs structure might have an additional role in defining their ability to partition into the LP membrane. In this regard, if we look at the pH range 4.0-7.4 (Table 4 from Discussion) we can see that whilst PQ is mainly found in its monoprotonated form (PQ H^+), CQ becomes fully protonated (CQ $2H^+$). Such differences are attributed to drugs pKa_2 3.2 (PQ) vs. 8.4 (CQ) and, presumably, the intermediate ionization state of drugs monoprotonated species enables their solubilization into the lipid bilayer hydrocarbon core (drugs oriented in parallel to phospholipid tails) while simultaneously exposing their cationic protonated end at the membrane surface in association with the anionic phosphate moieties from the surrounding lipid headgroups. In fact, similar drug-membrane interactions have been theorized as the most thermodynamically favorable for cylinder-shaped hydrophobic compounds (Fahr et al. 2005).

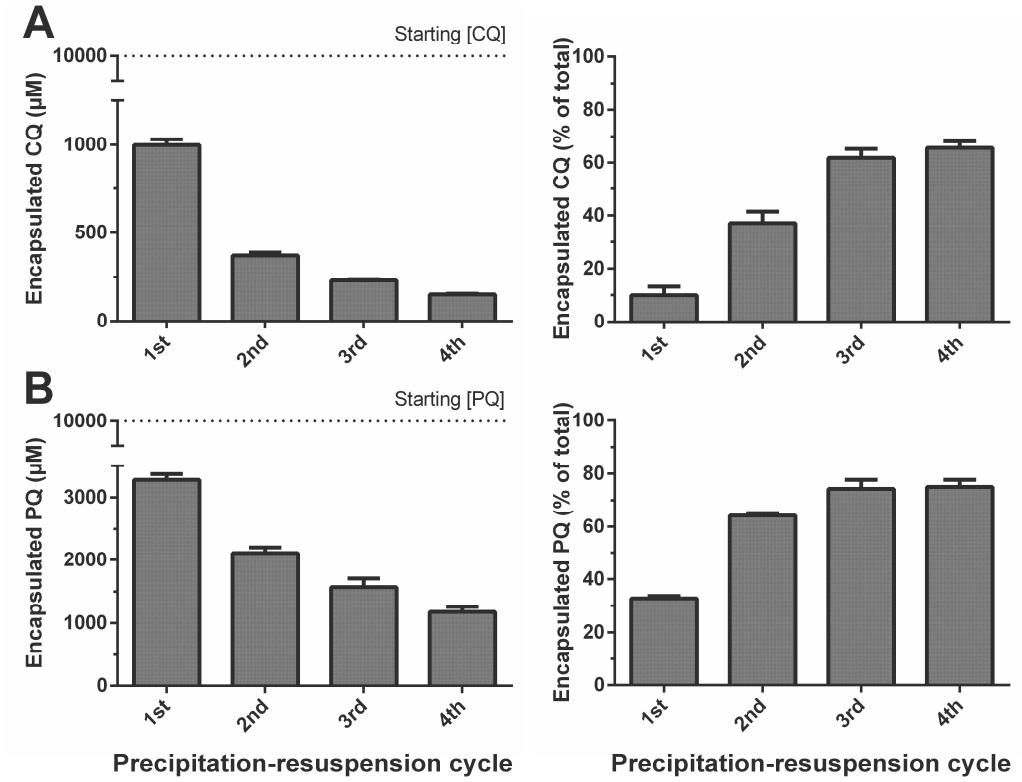

Figure 36. *Determination of (A) CQ and (B) PQ encapsulated amounts at non-membrane-saturating concentrations into LPs (DOPC:cholesterol, 80:20 mol%).* LP samples from Chapter 1, assayed at 10 mM total lipid and suspended in PBS, pH 7.4. In this experiment, the same drug-loaded LP samples were subjected to 4 precipitation-resuspension cycles. Released material into the LP-external solution was removed from supernatants in each cycle and pelleted LPs were redissolved and subsequently incubated for 1 h at room temperature in order to allow LP/solution drug partitioning to reach equilibrium.

1.4. Determination of the new partitioning model for proton-ionizable drugs

In order to provide a more accurate partitioning model for proton-ionizable compounds, we firstly considered an additional organic/aqueous partition coefficient named *P** accounting for the solubilization of partially ionized molecules into the LP-membrane hydrophobic core. In this regard, if we look at the position occupied by the first weakly basic group to be protonated within the structure of CQ and PQ antimalarials (pKa_1, Fig. 2 from Chapter 1), its ionization in CQ H^+ and PQ H^+ species would only affect a minor part of the drug (about 25% of the whole structure), leaving in this manner most of the molecule still lipophilic.

The novel theorized partitioning model bearing in mind the above-mentioned suggestions and considering a diprotic weak base similar in structure to the aminoquinoline antimalarials is illustrated in Fig. 37. This model together with the previously obtained drug encapsulation percentages at non-saturating amounts (Fig. 36) were employed to calculate the organic/aqueous *P** partition coefficient for CQ H^+ (log *P** of 3.34) and PQ H^+ (log *P** of 2.5). A detailed exemplification of the new partitioning model is included in Table 7.

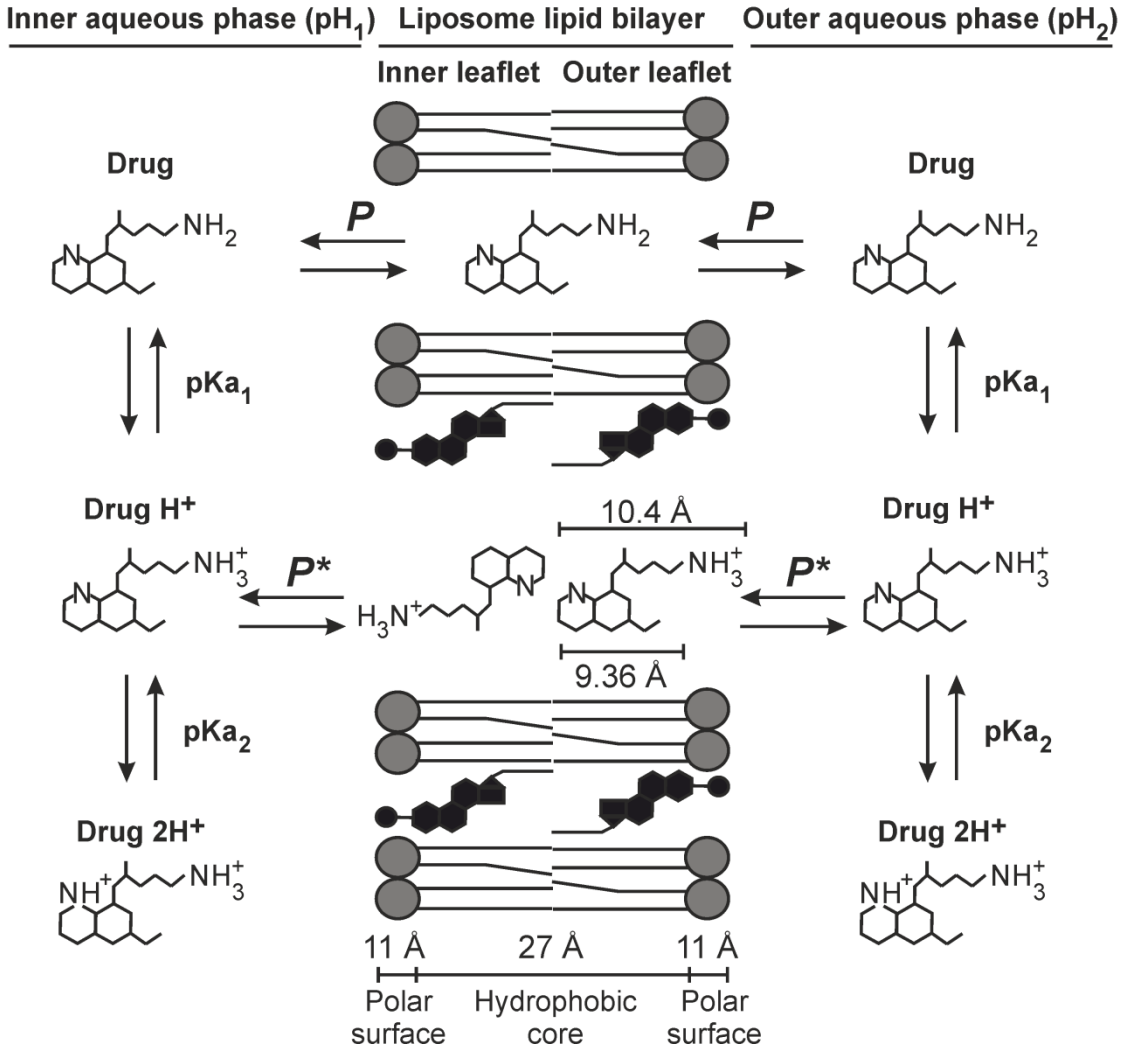

Figure 37. *New partitioning model illustrating the main interaction events taking place between a diprotic weak base and a PC:cholesterol-based LP membrane*. Lipid bilayer solubilization of the deprotonated and monoprotonated forms is described by *P* and *P** organic/aqueous partition coefficients, respectively. Hydrophobic core thickness and headgroup size of PC has been retrieved from (Lewis & Engelman 1983; Leitmannova Liu 2006). Drug dimensions (10.4 Å long, 6.36 Å wide) were selected using PQ as model with a mean projection area of 66.2 $Å^2$, http://www.chemicalize.org.

Due to the partial ionization state of drugs monoprotonated species, a slightly reduced solubility into the LP membrane compared to their unionized forms was expected. Such evidence is in accordance with the log *P** values obtained, which were approximately 30% and 22% smaller in comparison with CQ (4.72) and PQ (3.2) log *P* values. Remarkably, an analogous performance might be taking place when encapsulating LMF, for which we obtained in Chapter 2 an Exp EE of 89% into LPs DSPC:cholesterol (90:10 mol%, pH 6.5) in spite of being found mainly in its monoprotonated species (LMF H^+ corresponding to >95% of all drug molecules in solution for the pH range 4.0-7.4, Table 4 from Discussion). Furthermore, if we bear in mind the disposition of its weakly basic group at the molecule end (feature comparable to CQ and PQ), similar hydrophobic properties for LMF H^+ compared to its unionized form would be expected.

CQ pH 7.4	LP aqueous cargo	Inner LB	Outer LB	External solution
	Vol %	**Vol %**	**Vol %**	**Vol %**
	2.40	0.41	0.48	96.71
	pH	-	-	**pH**
	7.40	-	-	7.40
	Drug	**Drug**	**Drug**	**Drug**
Mol	2.48E-02	221.89	260.47	1
% total Drug	1.21E-04	1.08	1.27	4.88E-03
	Drug H^+	**Drug H^+**	**Drug H^+**	**Drug H^+**
Mol	15.66	5.86E+03	6.88E+03	630.96
% total Drug	7.64E-02	28.61	33.59	3.08
	Drug $2H^+$	-	-	**Drug $2H^+$**
Mol	160.23	-	-	6.46E+03
% total Drug	0.78	-	-	31.51
			Mol	% total Drug
		Total Drug	2.05E+04	100.00
		Encapsulated	1.34E+04	65.41
		Released	7.09E+03	34.59

CQ pH 4.0-7.4	LP aqueous cargo	Inner LB	Outer LB	External solution
LPs dilution	**Vol %**	**Vol %**	**Vol %**	**Vol %**
2500	9.60E-04	1.64E-04	1.92E-04	100.00
	pH	-	-	**pH**
	4.00	-	-	7.40
	Drug	**Drug**	**Drug**	**Drug**
Mol	9.60E-06	0.09	0.10	1
% total Drug	2.38E-09	2.13E-05	2.49E-05	2.48E-04
	Drug H^+	**Drug H^+**	**Drug H^+**	**Drug H^+**
Mol	15.22	5.70E+03	2.66	630.96
% total Drug	3.77E-03	1.41	6.59E-04	0.16
	Drug $2H^+$	-	-	**Drug $2H^+$**
Mol	3.91E+05	-	-	6.46E+03
% total Drug	96.83	-	-	1.60
			Mol	% total Drug
		Total Drug	4.04E+05	100.00
		Encapsulated	3.97E+05	98.24
		Released	7.09E+03	1.76

Table 7. *Exemplification of the LP/solution novel partitioning model for CQ diprotic weak base if passively encapsulated at physiological pH (undiluted) or actively encapsulated through a pH 4.0-7.4 gradient (2,500-fold diluted) and considering the same liposomal system as in Table 6*. The 2,500-fold dilution has been selected corresponding to the maximum lipid amount employed during *P. falciparum* growth inhibition assays with GPA-iLPs, 4 µM lipid and 200 nM CQ in culture, Chapter 1.

Finally, new and more realistic theoretical EE% (Theo* EE %, Table 5) and modified distribution coefficients *D** were calculated for CQ and PQ. *D** determination is specified in Eq. 6-8 and *D* vs. *D** values are represented as a function of solution pH in Fig. 38. We can see how by means of this novel partitioning model, the encapsulation behavior of CQ and PQ into LPs is better explained. Whereas their lipophilicity hugely decays at acidic pH when considering *D* as partitioning model of choice, such effect is considerably diminished if based on the corrected *D** approach (Fig. 38). Furthermore, when using *D** as model, PQ hydrophobicity remains almost unaffected in the pH range 6.5-7.4 (in agreement with the Exp EE% shown in Table 5) and the same behavior might be theoretically maintained until pH 4.0. However, we have only validated drugs *P** values in PBS at physiological pH and at room temperature. Additional LP-encapsulation experiments should be performed in this regard at distinct solution pH values, temperatures and osmolarity in order to provide more precise *P** values and acquire a better knowledge about *P** dependence on the conditions of the system.

(6)

$$D^* = \frac{\dfrac{\text{mol Drug}_{org} + \text{mol Drug}^{H+}{}_{org}}{\text{Vol}_{org}}}{\dfrac{\text{mol Drug}_{aq} + \text{mol Drug}^{H+}{}_{aq} + \text{mol Drug}^{2H+}{}_{aq}}{\text{Vol}_{aq}}}$$

(7)

$$\log D^* = \log\left[\frac{\text{mol Drug}_{org}\times\text{Vol}_{aq}}{\text{Vol}_{org}\times\text{mol Drug}_{aq}} + \frac{\text{mol Drug}^{H+}{}_{org}\times\text{Vol}_{aq}}{\text{Vol}_{org}\times\text{mol Drug}_{aq}}\right] - \log\left[1 + \frac{\text{mol Drug}^{H+}{}_{aq}}{\text{mol Drug}_{aq}} + \frac{\text{mol Drug}^{2H+}{}_{aq}}{\text{mol Drug}_{aq}}\right]$$

(8)

$$\log D^* = \log\left[P + \left(10^{(pKa1-pH)}\times P^*\right)\right] - \log\left[1 + 10^{(pKa1-pH)} + 10^{(pKa1+pKa2-2\times pH)}\right]$$

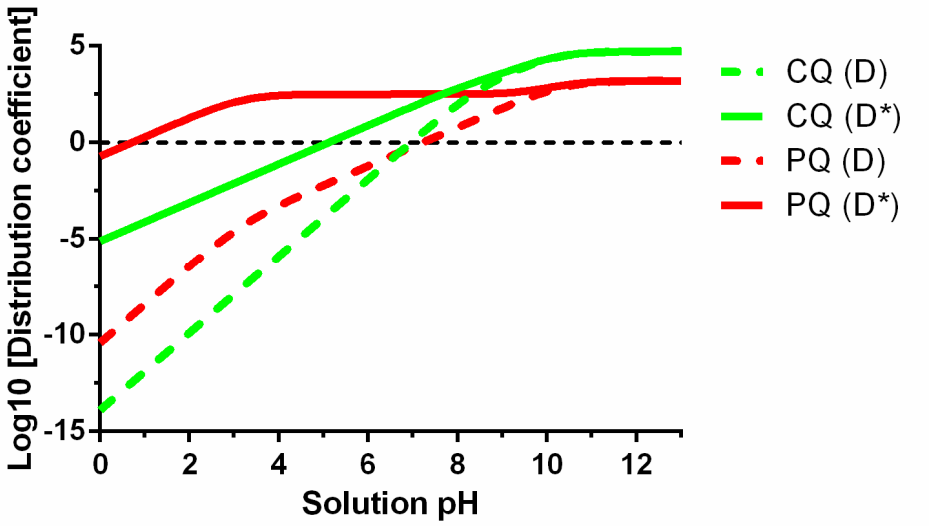

Figure 38. *Determination of D and D* distribution coefficients for CQ and PQ drugs as a function of solution pH.* Equations Eq. 4 from Introduction and Eq. 8 were employed for *D* and *D** calculation, respectively. CQ: pKas 10.2 and 8.4, log *P* 4.72 and log *P** 3.34. PQ: pKas 10.4 and 3.2, log *P* 3.2 and log *P** 2.5.

2. Theoretical calculation of LP numbers as a function of lipid molarity and the size of the nanoparticle

The number of LP particles in solution was theoretically determined in Chapter 1 using the equations (Eq. 9-10) provided by Encapsula NanoSciences LLC (http://www.liposomes.org) and employed as well in other works (Maurer et al. 2001) for the calculation of the number of lipid molecules comprising a single unilamellar vesicle (N_{lipid}) as a function of its radius (r) and lipid bilayer thickness (h). Considering our LP model of 170 nm in diameter and bearing a ~5 nm thick membrane composed mostly of either DOPC or DSPC phospholipids (PC headgroup area in both cases of about 0.71 nm^2, http://www.liposomes.org), features illustrated in Fig. 37, a total number of 2.41×10^5 lipids/LP vesicle is obtained.

(9)
$$N_{lipid} = \frac{\left[\text{Outer leaflet area} + \text{Inner leaflet area}\right]}{\text{Lipid headgroup area}}$$

(10)
$$N_{lipid} = \frac{\left[4\pi r^2 + 4\pi\left(r-h\right)^2\right]}{a}$$

(11)
$$\frac{N_{LPs}}{ml} = \frac{\left[lipid\right]\times N_A}{N_{lipid}\times 1000}$$

The number of LP particles (N_{LPs}) per milliliter (Eq. 11) can be subsequently determined from knowledge of (i) total lipid concentration, (ii) the Avogadro number (6.02×10^{23} N_A), and (iii) the previously calculated N_{lipid}. In this regard, a 10 mM lipid concentration gives a total of 2.5×10^{13} LPs/ml for our DSPC-based, 170 nm LP model. This theoretical N_{LPs}/ml was utilized for the determination of the number of LPs in cell culture as a function of lipid concentration (Fig. S19 from Chapter 1) and the number of antibodies attached per LP particle (Table 2 from Chapter 1). Finally, a RBC amount of 1.3×10^8 RBCs/ml corresponding to 2% hematocrit was considered during LP incubation with cells (parameter obtained by using the Guava EasyCyte™ mini flow cytometer, Merck Millipore Corporation).

3. Alternative determination of LP numbers by nanoparticle tracking analysis (NTA)

The amount of LPs/ml as a function of lipid concentration was determined more accurately in Chapter 2 by analyzing the movement of particles in suspension through the NanoSight NS500 system (Malvern Instruments Ltd, material kindly provided by the Department of Laboratory Medicine, Karolinska Institutet, Huddinge, Sweden). The integrated camera within this instrument allows to the determination of particles size and their concentration as well as a clear

differentiation of LPs from other interfering particles in suspension. A total of 1.2×10^{13} LPs/ml was obtained through the NTA approach for 10 mM total lipid (Table S1 from Chapter 2). This experimental N_{LPs}/ml value was employed for the calculation of LP amounts per pRBC in Chapter 2 (Fig. S3 from the same Chapter). Finally, it is important to note that this N_{LPs}/ml experimentally obtained was rather similar to the theoretical 2.5×10^{13} LPs/ml value previously determined through Eq. 11, which is remarkable if we bear in mind the scale we are working with of nearly 1×10^{13} liposome particles/ml.

ANNEX II

Exploration of amphiphilic dendritic nanoparticles as alternative antimalarial drug delivery system to LP-based approaches

RESULTS

Biomaterials 35 (2014) 7940–7950

Contents lists available at ScienceDirect

Biomaterials

journal homepage: www.elsevier.com/locate/biomaterials

Amphiphilic dendritic derivatives as nanocarriers for the targeted delivery of antimalarial drugs

Julie Movellan [a, 1], Patricia Urbán [b, c, 1], Ernest Moles [b, c], Jesús M. de la Fuente [d, e], Teresa Sierra [f], José Luis Serrano [a, *], Xavier Fernàndez-Busquets [b, c, **]

[a] Departamento de Química Orgánica-Institute of Nanoscience of Aragon (INA), University of Zaragoza, Pedro Cerbuna 12, ES-50009 Zaragoza, Spain
[b] Nanomalaria Group, Institute for Bioengineering of Catalonia (IBEC), Baldiri Reixac 10-12, ES-08028 Barcelona, Spain
[c] Barcelona Centre for International Health Research (CRESIB, Hospital Clínic-Universitat de Barcelona), Rosselló 149-153, ES-08036 Barcelona, Spain
[d] Fundación Agencia Aragonesa para la Investigación y el Desarollo (ARAID), María de Luna 11, 1ª planta, Edificio CEEI Aragón, ES-50018 Zaragoza, Spain
[e] Institute of Nanoscience of Aragon (INA), University of Zaragoza, Mariano Esquillor, Edificio I+D, ES-50018 Zaragoza, Spain
[f] Instituto de Ciencia de Materiales de Aragón (ICMA), University of Zaragoza-CSIC, Pedro Cerbuna 12, ES-50009 Zaragoza, Spain

ARTICLE INFO

Article history:
Received 25 March 2014
Accepted 21 May 2014
Available online 13 June 2014

Keywords:
Plasmodium
Dendrimers
Malaria
Nanomedicine
Polymeric nanoparticles
Antimalarial targeted drug delivery

ABSTRACT

It can be foreseen that in a future scenario of malaria eradication, a varied armamentarium will be required, including strategies for the targeted administration of antimalarial compounds. The development of nanovectors capable of encapsulating drugs and of delivering them to *Plasmodium*-infected cells with high specificity and efficacy and at an affordable cost is of particular interest. With this objective, dendritic derivatives based on 2,2-*bis*(hydroxymethyl)propionic acid (*bis*-MPA) and Pluronic® polymers have been herein explored. Four different dendritic derivatives have been tested for their capacity to encapsulate the antimalarial drugs chloroquine (CQ) and primaquine (PQ), their specific targeting to *Plasmodium*-infected red blood cells (pRBCs), and their antimalarial activity *in vitro* against the human pathogen *Plasmodium falciparum* and *in vivo* against the rodent malaria species *Plasmodium yoelii*. The results obtained have allowed the identification of two dendritic derivatives exhibiting specific targeting to pRBCs vs. non-infected RBCs, which reduce the *in vitro* IC_{50} of CQ and PQ by ca. 3- and 4-fold down to 4.0 nM and 1.1 μM, respectively. This work on the application of dendritic derivatives to antimalarial targeted drug delivery opens the way for the use of this new type of chemicals in future malaria eradication programs.

1. Introduction

Because the blood-stage infection is responsible for all symptoms and pathologies of malaria, *Plasmodium*-infected red blood cells (pRBCs) are a main chemotherapeutic target [1]. However, the success of antimalarial therapies is significantly reduced due to a variety of factors mostly derived from the complexity of the parasite life cycle and the emergence of drug resistance [2]. Consequently, new antimalarial drugs with ever increasing potency are being developed [3], many of them with a narrow therapeutic window. Drug delivery strategies could play an important role in the treatment of malaria because they might allow (i) low overall doses to limit the toxicity of the drug for the patient, (ii) delivery of sufficiently high local amounts to avoid the development of resistant parasite strains [4,5], (iii) improvement of the efficacy of currently used hydrophilic (low membrane trespassing capacity) and lipophilic antimalarials (poor aqueous solubility), (iv) use of orphan drugs never assayed as malaria therapy, e.g. because of their high and unspecific toxicity, and (v) increased immune responses in vaccine formulations.

Malaria parasites have evolved resistance (first reported from the field between 1 and 15 years after introduction, depending on the drug) to all classes of antimalarials that have gone into widespread use [6]. The physiopathology of *Plasmodium* has mechanisms oriented to develop such resistance [7], which suggests that most future new drugs will follow the same fate of rapidly losing efficacy. A strategy to maintain for a longer time the activity of yet to be discovered antimalarials is to design in advance new biomaterials for administration methods allowing the highly targeted delivery of drugs to infected cells. The development of novel drug

* Corresponding author.
** Corresponding author. Nanomalaria Group, Institute for Bioengineering of Catalonia (IBEC), Baldiri Reixac 10-12, ES-08028 Barcelona, Spain.
E-mail addresses: joseluis@unizar.es (J.L. Serrano), xfernandez_busquets@ub.edu (X. Fernàndez-Busquets).
[1] These authors contributed equally.

http://dx.doi.org/10.1016/j.biomaterials.2014.05.061
0142-9612/

delivery systems is not only less expensive than finding new drugs, but may also improve release of antimalarials at the desired rates [8]. Nanomedicine, which uses nanosized tools for the treatment of disease [9], has not been extensively applied to malaria yet, but the administration of antimalarial compounds would largely benefit from a method based on nanoparticles able to deliver their encapsulated drugs into pRBCs with high specificity. Nanoparticulate systems are a miscellaneous family of submicron structures, typically self-assembling and unable to self-replicate, and the main feature that makes them attractive drug carriers is their small size, up to several hundred nm, which allows them to cross biological barriers. Furthermore, nanoaggregates play a protective role for the drugs that helps to increase their circulating half lifes and water solubility, thus improving their therapeutic efficacy [10].

Polymer-based nanoaggregates are among the most promising carriers for drug delivery applications [11–13]. Recently, polyamidoamine (PAA)-derived polymers have been studied for the administration of antimalarials to pRBCs [14]. The PAAs AGMA1 and ISA23 exhibited specific binding and entry into target cells, but their *in vitro* IC_{50} improvement of encapsulated drugs was modest. This, in addition to their relatively small drug encapsulation capacity led us to explore new polymeric structures that could offer an alternative to PAAs. In particular, dendrimers and dendrons form a especial type of monodisperse polymers synthesized through generational growth [15–17], which have shown great potential for the design of efficient vehicles for drug delivery, mainly forming either covalent or guest-host drug-dendrimer conjugates [18–23]. The possibility of precisely tailoring the structure of dendritic molecules makes them excellent candidates to design self-assembling units that form nanoaggregates in solution [24–27], which in turn could trap molecules. Amphiphilic dendrimers (including dendrimers and dendritic polymers) have been described to form a variety of supramolecular nanostructures [28–30], enabling the effective internalization of their encapsulated drugs into cells [31].

On the basis of these considerations, we have addressed the development of efficient antimalarial carriers towards the design of two types of dendritic systems susceptible of self-aggregating in water while encapsulating the drug: amphiphilic segmented dendrimers, also called Janus dendrimers [28,30,32], consisting of two dendritic blocks of different polarity, and hybrid dendritic-linear-dendritic block copolymers [33–35] formed by a linear amphiphilic polymer functionalized at both ends with dendritic blocks. In the search of advantageous dendritic building blocks for the amphiphilic systems, we focused our attention on polyester dendrimers based on 2,2-*bis*(hydroxymethyl)propionic acid (*bis*-MPA) monomers [36]. Hult and colleagues first described this type of structures in 1996 [37] and their application in the biomedical field has been developed since then [38–42]. Some characteristics of *bis*-MPA derivatives, among which their biocompatibility *in vitro* and *in vivo*, their solubility in biological environment, their ability to be degraded by enzymes or by nonenzymatic hydrolysis and their ease of functionalization, make them good candidates for drug delivery.

2. Materials and methods

2.1. Reagents

Unless otherwise indicated, all reagents were purchased from Sigma–Aldrich (St. Louis, MO, USA) and used as received.

2.2. Synthesis and characterization of the dendritic derivatives A, B, C and D

The experimental details concerning the synthesis and characterization of all final and intermediate compounds synthesized are included in the Supplementary Information. Janus dendrimers A and B (Fig. 1) were synthesized by copper-catalyzed 1,3-dipolar azide-alkyne cycloaddition [43] of the azido-terminated glycine containing dendron and the alkyne-terminated stearic acid-functionalized dendron. A and B were obtained with total yields of 16% and 3%, respectively. Hybrid dendritic-linear-dendritic block copolymers C and D (Fig. 1) were prepared from the commercial amphiphilic block copolymer Pluronic® F127. Compound C was obtained in three steps, starting with the synthesis of the bis-MPA anhydride. The anhydride reacted directly with the terminal hydroxyl groups of the polymer to give a derivative with a first-generation bis-MPA dendron at each end of the polymeric chain. Finally, the hydroxyl terminal groups of the bis-MPA moieties were functionalized with glycine giving rise to the final compound C with a total yield of 53%. Compound D was also obtained in three steps. During the first step, the terminal hydroxyl groups of Pluronic® F127 were esterified with 4-(prop-2-ynyloxy)benzoic acid. In a second step, the alkyne terminal groups were coupled via 1,3-dipolar cycloaddition with an azido-terminated dendron derived from the third generation bis-MPA, which had the terminal hydroxyl groups protected with Boc-glycine groups (See the synthesis of compound B-3a in the Supplementary Information). Finally, the deprotection of the amine groups gave compound D in a total yield of 38%. The compounds A, B, C and D, as well as the intermediates, were characterized by ^{1}H NMR, ^{13}C NMR, FTIR, mass spectroscopy and elemental analysis (details in Supplementary Information).

2.3. Encapsulation of drugs and rhodamine B and release assays

The oil/water method described by Vrignaud et al. [12], based on the emulsification of an organic phase including the corresponding dendritic derivative (compound A, B, C or D) and an aqueous phase including the drug, chloroquine (CQ) or primaquine (PQ), or rhodamine B was used to form the nanovectors (Fig. 2). Chloroquine diphosphate, primaquine diphosphate and rhodamine B were solubilized in water and the polymer was added in a small amount of dichloromethane at a molar ratio drug:polymer 5:1. After 1 h stirring and the complete evaporation of dichloromethane, the sample was dialyzed (24 h, 4 °C) against double deionized water (MilliQ system, Millipore) in order to remove free drug and free rhodamine B (cellulose membrane, 2000 Da cutoff, Spectrum® Laboratories). These nanoparticles could be stored frozen up to several months. The amount of encapsulated compounds was calculated in an indirect way by subtracting their content in the dialysis water, measuring the absorbance at 345 nm or 340 nm for chloroquine and primaquine, respectively, and the fluorescence emission of rhodamine B at 580 nm. The encapsulation efficiency (EE) is expressed as mole of encapsulated compound/mole of initially added compound × 100.

For release assays, dendritic derivatives conjugated to chloroquine, primaquine, or rhodamine B were diluted in 250 μL of Roswell Park Memorial Institute (RPMI) complete medium supplemented with 0.5% Albumax and dialyzed (Slide-A-Lyzer MINI Dialysis Device, 10K MWCO, 0.1 mL, Thermo Scientific) at room temperature against 5 mL of the same medium for up to 48 h. 100-μL samples were taken at the specified times from the waters of dialysis and placed in a 96-well plate for determination of the different compounds as specified above.

2.4. Scanning electron microscopy (SEM)

For SEM analyses, 20 μL of the suspension of nanovectors in water was deposited on a glass plate and the solvent was evaporated at room temperature. Gold coating was done with an SC7620 Mini Sputter Coater (Quorum Technologies), and the samples were imaged with an Inspect TM550 SEM (FEI Company). The average aspect ratio (AR) was calculated for the different nanovectors following the formula AR = length/width, with 1 corresponding to a perfect sphere. The structures have been considered spherical when $1 < AR \leq 1.2$, ovoid when $1.2 < AR \leq 3$, and elongated when $AR > 3$.

2.5. Plasmodium falciparum cell culture and growth inhibition assays (GIAs)

Plasmodium falciparum 3D7 was grown *in vitro* in rinsed human RBCs of blood group type B prepared as described elsewhere [44] using previously established conditions [45]. Briefly, parasites (thawed from glycerol stocks) were cultured at 37 °C in Petri dishes containing RBCs in RPMI complete medium under a gas mixture of 92% N_2, 5% CO_2, and 3% O_2. Synchronized cultures were obtained by 5% sorbitol lysis [46], and the medium was changed every 2 days maintaining 3% hematocrit. For culture maintenance, parasitemias were kept below 5% late forms by dilution with washed RBCs. For GIAs, parasitemia was adjusted to 1.5% with more than 90% of parasites at ring stage after sorbitol synchronization. 200 μL of these living *Plasmodium* cultures were plated in 96-well plates and incubated for 48 h at 37 °C in the presence of free drugs, polymers, or polymer-encapsulated drugs. Parasitemia was determined by microscopic counting of blood smears or by fluorescence-assisted cell sorting as previously described [44].

2.6. Confocal fluorescence microscopy

Living *P. falciparum* cultures with mature stages of the parasite were incubated in phosphate buffered saline (PBS) in the presence of 100 μg/mL of polymers encapsulating rhodamine B for 90 min at 37 °C with gentle stirring. After washing, blood smears were prepared and cells were fixed in acetone:methanol (90:10). Parasite nuclei were stained with 4′,6-diamino-2-phenylindole (DAPI, Invitrogen) and the RBC membrane was labeled with wheat germ agglutinin (WGA)-Alexa 488

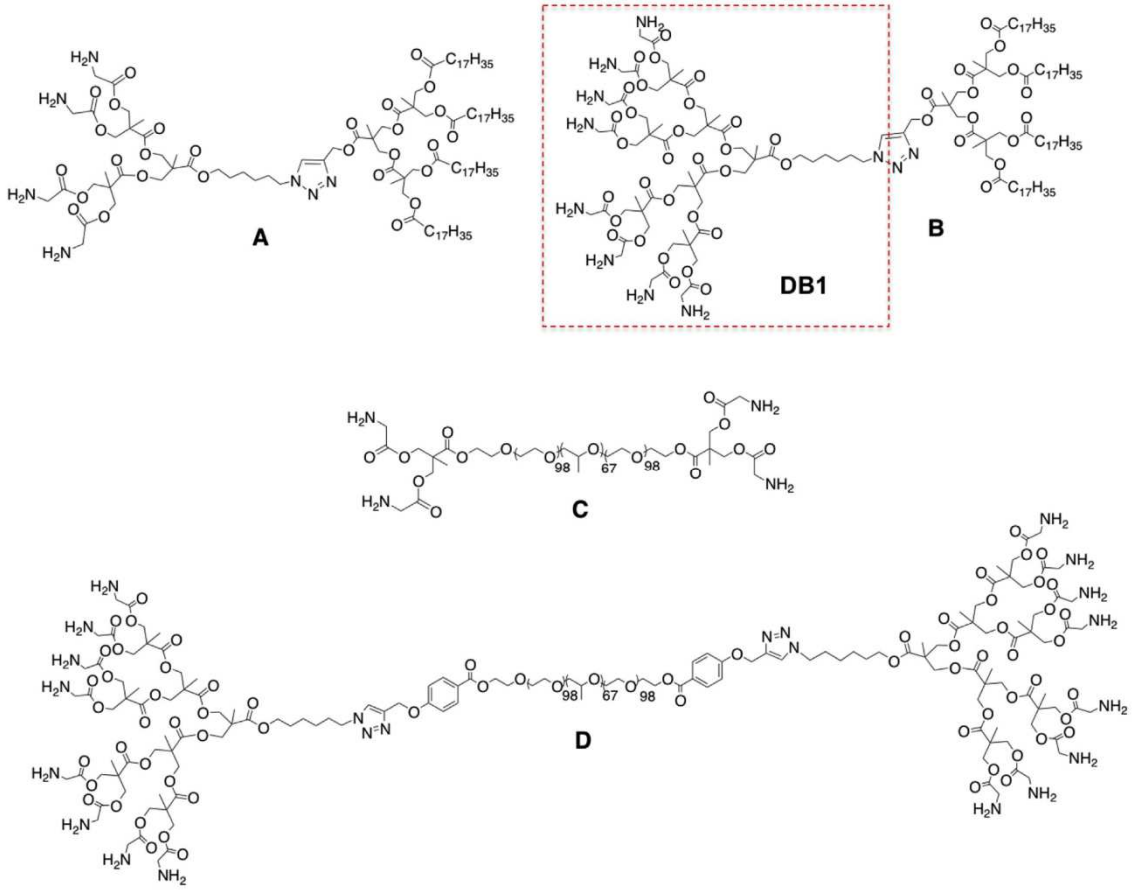

Fig. 1. Molecular structures of the two Janus dendrimers A and B, the dendron DB1, and the two hybrid dendritic-linear-dendritic block copolymers C and D.

conjugate (Molecular Probes, Eugene, OR, USA). Slides were finally mounted with Fluoroprep Mounting Medium (BioMérieux), and analyzed with a Leica TCS SP5 laser scanning confocal microscope. DAPI, reflection, WGA-Alexa 488 and rhodamine B images were acquired sequentially using 405, 488, 488 and 561 laser lines, and emission detection ranges 415–480 nm, 500–550 nm, 480–500 nm, and 571–625 nm, respectively, with the confocal pinhole set at 1 Airy units. Bright field transmitted light images were acquired simultaneously.

2.7. Hemolysis assays

RBCs were diluted in PBS to yield a solution with 3% hematocrit. 200 μL of RBCs from this suspension and 2 μL of each polymer solution were added to a 96-well plate. Each assay was performed in triplicate, including positive (1% Triton X-100) and negative (PBS) controls. After incubating for 3 h, 6 h and 24 h at 37 °C, samples were collected in Eppendorf tubes, spun at 16,000 ×*g* for 5 min, and the supernatant absorbance was measured at 541 nm.

2.8. Unspecific cytotoxicity assays

Human umbilical vein endothelial cells (HUVEC, 5000 cells/well) were plated in 96-well plates and grown for 24 h at 37 °C in 5% CO_2. After that, the medium was substituted by 100 μL of polymer-containing culture medium without fetal bovine serum, and incubation was resumed for 48 h. 10 μL of 4-[3-(4-iodophenyl)-2-(4-nitrophenyl)-2H-5-tetrazolio]-1,3-benzene disulfonate labeling reagent (WST-1) was added to each well, and the plate was incubated in the same conditions for 3 h. After thoroughly mixing for 1 min on a shaker, the absorbance of the samples was measured at 440 nm using a Benchmark Plus microplate reader. WST-1 in the absence of cells was used as blank and samples were prepared in triplicate for each

Fig. 2. Scheme representing the oil/water encapsulation method.

experiment. Percentages of viability were obtained using non-treated cells as control of survival.

2.9. Determination of polymer blood residence time and toxicity assay in mice

Inbred BALB/cAnNHsd female, 6–8 week-old mice were purchased from Harlan Laboratories and housed under standard conditions of light and temperature at the Animal House of the Universitat de Barcelona. All mice were fed a commercial diet *ad libitum*. Mice were injected intraperitoneally with a 100-μL solution in PBS of C-rhoB (12 μg rhoB/mL) or D-rhoB (2.1 μg rhoB/mL; both 50 mg dendrimer/kg). The pH of all samples was checked prior to administration and, when needed, adjusted to between 6 and 7 by addition of NaOH. 20-μL blood samples were collected in Microvette® heparinized tubes (Sarstedt) using the cross-sectional cut method, before injection (t_0) and up to 48 h post-administration. Blood samples were centrifuged for 5 min (4000 ×*g*), and 10 μL of the supernatant were used to measure rhoB fluorescence ($\lambda_{ex} = 530$ nm, $\lambda_{em} = 590$ nm) in the presence of 2% Triton X-100. For sample calibration, the respective C-rhoB and D-rhoB conjugates were used as standard. For *in vivo* toxicity assays, polymer solutions were prepared in PBS at pH 7.4 and each sample was injected intraperitoneally in three mice. Mice weight and behavior was followed daily during one week.

2.10. Antimalarial activity assay in vivo

The *in vivo* antimalarial activity of free chloroquine and primaquine and of D-CQ and C-PQ was analyzed by using a 4-day-blood suppressive test as previously described [47]. Briefly, mice were inoculated 2×10^6 RBC from *P. yoelii* 17XL (PyL) MRA-267-infected mice by intraperitoneal injection. Treatment started 2 h later (day 0) with a single dose of 0.5 or 1 mg kg^{-1} day^{-1} chloroquine ($n = 3$), or 0.9 or 1.8 mg kg^{-1} day^{-1} primaquine ($n = 3$), administered as free drug, D-CQ or C-PQ by an intraperitoneal injection followed by identical dose administration for the following 3 days. Tested compounds were prepared at appropriate doses in PBS. The control groups received PBS ($n = 3$). Parasitemia was monitored daily by microscopic examination of Wright's-stained thin-blood smears. Activity was calculated by microscopic counting of blood smears from day 4. Mice were treated in accordance with the official guidelines and Spanish laws regulating the care and use of laboratory animals. All the protocols involving animal use were approved by the Animal Experimentation Ethics Committee at the Universitat de Barcelona (http://www.ub.edu/ceea).

2.11. Statistical analysis

Data are presented as the mean ± standard error of at least three independent experiments, and the corresponding standard errors in histograms are represented by error bars. IC_{50} values were calculated by nonlinear regression with an inhibitory dose–response model using GraphPad Prism5 software.

3. Results

3.1. Selection, design and synthesis of dendritic derivatives

Previous studies in our laboratory on glycine containing dendrons with relation to their unspecific cytotoxicity, as well as their hemolytic or inherent antimalarial activities, led us to select glycine containing bis-MPA dendrons as promising candidates to be incorporated into the amphiphilic structures as a hydrophilic block

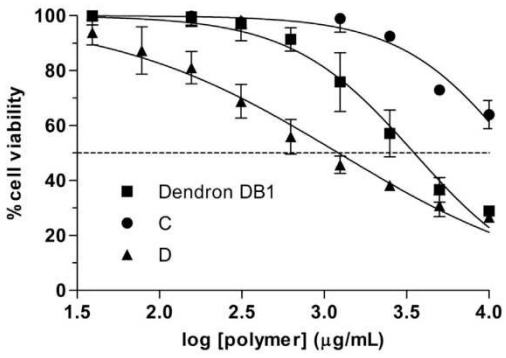

Fig. 3. Unspecific *in vitro* cytotoxicity for human umbilical vein endothelial cells of copolymers C and D and of dendron DB1.

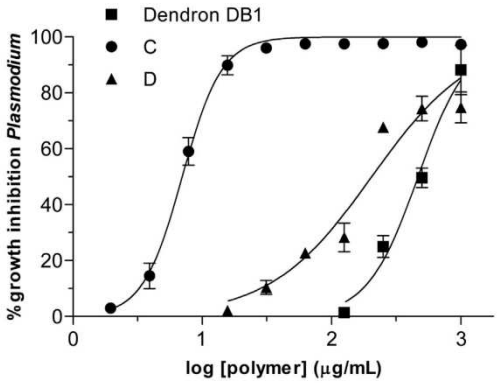

Fig. 4. *P. falciparum* growth inhibition activity of copolymers C and D and of dendron DB1.

[48]. Accordingly, we coupled two different generations, G2 and G3, of glycine containing dendrons with a hydrophobic G2 bis-MPA dendron, bearing four estearic acid chains as peripheral groups, to prepare the amphiphilic Janus dendrimers A and B, respectively (Fig. 1 and Supplementary Information).

For the design of amphiphilic hybrid dendritic-linear-dendritic block copolymers (HDLDBC) we chose Pluronic® F127, a triblock copolymer formed by two external hydrophilic blocks of poly(ethylene oxide) and a central lipophilic block of poly(propylene oxide). Due to their amphiphilic nature, Pluronic® block copolymers have the ability to self-arrange in aqueous solutions forming micelles and micellar aggregates, which have proven to be excellent candidates for the physical encapsulation of drugs [49–55]. Moreover, Pluronic® block copolymers have shown to enhance drug transport across cellular barriers through the interaction with lipidic membranes inducing membrane destabilization and permeabilization to small molecules [56]. As depicted in Fig. 1, two HDLDBCs were synthesized, copolymers C and D, which consist of Pluronic® F127 coupled at both ends with a glycine-terminated dendron of two generations, G1 in C and G3 in D.

3.2. Cytotoxicity studies

The unspecific *in vitro* cytotoxicity of the dendritic derivatives was studied on human umbilical vein endothelial cells (HUVEC) in a WST-1 toxicity assay. Due the insolubility of compounds A and B in aqueous media the cytotoxicity studies for them were made using as a model the azide-dendron derived from the third generation of bis-MPA that bears the terminal hydroxyl groups functionalized with glycine, i.e. DB1 in Fig. 1. The results obtained (Fig. 3) indicate that IC_{50} values for copolymer D and dendron DB1 are 1.2 and 3.5 mg/mL, whereas assays with copolymer C did not reach IC_{50} at the highest concentration assayed of 14.5 mg/mL. At a concentration of 2 mg/mL, none of the copolymers presented hemolytic

Table 1
Amount of chloroquine (CQ), primaquine (PQ), or rhodamine B (RhoB) conjugated to the particles formed with the dendritic derivatives A, B, C and D, expressed in weight percentage of drug. Encapsulation efficiency (EE) is also provided.

Polymer	CQ/Polymer		PQ/Polymer		RhoB/Polymer	
	w/w (%)	*EE (%)*	w/w (%)	*EE (%)*	w/w (%)	*EE (%)*
A	47.1	*81*	31.5	*47*	16.0	*19*
B	43.8	*96*	30.1	*60*	1.0	*0.4*
C	13.0	*81*	13.8	*98*	19.4	*24*
D	13.8	*100*	11.5	*92*	7.4	*8*

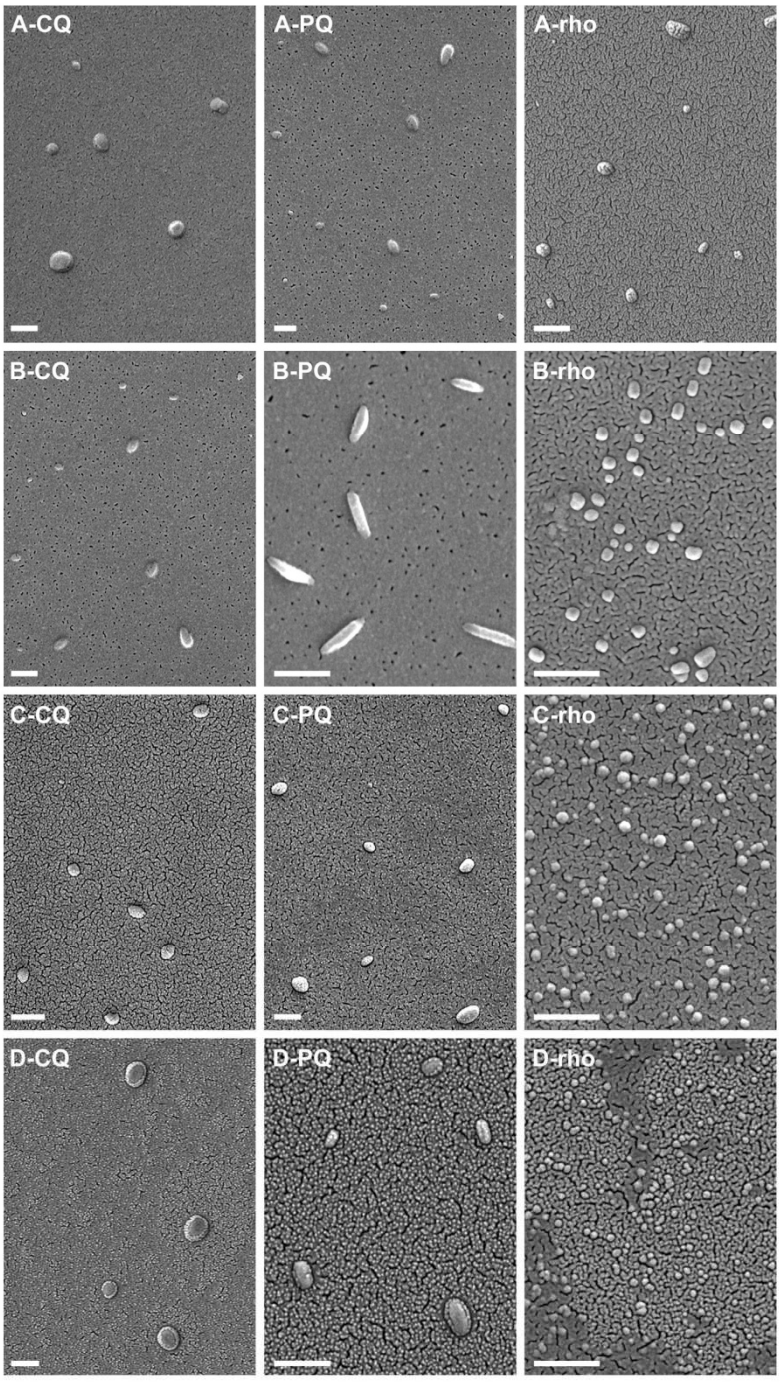

Fig. 5. Scanning electron microscopy analysis of the dendritic derivatives encapsulating chloroquine, primaquine, and rhodamine B at the ratios from Table 1. Size bar: 500 nm.

Table 2
Mean length, shape, and aspect ratio (AR = length/width), as determined by SEM, for all nanoparticles used in this work. Fifty randomly chosen nanoparticles were measured and number averaged for each type of structure to determine their mean length and aspect ratio.

Compound	Length (nm)	Shape	AR
A-CQ	415 ± 109	Spherical	1.13 ± 0.16
B-CQ	500 ± 226	Spherical	1.17 ± 0.11
C-CQ	172 ± 87	Ovoid	1.46 ± 0.25
D-CQ	360 ± 131	Ovoid	1.30 ± 0.15
A-PQ	386 ± 257	Ovoid	1.71 ± 0.28
B-PQ	641 ± 277	Elongated	4.66 ± 1.84
C-PQ	290 ± 78	Ovoid	1.23 ± 0.17
D-PQ	178 ± 53	Ovoid	1.73 ± 0.15
A-rhoB	188 ± 91	Spherical	1.09 ± 0.11
B-rhoB	94 ± 29	Spherical	1.17 ± 0.10
C-rhoB	70 ± 16	Spherical	1.06 ± 0.05
D-rhoB	50 ± 7	Spherical	1.12 ± 0.09

activity, with 0.0 ± 0.9%, 0.0 ± 0.8%, and 0.0 ± 0.4% hemolysis for dendron DB1 and copolymers C and D, respectively.

The three dendritic derivatives were assayed for their *in vitro* activity against *P. falciparum* in a GIA that revealed intrinsic antimalarial activity for all of them. The results obtained (Fig. 4) indicate that the respective *P. falciparum* IC_{50} values for copolymers C and D and the dendron DB1 are 7, 204, and 466 μg/mL. Copolymer C showed significant antimalarial activity *in vitro* at concentrations at which no cytotoxicity was observed in HUVEC cells.

3.3. Encapsulation of antimalarial drugs and rhodamine B in nanoparticles

The four amphiphilic dendritic derivatives have been used to prepare nanocarriers that encapsulate the antimalarial drugs chloroquine (CQ) or primaquine (PQ), and the fluorescent dye rhodamine B (rhoB). The oil/water emulsion method [12], based on the emulsification of an organic phase including the dendritic derivatives and an aqueous phase including rhodamine B or the

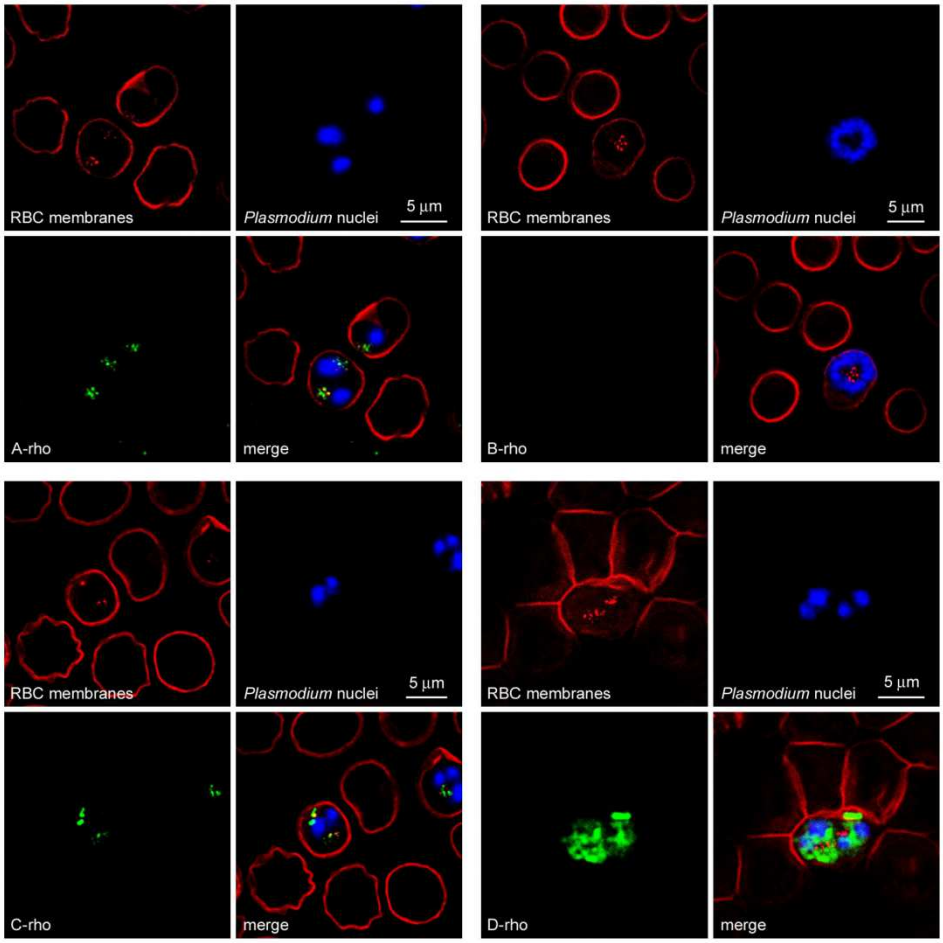

Fig. 6. Confocal fluorescence microscopy study of the targeting of dendritic derivatives to pRBCs vs. RBCs. Rhodamine B-labeled dendritic derivatives were incubated for 90 min with living RBC + pRBC cocultures before sample processing. Blue DAPI fluorescence indicates *Plasmodium* DNA inside pRBCs and the fluorescence of rhodamine B is shown in green to avoid overlapping with WGA membrane staining (red).

corresponding drug in its diphosphate form, was used for the formation of heterologous nanoaggregates. The highest amounts of conjugated drug (w/w percentage ratios active molecule/polymer) were achieved with dendrimers A and B, whereas rhodamine B was best incorporated into structures A and C (Table 1, Tables S4 and S5).

In order to achieve optimal encapsulation efficiency (EE) with these systems, different drug/dendritic derivative ratios were assayed (Tables S2 and S3). These preliminary studies allowed establishing a drug/dendritic derivative molar ratio of 5:1 yielding the highest EEs, which ranged from ca. 50%–100% depending on their structure (Tables S2). By increasing the drug/dendritic derivative molar ratio to values around 30:1, a higher amount of drug could be encapsulated in the case of copolymers C and D (Tables S3), although this occurred simultaneously with a significant decrease of the EE and a consequent complication in the purification of the resulting nanocarriers.

3.4. Determination of nanoparticle morphology

The nanoparticles formed with the dendritic derivatives encapsulating chloroquine, primaquine, and rhodamine B were analyzed by SEM (Fig. 5). The different chemical structures of the molecules encapsulated resulted in nanoparticles of different size and shape (Table 2). Those containing PQ and CQ presented ovoid or spherical shapes with mean long axes/diameters, respectively, ranging from ca. 170–500 nm, with the only exception of B-PQ, which yielded elongated structures. Rhodamine B-encapsulating structures were all spherical and significantly smaller. A-rhoB aggregates were polydisperse, ranging in size from 100 to 300 nm, whereas the structures formed by B-rhoB were more regular, around 100 nm across. The compounds derived from Pluronic® F127 polymer formed more spherical and smaller assemblies, with respective diameters around 70 and 50 nm for C-rhoB and D-rhoB .

3.5. Cell targeting analysis of dendritic derivatives

With the objective of exploring whether a specific pRBC targeting due to the chemical structure of the carrier existed, rhodamine B-loaded nanoparticles prepared from A, B, C and D amphiphilic dendritic derivatives were used in fluorescence microscopy assays. Living pRBC/RBC cocultures were incubated for 90 min in the presence of the four nanocarriers encapsulating rhodamine B prior to fixation and processing of the sample for fluorescence microscopy (Fig. 6). Whereas fluorescence was never observed inside RBCs, rhodamine B signal could be detected inside pRBCs when the cocultures were incubated with A-rhoB, C-rhoB, and D-rhoB nanoparticles. No labeled cells were present in cocultures incubated with B-rhoB, likely due to the limited incorporation of rhodamine B in B aggregates. The highest intracellular rhodamine B signal was obtained with D-rhoB, with a fluorescent pattern distributed throughout the cytoplasm of the parasitized pRBC. Rhodamine B in this experiment acted as a drug surrogate, showing that dendrimeric derivative-transported compounds could specifically enter pRBCs vs. RBCs *in vitro*.

3.6. Evaluation of the in vitro antimalarial activity of drug-loaded nanoparticles

Equal drug concentrations in the form of both control free drugs and drug-loaded carriers were tested for their ability to inhibit the growth of *P. falciparum in vitro* (Fig. 7). The results obtained with chloroquine-containing nanoparticles (Fig. 7A) showed that, whereas no efficacy improvement occurred with A-CQ, B-CQ and C-CQ, a three-fold increase with respect to free chloroquine was observed for D-CQ. In agreement with growth inhibition activity

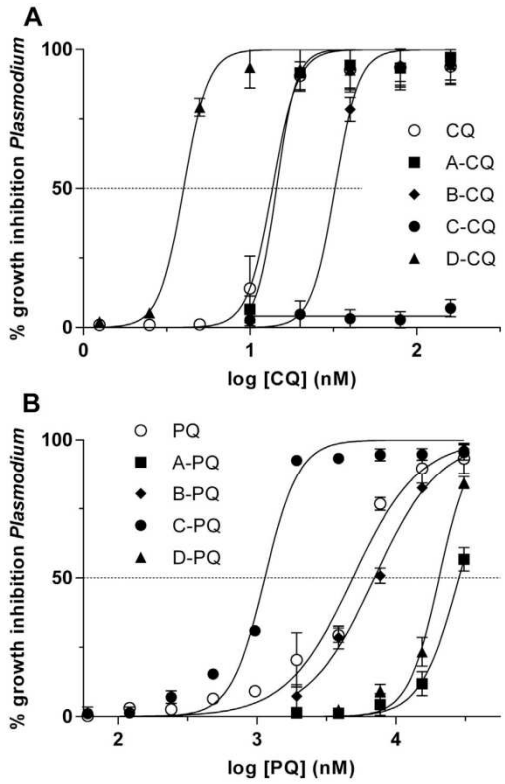

Fig. 7. Antimalarial activity *in vitro* of the particles encapsulating chloroquine (A) or primaquine (B).

data, *P. falciparum* cultures that had been treated with D-CQ were almost free of pRBCs according to microscopic examination (Fig. S3). This chloroquine-loaded system provided optimal antimalarial activity at all tested concentrations, reducing the IC_{50} from 13.6 nM for free chloroquine to 4.0 nM for the encapsulated drug (Table 3). The observed targeting specificity of D-rhoB towards pRBCs could contribute to the good performance in GIAs of copolymer D when encapsulating chloroquine. At the concentration used (13 ng/mL) copolymer D has low toxicity for *Plasmodium*, indicating that the antimalarial effect observed is mainly due to the activity of chloroquine, which is significantly increased when the drug is delivered within this nanostructure.

Data obtained from delivery systems encapsulating primaquine (Fig. 7B) reveal that A-PQ and D-PQ have significantly less efficacy than an equal amount of primaquine in solution, whereas B-PQ displays an activity similar to that of the free drug. C-PQ exhibits the highest activity, reducing the IC_{50} from 4.9 μM for free primaquine to 1.1 μM for the encapsulated drug (Table 3). In this case the

Table 3
IC_{50} values of the different nanovectors and their corresponding free drugs.

	IC_{50} (nM)	95% Confidence intervals		IC_{50} (μM)	95% Confidence intervals
CQ	13.6	12.2–15.2	PQ	4.9	4.0–5.9
A-CQ	14.4	11.3–18.3	A-PQ	28.5	26.5–30.6
B-CQ	32.4	26.4–39.7	B-PQ	7.0	5.9–8.3
C-CQ	–	–	C-PQ	1.1	0.9–1.3
D-CQ	4.0	3.5–4.4	D-PQ	20.5	17.4–24.1

concentration of copolymer C used (3 μg/mL) is not far from its IC_{50} for *Plasmodium* (7 μg/mL, Fig. 4), suggesting that part of the antimalarial activity of C-PQ might be due to the endogenous activity of copolymer C itself.

According to release assays (Fig. 8), after 24 h in the medium used for *P. falciparum* GIAs all the drug has leaked from drug/polymer conjugates. The release of drug that had been trapped within the nanostructures during their preparation in water, might be due to drug–solvent interactions at the physiological ionic strength of GIAs. Drug release could also be favored by the degradation of dendritic structures at the temperature (37 °C) and pH (7.4) of GIAs. Mass spectroscopy analysis in these conditions proved the ester cleavage of the glycine units from the dendritic block after only 1 h of incubation (Fig. S4).

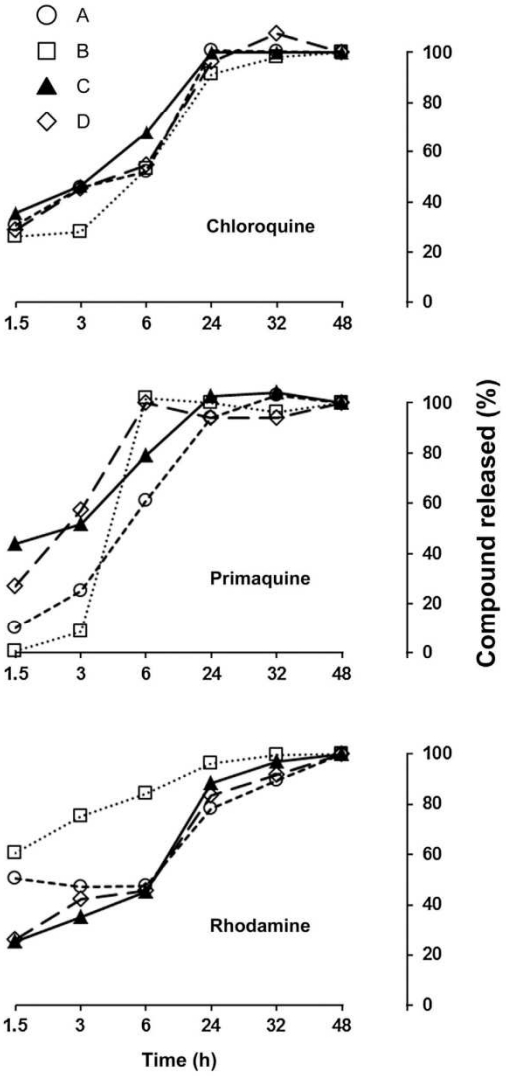

Fig. 8. Release from dendritic derivatives of chloroquine, primaquine and rhodamine B in the medium used for *P. falciparum* growth inhibition assays.

3.7. *In vivo* assays in malaria-infected mice

Preliminary *in vivo* assays in mice did not show a significant improvement of drug efficacy for D-CQ when compared to free chloroquine. At the intraperitoneally administered doses of 0.5 and 1 mg kg^{-1} day^{-1} free chloroquine reduced parasitemia by 38.2 ± 23.0% and 52.1 ± 35.6% respectively, whereas the same amount of drug encapsulated in D yielded the respective activities of 34.0 ± 21.7% and 43.6 ± 8.3%. The mice survival data, however, were better for D-CQ-treated mice, which survived for respective mean times of 5.7 and 9.7 days vs. 3.3 and 7 days for the animals treated with free chloroquine. In the same assay done for C-PQ, at the intraperitoneally administered dose of 0.9 mg kg^{-1} day^{-1} free primaquine had no activity against *P. falciparum*, whereas the same amount of conjugated drug reduced parasitemia by 22.6 ± 9.1%; upon administration of 1.8 mg kg^{-1} day^{-1} the activities were 13.9 ± 15.3% and 49.7 ± 21.4% respectively. Mice survival data also indicated a better efficacy of PQ encapsulated in C: free PQ-treated mice survived for respective mean times of 4.3 and 5.0 days in comparison to 5.7 and 9.3 days for the animals treated with C-PQ.

A pharmacokinetic study of the presence in blood of intraperitoneally administered C-rhoB and D-rhoB (Fig. 9) revealed that both nanovectors were detected in the blood circulation as soon as 2 min post-administration, with about 20% of their maximum level still detected after 8.5 h and a blood half-life of ca. 4.5 h.

4. Discussion

The antimalarial drug-encapsulating dendritic derivatives C-PQ and D-CQ significantly reduce the *in vitro* IC_{50} of free primaquine and chloroquine. This might be related to structures C and D being poloxamer derivatives that have been previously reported to form micelles [51] and to interact with cell membranes thus facilitating the internalization of compounds [56]. The result obtained with D-CQ is particularly relevant because CQ has an endogenous carrier across erythrocyte membranes that accumulates the drug selectively in these cells [57], which makes improving CQ activity a challenging task. Also the data obtained for primaquine encapsulation are promising because in patients with glucose-6-phosphate dehydrogenase (G6PD) deficiency primaquine generally produces a hemolysis which may be severe [58,59], and this toxicological concern has led to restrictions in the use of this drug since the

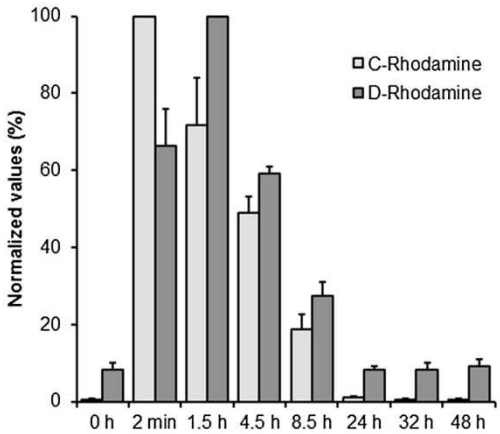

Fig. 9. Time profile determination of the presence in blood of intraperitoneally administered C-rhoB and D-rhoB.

incidence of G6PD genetic anomaly is particularly high in areas where malaria is endemic [60]. The possibility of delivering the drug encapsulated might contribute to eliminating this problem, since at the concentrations used in *in vitro Plasmodium* GIAs the dendritic derivatives used are neither cytotoxic nor hemolytic.

Antibody-functionalized liposomal nanovectors for the targeted delivery of drugs specifically to pRBCs have shown complete discrimination *in vitro* for pRBCs vs. non-infected erythrocytes, increasing tenfold the activity of chloroquine. But some properties of antibodies limit their role as targeting elements in antimalarial therapeutic strategies: they have a lengthy and relatively expensive production, are highly immunogenic unless genetically engineered humanized forms are used, and, as a result of the high variability of *Plasmodium* proteins exposed on pRBC surfaces, as the parasite switches to new antigenic repertoires any antibody will likely lose targeting efficacy and will have to be replaced. In this context, the endogenous pRBC targeting specificity vs. non-infected RBCs observed for derivatives A, C, and D, eliminates the need for adding targeting molecules to the nanovector, thus reducing production costs and complexity of the system. These are important parameters to consider when designing medicines for malaria, which will be mainly deployed in low per-capita income regions and will require long shelf lives.

The sizes of the drug-loaded carriers used for GIAs were in all cases above 70 nm, which is the upper limit described for the entry of nanoparticles into pRBCs through the new permeation pathways (NPPs) which *Plasmodium* generates in its host cell [61]. The chemical interplay between copolymer and drug must be a key factor regarding the interactions of the nanoparticles with pRBCs and the targeted specificity of drug delivery, since structure C improves the activity of PQ but not of CQ, whereas the opposite has been observed for structure D. Similarly, in the case of rhodamine B-loaded nanocarriers, C-rhoB had a rhodamine B load three times higher than D-rhoB according to rhodamine B emission, but rhodamine B fluorescence was much higher inside pRBCs treated with D-rhoB. In this case, though, the smaller size of D-rhoB (50 ± 7 nm vs. 70 ± 16 nm for C-rhoB) suggests that this adduct could more easily enter pRBCs through NPPs, although our data do not permit discriminating between D-rhoB entering pRBCs and its binding to pRBCs and releasing rhodamine B there, which would result in a high rhodamine B concentration in the close vicinity of pRBCs that might favor its entry in these cells.

It has been shown that the shape of the nanoparticles influences their targeting ability, internalization capacity and degradation for the release of drugs [62,63]. The dendrimeric derivatives assayed here showing higher activity than free drugs have an aspect-ratio closer to 1, which corresponds to a more spherical shape. Worm-shaped nanoparticles composed of a diblock copolymer circulate in the mouse blood with a long half-life of ca. 5 days [64]. The underlying mechanism seems to be the strong drag force experienced in the fluid flow by the elongated structures such that the macrophages cannot engulf them before they are carried away by the blood circulation. It is then conceivable that a further improved efficacy of polymer-encapsulated drugs might be obtained by increasing blood residence times through the synthesis of more elongated polymers.

Galactose-coated dendrimers had been assayed for chloroquine delivery [65], having shown reduced phagocytosis, immunogenicity and hemolytic toxicity, thus being a safer alternative compared to their uncoated formulations. In spite of their broad applicability, associated toxicity due to the terminal amino groups and cationic charge of some dendrimers hampers their clinical applications [66]. One approach to improve dendrimer biocompatibility contemplates surface modifications [67], including capping of the terminal $-NH_2$ groups with neutral or anionic moieties such as poly(ethylene glycol) (PEG). A PEG-lysine type dendritic micelle presented a prolonged release of the antimalarial drug artemether [68], increasing drug stability and solubility. These good properties were also observed for chondroitin sulfate A (CSA)-coated poly-L-lysine-based dendrimers having a PEG amino core for the controlled release of chloroquine after intravenous administration [69]. CSA coating increased the amount of drug loading and its sustained release, decreased the unspecific cytotoxicity of the dendrimer and showed higher activity in *in vitro* studies. Despite these promising *in vitro* results, to the best of our knowledge there are no published studies on the *in vivo* efficacy of dendrimer-antimalarial drug conjugates. Only one report describes the evaluation of Pluronic® F127 for the encapsulation of artemether in a nasal delivery formulation [70]. The *in vivo* behavior hinted here in preliminary assays for structure D, which equals (in parasitemia reduction) and even slightly improves (in mice survival time) the activity of such a good antimalarial in solution as chloroquine, represents an important pioneering step towards the use of dendritic structures in antimalarial therapeutic strategies. The promising *in vivo* data obtained for adduct C-PQ are also important regarding the above mentioned problems of PQ therapy in G6PD-deficient patients.

5. Conclusion

In a previous work where we studied the capacity of polyamidoamine-derived polymers for the targeted delivery of antimalarials to pRBCs [14], we obtained a modest amelioration in the *in vitro* activity of encapsulated chloroquine or primaquine compared to the free drug, up to drug:polymer ratios of ca. 30% (w/w). In contrast, here we have observed a clear improvement in the *in vitro* IC_{50} of both drugs at drug:polymer ratios of only 16% (w/w). Preliminary assays indicate that the drug loading capacity limit of the dendritic derivatives is considerably higher, suggesting that drug efficacy can still be further improved. Finally, a crucial practical aspect to consider when designing nanomedicines to be administered in a malaria setting of low per-capita income regions is their cost. Nanomedicines in general and dendrimers in particular are usually thought to be expensive and therefore difficult to apply to diagnose, prevent, or treat malaria. However, the synthesis cost of 1 g of structures C and D is 14 and 67 € respectively, which means that the added cost of the observed reduction in the *in vitro* IC_{50} of PQ and CQ is of less than 0.5 cents of € for a culture volume of 6 L, a figure likely to be cut down for larger batch sizes.

Author contributions

The manuscript was written through contributions of all authors. All authors have given approval to the final version of the manuscript.

Acknowledgments

This work was supported by grants BIO2008-01184, BIO2011-25039, CTQ2012-35692 and MAT2012-38538-CO3-01 from the Ministerio de Economía (MINECO), Spain, which included FEDER funds, by grant 2009SGR-760 from the Generalitat de Catalunya and the Aragon Government-FSE (Project E04) and by the European Union with the FP7 PEOPLE PROGRAMME, The Marie Curie Actions, ITN, no. 215884-2. Thanks are given to: LMA Service of the Instituto de Nanociencia Aragon, University of Zaragoza (Spain) and Nuclear Magnetic Resonance and Mass Spectrometry Services from the CEQMA, Universidad de Zaragoza-CSIC (Spain). A fellowship from Instituto de Salud Carlos III is acknowledged by P.U. J.M.

acknowledges support from EU as an ESR fellowship. Julie Movellan and Patricia Urbán contributed equally to this work.

Appendix A. Supplementary data

Supplementary data related to this article can be found at http://dx.doi.org/10.1016/j.biomaterials.2014.05.061.

References

[1] Griffith KS, Lewis LS, Mali S, Parise ME. Treatment of malaria in the United States: a systematic review. JAMA 2007;297:2264–77.
[2] World Health Organization World Malaria Report 2013. Available from: URL, http://www.who.int/malaria/publications/world_malaria_report_2013/report/en/; May 2014.
[3] Gamo FJ, Sanz LM, Vidal J, de Cozar C, Alvarez E, Lavandera JL, et al. Thousands of chemical starting points for antimalarial lead identification. Nature 2010;465:305–10.
[4] Baird JK. Effectiveness of antimalarial drugs. N Engl J Med 2005;352:1565–77.
[5] White NJ. Assessment of the pharmacodynamic properties of antimalarial drugs in vivo. Antimicrob Agents Chemother 1997;41:1413–22.
[6] Mackinnon MJ, Marsh K. The selection landscape of malaria parasites. Science 2010;328:866–71.
[7] Read AF, Huijben S. Evolutionary biology and the avoidance of antimicrobial resistance. Evol Appl 2009;2:40–51.
[8] Murambiwa P, Masola B, Govender T, Mukaratirwa S, Musabayane CT. Antimalarial drug formulations and novel delivery systems: a review. Acta Trop 2011;118:71–9.
[9] Duncan R, Gaspar R. Nanomedicine(s) under the microscope. Mol Pharmacol 2011;8:2101–41.
[10] Owen SC, Chan DPY, Shoichet MS. Polymeric micelle stability. Nano Today 2012;7:53–65.
[11] Kedar U, Phutane P, Shidhaye S, Kadam V. Advances in polymeric micelles for drug delivery and tumor targeting. Nanomedicine: NBM 2010;6:714–29.
[12] Vrignaud S, Benoit JP, Saulnier P. Strategies for the nanoencapsulation of hydrophilic molecules in polymer-based nanoparticles. Biomaterials 2011;32:8593–604.
[13] Kamaly N, Xiao Z, Valencia PM, Radovic-Moreno AF, Farokhzad OC. Targeted polymeric therapeutic nanoparticles: design, development and clinical translation. Chem Soc Rev 2012;41:2971–3010.
[14] Urbán P, Valle-Delgado JJ, Mauro N, Marques J, Manfredi A, Rottmann M, et al. Use of poly(amidoamine) drug conjugates for the delivery of antimalarials to *Plasmodium*. J Control Release 2014;177:84–95.
[15] Grayson SM, Fréchet JMJ. Convergent dendrons and dendrimers: from synthesis to applications. Chem Rev 2001;101:3819–68.
[16] Carlmark A, Hawker C, Hult A, Malkoch M. New methodologies in the construction of dendritic materials. Chem Soc Rev 2009;38:352–62.
[17] Tomalia DA. Dendrons/dendrimers: quantized, nano-element like building blocks for soft-soft and soft-hard nano-compound synthesis. Soft Matter 2010;6:456–74.
[18] Boas U, Heegaard PMH. Dendrimers in drug research. Chem Soc Rev 2004;33:43–63.
[19] Patri AK, Kukowska-Latallo JF, Baker JRJ. Targeted drug delivery with dendrimers: comparison of the release kinetics of covalently conjugated drug and non-covalent drug inclusion complex. Adv Drug Deliv Rev 2005;57:2203–14.
[20] Paleos CM, Tsiourvas D, Sideratou Z. Molecular engineering of dendritic polymers and their application as drug and gene delivery systems. Mol Pharm 2007;4:169–88.
[21] Tekade RK, Kumar PV, Jain NK. Dendrimers in oncology: an expanding horizon. Chem Rev 2008;109:49–87.
[22] Medina SH, El-Sayed MEH. Dendrimers as carriers for delivery of chemotherapeutic agents. Chem Rev 2009;109:3141–57.
[23] Mintzer MA, Grinstaff MW. Biomedical applications of dendrimers: a tutorial. Chem Soc Rev 2011;40:173–90.
[24] Tomalia DA. Dendrimeric supramolecular and supramacromolecular assemblies. In: Ciferri A, editor. Supramolecular Polymers. Boca Raton, FL: CRC Press Taylor & Francis Group; 2005. pp. 187–256.
[25] Al-Jamal KT, Ramaswamy C, Florence AT. Supramolecular structures from dendrons and dendrimers. Adv Drug Deliv Rev 2005;57:2238–70.
[26] Rosen BM, Wilson CJ, Wilson DA, Peterca M, Imam MR, Percec V. Dendron-mediated self-assembly, disassembly, and self-organization of complex systems. Chem Rev 2009;109:6275–540.
[27] Dong CM, Liu G. Linear-dendritic biodegradable block copolymers: from synthesis to application in bionanotechnology. Polym Chem 2013;4:46–52.
[28] Percec V, Wilson DA, Leowanawat P, Wilson CJ, Hughes AD, Kaucher MS, et al. Self-assembly of Janus dendrimers into uniform dendrimersomes and other complex architectures. Science 2010;328:1009–14.
[29] Meyers SR, Juhn FS, Griset AP, Luman NR, Grinstaff MW. Anionic amphiphilic dendrimers as antibacterial agents. J Am Chem Soc 2008;130:14444–5.
[30] Wang Y, Grayson SM. Approaches for the preparation of non-linear amphiphilic polymers and their applications to drug delivery. Adv Drug Deliv Rev 2012;64:852–65.
[31] Hillaireau H, Couvreur P. Nanocarriers' entry into the cell: relevance to drug delivery. Cell Mol Life Sci 2009;66:2873–96.
[32] Caminade AM, Laurent R, Delavaux-Nicot B, Majoral JP. "Janus" dendrimers: syntheses and properties. New J Chem 2012;36:217–26.
[33] Gitsov I, Wooley KL, Fréchet JMJ. Novel polyether copolymers consisting of linear and dendritic blocks. Angew Chem Int Ed Engl 1992;31:1200–2.
[34] Amir RJ, Albertazzi L, Willis J, Khan A, Kang T, Hawker CJ. Multifunctional trackable dendritic scaffolds and delivery agents. Angew Chem Int Ed 2011;50:3425–9.
[35] Wurm F, Frey H. Linear–dendritic block copolymers: the state of the art and exciting perspectives. Prog Polym Sci 2011;36:1–52.
[36] Carlmark A, Malmström E, Malkoch M. Dendritic architectures based on bis-MPA: functional polymeric scaffolds for application-driven research. Chem Soc Rev 2013;42:5858–79.
[37] Ihre H, Hult A, Söderlind E. Synthesis, characterization, and ^{1}H NMR self-diffusion studies of dendritic aliphatic polyesters based on 2,2-bis(hydroxymethyl)propionic acid and 1,1,1-tris(hydroxyphenyl)ethane. J Am Chem Soc 1996;118:6388–95.
[38] Gillies ER, Fréchet JMJ. Designing macromolecules for therapeutic applications: polyester dendrimer-poly(ethylene oxide) "bow-tie" hybrids with tunable molecular weight and architecture. J Am Chem Soc 2002;124:14137–46.
[39] Lee CC, MacKay JA, Fréchet JMJ, Szoka FC. Designing dendrimers for biological applications. Nat Biotechnol 2005;23:1517–26.
[40] Lee CC, Gillies ER, Fox ME, Guillaudeu SJ, Fréchet JMJ, Dy EE, et al. A single dose of doxorubicin-functionalized bow-tie dendrimer cures mice bearing C-26 colon carcinomas. Proc Natl Acad Sci U S A 2006;103:16649–54.
[41] Goodwin AP, Lam SS, Fréchet JMJ. Rapid, efficient synthesis of heterobifunctional biodegradable dendrimers. J Am Chem Soc 2007;129:6994–5.
[42] van der Poll DG, Kieler-Ferguson HM, Floyd WC, Guillaudeu SJ, Jerger K, Szoka FC, et al. Design, synthesis, and biological evaluation of a robust, biodegradable dendrimer. Bioconjug Chem 2010;21:764–73.
[43] Himo F, Lovell T, Hilgraf R, Rostovtsev VV, Noodleman L, Sharpless KB, et al. Copper(I)-catalyzed synthesis of azoles. DFT study predicts unprecedented reactivity and intermediates. J Am Chem Soc 2004;127:210–6.
[44] Urbán P, Estelrich J, Cortés A, Fernàndez-Busquets X. A nanovector with complete discrimination for targeted delivery to *Plasmodium falciparum*-infected versus non-infected red blood cells *in vitro*. J Control Release 2011;151:202–11.
[45] Cranmer SL, Magowan C, Liang J, Coppel RL, Cooke BM. An alternative to serum for cultivation of *Plasmodium falciparum in vitro*. Trans R Soc Trop Med Hyg 1997;91:363–5.
[46] Lambros C, Vanderberg JP. Synchronization of *Plasmodium falciparum* erythrocytic stages in culture. J Parasitol 1979;65:418–20.
[47] Fidock DA, Rosenthal PJ, Croft SL, Brun R, Nwaka S. Antimalarial drug discovery: efficacy models for compound screening. Nat Rev Drug Discov 2004;3:509–20.
[48] Movellan J. Dendritic derivatives as building blocks for biomedical applications, 2013. PhD dissertation. Universidad de Zaragoza; May 2014. Available from: URL: http://zaguan.unizar.es/record/10464.
[49] Batrakova EV, Kabanov AV. Pluronic block copolymers: evolution of drug delivery concept from inert nanocarriers to biological response modifiers. J Control Release 2008;130:98–106.
[50] Wei Z, Hao J, Yuan S, Li Y, Juan W, Sha X, et al. Paclitaxel-loaded Pluronic P123/F127 mixed polymeric micelles: formulation, optimization and in vitro characterization. Int J Pharm 2009;376:176–85.
[51] Lee ES, Oh YT, Youn YS, Nam M, Park B, Yun J, et al. Binary mixing of micelles using pluronics for a nano-sized drug delivery system. Colloids Surf B 2011;82:190–5.
[52] Dahmani FZ, Yang H, Zhou J, Yao J, Zhang T, Zhang Q. Enhanced oral bioavailability of paclitaxel in pluronic/LHR mixed polymeric micelles: preparation, in vitro and in vivo evaluation. Eur J Pharm Sci 2012;47:179–89.
[53] Yoncheva K, Calleja P, Agüeros M, Petrov P, Miladinova I, Tsvetanov C, et al. Stabilized micelles as delivery vehicles for paclitaxel. Int J Pharm 2012;436:258–64.
[54] Kabanov AV, Batrakova EV, Alakhov VY. Pluronic® block copolymers for overcoming drug resistance in cancer. Adv Drug Deliv Rev 2002;54:759–79.
[55] Kabanov AV, Batrakova EV, Alakhov VY. Pluronic® block copolymers as novel polymer therapeutics for drug and gene delivery. J Control Release 2002;82:189–212.
[56] Pembouong G, Morellet N, Kral T, Hof M, Scherman D, Bureau MF, et al. A comprehensive study in triblock copolymer membrane interaction. J Control Release 2011;151:57–64.
[57] Yayon A, Ginsburg H. The transport of chloroquine across human erythrocyte membranes is mediated by a simple symmetric carrier. Biochim Biophys Acta 1982;686:197–203.
[58] Beutler E, Duparc S. Glucose-6-phosphate dehydrogenase deficiency and antimalarial drug development. Am J Trop Med Hyg 2007;77:779–89.
[59] Burgoine KL, Bancone G, Nosten F. The reality of using primaquine. Malar J 2010;9:376.
[60] Chan TK, Todd D, Tso SC. Drug-induced haemolysis in glucose-6-phosphate dehydrogenase deficiency. BMJ 1976;2:1227–9.
[61] Goodyer ID, Pouvelle B, Schneider TG, Trelka DP, Taraschi TF. Characterization of macromolecular transport pathways in malaria-infected erythrocytes. Mol Biochem Parasitol 1997;87:13–28.

[62] Champion JA, Katare YK, Mitragotri S. Particle shape: a new design parameter for micro- and nanoscale drug delivery carriers. J Control Release 2007;121:3–9.
[63] Gratton SEA, Ropp P, Pohlhaus PD, Luft JC, Madden VJ, Napier ME, et al. The effect of particle design on cellular internalization pathways. Proc Natl Acad Sci U S A 2008;105:11613–8.
[64] Geng Y, Discher DE. Hydrolytic degradation of poly(ethylene oxide)-block-polycaprolactone worm micelles. J Am Chem Soc 2005;127:12780–1.
[65] Agrawal P, Gupta U, Jain NK. Glycoconjugated peptide dendrimers-based nanoparticulate system for the delivery of chloroquine phosphate. Biomaterials 2007;28:3349–59.
[66] Bhadra D, Yadav AK, Bhadra S, Jain NK. Glycodendrimeric nanoparticulate carriers of primaquine phosphate for liver targeting. Int J Pharm 2005;295:221–33.
[67] Ciolkowski M, Petersen JF, Ficker M, Janaszewska A, Christensen JB, Klajnert B, et al. Surface modification of PAMAM dendrimer improves its biocompatibility. Nanomedicine 2012;8:815–7.
[68] Bhadra D, Bhadra S, Jain NK. PEGylated lysine based copolymeric dendritic micelles for solubilization and delivery of artemether. J Pharm Pharm Sci 2005;8:467–82.
[69] Bhadra D, Bhadra S, Jain NK. PEGylated peptide dendrimeric carriers for the delivery of antimalarial drug chloroquine phosphate. Pharm Res 2006;23:623–33.
[70] Mahajan HS, Shah SK, Surana SJ. Nasal in situ gel containing hydroxy propyl β-cyclodextrin inclusion complex of artemether: development and in vitro evaluation. J Incl Phenom Macrocycl Chem 2011;70:49–58.

SUPPLEMENTARY DATA

Synthesis of *bis*-MPA and Pluronic® derivatives

The same synthetic processes have been used for the preparation of several compounds. The general procedures are described as follows and each compound is referred to the appropriate one.

General procedure for the synthesis of compounds A and B

The synthesis of products A and B began with the preparation of two bis-MPA dendrons by Steglich esterifications, both of them functionalized with an azide group or an alkyne group in order to be coupled by CuAAC. Both dendrimers were synthesized following the same strategy and were prepared from the commercial bis-MPA monomer as described below (see Scheme 1 for the synthesis of compound B). As a first step, the bis-MPA carboxylic acid was functionalized with either azide- (**1a**) or alkyne-containing moieties (**1b**). In order to do so, the hydroxyl groups of the bis-MPA monomer were protected by the formation of an acetal with 2,2-dimethoxypropane catalyzed by p-toluenesulfonic acid in acetone. Then, the esterification of the carboxylic acid with 6-azidohexan-1-ol (**1a**) or propargyl alcohol (**1b**) in the presence of N,N'-dicyclohexylcarbodiimide (DCC) and 4-(dimethylamino)pyridinium p-toluenesulfonate (DPTS) in dichloromethane gave the functionalized products, which were purified by filtration to eliminate the N,N'-dicyclohexylurea (DCU) formed and by column chromatography for removal of the alcohol excess. The hydroxyl groups of the dendrons were deprotected in acidic environment using a Dowex-H^+ resin in methanol to obtain **B-1a** (53%) and **B-1b** (75%).

The generation growth was obtained by esterification of the hydroxyl groups with the protected *bis*-MPA monomer in the presence of DCC and DPTS in dichloromethane (**2a, 2b**). After each esterification, the crudes were purified by column chromatography and the hydroxyl groups of the dendrons were deprotected in acidic environment (**B-2a**: 13%, **B-2b**: 74%).

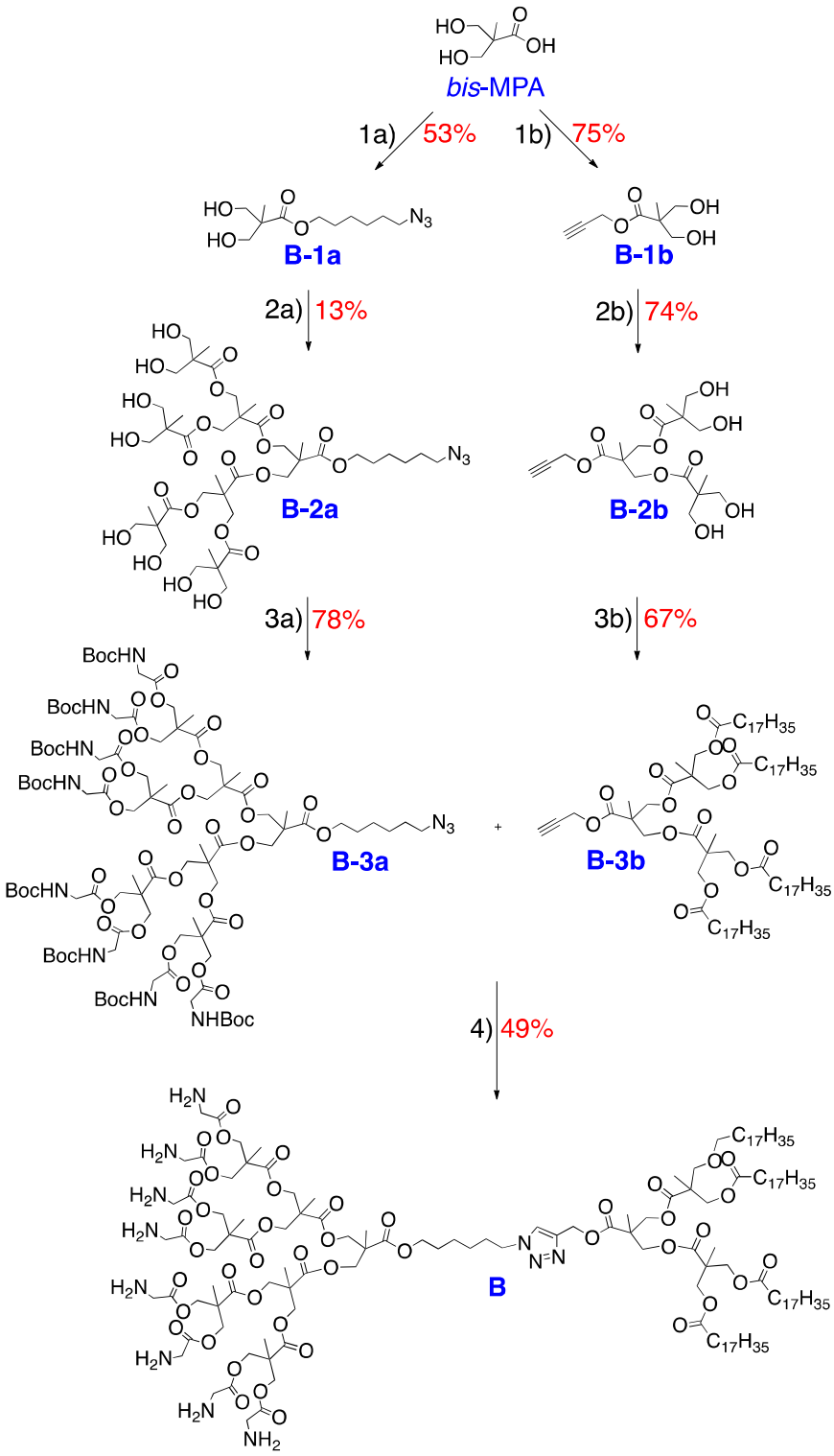

Scheme S1. Synthetic scheme for product **B**. 1a) i) 2,2-dimethoxypropane, p-TsOH, acetone; ii) 6-azidohexanol, DCC, DMAP, CH_2Cl_2; iii) Dowex-H^+, MeOH.1b) i) 2,2-dimethoxypropane, p-TsOH, acetone; ii) propargyl alcohol, DCC, DPTS, CH_2Cl_2; iii) Dowex-H^+, MeOH.2a and 2b) i) isopropylidene bis-MPA, DCC, DPTS, CH_2Cl_2; ii) Dowex-H^+, MeOH.3a) GlyBoc, DCC, DPTS, CH_2Cl_2.3b) stearic acid, DMAP, CH_2Cl_2. 4) i) $CuSO_4 \cdot 5H_2O$, sodium ascorbate, dimethylformamide (DMF); ii) MeOH/HCl, quant.

The next step consisted of the functionalization of the dendron surface. The azido-modified dendron (**B-2a**) was functionalized with protected glycine in order to obtain the aminated derivative **B-3a** (78%). The alkyne-modified dendron (**B-2b**) was functionalized with stearic acid forming the apolar part of the dendron. The reaction of esterification was carried out in dichloromethane in the presence of DCC and 4-(dimethylamine)pyridine (DMAP) as catalyst and was purified by filtration (removal of DCU) and precipitation in cold acetone (elimination of the excess of stearic acid) to give the pure product (**B-3b**: 67%).

The last step of the synthesis (4, 49%) involved the copper-catalyzed 1,3-dipolar cycloaddition between the azido-dendron (**B-3a**) and the alkyno-dendron (**B-3b**). The copper (I) catalyst was generated *in situ* by reduction of the copper (II) salt ($CuSO_4 \cdot 5H_2O$) with sodium ascorbate in dimethylformamide. Then, the dendrons were added and the reaction mixture was stirred during two days. The crude product was purified by precipitation in acetone. Finally, the amine groups were deprotected in acidic environment (AcOEt saturated with HCl) to give the final product in a quantitative yield. The products **A** and **B** were obtained in **total yields** of **16%**and**3%** respectively, from the *bis*-MPA monomer.

General procedure for the synthesis of compound C

The product **C** was obtained in 3 steps: synthesis of *bis*-MPA anhydride (**C-1**, **C-2**), reaction with Pluronic® (**C-3**, **C-4**) and, finally, functionalization with glycine (**C-5**, **C**) (Scheme S2). The first step was the protection of the *bis*-MPA hydroxyl groups to form the benzylidene-protected derivative (**C-1**, 73%) followed by the formation of the corresponding anhydride (**C-2**, 98%) as first described by Fréchet and co-workers in 2001.[44] Then, the reaction between the commercial F127 Pluronic® and *bis*-MPA anhydride in presence of DMAP in dichloromethane (**C-3**, 84%) followed by the deprotection of the hydroxyl groups by hydrogenolysis on palladium on carbon (Pd/C) gave the *bis*-MPA-functionalized Pluronic® (**C-4**, 92%). Subsequently, the Steglish esterification with protected glycine (GlyBoc) in presence of DCC and DMAP in dichloromethane produced**C-5** (95%).

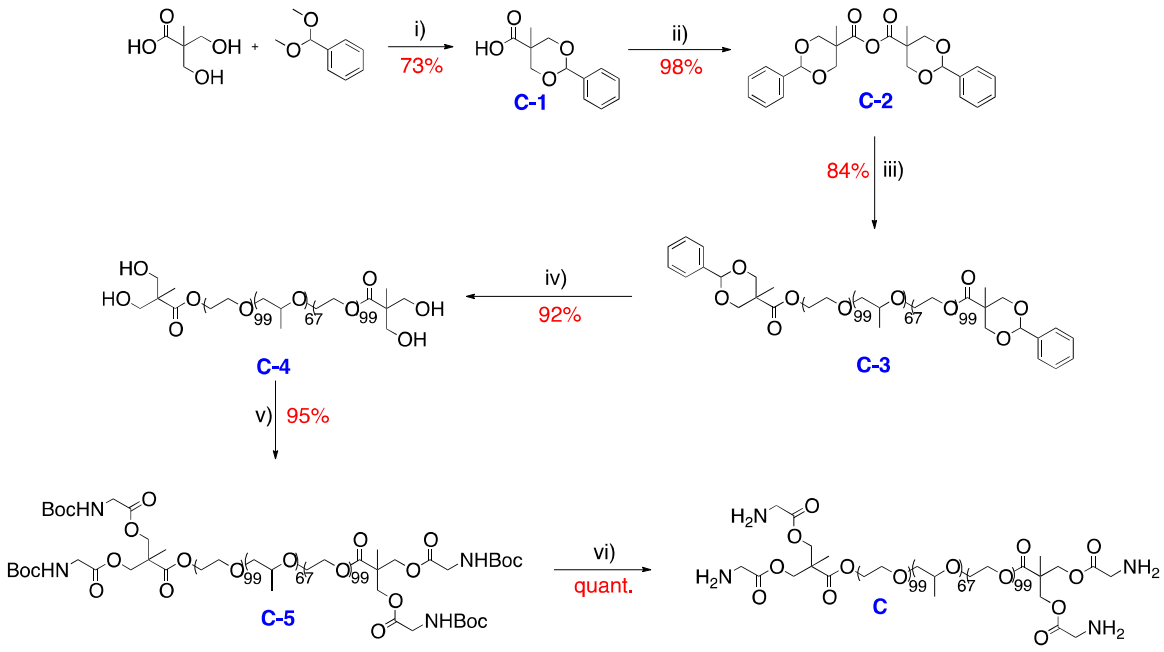

Scheme S2. Synthetic scheme for product **C**. i) TsOH, acetone; ii) DCC, CH_2Cl_2; iii) Pluronic® F127, DMAP, CH_2Cl_2; iv) H_2, Pd/C, CH_2Cl_2/MeOH 1:2; v) GlyBoc, DCC, DMAP, CH_2Cl_2; vi) MeOH/HCl.

Deprotection of amine groups in acidic environment offered the final product **C** in a total yield of **53%**. All the products were purified by precipitation except **C-5**, which was purified by dialysis against methanol (cellulose membrane, 1000 Da cutoff, Spectrum® Laboratories, USA).

General procedure for the synthesis of compound D

Compound **D** was obtained in three steps (Scheme S3). The first step consisted on the esterification of Pluronic® hydroxyl groups with 4-(prop-2-ynyloxy)benzoic acid in presence of DCC and DMAP in order to obtain the polymer functionalized with alkyne groups at both extremities (**D-1**, 56%). These end groups allowed to couple the third generation dendron previously synthetized (**B-3a**) by copper catalysed click-chemistry 1,3-dipolar cycloaddition in dimethylformamide (**ii**). The crude product was purified by dialysis against methanol (1000 Da cutoff cellulose membrane, Spectrum® Laboratories). Deprotection of the amine groups in acidic environment (**iii**) gave the final product **D** without further purification in a total yield of **38%**.

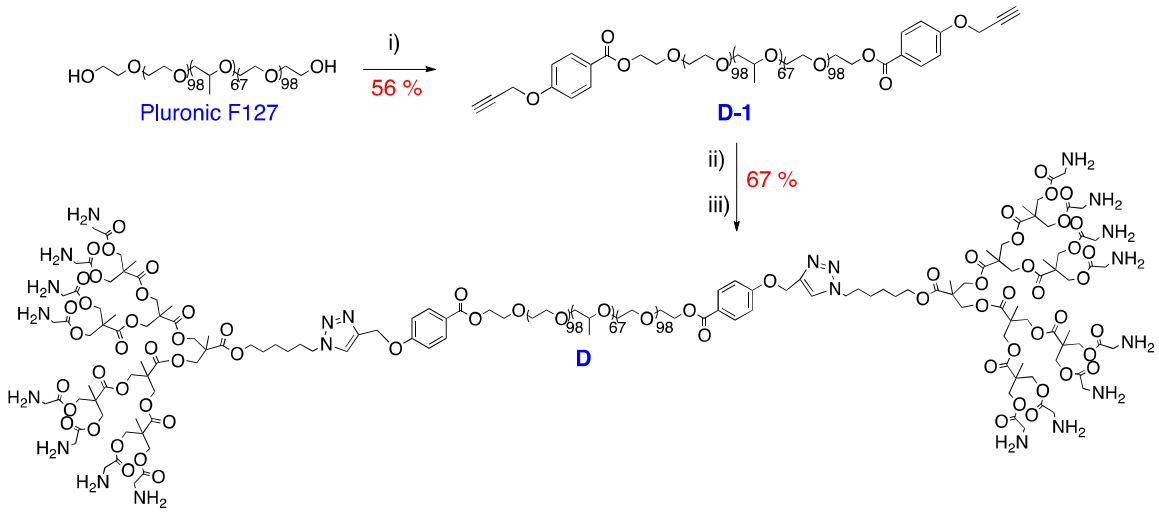

Scheme S3. Synthetic scheme of Pluronic® hybrid linear dendritic block copolymer derivative **D**. i) DCC, DMAP, 4-(prop-2-ynyloxy)benzoic acid, CH_2Cl_2; ii) $CuSO_4$ $5H_2O$, sodium ascorbate, DMF, B-3a; iii) MeOH/HCl.

Experimental procedures

a-Typical procedure for Steglish esterification – generational growth (A):

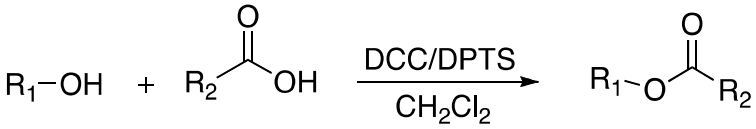

1 eq of the alcohol and 1.2 eq of the carboxylic acid were dissolved in dry dichloromethane with 0.4 eq of DPTS (per hydroxyl group to functionalize), under argon atmosphere. When the products were not totally soluble in dichloromethane, a few amount of dry dimethylformamide was added. After complete dissolution of the products, the flask was cooled to 0°C and 1.2 eq of DCC (per hydroxyl group to functionalize) in dry dichloromethane was added dropwise. The reaction mixture was stirred at room temperature and under argon atmosphere for 24 h. Then, the DCU formed was removed by filtration and the solvent evaporated to give the crude product, which was purified by column chromatography.

b-Typical procedure for deprotection of bis-MPA alcohol groups (B):

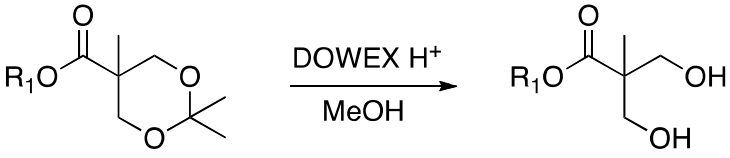

Before reaction, Dowex-H^+ resin was washed with methanol and filtered. The protected product was dissolved in methanol and Dowex-H^+ resin was added (dendron/Dowex-H^+ 1:2 w/w). The reaction was allowed to stir at room temperature for 2 to 24 h depending on the dendron

generation (Table S1). Then, the residue of Dowex-H^+ was filtered off and the solvent was evaporated under reduced pressure to give the pure product.

Hydroxyl groups	Time of reaction
2	2h
4	8h
8	24h

Table S1. Time of reaction related to the hydroxyl group number of the compounds.

c-Typical procedure for deprotection of amine groups (C):

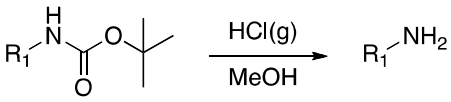

The product was dissolved in a solution of methanol or ethyl acetate saturated with hydrochloric acid (gaz) and was stirred for 30 min, when the formation of a white precipitate was observed. The residue was concentrated and dried under reduced pressure to give the pure product as a pale yellow or white solid in a quantitative yield.

d-Typical procedure for dendrimer generation growth (D):

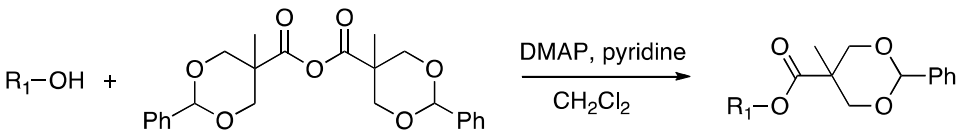

Pentaerythritol or G-1 dendrimer (1 eq) and DMAP (0.8 eq/OH) were dissolved in anhydrous pyridine and then diluted with anhydrous dichloromethane (1:3 v/v pyridine/dichloromethane). Solid *bis*-MPA anhydride (6 eq/OH) was added and the reaction mixture was allowed to stir at room temperature for 5 h. The excess of anhydride was quenched by stirring the reaction mixture with 1:1 H_2O:pyridine solution overnight. The organic phase was diluted with 200 mL of CH_2Cl_2 and extracted with $NaHSO_4$ 1M (3 × 50 mL), Na_2CO_3 10% (3 × 50 mL) and brine (1 × 50 mL). The organic phase was dried over anhydrous $MgSO_4$ and the solvent evaporated to give the pure product as a white solid.

e-Typical procedure for deprotection of dendrimer OH groups (E):

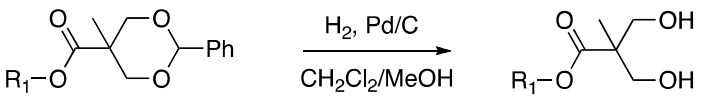

The protected dendrimer was dissolved in a small amount of dichloromethane and the solution was diluted with methanol. 10% Pd/C (20% in weight of dendrimer) was added to the solution and the reaction mixture was stirred under H_2 atmosphere (1 atm) overnight. Then, the catalyst

was filtered off over celite and washed with methanol. The solvent was evaporated to give the pure product as a white solid.

Synthesis and characterization of intermediate derivatives

Isopropylidene-2,2-bis(methoxy)propionic acid

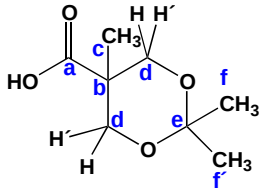

30.1 g (219.9 mmol) of commercial *bis*-MPA, 41.4 mL (330.0 mmol) of 2,2-dimethoxipropane and 2.30 g (11.9 mmol) of *p*-toluenesulfonic acid monohydrate were dissolved in 150 mL of anhydrous acetone. The reaction mixture was stirred for 2 h at room temperature. The catalyst was then neutralized using 3 mL of a NH_4OH (25%)/EtOH (4:1) solution. The acetone was evaporated to give a white solid that was dissolved in 500 mL of EtOAc and extracted 3 times with 100 mL of water. The organic phase was dried over anhydrous $MgSO_4$ and the solvent was evaporated to give 30.9 g (177 mmol) of the pure product as a white solid in 81% yield.

NMR ^{1}H (CDCl3, 400 MHz) δ *(ppm):*1.21 (s, 3H, H_c), 1.42 (s, 3H, H_f), 1.45 (s, 3H, $H_{f'}$), 3.68 (d, *J* =12 Hz, 2H, H_d), 4.18 (d, *J* =12 Hz, 2H, $H_{d'}$).

NMR ^{13}C (CDCl3, 400 MHz) δ *(ppm):*18.4 (C_c), 21.8 (C_f), 25.3 ($C_{f'}$), 41.7 (C_b), 65.9 (C_d), 98.3 (C_e), 180.0 (C_a).

*IR (cm^{-1}, Nujol):*3126 (COO-H st), 2854-2924 (C-H st), 1722 (C=O).

*Calculated $[M]^+$ ($C_8H_{14}O_4$)*m/z= 174.09. *Found:* ESI+: $[M+Na]^+$ m/z= 196.9.

*Elem. analysis calc.:*C, 55.16; H, 8.10; O, 36.74. *Found:* C, 55.40; H, 8.36.

prop-2-ynyl 2,2,5-trimethyl-1,3-dioxane-5-carboxylate

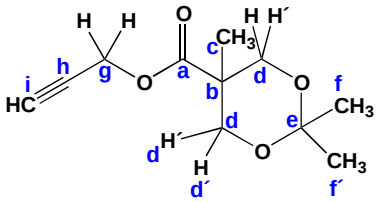

5 g (28.70 mmol) of isopropylidene-2,2-*bis*(methoxy)propionic acid, 1.75 mL (30.14 mmol) of propargyl alcohol and 3.38 g (11.48 mmol) of DPTS were dissolved in 50 mL of anhydrous dichloromethane. The flask was flushed with argon, cooled to 0°C, and a solution of 8.88 g (43.05 mmol) of DCC in 10 mL of dichloromethane was added dropwise. The reaction was

allowed to stir at room temperature, under argon atmosphere for 24 h. The reaction mixture was then filtered and the solvent was evaporated. The oil/solid mixture obtained was stirred with hexane, and the solid filtered off. The product was then purified by column chromatography eluting with dichloromethane to obtain 4.70 g (22.14 mmol, 77 %) of the pure product as a green oil.

*NMR ^{1}H (CDCl3, 300 MHz) δ (ppm):*1.21 (s, 3H, H_c), 1.38 (s, 3H, H_f), 1.42 (s, 3H, $H_{f'}$), 2.46 (t, *J* = 2.4 Hz, 1H, H_i), 3.65 (d, *J* = 11.7 Hz, 2H, H_d), 4.20 (d, *J* = 12 Hz, 2H, $H_{d'}$), 4.73 (d, *J* = 2.4 Hz, 2H, H_g).

*NMR ^{13}C (CDCl3, 400 MHz) δ (ppm):*18.3 (C_c), 22.5 (C_f), 24.5 ($C_{f'}$), 41.8 (C_b), 52.3 (C_g), 65.8 (C_d), 74.9 (C_i), 77.4 (C_h), 98.0 (C_e), 173.3 (C_a).

IR (KBr, cm^{-1}): 3273 (≡C-H), 2876-2941-2992 (C-H), 2129 (C≡C), 1739 (C=O).

Calculated $[M]^+$ ($C_{11}H_{16}O_4$):m/z = 212.10. *Found: MALDI+:* $[M+Na]^+$*m/z* = 225.1.

Elem. analysis calc.: C, 62.25; H, 7.60. *Found:* C, 61.81; H, 7.67.

≡-G1(OH)$_2$, B-1b

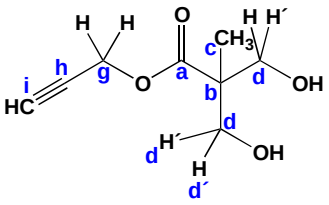

The product was obtained following the synthetic method (B) of deprotection of the hydroxyl groups. White solid. 98% yield.

*NMR ^{1}H (CDCl3, 300 MHz) δ (ppm):*1.09 (s, 3H, H_c), 2.49 (t, J = 2.7 Hz, H_d), 2.76 (br s, OH), 3.72 (d, J = 11.4 Hz, H_d), 3.92 (d, J = 11.4 Hz, $H_{d'}$), 4.75 (d, J = 2.4 Hz, 2H, H_g).

NMR ^{13}C (CDCl3, 400 MHz) δ (ppm): 16.9 (C_c), 49.3 (C_b), 52.4 (C_f), 67.0 (C_d), 75.2 (C_i), 77.3 (C_h), 174.9 (C_a).

IR (KBr, cm^{-1}): 3396 (O-H), 3293 (≡C-H), 2945-2885 (C-H), 2127 (C≡C), 1729 (C=O).

Calculated $[M]^+$ ($C_8H_{12}O_4$):m/z = 172.18. *Found: ESI+:* $[M+H]^+$*m/z*=173.0, $[M+Na]^+$ m/z=195.0.

Elem. analysis calc.: C, 55.81; H, 7.02. *Found:* C, 55.42; H, 7.29.

≡G2

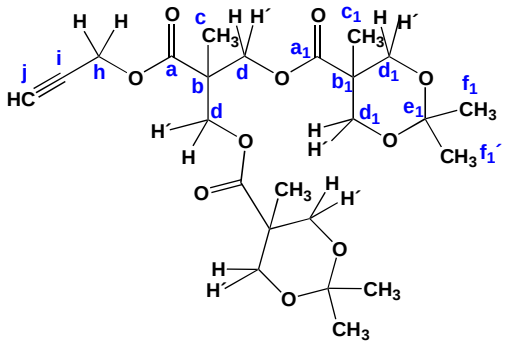

The product was obtained following the synthetic method (A) for Steglish esterification. The crude product was purified by column chromatography eluting gradually with a mixture of 4:1 Hexane:EtOAc to a mixture of 1:1 Hexane:EtOAc (R_f = 0.5). The pure product was obtained as a yellow oil in a 79% yield (4.03 g, 8.37 mmol).

NMR ^{1}H (CDCl3, 300 MHz) δ *(ppm):*1.16 (s, 6H, H_{c1}), 1.31 (s, 3H, H_c), 1.36 (s, 6H, H_{f1}), 1.41 (s, 6H, $H_{f1'}$), 2.46 (t, *J* = 2.4 Hz, 1H, H_j), 3.61 (d, *J* = 12 Hz, 4H, H_{d1}), 4.15 (d, *J* = 12 Hz, 4H, $H_{d1'}$), 4.33 (s, 4H, H_d), 4.71 (d, *J* = 2.4 Hz, 2H, H_h).

NMR ^{13}C (CDCl3, 400 MHz) δ *(ppm):*17.5 (C_c), 18.4 (C_{c1}), 21.6 (C_{f1}), 25.4 ($C_{f1'}$), 43.6 (C_b), 46.7 (C_{b1}), 52.6 (C_h), 65.2 (C_d), 65.9 (C_{d1}), 75.3 (C_h), 77.1 (C_i), 98.0 (C_{e1}), 171.8 (C_a), 173.4 (C_{a1}).

IR (KBr, cm^{-1}): 3249 (≡C-H), 2993-2923-2857 (C-H), 2121 (C≡C), 1733 (C=O).

Calculated $[M]^+$ ($C_{24}H_{36}O_{10}$):m/z = 484.54. *Found:* MALDI+: $[M+Na]^+$*m/z*=507.2.

Elem. analysis calc.: C, 59.49; H, 7.49. *Found:* C, 59.94; H, 7.77.

≡G2(OH)$_4$, B-2b

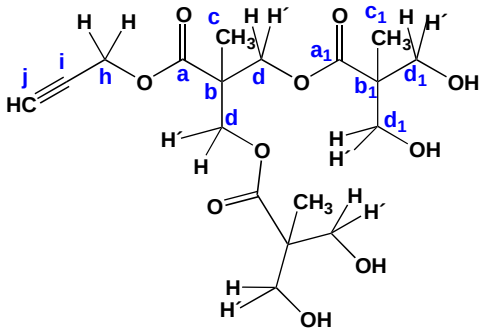

The product was obtained following the synthetic method (B) of deprotection of the *bis*-MPA hydroxyl groups. The pure product was obtained in a 94% yield (3.02 g, 7.46 mmol).

*NMR ^{1}H (CDCl3, 300 MHz) δ (ppm):*1.05 (s, 6H, H_{c1}), 1.34 (s, 3H, H_c), 2.49 (t, *J* = 2.4 Hz, 1H, H_j), 3.71 (dd, *J* = 6 Hz, *J* = 11.4 Hz, 4H, H_{d1}), 3.87 (dd, *J* = 5.1 Hz, *J* = 10.5 Hz, 4H, $H_{d1'}$), 4.30 (d, *J* = 11.1 Hz, 2H, H_d), 4.47 (d, *J* = 11.1 Hz, 2H, $H_{d'}$), 4.74 (d, *J* = 2.4 Hz, 2H, H_h).

NMR ^{13}C (MeOD, 400 MHz) δ (ppm): 17.3 (C_c), 18.1 (C_{c1}), 40.5 (C_b), 47.9 (C_{b1}), 53.6 (C_h), 65.8 (C_{d1}), 66.3 (C_d), 76.7 (C_j), 78.5 (C_i), 173.7 (C_a), 175.9 (C_{a1}).

IR (KBr, cm^{-1}): 3310-3402 (O-H), 3258 (≡C-H), 2923-2853 (C-H), 2125 (C≡C), 1731 (C=O).

Calculated $[M]^+$ ($C_{18}H_{28}O_{10}$):m/z = 404.41. *Found:* MALDI+: $[M+Na]^+$*m/z*=427.2.

Elem. analysis calc.: C, 53.46; H, 6.98. *Found:* C, 53.16; H, 7.25.

$(C_{17}H_{35})_4$[G#3]-$CH_2C{\equiv}CH$, B-3b

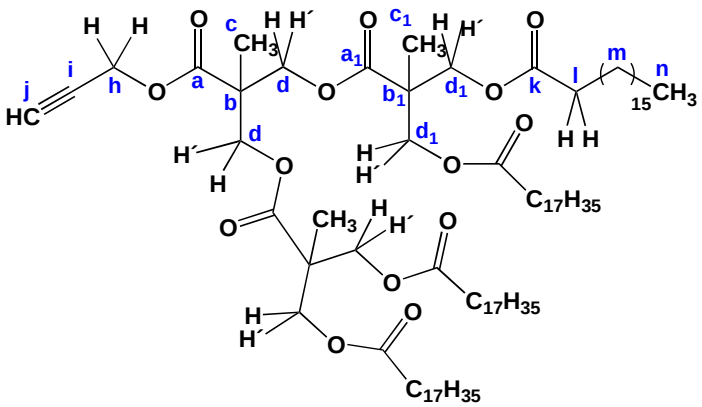

The second generation dendron with free hydroxyl groups B-2b (1.50 g, 3.7 mmol, 1 eq) was dissolved in dry dichloromethane (75 mL). DMAP (1.36 g, 11.1 mmol, 6 eq) and stearic acid (6.34 g, 22.3 mmol, 6 eq) were added. The reaction was allowed to stir under argon atmosphere and was cooled to 0 °C. DCC (4.59 g, 22.27 mmol, 6.0 eq) was dissolved in dry dichloromethane (25 mmol) and was added dropwise. The reaction was allowed to stir at room temperature during 7 days. Then, the formed DCU was filtered off and the solvent was evaporated under reduce pressure. A mixture of oil and solid was obtained. A small amount of THF was added and the crude was allowed to stir during 20 min at room temperature. Then, the precipitate was filtered off and the solvent was evaporated under vacuum to get a yellow solid which was dissolved in a small amount of dichloromethane and precipitated in cold acetone into a white solid (3.67 g, 67%).

^{1}H (300 MHz, $CDCl_3$) δ (ppm): 0.88 (t, *J* = 6.6 Hz, 12H, H_n), 1.25 (m, 121 H, H_c, H_{c1}, H_m), 1.57 (m, 8H, H_m), 2.29 (t, *J* = 7.5 Hz, 8H, H_l), 2.50 (t, *J* = 2,4 Hz, 1H, H_j), 4.19 (s, 8H, H_d, H_{d1}), 4.27 (d, *J* =5.1 Hz, 4H, $H_{d1'}$), 4.72 (d, *J* = 2.4 Hz, 2H, H_h).

^{13}C (300 MHz, $CDCl_3$) δ (ppm): 14.0 (C_n), 17.4 (C_c), 17.7 (C_{c1}), 22.6 (C_m), 24.8 (C_m), [29.1, 29.2, 29.4, 29.6] (C_m), 31.9 (C_m), 34.0 (C_l), 46.4 (C_{b1}), 46.7 (C_b), 52.7 (C_h), 65.0 (C_{d1}), 65.6 (C_d), 75.4 (C_j), 77.1 (C_i), 171.4 (C_a), 172.0 (C_{a1}), 173.1 (C_k).

IR (cm^{-1}, KBr): 3307 (≡C-H), 2919-2851 (C-H), 1736 (C=O).

Calculated $[M]^+$ ($C_{90}H_{164}O_{14}$): m/z = 1469.2. *Found:* ESI+: $[M+Na]^+$ m/z = 1492.4.

Elem. analysis calc.: C, 73.52; H, 11.24. *Found:* C, 73.33; H, 11.81.

6-azidohexan-1-ol

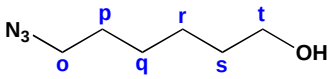

10.00 g (73 mmol) of 6-chlorohexan-1-ol were dissolved in 30 mL of DMF and 14.25 g (219 mmol) of NaN_3 were added. The reaction mixture was stirred at 140°C for 24 h, and at room temperature for a further 24 h. 100 mL of Et_2O were added and the crude was extracted 3 times with 100 mL of water. The organic layer was dried over anhydrous $MgSO_4$ and the solvent was evaporated under reduced pressure. The crude was purified by column chromatography eluting with Hexane/EtOAc 1:1 (R_f = 0.4) to give the pure product as a yellow liquid in a 84% yield (8.79 g, 61 mmol).

*NMR ^1H (CDCl3, 300 MHz) δ (ppm):*1.35 (m, 4H, H_q, H_r), 1.56 (m, 4H, H_p, H_s), 1.96 (s, 1H, OH), 3.24 (t, J = 6.9 Hz, 2H, H_o), 3.6 (t, J = 6.6 Hz, 2H, H_t).

NMR ^{13}C (CDCl3, 400 MHz) δ (ppm): 25.2 (C_r), 26.4 (C_q), 28.7 (C_p), 32.4 (C_s), 51.3 (C_o), 62.6 (C_t).

*IR (cm^{-1}, KBr):*3339 (O-H st), 2861-2936 (C-H st), 2097 (N_3).

*Calculated $[M]^+$ ($C_6H_{13}N_3O$)*m/z= 143.11. *Found:* ESI+: $[M+Na]^+$ m/z= 166.0.

Elem. analysis calc.: C, 50.33; H, 9.15; N, 29.35. *Found:* C, 49.91; H, 9.17; N, 29.54.

6-azidohexyl 2,2,5-trimethyl-1,3-dioxane-5-carboxylate

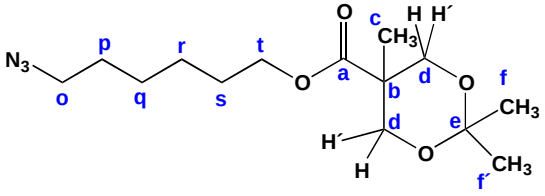

The product was obtained by Steglish esterification (A) and purified by column chromatography eluting with dichloromethane. Yield: 66%. Green oil.

*NMR ^{1}H (CDCl3, 400 MHz) δ (ppm):*1.17 (s, 3H, H_c), 1.37 (s, 3H, H_f), 1.39(m, 4H, H_q, H_r), 1.41 (s, 3H, $H_{f'}$), 1.60 (m, 4H, H_p, H_s), 3.25 (t, *J* = 6.9 Hz, 2H, H_o), 3.62 (d, *J* = 12 Hz, 2H, H_d), 4.13 (t, *J* = 6.3 Hz, 2H, H_t), 4.17 (d, *J* = 11.7 Hz, 2H, $H_{d'}$).

*NMR ^{13}C (CDCl3, 400 MHz) δ (ppm):*18.6 (C_c), 22.7 (C_f), 24.6 ($C_{f'}$), 25.4 (C_r), 26.3 (C_q), 28.4 (C_p), 28.7 (C_s), 41.8 (C_b), 51.3 (C_o), 64.6 (C_t), 66.0 (C_d), 98.0 (C_e), 174.2 (C_a).

*IR (cm^{-1}, KBr):*2864-2939 (C-H st), 2096 (N_3 st), 1731 (C=O).

*Calculated $[M]^+$ ($C_{14}H_{25}N_3O_4$)*m/z= 299.18. *Found:* Maldi+: $[M+Na]^+$ m/z= 322.2.

Elem. analysis calc.: C, 56.17; H, 8.42; N, 14.04. *Found:* C, 55.91; H, 8.71; N, 13.83.

$(OH)_2$-[G#1]-$C_6H_{12}N_3$, B-1a

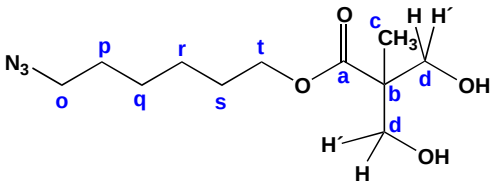

The product B-1a was obtained by the deprotection method (B). Yield: 99%. White solid.

*NMR ^{1}H (CDCl3, 400 MHz) δ (ppm):*1.05 (s, 3H, H_c), 1.40 (m, *J* = 3.6 Hz, 4H, H_q, H_r), 1.63 (m, 4H, H_p, H_s), 2.78 (s, 2H, OH), 3.27 (t, *J* = 6.6 Hz, 2H, H_o), 3.71 (d, *J* = 11.1 Hz, 2H, H_d), 3.89 (d, *J* = 11.2 Hz, 2H, $H_{d'}$), *4*.17 (t, *J* = 6.6 Hz, 2H, H_t).

NMR ^{13}C (CDCl3, 400 MHz) δ (ppm): 17.1 (C_c), 25.3 (C_r), 26.2 (C_q), 28.3 (C_s), 28.6 (C_p), 49.1 (C_d), 51.2 (C_o), 64.8 (C_t), 67.8 (C_d), 175.9 (C_a).

IR (cm^{-1}, KBr): 3381 (O-H st), 2854-2924 (C-H st), 2097 (N_3 st), 1726 (C=O st).

*Calculated $[M]^+$ ($C_{11}H_{21}N_3O_4$)*m/z= 259.15. *Found:* MALDI+: $[M+Na]^+$ m/z= 282.2.

Elem. analysis calc.: C, 50.95; H, 8.16; N, 16.21. *Found:* C, 50.37; H, 8.21; N, 16.53.

[G#2]-$C_6H_{12}N_3$

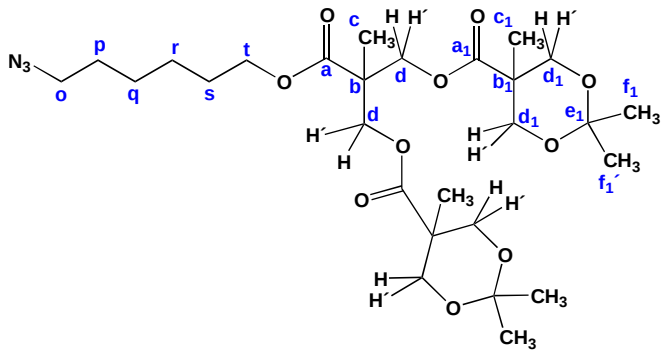

The product was obtained by Steglish esterification method (A) and was purified by column chromatography eluting with dichloromethane (R_f = 0.7). Yield: 19%. White solid.

NMR ^{1}H (CDCl3, 300 MHz) δ (*ppm):*1.15 (s, 6H, H_{c1}), 1.28 (s, 3H, H_c), 1.35 (s, 6H, H_{f1}), 1.38 (m, 4H, H_q, H_r), 1.41 (s, 6H, $H_{f1'}$), 1.63 (m, *J* = 6.9 Hz, 4H, H_p, H_s), 3.27 (t, *J* = 6.6 Hz, 2H, H_o), 3.61 (d, *J* = 12 Hz, 4H, H_{d1}), 4.11 (t, *J* = 6.6 Hz, 2H, H_t), 4.14 (d, *J* = 11.7 Hz, 4H, $H_{d1'}$), 4.32 (s, 4H, H_d).

NMR ^{13}C (CDCl3, 400 MHz) δ (*ppm):*17.7 (C_c), 18.5 (C_{c1}), 22.1 (C_{f1}), 24.9 ($C_{f1'}$), 25.4 (C_r), 26.3 (C_q), 28.3 (C_s), 28.6 (C_p), 42.0 (C_{b1}), 46.7 (C_b), 51.2 (C_o), 65.1 (C_t), 65.2 (C_d), 65.6 ($C_{d'}$), 65.8 (C_{d1}), 65.9 ($C_{d1'}$), 98.0 (C_o), 172.5 (C_a), 173.5 (C_{a1}).

*IR (cm^{-1}, KBr):*2868-2939 (C-H st), 2097 (N_3 st), 1736 (C=O).

Calculated $[M]^+$ ($C_{27}H_{45}N_3O_{10}$):m/z = 571.31. *Found: ESI+:* $[M+H]^+$ *m/z* = 572.0.

Elem. analysis calc.: C, 56.73; H, 7.93; N, 7.35. *Found:* C, 56.48; H, 7.79; N, 6.96.

$(OH)_4$-[G#2]-$C_6H_{12}N_3$

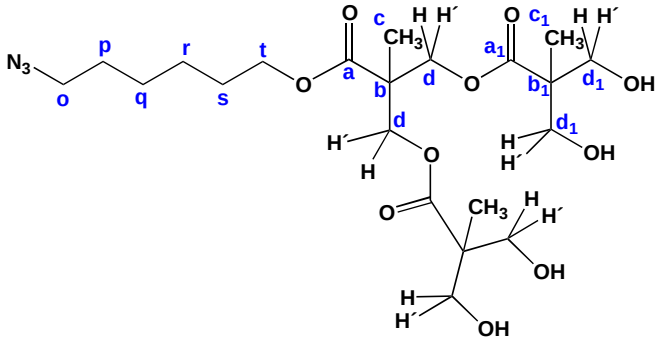

The product was obtained following the synthetic method (B). Yield: 95%. White solid.

NMR ^{1}H (MeOD, 300 MHz) δ (*ppm):*1.14 (s, 6H, H_{c1}), 1.29 (s, 3H, H_c), 1.43 (m, 4H, H_q, H_r), 1.61-1.71 (m, 4H, H_p, H_s), 3.31 (t, 2H, H_o), 3.61 (d, *J* = 10.8 Hz, 4H, H_{d1}), 3.65 (d, *J* = 10.8 Hz, 4H, $H_{d1'}$), 4.15 (t, *J* = 6.6 Hz, 2H, H_t), 4.25 (d, *J* = 11.1 Hz, 2H, H_d), 4.30 (d, *J* = 11.1 Hz, 2H, $H_{d'}$).

NMR ^{13}C (CDCl3, 400 MHz) δ (*ppm):* 17.3 (C_{d1}), 18.3 (C_d), 26.7 (C_r), 27.5 (C_q), 29.6 (C_s), 29.9 (C_p), 47.8 (C_b), 51.8 (C_{b1}), 52.4 (C_o), 65.8 (C_{d1}), 66.4 (C_t), 66.5 (C_d), 174.6 (C_a), 175.9 (C_{a1}).

*IR (cm^{-1}, KBr):*3283 (O-H st), 2923-2854 (C-H st), 2098 (N_3 st), 1731 (C=O st).

*Calculated $[M]^+$ ($C_{21}H_{37}N_3O_{10}$):*m/z= 491.25. *Found:* MALDI+: $[M+Na]^+$ m/z= 514.2.

Elem. analysis calc.: C, 51.31; H, 7.59; N, 8.55. *Found:* C, 51.16; H, 7.40; N, 8.78.

$(NHBoc)_4[G\#2]$-$(CH_2)_6N_3$

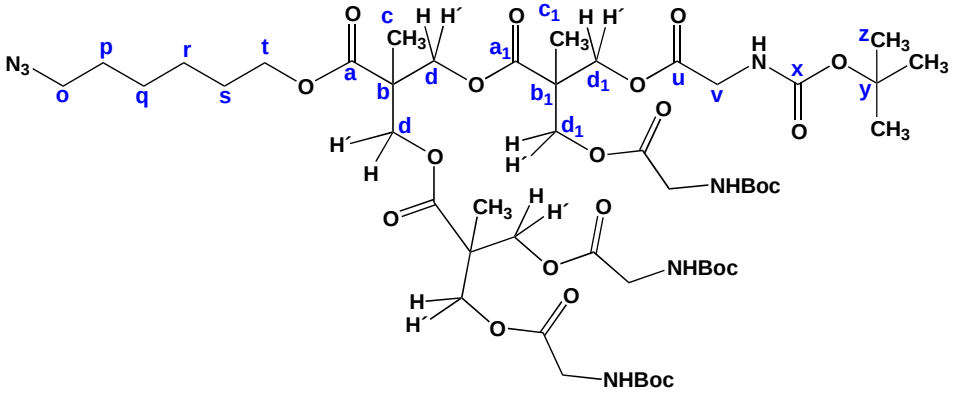

The product was obtained following the synthetic method (B). The crude was purified by column chromatography eluting with a mixture 5:5 of Hexane:EtOAc (R_f = 0.43). Yield: 86%. Green oil.

NMR ^1H (CDCl3, 300 MHz) δ *(ppm):*1.23-1.24 (m, 9H, H_c, H_{c1}), 1.43 (m, 40H, H_z, H_q, H_r), 1.60-1.65 (m, 4H, H_p, H_s), 3.27 (t, *J* = 6.6 Hz, 2H, H_o), 3.87 (d, *J* = 5.4 Hz, 8H, H_v), 4.09-4.13 (m, 2H, H_t), 4.23-4.25 (m, 12H, H_d, H_{d1}), 5.24 (br s, 4H, NH).

NMR ^{13}C (CDCl3, 400 MHz) δ *(ppm):*17.6, 17.8, 25.4, 26.3, 28.1, 28.7, 42.3, 46.4, 46.6, 65.5, 65.6, 80.0, 155.8, 169.9, 171.8, 172.2.

IR (cm^{-1}, KBr): 3389 (N-H), 2978-2936 (C-H), 2097 (N_3), 1717 (C=O).

Calculated $[M]^+$ ($C_{49}H_{81}N_7O_{22}$):m/z = 1120,20. *Found:* Maldi+: $[M+Na]^+$*m/z* =1147.2.

Elem. analysis calc: C, 52.54; H, 7.29; N, 8.75. *Found:* C, 52.64; H, 7.30; N, 8.55.

$3Gpolar(NHBoc)_8$-$3Gapolar(C_{17}H_{35})_8$

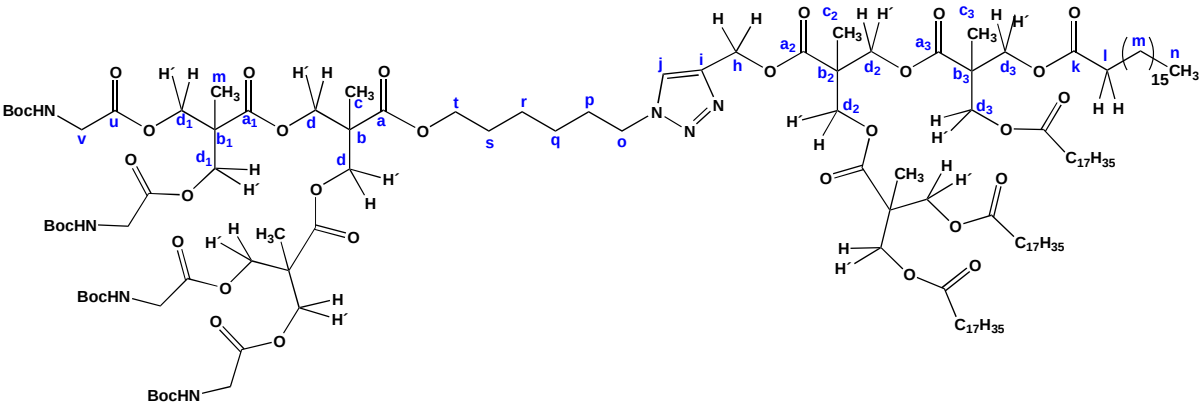

Penta-hydrated copper sulfate (2.7 mg, 9.2 µmol) and sodium ascorbate (3.9 mg, 19.7 µmol) were agitated in DMF during 1 h in order to form Cu(I). Meanwhile, the polar dendron (200 mg,

179 µmol) and the apolar dendron (289 mg, 196 µmol) were solubilized in DMF. Then, the two solutions were mixed and agitated for 2 days at room temperature, under argon atmosphere. 50 mL of dichloromethane were added and the reaction mixture was washed with brine and water (4 × 10 mL) to remove DMF. The crude was concentrated under reduced pressure and precipitated in cold MeOH as a white solid and purified by column chromatography eluting with 8:2 hexane/EtOAc . Yield: 49%.

*NMR ^{1}H (CDCl3, 400 MHz) δ (ppm):*0.88 (t, *J* = 6.5 Hz, 12H), 1.18 (s, 6H), 1.25 (m, 122H), 1.39-1.42 (m, 38H), 1.57-1.65 (m, 14H), 1.94 (q, *J* = 3.6 Hz, 2H), 2.28 (t, *J* = 7.5 Hz, 8H), 3.89 (d, J = 5.7 Hz, 8H), 4.04-4.30 (m, 24H), 4.37 (t, *J* = 7.2 Hz, H_o), 5.24 (m, 6H, H_h) 7.68 (s, 1H, H_j).

*NMR ^{13}C (CDCl3, 400 MHz) δ (ppm):*14.1, 17.5, 17.2, 17.7, 17.9, 22.6, 24.8, 25.3, 26.1, 28.3, 29.1, 29.2, 29.3, 29.5, 29.6, 29.7, 30.1, 31.9, 34.0, 42.2, 46.3, 46.4, 46.5, 46.6, 50.2 (C_o), 58.4 (C_h), 64.9, 65.4, 65.5, 65.6, 65.7, 79.9, 124.1 (C_j), 142.0 (C_i), 155.8, 170.0, 171.8, 172.0, 172.1, 172.2, 173.2.

*IR (cm^{-1}, KBr):*3418 (N-H), 2919-2850 (C-H), 1742 (C=O).

Calculated $[M]^+$ ($C_{139}H_{245}N_7O_{36}$):m/z = 2590.46. *Found*: MALDI+: $[M+Na]^+$*m/z* = 2612.8.

Elem. analysis calc.: C, 64.45; H, 9.53; N, 3.78. *Found:* C, 64.88; H, 9.32; N, 4.05.

3Gpolar$(NH_2)_8$-3Gapolar$(C_{17}H_{35})_8$, compound A

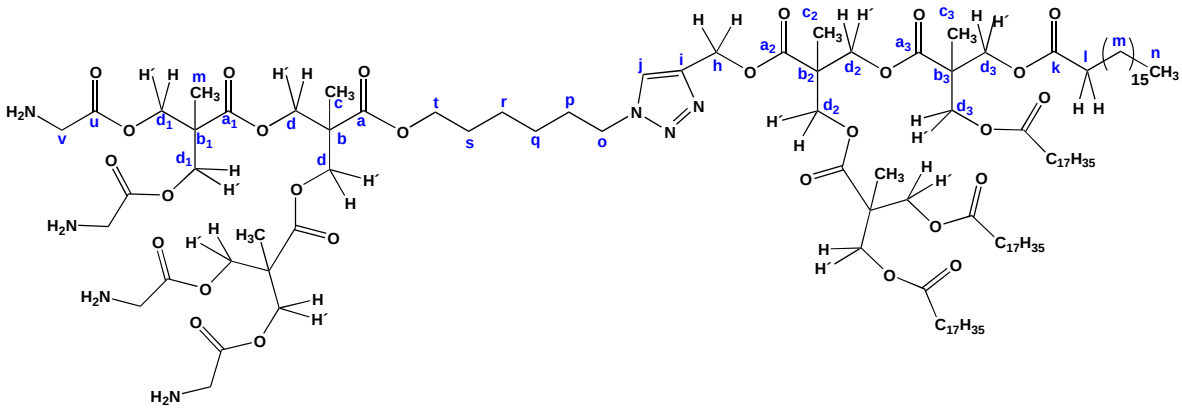

The compound A was obtained following the procedure (C) of deprotection of amine groups and obtained as a white solid, in a quantitative yield.

*NMR ^{1}H (CDCl3, 400 MHz) δ (ppm):*0.85 (t, *J* = 5.7 Hz, 12H), 1.18-1.40 (m, 140H), 1.58 (m, 12H), 1.80-1.98 (m, 22H), 2.28 (t, *J* = 7.5 Hz, 8H), 4.10-4.37 (m, 34H), 5.24 (s, 2H, H_h), 7.67 (s, 1H, H_j), 8.38 (br s, 8H, NH).

NMR ^{13}C (CDCl3, 400 MHz) δ *(ppm):*14.0, 17.5, 17.7, 22.6, 24.8, 25.3, 26.1, 28.3, 29?1, 29.2, 29.3, 29.4, 29.6, 29.7, 30.1, 31.9, 34.0, 46.3, 46.6, 50.2 (C_o), 58.3 (C_h), 64.9, 65.3, 124.1 (C_j), 141.9 (C_i), 167.4, 171.9, 172.1, 173.1.

IR (cm^{-1}, KBr): 3430 (N-H), 2919-2851 (C-H), 1740 (C=O).

Calculated $[M]^+$ ($C_{119}H_{213}N_{16}O_{28}$):m/z = 2188.55. *Found*: MALDI+: $[M+Na]^+$ *m/z* = 2213.2.

The ^{1}H-NMR spectrum of compound **A** is shown in **Fig. S1**. The singlet peak at 7.67 ppm integrating for one proton (**Hj**) confirmed the formation of the triazide cycle resulting from the CuAAC reaction. Between 4.10 ppm and 4.55 ppm are situated the peaks corresponding to the C**H**$_2$ of the *bis*-MPA dendrons (12 CH_2, **Hd-d$_4$**), with the -C**H$_2$**-NH_2 (4 CH_2, **Hv**) and the -C**H$_2$**-O-**Ht**. At 5.24 ppm is located the peak due to the CH_2 in α of the triazide cycle **Ho**. The peaks corresponding to the methyl groups of the *bis*-MPA appear at ca. 1.2 ppm (**Hc-c$_3$**) with the peak due to the -C**H$_2$**- groups from the apolar chains **Hm**. The peak corresponding to the -C**H$_2$-** groups in α of the C=O, **Hr**, is situated at 2.28 ppm.

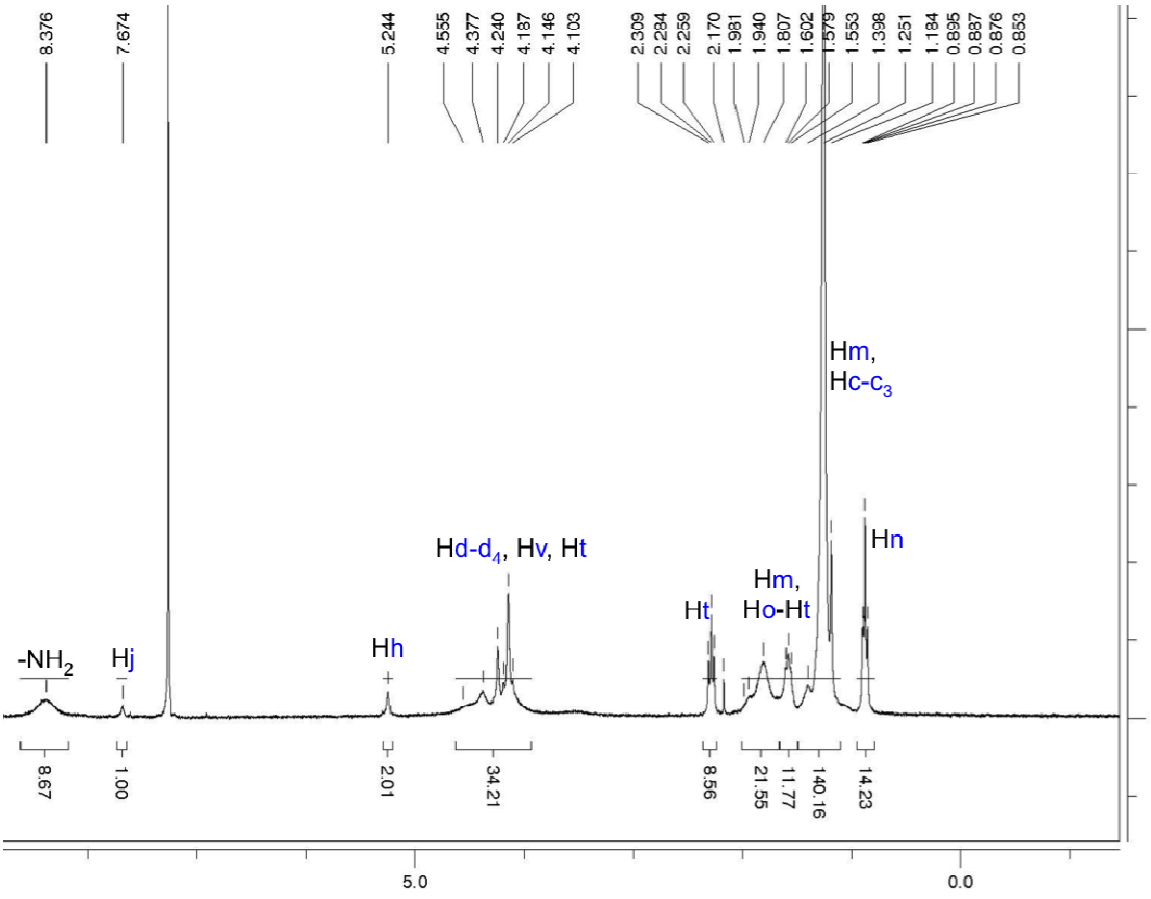

Fig. S1.^{1}H-NMR spectrum of the compound A. 300 MHz, $CDCl_3$ (solvent residual peak at 7.26 ppm), shift in ppm.

[G#3]-$C_6H_{12}N_3$

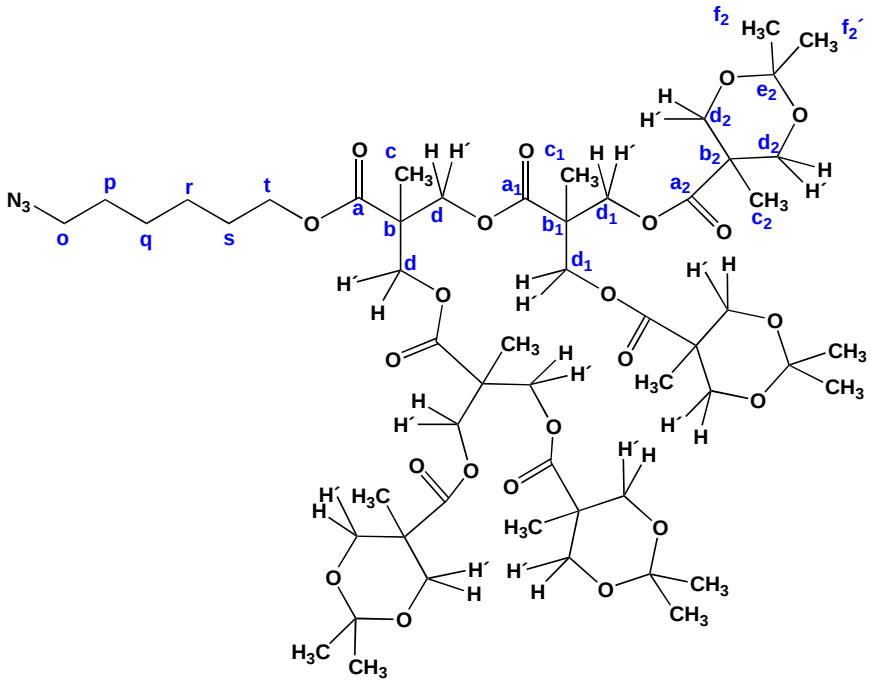

The product was obtained by Steglish esterification (A). The crude product was purified by column chromatography eluting with a mixture 7:3 of Hexane:EtOAc. Yield: 75%. Transparent oil.

*NMR ^1H (CDCl3, 400 MHz) δ (ppm):*1.13 (s, 12H, H_{c2}), 1.25 (s, 3H, H_c), 1.26 (s, 6H, H_{c1}), 1.34 (s, 12H, H_{f2}), 1.40 (m, 16H, $H_{f2'}$, H_q, H_r), 1.62 (m, 4H, H_p, H_s), 3.27 (t, *J* = 6.8 Hz, 2H, H_o), 3.61 (d, *J* = 12.8 Hz, 8H, H_{d2}), 4.11 (m, 10H, $H_{d2'}$, H_t), 4.26 (d, *J* = 6.8 Hz, 4H, H_{d1}), 4.29 (m, 8H, $H_{d1'}$, H_d).

*NMR ^{13}C (CDCl3, 400 MHz) δ (ppm):*17.6 (C_c), 17.7 (C_{c1}), 18.5 (C_{c2}), 22.0 (C_{f2}), 25.1 ($C_{f2'}$), 25.4 (C_r), 26.3 (C_q), 28.4 (C_s), 28.7 (C_p), 42.0 (C_{b2}), 46.6 (C_b), 46.8 (C_{b1}), 51.3 (C_o), 64.9 (C_d), 65.4 (C_t), 65.8 (C_{d1}), 65.9 (C_{d2}), 98.1 (C_{e2}), 171.8 (C_a), 172.0 (C_{a1}), 173.4 (C_{a2}).

*IR (cm^{-1}, Nujol):*2990-2940-2876 (C-H), 2097 (N_3), 1739 (C=O).

*Calculated $[M]^+$ ($C_{53}H_{85}N_3O_{22}$):*m/z= 1115.56. *Found:* ESI+: $[M+Na]^+$*m/z*=1138.4.

Elem. analysis calc.: C, 58.35; H, 7.44. *Found:* C, 58.20; H, 7.58.

$(OH)_8$-[G#3]-$C_6H_{12}N_3$, B-2a

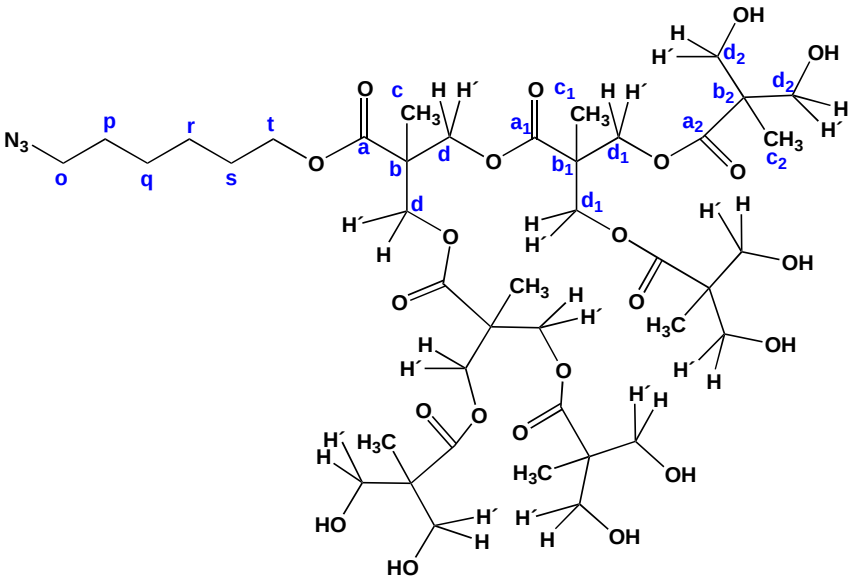

The product was obtained following the procedure (B) and obtained in 93% yield as white solid.

NMR ^1H (MeOD, 400 MHz) δ (*ppm):*1.15 (s, 12H, H_{c2}), 1.29 (s, 6H, H_{c1}), 1.30 (s, 3H, H_c), 1.44 (m, 4H, H_q, H_r), 1.61 (m, 2H, H_p), 1.70 (m, 2H, H_s), 3.32 (m, 2H, H_o), 3.59 (d, *J* = 6.8 Hz, 8H, H_{d2}), 3.67 (d, *J* = 6.8 Hz, 8H, $H_{d2'}$), 4.16 (t, *J* = 7.2 Hz, 2H, H_o), 4.23 (m, 4H, H_{d1}), 4.30 (m, 8H, $H_{d1'}$, H_d).

NMR ^{13}C (MeOD, 400 MHz) δ (*ppm):*17.3 (C_{c2}), 18.2 (C_c), 18.3 (C_{c1}), 26.7 (C_r), 27.5 (C_q), 29.6 (C_s), 29.8 (C_p), 48.0 (C_b, C_{b1}), 51.8 (C_{b2}), 52.4 (C_o), 65.9 (C_{d2}), 66.2 (C_{d1}), 66.7 (C_d), 67.4 (C_t), 173.8 (C_{a1}), 174.1 (C_a), 175.9 (C_{a2}).

*IR (cm^{-1}, KBr):*3288 (O-H st), 2923-2853 (C-H st), 2099 (N_3 st), 1732 (C=O st).

Calculated $[M]^+$ ($C_{41}H_{69}N_3O_{22}$): m/z= 955.44. *Found:* ESI+: $[M+H]^+$ m/z= 956.7.

Elem. analysis calc.: C, 52.53; H, 6.96. *Found*: C, 52.10; H, 7.22.

$(GlyBoc)_8$-[G#3]-$C_6H_{12}N_3$, B-3a

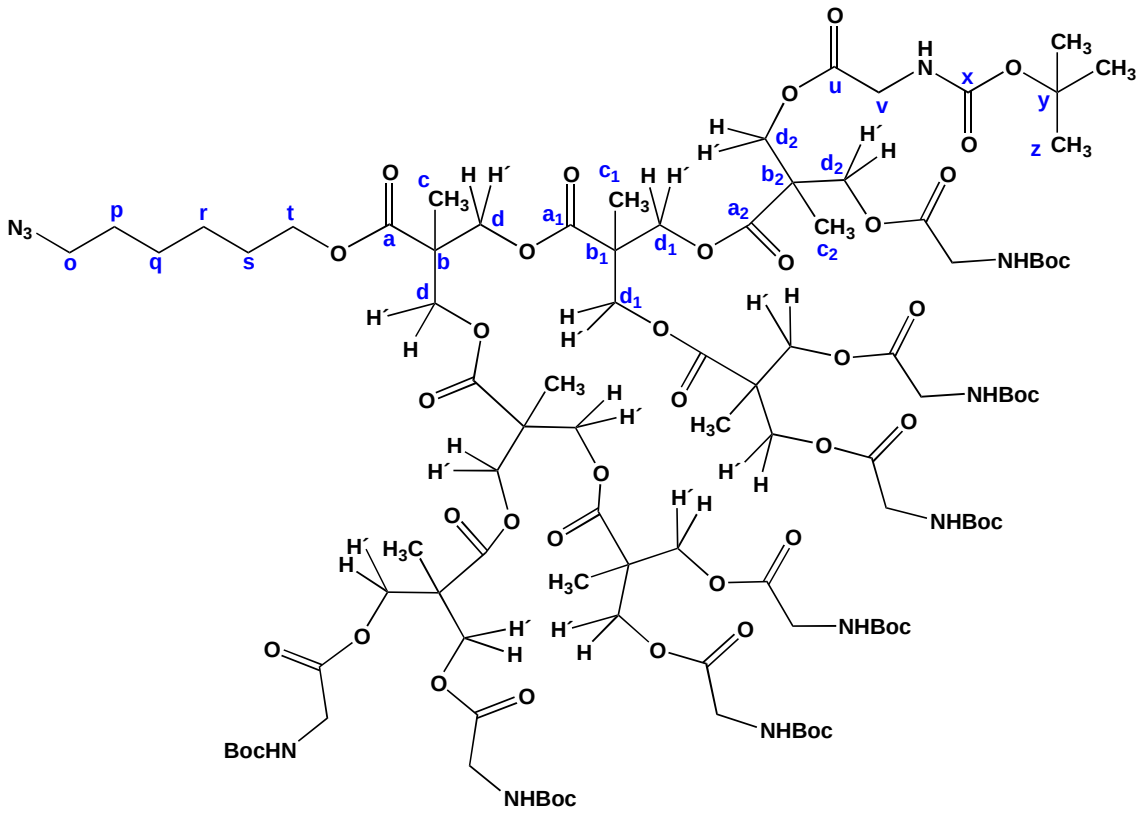

The product B-3a was obtained by Steglish esterification (A). The crude product was purified by column chromatography eluting with a mixture 1:1 of Hexane:EtOAc (R_f = 0.5). Yield: 78%. White solid.

*NMR ^1H (CDCl3, 400 MHz) δ (ppm):*1.23-1.27 (m, 21H, H_c, H_{c1}, H_{c2}), 1.43 (m, 76H, H_q, H_r, H_z), 1.60 (m, 2H, H_p), 1.66 (m, 2H, H_s), 3.27 (t, *J* = 6.8 Hz, 2H, H_o), 3.88 (d, *J* = 5.6 Hz, 16H, H_v), 4.11 (t, *J* = 6.4 Hz, 2H, H_t), 4.27 (m, 28H, H_d, H_{d1}, H_{d2}), 5.34 (s, 8H, NH).

*NMR ^{13}C (CDCl3, 400 MHz) δ (ppm):*17.6 (C_{d2}), 17.8 (C_d, C_{d1}), 25.4 (C_r), 26.3 (C_q), 28.3 (C_z, C_s), 28.6 (C_p), 42.2 (C_v), 46.3 (C_{b2}), 46.4 (C_b), 46.6 (C_{b1}), 51.2 (C_o), 65.3 (C_{d1}), 65.5 (C_t), 65.6 (C_{d2}), 66.1 (C_d), 79.9 (C_y), 155.8 (C_x), 170.0 (C_u), 171.5 (C_{a2}), 171.8 (C_{a1}), 172.0 (C_a).

IR (cm^{-1}, KBr): 3384 (N-H), 2978-2936 (C-H), 2098 (N_3), 1717-1734 (C=O).

Calculated $[M]^+$ ($C_{97}H_{157}N_{11}O_{46}$):m/z = 2212.03. *Found: ESI+:*$[M+Na]^+$ *m/z* = 2235.7.

Elem. analysis calc.: C, 52.64; H, 7.15; N, 6.96. *Found:* C, 52.90; H, 6.95; N, 6.64.

3Gpolar(NHBoc)-2Gapolar($C_{17}H_{35}$)$_4$

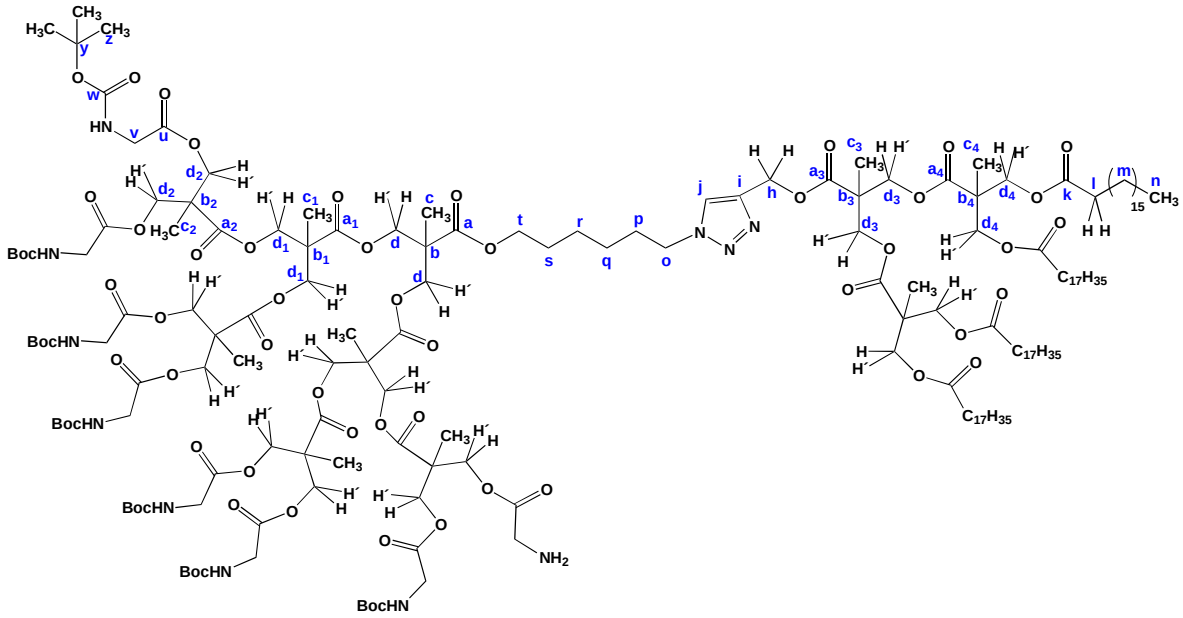

Penta-hydrated copper sulfate (3 mg, 1.13 µmol) and sodium ascorbate (0.45 mg, 2.26 µmol) were agitated in DMF during 1 h in order to form Cu(I). At the same time the apolar dendron (37 mg, 25 µmol) and the polar dendron (50 mg, 23 µmol) were solubilized in DMF. After that, the solutions were mixed and agitated for 2 days at room temperature under argon atmosphere. 50 mL of dichloromethane were added and the reaction mixture was washed with brine and water (4 × 10 mL) to remove residues and DMF. The crude was concentrated under reduced pressure and the product was precipitated in cold acetone as a white solid. Yield: 49%.

NMR ^{1}H (CDCl3, 300 MHz) δ (ppm): 0.80-0.85 (m, 12H, H_n), 1.14-1.20 (m, 142H, H_m, $H_{c\text{-}c4}$), 1.39 (s, 72H, H_z), 1.54 (m, 8H), 1.91 (m, 8H, H_{chains}), 2.24 (t, J = 7.5 Hz, 8H, H_{chains}), 3.84 (d, J =4.8 Hz, 16H, H_v), 4.07-4.35 (m, 42H, H_o, $H_{d\text{-}d4}$), 5.19 (s, 2H, H_h), 5.47 (br s, 8H, NH), 7.67 (s, 1H, H_j).

NMR ^{13}C (CDCl3, 400 MHz) δ (ppm): 14.0, 14.1, 17.5, 17.7, 17.8, 20.9, 21.0, 22.6, 24.8, 25.3, 26.1, 28.3, 29.1, 29.2, 29.3, 29.5, 29.7, 30.1, 31.9, 34.0, 42.2, 46.3, 46.4, 46.5, 46.6, 46.7, 50.2, 58.4, 60.3, 64.9, 65.1, 65.4, 65.6, 66.1, 79.9, 124.1 (C_j), 141.9 (C_i), 155.9, 170.1, 171.1, 171.5, 171.8, 171.8, 172.0, 172.1, 173.2.

IR (cm^{-1}, KBr): 3399 (N-H st), 2918-2850 (C-H), 1744 (C=O).

Calculated $[M]^+$ ($C_{187}H_{321}N_{11}O_{60}$): m/z = 3683.59. *Found:* MALDI+: $[M+Na]^+$ m/z = 3707.01.

Elem. analysis calc.: C, 60.97; H, 8.78; N, 4.18. *Found:* C, 60.51; H, 8.46; N, 4.05.

3Gpolar(NH_2)$_8$-2Gapolar($C_{17}H_{35}$)$_4$, compound B

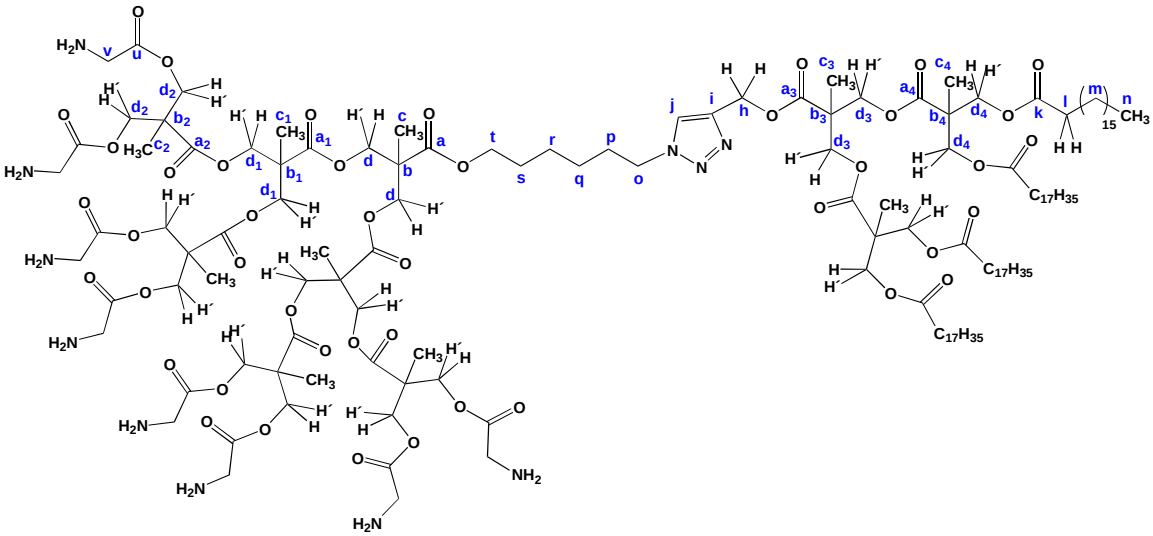

The compound B was obtained following the procedure (C) of deprotection of amine groups as a pale yellow solid in quantitative yield.

NMR ^{1}H (DMSO, 300 MHz) δ (*ppm):*0.82-0.86 (m, 12H, CH_n), 0.99-1.10 (m, 30H, $H_{c\text{-}c4}$), 1.15-1.22 (m, 90H, $CH_{2chains}$,), 1.45-1.52 (m, 8H, $CH_{2chains}$), 1.76-1.81 (m, 8H, H_p), 2.24 (t, *J* = 7.2 Hz, 8H, H_{chains}), 3.44 (d, *J* =4.8 Hz, 16H, H_v), 4.07-4.35 (m, 42H, H_o, H*d-d4*), 5.75 (s, 2H, H_h), 5.47 (br s, 8H, NH), 7.95 (s, 1H, H_j), 8.29 (br s, 16H, NH_2).

NMR ^{13}C (CDCl3, 300 MHz) δ (*ppm):*13.8, 16.7-17.0, 22.0, 24.3, 24.4, 28.3-28.9, 31.2, 33.2, 33.6, 34.0, 47.9, 48.1-48.3, 49.3, 50.1, 63.5-63.9, 65.5-65.8, 147.8 (C_d), 168.8, 172.9-173.3, 174.3, 174.4, 175.2, 176.6.

IR (cm^{-1}, KBr): 3433 (N-H), 2917-2850 (C-H), 1741 (C=O).

5-methyl-2-phenyl-1,3-dioxane-5-carboxylic acid, C-1

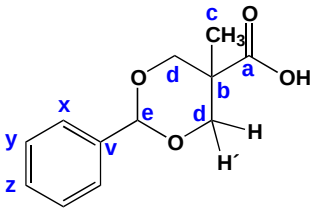

15 g (111.84 mmol) of commercial *bis*-MPA and 1.05 g (5.55 mmol) of *p*-TsOH were dissolved in 120 mL of acetone. 25.5 mL (166.62 mmol) of (dimethoxymethyl)benzene were added and the reaction mixture was stirred for 4 h. Then, the reaction was cooled to 0°C during one night and

the white precipitate was filtered and washed with cold acetone. After drying under vacuum, the product was obtained in a 73% yield (18.10 g, 81.46 mmol) as a white solid.

NMR ^{1}H (CDCl3, 400 MHz) δ (*ppm):*0.95 (s, 3H, H_c), 3.67 (d, *J* = 11.2 Hz, 2H, H_d), 4.45 (d, *J* = 11.2 Hz, 2H, $H_{d'}$), 5.50 (s, 1H, H_e), 7.35 (m, 5H, H_x, H_y, H_z).

NMR ^{13}C (CDCl3, 400 MHz) δ (*ppm):*17.5 (C_c), 41.5 (C_b), 72.8 (C_d), 100.3 (C_e), 126.0 (C_x), 127.9 (C_z), 128.6 (C_y), 138.3 (C_v), 175.5 (C_a).

*IR (cm^{-1}, KBr):*2924-2854 (C-H st), 1698 (C=O st).

Calculated $[M]^+$ ($C_{12}H_{14}O_4$) m/z = 222.09. *Found*: ESI+: $[M+Na]^+$ *m/z* = 245.1.

Elem. analysis calc.: C, 64.85; H, 6.35. *Found:*C, 64.78; H, 6.26.

5-methyl-2-phenyl-1,3-dioxane-5-carboxylic anhydride, C-2

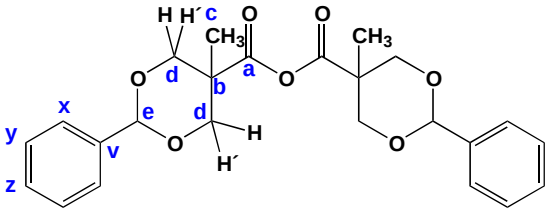

12.38 g (55.69 mmol) of C-1 and 17.80 g (86.32 mmol) of DCC were dissolved in 70 mL of dry dichloromethane. The flask was flushed with argon and the reaction mixture was stirred overnight at room temperature. The precipitate was filtered off and washed with 20 mL of dichloromethane. The filtrate was precipitated over 1 L of cold diethylic ether. The white precipitate was filtered and dried to give the pure product in a 98% yield (11.67 g, 27.36 mmol).

NMR ^{1}H (CDCl3, 400 MHz) δ (*ppm):*1.12 (s, 6H, H_c), 3.68 (d, *J* = 12 Hz, 4H, H_d), 4.65 (d, *J* = 11.6 Hz, 4H, $H_{d'}$), 5.48 (s, 2H, H_e), 7.32 (m, 6H, H_y, H_z), 7.45 (m, 4H, H_x).

NMR ^{13}C (CDCl3, 400 MHz) δ (*ppm):*16.8 (C_c), 44.2 (C_b), 73.2 (C_d), 102.1 (C_e), 126.3 (C_x), 128.2 (C_z), 129.1 (C_y), 137.5 (C_v), 169.1 (C_a).

*IR (cm^{-1}, KBr):*2923-2854 (C-H st), 1817 (C=O st sim).

Calculated $[M]^+$ ($C_{24}H_{26}O_7$):m/z = 426.17. *Found*: MALDI+: $[M+Na]^+$ *m/z* = 449.2.

Elem. analysis calc.: C, 67.59; H, 6.15. *Found:* C, 67.60; H, 6.23.

[G#1]Pluronic[G#1], C-3

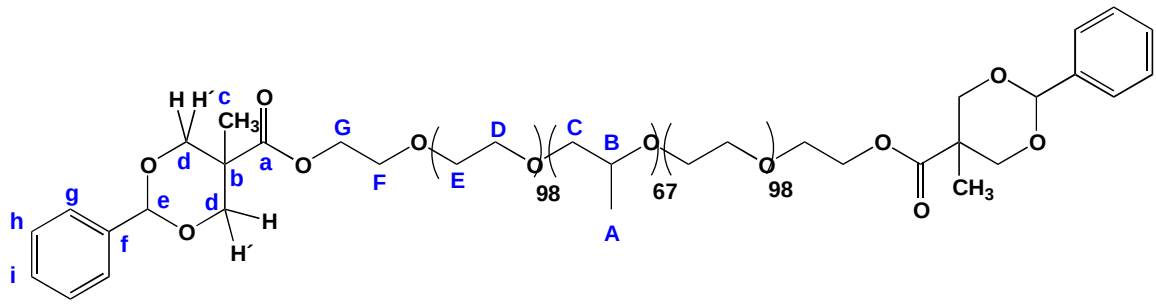

10.04 g (0.80 mmol) of F127 Pluronic® were dried at 110°C under vacuum during 1 h. The product was then dissolved in 50 mL of dry dichloromethane and 116 mg (0.95 mmol) of DMAP was added. After dissolution, 2.03 g (4.76 mmol) of *bis*-MPA benzylidene anhydride C-2 were added to the reaction mixture. The reaction was allowed to stir at room temperature, under argon atmosphere during 1 night. Then, 5 mL of methanol were added to the reaction to eliminate the excess of anhydride and the reaction mixture was allowed to stir at room temperature for 6 h. The crude product was then precipitated dropwise over 1 L of diethylic ether. The precipitate was filtered after one night at 5°C, and washed with cold diethylic ether. The product was obtained in a 84% yield (8.73 g, 0.67 mmol) as a white solid after pump drying. The structure of the compound **C-3** was confirmed in ^{1}H-NMR (**Fig. S2**), ^{13}C-NMR and IR.

*NMR ^{1}H (CDCl3, 400 MHz) δ (ppm):*1.02 (s, 6H, H_c), 1.10 (m, 201H, H_A), 3.36-3.38 (m, 67H, H_B), 3.46-3.79 (m, ≈1030H, H_C, H_D, H_E, H_F, H_d), 4.32 (t, *J* = 4.8 Hz, 4H, H_G), 4.62 (d, *J* = 11.6 Hz, 4H, $H_{d'}$), 5.41 (s, 2H, H_e), 7.28 (m, 6H, H_h, H_i), 7.39 (m, 4H, H_g).

*NMR ^{13}C (CDCl3, 400 MHz) δ (ppm):*17.1 (C_A), 17.3 (C_A), 17.7 (C_c), 42.2 (C_b), 64.1 (C_G), 68.3 (C_F), 68.4 (C_F), 68.9 (C_F), 70.4 (C_E, C_D), 72.7-73.4 (C_C, C_D), 75.0-75.5 (C_B), 101.6 (C_E), 126.1 (C_g), 128.1 (C_h), 128.8 (C_i), 137.7 (C_f), 173.7 (C_a).

*IR (cm^{-1}, thin film over NaCl):*2882 (C-H st), 1734 (C=O), 1114 (C-O-C).

MALDI+: distribution with max at *m/z* = 13649 and *m/z* = 5250.

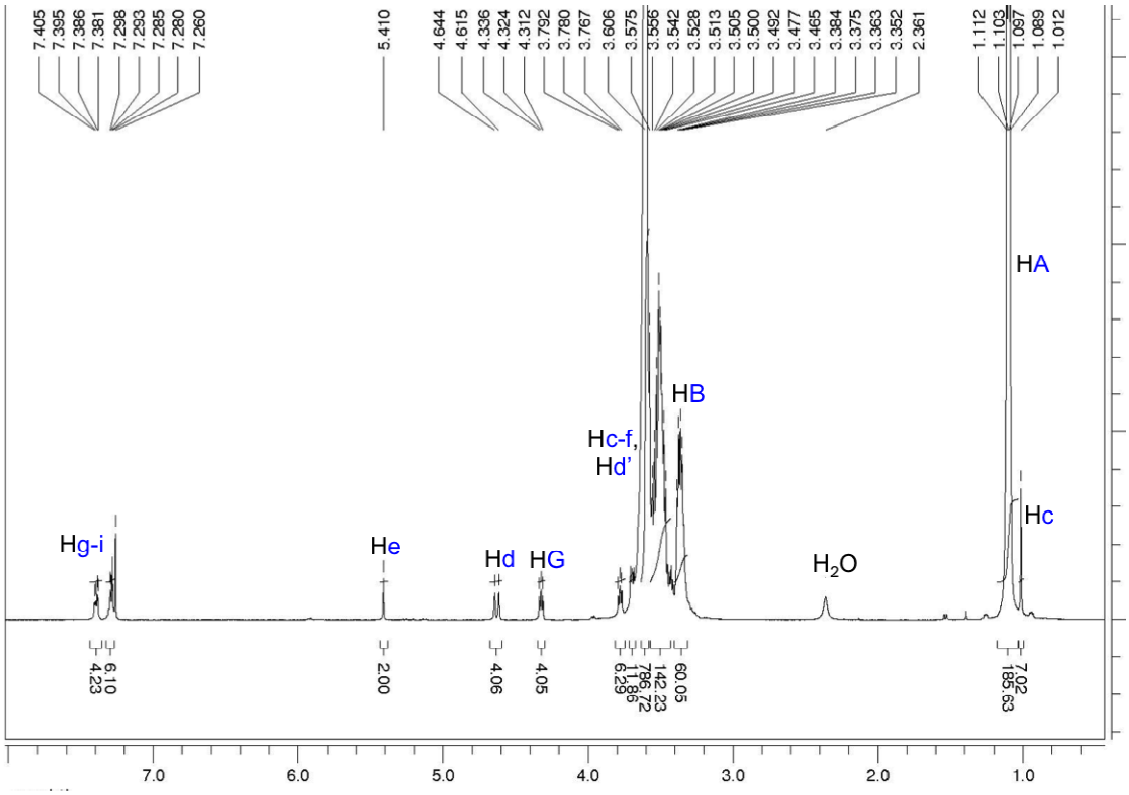

Fig. S2. ^{1}H-NMR spectrum of compound C-3. 400 MHz, $CDCl_3$ (solvent residual peak at 7.26 ppm), shift in ppm.

In ^{1}H-NMR, the union of the protected *bis*-MPA is shown by the shift of $\mathbf{H_G}$ to upper spectrum (from ca. 3.6 ppm in the commercial Pluronic® to 4.32 ppm). The peaks due to the *bis*-MPA monomer structure are situated at 1.01 ppm (s, 6H, **Hc**) and 4.63 ppm (d, 4H, **Hd**). The peak corresponding to the other diastereotopic protons, **Hd'**, appears with the peaks due to the protons of the Pluronic® structure($\mathbf{H_C}$, $\mathbf{H_D}$, $\mathbf{H_E}$, $\mathbf{H_F}$,$\mathbf{H_B}$), between 3.35 ppm and 3.79 ppm. The peaks corresponding to the protons of the benzyldene protecting groups can be observed at 5.14 ppm (s, C**H**, 2H, **He**), and at 7.28 ppm (m, and 7.39 ppm in the case of the aromatic protons **Hg**,**Hh**, **Hi**.

$(OH)_2$[G#1]Pluronic[G#1]$(OH)_2$, C-4

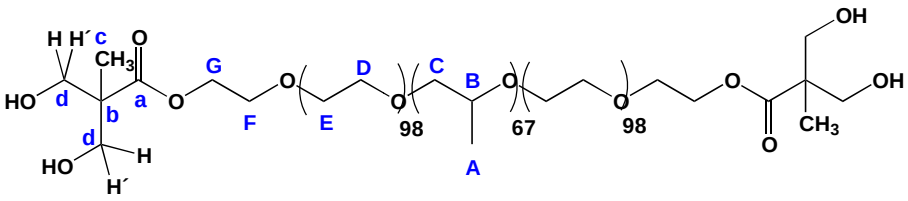

1.88 g (0.14 mmol) of [G#1]Pluronic[G#1] (C-3) were dissolved in 20 mL of ethyl acetate and 200 mg of Pd/C (20% w) were added. The reaction mixture was allowed to stir at room temperature under hydrogen atmosphere for 1 day. The residue of palladium was filtered over

Celite® and the solvent evaporated under reduced pressure to give the pure product in a 92% yield (1.68 g, 0.13 mmol) as a white solid.

*NMR ^{1}H (CDCl3, 400 MHz) δ (ppm):*1.10 (m, 207H, H_A, H_c), 3.36 (m, 67H, H_B), 3.48-3.72 (m, ≈1050, H_C, H_D, H_E, H_F, H_d), 4.32 (t, *J* = 4.8 Hz, 4H, H_G).

*NMR ^{13}C (CDCl3, 400 MHz) δ (ppm):*17.1 (C_A), 17.3 (C_A), 17.4 (C_c), 63.3 (C_G), 67.5 (C_d), 68.7 (C_F), 70.5 (C_E, C_D), 72.8-75.5 (C_B, C_C), 175.6 (C_a).

*IR (cm^{-1}, thin film over NaCl):*3482 (O-H), 2883 (C-H), 1732 (C=O), 1112 (C-O-C).

MALDI+: distribution with max at *m/z* = 13640.

$(NHBoc)_2$[G#1]Pluronic[G#1]$(NHBoc)_2$, C-5

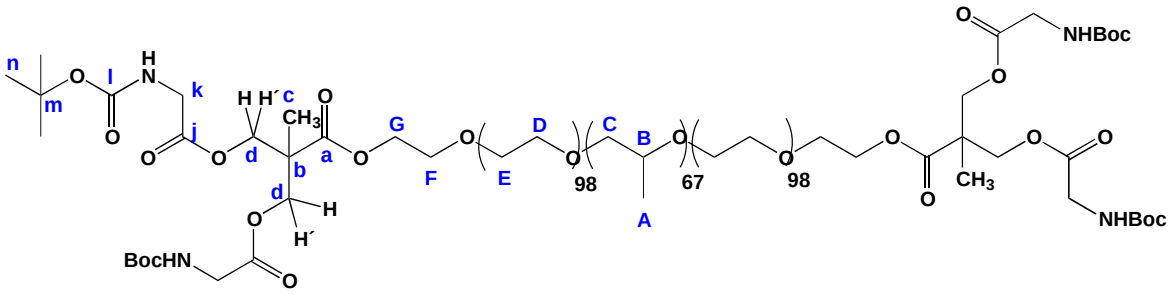

1 g (78 µmol) of $(OH)_2$[G#1]Pluronic[G#1]$(OH)_2$(C-4)were dissolved in 50 mL of dry dichloromethane, to which 164 mg (934 µmol) of GlyBoc and 38 mg (311 µmol) of DMAP were added. After dissolution, 193 mg (934 µmol) of DCC in 10 mL of dry dichloromethane were added to the reaction mixture. The reaction was allowed to stir at room temperature under argon atmosphere for 2 days. Then, the reaction mixture was cooled to 5°C and the precipitate filtered off. The solvent was evaporated under reduced pressure and the crude product was dissolved in water and dialyzed against 300 mL of dichloromethane. After 3 days the dialyzed product was collected and the solvent evaporated under reduced pressure. The product was obtained in 95% yield (997 mg, 74 µmol) as a pale yellow solid after pump drying.

The functionalization of the *bis*-MPA modified Pluronic®**C-4** by the protected glycine (**C-5**) was shown by the appearance in ^{1}H-NMR of the peak corresponding to the –OCO-C**H_2**-NHBoc at 3.81 ppm (d, *J* = 5.6Hz, 8H) and the peak due to the -C**H_3**(Boc) at 1.39 ppm (s, 36H). The deprotection of the amines was confirmed by the absence of the -C**H_3**(Boc) peak in ^{1}H-NMR and in IR by presence of the band at 2969 cm^{-1} corresponding to the NH_2 (disappearance of the band at 3328 cm^{-1} corresponding to the **N-H-**Boc).

NMR ^{1}H ($CDCl_3$, 400 MHz) δ *(ppm):* 1.08 (m, 207H, H_A, H_c), 1.39 (s, 36H, H_n), 3.33-3.36 (m, 67H, H_B), 3.45-3.77 (m, ≈ 1030H, H_C, H_D, H_E, H_F, H_d), 3.81 (d, *J* = 5.6 Hz, 8H, H_k), 4.20-4.29 (m, 8H, $H_{d'}$, H_G).

NMR ^{13}C (MeOD, 400 MHz) δ *(ppm):* 17.3-17.4 (C_A, C_d), 28.3 (C_n), 42.3 (C_b), 46.3 (C_k), 64.2 (C_G), 65.7 (C_d), 68.8 (C_F), 70.5-70.8 (C_D, C_E), 72.8-73.4 (C_B), 75.1-75.5 (C_C), 79.9 (C_m), 169.9 (C_j, C_l), 172.3 (C_a).

*IR (cm^{-1}, thin film over NaCl):*3328 (N-H), 2881 (C-H), 1721 (C=O), 1114 (C-O-C).

MALDI+: distribution with max at *m/z* = 13884 and *m/z* = 5223.

$(NH_2)_2$[G#1]Pluronic[G#1]$(NH_2)_2$, compound C

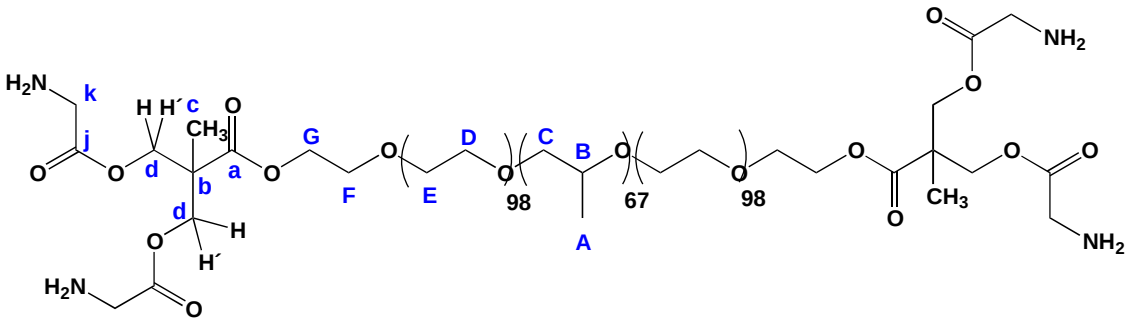

The compound C was obtained following the procedure (C) of deprotection of amines.

NMR ^{1}H ($CDCl_3$, 400 MHz) δ *(ppm):* 1.13 (m, 207H, H_A, H_c), 3.29-3.43. (m, 67H, H_B), 3.45-3.77 (m, ≈ 1030H, H_C, H_D, H_E, H_F, H_K), 4.20-4.29 (m, 8H, $H_{d'}$, H_G), 8.36 (br s, 4H, NH_2).

NMR ^{13}C (MeOD, 400 MHz) δ *(ppm):* 17.3 (C_A), 17.4 (C_c), 70.2-70.5 (C_D, C_E), 72.8, 72.9, 73.3, 75.1, 75.3, 75.5, 167.4 (C_a), 167.7 (C_j).

IR (cm^{-1}, thin film over NaCl): 2969 (-NH^{3+}, st), 2883 (C-H st), 1750 (C=O), 1114 (C-O-C).

MALDI+: distribution with max at *m/z* = 13987 and *m/z* = 4764.

$(HC{\equiv}CH_2OPh)$-Pluronic-$(PhOCH_2{\equiv}CH)$, D-1

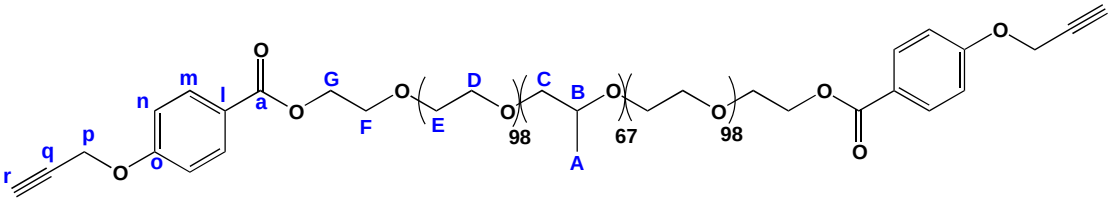

3.58 g (284 µmol) of F127 Pluronic® were dried at 110 °C under vacuum during 1 h. The product was cooled at room temperature and dissolved in 10 mL of dry dichloromethane. 166 mg (1.13 mmol) of DMAP and 200 mg (1.13 mmol) of 4-(prop-2-ynyloxy)benzoic acid were added after dissolution, the reaction mixture was cooled to 0 °C, and 234 mg (1.36 mmol) of DCC in dry dichloromethane were added. The reaction was allowed to stir at room temperature under argon atmosphere during 1 night. The crude product was then precipitated dropwise over 1 L of diethylic ether. The precipitate was filtered after one night at 5 °C, and washed with cold diethylic ether. The crude was then dissolved in methanol and dialyzed with a MWCO 1000 cellulose membrane (Spectrum® Laboratories, USA) against methanol during 2 days. After evaporation under reduced pressure, the pure product was obtained in a 56% yield (2.06 g, 150 µmol) as a pale yellow solid.

NMR ^{1}H ($CDCl_3$, 400 MHz) δ *(ppm):* 1.12 (m, 201H, H_A), 3.36 (m, 67H, H_B), 3.26-3.80 (m, ≈1050, H_C, H_D, H_E, H_F, H_r), 4.41 (t, *J* = 4.4 Hz, 4H, H_G), 4.72 (d, *J* = 2.4 Hz, 4H, H_p), 6.97 (d, *J* = 8.8 Hz, 4H, H_m), 7.99 (d, *J* = 8.8 Hz, 4H, H_n).

NMR ^{13}C ($CDCl_3$, 400 MHz) δ *(ppm):* 17.3-17.4 (C_A), 55.8 (C_p), 63.9 (C_G), 70.6 (C_E, C_D), 72.9-73.3 (C_C), 75.1-75.5 (C_B), 114.5 (C_n), 131.6 (C_m).

IR (cm^{-1}, thin film over NaCl): 2985 (arC-H), 2881 (C-H), 2687 (C≡C), 1113 (C-O-O).

MALDI+: distribution with max at *m/z* = 4692.

$(NHBoc)_8$[G#3]Pluronic[G#3]$(NHBoc)_8$, D-2

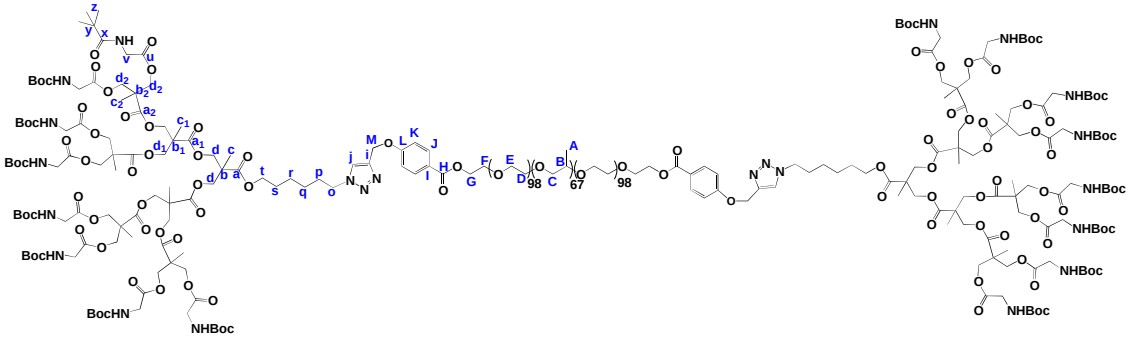

243 mg (18.8 µmol) of D-1 and 100 mg (51.2 µmol) of B-3a were dissolved in 3 mL of DMF. In another flask, 2.35 mg (9.4 µmol) of pentahydrated copper sulfate and 3.73 mg (18.8 µmol) of sodium ascorbate were mixed in 1 mL of DMF to generate copper (I). After 10 min, both solutions were mixed and stirred over night under argon atmosphere. The resulting crude product was dialyzed (cellulose membrane MWCO 12000, Spectrum® Laboratories, USA) against methanol during 2 days. The pure product was obtained in a 76% yield as a white solid.

NMR ^{1}H ($CDCl_3$, 400 MHz) δ (*ppm*): 1.12-1.14 (m, 201H, H_A), 1.24 (s, 36H, H_{c1}, H_{c2}), 1.28 (s, 6H, H_c), 1.43 (m, 144H, H_z), 1.58-1.67 (m, 8H, H_q, H_r), 3.30-3.41 (m, 69H, H_B, H_o), 3.49-3.68 (m, ≈1050H, H_C, H_D, H_E, H_F), 3.88 (d, *J* = 5.2 Hz, 32H, H_v), 4.11 (m, 4H, H_G), 4.22-4.28 (m, 56H, H_d, H_{d1}, H_{d2}), 5.24 (s, 4H, H_{c1}), 5.37 (br s, 16H, NH), 7.02 (m, 4H, H_K), 7.67 (s, 2H, H_j), 8.01 (m, 4H, H_J).

NMR ^{13}C ($CDCl_3$, 300 MHz) δ (*ppm*): 17.3, 17.4, 17.8, 28.3, 42.2, 46.4, 46.6, 65.3, 65.7, 70.5, 72.8, 72.9, 73.3, 75.0, 75.2, 75.6, 79.9, 114.3 (C_K), 123.0 (C_H), 131.7 (C_J), 143.1 (C_i), 155.9 (C_x), 162.0 (C_L), 166.1 (C_l), 170.0 (C_u), 171.5, 171.8.

IR (cm^{-1}, thin film over NaCl): 3360 (N-H), 2883 (C-H st), 1717-1743 (C=O), 1111 (C-O-C).

MALDI+: distribution with max at *m/z* = 15601 and m/z = 5179.

$(NH_2)_8$[G#3]Pluronic[G#3]$(NH_2)_8$, compound D

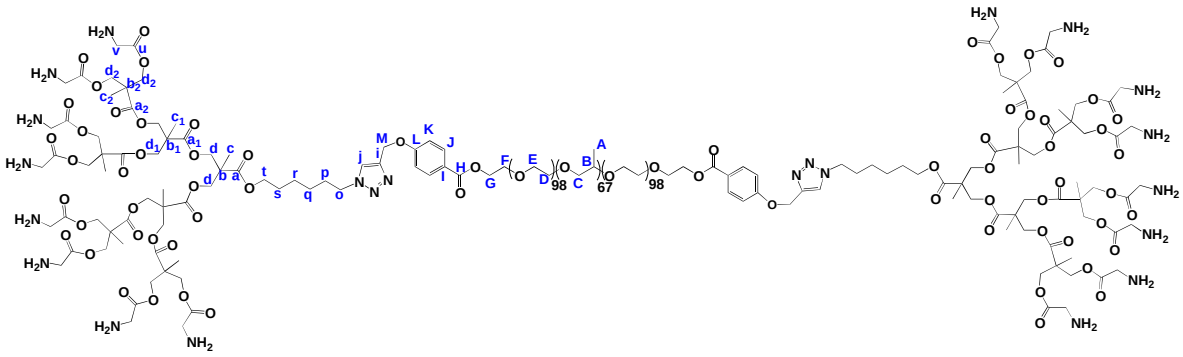

The compound D was obtained from D-1 following the synthesis method (C). Quantitative yield. Yellow solid.

NMR ^{1}H (MeOD, 400 MHz) δ (*ppm*): 1.13-1.15 (m, 201H, H_A), 1.29-1.34 (m, 36H, H_{c1}, H_{c2}), 1.36-1.67 (m, 8H, H_q, H_r), 3.30-3.33 (m, 69H, H_B, H_o), 3.42-3.69 (m, ≈1080H, H_C, H_D, H_E, H_F), 4.02-4.06 (m, 18H, H_d, H_{d1}), 4.11 (m, 4H, H_G), 4.33-4.35 (m, 32H, H_{d2}), 4.96 (m, 32H, H_v), 5.32 (s, 4H, H_M), 5.49 (s, 2H, H_j), 7.02 (m, 4H, H_l), 8.01 (m, 4H, H_J).

NMR ^{13}C (MeOD, 400 MHz) δ (*ppm*): 17.7, 71.3-71.5, 74.1, 74.4, 76.6-76.8, 111.4.

*IR (cm^{-1}, thin film over NaCl):*2970 (N-H, NH_3^+, st), 2880 (C-H st), 1742 (C=O), 1112 (C-O-C).

MALDI+: distribution with max at *m/z* = 15264.

Polymer			CQ added			CQ encapsulated				
P	**mg[a]**	**µmol[b]**	**mg[c]**	**µmol[d]**	**molCQ /molP**	**µmolCQ /mgP[e]**	**mgCQ /mgP[f]**	**molCQ /molP[g]**	**w (%) CQ in carrier[h]**	**EE[i] (%)**
A	1	0.428	1.10	2.14	5	1.73	0.89	4.0	47.1	81
B	1	0.315	0.81	1.57	5	1.51	0.78	4.8	43.8	96
C	1	0.072	0.19	0.36	5	0.29	0.15	4.0	13.0	81
D	1	0.061	0.16	0.31	5	0.32	0.16	5.0	13.8	100

Polymer			PQ added			PQ encapsulated				
P	**mg[a]**	**µmol[b]**	**mg[c]**	**µmol[d]**	**mol PQ /molP**	**µmolPQ /mgP[e]**	**mgPQ /mgP[f]**	**molPQ /molP[g]**	**w (%) PQ in carrier[h]**	**EE[i] (%)**
A	1	0.428	0.97	2.14	5	1.01	0.46	2.4	31.5	47
B	1	0.315	0.72	1.57	5	0.95	0.43	3.0	30.1	60
C	1	0.072	0.16	0.36	5	0.34	0.16	4.7	13.8	98
D	1	0.061	0.14	0.31	5	0.28	0.13	4.6	11.5	92

Table S2. Amount of drug encapsulated using the ratio 5:1 mol of drug/mol of polymer. All the quantities are expressed per mL of water: [a]quantity of polymer in mg; [b]quantity of polymer in mol; [c]quantity of drug added in mg; [d]quantity of drug added in mol; [e]ratio of drug encapsulated in mol per mg of polymer; [f]ratio of drug encapsulated in mg per mg of polymer; [g]ratio of drug encapsulated in mol per mol of polymer; [h]drug contents in the carrier expressed in weight percentage of drug, [i]encapsulation efficiency (EE = 100 × mol of drug loaded/mol of drug added).

Polymer			CQ added			CQ encapsulated				
P	**mg[a]**	**µmol[b]**	**mg[c]**	**µmol[d]**	**molCQ /molP**	**µmolCQ /mgP[e]**	**mgCQ /mgP[f]**	**molCQ /molP[g]**	**w (%) CQ in carrier[h]**	**EE[i] (%)**
B	1	0.315	1	1.94	6.2	1.94	1.00	6.2	50.0	100
C	1	0.072	1	1.94	26.9	1.07	0.55	14.9	35.5	55
D	1	0.061	1	1.94	31.8	1.30	0.67	21.2	40.1	67

Polymer			PQ added			PQ encapsulated				
P	**mg[a]**	**µmol[b]**	**mg[c]**	**µmol[d]**	**molPQ /molP**	**µmolPQ /mgP[e]**	**mgPQ /mgP[f]**	**molPQ /molP[g]**	**w (%) PQ in carrier[h]**	**EE[i] (%)**
B	1	0.315	1	2.20	7.0	1.31	0.60	4.1	37.5	60
C	1	0.072	1	2.20	30.5	1.94	0.88	27.0	46.8	88
D	1	0.061	1	2.20	36.1	1.29	0.59	21.1	37.1	59

Table S3. Amount of drug encapsulated using the ratio drug/polymer 1:1 w/w. Compound A has not been tested here because its w/w drug/polymer ratios in Table S2 were already close to 1:1.All the quantities are expressed per mL of water: [a]quantity of polymer in mg; [b]quantity of polymer in mol; [c]quantity of drug added in mg; [d]quantity of drug added in mol; [e]ratio of drug encapsulated in mol per mg of polymer; [f]ratio of drug encapsulated in mg per mg of polymer; [g]ratio of drug encapsulated in mol per mol of polymer;[h]drug contents in the carrier expressed in weight percentage of drug,[i]encapsulation efficiency.

Nanovectors	Fluorescence emission
A-rhoB	597
B-rhoB	30
C-rhoB	753
D-rhoB	256

Table S4. Fluorescence emission values (arbitrary units) of the nanovectors encapsulating rhodamine B (λ_{ex} = 540 nm, λ_{em} = 580 nm).

Polymer			RhoB added			RhoB encapsulated				
P	**mg[a]**	**µmol[b]**	**mg[c]**	**µmol[d]**	**mol RhoB /mol P**	**µmolRhoB /mgP[e]**	**mgRhoB /mgP[f]**	**molRhoB /molP[g]**	**w (%) RhoB in carrier[h]**	**EE[i] (%)**
A	1	0.428	1	2.09	4.9	0.403	0.19	0.9	16.0	19
B	1	0.315	1	2.09	6.9	0.08	0.01	0.03	1.0	0.4
C	1	0.072	1	2.09	29.0	0.511	0.24	7.1	19.4	24
D	1	0.061	1	2.09	34.3	0.165	0.08	2.7	7.4	8

Table S5. Amount of rhodamine B encapsulated using the ratio RhoB/polymer 1:1 w/w. All the quantities are expressed per mL of water: [a]quantity of polymer in mg; [b]quantity of polymer in mol; [c]quantity of rhodamine B added in mg; [d]quantity of rhodamine B added in mol; [e]ratio of rhodamine B encapsulated in mol per mg of polymer; [f]ratio of rhodamine B encapsulated in mg per mg of polymer; [g]ratio of rhodamine B encapsulated in mol per mol of polymer; [h]rhodamine B contents in the carrier expressed in weight percentage of rhodamine B, [i]encapsulation efficiency.

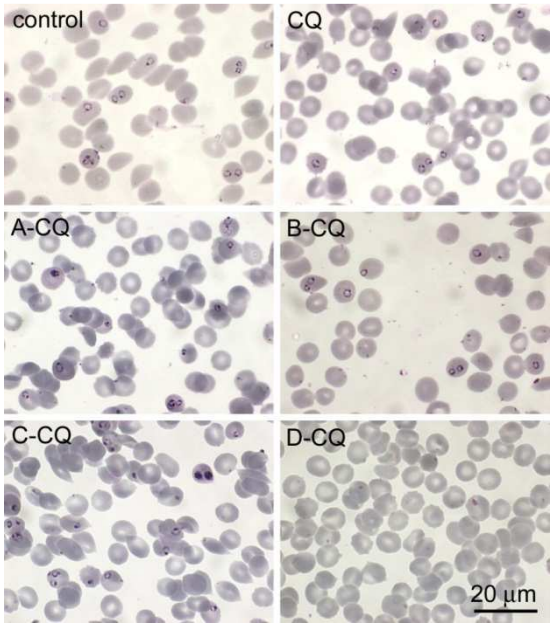

Fig. S3. Bright field microscope pictures of Giemsa-stained pRBC cultures treated with free chloroquine and with A-CQ, B-CQ, C-CQ, and D-CQ at a CQ concentration of 10 nM.

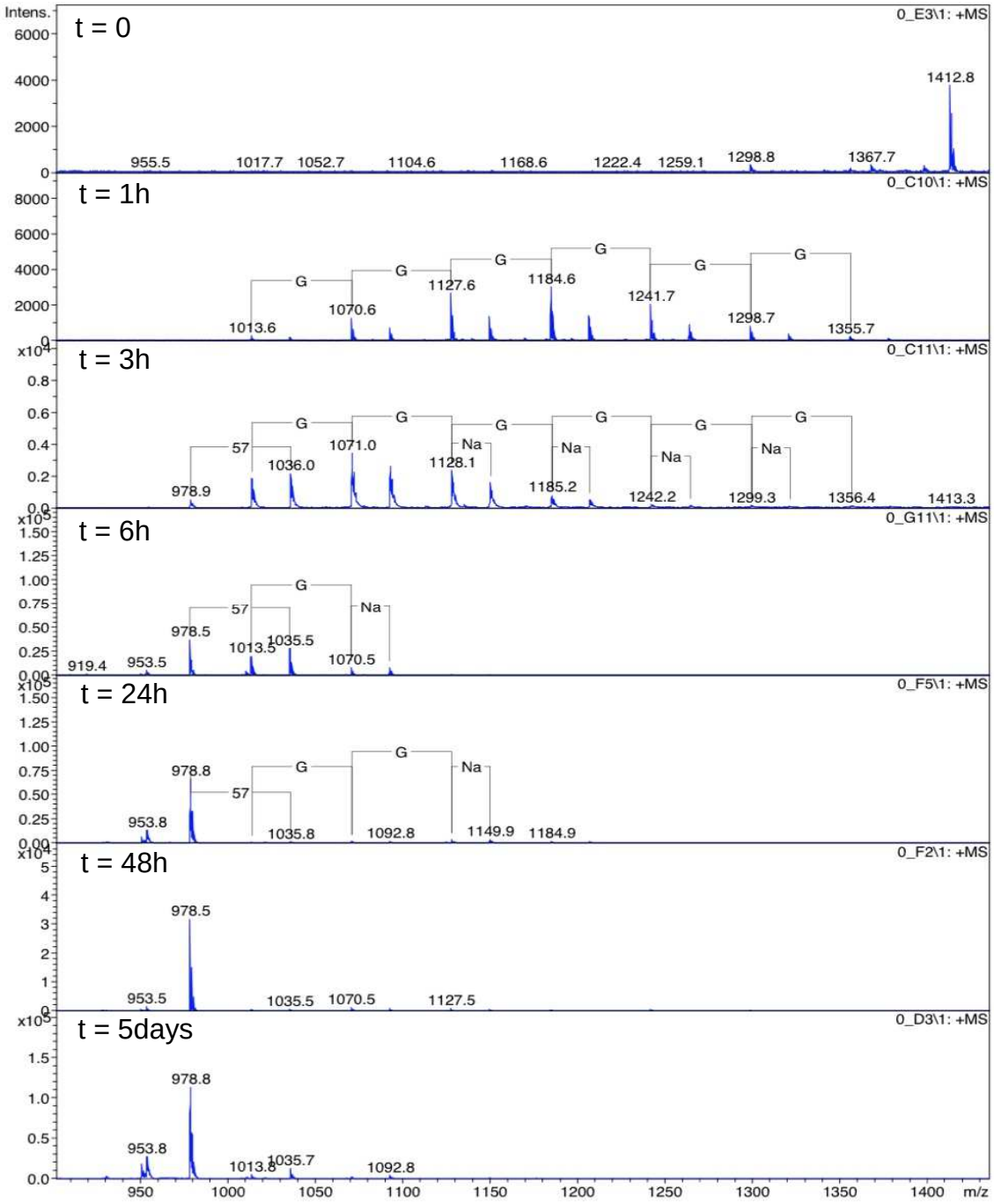

Fig. S4. Mass spectrometry study of the degradation of dendron DB1 (1 mg/mL) along time, performed at 37 °C in 0.1 M citrate phosphate buffer, pH 7.0. After only 1 h of incubation, the molecular peak has disappeared with the concomitant appearance of peaks corresponding to the loss of one or various glycine moieties (G). After 5 days, the degradation seems to be complete, remaining only the nude dendron with hydroxyl groups.

SUMMARY OF RESULTS

Amphiphilic dendritic nanoparticles obtained through (i) derivatization of 2,2-*bis*(hydroxymethyl)propionic acid (*bis*-MPA) and Pluronic® as fundamental subunits and (ii) their subsequent aggregation, were explored as **supplementary antimalarial drug nanocarriers cheaper to produce than liposomes and as an alternative to the polyamidoamine(PAA)-derived polymers** already reported. The latter polymer-based approach had provided a marginal increase in CQ and PQ drugs efficacy *in vitro* against *P. falciparum* (<2-fold decrease in IC50) but considerably increased the number of surviving *P. yoelii*-infected animals in comparison with drugs delivered on their own (Urbán et al. 2014).

Pluronic®-derived, dendritic-linear-dendritic block copolymers showed a **selective accumulation into pRBCs** and **improved** as well **CQ and PQ activity** by approximately **3- and 4-fold reduction of drugs IC50** when assayed ***in vitro* in *P. falciparum* cultures**. Among the dendritic derivatives employed, the copolymer C exhibited antimalarial activity in itself (IC50 of 7 µg/ml polymer) at a non-toxic concentration (*in vitro* cytotoxicity observed for >2 mg/ml polymer) and, together with copolymer D and similarly to PAA-polymers, **both C and D dendritic polymers prolonged *P. yoelii*-infected mice survival times** when encapsulating PQ and CQ antimalarials, respectively. Furthermore, these two particular dendrimers displayed an extraordinary drug trapping capacity with encapsulation efficiencies ranging from 80% to 100%.

DISCUSSION

1. Amphiphilic dendritic nanoparticles as antimalarial agents

Dendrimers have been extensively employed as drug delivery and cell transfection systems on the basis of their capacity to: (i) encapsulate drugs and DNA, feature provided by including amphipathic structures and/or weakly basic groups at the dendrimer surface (Nanjwade et al. 2009), and (ii) become internalized into cells. The cytoplasmic delivery of dendrimers being primarily driven by cell-mediated endocytic events and particularly enhanced when conjugated with cell penetrating peptides (Olson et al. 2010). Antimicrobial and antiviral activities have been additionally reported for dendrimers assayed on their own, fact that increases even more their biomedical application repertoire (Mintzer & Grinstaff 2011).

In the light of the above, we have explored in this PhD thesis the application of dendritic nanoaggregates as nanocarriers for the delivery of antimalarials into pRBCs (i) cheaper to produce compared to immunoliposomal vectors (such as the liposomal approaches presented in Chapters 1 and 2) and (ii) as an alternative to polyamidoamine(PAA)-based polymers by which a moderate improvement in drug activity *in vitro* had been reported against *P. falciparum* cultures (Urbán et al. 2014).

2. Physicochemical properties of dendrimers and encapsulation of active molecules

Polarized dendritic monomers (Janus-type dendrimers termed A and B, approx. 2-3 kDa MW) (Caminade et al. 2012) as well as dendritic-linear-dendritic block copolymers (named C and D) were synthesized by Julie Movellan (Department of Organic Chemistry-Institute of Nanoscience of Aragon) following a convergent strategy and employing 2,2-Bis(hydroxymethyl)propionic acid (*bis*-MPA) as principal branching molecule. Besides, Pluronic® F127 was used as internal amphiphilic core for C and D copolymers (approximately 14-16 kDa MW). These dendrimeric subunits were thereafter self-arranged in aqueous solution, forming micelle-like aggregates of a few hundred nanometers in length, while simultaneously entrapping other amphipathic molecules already present in solution (process named as 'oil/water method') (Vrignaud et al. 2011).

2.1. Encapsulation of drugs and rhodamine B

The aforementioned self-aggregating mechanism was employed for the encapsulation of CQ and PQ antimalarials as well as the rhodamine B (rhoB) fluorescent dye for tracking purposes. Remarkably, both EE% and the supramolecular structure of the resulting conjugates largely depended on the initial compound/polymer molar ratio and the physicochemical properties of the entrapped molecule. In this regard, best drug EE of >80% were obtained for (i) CQ in all four dendrimeric structures and (ii) PQ in the Puronic®-based, C and D copolymers when employing a starting 5:1 drug/polymer molar ratio. The aforesaid dendrimer-drug conjugates displayed spherical-ovoid shapes and sizes ranging from 170 to 640 nm in length. By contrast, EE lower than 20% and complete spherical adducts of 50 to 200 nm in diameter were obtained when encapsulating rhoB.

Remarkably, such differences in EE%, size and shape might be explained by drugs physicochemical properties. Whereas rhoB is triangularly shaped and fully ionized (though displaying a net zero overall charge at physiological pH), CQ and PQ drugs structure is more stretched and contain highly lipophilic regions that are found in their unionized and monoprotonated species (discussed more in detail in Annex I). Consequently, drugs might be able to partition into the apolar core of the dendritic-micellar aggregates and remain entrapped more easily than rhoB. Furthermore, the positively-charged groups of CQ and PQ would become stabilized due to the highly abundant esters present in *bis*-MPA derived dendrons (ion-dipole interaction). Finally, the elongated shape of drugs would explain as well the more ovoid nanoparticles formed compared to the spherical-shaped, rhoB-containing adducts.

2.2. Disaggregation of dendritic nanoparticles and release of the entrapped material

In comparison with vesicular structures such as liposomes, dendrimer-based nanoparticles do not provide a membrane-closed system, fact that considerably exposes those encapsulated compounds to the external aqueous environment. In addition to this, the packing degree of composing dendritic monomers is not as uniform as in phospholipid-based bilayers. Moreover, the weak amino groups from glycine units present at the dendrimers surface (pKa_2 ~9.6) as well as the weakly basic moieties of CQ and PQ encapsulated drugs, will display distinct ionization states as a function of solution pH: slightly neutral at physiological conditions but completely ionized in an acidic environment. Nanoparticle overall charge, structure and stability will therefore be defined by solution pH and the presence of small ions. The latter factor would improve the solubility of both dendrimers and drugs by means of ion-dipole and ion-induced dipole forces.

The aforementioned properties of dendritic nanoparticles and drugs might explain why drug-polymer conjugates are stably formed in water (EE >80% after overnight sample dialysis against MilliQ water) but, at the same time, these micellar aggregates release more than one-half of the initially entrapped material in a few hours when dialyzed against *P. falciparum* complete culture medium. Drug leakage could be further accelerated due to the non-enzymatic degradation of dendrimers, which is principally triggered through acid-catalyzed hydrolysis of the esters located between *bis*-MPA branching units and within the surface-exposed glycines (Grajales & Jasty 2012). In this regard, >50% of glycine moieties were released from DB1 dendrons after 1 h incubation at 37 ºC in 0.1 M citrate phosphate buffer, pH 7.0.

3. Targetability and antimalarial activity of dendritic nanoparticles

3.1. Targetability and pRBC-intracellular delivery

Specific targeting towards pRBCs was observed for rhoB-laden dendritic nanocarriers and the internalization rate of these nanoparticles was suggested to be influenced by their size and structure. In this regard, the most significant rhoB intracellular signal was observed when delivered through copolymer D, conjugate that displayed the smallest size obtained of 50 nm in diameter along with a considerable positive charge (the latter attribute provided by its lateral amine-rich DB1 dendrons). Given these particular features, D-rhoB might efficiently interact with the negatively-charged glycocalyx of the RBC (Fernandes et al. 2011) as well as those phosphatidylserine lipids exposed on pRBCs (Maguire et al. 1991). This conjugate would become finally internalized into parasitized cells by means of a not well understood uptake mechanism that has been described to occur for several nanoparticles of <100 nm in size. A similar pRBC-internalization process might be followed by PAA-based polymers and heparin, whose sizes were in all cases below 40 nm in diameter (Urbán et al. 2014; Marques et al. 2014).

Bearing in mind the absence of endocytosis in pRBCs, the existence of a parasitophorous duct or small apertures formed at the surface of late stage-pRBCs had been considered responsible for the uptake of macromolecules (Goodyer et al. 1997; Pouvelle et al. 1991). Nevertheless, such features were not identified when studying the ultrastructure of pRBCs through electron tomography and 3D reconstruction (Hanssen, Carlton, et al. 2010). The likeliest reported structure to a possible duct, though, were electron-dense tethers of 30 nm in diameter and up to 300 nm in length physically connecting the Maurer's clefts with the cytoplasmic leaflet of the pRBCM but lacking of surface exposition. Besides, a role in intracellular protein trafficking was attributed to these tubes.

As an alternatively proposed mechanism, dendritic aggregates might nonspecifically release rhoB onto the pRBC surface, as described in 2.2., and the free dye could in turn accumulate into the parasitized cell by means of the parasite-induced new permeability pathways or through its passive diffusion across the pRBCM. This indirect uptake mechanism might be less efficient and probably followed by those nanoparticles bigger in size than D-rhoB: A-rhoB and C-rhoB with 188 and 70 nm in diameter, respectively; for which a considerable diminished intracellular signal was obtained. Remarkably, a similar fate would be attributable to drug-polymer conjugates, whose sizes were in all cases larger than 170 nm in length.

3.2. Antimalarial activity

The best activity against *P. falciparum* intraerythrocytic growth *in vitro* was obtained for the D-CQ and C-PQ drug-polymer conjugates, improving drug efficacy by means of a 3- to 4-fold reduced IC50 compared to freely delivered antimalarials. Such eventual enhanced activities (2 from 8 total assayed conjugates) indicated a major role of the combined properties of the encapsulated compound and the hosting dendritic nanoparticle for an efficient parasite growth inhibition. Moreover, copolymer C is the best positioned structure to reach clinical assays on the basis of its own antimalarial activity (IC50 of 7 µg polymer C/ml) together with a remarkably low *in vitro* cytotoxicity (IC50 >10 mg polymer C/ml). In comparison, copolymer D was much less active against *P. falciparum* on itself (IC50 of 200 µg polymer D/ml) and more cytotoxic (IC50 ~1 mg polymer D/ml), though at a concentration far away from the amount of copolymer required to obtain a 100% parasite growth inhibition in combination with CQ (which corresponds to about 3.1E-05 mg polymer D/ml in culture, 0.32 µmol CQ/mg D).

However, the particular features leading to antiparasitic activity and/or endothelial cell toxicity remain unknown. Given the similar building blocks employed in all polymers (i.e. *bis*-MPA and Pluronic® units), the final structure adopted by dendrimers after their self-aggregation and drug entrapment seems to be the principal factor defining their activity. Finally, additional *P. falciparum* growth inhibition assays should be performed with drug-polymer conjugates incubated during different time periods (not the fully 48 h replication cycle) and added at distinct intraerythrocytic

stages of the parasite in order to ascertain which is the mechanism driving the aforementioned improvement in drug efficacy.

In summary, taking into account the aforementioned limited pRBC-internalization of nanoparticles bigger in size than 100 nm as well as the release of drugs and degradability of dendrimers in a few hours, the most likely events taking place during *P. falciparum* growth inhibition assays would be (i) the leakage of drugs over time at the pRBC nearby area along with (ii) a possible blockage of RBCs invasion by merozoites. Importantly, the latter process has been observed to occur for PAA-based polymers (Urbán et al. 2014) and might be mediated through the already mentioned interaction of positively-charged nanocarriers with the anionic glycocalyx of host RBCs.

4. In vivo antimalarial activity and clinical applicability of dendritic nanoparticles

4.1. *In vivo* antimalarial activity

Marginal parasitemia reduction at day 4th post-infection together with prolonged survival times of a few days were obtained for D-CQ and C-PQ conjugates when assayed in *P. yoelii* 17XL-infected mice and in comparison with freely administered drugs. An absence of toxicity was additionally observed at the amounts of copolymers assayed: 4 administrations of 125 µg D or 225 µg C to a 20 g mouse, which corresponds to 1 mg CQ/kg or 1.8 mg PQ/kg maximum doses, respectively (0.16 mg encapsulated drug per mg of copolymer). Similar results have been reported in (Urbán et al. 2014), though using PAA-based nanocarriers instead. Improved parasite clearance and mice survival times (>1 month) were obtained in this work for encapsulated CQ. In the same assay, animals receiving free CQ died between 7 and 12 days post-infection.

Moreover, C-rhoB and D-rhoB conjugates reached their maximum levels in plasma between 2 min and 1.5 h post intraperitoneal-administration (50 mg copolymer/kg dose) and displayed circulation half-lives of about 4.5 h. Nevertheless, *in vivo* pharmacokinetics might be affected as well by the encapsulated compound/dendrimer combination and, therefore, subsequent assays should be performed with drug-loaded copolymers. In such case, nanoparticles might be radioactive-labeled in order to minimize the otherwise alteration of conjugates structure caused by the inclusion of fluorescent dyes.

4.2. Clinical application

In the light of the above, dendritic aggregates appear as a potential alternative to the already proposed liposomal (Chapter 1 and 2) and PAA-based nanocarriers (Urbán et al. 2014) for the treatment of malaria. Their most remarkable features include:

1. **Considerable improvement in CQ and PQ drug activity *in vitro*** (48 h incubation with *P. falciparum* cultures) when **compared to PAA polymers** though **less efficient *in vivo***

against *P. yoelii*. Moreover, for a proper comparison with the GPA-iLP model (Chapter 1), *in vitro* kinetic assays should be performed in order to know (i) the amounts of conjugates internalized and/or retained onto pRBCs as a function of time and nanoparticle concentration, as well as (ii) the minimum incubation time required for an effective antimalarial activity (the shortest we have ever observed has been 15 min for GPA-iLPs).

2. Similarly to PAA-based nanoparticles, **drug-dendrimer conjugates are active against both *P. falciparum* and *P. yoelii***, which allows to their *in vivo* validation using more affordable malaria murine models than the *P. falciparum*-infected, humanized mouse. Nevertheless, drug-laden dendrimers should also be tested in the latter model in order to confirm their *in vivo* efficacy against human-infecting *Plasmodium* spp.
3. **Low production cost** of nearly <8 cents of € for the 100% growth inhibition of 1L of *P. falciparum* culture using either C-PQ or D-CQ. Extraordinarily smaller when compared to iLP-based antimalarial therapies.
4. **CQ and PQ EE of >80% for the 5:1 drug/polymer molar ratio**, being similar to the liposomal pH gradient method. EEs% have not been reported for PAA-based nanoparticles. Moreover, dendritic aggregates provide similar drug loading capacities to PAA polymers (160 mg/g copolymer vs. 150-300 mg/g PAA, respectively) but considerably higher than pH gradient-containing LPs (20-40 mg/g phospholipid).
5. **Easy adjustability of dendrimers composition, activity and structure** by changing their branching and functional units. Lego-like process similar to liposomal nanoparticles but requiring several time-consuming steps and specific knowledge in chemistry.

Nevertheless, several improvements in dendrimer composition must be done if we consider a future clinical application. Having a look at our dendritic nanoparticles showing best pRBC-internalization as well as the previously reported PAA-derived polymers, the first issue to address will be the reduction of the size of the drug-copolymer conjugates below the 50 nm limit (maximum diameter we have observed for an effective uptake). If we take into account that the length of copolymers C and D is defined by their central lipophilic region, a shorter polymer than Pluronic® F127 (linear structure containing approximately 526 carbon + 263 oxygen atoms) would consequently result in smaller conjugates. Moreover, sterically stabilizing agents (e.g. PEG, chondroitin sulfate A or gangliosides) might be attached to the surface of dendritic nanoparticles in order to improve their *in vivo* pharmacokinetics, simultaneously avoiding in this manner nonspecific interactions with host cells and the binding of serum components to dendrimer cationic moieties (Bhadra et al. 2006). Those conjugates preserving a small size and minimal drug leakage as well as efficiently internalized into parasitized cells would be optimal. Finally, the mechanism by which macromolecules of a few nanometers in size are taken up by pRBCs and the possible existence of either specific active groups or cell receptors mediating this process should be explored without preconceptions.

ANNEX III

Possible roles of amyloids in malaria pathophysiology

SPECIAL FOCUS I Protein Misfolding Diseases

Special Report

For reprint orders, please contact reprints@future-science.com

Future Science OA

Possible roles of amyloids in malaria pathophysiology

The main therapeutic and prophylactic tools against malaria have been locked for more than a century in the classical approaches of using drugs targeting metabolic processes of the causing agent, the protist *Plasmodium* spp., and of designing vaccines against chosen antigens found on the parasite's surface. Given the extraordinary resources exhibited by *Plasmodium* to escape these traditional strategies, which have not been able to free humankind from the scourge of malaria despite much effort invested in them, new concepts have to be explored in order to advance toward eradication of the disease. In this context, amyloid-forming proteins and peptides found in the proteome of the pathogen should perhaps cease being regarded as mere anomalous molecules. Their likely functionality in the pathophysiology of *Plasmodium* calls for attention being paid to them as a possible Achilles' heel of malaria. Here we will give an overview of *Plasmodium*-encoded amyloid-forming polypeptides as potential therapeutic targets and toxic elements, particularly in relation to cerebral malaria and the blood–brain barrier function. We will also discuss the recent finding that the genome of the parasite contains an astonishingly high proportion of prionogenic domains.

Keywords: amyloids • intrinsically unstructured proteins • malaria • prions

Ernest Moles[†,1,2], Juan José Valle-Delgado[†,1,2], Patricia Urbán[1,2], Isabel G Azcárate[3,4], José M Bautista[3,4], Javier Selva[5], Gustavo Egea[5], Salvador Ventura[6] & Xavier Fernàndez-Busquets*[,1,2]

[1]Nanomalaria Group, Institute for Bioengineering of Catalonia (IBEC), Baldiri Reixac 10–12, ES-08028 Barcelona, Spain

[2]Barcelona Institute for Global Health (ISGlobal, Hospital Clínic-Universitat de Barcelona), Rosselló 149–153, ES-08036 Barcelona, Spain

[3]Department of Biochemistry & Molecular Biology IV, Universidad Complutense de Madrid, Ciudad Universitaria, ES-28040 Madrid, Spain

[4]Research Institute Hospital 12 de Octubre, Universidad Complutense de Madrid, Ciudad Universitaria, ES-28040 Madrid, Spain

[5]Department of Cell Biology, Immunology & Neurosciences, University of Barcelona School of Medicine & Institut d'Investigacions Biomèdiques August Pi i Sunyer (IDIBAPS), ES-08036 Barcelona, Spain

[6]Institut de Biotecnologia i Biomedicina & Departament de Bioquímica i Biologia Molecular, Universitat Autònoma de Barcelona, ES-08193 Bellaterra, Spain

*Author for correspondence: xfernandez_busquets@ub.edu

[†]Authors contributed equally

Malaria pathophysiology

Malaria infection starts when a parasitized female *Anopheles* mosquito inoculates during a blood meal sporozoites of the malaria parasite, the apicomplexan protist *Plasmodium* spp., which migrate through the skin into the circulation and then to the liver. In a few minutes, sporozoites invade hepatocytes, where they will transform into merozoites that enter the circulation to invade red blood cells (RBCs) [1]. Merozoites replicate asexually to produce daughter cells that infect new erythrocytes to perpetuate the blood-stage cycle. Some parasites eventually differentiate into sexual stages, micro- and macro-gametocytes that are ingested by a mosquito from peripheral blood, and reach the insect's midgut where they develop into male and female gametes. Following fertilization, the zygote differentiates into an ookinete that moves through the midgut epithelium of the mosquito host and forms an oocyst from which sporozoites are released and migrate to the salivary glands to restart the cycle at the next bite. Because RBCs are unable to process and present antigens, the intraerythrocytic parasite remains invisible to the immune system until it starts modifying the parasitized RBCs (pRBCs) in order to meet its needs for membrane transport processes [1]. Even then, the proteins exported to the pRBC plasma membrane have a very high antigenic variation [2] which leads to waves of parasitemia and persistent infections despite antibody-mediated immune pressure.

Amyloidogenic proteins & peptides in the malaria parasite

Sequence analysis has shown that apicomplexan parasite proteomes are enriched in intrinsically unstructured proteins (IUPs) [3], which contain large segments of disordered

FUTURE SCIENCE part of fsg

structure under physiological conditions. The IUP contents in mammalian-infecting *Plasmodium* species are particularly high, especially in the proteome of the *Plasmodium falciparum* sporozoite. Several *Plasmodium* IUPs have been examined as potential targets of interest for protective immune responses because repeats present in many of them are highly immunogenic showing strong reactivity with antibodies. However, antibodies raised against these repeats do not mediate protection in front of the parasite, probably because IUPs adopt more ordered structures when interacting with different ligands, and antibodies induced by such regions may recognize a variety of antigen conformers and thus react poorly with the antigen on the parasite surface. The structural plasticity of IUPs, which allows promiscuous binding interactions, may favor parasite survival both by inhibiting the generation of effective high affinity antibody responses and by facilitating the interactions with host molecules necessary for attachment to the vascular endothelium and for the invasion of host cells. Amyloidogenesis is undergone by a diverse group of evolutionarily unrelated proteins from different organisms, all sharing permanent or transiently disordered structural regions with propensity to form β-sheet aggregates in their complete or fragmented forms.

Among several merozoite surface proteins being assessed as potential components of a vaccine against *P. falciparum*, merozoite surface protein 2 (MSP2) is unusually hydrophilic and contains tandem sequence repeats characteristic of IUPs [4]. MSP2 is highly polymorphic, with conserved N- and C-terminal domains flanking a central variable region, and is anchored into the plasma membrane of the merozoite by a C-terminal glycosylphosphatidylinositol (GPI) moiety. MSP2 was one of three components in a combination vaccine that significantly reduced parasite densities in Papua New Guinean children living in an area where the transmission intensity of *P. falciparum* is high,

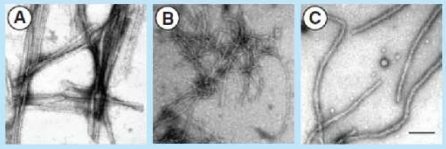

Figure 1. Electron micrographs of the fibrils formed by (A) MSP2 8–15 peptide, (B) MSP2 1–25 peptide and (C) recombinant full-length FC27 MSP2. Peptides and protein were incubated in PBS at 1 mg/ml. Samples were negatively stained and viewed using transmission electron microscopy. The scale bar represents 100 nm. Reproduced with permission from [6] © European Peptide Society and John Wiley & Sons, Ltd. (2007).

and the MSP2 isoforms 3D7 and FC27 have been shown to elicit significant antibody responses in clinical studies [5]. Recombinant forms of MSP2 have been recently described to polymerize into amyloid-like fibrils *in vitro* [4]. The formation of MSP2 fibrils seems to be driven by cross-β aggregation of the N-terminal regions, as suggested by the observations that the protein contains there a proteinase K-resistant core, and that synthetic peptides from that region self-assemble *in vitro* into fibrils with amyloid-like properties [6] (Figure 1). The fibrillar aggregation of MSP2 would significantly increase the conformational order of the monomeric subunit with consequences for the protein's antigenicity, and the propensity of MSP2 to form fibrils in solution has been suggested to be an obstacle for its development as a malaria vaccine candidate [7].

Amyloid-like protein aggregates are associated with the surface of several microorganisms [8]. Functional amyloids have been found in bacteria, fungi and mammals with roles as diverse as biofilm formation, development of aerial structures, scaffolding, regulation of melanin synthesis, and activation of haemostatic factors, among others [9]. The *P. falciparum* merozoite surface bears a thick bristly coat, each bristle being a clump of thin (2–3 nm) filaments anchored at their bases to the plasma membrane, as in other species of *Plasmodium*, such as *P. knowlesi* [10] (Figure 2). Their removal by trypsin and papain enzymes points to a proteinaceous nature of those filaments.

Indirect evidence that MSP2 could form oligomers on the merozoite surface has been obtained from immunofluorescence experiments with monoclonal antibodies 6D8 and 11E1. 6D8, which preferentially recognized monomeric MSP2, failed to bind merozoites, in contrast to 11E1, which recognized both monomeric and polymeric MSP2 [4]. Amyloid-like protein aggregates on other microorganisms have roles in attachment and invasion of substrates. It will be of considerable interest to determine whether putative MSP2 amyloids on the surface of *P. falciparum* merozoites had similar functions, particularly given the reports of some forms of amyloid interacting with red blood cells [11,12]. However, the recent observation that MSP2 is carried into the host erythrocyte on the surface of the invading merozoite and then rapidly degraded [13] makes it unlikely that the mature protein has any toxic effects even in the case that it were found to form amyloids *in vivo*.

Somewhat surprisingly, analysis of the peptide sequence of MSP2 isoforms 3D7 and FC27 with the amyloid sequence-predicting algorithms [14] *FoldAmyloid*, *Tango*, *Waltz*, *Aggrescan* and *Zhang's method* indicated that the main amyloid-prone regions are actually found within the N-terminus signal peptide and the C-terminus GPI anchor signal peptide, which are not

present on the processed mature protein (Figure 3). In Table 1 are shown the scores obtained using the *Waltz* algorithm, which is one of the most specific servers for the prediction of amyloid structure. Taking into account the values and also the peptide lengths (since the average score is per residue), we can possibly conclude that both MSP2 signal peptides are at least as amyloidogenic as the amyloid β peptide (Aβ). The N-terminus amyloidogenic region within the signal peptide is probably lost at the beginning of the protein transit through the endoplasmic reticulum (ER), whereas the C-terminus sequence within the GPI anchor signal peptide is excised later in the polypeptide processing. Because MSP2 is very abundant on the merozoite surface [15], these two peptides will likely be present at high concentrations within the ER, where they could start forming amyloid-like fibrils.

We performed *in vitro* assays to explore if both peptides formed amyloid-like structures in agreement with the theoretical predictions presented above. Two peptides derived from the MSP2 GPI anchor and signal sequences, SSNIASINKFVVLISATLVLSFAIFI-KKKK (Peptide Synthesis Unit, Scientific and Technological Centers of the University of Barcelona, Spain), and MKVIKTLSIINFFIFVTFNI-KKKK (Caslo Laboratory ApS, Lyngby, Denmark), both >95% purity according to chromatographic analysis, were incubated in phosphate buffered saline (PBS) at 37°C for 2–3 weeks. Since in both peptides the amyloidogenic region starts after or with a lysine (Figure 3), a second sample was incubated after trypsin digestion. Atomic force microscope (AFM) images on graphite (Figure 4) showed a propensity of the GPI anchor signal peptide to form globular structures, especially after trypsin cleavage, whereas the MSP2 signal peptide was observed to form amyloid-like fibrils up to several hundred nanometer in length. The presence of MSP2 on the merozoite surface suggests that its processing will occur during the terminal phase of the pRBC; the excised signal and GPI anchor peptides will likely have a very short time to be metabolized and thus might have the chance to form fibrils and oligomers that would be released in the blood when the pRBC bursts.

Circular dichroism analysis of the MSP2 signal peptide showed a minimum at 218 nm both before and after trypsin digestion (Figure 5), indicative of the presence of β-sheet structure characteristic of amyloid fibrils. The GPI anchor peptide did not exhibit a circular dichroism profile consistent with the existence of significant β-sheet structure, in agreement with AFM data indicating a reduced fibril formation propensity in comparison to the signal peptide.

As a first approximation to study the possible *in vivo* existence of amyloidogenic signal and GPI anchor

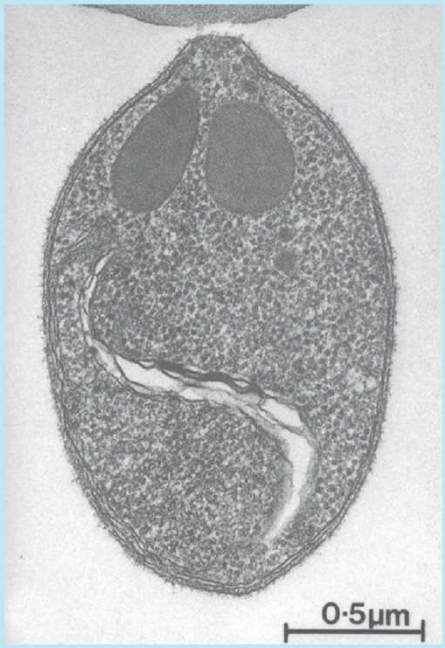

Figure 2. Longitudinal section of a *Plasmodium knowlesi* merozoite showing the bristly appearance of the cell coat which covers the entire surface. In this example, the parasite is attached apically to a red cell by a few long thread-like projections.
Image reprinted with kind permission from [10]. Springer Science+Business Media B.V.

MSP2 peptides, the plasma of malaria-infected persons was screened for the presence of antibodies against *in vitro* formed amyloid structures. ELISA analysis of the aggregated forms of MSP2 signal and GPI anchor peptides was performed using 71 sera samples from several sources as follows. Sixty sera were obtained from patients collected at a high-transmission region in Ghana, that were classified by the level of *P. falciparum* specific IgGs as high (7×10^6–2×10^6 ng/ml; n = 20), medium (1.5×10^6–0.3×10^6 ng/ml; n = 20) and low immunoreactive (5×10^4 ng/ml; n = 20). In each group, half of the samples were malaria positive by PCR. In addition, 11 sera from Equatorial Guinea patients with MSP1 and/or MSP9-specific IgGs were also examined. Malaria nonexposed control sera were used to determine the baseline signal; all serum samples were from blood donors that had provided informed consent and the procedure was approved by the clinical research ethical committee at the University Hospital of Getafe (Spain). The analysis of the recognition of the aggregated forms of MSP2 signal and anchor peptides by all sera did not show any val-

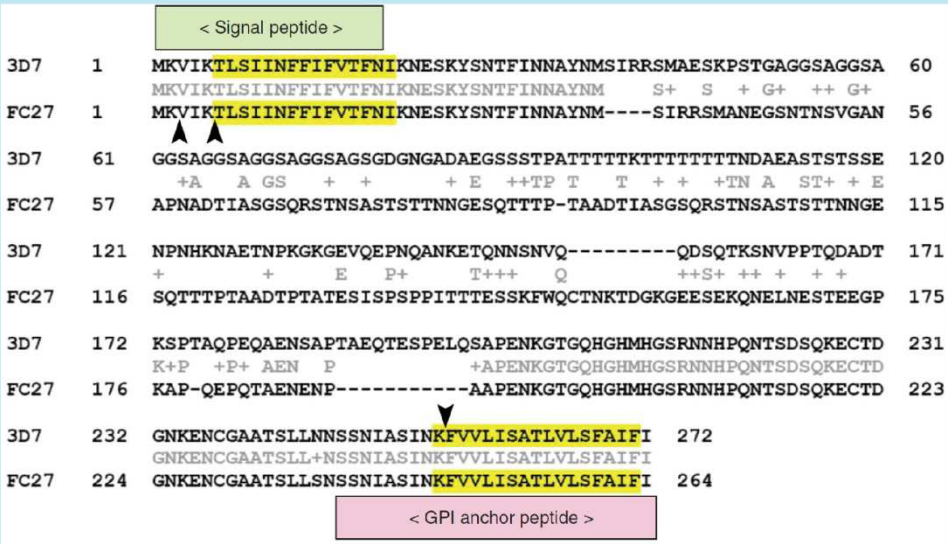

Figure 3. Prediction of amyloid-forming sequences in the MSP2 isoforms 3D7 and FC27. Highlighted in yellow are the sequences with strong consensus prediction according to *FoldAmyloid*, *Tango*, *Waltz*, *Aggrescan* and *Zhang's method* algorithms. The arrowheads indicate trypsin cleaving sites.

ues above the threshold in ELISA assays. Although one interpretation of this result is that such forms are not present *in vivo*, we cannot rule out the possibility that amyloidogenic peptide forms have low immunogenicity, as it has been described previously [7]. If amyloidogenesis reduces immunogenicity, *Plasmodium* might have evolved amyloid-forming regions in proteins that are at some time exposed to the plasma.

Cerebral malaria & integrity of the blood–brain barrier

Pathogenesis in Alzheimer's disease (AD) is linked to the accumulation of the highly amyloidogenic self-associating Aβ, whose oligomers, which are intermediate species in the assembly of fibrils, are powerful neurotoxins and might therefore be the key effectors of cytotoxicity [16]. We decided that it would be worth exploring the possibility that the presence of soluble amyloids encoded by the *Plasmodium* genome were related to some aspect of malaria pathophysiology, such as cerebral malaria (CM), the most severe neurological complication of falciparum malaria. Gene expression analysis suggested that CM and AD share common mechanisms of pathogenesis, as indicated by the accumulation of Aβ in brains of CM-susceptible (CM-S) but not in CM-resistant (CM-R) mice [17], in agreement with former reports showing detection of the Aβ precursor protein in humans with CM [18]. This result is consistent with the downregulation in CM-S animals of genes whose products inhibit the production of Aβ [17]. The reelin pathway that inhibits Tau protein phosphorylation, proposed as a protective mechanism against AD [19], has been found to be overexpressed in CM-R mice together with other genes involved in neurogenesis, suggesting that CM-S mice are less efficient in repairing neuronal damage [17]. In addition,

Table 1. Average scores obtained using the *Waltz* algorithm for the prediction of amyloid regions in MSP2 GPI anchor and signal peptides and in the two amyloidogenic stretches of the amyloid β peptide.

Peptide	Positions	Sequence	Average score per residue
MSP2 GPI anchor	10–26	FVVLISATLVLSFAIFI	97.226048
MSP2 signal	6–19	TLSIINFFIFVTFNI	98.351648
Amyloid β	16–21	KLVFFA	97.993311
Amyloid β	37–42	GGVVIA	92.307692

decreased ribosomal RNA levels and decreased rates for protein synthesis have been described in AD, whereas downregulation of several genes encoding ribosomal proteins has been found in CM-S mice [17].

Erythrocytes infected with mature stages of the malaria parasite bind to the endothelial cells in the capillaries of tissues in a phenomenon known as sequestration, which allows *Plasmodium* to replicate while evading splenic clearance [20]. pRBCs can also adhere to noninfected RBCs giving rise to rosettes, and they can form clumps through platelet-mediated binding to other pRBCs. These events, which may lead to occlusion of the microvasculature, are thought to play a major role in the fatal outcome of CM. Because parasites are largely confined to intravascular spaces without entering the brain parenchyma, one main question regarding the pathogenesis of cerebral malaria is how neuronal dysfunction is caused [21]. There is growing evidence that *Plasmodium*-induced sequestration of infected and uninfected erythrocytes changes blood–brain barrier (BBB) function [22]. Entry of solutes from the blood into the CNS is characterized by a restricted permeability and active transport mechanism through the BBB formed by tight junctions between adjacent cerebrovascular endothelial cells (ECs). Postmortem analysis of CM brains has shown widespread disruption of these tight junctions, particularly in vessels containing pRBCs, which could result in the exposure of sensitive perivascular neuronal cells to toxic plasma metabolites [23]. pRBC binding to receptors on cerebral endothelial cells might cause changes in the integrity of the BBB, making it more permeable to molecules released upon egression of *Plasmodium* merozoites from the pRBC, among which perhaps neurotoxic amyloids formed by MSP2 signal peptides. Amyloid

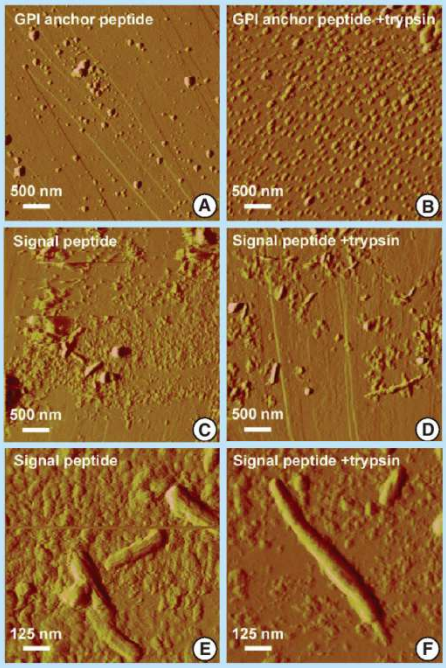

Figure 4. Atomic force microscope images of aggregates of MSP2-derived peptides (digested or not with trypsin) formed after incubation in PBS at 37°C for 2–3 weeks. The images were obtained using a Dimension 3100 atomic force microscope (Veeco Instruments, Inc., CA, USA) and NP-S probes (Veeco) with nominal spring constants of 0.06 N/m to scan the samples in tapping mode in liquid at 0.5–1.0 Hz scan rates. Highly oriented pyrolytic graphite (NT-MDT Co., Moscow, Russia) was used as a substrate.

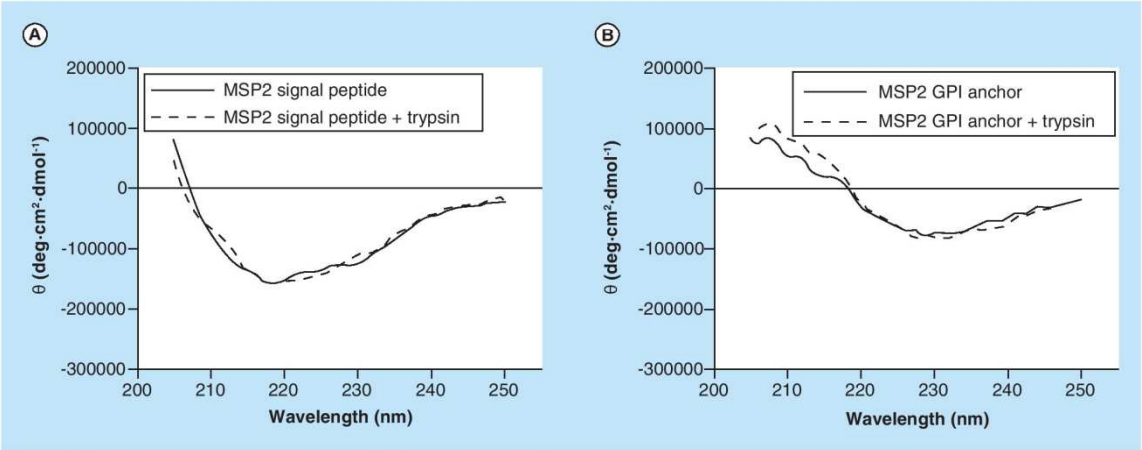

Figure 5. Circular dichroism analysis of MSP2 (A) signal and (B) GPI anchor peptides, before and after trypsin digestion.

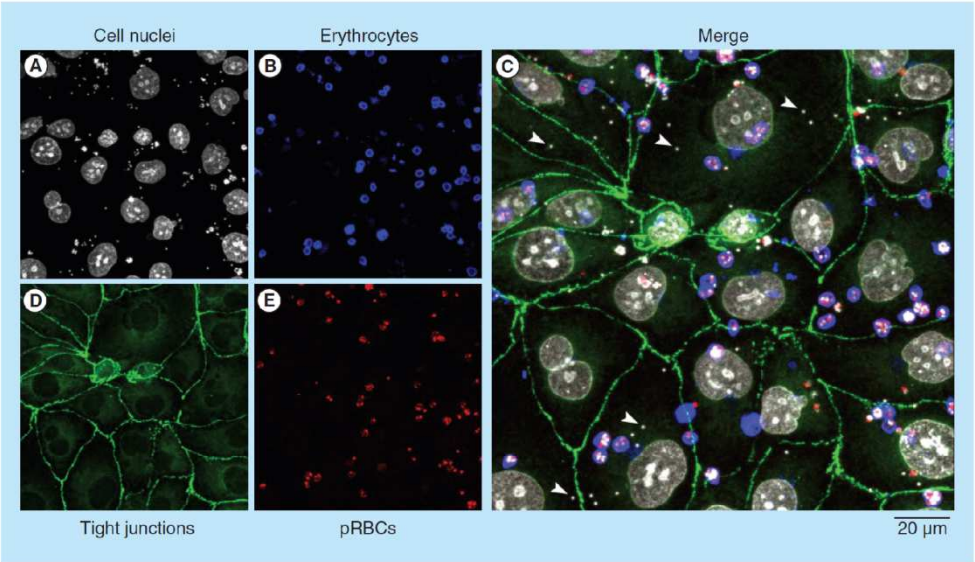

Figure 6. Adhesion of parasitized red blood cells and of free *Plasmodium falciparum* parasites to an *in vitro* blood–brain barrier model. HBMECs were initially expanded in a 75-cm^2 flask precoated with fibronectin. *Plasmodium falciparum* strain E8B was grown *in vitro* in group B human erythrocytes using previously described conditions [26]. For the selection of cytoadherent parasites, pRBCs were passed over human umbilical vein endothelial cells (HUVECs) in two selection rounds. Late trophozoite- and schizont-containing pRBCs were selected in 70% Percoll and seeded at approximately 2 × 10^7 pRBCs/cm^2 on an HUVEC monolayer. The co-culture model of the BBB was adapted from a previously described protocol [27]. Briefly, rat astrocytes (RA) obtained from 2-day newborn rats were initially seeded at 60,000 cells/well onto a poly-D-lysine-coated plate. After 4 days, HBMECs were seeded at 16,500 cells/well onto collagen-coated 0.4 µm pore membrane inserts. This EC monolayer separated the system into an apical (bloodstream) and basolateral (brain tissue) compartments. The growth medium was changed every 3 days until cells reached confluence and tight junctions appeared. On the 9th HBMECs-RA co-culture day, pRBCs were purified in 70% Percoll, stained with wheat germ agglutinin-tetramethylrhodamine conjugate, and seeded at 1 × 10^6 cells/well onto membrane inserts (apical compartment of the BBB model containing the EC layer). The system was co-cultured overnight at 37°C in a humidified atmosphere with 5% CO_2 (protocol adapted from [28]). The day after, HBMECs and pRBCs were fixed and stained for the analysis by confocal microscopy of the tight junction marker protein zonula occludens-1 (ZO-1) [29]. Cell nuclei were stained with DAPI, and pRBCs were specifically detected with a monoclonal antibody against schizont-infected RBCs [26]. Arrowheads in the Merge panel indicate individual *P. falciparum* merozoites.

structures have been described to bind glycosaminoglycans such as the chondroitin and heparan sulfates of cell-bound glycoproteins and proteoglycans, including those present on ECs of the BBB [24]. Erythrocytes infected by the *P. falciparum* E8B strain and free parasites showed significant adherence to confluent human brain microvascular endothelial cells (HBMECs) in an *in vitro* BBB model (Figure 6). Although in this particular experiment no obvious alteration of tight junctions was observed, other studies performed under different conditions indicated disruption of the BBB induced by the malaria parasite [25].

Prionogenic domains encoded in the malaria parasite genome

MSP2 has been the first *Plasmodium*-encoded protein unequivocally related to amyloid structures of potential pathological importance in malaria. However, recent data strongly suggest that in the short term, we will witness an important increase in the number of works dealing with the role in *Plasmodium* cell biology of a particular type of amyloids. When amyloid fibrils grow and divide with high efficiency they can propagate, become infective and transmit aggregative folds and are then termed prions [30]. While prions identified in mammals act usually as pathogens, prions in lower eukaryotes can be beneficial to the host [31]. There are organisms in which prion-like self-assembly might play important functions, as can be inferred from the rather high number of prions in their genomes. The inspection of incomplete sequenced genomes of some members of the genus *Plasmodium* proved that they might encode abundant hydrophilic low-complexity protein fragments corresponding to species-specific, rapidly diverging regions

that could form nonglobular domains helping the parasites to evade the host's immune response [3]. Analysis of the complete proteomes of various members of this genus suggested that most of these stretches may be prionogenic domains [32]. In most cases, the fraction of proteins bearing prion-forming domains is less than 1% of the size of the proteome, but in *P. falciparum* the proportion of putative prions rises to an astonishing 10%. One in four proteins in this organism contains asparagine repeats, whose functions are still unknown [33], but are found in all protein families in all developmental stages. The life cycle of *Plasmodium* forces the organism through drastic changes in its environmental temperature, including cyclical fever episodes that can last several hours and exceed 40°C. Because heat shock increases the propensity of proteins to misfold and form aggregates, if only a fraction of the abundant prion-like domains in the malaria parasite aggregates during heat shock, this would certainly lead to the pathogen's demise. However, *Plasmodium* is able to survive with one of the most aggregation-prone proteomes in nature. This is due to the presence of specialized chaperones which prevent aggregation and are essential for parasite survival within RBCs [34]. Although prionogenic domains are potentially deleterious for the organism, their abundance in *Plasmodium* suggests that they might provide certain advantages, but the functional implications of such an amount of aggregation-prone proteins are still unclear. Identifying their so far unknown roles and mechanisms of action can provide new unexpected targets for future chemotherapeutic and prophylactic antimalarial approaches.

Conclusion

The growing experimental evidence for the presence in the *Plasmodium* proteome of amyloidogenic peptides suggests that these entities have a physiological function in the life cycle of the pathogen. Functional amyloids might have roles in the adhesion of the parasite to its host cells during invasion, or participate in some of the pathological effects of malaria related, for example, to blood–brain barrier alteration or the triggering of immune responses. However, *Plasmodium*-derived amyloids could also provide new prophylactic or therapeutic possibilities if we are capable of harnessing them for future innovative antimalarial strategies.

Financial & competing interests disclosure

This work was supported by grants BIO2011–25039, BIO2014–52872-R and BFU2012–33932, from the Ministerio de Economía y Competitividad, Spain, which included FEDER funds, and 2014-SGR-938 from the Generalitat de Catalunya, Spain. The authors have no other relevant affiliations or financial involvement with any organization or entity with a financial interest in or financial conflict with the subject matter or materials discussed in the manuscript apart from those disclosed.

No writing assistance was utilized in the production of this manuscript.

Executive summary

- At least one protein expressed by *Plasmodium*, MSP2, forms amyloid-like fibrils *in vitro*.
- Amyloid-like structures formed by certain signal peptides of *Plasmodium* proteins might be released in the plasma.
- Cerebral malaria and amyloid-related Alzheimer's disease share common mechanisms of pathogenesis.
- *Plasmodium*-infected erythrocytes show adhesion to the blood–brain barrier according to *in vitro* assays.
- The genome of *Plasmodium* encodes one of the highest proportions of putative prion sequences.

References

1 Cowman AF, Crabb BS. Invasion of red blood cells by malaria parasites. *Cell* 124(4), 755–766 (2006).

2 Rovira-Graells N, Gupta AP, Planet E *et al.* Transcriptional variation in the malaria parasite *Plasmodium falciparum*. *Genome Res.* 22(5), 925–938 (2012).

3 Feng ZP, Zhang X, Han P, Arora N, Anders RF, Norton RS. Abundance of intrinsically unstructured proteins in *P. falciparum* and other apicomplexan parasite proteomes. *Mol. Biochem. Parasitol.* 150(2), 256–267 (2006).

4 Adda CG, Murphy VJ, Sunde M *et al. Plasmodium falciparum* merozoite surface protein 2 is unstructured and forms amyloid-like fibrils. *Mol. Biochem. Parasitol.* 166(2), 159–171 (2009).

5 Iriemenam NC, Khirelsied AH, Nasr A *et al.* Antibody responses to a panel of *Plasmodium falciparum* malaria blood-stage antigens in relation to clinical disease outcome in Sudan. *Vaccine* 27(1), 62–71 (2009).

6 Yang X, Adda CG, Keizer DW *et al.* A partially structured region of a largely unstructured protein, *Plasmodium falciparum* merozoite surface protein 2 (MSP2), forms amyloid-like fibrils. *J. Pept. Sci.* 13(12), 839–848 (2007).

7 Chandrashekaran IR, Adda CG, MacRaild CA, Anders RF, Norton RS. EGCG disaggregates amyloid-like fibrils formed by *Plasmodium falciparum* merozoite surface

protein 2. *Arch. Biochem. Biophys.* 513(2), 153–157 (2011).

8 Gebbink MF, Claessen D, Bouma B, Dijkhuizen L, Wosten HA. Amyloids – a functional coat for microorganisms. *Nat. Rev. Microbiol.* 3(4), 333–341 (2005).

9 Maury CP. The emerging concept of functional amyloid. *J. Intern. Med.* 265(3), 329–334 (2009).

10 Bannister LH, Mitchell GH, Butcher GA, Dennis ED, Cohen S. Structure and development of the surface coat of erythrocytic merozoites of *Plasmodium knowlesi*. *Cell Tissue Res.* 245(2), 281–290 (1986).

11 Jayakumar R, Kusiak JW, Chrest FJ *et al.* Red cell perturbations by amyloid beta-protein. *Biochim. Biophys. Acta* 1622(1), 20–28 (2003).

12 Murali J, Koteeswari D, Rifkind JM, Jayakumar R. Amyloid insulin interaction with erythrocytes. *Biochem. Cell Biol.* 81(1), 51–59 (2003).

13 Boyle MJ, Langer C, Chan JA *et al.* Sequential processing of merozoite surface proteins during and after erythrocyte invasion by *Plasmodium falciparum*. *Infect. Immun.* 82(3), 924–936 (2014).

14 Fernàndez-Busquets X, de Groot NS, Fernandez D, Ventura S. Recent structural and computational insights into conformational diseases. *Curr. Med. Chem.* 15(13), 1336–1349 (2008).

15 Low A, Chandrashekaran IR, Adda CG *et al.* Merozoite surface protein 2 of *Plasmodium falciparum*: expression, structure, dynamics, and fibril formation of the conserved N-terminal domain. *Biopolymers* 87(1), 12–22 (2007).

16 Lambert MP, Barlow AK, Chromy BA *et al.* Diffusible, nonfibrillar ligands derived from $A\beta_{1-42}$ are potent central nervous system neurotoxins. *Proc. Natl Acad. Sci. USA* 95(11), 6448–6453 (1998).

17 Delahaye N, Coltel N, Puthier D *et al.* Gene expression analysis reveals early changes in several molecular pathways in cerebral malaria-susceptible mice versus cerebral malaria-resistant mice. *BMC Genomics* 8(1), 452 (2007).

18 Medana IM, Day NP, Hien TT *et al.* Axonal injury in cerebral malaria. *Am. J. Pathol.* 160(2), 655–666 (2002)

19 Deutsch SI, Rosse RB, Deutsch LH. Faulty regulation of tau phosphorylation by the reelin signal transduction pathway is a potential mechanism of pathogenesis and therapeutic target in Alzheimer's disease. *Eur. Neuropsychopharmacol.* 16(8), 547–551 (2006)

20 Miller LH, Baruch DI, Marsh K, Doumbo OK. The pathogenic basis of malaria. *Nature* 415(6872), 673–679 (2002).

21 Gitau EN, Newton CRJC. Blood–brain barrier in falciparum malaria. *Trop. Med. Int. Health* 10(3), 285–292 (2005).

22 Medana IM, Turner GDH. Human cerebral malaria and the blood–brain barrier. *Int. J. Parasitol.* 36(5), 555–568 (2006).

23 Idro R, Jenkins NE, Newton CR. Pathogenesis, clinical features, and neurological outcome of cerebral malaria. *Lancet Neurol.* 4(12), 827–840 (2005).

24 Valle-Delgado JJ, Alfonso-Prieto M, de Groot NS *et al.* Modulation of $A\beta_{42}$ fibrillogenesis by glycosaminoglycan structure. *FASEB J.* 24(11), 4250–4261 (2010).

25 Treeratanapiboon L, Psathaki K, Wegener J, Looareesuwan S, Galla HJ, Udomsangpetch R. *In vitro* study of malaria parasite induced disruption of blood–brain barrier. *Biochem. Biophys. Res. Commun.* 335(3), 810–818 (2005).

26 Urbán P, Estelrich J, Cortés A, Fernàndez-Busquets X. A nanovector with complete discrimination for targeted delivery to *Plasmodium falciparum*-infected versus non-infected red blood cells *in vitro*. *J. Control. Release* 151(2), 202–211 (2011).

27 Bachmeier C, Mullan M, Paris D. Characterization and use of human brain microvascular endothelial cells to examine β-amyloid exchange in the blood–brain barrier. *Cytotechnology* 62(6), 519–529 (2010).

28 Viebig NK, Wulbrand U, Förster R, Andrews KT, Lanzer M, Knolle PA. Direct activation of human endothelial cells by *Plasmodium falciparum*-infected erythrocytes. *Infect. Immun.* 73(6), 3271–3277 (2005).

29 Rüffer C, Strey A, Janning A, Kim KS, Gerke V. Cell–cell junctions of dermal microvascular endothelial cells contain tight and adherens junction proteins in spatial proximity. *Biochemistry* 43(18), 5360–5369 (2004).

30 Chien P, Weissman JS, DePace AH. Emerging principles of conformation-based prion inheritance. *Annu. Rev. Biochem.* 73(1), 617–656 (2004).

31 Newby GA, Lindquist S. Blessings in disguise: biological benefits of prion-like mechanisms. *Trends Cell Biol.* 23(6), 251–259 (2013)

32 Espinosa Angarica V, Ventura S, Sancho J. Discovering putative prion sequences in complete proteomes using probabilistic representations of Q/N-rich domains. *BMC Genomics* 14(1), 316 (2013).

33 Muralidharan V, Goldberg DE. Asparagine repeats in *Plasmodium falciparum* proteins: good for nothing? *PLoS Pathog.* 9(8), e1003488 (2013).

34 Muralidharan V, Oksman A, Pal P, Lindquist S, Goldberg DE. *Plasmodium falciparum* heat shock protein 110 stabilizes the asparagine repeat-rich parasite proteome during malarial fevers. *Nat. Commun.* 3, 1310 (2012).

ANNEX IV: PhD STUDENT PARTICIPATION IN PUBLICATIONS AND THEIR IMPACT FACTOR

During his PhD in my group, Mr. Ernest Moles has contributed to eight papers, six of them published, one submitted, and one in preparation. His contribution in these works is described below:

1. Moles, E., Urbán, P., Jiménez-Díaz, M.B., Viera-Morilla, S., Angulo-Barturen, I., Busquets, M.A., Fernàndez-Busquets, X. (2015) Immunoliposome-mediated drug delivery to *Plasmodium*-infected and non-infected red blood cells as a dual therapeutic/prophylactic antimalarial strategy. *J. Control. Release* **210**, 217-229.

IF 2014: 7.7

Ernest has done an impressive amount of work in this excellent paper, where he has been responsible for all the experiments presented in the 30 figures of the manuscript (including those in the supplementary material), except for Figure 1A.

2. Moles, E. and Fernàndez-Busquets, X. (2015) Loading antimalarial drugs into non-infected red blood cells: an undesirable roommate for *Plasmodium*. *Future Med. Chem.* **7**, 837-840.

IF 2014: 3.7

Ernest contributed with a 50% participation to the preparation of this Editorial.

3. Moles, E., Valle-Delgado, J.J., Urbán, P., Azcárate, I.G., Bautista, J.M., Selva, J., Egea, G., Ventura, S., and Fernàndez-Busquets, X. (2015) Possible roles of amyloids in malaria pathophysiology. *Future Science OA*, **1**, FSO43.

IF 2014: not available (this journal has started being published in 2015).

Ernest contributed Figure 6 of this paper, which represents a considerable effort in the preparation of a blood brain barrier in vitro model.

4. Marques, J., **Moles, E.**, Urbán, P., Prohens, R., Busquets, M.A., Sevrin, C., Grandfils, C., and Fernàndez-Busquets, X. (2014) Application of heparin as a dual agent with antimalarial and liposome targeting activities toward *Plasmodium*-infected red blood cells. *Nanomedicine: NBM* **10**, 1719-1728.

IF 2014: 6.2

Ernest contributed here his expertise in liposome preparation. This paper has been used in the PhD Thesis of Ms. Joana Marques.

An important result derived from this work is the registration of a patent:

Patent application: ***Heparin-lipidic nanoparticle conjugates****. Inventors: Fernàndez-Busquets, X., Marques, J.,* ***Moles, E.*** *Institutions: IBEC, CRESIB. Application number: EP13152187.4; priority countries: Europe; priority date: January 22, 2013.*

5. Movellan, J., Urbán, P., **Moles, E.**, de la Fuente, J.M., Sierra, T., Serrano, J.L., and Fernàndez-Busquets, X. (2014) Amphiphilic dendritic derivatives as nanocarriers for the targeted delivery of antimalarial drugs. *Biomaterials* **35**, 7940-7950.

IF 2014: 8.6

In this paper Ernest contributed (i) the drug release assays (Fig. 8, Materials and Methods 2.3.), (ii) the determination of polymer blood residence time (Fig. 9, Materials and Methods 2.9.), and (iii) the in vivo assays with P. yoelii-infected mice (Results 3.7 and Materials and Methods 2.10.).

6. Urbán, P., Valle-Delgado, J.J., **Moles, E.**, Marques, J., Díez, C., and Fernàndez-Busquets, X. (2012) Nanotools for the delivery of antimicrobial peptides. *Curr. Drug Targets* **13**, 1158-1172.

IF 2012: 3.8

Ernest contributed significantly to the preparation of this review.

7. Moles, E., Moll, K., Ch'ng J., Parini, P., Wahlgren, M., and Fernàndez-Busquets, X. Development of drug-loaded immunoliposomes for the selective targeting and elimination of rosetting *Plasmodium falciparum*-infected RBCs. *In preparation for submission to J. Control. Release.*

Ernest has done an impressive amount of work in this excellent paper, where he has been responsible for all the experiments presented in the manuscript.

8. **Moles, E.**, Marcos, J., Imperial, S., Pozo, O.J., and Fernàndez-Busquets, X.

Proposal of 2-picolylamine derivatization and LC-ESI-MS/MS analysis for the ultra-sensitive detection of abscisic acid in apicomplexan blood-infecting parasites and first validation test in *Plasmodium falciparum* extracts. *In preparation for submission to Analytical Chemistry.*

Ernest has contributed all the work involving P. falciparum cultures.

Barcelona, October 22, 2015

Xavier Fernàndez Busquets

PhD Thesis advisor

BIBLIOGRAPHY

Abraham, R. et al., 1991. The influence of periodate oxidation on monoclonal antibody avidity and immunoreactivity. *Journal of Immunological Methods*, 144(1), pp.77–86.

Adams, Y. et al., 2014. Rosetting Plasmodium falciparum-infected erythrocytes bind to human brain microvascular endothelial cells in vitro, demonstrating a dual adhesion phenotype mediated by distinct P. falciparum erythrocyte membrane protein 1 domains. *Infection and Immunity*, 82(3), pp.949–959.

Adda, C.G. et al., 2009. Plasmodium falciparum merozoite surface protein 2 is unstructured and forms amyloid-like fibrils. *Molecular and Biochemical Parasitology*, 166(2), pp.159–171.

Agarwal, S. et al., 2013. Ca2+-mediated exocytosis of subtilisin-like protease 1: A key step in egress of Plasmodium falciparum merozoites. *Cellular Microbiology*, 15(6), pp.910–921.

Agrawal, A.K., Singhal, A. & Gupta, C.M., 1987. Functional drug targeting to erythrocytes in vivo using antibody bearing liposomes as drug vehicles. *Biochemical and Biophysical Research Communications*, 148(1), pp.357–361.

Albrecht, L. et al., 2011. var gene transcription and PfEMP1 expression in the rosetting and cytoadhesive Plasmodium falciparum clone FCR3S1.2. *Malaria journal*, 10, p.17.

Alkhalil, A. et al., 2004. Plasmodium falciparum likely encodes the principal anion channel on infected human erythrocytes. *Blood*, 104(13), pp.4279–4286.

Allen, T.M., 2002. Ligand-targeted therapeutics in anticancer therapy. *Nature reviews. Cancer*, 2(10), pp.750–763.

Allen, T.M. & Hansen, C., 1991. Pharmacokinetics of stealth versus conventional liposomes: effect of dose. *Biochimica et biophysica acta*, 1068(2), pp.133–141.

Allen, T.M., Hansen, C.B. & Guo, L.S.S., 1993. Subcutaneous administration of liposomes: a comparison with the intravenous and intraperitoneal routes of injection. *Biochim Biophys Acta*, 1150(1), pp.9–16.

Allison, A.C., 1960. Glucose-6-phosphate dehydrogenase deficiency in red bloods cells of East Africans. *Nature*, 186, pp.531–532.

Alving, A. et al., 1956. Enzymatic deficiency in primaquine-sensitive erythrocytes. *Science*, 124(3220), pp.484–485.

Amin, N.C. et al., 2013. Determination of artemether and lumefantrine in anti-malarial fixed-dose combination tablets by microemulsion electrokinetic chromatography with short-end injection procedure. *Malaria Journal*, 12, p.202.

Ancsin, J.B. & Kisilevsky, R., 2004. A binding site for highly sulfated heparan sulfate is identified in the N terminus of the circumsporozoite protein: Significance for malarial sporozoite attachment to hepatocytes. *Journal of Biological Chemistry*, 279(21), pp.21824–21832.

Andreopoulou, E. et al., 2007. Pegylated liposomal doxorubicin HCL (PLD; Caelyx/Doxil®): Experience with long-term maintenance in responding patients with recurrent epithelial ovarian cancer. *Annals of Oncology*, 18(4), pp.716–721.

Angeletti, D. et al., 2013. Analysis of antibody induction upon immunization with distinct NTS-DBL1α-domains of PfEMP1 from rosetting Plasmodium falciparum parasites. *Malaria journal*, 12, p.32.

Angeletti, D. et al., 2015. Binding of subdomains 1/2 of PfEMP1-DBL1α to heparan sulfate or heparin mediates Plasmodium falciparum rosetting. *Plos One*, 10(3), p.e0118898.

Angeletti, D. et al., 2012. Plasmodium falciparum rosetting epitopes converge in the SD3-loop of PfEMP1-DBL1α. *PLoS ONE*, 7(12).

Angulo-Barturen, I. et al., 2008. A murine model of falciparum-malaria by in vivo selection of competent strains in non-myelodepleted mice engrafted with human erythrocytes. *PLoS ONE*, 3(5).

Ansell, S.M. et al., 2000. Antibody conjugation methods for active targeting of liposomes. *Methods in molecular medicine*, 25, pp.51–68.

Ansell, S.M., Tardi, P.G. & Buchkowsky, S.S., 1996. 3-(2-pyridyldithio)propionic acid hydrazide as a cross-linker in the formation of liposome-antibody conjugates. *Bioconjugate Chemistry*, 7(4), pp.490–496.

Arbustini, E., 2007. Total erythrocyte membrane cholesterol: an innocent new marker or an active player in acute coronary syndromes? *Journal of the American College of Cardiology*, 49(21), pp.2090–2092.

Ashley, C.E. et al., 2011. The targeted delivery of multicomponent cargos to cancer cells by nanoporous particle-supported lipid bilayers. *Nature materials*, 10(5), pp.389–397.

Asthana, A. et al., 2005. Poly(amidoamine) (PAMAM) dendritic nanostructures for controlled site-specific delivery of acidic anti-inflammatory active ingredient. *AAPS PharmSciTech*, 6(3), pp.E536–E542.

Augusto, O. et al., 1986. Hydroxyl radical formation as a result of the interaction between primaquine and reduced pyridine nucleotides. Catalysis by hemoglobin and microsomes. *Archives of biochemistry and biophysics*, 244(1), pp.147–155.

Avnir, Y. et al., 2008. Amphipathic weak acid glucocorticoid prodrugs remote-loaded into sterically stabilized nanoliposomes evaluated in arthritic rats and in a Beagle dog: A novel approach to treating autoimmune arthritis. *Arthritis and Rheumatism*, 58(1), pp.119–129.

Avnir, Y. et al., 2011. Fabrication principles and their contribution to the superior in vivo therapeutic efficacy of nano-liposomes remote loaded with glucocorticoids. *PLoS ONE*, 6(10).

Avnir, Y. & Barenholz, Y., 2005. pH determination by pyranine: Medium-related artifacts and their correction. *Analytical Biochemistry*, 347(1), pp.34–41.

Avril, M. et al., 2012. A restricted subset of var genes mediates adherence of Plasmodium falciparum-infected erythrocytes to brain endothelial cells. *Proceedings of the National Academy of Sciences*, 109(26), pp.10130–10131.

Bailey, A.L. & Cullis, P.R., 1997. Liposome Fusion. In R. M. Epand, ed. *Current Topics in Membranes (Lipid polymorphism and membrane properties)*. Vancouver, Canada: Elsevier Inc., Academic Press, pp. 359–373, vol. 44.

Bakry, R. et al., 2007. Medicinal applications of fullerenes. *International Journal of Nanomedicine*, 2(4), pp.639–649.

Bangham, A.D. & Horne, R.W., 1964. Negative staining of phospholipids and their structural modification by surface-active agents as observed in the electron microscope. *Journal of molecular biology*, 8(5), pp.660–668.

Bangham, A.D., Standish, M.M. & Weissmann, G., 1965. The action of steroids and streptolysin S on the permeability of phospholipid structures to cations. *Journal of molecular biology*, 13(1), pp.253–259.

Barenholz, Y., 2012. Doxil® - The first FDA-approved nano-drug: Lessons learned. *Journal of Controlled Release*, 160(2), pp.117–134.

Barr, P.J. et al., 1991. Recombinant Pfs25 protein of Plasmodium falciparum elicits malaria transmission-blocking immunity in experimental animals. *The Journal of experimental medicine*, 174(5), pp.1203–1208.

Barragan, A. et al., 1999. Plasmodium falciparum: molecular background to strain-specific rosette disruption by glycosaminoglycans and sulfated glycoconjugates. *Experimental parasitology*, 91(2), pp.133–143.

Barragan, A. et al., 2000. The duffy-binding-like domain 1 of Plasmodium falciparum erythrocyte membrane protein 1 (PfEMP1) is a heparan sulfate ligand that requires 12 mers for binding. *Blood*, 95(11), pp.3594–3599.

Barrett, M.P., 1997. The pentose phosphate pathway and parasitic protozoa. *Parasitology Today*, 13(1), pp.11–16.

Barry, A.E. et al., 2009. Contrasting population structures of the genes encoding ten leading vaccine-candidate antigens of the human malaria parasite, Plasmodium falciparum. *PloS one*, 4(12), p.e8497.

Barry, A.E. & Arnott, A., 2014. Strategies for designing and monitoring malaria vaccines targeting diverse antigens. *Frontiers in Immunology*, 5(Article 359).

Bartoloni, A. & Zammarchi, L., 2012. Clinical aspects of uncomplicated and severe malaria. *Mediterranean Journal of Hematology and Infectious Diseases*, 4(1).

Baruch, D.I. et al., 1997. Identification of a region of PfEMP1 that mediates adherence of Plasmodium falciparum infected erythrocytes to CD36: conserved function with variant sequence. *Blood*, 90(9), pp.3766–3775.

Baruch, D.I. et al., 2002. Immunization of Aotus monkeys with a functional domain of the Plasmodium falciparum variant antigen induces protection against a lethal parasite line. *Proceedings of the National Academy of Sciences of the United States of America*, 99(6), pp.3860–3865.

Baryshnikova, M.A. & Baryshnikov, A.Y., 2013. Immunoliposomes and their targets. *Russian Journal of General Chemistry*, 83(12), pp.2565–2570.

Bates, M.D. et al., 1990. In vitro effects of primaquine and primaquine metabolites on exoerythrocytic stages of Plasmodium berghei. *American Journal of Tropical Medicine and Hygiene*, 42(6), pp.532–537.

Baum, J. et al., 2009. Reticulocyte-binding protein homologue 5 - An essential adhesin involved in invasion of human erythrocytes by Plasmodium falciparum. *International Journal for Parasitology*, 39(3), pp.371–380.

Baumeister, S. et al., 2011. Fosmidomycin uptake into Plasmodium and Babesia-infected erythrocytes is facilitated by parasite-induced new permeability pathways. *PLoS ONE*, 6(5).

Baumgart, T. et al., 2007. Fluorescence probe partitioning between Lo/Ld phases in lipid membranes. *Biochimica et Biophysica Acta - Biomembranes*, 1768(9), pp.2182–2194.

De Beaudrap, P. et al., 2013. Impact of malaria during pregnancy on pregnancy outcomes in a Ugandan prospective cohort with intensive malaria screening and prompt treatment. *Malaria journal*, 12, p.139.

Bechara, C. & Sagan, S., 2013. Cell-penetrating peptides: 20 years later, where do we stand? *FEBS Letters*, 587(12), pp.1693–1702.

Benatti, U. et al., 1996. Azidothymidine homodinucleotide-loaded erythrocytes and bioreactors for slow delivery of the antiretroviral drug azidothymidine. *Biochemical and biophysical research communications*, 220(1), pp.20–25.

Bernabeu, M. et al., 2012. Functional analysis of Plasmodium vivax VIR proteins reveals different subcellular localizations and cytoadherence to the ICAM-1 endothelial receptor. *Cellular Microbiology*, 14(3), pp.386–400.

Bertin, G.I. et al., 2013. Expression of the domain cassette 8 Plasmodium falciparum erythrocyte membrane protein 1 is associated with cerebral malaria in Benin. *PLoS ONE*, 8(7).

Bhadra, D., Bhadra, S. & Jain, N.K., 2006. PEGylated peptide dendrimeric carriers for the delivery of antimalarial drug chloroquine phosphate. *Pharmaceutical Research*, 23(3), pp.623–633.

Bhattacharjee, S. et al., 2008. Maurer's clefts of Plasmodium falciparum are secretory organelles that concentrate virulence protein reporters for delivery to the host erythrocyte. *Blood*, 111(4), pp.2418–2425.

Binnig, G. & Rohrer, H., 1983. Scanning tunneling microscopy. *Surface Science*, 126(1-3), pp.236–244.

Bodammer, J.E. & Bahr, G.F., 1973. The initiation of a "metabolic window" in the surface of host erythrocytes by Plasmodium berghei NYU-2. *Lab Invest.*, 28(6), pp.708–718.

Bolchoz, L.J.C. et al., 2002. Primaquine-induced hemolytic anemia: formation of free radicals in rat erythrocytes exposed to 6-methoxy-8-hydroxylaminoquinoline. *The Journal of pharmacology and experimental therapeutics*, 303(3), pp.1121–1129.

Bopp, S.E.R. et al., 2013. Mitotic evolution of Plasmodium falciparum shows a stable core genome but recombination in antigen families. *PLoS Genetics*, 9(2), e1003293.

Borrmann, S. & Matuschewski, K., 2011. Targeting Plasmodium liver stages: better late than never. *Trends in Molecular Medicine*, 17(9), pp.527–536.

Boyle, M.J. et al., 2010. Interactions with heparin-like molecules during erythrocyte invasion by Plasmodium falciparum merozoites. *Blood*, 115(22), pp.4559–4568.

Boyle, M.J. et al., 2014. Sequential processing of merozoite surface proteins during and after erythrocyte invasion by Plasmodium falciparum. *Infection and Immunity*, 82(3), pp.924–936.

Buffet, P.A. et al., 2011. The pathogenesis of Plasmodium falciparum malaria in humans: Insights from splenic physiology. *Blood*, 117(2), pp.381–392.

Burbidge, A. et al., 1997. Structure and expression of a cDNA encoding a putative neoxanthin cleavage enzyme (NCE), isolated from a wilt-related tomato (Lycopersicon esculentum Mill.) library. *Journal of Experimental Botany*, 48(12), pp.2111–2112.

Bustamante, L.Y. et al., 2013. A full-length recombinant Plasmodium falciparum PfRH5 protein induces inhibitory antibodies that are effective across common PfRH5 genetic variants. *Vaccine*, 31(2), pp.373–379.

Callahan, M.K., Williamson, P. & Schlegel, R.A., 2000. Surface expression of phosphatidylserine on macrophages is required for phagocytosis of apoptotic thymocytes. *Cell death and differentiation*, 7(7), pp.645–653.

Caminade, A.M. et al., 2012. “Janus” dendrimers: syntheses and properties. *New Journal of Chemistry*, 36(2), p.217.

Cao, A., Briane, D. & Coudert, R., 2006. Chapter 5: Cationic liposomes as transmembrane carriers of nucleic acids. *Advances in Planar Lipid Bilayers and Liposomes*, 4, pp.135–190.

Carlson, J. et al., 1990. Human cerebral malaria: association with erythrocyte rosetting and lack of anti-rosetting antibodies. *Lancet*, 336(8729), pp.1457–1460.

Carvalho, B.O. et al., 2010. On the cytoadhesion of Plasmodium vivax-infected erythrocytes. *The Journal of infectious diseases*, 202(4), pp.638–647.

Cassera, M.B. et al., 2004. The methylerythritol phosphate pathway is functionally active in all intraerythrocytic stages of Plasmodium falciparum. *Journal of Biological Chemistry*, 279(50), pp.51749–51759.

Chabanel, A., Flamm, M. & Sung, K.L.P., 1983. Influence of cholesterol content on red cell membrane viscoelasticity and fluidity. *Biophysical Journal*, 44(2), pp.171–176.

Chan, J.A. et al., 2012. Targets of antibodies against Plasmodium falciparum-infected erythrocytes in malaria immunity. *Journal of Clinical Investigation*, 122(9), pp.3227–3238.

Chan, X.W.A. et al., 2013. Chemical and genetic validation of thiamine utilization as an antimalarial drug target. *Nature communications*, 4, p.2060.

Chandra, S., Agrawal, A.K. & Gupta, C.M., 1991. Chloroquine delivery to erythrocytes in Plasmodium berghei-infected mice using antibody-bearing liposomes as drug vehicles. *Journal of Biosciences*, 16(3), pp.137–144.

Chen, C. et al., 2010. An overview of liposome lyophilization and its future potential. *Journal of Controlled Release*, 142(3), pp.299–311.

Chimanuka, B. et al., 2002. Preparation of β-artemether liposomes, their HPLC-UV evaluation and relevance for clearing recrudescent parasitaemia in Plasmodium chabaudi malaria-infected mice. *Journal of Pharmaceutical and Biomedical Analysis*, 28(1), pp.13–22.

Chin, W. et al., 1965. A naturally acquired quotidian-type malaria in man transferable to monkeys. *Science*, 149(3686), p.865.

Chotivanich, K. et al., 2002. Central role of the spleen in malaria parasite clearance. *The Journal of infectious diseases*, 185(10), pp.1538–1541.

Chou, A.C. & Fitch, C.D., 1993. Control of heme polymerase by chloroquine and other quinoline derivatives. *Biochemical and biophysical research communications*, 195(1), pp.422–427.

Chou, H.H. et al., 2006. Pegylated liposomal doxorubicin (Lipo-Dox) for platinum-resistant or refractory epithelial ovarian carcinoma: a Taiwanese gynecologic oncology group study with long-term follow-up. *Gynecologic oncology*, 101(3), pp.423–428.

Christianson, H.C. & Belting, M., 2014. Heparan sulfate proteoglycan as a cell-surface endocytosis receptor. *Matrix Biology*, 35, pp.51–55.

Claessens, a. et al., 2012. From the Cover: PNAS Plus: A subset of group A-like var genes encodes the malaria parasite ligands for binding to human brain endothelial cells. *Proceedings of the National Academy of Sciences*, 109(26), pp.E1772–E1781.

Clerc, S. & Barenholz, Y., 1995. Loading of amphipathic weak acids into liposomes in response to transmembrane calcium acetate gradients. *Biochimica et biophysica acta*, 1240(2), pp.257–265.

Collander, R. et al., 1951. The partition of organic compounds between higher alcohols and water. *Acta Chemica Scandinavica*, 5, pp.774–780.

Collins, C.R. et al., 2013. Malaria parasite cGMP-dependent protein kinase regulates blood stage merozoite secretory organelle discharge and egress. *PLoS Pathogens*, 9(5), e1003344.

Conniot, J. et al., 2014. Cancer immunotherapy: nanodelivery approaches for immune cell targeting and tracking. *Frontiers in Chemistry*, 2(Article 105), pp.1–27.

Cooke, B.M. et al., 1994. Rolling and stationary cytoadhesion of red blood cells parasitized by Plasmodium falciparum: separate roles for ICAM-1, CD36 and thrombospondin. *British journal of haematology*, 87(1), pp.162–170.

Cox, F.E.G., 2002. History of human parasitology. *Clinical Microbiology Reviews*, 15(4), pp.595–612.

Creelman, R.A., Bell, E. & Mullet, J.E., 1992. Involvement of a lipoxygenase-like enzyme in abscisic Acid biosynthesis. *Plant physiology*, 99(3), pp.1258–1260.

Cromer, D. et al., 2006. Preferential invasion of reticulocytes during late-stage Plasmodium berghei infection accounts for reduced circulating reticulocyte levels. *International Journal for Parasitology*, 36(13), pp.1389–1397.

Crosnier, C. et al., 2011. Basigin is a receptor essential for erythrocyte invasion by Plasmodium falciparum. *Nature*, 480(7378), pp.534–7.

Cullis, P.R. et al., 1991. pH gradients and membrane transport in liposomal systems. *Trends in biotechnology*, 9(8), pp.268–72.

Cullis, P.R., Fenske, D.B. & Hope, M.J., 1996. Physical properties and functional roles of lipids in membranes. In D. E. Vance & J. E. Vance, eds. *Biochemistry of Lipids, Lipoproteins and Membranes*. Elsevier B.V., pp. 1–33.

Cyrklaff, M. et al., 2011. Hemoglobins S and C interfere with actin remodeling in Plasmodium falciparum-infected erythrocytes. *Science*, 334(6060), pp.1283–1286.

Daniels, G. & Bromilow, I., 2013. *Essential Guide to Blood Groups* 3rd Ed. Blackwell Publ, ed., Wiley-Blackwell.

Davis, F.F., 2002. The origin of pegnology. *Advanced Drug Delivery Reviews*, 54(4), pp.457–458.

Deamer, D.W. & Nichols, J.W., 1983. Proton-hydroxide permeability of liposomes. *Proceedings of the National Academy of Sciences of the United States of America*, 80(1), pp.165–168.

Dean, L., 2005. The MNS blood group. In N. C. for B. Information, ed. *Blood Groups and Red Cell Antigens*. Bethesda.

Dluzewski, A.R. et al., 1992. Origins of the parasitophorous vacuole membrane of the malaria parasite, Plasmodium falciparum, in human red blood cells. *J Cell Sci*, 102(Pt3), pp.527–532.

Dondorp, A.M. et al., 2010. Artesunate versus quinine in the treatment of severe falciparum malaria in African children (AQUAMAT): An open-label, randomised trial. *The Lancet*, 376(9753), pp.1647–1657.

Dordas, C. & Brown, P.H., 2000. Permeability of boric acid across lipid bilayers and factors affecting it. *Journal of Membrane Biology*, 175(2), pp.95–105.

Dorn, A. et al., 1995. Malarial haemozoin/beta-haematin supports haem polymerization in the absence of protein. *Nature*, 374(6519), pp.269–271.

Douglas, A. et al., 2015. A PfRH5-based vaccine is efficacious against Heterologous strain blood-stage Plasmodium falciparum infection in aotus monkeys. *Cell Host Microbe*, 17(1), pp.130–139.

Douglas, A.D. et al., 2014. Neutralization of Plasmodium falciparum merozoites by antibodies against PfRH5. *Journal of immunology (Baltimore, Md. : 1950)*, 192(1), pp.245–58.

Duffield, P.H. & Netting, A.G., 2001. Methods for the quantitation of abscisic acid and its precursors from plant tissues. *Analytical biochemistry*, 289(2), pp.251–259.

Duncan, R. et al., 1983. Polymers containing enzymatically degradable bonds, 7. Design of oligopeptide side-chains in poly [N-(2-hydroxypropyl)methacrylamide] copolymers to promote efficient degradation by lysosomal enzymes. *Makromol. Chem.*, 184(10), pp.1997–2008.

Duncan, R. et al., 1983 (1). Targeting of N-(2-hydroxypropyl)methacrylamide copolymers to liver by incorporation of galactose residues. *Biochimica et biophysica acta*, 755(3), pp.518–521.

Dutta, P. & Fitch, C.D., 1983. Diverse membrane-active agents modify the hemolytic response to ferriprotoporphyrin IX. *The Journal of pharmacology and experimental therapeutics*, 225(3), pp.729–734.

Düzgüneş, N. et al., 1985. Proton-induced fusion of oleic acid-phosphatidylethanolamine liposomes. *Biochemistry*, 24(13), pp.3091–3098.

Dvorin, J.D. et al., 2010. A plant-like kinase in Plasmodium falciparum regulates parasite egress from erythrocytes. *Science (New York, N.Y.)*, 328(5980), pp.910–912.

Egan, T.J. et al., 2002. Fate of haem iron in the malaria parasite Plasmodium falciparum. *The Biochemical journal*, 365(Pt 2), pp.343–347.

Egan, T.J. et al., 1997. Thermodynamic factors controlling the interaction of quinoline antimalarial drugs with ferriprotoporphyrin IX. *Journal of Inorganic Biochemistry*, 68(2), pp.137–145.

Elamrani, K. & Blume, a, 1983. Effect of the lipid phase transition on the kinetics of H+/OH- diffusion across phosphatidic acid bilayers. *Biochimica et Biophysica Acta*, 727, pp.22–30.

El-Assaad, F. et al., 2013. Cytoadherence of Plasmodium berghei-infected red blood cells to murine brain and lung microvascular endothelial cells in vitro. *Infection and Immunity*, 81(11), pp.3984–3991.

Eliaz, R.E. et al., 2004. Determination and modeling of kinetics of cancer cell killing by doxorubicin and doxorubicin encapsulated in targeted liposomes. *Cancer Research*, 64(2), pp.711–718.

Enomoto, M. et al., 2012. Blockage of spontaneous Ca2+ oscillation causes cell death in intraerythrocitic Plasmodium falciparum. *PLoS ONE*, 7(7), e39499.

Fade, V., 1998. Link between drug absorption solubility and permeability measurements in Caco-2 cells. *Journal of Pharmaceutical Sciences*, 87(12), pp.1604–1607.

Fahr, A. et al., 2005. Transfer of lipophilic drugs between liposomal membranes and biological interfaces: Consequences for drug delivery. *European Journal of Pharmaceutical Sciences*, 26, pp.251–265.

Fahr, A. & Seelig, J., 2001. Liposomal formulations of Cyclosporin A: a biophysical approach to pharmacokinetics and pharmacodynamics. *Critical reviews in therapeutic drug carrier systems*, 18(2), pp.141–172.

Famin, O. & Ginsburg, H., 2002. Differential effects of 4-aminoquinoline-containing antimalarial drugs on hemoglobin digestion in Plasmodium falciparum-infected erythrocytes. *Biochemical Pharmacology*, 63(3), pp.393–398.

Fan, Y. & Zhang, Q., 2013. Development of liposomal formulations: From concept to clinical investigations. *Asian Journal of Pharmaceutical Sciences*, 8(2), pp.79–90.

Feng, Z.P. et al., 2006. Abundance of intrinsically unstructured proteins in P. falciparum and other apicomplexan parasite proteomes. *Molecular and Biochemical Parasitology*, 150(2), pp.256–267.

Fernandes, H.P., Cesar, C.L. & Barjas-Castro, M. de L., 2011. Electrical properties of the red blood cell membrane and immunohematological investigation. *Revista Brasileira de Hematologia e Hemoterapia*, 33(4), pp.297–301.

Fernández-Becerra, C., Pinazo, M.J., et al., 2009. Increased expression levels of the pvcrt-o and pvmdr1 genes in a patient with severe Plasmodium vivax malaria. *Malaria journal*, 8, p.55.

Fernández-Becerra, C., Yamamoto, M.M., et al., 2009. Plasmodium vivax and the importance of the subtelomeric multigene vir superfamily. *Trends in Parasitology*, 25(1), pp.44–51.

Fernando, D., Rodrigo, C. & Rajapakse, S., 2011. Primaquine in vivax malaria: an update and review on management issues. *Malaria Journal*, 10(1), p.351.

Filion, M.C. & Phillips, N.C., 1997. Toxicity and immunomodulatory activity of liposomal vectors formulated with cationic lipids toward immune effector cells. *Biochimica et Biophysica Acta - Biomembranes*, 1329(2), pp.345–356.

Finkelstein, A., 1988. Water movement through lipid bilayers, pores and plasma membranes: Theory and reality. In P. H. Baylis, ed. *Cell Biochemistry and Function*. p. 223.

Fitch, C.D., 2004. Ferriprotoporphyrin IX, phospholipids, and the antimalarial actions of quinoline drugs. *Life Sciences*, 74(16), pp.1957–1972.

Fitch, C.D., Cai, G. zuan, et al., 2003. Relationship of chloroquine-induced redistribution of a neutral aminopeptidase to hemoglobin accumulation in malaria parasites. *Archives of Biochemistry and Biophysics*, 410(2), pp.296–306.

Fitch, C.D., Chen, Y. feng & Cai, G. zuan, 2003. Chloroquine-induced masking of a lipid that promotes ferriprotoporphyrin IX dimerization in malaria. *Journal of Biological Chemistry*, 278(25), pp.22596–22599.

Fleiner, M. et al., 2001. Studies on protein-liposome coupling using novel thiol-reactive coupling lipids: Influence of spacer length and polarity. *Bioconjugate Chemistry*, 12(4), pp.470–475.

Flores, M.V.C. et al., 1997. Inhibition of Plasmodium falciparum proliferation in vitro by ribozymes. *Journal of Biological Chemistry*, 272(27), pp.16940–16945.

Folkman, J. & Long, D.M., 1964. The use of silicone rubber as a carrier for prolonged drug therapy. *The Journal of surgical research*, 4, pp.139–142.

Foth, B.J. et al., 2005. The malaria parasite Plasmodium falciparum has only one pyruvate dehydrogenase complex, which is located in the apicoplast. *Molecular Microbiology*, 55(1), pp.39–53.

Francis, S.E., Sullivan, D.J. & Goldberg, D.E., 1997. Hemoglobin metabolism in the malaria parasite Plasmodium falciparum. *Annual Review of Microbiology*, 51(0066-4227 LA - eng), pp.97–123.

Frank, M. et al., 2007. Variable switching rates of malaria virulence genes are associated with chromosomal position. *Molecular Microbiology*, 64(6), pp.1486–1498.

Frevert, U. et al., 1993. Malaria circumsporozoite protein binds to heparan sulfate proteoglycans associated with the surface membrane of hepatocytes. *The Journal of Experimental Medicine*, 177(5), pp.1287–1298.

Futami, K. et al., 2014. Impacts of insecticide treated bed nets on Anopheles gambiae s.l. populations in Mbita district and Suba district, Western Kenya. *Parasites & vectors*, 7, p.63.

Gabizon, A., Horowitz, A.T., et al., 2003. In vivo fate of folate-targeted polyethylene-glycol liposomes in tumor-bearing mice. *Clinical Cancer Research*, 9(17), pp.6551–6559.

Gabizon, A. & Papahadjopoulos, D., 1988. Liposome formulations with prolonged circulation time in blood and enhanced uptake by tumors. *Proceedings of the National Academy of Sciences of the United States of America*, 85(18), pp.6949–6953.

Gabizon, A. & Papahadjopoulos, D., 1992. The role of surface charge and hydrophilic groups on liposome clearance in vivo. *Biochimica et Biophysica Acta - Biomembranes*, 1103(1), pp.94–100.

Gabizon, A., Shmeeda, H. & Barenholz, Y., 2003. Pharmacokinetics of pegylated liposomal doxorubicin: Review of animal and human studies. *Clinical Pharmacokinetics*, 42(5), pp.419–436.

Galappaththy, G.N., Tharyan, P. & Kirubakaran, R., 2013. Primaquine for preventing relapse in people with Plasmodium vivax malaria treated with chloroquine. *The Cochrane database of systematic reviews*, 10(Article CD004389).

Gallmetzer, M., Müller, B. & Burgstaller, W., 1998. Net efflux of citrate in Penicillium simplicissimum is mediated by a transport protein. *Archives of Microbiology*, 169(4), pp.353–359.

Gardner, M.J. et al., 2002. Genome sequence of the human malaria parasite Plasmodium falciparum. *Nature*, 419(6906), pp.498–511.

Gething, P.W. et al., 2011. A new world malaria map: Plasmodium falciparum endemicity in 2010. *Malaria journal*, 10(1), p.378.

Ghosh, J.K. et al., 1997. Selective cytotoxicity of dermaseptin S3 toward intraerythrocytic Plasmodium falciparum and the underlying molecular basis. *Journal of Biological Chemistry*, 272(50), pp.31609–31616.

Ghumra, A. et al., 2012. Induction of strain-transcending antibodies against group A PfEMP1 surface antigens from virulent malaria parasites. *PLoS Pathogens*, 8(4), e1002665.

Gill, J., Chitnis, C.E. & Sharma, A., 2009. Structural insights into chondroitin sulphate A binding Duffy-binding-like domains from Plasmodium falciparum: implications for intervention strategies against placental malaria. *Malaria journal*, 8, p.67.

Ginsburg, H. & Demel, R.A., 1984. Interactions of hemin, antimalarial drugs and hemin-antimalarial complexes with phospholipid monolayers. *Chemistry and Physics of Lipids*, 35(4), pp.331–347.

Glenn, M.P. et al., 2006. Structurally simple, potent, Plasmodium selective farnesyltransferase inhibitors that arrest the growth of malaria parasites. *Journal of Medicinal Chemistry*, 49(19), pp.5710–5727.

Goel, S. et al., 2015. RIFINs are adhesins implicated in severe Plasmodium falciparum malaria. *Nature Medicine*, 21(4), pp.314–317.

Goldberg, D.E. & Cowman, A.F., 2010. Moving in and renovating: exporting proteins from Plasmodium into host erythrocytes. *Nature reviews. Microbiology*, 8(9), pp.617–621.

Gombotz, W., Healy, M. & Brown, L., 1991. Very low temperature casting of controlled release microspheres. *US Patent 5,019,400*.

Goodyer, I.D. et al., 1997. Characterization of macromolecular transport pathways in malaria-infected erythrocytes. *Molecular and biochemical parasitology*, 87(1), pp.13–28.

Gowda, D.C. & Davidson, E.A., 1999. Protein glycosylation in the malaria parasite. *Parasitology Today*, 15(4), pp.147–152.

Grajales, S. & Jasty, S.G., 2012. Innovative polymers engineered for drug delivery and tissue engineering. *Material Matters, Aldrich Materials Science*, 7(3), p.51.

Grassi, B., 1901. *Studi di uno zoologo sulla malaria* 2nd Ed., Roma: R. Accademia dei lincei.

Graves, P. & Gelband, H., 2006. Vaccines for preventing malaria (blood-stage). *Cochrane Database of Systematic Reviews*, (4), CD006199.

Graves, P., Gelband, H. & Garner, P., 2014. Primaquine or other 8-aminoquinoline for reducing P. falciparum transmission. *Cochrane database of systematic reviews*, 19(2).

Gray, J.C. et al., 2003. Coordination of plastid and nuclear gene expression. *Philosophical transactions of the Royal Society of London. Series B, Biological sciences*, 358(1429), pp.135–145.

Griffiths, R.E., Kupzig, S., et al., 2012. Maturing reticulocytes internalize plasma membrane in glycophorin A-containing vesicles that fuse with autophagosomes before exocytosis. *Blood*, 119(26), pp.6296–6306.

Griffiths, R.E., Kupzig, S., et al., 2012 (1). The ins and outs of human reticulocyte maturation: Autophagy and the endosome/exosome pathway. *Autophagy*, 8(7), pp.1150–1151.

Gruszecki, W.I. & Strzałka, K., 2005. Carotenoids as modulators of lipid membrane physical properties. *Biochimica et Biophysica Acta - Molecular Basis of Disease*, 1740(2), pp.108–115.

Gulati, M. et al., 1998. Lipophilic drug derivatives in liposomes. *International Journal of Pharmaceutics*, 165(2), pp.129–168.

Gupta, B., Levchenko, T.S. & Torchilin, V.P., 2005. Intracellular delivery of large molecules and small particles by cell-penetrating proteins and peptides. *Advanced Drug Delivery Reviews*, 57(4), pp.637–651.

Hafez, I.M., Maurer, N. & Cullis, P.R., 2001. On the mechanism whereby cationic lipids promote intracellular delivery of polynucleic acids. *Gene therapy*, 8(15), pp.1188–1196.

Hage, D.S., 2000. Periodate oxidation of antibodies for site-selective immobilization in immunoaffinity chromatography. In P. Bailon et al., eds. *Affinity Chromatography, Methods and Protocols*. pp. 69–82.

Haldar, K. & Uyetake, L., 1992. The movement of fluorescent endocytic tracers in Plasmodium falciparum infected erythrocytes. *Molecular and Biochemical Parasitology*, 50(1), pp.161–178.

Han, S.-Y. et al., 2004. A novel inhibitor of 9-cis-epoxycarotenoid dioxygenase in abscisic acid biosynthesis in higher plants. *Plant physiology*, 135(3), pp.1574–1582.

Hansch, C., Leo, A. & Hoekman, D., 1995. *Exploring QSAR: Fundamentals and applications in chemistry and biology* A. C. Society, ed., University of Michigan.

Hanssen, E. et al., 2008. Electron tomography of the Maurer's cleft organelles of Plasmodium falciparum-infected erythrocytes reveals novel structural features. *Molecular Microbiology*, 67(4), pp.703–718.

Hanssen, E., Carlton, P., et al., 2010. Whole cell imaging reveals novel modular features of the exomembrane system of the malaria parasite, Plasmodium falciparum. *International Journal for Parasitology*, 40(1), pp.123–134.

Hanssen, E., Goldie, K.N. & Tilley, L., 2010. Ultrastructure of the asexual blood stages of Plasmodium falciparum. *Methods in Cell Biology*, 96, pp.93–116.

Hanssen, E., McMillan, P.J. & Tilley, L., 2010. Cellular architecture of Plasmodium falciparum-infected erythrocytes. *International Journal for Parasitology*, 40(10), pp.1127–1135.

Happi, C.T. et al., 2006. Confirmation of emergence of mutations associated with atovaquone-proguanil resistance in unexposed Plasmodium falciparum isolates from Africa. *Malaria journal*, 5, p.82.

Happi, C.T. et al., 2006 (1). Association between mutations in Plasmodium falciparum chloroquine resistance transporter and P. falciparum multidrug resistance 1 genes and in vivo amodiaquine resistance in P. falciparum malaria-infected children in Nigeria. *American Journal of Tropical Medicine and Hygiene*, 75(1), pp.155–161.

Harada, A., 1999. Chain length recognition: core-shell supramolecular assembly from oppositely charged block copolymers. *Science*, 283(5398), pp.65–67.

Harding, C., Heuser, J. & Stahl, P., 1983. Receptor-mediated endocytosis of transferrin and recycling of the transferrin receptor in rat reticulocytes. *Journal of Cell Biology*, 97(2), pp.329–339.

Harper, J.F. & Harmon, A., 2005. Plants, symbiosis and parasites: a calcium signalling connection. *Nature reviews. Molecular cell biology*, 6(7), pp.555–566.

Harris, J. V. et al., 2012. Sequential Plasmodium chabaudi and Plasmodium berghei infections provide a novel model of severe malarial anemia. *Infection and Immunity*, 80(9), pp.2997–3007.

Hastings, I.M., Watkins, W.M. & White, N.J., 2002. The evolution of drug-resistant malaria: the role of drug elimination half-life. *Philosophical transactions of the Royal Society of London. Series B, Biological sciences*, 357(1420), pp.505–519.

Hastings, P.J. et al., 2009. Mechanisms of change in gene copy number. *Nature reviews. Genetics*, 10(8), pp.551–564.

He, H. et al., 2014. Cell-penetrating peptides meditated encapsulation of protein therapeutics into intact red blood cells and its application. *Journal of Controlled Release*, 176(1), pp.123–132.

Hefesha, H. et al., 2011. Transfer mechanism of temoporfin between liposomal membranes. *Journal of Controlled Release*, 150(3), pp.279–286.

Hermanson, G.T., 2008. *Bioconjugate Techniques* 2nd Ed. G. T. Hermanson, ed., Academic Press.

Herrmann, I.K. et al., 2013. Endotoxin removal by magnetic separation-based blood purification. *Advanced Healthcare Materials*, 2(6), pp.829–835.

Hibbs, A.R., Stenzel, D.J. & Saul, A., 1997. Macromolecular transport in malaria - Does the duct exist? *European Journal of Cell Biology*, 72(2), pp.182–188.

Hill, D.R. et al., 2006. Primaquine: report from CDC expert meeting on malaria chemoprophylaxis I. *Am J Trop Med Hyg.*, 75(3), pp.402–15.

Hirai, N. et al., 2000. Biosynthesis of abscisic acid by the non-mevalonate pathway in plants, and by the mevalonate pathway in fungi. *Bioscience, biotechnology, and biochemistry*, 64(7), pp.1448–1458.

Hoffman, A.S., 2008. The origins and evolution of “controlled” drug delivery systems. *Journal of Controlled Release*, 132(3), pp.153–163.

Holovati, J.L., Gyongyossy-Issa, M.I.C. & Acker, J.P., 2008. Effect of liposome charge and composition on the delivery of trehalose into red blood cells. *Cell Preservation Technology*, 6(3), pp.207–218.

Hong, Y.L. et al., 1992. Activated oxygen generation by a primaquine metabolite: inhibition by antioxidants derived from Chinese herbal remedies. *Free radical biology & medicine*, 12(3), pp.213–218.

Van Hoogevest, P. & Wendel, A., 2014. The use of natural and synthetic phospholipids as pharmaceutical excipients. *European Journal of Lipid Science and Technology*, 116(9), pp.1088–1107.

Horrocks, P. et al., 2005. PfEMP1 expression is reduced on the surface of knobless Plasmodium falciparum infected erythrocytes. *Journal of cell science*, 118(Pt 11), pp.2507–2518.

Howe, R. et al., 2013. Isoprenoid biosynthesis inhibition disrupts Rab5 localization and food vacuolar integrity in Plasmodium falciparum. *Eukaryotic Cell*, 12(2), pp.215–223.

Hsiao, L.L. et al., 1991. Modification of host cell membrane lipid composition by the intra-erythrocytic human malaria parasite Plasmodium falciparum. *Biochemical Journal*, 274(Pt 1), pp.121–132.

Hsu, M.J. & Juliano, R.L., 1982. Interactions of liposomes with the reticuloendothelial system. II: Nonspecific and receptor-mediated uptake of liposomes by mouse peritoneal macrophages. *Biochimica et biophysica acta*, 720(4), pp.411–419.

Huber, S.M., Duranton, C. & Lang, F., 2005. Patch-clamp analysis of the “new permeability pathways” in malaria-infected erythrocytes. *International Review of Cytology*, 246, pp.59–134.

Hui, R., El Bakkouri, M. & Sibley, L.D., 2015. Designing selective inhibitors for calcium-dependent protein kinases in apicomplexans. *Trends in Pharmacological Sciences*, 36(7), pp.452–460.

Huy, N.T. et al., 2003. Neutralization of toxic heme by Plasmodium falciparum histidine-rich protein 2. *Journal of Biochemistry*, 133(5), pp.693–698.

Hwang, S.H. et al., 1999. Remote loading of diclofenac, insulin and fluorescein isothiocyanate labeled insulin into liposomes by pH and acetate gradient methods. *International Journal of Pharmaceutics*, 179(1), pp.85–95.

Idro, R. et al., 2010. Cerebral malaria: Mechanisms of brain injury and strategies for improved neurocognitive outcome. *Pediatric Research*, 68(4), pp.267–274.

Immordino, M.L., Dosio, F. & Cattel, L., 2006. Stealth liposomes: Review of the basic science, rationale, and clinical applications, existing and potential. *International Journal of Nanomedicine*, 1(3), pp.297–315.

Ishida, T., Harashima, H. & Kiwada, H., 2002. Liposome clearance. *Bioscience Reports*, 22(2), pp.197–224.

Ishida, T., Iden, D.L. & Allen, T.M., 1999. A combinatorial approach to producing sterically stabilized (Stealth) immunoliposomal drugs. *FEBS Letters*, 460(1), pp.129–133.

Iwai, K., Maeda, H. & Konno, T., 1984. Use of oily contrast medium for selective drug targeting to tumor: Enhanced therapeutic effect and X-ray image. *Cancer Research*, 44(5), pp.2115–2121.

Jacobs, P., Radzioch, D. & Stevenson, M.M., 1996. A Th1-associated increase in tumor necrosis factor alpha expression in the spleen correlates with resistance to blood-stage malaria in mice. *Infection and Immunity*, 64(2), pp.535–541.

Vander Jagt, D.L., Hunsaker, L.A. & Campos, N.M., 1986. Characterization of a hemoglobin-degrading, low molecular weight protease from Plasmodium falciparum. *Molecular and biochemical parasitology*, 18(3), pp.389–400.

Jain, N.K. & Asthana, A., 2007. Dendritic systems in drug delivery applications. *Expert opinion on drug delivery*, 4(5), pp.495–512.

Janthur, W.D., Cantoni, N. & Mamot, C., 2012. Drug conjugates such as antibody drug conjugates (ADCs), immunotoxins and immunoliposomes challenge daily clinical practice. *International Journal of Molecular Sciences*, 13(12), pp.16785–16795.

Joel Anne Chasis, N.M., 1992. Red Blood Cell Glycophorins. *Blood*, 80(8), pp.1869–1879.

Joet, T. et al., 2003. Validation of the hexose transporter of Plasmodium falciparum as a novel drug target. *Proceedings of the National Academy of Sciences of the United States of America*, 100(13), pp.7476–7479.

John, C.C. et al., 2008. Antibodies to pre-erythrocytic Plasmodium falciparum antigens and risk of clinical malaria in Kenyan children. *The Journal of infectious diseases*, 197(4), pp.519–526.

Jomaa, H. et al., 1999. Inhibitors of the nonmevalonate pathway of isoprenoid biosynthesis as antimalarial drugs. *Science (New York, N.Y.)*, 285(5433), pp.1573–1576.

Jones, J.D. & Thompson, T.E., 1989. Spontaneous phosphatidylcholine transfer by collision between vesicles at high lipid concentration. *Biochemistry*, 28(1), pp.129–134.

Jones, M.L., Cottingham, C. & Rayner, J.C., 2009. Effects of calcium signaling on Plasmodium falciparum erythrocyte invasion and post-translational modification of gliding-associated protein 45 (PfGAP45). *Molecular and Biochemical Parasitology*, 168(1), pp.55–62.

Kabanov, A.V. et al., 1989. The neuroleptic activity of haloperidol increases after its solubilization in surfactant micelles. Micelles as microcontainers for drug targeting. *FEBS letters*, 258(2), pp.343–345.

Kara, U.A.K. et al., 1988. Inhibitory monoclonal antibody against a (myristylated) small-molecular-weight antigen from Plasmodium falciparum associated with the parasitophorous vacuole membrane. *Infection and Immunity*, 56(4), pp.903–909.

Kaslow, D.C. et al., 1988. A vaccine candidate from the sexual stage of human malaria that contains EGF-like domains. *Nature*, 333(6168), pp.74–76.

Ke, H. et al., 2014. The heme biosynthesis pathway is essential for Plasmodium falciparum development in mosquito stage but not in blood stages. *Journal of Biological Chemistry*, 289(50), pp.34827–34837.

Kelly, C., Jefferies, C. & Cryan, S.-A., 2011. Targeted liposomal drug delivery to monocytes and macrophages. *Journal of drug delivery*, 2011(Article 727241), pp.1–11.

Kerlin, D.H. & Gatton, M.L., 2013. Preferential invasion by Plasmodium merozoites and the self-regulation of parasite burden. *PLoS ONE*, 8(2), e57434.

Khalil, I. et al., 2002. Pyrimethamine/sulfadoxine combination in the treatment of uncomplicated falciparum malaria: Relation between dihydropteroate synthase/dihydrofolate reductase genotypes, sulfadoxine plasma levels, and treatment outcome. *American Journal of Tropical Medicine and Hygiene*, 67(3), pp.225–229.

Kim, B.Y.S., Rutka, J.T. & Chan, W.C.W., 2010. Nanomedicine. *The New England journal of medicine*, 363(25), pp.2434–2443.

Kina, T. et al., 2000. The monoclonal antibody TER-119 recognizes a molecule associated with glycophorin A and specifically marks the late stages of murine erythroid lineage. *British Journal of Haematology*, 109(2), pp.280–287.

Kirk, K., 2001. Membrane transport in the malaria-infected erythrocyte. *Physiological reviews*, 81, pp.495–537.

Kirpotin, D. et al., 1997. Sterically stabilized anti-HER2 immunoliposomes: design and targeting to human breast cancer cells in vitro. *Biochemistry*, 36, pp.66–75.

Knop, K. et al., 2010. Poly(ethylene glycol) in drug delivery: Pros and cons as well as potential alternatives. *Angewandte Chemie - International Edition*, 49(36), pp.6288–6308.

Kobayashi, K. et al., 2013. Analyses of interactions between heparin and the apical surface proteins of Plasmodium falciparum. *Scientific reports*, 3(Article 3178).

Kokwaro, G., Mwai, L. & Nzila, A., 2007. Artemether/lumefantrine in the treatment of uncomplicated falciparum malaria. *Expert opinion on pharmacotherapy*, 8(1), pp.75–94.

Kondo, M. et al., 2004. Anti-neovascular therapy by liposomal drug targeted to membrane type-1 matrix metalloproteinase. *International Journal of Cancer*, 108(2), pp.301–306.

Kono, K., Igawa, T. & Takagishi, T., 1997. Cytoplasmic delivery of calcein mediated by liposomes modified with a pH-sensitive poly(ethylene glycol) derivative. *Biochimica et Biophysica Acta - Biomembranes*, 1325(2), pp.143–154.

Korsinczky, M. et al., 2000. Mutations in Plasmodium falciparum cytochrome b that are associated with atovaquone resistance are located at a putative drug-binding site. *Antimicrobial Agents and Chemotherapy*, 44(8), pp.2100–2108.

Kremsner, P.G. et al., 1995. Prediction of accelerated cure in Plasmodium falciparum malaria by the elevated capacity of tumor necrosis factor production. *American Journal of Tropical Medicine and Hygiene*, 53(5), pp.532–538.

Kroemer, G. et al., 2009. Classification of cell death: recommendations of the Nomenclature Committee on Cell Death 2009. *Cell death and differentiation*, 16(1), pp.3–11.

Krogstad, D.J. & Schlesinger, P.H., 1986. A perspective on antimalarial action: effects of weak bases on Plasmodium falciparum. *Biochemical pharmacology*, 35(4), pp.547–552.

Kroto, H.W. et al., 1985. C 60: buckminsterfullerene. *Nature*, 318, pp.162–163.

Külzer, S. et al., 2010. Parasite-encoded Hsp40 proteins define novel mobile structures in the cytosol of the P. falciparum-infected erythrocyte. *Cellular Microbiology*, 12(10), pp.1398–1420.

Külzer, S. et al., 2012. Plasmodium falciparum-encoded exported hsp70/hsp40 chaperone/co-chaperone complexes within the host erythrocyte. *Cellular Microbiology*, 14(11), pp.1784–1795.

Kuss, C. et al., 2012. Quantitative proteomics reveals new insights into erythrocyte invasion by Plasmodium falciparum. *Molecular & Cellular Proteomics*, 11(2), p.M111.010645.

Kyes, S.A., Kraemer, S.M. & Smith, J.D., 2007. Antigenic variation in Plasmodium falciparum: gene organization and regulation of the var multigene family. *Eukaryotic Cell*, 6(9), pp.1511–1520.

Lange, Y. et al., 1983. On the mechanism of transfer of cholesterol between human-erythrocytes and plasma. *Journal Of Biological Chemistry*, 258(11), pp.6920–6926.

Langer, R. & Folkman, J., 1976. Polymers for the sustained release of proteins and other macromolecules. *Nature*, 263(5580), pp.797–800.

Lau, L.W. et al., 2013. Pathophysiology of the brain extracellular matrix: a new target for remyelination. *Nature reviews. Neuroscience*, 14(10), pp.722–9.

Laveran, A., 1880. Note sur un nouveau parasite trouvé dans le sang de plusieurs malades atteints de fièvre palustre. *Bull.Acad.Méd*, 9, pp.1235–1236.

Lavstsen, T. et al., 2012. Plasmodium falciparum erythrocyte membrane protein 1 domain cassettes 8 and 13 are associated with severe malaria in children. *Proceedings of the National Academy of Sciences of the United States of America*, 109(26), pp.E1791–800.

Lawaczeck, R., 1988. Defect structures in membranes: routes for the permeation of small molecules. *Berichte der Bunsengesellschaft für physikalische Chemie*, 92(9), pp.961–963.

Lazarus, M.D., Schneider, T.G. & Taraschi, T.F., 2008. A new model for hemoglobin ingestion and transport by the human malaria parasite Plasmodium falciparum. *J Cell Sci*, 121(11), pp.1937–1949.

Lee, J.J. et al., 2014. Synthetic ligand-coated magnetic nanoparticles for microfluidic bacterial separation from blood. *Nano Letters*, 14(1), pp.1–5.

Leef, J.L. & Carlson, P.S., 1997. Carotenoid synthesis inhibiting herbicides and fatty acid synthesis inhibiting oxime herbicides as anti-Apicomplexa protozoan parasite agents (Patent US5877186 A).

Leitgeb, A.M. et al., 2011. Low anticoagulant heparin disrupts Plasmodium falciparum rosettes in fresh clinical isolates. *American Journal of Tropical Medicine and Hygiene*, 84(3), pp.390–396.

Leitmannova Liu, A., 2006. *Advances in Planar Lipid Bilayers and Liposomes, Volume 3* 1st Editio. A. Leitmannova Liu, ed., Academic Press.

Leo, A., Hansch, C. & Elkins, D., 1971. Partition coefficients and their Uses. *Chemical Reviews*, 71(6), pp.525–616.

Lewis, B.A. & Engelman, D.M., 1983. Lipid bilayer thickness varies linearly with acyl chain length in fluid phosphatidylcholine vesicles. *Journal of molecular biology*, 166(2), pp.211–217.

Li, J. et al., 2000. Regulation of abscisic acid-induced stomatal closure and anion channels by guard cell AAPK kinase. *Science (New York, N.Y.)*, 287(5451), pp.300–303.

Lindblom, G., Orädd, G. & Filippov, A., 2006. Lipid lateral diffusion in bilayers with phosphatidylcholine, sphingomyelin and cholesterol. An NMR study of dynamics and lateral phase separation. *Chemistry and Physics of Lipids*, 141(1-2), pp.179–184.

Liu, H. et al., 2013. Methemoglobin generation by 8-aminoquinolines: Effect of substitution at 5-position of primaquine. *Chemical Research in Toxicology*, 26(12), pp.1801–1809.

Liu, W. et al., 2010. Origin of the human malaria parasite Plasmodium falciparum in gorillas. *Nature*, 467(7314), pp.420–425.

Loew, S., Fahr, A. & May, S., 2011. Modeling the release kinetics of poorly water-soluble drug molecules from liposomal nanocarriers. *Journal of drug delivery*, 2011(Article 376548), pp.1–10.

Longmire, M., Choyke, P.L. & Kobayashi, H., 2008. Clearance properties of nano-sized particles and molecules as imaging agents: considerations and caveats. *Nanomedicine (London, England)*, 3(5), pp.703–717.

Longmuir, K.J. et al., 2006. Effective targeting of liposomes to liver and hepatocytes in vivo by incorporation of a Plasmodium amino acid sequence. *Pharmaceutical Research*, 23(4), pp.759–769.

Loughrey, H.C. et al., 1990. Optimized procedures for the coupling of proteins to liposomes. *Journal of immunological methods*, 132(1), pp.25–35.

Lourido, S., Tang, K. & Sibley, L.D., 2012. Distinct signalling pathways control Toxoplasma egress and host-cell invasion. *The EMBO journal*, 31(24), pp.4524–34.

Lovett, J.L. et al., 2002. Toxoplasma gondii microneme secretion involves intracellular Ca2+ release from inositol 1,4,5-triphosphate (IP3)/ryanodine-sensitive stores. *Journal of Biological Chemistry*, 277(29), pp.25870–25876.

Lü, J.M. et al., 2010. Molecular mechanisms and clinical applications of nordihydroguaiaretic acid (NDGA) and its derivatives: an update. *Medical science monitor : international medical journal of experimental and clinical research*, 16(5), pp.RA93–A100.

Lwetoijera, D.W. et al., 2014. Increasing role of Anopheles funestus and Anopheles arabiensis in malaria transmission in the Kilombero Valley, Tanzania. *Malaria Journal*, 13(1), p.331.

MacRae, J.I. et al., 2013. Mitochondrial metabolism of sexual and asexual blood stages of the malaria parasite Plasmodium falciparum. *BMC biology*, 11, p.67.

Madden, T.D. et al., 1990. The accumulation of drugs within large unilamellar vesicles exhibiting a proton gradient: a survey. *Chemistry and physics of lipids*, 53(1), pp.37–46.

Magnani, M. et al., 2002. Erythrocyte-mediated delivery of drugs, peptides and modified oligonucleotides. *Gene therapy*, 9(11), pp.749–751.

Maguire, P.A., Prudhomme, J. & Sherman, I.W., 1991. Alterations in erythrocyte membrane phospholipid organization due to the intracellular growth of the human malaria parasite, Plasmodium falciparum. *Parasitology*, 102(Pt 2), pp.179–186.

Mahmoudi, N. et al., 2008. New active drugs against liver stages of Plasmodium predicted by molecular topology. *Antimicrobial Agents and Chemotherapy*, 52(4), pp.1215–1220.

Maier, A.G. et al., 2009. Malaria parasite proteins that remodel the host erythrocyte. *Nature Reviews Microbiology*, 7(5), pp.341–354.

Makino, K. et al., 2003. Effects of liposomal phophatidylserine on phagocytic uptake of liposomes by macrophage-like HL-60RG cells. *Colloids and Surfaces B: Biointerfaces*, 29(4), pp.277–284.

Makobongo, M.O. et al., 2006. Immunization of Aotus monkeys with recombinant cysteine-rich interdomain region 1 alpha protects against severe disease during Plasmodium falciparum reinfection. *The Journal of infectious diseases*, 193(5), pp.731–740.

Manjappa, A.S. et al., 2011. Antibody derivatization and conjugation strategies: application in preparation of stealth immunoliposome to target chemotherapeutics to tumor. *Journal of controlled release : official journal of the Controlled Release Society*, 150(1), pp.2–22.

Manno, S., Takakuwa, Y. & Mohandas, N., 2002. Identification of a functional role for lipid asymmetry in biological membranes: Phosphatidylserine-skeletal protein interactions modulate membrane stability. *Proceedings of the National Academy of Sciences of the United States of America*, 99(4), pp.1943–1948.

Mantel, P.Y. et al., 2013. Malaria-infected erythrocyte-derived microvesicles mediate cellular communication within the parasite population and with the host immune system. *Cell Host and Microbe*, 13(5), pp.521–534.

Marques, J. et al., 2014. Application of heparin as a dual agent with antimalarial and liposome targeting activities toward Plasmodium-infected red blood cells. *Nanomedicine*, 10(8), pp.1719–1728.

Martin, F.J. & Papahadjopoulos, D., 1982. Irreversible coupling of immunoglobulin fragments to preformed vesicles. An improved method for liposome targeting. *The Journal of biological chemistry*, 257(1), pp.286–288.

Martin, R.E. & Kirk, K., 2007. Transport of the essential nutrient isoleucine in human erythrocytes infected with the malaria parasite Plasmodium falciparum. *Blood*, 109(5), pp.2217–2224.

Martín-Jaular, L. et al., 2013. Reticulocyte-prone malaria parasites predominantly invade CD71 hi immature cells : implications for the development of an in vitro culture for Plasmodium vivax. *Malaria journal*, 12, p.434.

Maruyama, K., 2002. PEG-immunoliposome. *Bioscience reports*, 22(2), pp.251–66.

Masotti, A. et al., 2009. Comparison of different commercially available cationic liposome-DNA lipoplexes: Parameters influencing toxicity and transfection efficiency. *Colloids and Surfaces B: Biointerfaces*, 68(2), pp.136–144.

Mastrobattista, E. et al., 2002. Functional characterization of an endosome-disruptive peptide and its application in cytosolic delivery of immunoliposome-entrapped proteins. *Journal of Biological Chemistry*, 277(30), pp.27135–27143.

Matsumura, Y. & Maeda, H., 1986. A new concept for macromolecular therapeutics in cancer chemotherapy: Mechanism of tumoritropic accumulation of proteins and the antitumor agent smancs. *Cancer Research*, 46(12 Pt 1), pp.6387–6392.

Maurer, N., Fenske, D.B. & Cullis, P.R., 2001. Developments in liposomal drug delivery systems. *Expert opinion on biological therapy*, 1(6), pp.923–47.

Mayer, D.C.G. et al., 2009. Glycophorin B is the erythrocyte receptor of Plasmodium falciparum erythrocyte-binding ligand, EBL-1. *Proceedings of the National Academy of Sciences of the United States of America*, 106(13), pp.5348–5352.

McLaren, C.E., Brittenham, G.M. & Hasselblad, V., 1987. Statistical and graphical evaluation of erythrocyte volume distributions. *The American journal of physiology*, 252(4 Pt 2), pp.H857–H866.

McLean, L.R. & Phillips, M.C., 1981. Mechanism of cholesterol and phosphatidylcholine exchange or transfer between unilamellar vesicles. *Biochemistry*, 20(10), pp.2893–2900.

Mcmillan, P.J. et al., 2013. Spatial and temporal mapping of the PfEMP1 export pathway in Plasmodium falciparum. *Cellular Microbiology*, 15(8), pp.1401–1418.

Van der Merwe, D. & Pickrell, J. a., 2012. Toxicity of nanomaterials. *Veterinary Toxicology*, 2015, pp.383–390.

Miller, J.D. et al., 2008. Perlecan: a major IL-2-binding proteoglycan in murine spleen. *Immunology and cell biology*, 86(2), pp.192–199.

Miller, L.H. et al., 2002. The pathogenic basis of malaria. *Nature*, 415(6872), pp.673–679.

Miller, L.H. & Su, X., 2011. Artemisinin: Discovery from the Chinese herbal garden. *Cell*, 146(6), pp.855–858.

Mintzer, M.A. & Grinstaff, M.W., 2011. Biomedical applications of dendrimers: a tutorial. *Chemical Society reviews*, 40(1), pp.173–190.

Miura, K. et al., 2007. Transmission-blocking activity induced by malaria vaccine candidates Pfs25/Pvs25 is a direct and predictable function of antibody titer. *Malaria journal*, 6, p.107.

Mogi, T. & Kita, K., 2010. Diversity in mitochondrial metabolic pathways in parasitic protists Plasmodium and Cryptosporidium. *Parasitology International*, 59(3), pp.305–312.

Mohandas, N. & Chasis, J.A., 1993. Red blood cell deformability, membrane material properties and shape: regulation by transmembrane, skeletal and cytosolic proteins and lipids. *Seminars in hematology*, 30(3), pp.171–192.

Mohandas, N. & Gallagher, P.G., 2008. Red cell membrane: Past, present, and future. *Blood*, 112(10), pp.3939–3948.

Moles, E. et al., 2015. Immunoliposome-mediated drug delivery to Plasmodium-infected and non-infected red blood cells as a dual therapeutic/prophylactic antimalarial strategy. *Journal of Controlled Release*, 210, pp.217–229.

Moll, G.N. et al., 1990. Phospholipid asymmetry in the plasma membrane of malaria infected erythrocytes. *Biochemistry and cell biology*, 68(2), pp.579–585.

Mondal Roy, S. & Sarkar, M., 2011. Membrane fusion induced by small molecules and ions. *Journal of lipids*, 2011, p.528784.

Montero, A., 2013. *Medicina tropical. Abordaje práctico e integral* 1st Ed. Elsevier, ed., Barcelona: Elsevier.

Montrose, K. et al., 2013. Xentry, a new class of cell-penetrating peptide uniquely equipped for delivery of drugs. *Scientific reports*, 3, p.1661.

Moorthy, V.S., Newman, R.D. & Okwo-Bele, J.M., 2013. Malaria vaccine technology roadmap. *Lancet*, 382(9906), pp.1700–1701.

Moreira, J.N. et al., 2002. Use of the post-insertion technique to insert peptide ligands into pre-formed stealth liposomes with retention of binding activity and cytotoxicity. *Pharmaceutical Research*, 19(3), pp.265–269.

Murray, C.J.L. et al., 2012. Global malaria mortality between 1980 and 2010: A systematic analysis. *The Lancet*, 379(9814), pp.413–431.

Muzykantov, V.R., 2010. Drug delivery by red blood cells: vascular carriers designed by Mother Nature. *Expert Opinion on Drug Delivery*, 7(4), pp.403–427.

Nagamune, K. et al., 2008. Abscisic acid controls calcium-dependent egress and development in Toxoplasma gondii. *Nature*, 451(7175), pp.207–210.

Nagamune, K. & Sibley, L.D., 2006. Comparative genomic and phylogenetic analyses of calcium ATPases and calcium-regulated proteins in the Apicomplexa. *Molecular Biology and Evolution*, 23(8), pp.1613–1627.

Nair, A. et al., 2012. Biowaiver monographs for immediate-release solid oral dosage forms: primaquine phosphate. *Journal of pharmaceutical sciences*, 101(3), pp.936–45.

Nakase, I., Kobayashi, S. & Futaki, S., 2010. Endosome-disruptive peptides for improving cytosolic delivery of bioactive macromolecules. *Biopolymers*, 94(6), pp.763–770.

Nakornchai, S. et al., 1983. Mechanism of enhanced fusion capacity of mouse red cells infected with Plasmodium berghei. *Journal of cell science*, 63, pp.147–154.

Nallan, L. et al., 2005. Protein farnesyltransferase inhibitors exhibit potent antimalarial activity. *Journal of Medicinal Chemistry*, 48(11), pp.3704–3713.

Nanjwade, B.K. et al., 2009. Dendrimers: emerging polymers for drug-delivery systems. *European journal of pharmaceutical sciences : official journal of the European Federation for Pharmaceutical Sciences*, 38(3), pp.185–96.

Nguyen, D.B. et al., 2011. Regulation of phosphatidylserine exposure in red blood cells. *Cellular Physiology and Biochemistry*, 28(5), pp.847–856.

Nicolas, E., Goodyer, I.D. & Taraschi, T.F., 1997. An additional mechanism of ribosome-inactivating protein cytotoxicity: degradation of extrachromosomal DNA. *The Biochemical journal*, 327(Pt 2), pp.413–417.

Nixon, G.L. et al., 2013. Antimalarial pharmacology and therapeutics of atovaquone. *Journal of Antimicrobial Chemotherapy*, 68(5), pp.977–985.

Ntumngia, F.B. et al., 2013. Immunogenicity of single versus mixed allele vaccines of Plasmodium vivax duffy binding protein region II. *Vaccine*, 31(40), pp.4382–4388.

Nussenzweig, V. & Nussenzweigt, R.S., 1985. Circumsporozoite proteins of malaria parasites. *Cell*, 42(2), pp.401–403.

O'Neill, P.M., Barton, V.E. & Ward, S.A., 2010. The molecular mechanism of action of artemisinin--the debate continues. *Molecules*, 15(3), pp.1705–1721.

Ochola, L.B. et al., 2011. Specific receptor usage in Plasmodium falciparum cytoadherence is associated with disease outcome. *PLoS ONE*, 6(3).

Olson, E.S. et al., 2010. Activatable cell penetrating peptides linked to nanoparticles as dual probes for in vivo fluorescence and MR imaging of proteases. *Proceedings of the National Academy of Sciences of the United States of America*, 107(9), pp.4311–4316.

Olszewski, K.L. et al., 2010. Branched tricarboxylic acid metabolism in Plasmodium falciparum. *Nature*, 466(7307), pp.774–778.

Omodeo-Salè, F. et al., 2009. Novel antimalarial aminoquinolines: heme binding and effects on normal or Plasmodium falciparum-parasitized human erythrocytes. *Antimicrobial agents and chemotherapy*, 53(10), pp.4339–4344.

Ord, R.L. et al., 2014. A malaria vaccine candidate based on an epitope of the Plasmodium falciparum RH5 protein. *Malaria journal*, 13(1), p.326.

Oritani, T. & Kiyota, H., 2003. Biosynthesis and metabolism of abscisic acid and related compounds. *Natural product reports*, 20(4), pp.414–425.

Orjih, A.U. et al., 1981. Hemin lyses malaria parasites. *Science*, 214(4521), pp.667–669.

Otto, T.D. et al., 2014. Genome sequencing of chimpanzee malaria parasites reveals possible pathways of adaptation to human hosts. *Nature Communications*, 5, p.4754.

Owais, M. et al., 1995. Chloroquine encapsulated in malaria-infected erythrocyte-specific antibody-bearing liposomes effectively controls chloroquine-resistant Plasmodium berghei infections in mice. *Antimicrobial Agents and Chemotherapy*, 39(1), pp.180–184.

Pachlatko, E. et al., 2010. MAHRP2, an exported protein of Plasmodium falciparum, is an essential component of Maurer's cleft tethers. *Molecular microbiology*, 77(5), pp.1136–1152.

Paget-McNicol, S. et al., 2002. The Plasmodium falciparum var gene switching rate, switching mechanism and patterns of parasite recrudescence described by mathematical modelling. *Parasitology*, 124(Pt 3), pp.225–235.

Painter, H.J. et al., 2007. Specific role of mitochondrial electron transport in blood-stage Plasmodium falciparum. *Nature*, 446(7131), pp.88–91.

Painter, H.J., Morrisey, J.M. & Vaidya, A.B., 2010. Mitochondrial electron transport inhibition and viability of intraerythrocytic Plasmodium falciparum. *Antimicrobial Agents and Chemotherapy*, 54(12), pp.5281–5287.

Pandey, A.V. et al., 1999. Artemisinin, an endoperoxide antimalarial, disrupts the hemoglobin catabolism and heme detoxification systems in malarial parasite. *Journal of Biological Chemistry*, 274(27), pp.19383–19388.

Pang, A.J. & Reithmeier, R.A.F., 2009. Interaction of anion exchanger 1 and glycophorin A in human erythroleukaemic K562 cells. *The Biochemical journal*, 421(3), pp.345–356.

Panneerselvam, S. & Choi, S., 2014. Nanoinformatics: emerging databases and available tools. *International journal of molecular sciences*, 15(5), pp.7158–82.

Papahadjopoulos, D. et al., 1991. Sterically stabilized liposomes: improvements in pharmacokinetics and antitumor therapeutic efficacy. *Proceedings of the National Academy of Sciences of the United States of America*, 88(24), pp.11460–11464.

Papahadjopoulos, D., Nir, S. & Düzgünes, N., 1990. Molecular mechanisms of calcium-induced membrane fusion. *Journal of Bioenergetics and Biomembranes*, 22(2), pp.157–179.

Papahadjopoulos, D., Poste, G. & Schaeffer, B.E., 1973. Fusion of mammalian cells by unilamellar lipid vesicles: Influence of lipid surface charge, fluidity and cholesterol. *Biochim Biophys Acta*, 323(1), pp.23–42.

RTS,S Clinical Trials Partnership, 2015. Efficacy and safety of RTS,S/AS01 malaria vaccine with or without a booster dose in infants and children in Africa: final results of a phase 3, individually randomised, controlled trial. *The Lancet*, 386(9988), pp.31–45.

Pasini, E.M. et al., 2013. Proteomic and genetic analyses demonstrate that Plasmodium berghei blood stages export a large and diverse repertoire of proteins. *Molecular & cellular proteomics : MCP*, 12(2), pp.426–48.

Pasvol, G., 2010. Protective hemoglobinopathies and Plasmodium falciparum transmission. *Nature genetics*, 42(4), pp.284–285.

Paula, S. et al., 1996. Permeation of protons, potassium ions, and small polar molecules through phospholipid bilayers as a function of membrane thickness. *Biophysical journal*, 70(1), pp.339–348.

Payne, S.H. & Loomis, W.F., 2006. Retention and loss of amino acid biosynthetic pathways based on analysis of whole-genome sequences. *Eukaryotic Cell*, 5(2), pp.272–276.

Peeters, P.A. et al., 1988. Immunospecific targeting of immunoliposomes, F(ab')2 and IgG to red blood cells in vivo. *Biochimica et biophysica acta*, 943(2), pp.137–147.

Persson, K.E.M. et al., 2008. Variation in use of erythrocyte invasion pathways by Plasmodium falciparum mediates evasion of human inhibitory antibodies. *Journal of Clinical Investigation*, 118(1), pp.342–351.

Peters, J.M. et al., 2002. Mutations in cytochrome b resulting in atovaquone resistance are associated with loss of fitness in Plasmodium falciparum. *Antimicrobial Agents and Chemotherapy*, 46(8), pp.2435–2441.

Peterson, D.S., Milhous, W.K. & Wellems, T.E., 1990. Molecular basis of differential resistance to cycloguanil and pyrimethamine in Plasmodium falciparum malaria. *Proceedings of the National Academy of Sciences of the United States of America*, 87(8), pp.3018–3022.

Pires, P. et al., 1999. Interaction of cationic liposomes and their DNA complexes with monocytic leukemia cells. *Biochim Biophys Acta*, 1418(1), pp.71–84.

Pirson, P. et al., 1979. Liposomes in the chemotherapy of experimental murine malaria. *Trans R Soc Trop Med Hyg.*, 73(3), p.347.

Poole, R.C. & Halestrap, A.P., 1993. Transport of lactate and other monocarboxylates across mammalian plasma membranes. *The American journal of physiology*, 264(4 Pt 1), pp.C761–C782.

Del Portillo, H.A. et al., 2004. Variant genes and the spleen in Plasmodium vivax malaria. *International Journal for Parasitology*, 34(13-14), pp.1547–1554.

Postma, N.S. et al., 1999. Treatment with liposome-bound recombinant human tumor necrosis factor-alpha suppresses parasitemia and protects against Plasmodium berghei k173-induced experimental cerebral malaria in mice. *The Journal of pharmacology and experimental therapeutics*, 288(1), pp.114–120.

Pouvelle, B. et al., 1991. Direct access to serum macromolecules by intraerythrocytic malaria parasites. *Nature*, 353(6339), pp.73–75.

Pouvelle, B., Gormley, J.A. & Taraschi, T.F., 1994. Characterization of trafficking pathways and membrane genesis in malaria-infected erythrocytes. *Molecular and Biochemical Parasitology*, 66(1), pp.83–96.

Prabhakar, U. et al., 2013. Challenges and key considerations of the enhanced permeability and retention effect for nanomedicine drug delivery in oncology. *Cancer Research*, 73(8), pp.2412–2417.

Premji, Z.G., 2009. Coartem: the journey to the clinic. *Malaria journal*, 8(Suppl 1), p.S3.

Preuss, J., Jortzik, E. & Becker, K., 2012. Glucose-6-phosphate metabolism in Plasmodium falciparum. *IUBMB Life*, 64(7), pp.603–611.

Prugnolle, F. et al., 2011. African monkeys are infected by Plasmodium falciparum nonhuman primate-specific strains. *Proceedings of the National Academy of Sciences of the United States of America*, 108(29), pp.11948–11953.

Qin, S.S., Yu, Z.W. & Yu, Y.X., 2009. Structural characterization on the gel to liquid-crystal phase transition of fully hydrated DSPC and DSPE bilayers. *Journal of Physical Chemistry B*, 113(23), pp.8114–8123.

Qiu, L., Jing, N. & Jin, Y., 2008. Preparation and in vitro evaluation of liposomal chloroquine diphosphate loaded by a transmembrane pH-gradient method. *International Journal of Pharmaceutics*, 361(1-2), pp.56–63.

Quashie, N.B., Ranford-Cartwright, L.C. & de Koning, H.P., 2010. Uptake of purines in Plasmodium falciparum-infected human erythrocytes is mostly mediated by the human equilibrative nucleoside transporter and the human facilitative nucleobase transporter. *Malaria journal*, 9, p.36.

Raj, D.K. et al., 2014. Antibodies to PfSEA-1 block parasite egress from RBCs and protect against malaria infection. *Science*, 344(6186), pp.871–877.

Reddy, K.S. et al., 2015. Multiprotein complex between the GPI-anchored CyRPA with PfRH5 and PfRipr is crucial for Plasmodium falciparum erythrocyte invasion. *Proceedings of the National Academy of Sciences*, 112(4), pp.1179–1184.

Regev-Rudzki, N. et al., 2013. Cell-cell communication between malaria-infected red blood cells via exosome-like vesicles. *Cell*, 153(5), pp.1120–1133.

Reid, M.E., 2009. MNS blood group system: A review. *Immunohematology*, 25(3), pp.95–101.

Reis, A. & Spickett, C.M., 2012. Chemistry of phospholipid oxidation. *Biochimica et Biophysica Acta - Biomembranes*, 1818(10), pp.2374–2387.

Rener, J. et al., 1983. Target antigens of transmission-blocking immunity on gametes of plasmodium falciparum. *The Journal of experimental medicine*, 158(3), pp.976–981.

Ringsdorf, H., 1975. Structure and properties of pharmacologically active polymers. *Journal of Polymer Science: Polymer Symposia*, 51(1), pp.135–153.

Riske, K.A. et al., 2009. Lipid bilayer pre-transition as the beginning of the melting process. *Biochimica et Biophysica Acta - Biomembranes*, 1788(5), pp.954–963.

Robertson, R.T. et al., 2008. Liposomes incorporating a Plasmodium amino acid sequence target heparan sulfate binding sites in liver. *Journal of Pharmaceutical Sciences*, 97(8), pp.3257–3273.

Robinson, B.A., Welch, T.L. & Smith, J.D., 2003. Widespread functional specialization of Plasmodium falciparum erythrocyte membrane protein 1 family members to bind CD36 analysed across a parasite genome. *Molecular Microbiology*, 47(5), pp.1265–1278.

Ross, R., 1897. On some peculiar pigmented cells found in two mosquitoes fed on malarial blood. *Br Med J.*, 18(2), pp.1786–1788.

Rowe, A. et al., 1995. Plasmodium falciparum rosetting is associated with malaria severity in Kenya. *Infection and Immunity*, 63(6), pp.2323–2326.

Rowe, J.A. et al., 2002. Nonimmune IgM but not IgG binds to the surface of Plasmodium falciparum-infected erythrocytes and correlates with rosetting and severe malaria. *American Journal of Tropical Medicine and Hygiene*, 66(6), pp.692–699.

Rowe, J.A. et al., 1997. P. falciparum rosetting mediated by a parasite-variant erythrocyte membrane protein and complement-receptor 1. *Nature*, 388(6639), pp.292–295.

Rug, M. et al., 2014. Export of virulence proteins by malaria-infected erythrocytes involves remodelling of host actin cytoskeleton. *Blood*, 124(23), pp.3459–3468.

Ruoslahti, E., 1996. RGD and other recognition sequences for integrins. *Annual review of cell and developmental biology*, 12, pp.697–715.

Salanti, A. et al., 2004. Evidence for the involvement of VAR2CSA in pregnancy-associated malaria. *The Journal of experimental medicine*, 200(9), pp.1197–1203.

Salomao, M. et al., 2008. Protein 4.1R-dependent multiprotein complex: new insights into the structural organization of the red blood cell membrane. *Proceedings of the National Academy of Sciences of the United States of America*, 105(23), pp.8026–8031.

Santiago, C.M. et al., 2012. The role of matrix effects on the quantification of abscisic acid and its metabolites in the leaves of Bauhinia variegata L. using liquid chromatography combined with tandem mass spectrometry. *Brazilian Journal of Plant Physiology*, 24(3), pp.223–232.

Sapra, P. & Allenz, T.M., 2002. Internalizing antibodies are necessary for improved therapeutic efficacy of antibody-targeted liposomal drugs. *Cancer Research*, 62(24), pp.7190–7194.

Van Schaijk, B.C.L. et al., 2014. Type II fatty acid biosynthesis is essential for Plasmodium falciparum sporozoite development in the midgut of Anopheles mosquitoes. *Eukaryotic cell*, 13(5), pp.550–559.

Scherf, A. et al., 1998. Antigenic variation in malaria: In situ switching, relaxed and mutually exclusive transcription of var genes during intra-erythrocytic development in Plasmodium falciparum. *EMBO Journal*, 17(18), pp.5418–5426.

Scherrer, R.A. & Howard, S.M., 1977. Use of distribution coefficients in quantitative structure-activity relationships. *Journal of medicinal chemistry*, 20(1), pp.53–58.

Schipper, M.L. et al., 2009. Particle size, surface coating, and PEGylation influence the biodistribution of quantum dots in living mice. *Small*, 5(1), pp.126–134.

Schrier, S.L., 2012. What does the spleen see? *Blood*, 120(2), pp.242–243.

Schwartz, L. et al., 2012. A review of malaria vaccine clinical projects based on the WHO rainbow table. *Malaria Journal*, 11(1), p.11.

Semple, S.C., Chonn, A. & Cullis, P.R., 1998. Interactions of liposomes and lipid-based carrier systems with blood proteins: Relation to clearance behaviour in vivo. *Advanced Drug Delivery Reviews*, 32(1-2), pp.3–17.

Shah, S.N.H. et al., 2012. Permeation kinetics studies of physical mixtures of artemisinin in polyvinylpyrrolidone. *Dissolution Technologies*, 19(4), pp.6–13.

Sharifi, S. et al., 2012. Toxicity of nanomaterials. *Chemical Society reviews*, 41(6), pp.2323–2343.

Sharma, B., 2008. Structure and mechanism of a transmission blocking vaccine candidate protein Pfs25 from P. falciparum: a molecular modeling and docking study. *In silico biology*, 8(3-4), pp.193–206.

Sherman, I.W., 1979. Biochemistry of Plasmodium (malarial parasites). *Microbiological reviews*, 43(4), pp.453–495.

Shortt, H.E., 1948. Pre-erythrocytic stage in mammalian malaria parasites. *Garnham, P.C.*, 24(161), p.126.

Shviro, Y., Zilber, I. & Shaklai, N., 1982. The interaction of hemoglobin with phosphatidylserine vesicles. *Biochimica et biophysica acta*, 687(1), pp.63–70.

Silva, D.C.N. et al., 2012. Optical tweezers as a new biomedical tool to measure zeta potential of stored red blood cells. *PLoS ONE*, 7(2).

Singh, V., Gupta, P. & Pande, V., 2014. Revisiting the multigene families: Plasmodium var and vir genes. *Journal of Vector Borne Diseases*, 51(2), pp.75–81.

Singhal, A., Bali, A. & Gupta, C.M., 1986. Antibody-mediated targeting of liposomes to erythrocytes in whole blood. *Biochimica et biophysica acta*, 880(1), pp.72–77.

Singhal, A. & Gupta, C.M., 1986. Antibody-mediated targeting of liposomes to red cells in vivo. *FEBS letters*, 201(2), pp.321–326.

Siregar, J.E. et al., 2008. Mutation underlying resistance of Plasmodium berghei to atovaquone in the quinone binding domain 2 (Qo2) of the cytochrome b gene. *Parasitology International*, 57(2), pp.229–232.

Skorokhod, O.A. et al., 2007. Doxorubicin pharmacokinetics in lymphoma patients treated with doxorubicin-loaded eythrocytes. *Haematologica*, 92(4), pp.570–571.

Smith, J.D. et al., 2001. Decoding the language of var genes and Plasmodium falciparum sequestration. *Trends in Parasitology*, 17(11), pp.538–545.

Smith, J.D. et al., 1995. Switches in expression of Plasmodium falciparum var genes correlate with changes in antigenic and cytoadherent phenotypes of infected erythrocytes. *Cell*, 82(1), pp.101–110.

Smith, J.D., 2014. The role of PfEMP1 adhesion domain classification in Plasmodium falciparum pathogenesis research. *Molecular and Biochemical Parasitology*, 195(2), pp.82–87.

Soriano, J. et al., 2010. Cell uptake of Zn(II)-phthalocyanine-containing liposomes by clathrin-mediated endocytosis. *Histochem Cell Biol*, 133(4), pp.449–454.

Sridaran, S. et al., 2010. Anti-folate drug resistance in Africa: meta-analysis of reported dihydrofolate reductase (dhfr) and dihydropteroate synthase (dhps) mutant genotype frequencies in African Plasmodium falciparum parasite populations. *Malaria journal*, 9, p.247.

Srinivasan, P. et al., 2011. Binding of Plasmodium merozoite proteins RON2 and AMA1 triggers commitment to invasion. *Proceedings of the National Academy of Sciences of the United States of America*, 108(32), pp.13275–13280.

Staines, H.M., Ellory, J.C. & Kirk, K., 2001. Perturbation of the pump-leak balance for Na(+) and K(+) in malaria-infected erythrocytes. *American journal of physiology. Cell physiology*, 280(6), pp.C1576–C1587.

Stebelska, K., Wyrozumska, P. & Sikorski, A.F., 2006. PS exposure increases the susceptibility of cells to fusion with DOTAP liposomes. *Chemico-Biological Interactions*, 160(2), pp.165–174.

Steinberg, M.H. et al., 2009. *Disorders of Hemoglobin Genetics, Pathophysiology, and Clinical Management* 2nd Ed. M. H. Steinberg et al., eds., Cambridge University Press.

Steiner, E. et al., 2014. The heparan sulfate proteoglycan agrin contributes to barrier properties of mouse brain endothelial cells by stabilizing adherens junctions. *Cell and Tissue Research*, 358(2), pp.465–79.

Stensrud, G. et al., 2000. Formulation and characterisation of primaquine loaded liposomes prepared by a pH gradient using experimental design. *International Journal of Pharmaceutics*, 198(5), pp.213–228.

Straubinger, R.M., Papahadjopoulos, D. & Hong, K.L., 1990. Endocytosis and intracellular fate of liposomes using pyranine as a probe. *Biochemistry*, 29(20), pp.4929–39.

Strebhardt, K. & Ullrich, A., 2008. Paul Ehrlich's magic bullet concept: 100 years of progress. *Nature reviews. Cancer*, 8(6), pp.473–480.

Stubbs, J. et al., 2005. Molecular mechanism for switching of P. falciparum invasion pathways into human erythrocytes. *Science*, 309(5739), pp.1384–1387.

Sullivan, D.J., Gluzman, I.Y. & Goldberg, D.E., 1996. Plasmodium hemozoin formation mediated by histidine-rich proteins. *Science*, 271(5246), pp.219–222.

Summers, R.L. et al., 2014. Diverse mutational pathways converge on saturable chloroquine transport via the malaria parasite's chloroquine resistance transporter. *Proceedings of the National Academy of Sciences of the United States of America*, 111(17), pp.E1759–67.

Sun, H. et al., 2014. Oligonucleotide aptamers: new tools for targeted cancer therapy. *Molecular therapy. Nucleic acids*, 3(Article e182).

Tachibana, S.I. et al., 2012. Plasmodium cynomolgi genome sequences provide insight into Plasmodium vivax and the monkey malaria clade. *Nature Genetics*, 44(9), pp.1051–1055.

Taraschi, T.F. et al., 2001. Vesicle-mediated trafficking of parasite proteins to the host cell cytosol and erythrocyte surface membrane in Plasmodium falciparum infected erythrocytes. *International Journal for Parasitology*, 31(12), pp.1381–1391.

Terajima, M. et al., 1994. Structural organization of the mouse glycophorin A gene. *Journal of biochemistry*, 116(5), pp.1105–1110.

Tewari, R. et al., 2002. Function of region I and II adhesive motifs of Plasmodium falciparum circumsporozoite protein in sporozoite motility and infectivity. *Journal of Biological Chemistry*, 277(49), pp.47613–47618.

Thakur, R., Das, A. & Chakraborty, A., 2014. Interaction of human serum albumin with liposomes of saturated and unsaturated lipids with different phase transition temperatures: a spectroscopic investigation by membrane probe PRODAN. *RSC Advances*, 4(28), p.14335.

Tham, W.H. et al., 2010. Complement receptor 1 is the host erythrocyte receptor for Plasmodium falciparum PfRh4 invasion ligand. *Proceedings of the National Academy of Sciences of the United States of America*, 107(40), pp.17327–17332.

Thomas, D.C. et al., 2012. Regulation of Plasmodium falciparum glideosome associated protein 45 (PfGAP45) phosphorylation. *PLoS ONE*, 7(4), e35855.

Thybo, S. et al., 2004. Atovaquone-proguanil (malarone): an effective treatment for uncomplicated Plasmodium falciparum malaria in travelers from Denmark. *J Travel Med*, 11(4), pp.220–223.

Tilley, L. & McConville, M., 2013. Malaria: Sensing when it's time for sex. *Nature*, 499(7456), pp.38–40.

Tonhosolo, R. et al., 2009. Carotenoid biosynthesis in intraerythrocytic stages of Plasmodium falciparum. *The Journal of biological chemistry*, 284(15), pp.9974–9985.

Torchilin, V.P., 2005. Recent advances with liposomes as pharmaceutical carriers. *Nature reviews. Drug discovery*, 4(2), pp.145–160.

Tosta, C.E., Ruiz, G. & Wedderburn, N., 1984. The role of spleen macrophages in malaria: An ultrastructural study. *Revista da Sociedade Brasileira de Medicina Tropical*, 17(1), pp.31–36.

Trabulo, S. et al., 2010. Cell-penetrating peptides-mechanisms of cellular uptake and generation of delivery systems. *Pharmaceuticals*, 3(4), pp.961–993.

Tripathi, A.K., Garg, S.K. & Tekwani, B.L., 2002. A physiochemical mechanism of hemozoin (beta-hematin) synthesis by malaria parasite. *Biochemical and biophysical research communications*, 290(1), pp.595–601.

Tsai, M.S. et al., 2011. Binding patterns of peptide-containing liposomes in liver and spleen of developing mice: comparison with heparan sulfate immunoreactivity. *Journal of drug targeting*, 19(7), pp.506–515.

Turner, G.D. et al., 1994. An immunohistochemical study of the pathology of fatal malaria. Evidence for widespread endothelial activation and a potential role for intercellular adhesion molecule-1 in cerebral sequestration. *The American journal of pathology*, 145(5), pp.1057–1069.

Turner, L. et al., 2013. Severe malaria is associated with parasite binding to endothelial protein C receptor. *Nature*, 498(7455), pp.502–5.

Tusting, L.S. et al., 2013. Mosquito larval source management for controlling malaria. *The Cochrane database of systematic reviews*, 8(Article CD008923).

Tuteja, R., 2007. Malaria - An overview. *FEBS Journal*, 274(18), pp.4670–4679.

Ulbrich, K. et al., 1980. Polymers containing enzymatically degradable bonds. V. Hydrophilic polymers degradable by papain. *Biomaterials*, 1(4), pp.199–204.

Umeda, T. et al., 2011. Molecular basis of fosmidomycin's action on the human malaria parasite Plasmodium falciparum. *Scientific Reports*, 1(Article 9).

Urbán, P., Estelrich, J., Cortés, A., et al., 2011. A nanovector with complete discrimination for targeted delivery to Plasmodium falciparum-infected versus non-infected red blood cells in vitro. *Journal of controlled release*, 151(2), pp.202–11.

Urbán, P., Estelrich, J., Adeva, A., et al., 2011. Study of the efficacy of antimalarial drugs delivered inside targeted immunoliposomal nanovectors. *Nanoscale research letters*, 6(1), p.620.

Urbán, P. et al., 2014. Use of poly(amidoamine) drug conjugates for the delivery of antimalarials to Plasmodium. *Journal of Controlled Release*, 177, pp.84–95.

Valle-Delgado, J.J. et al., 2010. Modulation of Abeta42 fibrillogenesis by glycosaminoglycan structure. *The FASEB journal : official publication of the Federation of American Societies for Experimental Biology*, 24(11), pp.4250–4261.

Valle-Delgado, J.J., Urbán, P. & Fernàndez-Busquets, X., 2013. Demonstration of specific binding of heparin to Plasmodium falciparum-infected vs. non-infected red blood cells by single-molecule force spectroscopy. *Nanoscale*, 5(9), pp.3673–80.

Vangapandu, S. et al., 2007. Recent advances in antimalarial drug development. *Medicinal Research Reviews*, 27(1), pp.65–107.

Vaughan, A.M. et al., 2012. Development of humanized mouse models to study human malaria parasite infection. *Future microbiology*, 7(5), pp.657–65.

Vigan-Womas, I. et al., 2008. An in vivo and in vitro model of Plasmodium falciparum rosetting and autoagglutination mediated by varO, a group A var gene encoding a frequent serotype. *Infection and Immunity*, 76(12), pp.5565–5580.

Vigan-Womas, I. et al., 2010. The humoral response to Plasmodium falciparum VarO rosetting variant and its association with protection against malaria in Beninese children. *Malaria journal*, 9, p.267.

Virtanen, J.A., Cheng, K.H. & Somerharju, P., 1998. Phospholipid composition of the mammalian red cell membrane can be rationalized by a superlattice model. *Proceedings of the National Academy of Sciences of the United States of America*, 95(9), pp.4964–4969.

Vogt, A.M. et al., 2003. Heparan sulfate on endothelial cells mediates the binding of Plasmodium falciparum-infected erythrocytes via the DBL1alpha domain of PfEMP1. *Blood*, 101(6), pp.2405–2411.

Vogt, A.M. et al., 2004. Heparan sulphate identified on human erythrocytes: a Plasmodium falciparum receptor. *The Biochemical journal*, 381(Pt 3), pp.593–597.

De Vries, A.H. et al., 2005. Molecular structure of the lecithin ripple phase. *Proceedings of the National Academy of Sciences of the United States of America*, 102(15), pp.5392–5396.

Vrignaud, S., Benoit, J.P. & Saulnier, P., 2011. Strategies for the nanoencapsulation of hydrophilic molecules in polymer-based nanoparticles. *Biomaterials*, 32(33), pp.8593–8604.

Wahajuddin et al., 2014. Investigation of the functional role of P-glycoprotein in limiting the oral bioavailability of lumefantrine. *Antimicrobial Agents and Chemotherapy*, 58(1), pp.489–494.

Walker, H. k., Hall, W.D. & Hurst, J.W., 1990. *Clinical Methods: The History, Physical, and Laboratory Examinations* 3rd Ed., Boston: Butterworth.

Wallach, D.F., Mikkelsen, R.B. & Schmidt-Ullrich, R., 1981. Plasmodial modifications of erythrocyte surfaces. *Ciba Foundation symposium*, 80, pp.220–233.

Walling, M.A., Novak, J.A. & Shepard, J.R.E., 2009. Quantum dots for live cell and in vivo imaging. *International Journal of Molecular Sciences*, 10(2), pp.441–491.

Warhurst, D.C. et al., 2003. The relationship of physico-chemical properties and structure to the differential antiplasmodial activity of the cinchona alkaloids. *Malaria journal*, 2, p.26.

Webster, R. et al., 2009. PEG and PEG conjugates toxicity: towards an understanding of the toxicity of PEG and its relevance to PEGylated biologicals. In F. M. Veronese, ed. *PEGylated Protein Drugs Basic Science and Clinical Applications*. Switzerland: Birkhäuser Basel, pp. 127–146.

Webster, R. et al., 2007. PEGylated proteins: Evaluation of their safety in the absence of definitive metabolism studies. *Drug Metabolism and Disposition*, 35(1), pp.9–16.

Wei, N. & Hossein Sadrzadeh, S.M., 1994. Enhancement of hemin-induced membrane damage by artemisinin. *Biochemical Pharmacology*, 48(4), pp.737–741.

Wells, T.N.C., Alonso, P.L. & Gutteridge, W.E., 2009. New medicines to improve control and contribute to the eradication of malaria. *Nature reviews. Drug discovery*, 8(11), pp.879–891.

Wells, T.N.C., van Huijsduijnen, R.H. & Van Voorhis, W.C., 2015. Malaria medicines: a glass half full? *Nature Reviews Drug Discovery*, 14, pp.424–442.

Wickham, M.E. et al., 2001. Trafficking and assembly of the cytoadherence complex in Plasmodium falciparum-infected human erythrocytes. *EMBO Journal*, 20(20), pp.5636–5649.

Williams, A.R. et al., 2012. Enhancing blockade of Plasmodium falciparum erythrocyte invasion: assessing combinations of antibodies against PfRH5 and other merozoite antigens. *PLoS Pathogens*, 8(11).

Wilson, D.W. et al., 2013. Defining the timing of action of antimalarial drugs against Plasmodium falciparum. *Antimicrobial Agents and Chemotherapy*, 57(3), pp.1455–1467.

Woodle, M.C., Newman, M.S. & Cohen, J.A., 1994. Sterically stabilized liposomes: physical and biological properties. *Journal of drug targeting*, 2(5), pp.397–403.

World Health Organization, 2010. *Guidelines for the treatment of malaria, 2nd edition*,

World Health Organization, 2015a. *Guidelines for the treatment of malaria, 3rd edition*, Geneva.

World Health Organization, 2015b. Tables of malaria vaccine projects globally. *WHO website*. Available at: http://www.who.int/immunization/research/development/Rainbow_tables.

World Health Organization, 2014. *World malaria report 2014*, Switzerland.

Wright, G.J. & Rayner, J.C., 2014. Plasmodium falciparum erythrocyte invasion: combining function with immune evasion. *PLoS Pathogens*, 10(3), e1003943.

Wunderlich, J., 2012. The malaria digestive vacuole. *Frontiers in Bioscience*, S4(4), p.1424.

Xiang, T.X. & Anderson, B.D., 1998. Influence of chain ordering on the selectivity of dipalmitoylphosphatidylcholine bilayer membranes for permeant size and shape. *Biophysical journal*, 75(6), pp.2658–2671.

Xiang, T.X. & Anderson, B.D., 1997. Permeability of acetic acid across gel and liquid-crystalline lipid bilayers conforms to free-surface-area theory. *Biophysical journal*, 72(1), pp.223–237.

Xiong, X.B. et al., 2005. Intracellular delivery of doxorubicin with RGD-modified sterically stabilized liposomes for an improved antitumor efficacy: In vitro and in vivo. *Journal of Pharmaceutical Sciences*, 94(8), pp.1782–1793.

Yamaja Setty, B.N., Kulkarni, S. & Stuart, M.J., 2002. Role of erythrocyte phosphatidylserine in sickle red cell-endothelial adhesion. *Blood*, 99(5), pp.1564–1571.

Yamazaki, M. et al., 1992. Phase transitions of phospholipid vesicles under osmotic stress and in the presence of ethylene glycol. *Biophysical Chemistry*, 43(1), pp.29–37.

Yang, X. et al., 2010. Identification of key residues involved in fibril formation by the conserved N-terminal region of Plasmodium falciparum merozoite surface protein 2 (MSP2). *Biochimie*, 92(10), pp.1287–1295.

Ying, L. & Wang, Q., 2013. Microfluidic chip-based technologies: emerging platforms for cancer diagnosis. *BMC biotechnology*, 13(1), p.76.

Yu, M. et al., 2008. The fatty acid biosynthesis enzyme FabI plays a key role in the development of liver-stage malarial parasites. *Cell host & microbe*, 4(6), pp.567–578.

Zaitsev, S. et al., 2006. Human complement receptor type 1-directed loading of tissue plasminogen activator on circulating erythrocytes for prophylactic fibrinolysis. *Blood*, 108(6), pp.1895–1902.

Zalipsky, S., 1993. Synthesis of an end-group functionalized polyethylene glycol-lipid conjugate for preparation of polymer-grafted liposomes. *Bioconjugate Chemistry*, 4(4), pp.296–299.

Zeevaart, J. a D. & Creelman, R. a, 1988. Metabolism and Physiology of Abscisic Acid. *Annual Review of Plant Physiology and Plant Molecular Biology*, 39(1), pp.439–473.

Zeng, J., Smith, K.E. & Chong, P.L., 1993. Effects of alcohol-induced lipid interdigitation on proton permeability in L-alpha-dipalmitoylphosphatidylcholine vesicles. *Biophysical journal*, 65(4), pp.1404–1414.

Zhang, B. et al., 2011. A second target of the antimalarial and antibacterial agent fosmidomycin revealed by cellular metabolic profiling. *Biochemistry*, 50(17), pp.3570–3577.

Zhang, L. & Webster, T.J., 2009. Nanotechnology and nanomaterials: Promises for improved tissue regeneration. *Nano Today*, 4(1), pp.66–80.

Zhang, R. et al., 2013. Spectrin: Structure, function and disease. *Science China Life Sciences*, 56(12), pp.1076–1085.

Zhang, Y. et al., 2013. Proteomic analysis of Plasmodium falciparum schizonts reveals heparin-binding merozoite proteins. *Journal of Proteome Research*, 12(5), pp.2185–2193.

Zhou, R. et al., 2003. Rapid extraction of abscisic acid and its metabolites for liquid chromatography-tandem mass spectrometry. *Journal of Chromatography A*, 1010(1), pp.75–85.

Zhu, L., Kate, P. & Torchilin, V.P., 2012. Matrix metalloprotease 2-responsive multifunctional liposomal nanocarrier for enhanced tumor targeting. *ACS Nano*, 6(4), pp.3491–3498.

Zuhorn, I.S., Engberts, J.B.F.N. & Hoekstra, D., 2007. Gene delivery by cationic lipid vectors: Overcoming cellular barriers. *European Biophysics Journal*, 36(4-5), pp.349–362.